

Whether it is the action of dopamine or dope: it is all about interaction

Elise WOUTERS

2019

Promoter: Prof. Dr. Christophe Stove

Thesis submitted to obtain the degree of Doctor in Pharmaceutical Sciences

Copyright

The author and promoters give authorization to consult and copy parts of this thesis for personal use only. Any other use is limited by the laws of copyright, especially concerning the obligation to refer to the source whenever results are cited from this thesis.

De auteur en promotoren geven de toelating dit proefschrift voor consultatie beschikbaar te stellen en delen ervan te kopiëren voor persoonlijk gebruik. Elk ander gebruik valt onder de beperkingen van het auteursrecht, in het bijzonder met betrekking tot de verplichting uitdrukkelijk de bron te vermelden bij het aanhalen van resultaten uit dit proefschrift.

Ghent, 2019,

The promoter,

Prof. Dr. Christophe Stove

The author,

Elise Wouters

Een woordje van dank
En enkele lieve woorden
Recht uit het hart

Onwerkelijk. Onwerkelijk is het, dat na 4,5 jaar van bloed, zweet en tranen en na meerdere collega's het einde te zien behalen, het eindelijk aan mij is. Het was me wel een padje om te bewandelen: het leren omgaan met onzekerheid en tegenslag maar ook het leren geloven in een goede afloop. En ik moet toegeven, ik ben er sterker uitgekomen. En als ik het nog even zeggen mag: ik ben voor het eerst écht trots op mezelf.

Nu was dit natuurlijk niet allemaal gelukt als ik niet op de steun en advies van heel wat supporters rondom mij kon rekenen. Daarom kijk ik ernaar uit om jullie allemaal van harte te bedanken.

- - -

Eerst en vooral wil ik mijn promotoren bedanken: Dr. Kathleen Van Craenenbroeck, bedankt om mij de kans te geven te starten met een doctoraat en mij de 'kneepjes van het vak' te leren gedurende de eerste 2,5 jaar. Prof. Dr. Christophe Stove, bedankt om mij 'te adopteren' en mij de kans te geven mijn doctoraat te laten afwerken. Er is ontzettend veel werk verzet geweest gedurende het laatste jaar van mijn doctoraat. Dit bracht ook een kleine 300-tal pagina's met zich mee, die allemaal zeer kritisch en gedetailleerd nagekeken zijn geweest door jou. Bedankt hiervoor!

- - -

Aan alle leden van de examenjury: bedankt om mijn werk nauwgezet te lezen en grondig te bediscussiëren tijdens de gesloten verdediging.

- - -

Bedankt aan alle (ex-)L-GEST-collega's: Karen, Kamila, An, Lakshmi en René. Karen, jij hebt me geleerd kritisch mijn onderzoeksresultaten te benaderen en aan alle controles te denken vooraleer er besluiten genomen werden. Bedankt! Dear Kamila, thank you so much for your advice, your help, your expertise, but most of all your company. It was a great pleasure working with you. I wish you all the best with your husband and your lovely daughter Julia. Lieve lieve An, jou beschouw ik als mijn 'L-GEST mama' met een hart van goud. Jouw onvoorwaardelijke en continue steun via mailtjes hebben meer betekend dan je je kan inbeelden. Een welgemeende dankjewel! Dear Lakshmi, my friend. You crossed borders to

obtain your doctoral degree in Belgium, and I am so happy you did, as you ended up to be my colleague. Indeed, I am thrilled I have taken this journey with you (and with René, a.k.a. the three musketeers) until the very end for all three of us. Thank you for being by my side and always remember: you have my back! I wish you and Mani the very best (and a lot of kids ☺)! En dan finaal, René. Waar moet ik beginnen? Oh ja, eerst en vooral bedankt voor elke keer dat ik met een vraag afkwam, jij mij altijd wijselijk doorverwees naar de 'datasheet'. Nee serieus, je hebt me meer geholpen dan je je bewust bent. Bedankt voor altijd klaar te staan met je goede humeur en je onnozele grapjes. Je 'relativeringsvermogen' en je humor hebben het zeker aangenamer gemaakt voor mij. Jij bent me d'r eentje! ;)

- - -

Ex- en huidige TeamTox collega's, bedankt! Eerst en vooral een dankjewel aan mijn 'cel'-collega's Jolien, Annelies en Eline. Jolien, je bent een mooi persoon(tje) en ik weet dat ik aan jou niet enkel een ex-collega maar ook een vriendin heb overgehouden. Annelies, een dikke merci om altijd meer dan klaar te staan voor eender welke hulp ook! Eline, ons project-verzamelaartje, jij gaat het goed doen. Daar heb ik alle vertrouwen in. Het was aangenaam 'samen te werken' met jou! Ook een dankjewel aan Elly en Elke voor de aangename babbels. Verder wil ik nog Jana, Lisa, Sigrid, Rani, Sara, Sofie en Katleen bedanken voor de hulp of steun waar nodig. En finaal, ook zeker een dankjewel aan Valerie, Goedele en Ann. Alle drie stonden jullie wel klaar om af en toe eens een gezellige en vriendelijke babbel te voeren.

- - -

Mijn vriend(inn)en. Wat ben ik blij dat ik terug wat meer tijd kan maken voor jullie! Bij wie moet ik beginnen? Bedankt aan Esther, Florence, Sophie en Catherine. Jullie vriendschap, jullie steun en jullie gezelschap is iets dat ik niet meer wil missen. Bedankt Julieke, om er altijd voor mij te zijn en bedankt voor de vele leuke momenten samen! Een dikke dankjewel aan Saelfi, aka Sari en Fien, voor een studieperiode samen die uitgegroeid is tot een mooie vriendschap. Bedankt aan al mijn dansmaatjes, Vicky, Sofie, Svea, Mounia, Eshly en Laura, om speciaal af te komen naar Gent om dit moment met mij te delen. Bedankt voor, wanneer ik afkom naar Grimbergen, het altijd even leuk te maken! Bedankt aan mijn lieve ex-kotgenoten én vrienden, zeker Sofie maar ook Jasper ☺, voor de ongelooflijk leuke tijden samen in Gent. Een periode die ik niet snel zal vergeten. Sofie, jij bent een ongelooflijk goede vriendin geworden, ik geniet telkens van onze babbels.

- - -

En last but not least: mijn familie, mijn grootste steun in dit alles! Het vat niet in woorden samen te vatten hoe graag ik jullie zie. Eerst en vooral bedankt aan mijn ouders, voor de steun, de liefde, het luisterend oor, het lekkere eten en nog zoveel meer. Mijn broer, Yves, voor de onvoorwaardelijke en onbreekbare zus-broer-band. Mijn (suiker)tante, voor de enorme steun en de vele mooie belevingen en reizen die Yves en ik al van kleins af aan hebben mogen meemaken dankzij jou. Mijn oma en opa, het feit dat jullie zó ongelooflijk trots zijn dat ik hier geraakt ben, betekent de wereld voor mij! Mijn mamy, mijn kleinste maar dapperste familielid, jouw liefde voor je kleinkinderen is onbeschrijfelijk. Bedankt allemaal voor alles! Ik zou dit werk dan ook graag aan jullie opdragen.

- - -

Ook wil ik graag 'aangetrouwde' familie bedanken. Philip, bedankt voor je steun! Ik apprecieer het enorm, hoe je ons ook telkens welkom heet in Bever. Bedankt Erikaatje, voor je eeuwige enthousiasme. Veerle, ook jou wil ik bedanken voor jouw steun en lieve attenties/kaartjes die je me bezorgde. Ook bedankt aan Leontien, Martine, Christel en Katrien voor de gezellige samenkomsten en steun!

- - -

Lorenz, mijn grootste steun en toeverlaat. Je oprechtheid, je recht-door-zee manier, je zorgzaamheid en je groot hart apprecieer ik enorm! Bedankt om er voor me te zijn, me te troosten wanneer nodig, me op te beuren en me advies te geven (waar ik meestal naar luisterde ☺) gedurende deze periode. Ik kijk uit naar een toekomst samen met jou.

The end.

Ah!

Wat een zalig gevoel.

Table of Contents

List of abbreviations	XV-XVIII
CHAPTER 1: GENERAL INTRODUCTION, AIMS AND OUTLINE	1
1.1 G protein-coupled receptors (GPCRs)	3
1.2 Aims and outline of this thesis	8
References	11
PART I	
CHAPTER 2: FOCUS ON THE DOPAMINE RECEPTOR	15
2.1 GPCR-GPCR interactions: a question still open	17
2.1.1 What is GPCR homo- or heteromerization?	17
2.1.2 Why should we target GPCR oligomers?	20
2.1.3 How can we examine GPCR oligomers?	22
2.2 Dopamine receptor complexes	26
2.2.1 Dopamine receptors	26
2.2.2 Dopamine Homomeric complexes	28
2.2.3 Dopamine Heteromeric complexes	28
2.2.4 Ligands of dopaminergic D ₂ R complexes	31
2.2.4.1 Bivalent ligands	31
2.2.4.2 Bitopic ligands	35
2.2.4.3 Biased ligands	36
References	38
CHAPTER 3: LUMINESCENCE- AND FLUORESCENCE-BASED COMPLEMENTATION ASSAYS TO SCREEN FOR GPCR OLIGOMERIZATION: CURRENT STATE OF THE ART	49
3.1 Introduction	53
3.2 Protein complementation assays	54
3.2.1 Fluorescence-based complementation assays	57
3.2.1.1 Fluorescent proteins	58
3.2.1.1.1 Green fluorescent protein (GFP)	58
3.2.1.1.2 Yellow fluorescent protein (YFP)	59
3.2.1.1.3 Cyan fluorescent protein (CFP)	62
3.2.1.1.4 Red, far-red and near-infrared fluorescent proteins	62
3.2.1.2 BiFC assays	64
3.2.1.2.1 Multicolour BiFC (MBiFC)	64
3.2.1.2.2 BiFC-RET	65
3.2.1.3 Ligand-dependent modulation of dimerization	66
3.2.2 Luminescence-based complementation assays	67
3.2.2.1 Luminescent proteins	68
3.2.2.1.1 <i>Renilla</i> /Firefly Luciferase (RLuc/FLuc)	68
3.2.2.1.2 NanoLuciferase (NanoLuc)	71
3.2.2.2 BiLC-RET	72
3.2.3 Combinatorial assays: BiFC and BiLC	73
3.3 Comparison of split protein approaches	75
3.3.1 Advantages of PCA	75

3.3.2 Limitations of PCA	76
3.4 Guidelines to perform accurate PCA-based assays	77
3.4.1 Possible fusions	78
3.4.2 Functionality and localization of the fusion proteins	81
3.4.3 Non-interacting partners	82
3.4.4 Normalization factor	82
3.4.5 Endogenous expression levels	83
3.4.6 Kinetics	83
3.5 High-throughput screening with cell-based PCAs	84
3.5.1 GPCR oligomerization screening	84
3.5.2 GPCR drug discovery	85
3.6 <i>In vivo</i> application	86
3.7 Conclusion	88
References	89

CHAPTER 4: ASSESSING GPCR DIMERIZATION IN LIVING CELLS: COMPARISON OF THE NANOBIT ASSAY WITH RELATED BIOLUMINESCENCE- AND FLUORESCENCE-BASED APPROACHES.

	97
4.1 Introduction	101
4.2 Materials	102
4.2.1 Plasmids	102
4.2.2 Cells	103
4.3 Reagents	103
4.4 Equipment	103
4.5 Methods	104
4.6 Notes	107
4.7 Conclusion	110
References	110

CHAPTER 5: DISTINCT DOPAMINE D₂ RECEPTOR ANTAGONISTS DIFFERENTIALLY IMPACT D₂ RECEPTOR OLIGOMERIZATION

	111
5.1 Introduction	115
5.2 Material and Methods	117
5.2.1 Chemicals and Reagents	117
5.2.2 Cloning of the dopamine D ₂ R into the NanoBiT [®] plasmids	118
5.2.3 Cell culture	119
5.2.3.1 <i>Expression in HEK293T cells</i>	119
5.2.3.2 <i>Cell preparation for dimerization assay with HEK293T cells in suspension</i>	119
5.2.3.3 <i>Cell preparation for dimerization assay with adherent HEK293T cells</i>	120
5.2.3.4 <i>Fluorescence normalization and signal-to-noise ratio</i>	120
5.2.4 NanoBiT [®] -based validation of the functionality of D _{2L} R luminescent fusion proteins by mini-Gα _i protein-mediated signaling	121
5.2.5 Detection of the expression levels of D _{2L} R dimers by western blot	121
5.2.6 Data analysis	122
5.2.7 Computational modeling	123
5.2.8 Molecular dynamic (MD) simulations	123

5.2.9 MD simulation analysis	124
5.3 Results	125
5.3.1 Pharmacological properties of the D _{2L} R fusion proteins	125
5.3.2 Targeting the dopamine D _{2L} R homodimer using the NanoBiT assay	126
5.3.3 Antagonist-dependent modulation of the level of D _{2L} R homodimer formation	127
5.3.3.1 Short-term effects	127
5.3.3.2 Long-term effects	128
5.3.3.3 Screening of a broader panel of D ₂ R ligands	130
5.3.4 Validation of the spiperone-modulating capacity on the D _{2L} R homodimer	130
5.3.5 Spiperone and clozapine achieve stable binding poses in D ₂ R during molecular dynamics simulations	133
5.3.6 Spiperone and clozapine select for different sidechain conformations in D ₂ R TM5 and TM6	137
5.3.7 Aromatic interactions stabilize D ₂ R homodimer model interface during MD simulation	139
5.3.8 D _{2L} R oligomerization	140
5.4 Discussion	142
References	148
 CHAPTER 6: SYNTHESIS TOWARDS BIVALENT LIGANDS FOR THE DOPAMINE D ₂ AND METABOTROPIC GLUTAMATE 5 RECEPTORS	 155
6.1 Introduction	159
6.2 Material and Methods	161
6.2.1 Chemistry	161
6.2.2 Generation of the stable mGluR ₅ -D ₂₅ R co-expressing cell line	161
6.2.3 Cell culture and transfection	162
6.2.4 Membrane preparation and protein determination	162
6.2.5 [³ H]Raclopride binding	162
6.2.6 [³ H]MPEP binding	163
6.2.7 Data analysis	163
6.2.8 GloSensor cAMP protocol	163
6.2.9 Computational modeling	164
6.2.9.1 Receptor structure preparation	164
6.2.9.2 Protein-protein docking	164
6.2.9.3 Bivalent ligand docking	165
6.3 Results and discussion	165
6.3.1 Design of heterobivalent ligands	165
6.3.2 Synthesis	168
6.3.3 Pharmacological evaluation	168
6.3.3.1 Affinity of the bivalent ligands for the D ₂₅ R	168
6.3.3.2 Affinity of the bivalent ligands for the mGluR ₅	170
6.3.3.3 cAMP assay to study potency of the selected D ₂ R ligands	172
6.3.4 Computational modeling of a bivalent ligand bound to an mGluR ₅ -D ₂ R heterodimer	174
6.4 Conclusion	178
References	179

PART II

CHAPTER 7: INSIGHTS INTO BIASED SIGNALING AT CANNABINOID RECEPTORS: SYNTHETIC CANNABINOID RECEPTOR AGONISTS

	185
7.1 Introduction	189
7.1.1 Synthetic cannabinoid receptor agonists	190
7.2 Biased signaling	196
7.2.1 What is known for SCRAAs?	198
7.2.2 Strategies for identifying biased signaling	207
7.2.2.1 Challenges in comparing different experimental set-ups	207
7.2.2.2 Ideal <i>in vitro</i> activity-based techniques for assessing biased signaling	211
7.2.3 Reference compounds selection for SCRA bias detection	212
7.2.4 Cell system selection	213
7.3 Concluding remarks	215
References	217

CHAPTER 8: ASSESSMENT OF BIASED AGONISM AMONGST DISTINCT SYNTHETIC CANNABINOID RECEPTOR AGONIST SCAFFOLDS

	225
8.1 Introduction	229
8.2 Materials and methods	231
8.2.1 Chemicals and Reagents	231
8.2.2 Development of mini-G α_i protein NanoBiT [®] construct plasmids	232
8.2.3 Development of the CB ₁ -NanoBiT [®] - mini-G α_i reporter bio-assay	233
8.2.4. Generation of a stable HEK293T cell line expressing CB ₁ and mini-G α_i protein	234
8.2.5 Screening of SCRAAs in bio-assays of mini-G α_i and β -arrestin2 signaling	236
8.2.6 Data analysis	236
8.2.7 Quantifying biased signaling	237
8.2.8 Molecular docking	238
8.2 Results and discussion	240
8.3.1 Development of the stable CB ₁ NanoBiT [®] reporter bio-assay for real-time monitoring of mini-G α_i recruitment in HEK293T cells	240
8.3.2 Selection of a non-biased reference compound in the NanoBiT [®] bio-assays	241
8.3.3 Screening of a panel of SCRAAs for biased signaling in β -arrestin2 and mini-G α_i recruitment assays	243
8.3 Conclusions	260
References	263

CHAPTER 9: FUNCTIONAL EVALUATION OF CARBOXY METABOLITES OF SYNTHETIC CANNABINOID RECEPTOR AGONISTS FEATURING SCAFFOLDS BASED ON L-VALINE OR L-*TERT*-LEUCINE.

	267
9.1 Introduction	271
9.2 Materials and methods	273
9.2.1 Chemicals and Reagents	273
9.2.2 Cannabinoid reporter bio-assay	275
9.2.3 Data processing	276
9.3 Results and discussion	276

9.3.1 1-Pentyl-1 <i>H</i> -indazole-3-carboxamide derivatives (PINACA)	277
9.3.2 1-(Cyclohexylmethyl)-1 <i>H</i> -indole-3-carboxamide (CHMICA) and 1-(cyclohexylmethyl)-1 <i>H</i> -indazole-3-carboxamide (CHMINACA)	280
9.3.3 1-[4-Fluorophenyl)methyl]-1 <i>H</i> -indole-3-carboxamide (FUBICA) and 1-[(4-fluorophenyl)methyl]-1 <i>H</i> -indazole-3-carboxamide derivatives (FUBINACA)	283
8.3 Conclusion	285
References	286
 CHAPTER 10: BROADER INTERNATIONAL CONTEXT, RELEVANCE AND FUTURE PERSPECTIVES	 291
 CHAPTER 11: CONCLUSION AND SUMMARY	 309
 SAMENVATTING	 315
 CURRICULUM VITAE	 321

List of abbreviations

2-AG	2-arachidonoylglycerol
[³⁵ S]GTPγS	³⁵ S-labelled guanosine triphosphate
4F-MDMB-BINACA	methyl (2 <i>S</i>)-2-{[1-(4-fluorobutyl)-1 <i>H</i> -indazole-3-carbonyl]amino}-3,3-dimethylbutanoate
5F-AB-PINACA	<i>N</i> -[(2 <i>S</i>)-1-(amino-3-methyl-1-oxobutan-2-yl)-1-(5-fluoropentyl)-1 <i>H</i> -indazole-3-carboxamide
5F-AB-PINACA-COOH	(2 <i>S</i>)-3-methyl-2-{[1-(5-fluoropentyl)-1 <i>H</i> -indazole-3-carbonyl]amino}butanoic acid
5F-ADB-PINACA	<i>N</i> -[(2 <i>S</i>)-1-amino-3,3-dimethyl-1-oxobutan-2-yl]-1-(5-fluoropentyl)-1 <i>H</i> -indazole-3-carboxamide
5F-ADB-PINACA-COOH	(<i>S</i>)-2-{[1-(5-fluoropentyl)-1 <i>H</i> -indazole-3-carbonyl]amino}-3,3-dimethylbutanoic acid
5F-AEB-PINACA	ethyl (2 <i>S</i>)-2-{[1-(5-fluoropentyl)-1 <i>H</i> -indazole-3-carbonyl]amino}-3-methylbutanoate
5F-AMB-PINACA	methyl (2 <i>S</i>)-2-{[1-(5-fluoropentyl)-1 <i>H</i> -indazole-3-carbonyl]amino}-3-methylbutanoate
5F-APINACA	<i>N</i> -(adamantan-1-yl)-1-(5-fluoropentyl)-1 <i>H</i> -indazole-3-carboxamide
5F-CUMYL-PINACA	1-(5-fluoropentyl)- <i>N</i> -(2-phenylpropan-2-yl)-1 <i>H</i> -indazole-3-carboxamide
5F-MDMB-PINACA	methyl (2 <i>S</i>)-2-{[1-(5-fluoropentyl)-1 <i>H</i> -indazole-3-carbonyl]amino}-3,3-dimethylbutanoate
5F-PB-22	quinolin-8-yl 1-(5-fluoropentyl)-1 <i>H</i> -indole-3-carboxylate
A ₁ /A _{2A}	Adenosine receptor type 1 / type 2A
AB-CHMINACA	<i>N</i> -[(2 <i>S</i>)-1-amino-3-methyl-1-oxobutan-2-yl]-1-(cyclohexylmethyl)-1 <i>H</i> -indazole-3-carboxamide
AB-CHMINACA-COOH	(2 <i>S</i>)-2-{[1-(cyclohexylmethyl)-1 <i>H</i> -indazole-3-carbonyl]amino}-3-methylbutanoic acid
AC	Adenylyl cyclase
ADB-CHMICA	<i>N</i> -[(2 <i>S</i>)-1-amino-3,3-dimethyl-1-oxobutan-2-yl]-1-(cyclohexylmethyl)-1 <i>H</i> -indole-3-carboxamide
ADB-CHMICA-COOH	(<i>S</i>)-2-{[1-(5-fluoropentyl)-1 <i>H</i> -indazole-3-carbonyl]amino}-3,3-dimethylbutanoic acid
ADB-CHMINACA	<i>N</i> -[(2 <i>S</i>)-1-amino-3,3-dimethyl-1-oxobutan-2-yl]-1-(cyclohexylmethyl)-1 <i>H</i> -indazole-3-carboxamide
ADB-CHMINACA-COOH	(2 <i>S</i>)-2-{[1-(cyclohexylmethyl)-1 <i>H</i> -indazole-3-carbonyl]amino}-3,3-dimethylbutanoic acid
ADB-FUBICA	<i>N</i> -[(2 <i>S</i>)-1-amino-3,3-dimethyl-1-oxobutan-2-yl]-1-[(4-fluorophenyl)methyl]-1 <i>H</i> -indole-3-carboxamide
ADB-FUBICA-COOH	(<i>S</i>)-2-{[1-(4-fluorobenzyl)-1 <i>H</i> -indole-3-carbonyl]amino}-3,3-dimethylbutanoic acid
ADB-FUBINACA	<i>N</i> -[(2 <i>S</i>)-1-amino-3,3-dimethyl-1-oxobutan-2-yl]-1-[(4-fluorophenyl)methyl]-1 <i>H</i> -indazole-3-carboxamide

AEA	anandamide
AMB-CHMINACA	methyl (2 <i>S</i>)-2-[[1-(cyclohexylmethyl)-1 <i>H</i> -indazole-3-carbonyl]amino]-3-methylbutanoate
AM-2201	[1-(5-fluoropentyl)-1 <i>H</i> -indol-3-yl](naphthalen-1-yl)methanone
AT ₁ /AT ₂	Angiotensin II receptor type 1 / type 2
AUC	Area under the curve
β factor	Bias factor
β2AR	β2 Adrenergic Receptor
β-arrest2	β-arrestin2
BB-22	quinolin-8-yl 1-(cyclohexylmethyl)-1 <i>H</i> -indole-3-carboxylate
BiFC	Bimolecular fluorescence complementation
BiLC	Bimolecular luminescence complementation
BRET	Bioluminescence resonance energy transfer
(C8)-CP47,497	2-[(1 <i>S</i> ,3 <i>R</i>)-3-hydroxycyclohexyl]-5-(2-methylnonan-2-yl)phenol
cAMP	Cyclic adenosine monophosphate
CB ₁	Cannabinoid receptor 1
CB ₂	Cannabinoid receptor 2
CC	C-terminal fragment of split Cerulean
CC2	C-C chemokine receptor type 2
CFP	Cyan fluorescent protein
CN	N-terminal fragment of split Cerulean
co-IP	Co-immunoprecipitation
CP55,940	2-[(1 <i>R</i> ,2 <i>R</i> ,5 <i>R</i>)-5-hydroxy-2-(3-hydroxypropyl)cyclohexyl]-5-(2-methyloctan-2-yl)phenol
CUMYL-PEGACLONE	5-pentyl-2-(2-phenylpropan-2-yl)-2,5-dihydro-1 <i>H</i> -pyrido[4,3- <i>b</i>]indol-1-one
DMEM	Dulbecco's modified Eagle's medium
dNGFR	Truncated nerve growth factor receptor
D ₂ R	Dopamine D ₂ receptor
D _{2L} R	Dopamine receptor type 2 Long isoform
D _{2S} R	Dopamine receptor type 2 Short isoform
EC ₅₀	Concentration resulting in 50% maximum response
ECL	Extracellular loop
EG-018	(naphthalen-1-yl)(9-pentyl-9 <i>H</i> -carbazol-3-yl)methanone
EG-2201	[9-(5-fluoropentyl)-9 <i>H</i> -carbazol-3-yl](naphthalen-1-yl)methanone
EGFP	Enhanced green fluorescent protein
E _{max}	Maximal response provoked by a ligand
EMCDDA	European Monitoring Centre for Drugs and Drug Addiction
ERK1/2	Extracellular signal-regulated kinases 1 and 2
FAAH	fatty acid amide hydrolase
FLuc	Firefly Luciferase

FRET	Förster resonance energy transfer
GDP	guanosine diphosphate
GLuc	<i>Gaussia princeps</i> luciferase
GPCR	G protein-coupled receptor
GRK	G protein-coupled receptor kinase
GTP	guanosine triphosphate
h	hour
HEK293T	Human embryonic kidney cell line
HTS	High-throughput screening
IC ₅₀	Inhibitor concentration resulting in 50% inhibition of enzyme activity
IRES	Internal ribosome entry site
JWH-018	Naphthalen-1-yl)(1-pentyl-1 <i>H</i> -indol-3-yl)methanone
JWH-250	2-(2-methoxyphenyl-1-(1-pentyl-1 <i>H</i> -indol-3-yl)ethan-1-one
K _i	Binding affinity of the non-radioactive ligand
LC-MS/MS	liquid chromatography with tandem mass spectrometry
LgBiT	Large BiT, large subunit of Nanoluciferase
MAGL	monoacylglycerol lipase
MAPK	Mitogen activated protein kinase
MBiFC	Multicolour Bimolecular fluorescence complementation assay
MDMB-CHMICA	methyl (2 <i>S</i>)-2-[[1-(cyclohexylmethyl)-1 <i>H</i> -indole-3-carbonyl]amino]-3,3-dimethylbutanoate
MDMB-CHMINACA	methyl (2 <i>S</i>)-2-[[1-(cyclohexylmethyl)-1 <i>H</i> -indazole-3-carbonyl]amino]-3,3-dimethylbutanoate
MDMB-FUBICA	methyl (2 <i>S</i>)-2-([1-[(4-fluorophenyl)methyl]-1 <i>H</i> -indole-3-carbonyl]amino)-3,3-dimethylbutanoate
MDMB-FUBINACA	methyl (2 <i>S</i>)-2-([1-[(4-fluorophenyl)methyl]-1 <i>H</i> -indazole-3-carbonyl]amino)-3,3-dimethylbutanoate
MMB-CHMICA	methyl (2 <i>S</i>)-2-[[1-(cyclohexylmethyl)-1 <i>H</i> -indole-3-carbonyl]amino]-3-methylbutanoate
MDMB-CHMCZCA	methyl (2 <i>S</i>)-2-[[9-(cyclohexylmethyl)-9 <i>H</i> -carbazole-3-carbonyl]amino]-3,3-dimethylbutanoate
MeOH	methanol
mini-Gα _i	Engineered GTPase domain of the Gα _i subunit
mGluR ₅	Metabotropic glutamate receptor 5
mL	milliliter
NanoBiT®	NanoLuc Binary Technology
n _H	Hill slope coefficient

NPS	New psychoactive substances
PCA	Protein complementation assay
PCR	Polymerase chain reaction
PD	Parkinson's Disease
PLA	Proximity ligation assay
POI	Protein of interest
PPI	protein-protein interaction
RA _i	Intrinsic relative activity
RCS-4	(4-methoxyphenyl)(1-pentyl-1 <i>H</i> -indol-3-yl)methanone
RCS-8	1-[1-(2-cyclohexylethyl-1 <i>H</i> -indol-3-yl)-2-(2-methoxyphenyl)ethan-1-one
RLU	Relative luminescence units
RLuc	<i>Renilla</i> Luciferase
SCRA	Synthetic Cannabinoid receptor agonist
SD	Standard deviation
SDS-PAGE	Sodium dodecyl sulfate-polyacrylamide gel electrophoresis
SEM	Standard error of the mean
SmBiT	Small BiT, small subunit of Nanoluciferase
SpIDA	Spatial Intensity Distribution Analysis
SRET	Sequential Resonance Energy Transfer
TAT	Transactivator of transcription
TM domains	Transmembrane domains
UNODC	United Nations Office on Drug and Crime
UR-144	(1-pentyl-1 <i>H</i> -indol-3-yl)(2,2,3,3-tetramethylcyclopropyl)methanone
VC	C-terminal fragment of split Venus
VN	N-terminal fragment of split Venus
WIN48,098	(4-methoxyphenyl{2-methyl-1-[2-(morpholin-4-yl)ethyl]-1 <i>H</i> -indol-3-yl})methanone
YC	C-terminal fragment of split Yellow fluorescent protein
YFP	Yellow fluorescent protein
YN	N-terminal fragment of split Yellow fluorescent protein
XLR-11	[1-(5-fluoropentyl)-1 <i>H</i> -indol-3-yl](2,2,3,3-tetramethylcyclopropyl)methanone

Chapter 1:

General introduction, Aims and Outline

- G protein-coupled receptors and their interaction partners -

1.1 G protein-coupled receptors (GPCRs)

The human body is made of almost 4 trillion individual cells [1]. Those cells, from different parts of our body, require sophisticated communication to maintain homeostasis. Hence, chemical signals, in the form of hormones or neurotransmitters, are continuously being sent and received by these cells. In order to trigger the desired response, the information encoded by these chemical messengers needs to be transmitted across the cell membrane. Back in the 1980s, Brian Kobilka and Robert Lefkowitz initiated research that formed the basis of some groundbreaking discoveries via which we eventually gained our first insights into the function and structure of a class of cell surface receptors capable of transferring this information. These receptors were termed 'G protein-coupled receptors' (GPCRs), also known as seven transmembrane domain receptors. As a result of their impressive achievements, Brian Kobilka and Robert Lefkowitz were awarded with the Nobel Prize in Chemistry in 2012. Despite tremendous research efforts and although substantial additional information has been gathered, to this day researchers still don't have a complete understanding of the signaling mechanism of these receptors.

GPCRs represent the largest and most diverse family of cell surface receptors, with more than 800 distinct GPCRs that are classified into five main families [2]. Those five families follow the 'GRAFS' classification system, as the families are referred to as Glutamate, Rhodopsin, Adhesion, Frizzled/Taste2 and Secretin. One thing all these GPCRs have in common is their structure, consisting of an N-terminal extracellular end, seven transmembrane domains which are coupled by three extracellular loops (ECL1-3) and three intracellular loops (ICL1-3), and a C-terminal intracellular end. Nevertheless, the N-terminus, ECL, ICL and C-terminus can vary widely in size and function, so that certain GPCRs consist of fewer than 350 residues, whereas others consist of more than 5900 residues [2].

GPCRs can be activated by numerous stimuli, including hormones, neurotransmitters, pheromones, light, peptides, proteins, small molecule odorants, nucleotides, lipids, among others [3]. A tremendous amount of research has focused on how, upon receptor activation, GPCRs transfer information from outside the cell to the cell interior. As a matter of fact, the name of this receptor family already reveals that GPCRs couple to intracellular transducers, of which the G protein is the best characterized. The heterotrimeric G protein consists of a $G\alpha$

subunit and a dimeric $G\beta\gamma$ subunit. In humans, 21 $G\alpha$ subunits exist that are encoded by 16 genes, 6 $G\beta$ subunits encoded by 5 genes, and 12 $G\gamma$ subunits [4]. These G proteins are typically subdivided into four classes, based on the primary sequence of the $G\alpha$ subunit: $G\alpha_s$, $G\alpha_{i/o}$, $G\alpha_{q/11}$ and $G\alpha_{12/13}$. All members of the G protein families encompass a conserved GTPase domain and a helical domain that is responsible for the interaction with the $G\beta\gamma$ subunit and the GPCR. Upon receptor activation, the largest conformational change occurs by an outward movement of transmembrane helix 6 (TM6), thus creating a binding pocket for the C-terminal $\alpha 5$ helix of the G protein [5, 6]. Consequently, a GDP-GTP exchange in the catalytic domain of the $G\alpha$ -protein takes place and the $G\beta\gamma$ subunit dissociates from the $G\alpha$ subunit [7]. Each of the subunits provokes specific downstream signaling. The $G\alpha$ subunits couple to a variety of effector molecules, such as adenylyl cyclase (activated by $G\alpha_s$ or inhibited by $G\alpha_i$), phospholipase C (activated by $G\alpha_q$) or Rho guanine nucleotide exchange factors (activated by $G\alpha_{12/13}$), and the activation or inhibition of these effector molecules subsequently influences the production of second messengers (e.g. cAMP, inositol triphosphate and diacylglycerol), leading to the modulation of the activation of transcription factors. Similarly, the $G\beta\gamma$ subunits are known to recruit kinases or modulate the activity of ion channels, such as the G protein-coupled inwardly-rectifying potassium (GIRK) channels, which provoke hyperpolarization of the plasma membrane [8].

Besides G proteins, other well-known interaction partners of GPCRs involve β -arrestins. These are primarily known for their function as negative regulators of the G protein-mediated signaling [9]. Four members of the arrestin family have been reported: the visual arrestins (arrestin 1 and arrestin 4, which are solely expressed at the retina) and the non-visual arrestins (β -arrestin1 and β -arrestin2, ubiquitously expressed in most tissues). Upon receptor activation, recruitment of β -arrestins is mostly provoked by the phosphorylation of serine and threonine residues that reside at the intracellular part of the GPCR (i.e. ICL1-3 and/or the C-terminus) [10-12]. The phosphorylation of these residues of ligand-activated GPCRs can be mediated by distinct G protein-coupled receptor kinases (GRK1-7). Nevertheless, also phosphorylation-independent recruitment of β -arrestins has been reported, for which it has been suggested that negatively charged residues present in the intracellular part of the GPCRs may act as phospho-mimetics [13]. Coupling of these transducers to GPCRs is known to cause internalization of the receptors and thus, desensitization. However, an increasing body of

evidence suggests that β -arrestins can also function as scaffold proteins that mediate intracellular signaling as well. For example, the activation of the mitogen-activated protein kinases (MAPKs) that typically regulate cell cycle progression, cell survival and proliferation [14] or association with cAMP-response element binding protein (CREB), to promote transcription of target genes [15], among others, have been reported.

GPCRs clearly play a fundamental role in the regulation of distinct physiological processes. Hence, altered regulation and/or expression as well as the occurrence of mutations have been associated with numerous diseases, including cancer and neurodegenerative diseases. As GPCRs are expressed on the plasma membrane and thus easily targetable, it might not be surprising that $\pm 34\%$ of the US Food and Drug Administration (FDA)-approved drugs target GPCRs [16, 17]. By the end of 2017, 134 of the ~800 identified GPCRs were targets of drugs approved in the United States and the European Union, whereas other agents are still in clinical trials (see

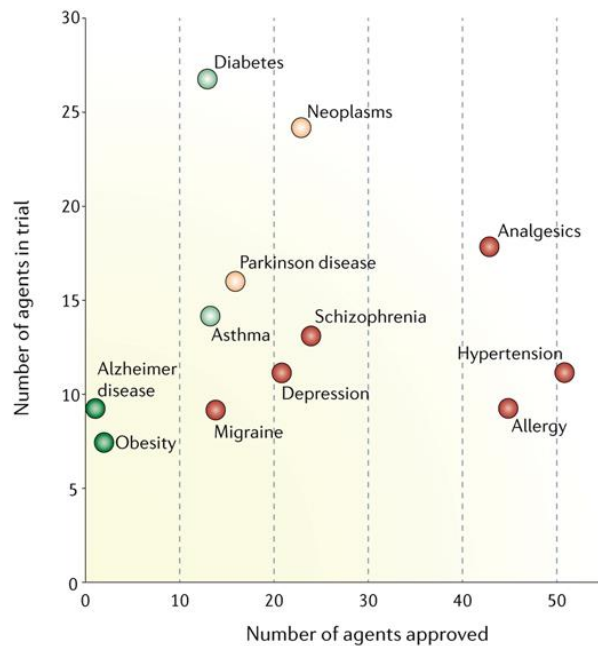


Figure 1.1 Number of approved GPCR-targeted drugs versus number of agents in clinical trials in 2017. A color gradient from red to green is applied to visualize a high ratio of approved over in-trial agents (red) as compared to a low ratio of approved over in-trial agents (green) for distinct diseases. Source: Hauser, 2017 [16].

Figure 1.1 as an example) [16]. In the human brain, antipsychotic drugs mainly act on the dopamine D_2 receptor (D_2R), as this receptor is one of the major neurological targets for the treatment of schizophrenia and Parkinson's disease [18-20]. As depicted in **Figure 1.1**, for schizophrenia more than 20 antipsychotic drugs were available on the drug market in 2017, whereas for Parkinson's disease an equal amount of drugs were approved or in-trial. On the other hand, for diseases such as obesity, which has been associated with activation of the cannabinoid receptor 1 (CB_1) [21], most drugs were in clinical trials.

These drug targets are often first identified and explored in academia. For approximately 40 distinct GPCRs, including the β 2-adrenergic receptor (β 2-AR), D₂R and CB₁, crystal structures in at least one functional state have been determined (**Figure 1.2 b**) [6, 22-24]. Consequently, new insights can be gained concerning structural rearrangements within the GPCR upon agonist or antagonist binding. However, as the drug development process has become more complex, with a higher risk of failure, a huge gap can be observed between the initial identification and its translation to the drug market (**Figure 1.2 a vs e**).

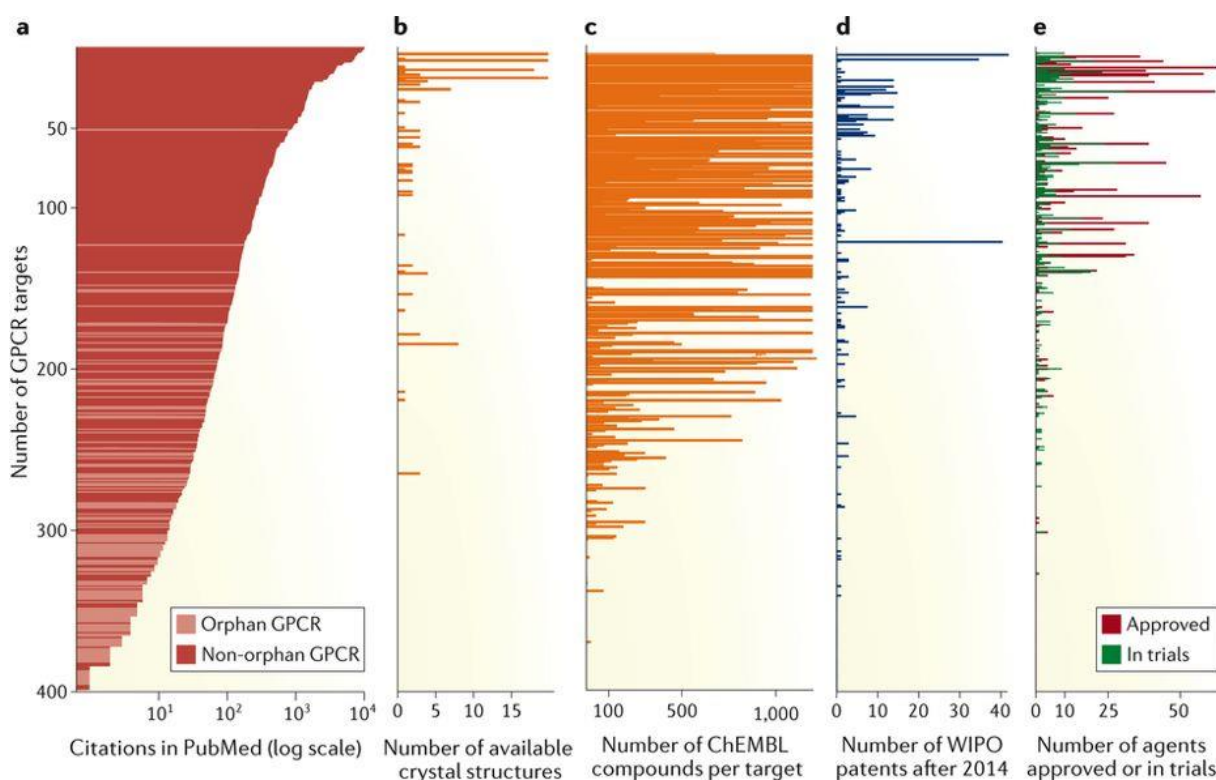


Figure 1.2 Number of GPCR targets that are reported in publications that eventually lead to approved drugs. The number of GPCR targets for which publications in PubMed are reported (**a**), crystal structures in the Protein Data Bank (**b**), ligands in the ChEMBL database (**c**), patents filed by the World Intellectual Property Organization (WIPO) since 2014 (**d**) and drugs approved or in clinical trial (**e**). Source: Hauser *et al.*, 2017 [16].

Nevertheless, as research is evolving at all times, new strategies for the development of novel drug therapies continuously arise. Within this context, this thesis aims at contributing knowledge regarding two particular aspects that are of broad and current interest:

- (i) As of today, pharmaceutical companies mostly focus on targeting a monomeric GPCR as such. However, it has been observed that GPCRs can interact with one another and thereby can potentially be considered as new entities with specific pharmacological, biochemical or functional properties. Consequently, targeting these new entities instead of the monomeric GPCRs could potentially open a new avenue for novel drug therapies. In this thesis, the focus will be on **GPCR-GPCR interactions involving the D₂R (Figure 1.3 A)**.
- (ii) From a drug discovery point of view, a key point of interest is to elucidate the signaling pattern provoked by certain drugs. It has been observed that certain ligands, upon activation of the GPCR, preferentially activate one signaling pathway, while attenuating or even blocking another signaling pathway. This phenomenon is known as ‘functional selectivity’, ‘biased signaling’ or ‘biased agonism’. Hence, exploring this field might result in pathway-selective drugs with abolished or reduced side effects. In this thesis, **biased signaling for CB₁** will be explored (**Figure 1.3 B**).

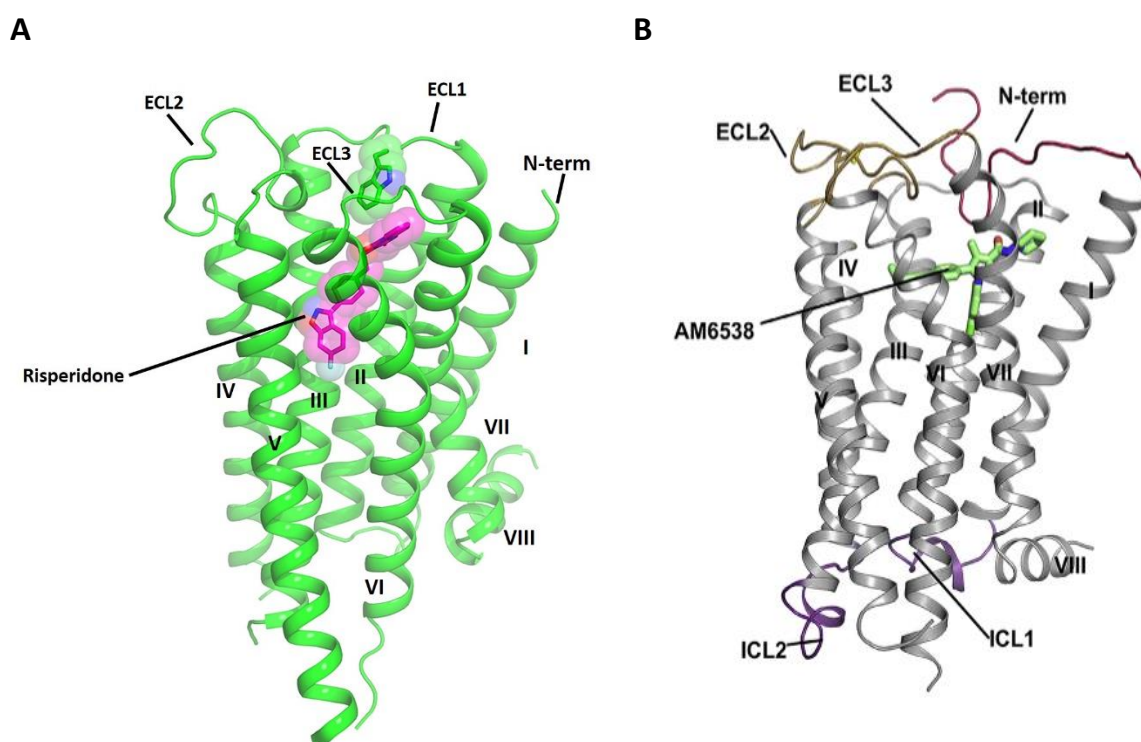


Figure 1.3 Side view of the D₂R (A) and the CB₁ (B) 3D structures. The GPCRs are represented in green and grey cartoon representation, respectively. (A) The D₂R is in complex with the antipsychotic risperidone (Figure adapted from Wang *et al.*, 2018[24]), and (B) the CB₁ is in complex with the AM6538 antagonist (Source: Hua *et al.*, 2016 [25]).

The objective of this thesis was to investigate whether - and how - certain compounds, more specifically dopamine-like ligands in the case of the D₂R or the newest synthetic drugs in the case of CB₁, influenced particular GPCR-mediated interactions within the cell. In other words, we wanted to investigate if it is safe to say: **“whether it is the action of dopamine or dope, is it all about interaction?”**

1.2 Aims and outline of this thesis

In **Part I** of this thesis the focus lies on GPCR-GPCR interactions, also referred to as *dimerization* in the case of two GPCRs interacting with each other or *oligomerization* in the case when multiple GPCRs interact. An introduction to this phenomenon is given in **Chapter 2**, in which the di- or oligomers involving D₂R, as the main GPCR of interest in this part of the thesis, are discussed more into detail.

A straightforward *in vitro* technique to investigate GPCR-GPCR interactions is the protein complementation assay (PCA). This technique is based on the fusion of split fragments of a luminescent or fluorescent protein to the GPCRs of interest. When the GPCRs interact, the split fragments come into close proximity and are able to complement to form a functional luminescent or fluorescent protein. Throughout time, distinct PCAs have been developed and applied for the investigation of these GPCR-GPCR interactions, of which an overview will be given in **Chapter 3**.

In **Chapter 4** several fluorescent and luminescent PCAs are compared and a stepwise guideline to correctly implement these PCAs is provided. One of these PCA techniques, namely the NanoLuc Binary Technology or NanoBiT[®] relies on the split fragments of a bright luminescent protein, NanoLuciferase [26]. This PCA was implemented in **Chapter 5** to investigate homodimerization of the D₂R and to evaluate whether ligand-dependent modulation of the D₂R homodimer could occur.

In the final chapter of Part I (**Chapter 6**), the heterodimer involving D₂R and the metabotropic glutamate receptor 5 (mGluR₅) is the main topic. Bivalent ligands, consisting of a D₂R agonist/antagonist and an mGluR₅ negative allosteric modulator connected by a linker, are tested for their ability to bridge the dimer.

In **Part II** of this thesis the focus lies on the interaction of CB₁ with downstream signaling molecules, i.e. the G protein or β -arrestin2. More specifically, the recruitment of these transducers to CB₁ will be used to evaluate the CB₁ activation by a broad panel of the newest synthetic drugs on the cannabinoid drug market, namely the synthetic cannabinoid receptor agonists (SCRAs).

In **Chapter 7** an overview is given on the rather limited knowledge that has been gathered *so far* on the potential of SCRAs to induce biased signaling at both the cannabinoid receptor CB₁ and CB₂. Moreover, it is discussed how this has been or could be investigated in *in vitro* assays.

In **Chapter 8** we have applied the above-mentioned (**Chapter 5**) NanoBiT[®] assay principle but instead of investigating GPCR-GPCR interactions, we have used this PCA to evaluate the preferred signaling through G α_i protein or β -arrestin2 upon activation of CB₁ by a structurally diverse panel of SCRAs.

In **Chapter 9** we demonstrate the utility of the CB₁- β -arrestin2 NanoBiT[®] assay for the activity profiling of carboxy metabolites of a certain group of SCRAs featuring scaffolds based on L-valine and L-*tert*-leucine. As these metabolites might potentially contribute to the toxicological profile of SCRAs *in vivo*, these *in vitro* activity studies are of paramount importance to help to better understand the adverse effects that have been associated with SCRA use.

Finally, in **Chapter 10** and **11** the future perspectives and final conclusion of the above-mentioned studies are given. A clear overview of the different chapters that will be discussed in this thesis is given in **Table 1.1**.

Table 1.1 Overview of the outline of this thesis

Part I	Chapter 1	–	General introduction
	Chapter 2	–	Focus on the dopamine D ₂ receptor
	Chapter 3	–	Luminescence- and fluorescence-based complementation assays to screen for GPCR oligomerization: current state of the art
	Chapter 4	–	Assessing GPCR dimerization in living cells: comparison of the NanoBiT® assay with related bioluminescence- and fluorescence-based approaches.
	Chapter 5	–	Distinct Dopamine D ₂ receptor antagonists differentially impact D ₂ receptor oligomerization
	Chapter 6	–	Synthesis towards bivalent ligands for the dopamine D ₂ and metabotropic glutamate 5 receptors
Part II	Chapter 7	–	Insights into biased signaling at cannabinoid receptors: synthetic cannabinoid receptor agonists
	Chapter 8	–	Assessment of biased agonism amongst distinct synthetic cannabinoid receptor agonist scaffolds
	Chapter 9	–	Functional evaluation of carboxy metabolites of synthetic cannabinoid receptor agonists featuring scaffolds based on L-valine or L- <i>tert</i> -leucine
	Chapter 10	–	Broader international context, relevance and future perspectives
	Chapter 11	–	Conclusion and summary

References

1. Bianconi, E., et al., *An estimation of the number of cells in the human body*. Annals of human biology, 2013. **40**(6): p. 463-71.
2. Fredriksson, R., et al., *The G-protein-coupled receptors in the human genome form five main families. Phylogenetic analysis, paralogon groups, and fingerprints*. Molecular pharmacology, 2003. **63**(6): p. 1256-72.
3. Bockaert, J. and J.P. Pin, *Molecular tinkering of G protein-coupled receptors: an evolutionary success*. The EMBO journal, 1999. **18**(7): p. 1723-9.
4. Downes, G.B. and N. Gautam, *The G protein subunit gene families*. Genomics, 1999. **62**(3): p. 544-52.
5. Oldham, W.M. and H.E. Hamm, *Heterotrimeric G protein activation by G-protein-coupled receptors*. Nature reviews. Molecular cell biology, 2008. **9**(1): p. 60-71.
6. Weis, W.I. and B.K. Kobilka, *The Molecular Basis of G Protein-Coupled Receptor Activation*. Annual review of biochemistry, 2018. **87**: p. 897-919.
7. Gether, U., *Uncovering molecular mechanisms involved in activation of G protein-coupled receptors*. Endocrine reviews, 2000. **21**(1): p. 90-113.
8. Mahoney, J.P. and R.K. Sunahara, *Mechanistic insights into GPCR-G protein interactions*. Current opinion in structural biology, 2016. **41**: p. 247-254.
9. Hausdorff, W.P., M.G. Caron, and R.J. Lefkowitz, *Turning off the signal: desensitization of beta-adrenergic receptor function*. The FASEB Journal, 1990. **4**(11): p. 2881-9.
10. Kim, K.M., et al., *Differential regulation of the dopamine D2 and D3 receptors by G protein-coupled receptor kinases and beta-arrestins*. Journal of Biological Chemistry, 2001. **276**(40): p. 37409-14.
11. Nakamura, K., R.W. Hipkin, and M. Ascoli, *The Agonist-Induced Phosphorylation of the Rat Follitropin Receptor Maps to the First and Third Intracellular Loops*. Molecular Endocrinology, 1998. **12**(4): p. 580-591.
12. Seibold, A., et al., *Localization of the sites mediating desensitization of the beta(2)-adrenergic receptor by the GRK pathway*. Molecular pharmacology, 2000. **58**(5): p. 1162-73.
13. Tobin, A.B., *G-protein-coupled receptor phosphorylation: where, when and by whom*. British Journal of Pharmacology, 2008. **153** Suppl 1: p. S167-76.
14. Lefkowitz, R.J. and S.K. Shenoy, *Transduction of receptor signals by beta-arrestins*. Science (New York, N.Y.), 2005. **308**(5721): p. 512-7.
15. Ma, L. and G. Pei, *Beta-arrestin signaling and regulation of transcription*. Journal of cell science, 2007. **120**(Pt 2): p. 213-8.
16. Hauser, A.S., et al., *Trends in GPCR drug discovery: new agents, targets and indications*. Nature reviews. Drug discovery, 2017. **16**(12): p. 829-842.
17. Sriram, K. and P.A. Insel, *G Protein-Coupled Receptors as Targets for Approved Drugs: How Many Targets and How Many Drugs?* Molecular pharmacology, 2018. **93**(4): p. 251-258.
18. Fernandez-Duenas, V., S. Ferre, and F. Ciruela, *Adenosine A2A-dopamine D2 receptor heteromers operate striatal function: impact on Parkinson's disease pharmacotherapeutics*. Neural regeneration research, 2018. **13**(2): p. 241-243.
19. Obeso, J.A., et al., *Pathophysiology of the basal ganglia in Parkinson's disease*. Trends in neurosciences, 2000. **23**(10 Suppl): p. S8-19.
20. Taura, J., et al., *Behavioral control by striatal adenosine A2A -dopamine D2 receptor heteromers*. Genes, brain, and behavior, 2018. **17**(4): p. e12432.
21. Engeli, S., *The clinical pharmacology of obesity*. Therapeutic advances in endocrinology and metabolism, 2012. **3**(3): p. 83-4.
22. Krishna Kumar, K., et al., *Structure of a signaling cannabinoid receptor 1-G protein complex*. Cell, 2019. **176**(3): p. 448-458 e12.
23. Masureel, M., et al., *Structural insights into binding specificity, efficacy and bias of a beta2AR partial agonist*. Nature chemical biology, 2018. **14**(11): p. 1059-1066.

24. Wang, S., et al., *Structure of the D2 dopamine receptor bound to the atypical antipsychotic drug risperidone*. Nature, 2018. **555**(7695): p. 269-273.
25. Hua, T., et al., *Crystal Structure of the Human Cannabinoid Receptor CB1*. Cell, 2016. **167**(3): p. 750-762 e14.
26. Dixon, A.S., et al., *NanoLuc Complementation Reporter Optimized for Accurate Measurement of Protein Interactions in Cells*. ACS chemical biology, 2016. **11**(2): p. 400-8.

Part I

Chapter 2:

Focus on the Dopamine receptor

- A role for dopamine D₂ receptor interactions: homo- and heteromerization -

Partly based on

Elise Wouters[‡], Lakshmi Vasudevan[‡], René A.J. Crans, Deepak K Saini and Christophe Stove. Luminescence- and fluorescence-based complementation assays to screen for GPCR oligomerization: current state of the art. *International Journal of Molecular Sciences*. 2019; 20(12), 2958. [‡]These authors contributed equally.

Chapter outline

2.1 GPCR-GPCR interactions: a question still open

2.1.1 What is GPCR homo- or heteromerization?

2.1.2 Why should we target GPCR oligomers?

2.1.3 How can we examine GPCR oligomers?

2.2 Dopamine receptor complexes

2.2.1 Dopamine receptors

2.2.2 Dopamine Homomeric complexes

2.2.3 Dopamine Heteromeric complexes

2.2.4 Ligands of dopaminergic D₂R complexes

2.2.4.1 Bivalent ligands

2.2.4.2 Bitopic ligands

2.2.4.3 Biased ligands

2.1 GPCR-GPCR interactions: a question still open

“The eminent German thinker Arthur Schopenhauer (1788 – 1860) wrote with philosophical clarity that all truth passes through three stages. First, it is ridiculed. Second, it is violently opposed. Third, it is accepted as being self-evident. These observations aptly apply to GPCRs: an understanding of their oligomerization has evoked much passion and continuing investigation.”(Palczewski, 2010)[1]

2.1.1 What is GPCR homo- or heteromerization?

While the traditional view on GPCRs was a ‘one ligand-one monomeric GPCR unit-one signaling protein’ model, an emerging body of evidence shows that GPCRs can form homo- or heterodimeric complexes. Within these complexes, one receptor is defined as a ‘protomer’. Hence, a dimeric complex which consists of a pair of the same protomers is termed a ‘homodimer’, while a ‘heterodimer’ is formed from distinct receptors.

In addition to dimerization, mounting evidence from biochemical techniques has suggested the existence of even higher-order oligomeric complexes or “receptor mosaics”, comprising more than two protomers. Agnati *et al.* (2005) [2, 3] distinguished 3 different types of receptor mosaics:

1. Receptor mosaics Type 1: comprise one type of GPCR (homo-oligomers) or of isoreceptors (i.e., hetero-oligomers formed by diverse subtypes of the same receptor, for example, subtypes of GABA_B or dopamine receptors). For example: the dopamine D₂ receptor (D₂R) oligomeric complexes (D₂R-D₂R-D₂R) [4].
2. Receptor mosaics Type 2: comprise diverse types of GPCRs (hetero-oligomers). The same type or subtypes of GPCRs can be present, but not in direct contact. For example: the adenosine A_{2a} receptor (A_{2a}), D₂R and metabotropic glutamate receptor 5 (mGluR₅) oligomeric complexes (A_{2a}-D₂R-mGluR₅) [5].
3. Receptor mosaics Type 3 or mixed types: comprise diverse types of GPCRs (hetero-oligomers). The same type or subtypes of GPCRs can be present and in contact, forming a Type 1-island within the GPCR assembly. For example: the cannabinoid CB₁ and D₂R oligomeric complexes (CB₁-CB₁-D₂R-D₂R) [6].

Although vibrant research on GPCR homo- and heteromerization dates back as far as the 1970s [7-9], the role and function of these receptor multimer complexes remains a subject of intense debate till this day [10-17]. More than 40 years ago, evidence of negative and positive cooperativity *via* receptor-receptor interactions among receptor dimeric or oligomeric complexes was already reported [7, 8, 18]. In the late 1990s, demonstration of the obligatory heterodimer formation of the GABA_B receptor, a prototypical member of Class C GPCRs, supported the notion that GPCRs may form dimers. As a direct consequence, a burst of studies on GPCR-GPCR interactions was initiated using biochemical, biophysical and functional techniques, assessing various aspects of GPCR-GPCR interactions, including dynamics of assembly and alterations in ligand binding or signaling pathways upon dimerization. Indeed, constant efforts are ever-expanding the number of revealed GPCR-GPCR interactions, as evidenced by the remarkable rise in publications in this field of research, with over 300 reports covering GPCR dimers or oligomers during the last 5 years (**Figure 2.1**).

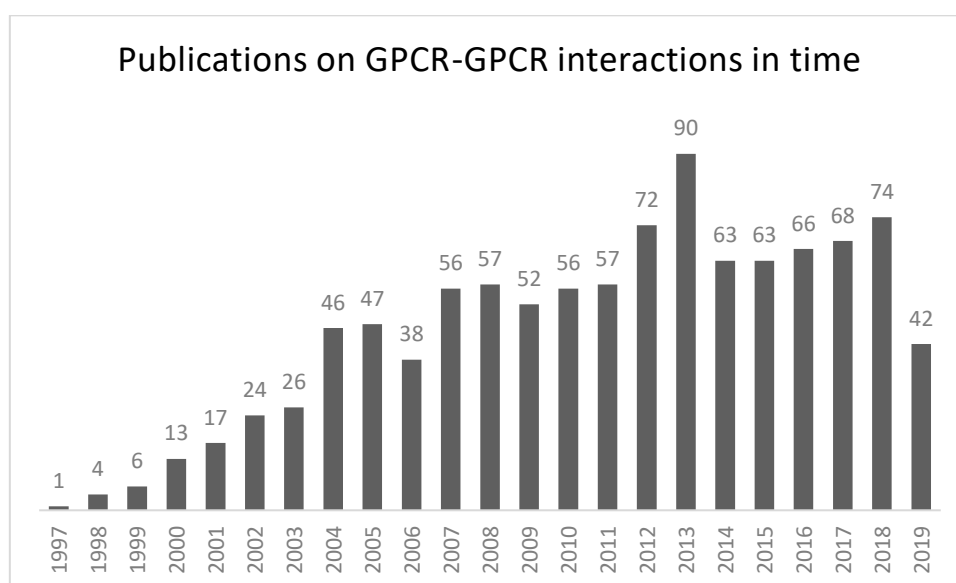


Figure 2.1 A search for the terms “GPCR* AND DIMER*” or “GPCR* AND OLIGOMER*” in the PubMed database (data incomplete for 2019).

Despite the increased interest and efforts, the phenomenon of GPCR-GPCR interactions remains a subject surrounded by healthy skepticism. Much of the uncertainty originates from the fact that techniques were used that suggest GPCR dimerization but do not necessarily prove a direct interaction (discussed more in detail in section **2.1.3**). Despite these limitations, complementary approaches of multiple research groups have provided

support for the existence of GPCR homo- or heteromeric complex formation of members of all GPCR subfamilies.

As a direct consequence, a list of recommendations for the recognition and acceptance of multimeric receptors has been published by *The International Union of Basic and Clinical Pharmacology* [19]. Before the acceptance by the scientific community, at least two criteria of the proposed list should be met: 1) evidence for the physical association in primary (1a) or native (1b) cells; 1a) co-localization of the two protomers composing the heteromer within the same subcellular compartment in the same cell, 1b) documentation of the physical interaction between the two protomers in native tissue, although most techniques, such as energy transfer technologies or transgenic (knock-in) animals expressing physiological levels of recombinant fluorescent-tagged protomers, would only prove close proximity of the protomers of interest in the multimer complex, 2) identification of a characteristic pharmacological property specific to the heteromer, e.g. allosteric modulation between the two binding sites or the identification of a ligand specific for the heteromer, and 3) validation of the *in vivo* heteromer using knockout animals or RNAi technology, so a modified response can be observed when either of the protomers is absent.

In addition to the broadly accepted and aforementioned obligate GPCR dimers observed in Class C receptors, an increasing amount of evidence suggests there is also -transient- dimer formation between Class A GPCRs [20-22]. Conflicting observations both in favor of and against oligomerization have been reviewed by Bouvier & Herbert (2014) [12] and by Lambert and Javitch (2014) [15]. Recent insight in Class A GPCR dimerization has shed light on this debated concept, i.e. a large-scale comparative study of 60 receptors of the Rhodopsin-family revealed that only a small fraction, i.e. 20%, forms dimers [23]. This dimer formation of Class A GPCRs seems to have a clustered distribution and furthermore an overall striking correlation is suggested between receptor organization and size of the GPCR family. A restricted family size as in the case of the small Glutamate family correlates with predominantly dimeric behavior. This also seems to be true for the receptors exhibiting less diversity like the Frizzled GPCRs [23]. Thus, the larger the family size, the less need for alterations in ligand binding or signaling pathways mediated by GPCR dimerization. Besides the fact that Class A GPCRs seem to dimerize to a lesser extent, the dimerization event itself is also much more complicated, i.e. Class A GPCRs often seem to interact at multiple

interfaces, thus causing a broad impact on functionality [24]. This has been noted in the case of muscarinic acetylcholine M₁ or M₂ receptor dimerization, wherein reports have suggested that the sites of contact are transitory and could involve multiple regions of the receptor [25-27]. For D₂R, this transient dimerization phenomenon has been studied in more detail, with a lifetime of 68 ms being assigned to the dimer. This dimer lifetime could be prolonged with a factor of ± 1.5 by agonist addition, indicating a role of the dimer in signaling cascades [28, 29]. Furthermore, also for the D₂R homodimeric complex multiple interfaces have already been proposed [30-34]. Dijkman and colleagues [35] introduced the 'rolling dimer' interface model for the GPCR neurotensin receptor 1 homodimer. This concept unites earlier seemingly conflicting data since multiple dimer conformations could co-exist and interconvert during the dimer lifetime, by rotation of the monomers relative to one another [35].

In general, the phenomenon of oligomerization can exert a significant impact on receptor-ligand binding, downstream signaling, crosstalk, internalization and trafficking. For instance, the interaction of D₂R with dopamine D₃ receptor (D₃R) results in a higher potency of certain antiparkinsonian agents, like pramipexole, compared to their monomers [20]. Furthermore, selective stimulation of D₁R or D₂R or both by the neurotransmitter dopamine triggered co-internalization of the D₁R-D₂R heterodimer [22].

Yet many questions remain partly or completely unanswered, of which the most important one will be to determine the relevance of GPCR oligomerization in healthy and pathological conditions *in vivo*. Thus indeed, GPCR dimerization is still a question open. Luckily, in several interesting cases, studies have been started to address this question.

2.1.2 Why should we target GPCR oligomers?

One might wonder why so many research groups do tremendous efforts to investigate such a complex phenomenon as GPCR dimer- or oligomerization. Since GPCR-GPCR interactions can potentially be considered as new entities with specific pharmacological, biochemical or functional properties, Franco *et al.* (2008) [36], defined the concept of 'dimer fingerprint'. Consequently, it should not be surprising that these dimers have been associated with multiple diseases, e.g. Parkinson's disease (A_{2a}-D₂R heterodimer)[37, 38], pre-eclampsia (angiotensin II type 1 and bradykinin receptor B2 heterodimer complexes) [39],

schizophrenia (D₂R homo- and heterocomplexes) [40], depression (serotonin 1A receptor 5-HT_{1A} and serotonin 7 receptor 5-HT₇ heterocomplexes and galanin receptor type 1 GalR₁, type 2 GalR₂ and 5-HT_{1A} heterocomplexes) [41-43], among others.

The most recognized dopamine-related disorder is Parkinson's disease (PD). This neurodegenerative disorder is characterized by the progressive loss of dopaminergic neurons in the *substantia nigra* of the human brain [44]. This results in a depletion of dopaminergic production, responsible for the specific PD symptoms, such as tremor, rigidity, bradykinesia and postural instability [45]. Dopamine replacement remains the mainstream therapy for attenuation of these symptoms. A metabolic precursor of dopamine, laevodihydroxyphenylalanine (L-DOPA), is able to cross the blood brain barrier and is efficiently converted into dopamine by enzymatic decarboxylation [46], making it the most effective dopamine replacement therapy. Unfortunately, chronic administration of these therapies have been associated with tolerance and increased L-DOPA dosage leads to adverse side-effects, including dyskinesia (abnormal movements), gastrointestinal symptoms, insomnia, hallucinations and even psychosis [47, 48]. As a consequence, research groups have shifted gears and focused on non-dopaminergic targets that play a possible key role in the pathophysiology of PD. Among those, A_{2a} has received a lot of attention. The D₂R and A_{2a} are known to form heterodimeric complexes and are co-expressed in post-synaptic striatopallidal neurons [38, 49-51]. Moreover, it has been demonstrated that activation of A_{2a} results in a decrease in affinity of D₂R agonists for their receptor [37, 52, 53]. Therefore, co-administration of A_{2a} antagonists results in the requirement of a lower dosage of the D₂R agonist L-DOPA, thereby reducing L-DOPA-induced dyskinesia. Since the action of A_{2a} antagonists has been shown to amplify the therapeutic effect, tremendous efforts have been made towards the development of new therapeutics for the treatment of PD symptoms. As a result, new dual-acting chemical entities have been designed to simultaneously target the A_{2a} and D₂R based on indole-piperazine-pyrimidine (IPP) derivatives [54]. Furthermore, these IPP scaffolds have been tested in the *Drosophila* model of PD and showed improvement in movement [54]. These new scaffolds can serve as lead compounds to get insight into structural requirements for new anti-parkinsonian drugs.

Also the pathological mechanisms underlying the development of the neuropsychiatric disorder schizophrenia are not yet fully understood. Different hypothesis, mostly involving

dopaminergic, glutamatergic and serotonergic pathways, have been proposed [55]. For the dopaminergic hypothesis, schizophrenia involves diminished frontal and increased striatal dopaminergic neurotransmission [55-57]. In addition, current hypotheses involve receptor oligomerization as well. As the D₂R is seen as a 'hub receptor', able to interact with many GPCRs among other proteins, several D₂R heteroreceptor complexes have been discovered of which some have been suggested to be involved in the development of schizophrenia. Disturbances in the balance of D₂R homo- and heteroreceptor complexes, including A_{2a}-D₂R, mGluR₅-A_{2a}-D₂R and 5-Hydroxytryptamine 2A (5-HT_{2A})-D₂R heteroreceptor complexes, may contribute to the development of schizophrenia [58]. Furthermore, an increase in D₂R homodimer formation has been seen in post-mortem striatal tissue of schizophrenia patients [59].

Although GPCRs represent the most common target on the drug market due to their remarkable diversity in biological actions, all current clinically available drugs have a GPCR monomeric unit as their target. As in many complex diseases, the single-target drugs for the treatment of schizophrenia and PD turned out to be failures due to their associated side effects. To conclude, targeting specific GPCR dimers could potentially be more efficient and may open new avenues for pharmaceutical companies in their development of novel drug therapies.

2.1.3 How can we examine GPCR oligomers?

Prior to targeting GPCR homo- or heterocomplexes, plenty of studies need to be executed to investigate the 'dimer fingerprint' and unravel specific dimer characteristics on the functional, pharmacological and biochemical level. As noted before, the debate about the functional significance, the extent or even the existence of GPCR dimers or oligomers originates from the implementation of techniques with certain limitations. Actually, several studies lack adequate controls or were only performed in transfected cell systems [60]. In addition, prior to any attempts to investigate levels of GPCR di- or oligomerization, possible changes in ligand binding or receptor signaling and trafficking characteristics, one should keep in mind that the *in vivo* co-localization of the GPCRs of interest is mandatory, and although this might seem obvious, this prerequisite is sometimes missing [61]. The underlying reason is often the lack of appropriate tools for *in vivo* investigation such as

selective receptor antibodies. Nevertheless, distinct techniques might highlight different aspects of GPCR-GPCR interactions and the emergence of a broader pallet of approaches could give rise to a full understanding of these complexes (**Table 2.1**).

The development of complementation- and Resonance Energy Transfer (RET)-based techniques has been of fundamental importance in the discovery and characterization of many GPCR-GPCR interactions. The principle of bioluminescence resonance energy transfer (BRET) and fluorescence resonance energy transfer (FRET) relies on the non-radiative energy transfer from a fluorescent donor protein to an acceptor protein [62]. In case of BRET, the donor protein is an enzyme (e.g. Firefly, *Renilla* or Nanoluciferase) that produces bioluminescence upon the degradation of its substrate (coelenterazine h, furimazine or derivatives). Whereas for FRET, the donor protein encompasses a fluorescent protein (e.g. cyan fluorescent protein (CFP), yellow fluorescent protein (YFP), among others). A similar technique, based on the complementation of one functional fluorescent or luminescent protein, whereby the split parts are fused to the GPCRs of interest, will be discussed more in detail in the section 'Protein complementation assays (PCAs)' in **Chapters 3 & 4**.

Although these approaches have been central in studying the quaternary organization of Class A GPCRs, the application of these techniques in transfected cell systems alone is often considered insufficient to determine the physiological relevance of an interaction. Therefore, these *in vitro* approaches should be combined/complemented with *in vivo* applications. It is likely that in future these techniques will be used more widely in tissue isolated from transgenic animals expressing labeled GPCRs, obtained by for example the CRISPR/Cas9 method. Other *ex vivo* biochemical techniques to further study and complement results observed from previously mentioned methods imply co-immunoprecipitation (co-IP) and proximity ligation assay (PLA). Although both techniques do not require GPCR labeling, they are thoroughly dependent on the specificity of available antibodies.

In addition, crystal structures of GPCRs and structure-based modeling of dimers or oligomers contribute to our understanding regarding receptor interfaces. As GPCRs mostly occur within the plasma membrane, with membranous phospholipids likely greatly contributing to the stability of existing dimers, it is likely that upon detergent solubilization only the most stable dimers will not dissociate [63]. These GPCRs could co-crystallize utilizing the same molecular

contacts upon diffusion in the cell membrane. Indeed, several potential dimer interfaces have been proposed [64-66]. Nevertheless, one should keep in mind that also crystallization artifacts may occur, due to a tendency of solubilized monomers to assemble in a non-physiological manner, such as the head to tail dimers seen in rhodopsin crystals [67]. Whether certain dimer interfaces might be physiologically relevant, could also be investigated with additional complementing techniques, such as cross-linking experiments [4, 30, 68, 69], isolated transmembrane (TM) peptide addition [70] and computational approaches [34, 70-74].

More advanced and accurate molecular techniques are single-molecule tracking or Spatial Intensity Distribution Analysis (SpIDA). Whereas single-molecule imaging can yield information on the spatio-temporal characteristics (e.g. dimer lifetime) [27, 28, 75], SpIDA allows quantification of the monomer-dimer ratio of fluorescently (eGFP)-labeled GPCRs [76-79]. Together with the investigation of possible allosteric modulation of downstream signaling pathways by each individual protomer in the multicomplex, a complete and convincing GPCR-GPCR interaction can be proven.

In some cases, different approaches have had different outcomes for one single GPCR-GPCR interaction. For example, when observed with total internal reflection microscopy (TIRFM) the muscarinic acetylcholine M₂ receptor predominantly existed as monomers but could reversibly form dimers in mice tissue slices [27]. TIRFM uses an evanescent wavelength to selectively illuminate only a thin region in the cell (± 100 nm) which results in a much higher signal-to-noise ratio as compared to conventional confocal microscopy. By contrast, FRET-based approaches reported this receptor as being organized predominantly as tetramers, both in a transfected cell system and in native tissue [80, 81]. Although comparison of these different outcomes would evoke a variety in opinions, one should consider that both expression levels and intrinsic affinity will potentially regulate the extent of interactions via mass-action [60].

Recently, this was confirmed by Walsh *et al.* (2018) [82], who investigated the homo-oligomerization characteristics of three Class A GPCRs (β_2 -adrenergic receptor, CB₁ and opsin) in single proteoliposomes. Using fluorescence microscopy-based approaches and a billion-fold less protein than conventional assays, the quantification of protomer-protomer

interactions revealed that the extent of receptor oligomerization is receptor type specific and, more importantly, sensitive to environmental conditions, including receptor density and membrane curvature.

Table 2.1 Overview of several approaches used to detect GPCR-GPCR interactions.

Technique	Applied in	Examples (Ref.)
Biophysical approaches		
BRET/FRET	<i>in vitro</i>	[80, 81, 83-85]
PCA	<i>in vitro</i>	[4, 86-89]
TR-FRET	<i>ex vivo</i>	[90, 91]
Physiological approaches		
SpIDA	<i>in vitro</i>	[76-79]
Single-Molecule Imaging (TIRFM)	<i>in vitro/ex vivo</i>	[27, 28, 75]
Physical approaches		
Isolated TM addition	<i>in vitro/ex vivo</i>	[33, 70, 92]
Bivalent ligands	<i>In vitro/in vivo</i>	[33, 74, 93-101]
Crystallography		
X-ray crystallography	NA*	[64-66]
Biochemical approaches		
Co-IP	<i>in vitro/ex vivo</i>	[61, 102-104]
PLA	<i>in vitro/ex vivo</i>	[84, 105-107]
Cross-linking experiments	<i>in vitro</i>	[4, 30, 68, 69]
Computational approaches		
Protein-protein docking	NA*	[70, 74]
All-atom MD simulations	NA*	[34, 108]

*NA= not applicable, Abbreviations: BRET/FRET: Bioluminescence or Fluorescence resonance energy transfer, PCA: protein complementation assay, TR-FRET: Time-resolved FRET, SpIDA: Spatial Intensity Distribution Analysis, TIRFM: total internal reflection microscopy, TM: transmembrane peptide, co-IP: co-immunoprecipitation, PLA: proximity ligation assay, MD: molecular dynamics

Although numerous interactions have been unraveled by the implementation of the above-mentioned techniques, we will limit the discussion in the following section only to the homo- and heteromeric complexes formed by D₂R, the main receptor of interest of Part I of this thesis.

2.2 Dopamine receptor complexes

Prior to summarizing recent literature concerning the dopamine homo- and heterodimeric complexes, a short introduction will be given on dopamine receptors as such.

2.2.1 Dopamine receptor

Dopamine (3-hydroxytyramine), a metabolite of the amino acid tyrosine, is the predominant catecholaminergic neurotransmitter in the mammalian brain (**Figure 2.2**). It plays a role in the central nervous system by controlling multiple functions, including locomotor activity, food intake, reward, sleep and learning [109]. In the periphery, dopamine modulates cardiovascular function, hormonal regulation, renal functions and gastrointestinal motility by the enteric dopaminergic neurons, among others. [110, 111]

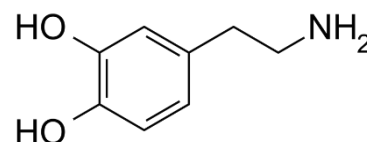


Figure 2.2 Dopamine

Upon release from the presynaptic neuronal terminals, dopamine mediates its effects through activation of members of the G protein-coupled dopamine receptor family. The dopamine receptors are five distinct but closely related GPCRs and can be divided into two major groups: the D₁-like dopamine receptors (D₁R [446 amino acids (aa), protein ID: P21728] and D₅R [477 aa, protein ID: P21918]) and the D₂-like dopamine receptors (D₂R [443 aa, protein ID: P14416], D₃R [400 aa, protein ID: 35462] and D₄R [419 aa, protein ID: P21917]) [112-114]. This classification was primarily based on their capacity to modulate adenylyl cyclase (AC) activity. Typically, D₁-like receptors are positively coupled to AC by the G $\alpha_{s/olf}$ - or G α_q -protein, mediating intracellular cyclic 3,5 adenine-monophosphate (cAMP) accumulation. The D₂-like receptors are negatively coupled to AC by the G $\alpha_{i/o}$ -protein, and as a result decrease the levels of cAMP.

The dopaminergic D₁- and D₂-like systems are expressed throughout different regions of the brain and periphery. In the brain, this broad expression pattern is the most widespread for the D₁R, with higher levels of expression compared to other dopamine receptors. In contrast, D₄R has the lowest expression levels in the brain (**Figure 2.3**). For the D₂R, expression is most abundant in the striatum, nucleus accumbens and the olfactory tubercle but this receptor is also found in the substantia nigra, ventral tegmental area, hypothalamus, cortical areas, septum, amygdala and hippocampus [115, 116].

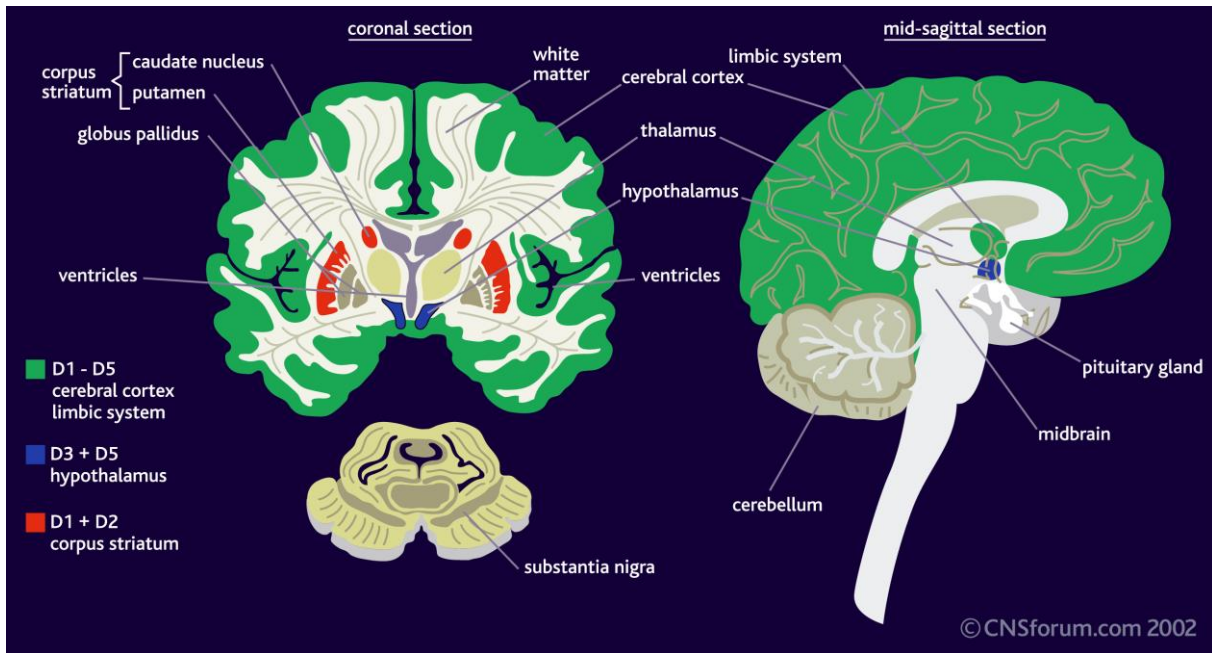


Figure 2.3 Distribution of the expression of dopamine receptors in the human brain. (Source: CNSforum.com)

The D_1 - and D_2 -like receptors do not only differ at the functional level and in expression levels in different brain areas, they also have distinct characteristics in their genetic and structural properties. At the genetic level, considerable homology has been observed within members of the same group. The D_1R and D_5R are 80% identical in their TM regions. The D_3R and D_4R are 75% and 53% homologous with the D_2R , respectively [115]. Furthermore, the D_1R and D_5R encoding genes do not contain any non-coding sequences (or introns), whereas the D_2 -like receptors do, with the most prominent amount of introns (6) present in the gene encoding D_2R (Gingrich and Caron, 1993). Alternative splicing of the D_2R results in two major D_2R variants with distinct physiological, signaling and pharmacological properties, due to the additional presence of a 29 amino acid stretch in the third intracellular loop of the $D_{2L}R$ compared to the $D_{2S}R$. Moreover, $D_{2L}R$ has been shown to be mostly expressed postsynaptically, whereas the $D_{2S}R$ is predominantly expressed presynaptically and is mostly involved in autoreceptor functions [117, 118].

The D_1 - and D_2 -like receptors have different structural properties as well. Whereas all dopamine receptors have an equal amount of amino acids in their amino-terminal domain, the carboxy-terminal domain is seven times longer in D_1 -like receptors compared to the D_2 -like receptors [119]. Interestingly, more insight in the structural differences among the dopamine receptors has been gathered due to the unraveled crystal structures of D_3R [120]

(protein data bank (PDB) ID: 3PBL), D₄R [121] (PDB ID: 5WIU) and most recently, the D₂R [122] (PDB ID: 6CM4) by X-ray diffraction.

Despite all these different characteristics, the dopamine receptors share a common receptor agonist, dopamine. This agonist is involved in a variety of critical functions in the human body, thus it may not be surprising that several pathological conditions have been related to dopaminergic dysfunctions. Hence, dopamine receptors are well-established clinical targets of numerous disorders, such as PD (see section 2.1.2), schizophrenia (see section 2.1.2), bipolar disorder, depression, hypertension, gastroparesis, attention deficit hyperactivity disorder (ADHD), Tourette's syndrome, Huntington's disease, among others [123].

Among other Class A GPCRs, the dopamine receptors have been reported to form dimer- and even higher-order oligomer complexes with distinct signaling profiles, ligand preferences and functions. As the interactions mediated by the D₁R, D₃R, D₄R and D₅R are not within the scope of this thesis, the focus will lie on D₂R-mediated homo- or hetero-oligomeric interactions.

2.2.2 Dopamine Homomeric complexes

The homo- or even higher order oligomerization of D₂R has been extensively studied since its first appearance in literature more than two decennia ago [113]. Both D₂R variants, D_{2S}R and D_{2L}R, have been shown to homodimerize. Details about D₂R homodimerization, as well as aspects involving ligand-dependent modulation of the D_{2L}R homodimer and –oligomer are discussed in detail in **Chapter 5**.

2.2.3 Dopamine Heteromeric complexes

Besides forming heteromers within the dopaminergic family, the D₂R has been shown to interact with many other GPCRs as well. **Table 2.2** gives an overview of GPCR heteromeric complexes that have been reported for the 'hub' D₂R. Several *in vitro*, *ex vivo* or *in vivo* techniques have been applied to characterize these complexes, ranging from *in vitro* biochemical techniques (FRET/BRET; bimolecular fluorescence or luminescence complementation (BiFC/BiLC) assay, bivalent ligands) to *in vivo* behavioral studies. The targeting of the D₂R-mGluR₅ dimer by implementation of bivalent ligands will be discussed more in detail in **Chapter 6**.

Table 2.2 An overview of the homo- and heteromeric dopamine D₂R complexes reported in literature.

Dopamine receptor complexes	Interactions	Examples of applied techniques	<i>in vitro</i> or <i>in vivo</i>	Associated diseases	Selected Ref.
Homodimer	D ₂ R-D ₂ R	Cross-linking, BRET	<i>in vitro</i> , <i>in vivo</i>	Schizophrenia	[4, 30, 31, 59]
Heterodimer	D ₂ R-D ₁ R	co-IP, (FLIM-)FRET, Ca ²⁺ mobilization	<i>in vitro</i> , <i>ex vivo</i>	Possible correlation with schizophrenia	[11, 22, 124-126]
	D ₂ R-D ₃ R	TR-FRET, co-IP	<i>in vitro</i>	Possible correlation with schizophrenia or PD	[91, 127]
	D ₂ R-D ₄ R	BRET, co-IP, PLA, MAPK	<i>in vitro</i> , <i>ex vivo</i>	Possible correlation with ADHD	[128, 129]
	D ₂ R-D ₅ R	FRET, Ca ²⁺ mobilization	<i>in vitro</i>	-	[130, 131]
Heteromeric receptor complexes	Interactions	Examples of applied techniques	<i>in vitro</i> or <i>in vivo</i>	Associated diseases	Selected Ref.
D ₂ R- adenosine receptor	D ₂ R-A _{2a}	BRET, PLA, behavioral studies, bivalent ligands, computational studies,...	<i>in vitro</i> , <i>ex vivo</i> , <i>in vivo</i>	PD	[38, 50, 52-54, 70, 83, 87-89, 132]
	D ₂ R-A _{2a} -mGluR ₅	BiFC + BRET, SRET ² , binding experiments	<i>in vitro</i> , <i>ex vivo</i>	Possible correlation with neuropsychiatric disorders and drug addiction	[5, 133]
	D ₂ R-CB ₁ -A _{2a}	BiFC + BRET	<i>in vitro</i>	-	[134]
D ₂ R-angiotensin II receptor	D ₂ R-AT1	BRET, PLA, cAMP, MAPK	<i>in vitro</i> , <i>ex vivo</i>	-	[84]
D ₂ R-bradykinin receptor	D ₂ R-B2	FLIM-FRET	<i>in vitro</i>	Possible correlation with the regulation of oxidative stress and inflammation	[135, 136]
D ₂ R-cannabinoid	D ₂ R-CB ₁	Co-IP, MAPK	<i>in vitro</i>	-	[6, 137]

receptor	D ₂ R-CB ₁ -A _{2a}	See 'D ₂ R- adenosine receptor' interactions.			[134]
D ₂ R- Cholecystokinin receptor	D ₂ R-CCK2	Ligand binding, PLA	<i>in vitro, ex vivo</i>	-	[138, 139]
D ₂ R-ghrelin receptor	D ₂ R-GHS1	(TR)-FRET confocal microscopy	<i>in vitro/ ex vivo</i> <i>In vivo</i>	Appetite	[140]
D ₂ R- histamine receptor	D ₂ R-H3	BRET, Radioligand binding	<i>in vitro, ex vivo</i>	-	[141]
D ₂ R- metabotropic glutamate receptor	D ₂ R-mGluR ₅	BiFC, BRET, Bivalent ligands	<i>in vitro</i>	-	[5, 74]
	D ₂ R-A _{2a} -mGluR ₅	See 'D ₂ R- adenosine receptor' interactions.			[5, 133]
D ₂ R- neurotensin receptor	D ₂ R-NTS1	Radioligand binding, BRET	<i>in vitro</i>	Schizophrenia and PD	[142, 143]
D ₂ R- oxytocin receptor	D ₂ R-OXT	PLA, MAPK	<i>in vitro, ex vivo, in vivo</i>	Anxiety	[106, 144]
D ₂ R- prosaposin gpr37 receptor	D ₂ R-GPR37	Fluorescence correlation spectroscopy (FCS), co-IP	<i>in vitro</i>	Possible correlation with PD	[145, 146]
D ₂ R- serotonin receptor	D ₂ R-5HT _{2A}	FRET, cAMP, MAPK	<i>in vitro</i>	Possible correlation with schizophrenia	[147-150]
D ₂ R- somatostatin receptor	D ₂ R-SST2	co-IP, FRET	<i>in vitro</i>	-	[151, 152]
	D ₂ R-SST5	FRET, PLA	<i>in vitro, ex vivo</i>	Possibly involved in mood regulation	[153, 154]
D ₂ R- trace amine-associated receptor	D ₂ R-TA1	BRET, cAMP, immunofluorescence, microdialysis	<i>in vitro, ex vivo, in vivo</i>	-	[155]

2.2.4 Ligands of dopaminergic D₂R complexes

Since the discovery of the existence of GPCR dimer complexes, many efforts have been made towards the development of new compounds targeting these receptor complexes. Among these, bivalent, biased and bitopic ligands have gathered interest in the scientific community. Interestingly, these types of compounds have a broad diversity in interaction modes, owing to their spacer length, pharmacophores and interaction site at the GPCR (dimer) of interest (**Figure 2.4**). Each of these ligand types will be discussed below, with special emphasis on their role in investigating or targeting homo- and heterocomplexes.

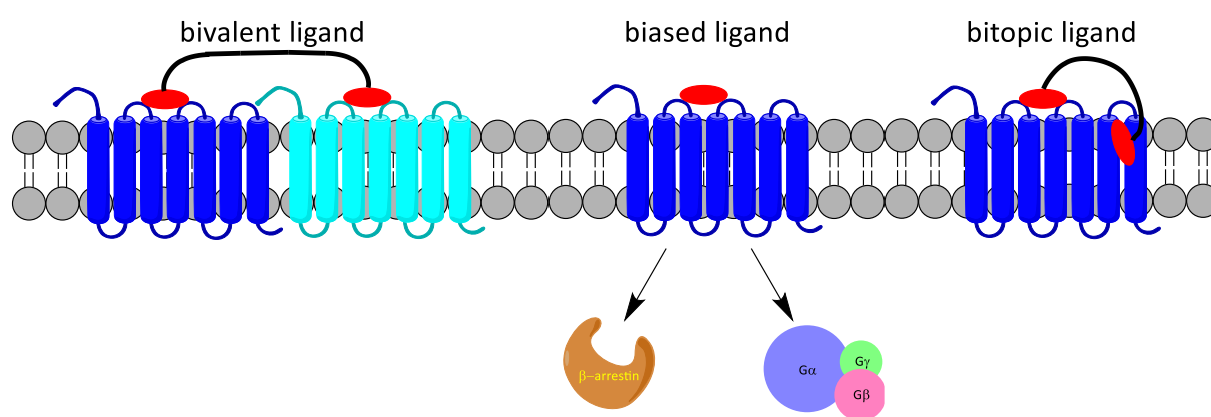


Figure 2.4 Different modes of interactions exerted by bivalent, biased and bitopic ligands.

2.2.4.1 Bivalent ligands

Besides the previously mentioned set of biochemical and biophysical techniques that can be implemented to gain insight into specific dimer characteristics, also chemical tools such as bivalent ligands can be used to evaluate the pharmacology of a given dimer. Bivalent ligands are defined as single entities consisting of two pharmacophores separated by an appropriately designed spacer. These ligands are designed to improve affinity and receptor subtype selectivity upon binding to the two orthosteric sites of a GPCR dimer [156]. When targeting a homodimer, the ligands contain two copies of the same pharmacophore and are referred as 'homobivalent ligands'. On the other hand, 'heterobivalent ligands' consist of two different pharmacophores, in order to target heterodimeric complexes.

The improved affinity that may be observed when implementing bivalent ligands, when compared to the individual binding of their monovalent equivalents, arises from a thermodynamic advantage; i.e. upon binding of the first pharmacophore to the protomer of the dimeric complex, the second pharmacophore is localized in closer vicinity to its respective receptor binding pocket. In this way, the overall entropy of the ligand-receptor complex is significantly lowered, which is inherent to a cooperative binding mode [156-158].

Pioneering work by Portoghesi *et al.* introduced the concept of bivalent ligands for the opioid receptors and further research elaborated on varying distances between subtype dimer complexes (i.e. μ , δ , κ opioid receptors), observed by the synthesis of different spacer lengths [157]. Indeed, the spacer, covalently linked to the two pharmacophores, is a key factor in mediating the simultaneous binding of the two pharmacophores to the orthosteric sites of the homo- or heterodimer.

Varying characteristics specific to the dimer of interest, such as the dimer interface, the structure of the pharmacophores and the geometry of the attachment points need to be taken into account [158]. Using computational models, built from crystal structures of GPCRs of interest, symmetric dimerization interfaces were identified as TM1/2, TM4/5, TM5 and TM5/6 [159, 160]. Notably, the shortest distance between the two orthosteric binding sites is observed between the TM5/6 dimerization interface (± 30 Å) [33, 160].

For the D₂R homodimer, several attempts were made to synthesize bivalent ligands using different pharmacophores. For the generation of homobivalent ligands the following pharmacophores have been used: amidoalkyl substituted phenylpiperazine [161], clozapine (79-fold gain in affinity relative to the original pharmacophore; 1.35 nM vs. 106 nM) [162], 5-hydroxy-2-(dipropylamino) tetralin (5-OH-DPAT) (2.0 nM vs. monovalent 59 nM) [163], apomorphine [164], haloperidol (310 nM vs. 0.81 nM monovalent) [165] and ropirinole [166].

Heterobivalent ligands targeting the D₂R homodimer were synthesized with different pharmacophores as well, including the partial agonists phenylpiperazine (K_i = 3.7 nM) [167], the antagonist 1,4-disubstituted aromatic piperazine (1,4-DAP) (K_i = 22 nM) [74, 100, 168], the agonist 5-hydroxy-2-(dipropylamino)tetralin (5-OH-DPAT) (see **Chapter 6**) [74, 100], the agonist propylaminoindane- and antagonist phenylpiperazine-derivative [169].

A gain in affinity or activity was observed for several of the above-mentioned bivalent ligands compared to their monovalent counterparts. For example, the homobivalent ligand consisting of two dopamine agonist 5-OH-DPAT moieties, showed a 95-fold increased potency and a 30-fold increased affinity, compared to the parent compound [163]. In other examples, such an increase in affinity and potency was not observed [169]. The latter might be explained by (i) a reduction in affinity of the pharmacophore due to impaired interaction of the ligand with the orthosteric site, owing to molecular changes made in the bivalent ligand (incorrect attachment points, spacer length) or (ii) negative cooperation between monomers in the specific dimer complex [170]:

- (i) Molecular changes within the bivalent ligand can have a significant influence on the affinity of bivalent ligands for the receptor complexes. Different binding modes can be adapted by bivalent ligands when varying lengths of spacers are incorporated (**Figure 2.5**) [160]. For instance, bivalent ligands with short spacers may adopt a simultaneous binding to the orthosteric and allosteric site of the same protomer (**Figure 2.5 A**) (also referred to as bitopic ligands, discussed in section 2.2.4.2). Extension of the spacer might result in a binding mode where the bivalent ligand binds to the orthosteric site of one protomer and to a secondary binding site of the second protomer (**Figure 2.5 B**). Last, optimal spacer lengths can lead to the simultaneous binding of both pharmacophores to both orthosteric binding sites of the dimeric complex (**Figure 2.5 C**), emphasizing the importance of spacer length.

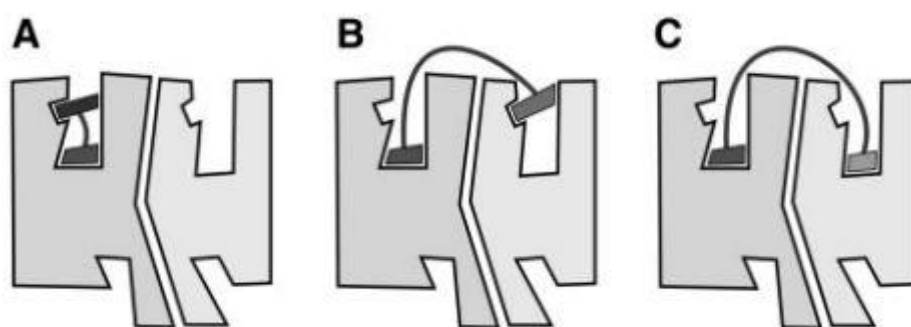


Figure 2.5 Different binding modes of bivalent ligands, reliant on the length of the linker. Figure was adapted from Pérez-Benito, 2018 [160].

- (ii) In experiments involving competitive radioactive ligands, negative or positive cooperativity can be quantified by the Hill slope (n_H). Extrapolated by ligand binding curves, a hill coefficient around 1 indicates an orthosteric ligand binding to a single receptor. Interestingly, for various synthesized bivalent ligands, a hill coefficient higher than 1 was observed [165, 168], indicating positive cooperativity.

Recently, a true D₂R homobivalent ligand with picomolar affinity ($K_D = 21$ pM) was developed by Pulido *et al.* (2018) [33]. Implementing a computational strategy by considering the TM interfaces, the distances between the D₂R orthosteric sites and the binding modes of the pharmacophores, a reduction in the amount of synthesized bivalent ligands could be conducted. Interestingly, in this case distances between the orthosteric sites with distinct interfaces including TM1/2, TM4/5 and TM5/6, were calculated as 36 Å, 43 Å and 33 Å, respectively. The homobivalent ligand consisted of two N-(paminophenethyl)siperone (NAPS) pharmacophores, a succinic acid linker, an oligoethylene glycol (OEG) spacer of 25-atoms and a nitrilotriacetic acid (NTA) scaffold (**Figure 2.6**). Compared to its monovalent counterpart, it showed a 37-fold increase in affinity. Scaffolds, such as NTA, can be introduced to allow an additional attachment of a reporter molecule for imaging studies or even a third pharmacophore to study trimers [171, 172].

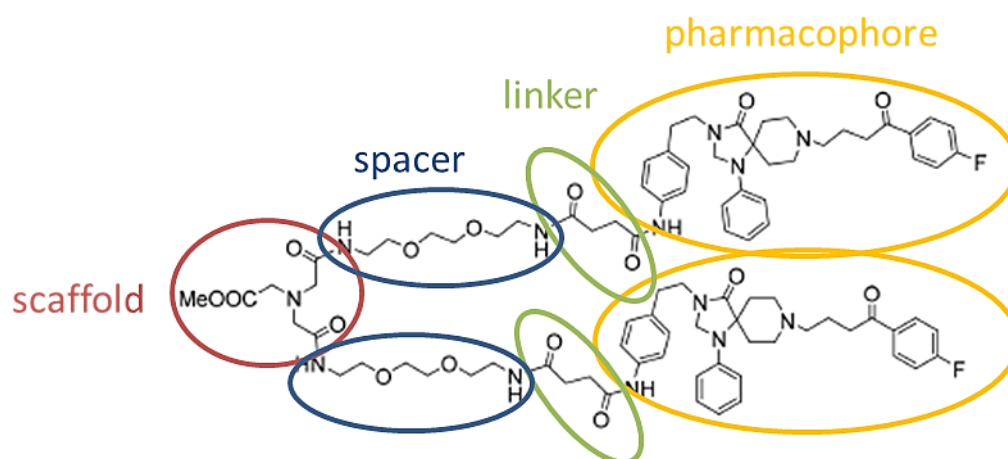


Figure 2.6 A homobivalent ligand for the D₂R homodimer, consisting of the same pharmacophores, a linker, a spacer and scaffold. Figure was adapted from Pulido, 2018 [33].

Although it had previously been observed that the addition of D₂R antagonistic bivalent ligands resulted in a shift in the equilibrium of D₂R homo-oligomerization towards the dimeric state and a reduced mobility of the receptor bivalent ligand complex [75], in this case the bivalent ligand did not significantly alter the dimerization state, as assessed by a fluorescence complementation assay.

A tricky fact associated with the use of bivalent ligands is to prove that both pharmacophores not only bridge the two protomers but also simultaneously interact with both orthosteric sites. To solve this issue, Pulido *et al.* [33] used a transactivator of transcription (TAT) fused to TM6 (TAT-TM6) to disturb the interprotomer interaction in the D₂R homodimer in sheep brain striatal tissue. Interestingly, as a direct consequence of the presence of TAT-TM6, the bivalent ligand showed the same affinity as the monovalent counterpart.

As negative controls often only the monovalent ligands containing capped spacers are investigated. Kühhorn *et al.* [168] incorporated another control for homobivalent ligands targeting the D₂R homodimer, namely 'dummy ligands', in which one of the pharmacophores is replaced by a non-binding structurally related moiety.

Due to their complex and large structure, bivalent ligands are associated with limited oral absorption profiles and impaired crossing of the blood-brain barrier [158]. Their molecular weight is most often significantly higher than that of conventionally marketed oral drugs. Nevertheless, these compounds have proven to be useful pharmacological tools in mice after intracerebroventricular administration, in multiple *in vivo* studies [94, 95, 97, 98]. Therefore, bivalent ligands could set the path to the successful development of novel therapeutic strategies, modulating multiple targets simultaneously with increased efficacy [173].

2.2.4.2 Bitopic ligands

An interesting variation on the strategy of bivalent ligands is the dual-acting ligand, also referred to as 'bitopic ligand'. In contrast to bivalent ligands, bitopic ligands comprise a shorter spacer and subsequently a simultaneous binding to the orthosteric and allosteric site in one (or two) monomeric receptor is favored (**Figure 2.4 & 2.5 B**). Interestingly, bitopic

ligands facilitate the generation of new subtype-selective drugs since allosteric regions are frequently less conserved among receptor family subtypes than the orthosteric binding pocket [161]. Hence, besides targeting homo- and heterodimers using bivalent ligands, significant progress has been made in the precise targeting of pathological processes related to the D₂R with minimal propensity of side effects. Such approaches include ‘biased agonism’ and ‘allosteric-based targeting of the D₂R and heteromers’, which could eventually result in a new generation of dopamine receptor-based therapies for a variety of dopamine-related disorders.

The bitopic ligand SB269,652 is the first allosteric molecule able to distinguish between D₂R monomers and homodimers. SB269,652 exerts the capacity of acting like an orthosteric antagonist for the monomer, while behaving as a negative allosteric modulator across receptor dimers [174]. This ‘dualsteric’ ligand is a new approach to target D₂R dimers and has been suggested to offer better therapeutic advantages regarding motor side-effects and anhedonia, which have been associated with the use of D₂R antagonists.

2.2.4.2.1 Biased bitopic ligands

Neuropsychiatric and neurologic disorders, such as PD, schizophrenia and restless legs syndrome (RLS), are associated with the hypo- or hyper-activation of dopaminergic pathways [175-178]. For the treatment of these D₂R subtype-related disorders, several candidates have been proposed in clinical trials, with varying degrees of success [179-182]. Limited success rates of these candidate lead compounds were often due to the lack in selectivity between D₂-like receptor subtypes or undesired side effects.

Recent investigations have revealed that GPCRs can not only signal through canonical G protein mediated signaling pathways, but also by the activation of the non-canonical, or G protein independent pathway by engaging β -arrestin recruitment. This phenomenon, whereby ligands are able to fully activate one specific signaling pathway while displaying limited activation of other pathways, is also referred to as ‘biased signaling’ or ‘functional selectivity’ (discussed more in detail in **Chapter 7 & 8**).

Hence, in the past few years there has been a growing interest in the synthesis of novel selective D₂R biased agonists targeting the D₂R monomer, since the development of such

compounds would significantly enlarge our knowledge and understanding of which (non-) canonical pathways are responsible for the therapeutic effects and which ones evoke the undesired side effects. Multiple lead compounds mediating selective β -arrestin recruitment to the D₂R have been identified as full or partial biased agonists [89, 183-186]. Nonetheless, to understand the involvement of these β -arrestin biased agonists in schizophrenia or PD, the comparison with highly selective G protein biased agonists is mandatory.

A highly selective D₂R-agonist, sumanirole ((*R*)-5,6-Dihydro-5-(methylamino)-4*H*-imidazo[4,5,1-*ij*]quinolin-2(1*H*)-one (2*Z*)-2-butenedioate), was developed for the treatment of PD and RLS [187-189]. Although it has never received FDA approval for clinical use, it has been used as a scaffold for lead optimization [190, 191]. The first developed G protein biased D₂R full agonist is a bitopic ligand, consisting of (i) a sumanirole-based primary pharmacophore binding to the orthosteric site and (ii) a secondary 2-indolylbutylamide pharmacophore binding to the secondary binding site of D₂R [190]. Subsequent, the authors optimized this lead compound to develop an even more selective G protein biased D₂R agonist, resulting in a 1000-fold G_o protein bias over β -arrestin (G_o protein \gg G_i protein $>$ β -arrestin), investigated by BRET-based recruitment assays [192]. Moreover, *ex vivo* electrophysiological experiments in midbrain dopamine D₂R-expressing neurons confirmed the biased agonism by prolonged G protein coupled inwardly rectifying potassium channel (GIRK) activity, evoked by the perfusion of G_o protein-selective agonists.

References

1. Palczewski, K., *Oligomeric forms of G protein-coupled receptors (GPCRs)*. Trends in biochemical sciences, 2010. **35**(11): p. 595-600.
2. Agnati, L.F., et al., *How proteins come together in the plasma membrane and function in macromolecular assemblies: focus on receptor mosaics*. Journal of molecular neuroscience 2005(2-3): p. 133-54.
3. Agnati, L.F., et al., *Receptor-receptor interactions, receptor mosaics, and basic principles of molecular network organization: possible implications for drug development*. Journal of molecular neuroscience, 2005. **26**(2-3): p. 193-208.
4. Guo, W., et al., *Dopamine D2 receptors form higher order oligomers at physiological expression levels*. The EMBO journal, 2008. **27**(17): p. 2293-304.
5. Cabello, N., et al., *Metabotropic glutamate type 5, dopamine D2 and adenosine A2a receptors form higher-order oligomers in living cells*. Journal of neurochemistry, 2009. **109**(5): p. 1497-507.
6. Kearn, C.S., et al., *Concurrent stimulation of cannabinoid CB1 and dopamine D2 receptors enhances heterodimer formation: a mechanism for receptor cross-talk?* Molecular pharmacology, 2005. **67**(5): p. 1697-704.
7. Limbird, L.E. and R.J. Lefkowitz, *Negative cooperativity among beta-adrenergic receptors in frog erythrocyte membranes*. The Journal of biological chemistry, 1976. **251**(16): p. 5007-14.
8. Limbird, L.E., P.D. Meyts, and R.J. Lefkowitz, *Beta-adrenergic receptors: evidence for negative cooperativity*. Biochemical and biophysical research communications, 1975. **64**(4): p. 1160-8.
9. Salahpour, A., S. Angers, and M. Bouvier, *Functional significance of oligomerization of G-protein-coupled receptors*. Trends in endocrinology and metabolism: TEM, 2000. **11**(5): p. 163-8.
10. Angers, S., et al., *Detection of β 2-adrenergic receptor dimerization in living cells using bioluminescence resonance energy transfer (BRET)*. Proceedings of the national academy of sciences, 2000. **97**(7): p. 3684-3689.
11. Blasiak, E., et al., *Genetic variants of dopamine D2 receptor impact heterodimerization with dopamine D1 receptor*. Pharmacological reports, 2017. **69**(2): p. 235-241.
12. Bouvier, M. and T.E. Hebert, *CrossTalk proposal: Weighing the evidence for Class A GPCR dimers, the evidence favours dimers*. Journal of physiology, 2014. **592**(12): p. 2439-41.
13. Faron-Gorecka, A., et al., *Understanding GPCR dimerization*. Methods in cell biology, 2019. **149**: p. 155-178.
14. Frederick, A.L., et al., *Evidence against dopamine D1/D2 receptor heteromers*. Molecular psychiatry, 2015. **20**(11): p. 1373-85.
15. Lambert, N.A. and J.A. Javitch, *CrossTalk opposing view: Weighing the evidence for class A GPCR dimers, the jury is still out*. The Journal of physiology, 2014. **592**(12): p. 2443–2445.
16. Lan, T.H., et al., *BRET evidence that beta2 adrenergic receptors do not oligomerize in cells*. Scientific reports, 2015. **5**: p. 10166.
17. Szidonya, L., M. Cserzo, and L. Hunyady, *Dimerization and oligomerization of G-protein-coupled receptors: debated structures with established and emerging functions*. Journal of endocrinology, 2008. **196**(3): p. 435-53.
18. Potter, L.T., et al., *Evidence of paired M2 muscarinic receptors*. Molecular pharmacology, 1991. **39**(2): p. 211-21.
19. Pin, J.P., et al., *International Union of Basic and Clinical Pharmacology. LXVII. Recommendations for the recognition and nomenclature of G protein-coupled receptor heteromultimers*. Pharmacological reviews, 2007. **59**(1): p. 5-13.
20. Maggio, R. and M.J. Millan, *Dopamine D2-D3 receptor heteromers: pharmacological properties and therapeutic significance*. Current opinion in pharmacology, 2010. **10**(1): p. 100-7.

21. Petrin, D. and T.E. Hebert, *The functional size of GPCRs - monomers, dimers or tetramers?* Subcellular biochemistry, 2012. **63**: p. 67-81.
22. So, C.H., et al., *D1 and D2 dopamine receptors form heterooligomers and cointernalize after selective activation of either receptor.* Molecular pharmacology, 2005. **68**(3): p. 568-78.
23. Felce, J.H., et al., *Receptor Quaternary Organization Explains G Protein-Coupled Receptor Family Structure.* Cell reports, 2017. **20**(11): p. 2654-2665.
24. Herrick-Davis, K., G. Milligan, and G. Di Giovanni, *G-protein-coupled Receptor Dimers.* 2017: Springer.
25. Hern, J.A., et al., *Formation and dissociation of M1 muscarinic receptor dimers seen by total internal reflection fluorescence imaging of single molecules.* Proceedings of the national academy of sciences of the United States of America, 2010. **107**(6): p. 2693-8.
26. Marsango, S., et al., *Muscarinic receptor oligomerization.* Neuropharmacology, 2017.
27. Nenasheva, T.A., et al., *Abundance, distribution, mobility and oligomeric state of M(2) muscarinic acetylcholine receptors in live cardiac muscle.* Journal of molecular and cellular cardiology, 2013. **57**: p. 129-36.
28. Kasai, R.S., et al., *The Class-A GPCR Dopamine D2 Receptor Forms Transient Dimers Stabilized by Agonists: Detection by Single-Molecule Tracking.* Cell biochemistry and biophysics, 2018. **76**(1-2): p. 29-37.
29. Kasai, R.S. and A. Kusumi, *Single-molecule imaging revealed dynamic GPCR dimerization.* Current opinion in cell biology, 2014. **27**: p. 78-86.
30. Guo, W., L. Shi, and J.A. Javitch, *The fourth transmembrane segment forms the interface of the dopamine D2 receptor homodimer.* The Journal of biological chemistry, 2003. **278**(7): p. 4385-8.
31. Lee, S.P., et al., *D2 dopamine receptor homodimerization is mediated by multiple sites of interaction, including an intermolecular interaction involving transmembrane domain 4.* Biochemistry, 2003. **42**(37): p. 11023-31.
32. Ng, G.Y., et al., *Dopamine D2 receptor dimers and receptor-blocking peptides.* Biochemical and biophysical research communications, 1996. **227**(1): p. 200-4.
33. Pulido, D., et al., *Design of a True Bivalent Ligand with Picomolar Binding Affinity for a G Protein-Coupled Receptor Homodimer.* Journal of medicinal chemistry, 2018. **61**(20): p. 9335-9346.
34. Wouters, E., et al., *Distinct Dopamine D(2) Receptor Antagonists Differentially Impact D(2) Receptor Oligomerization.* International journal of molecular sciences, 2019. **20**(7).
35. Dijkman, P.M., et al., *Dynamic tuneable G protein-coupled receptor monomer-dimer populations.* Nature communications, 2018. **9**(1): p. 1710.
36. Franco, R., et al., *G-protein-coupled receptor heteromers: function and ligand pharmacology.* British journal of pharmacology, 2008. **153** Suppl 1: p. S90-8.
37. Antonelli, T., et al., *Experimental studies and theoretical aspects on A2A/D2 receptor interactions in a model of Parkinson's disease. Relevance for L-dopa induced dyskinesias.* Journal of the neurological sciences, 2006. **248**(1-2): p. 16-22.
38. Fuxe, K., et al., *Adenosine A(2A) receptors, dopamine D(2) receptors and their interactions in Parkinson's disease.* Movement disorders : official journal of the movement disorder society, 2007. **22**(14): p. 1990-2017.
39. AbdAlla, S., et al., *Increased AT(1) receptor heterodimers in preeclampsia mediate enhanced angiotensin II responsiveness.* Nature methods, 2001. **7**(9): p. 1003-9.
40. Seeman, P., *Dopamine D2 receptors as treatment targets in schizophrenia.* Clinical schizophrenia and related psychoses, 2010. **4**(1): p. 56-73.
41. Borroto-Escuela, D.O., A.O. Tarakanov, and K. Fuxe, *FGFR1-5-HT1A Heteroreceptor Complexes: Implications for Understanding and Treating Major Depression.* Trends in neurosciences, 2016. **39**(1): p. 5-15.

42. Millon, C., et al., *Galanin (1-15) enhances the antidepressant effects of the 5-HT_{1A} receptor agonist 8-OH-DPAT: involvement of the raphe-hippocampal 5-HT neuron system*. Brain structure and function, 2016. **221**(9): p. 4491-4504.
43. Renner, U., et al., *Heterodimerization of serotonin receptors 5-HT_{1A} and 5-HT₇ differentially regulates receptor signalling and trafficking*. Journal of cell science, 2012. **125**(Pt 10): p. 2486-99.
44. Obeso, J.A., et al., *Pathophysiology of the basal ganglia in Parkinson's disease*. Trends in neurosciences, 2000. **23**(10 Suppl): p. S8-19.
45. Jankovic, J. and L.G. Aguilar, *Current approaches to the treatment of Parkinson's disease*. Neuropsychiatric disease and treatment, 2008. **4**(4): p. 743-57.
46. Djaldetti, R. and E. Melamed, *New therapies for Parkinson's disease*. Journal of neurology, 2001. **248**(5): p. 357-62.
47. Foster, H.D. and A. Hoffer, *The two faces of L-DOPA: benefits and adverse side effects in the treatment of Encephalitis lethargica, Parkinson's disease, multiple sclerosis and amyotrophic lateral sclerosis*. Medical hypotheses, 2004. **62**(2): p. 177-81.
48. Huot, P., et al., *The pharmacology of L-DOPA-induced dyskinesia in Parkinson's disease*. Pharmacological reviews, 2013. **65**(1): p. 171-222.
49. Ferre, S., *An update on the mechanisms of the psychostimulant effects of caffeine*. Journal of neurochemistry, 2008. **105**(4): p. 1067-79.
50. Fuxe, K., et al., *Adenosine receptor-dopamine receptor interactions in the basal ganglia and their relevance for brain function*. Physiology & behavior, 2007. **92**(1-2): p. 210-7.
51. Tozzi, A., et al., *The distinct role of medium spiny neurons and cholinergic interneurons in the D(2)/A(2)A receptor interaction in the striatum: implications for Parkinson's disease*. The Journal of neuroscience : the official journal of the Society for Neuroscience, 2011. **31**(5): p. 1850-62.
52. Fernandez-Duenas, V., S. Ferre, and F. Ciruela, *Adenosine A_{2A}-dopamine D₂ receptor heteromers operate striatal function: impact on Parkinson's disease pharmacotherapeutics*. Neural regeneration research, 2018. **13**(2): p. 241-243.
53. Taura, J., et al., *Behavioral control by striatal adenosine A_{2A} -dopamine D₂ receptor heteromers*. Genes, brain, and behavior, 2018. **17**(4): p. e12432.
54. Shao, Y.M., et al., *Discovery of indolylpiperazinylpyrimidines with dual-target profiles at adenosine A_{2A} and dopamine D₂ receptors for Parkinson's disease treatment*. PloS one, 2018. **13**(1): p. e0188212.
55. Stepnicki, P., M. Kondej, and A.A. Kaczor, *Current Concepts and Treatments of Schizophrenia*. Molecules (Basel, Switzerland), 2018. **23**(8).
56. Davis, K.L., et al., *Dopamine in schizophrenia: a review and reconceptualization*. The American journal of psychiatry, 1991. **148**(11): p. 1474-86.
57. Slifstein, M., et al., *Deficits in prefrontal cortical and extrastriatal dopamine release in schizophrenia: a positron emission tomographic functional magnetic resonance imaging study*. JAMA psychiatry, 2015. **72**(4): p. 316-24.
58. Borroto-Escuela, D.O., et al., *Multiple D₂ heteroreceptor complexes: new targets for treatment of schizophrenia*. Therapeutic advances in psychopharmacology, 2016. **6**(2): p. 77-94.
59. Wang, M., et al., *Schizophrenia, amphetamine-induced sensitized state and acute amphetamine exposure all show a common alteration: increased dopamine D₂ receptor dimerization*. Molecular brain, 2010. **3**: p. 25.
60. Milligan, G., R.J. Ward, and S. Marsango, *GPCR homo-oligomerization*. Current opinion in cell biology, 2018. **57**: p. 40-47.
61. Massotte, D., *In vivo opioid receptor heteromerization: where do we stand?* British journal of pharmacology, 2015. **172**(2): p. 420-34.
62. Ciruela, F., J.P. Vilardaga, and V. Fernandez-Duenas, *Lighting up multiprotein complexes: lessons from GPCR oligomerization*. Trends in biotechnology, 2010. **28**(8): p. 407-15.

63. Congreve, M. and F. Marshall, *The impact of GPCR structures on pharmacology and structure-based drug design*. British journal of pharmacology, 2010. **159**(5): p. 986-96.
64. Huang, J., et al., *Crystal structure of oligomeric beta1-adrenergic G protein-coupled receptors in ligand-free basal state*. Nature structural & molecular biology, 2013. **20**(4): p. 419-25.
65. Lodowski, D.T., et al., *Reprint of "Crystal packing analysis of Rhodopsin crystals" [J. Struct. Biol. 158 (2007) 455-462]*. Journal of structural biology, 2007. **159**(2): p. 253-60.
66. Wu, B., et al., *Structures of the CXCR4 chemokine GPCR with small-molecule and cyclic peptide antagonists*. Science (New York, N.Y.), 2010. **330**(6007): p. 1066-71.
67. Palczewski, K., et al., *Crystal structure of rhodopsin: A G protein-coupled receptor*. Science (New York, N.Y.), 2000. **289**(5480): p. 739-45.
68. Guo, W., et al., *Crosstalk in G protein-coupled receptors: changes at the transmembrane homodimer interface determine activation*. Proceedings of the national academy of sciences of the United States of America, 2005. **102**(48): p. 17495-500.
69. Xue, L., et al., *Major ligand-induced rearrangement of the heptahelical domain interface in a GPCR dimer*. Nature chemical biology, 2015. **11**(2): p. 134-40.
70. Borroto-Escuela, D.O., et al., *Mapping the Interface of a GPCR Dimer: A Structural Model of the A2A Adenosine and D2 Dopamine Receptor Heteromer*. Frontiers in pharmacology, 2018. **9**: p. 829.
71. Baltoumas, F.A., M.C. Theodoropoulou, and S.J. Hamodrakas, *Molecular dynamics simulations and structure-based network analysis reveal structural and functional aspects of G-protein coupled receptor dimer interactions*. Journal of computer-aided molecular design, 2016. **30**(6): p. 489-512.
72. Johnston, J.M. and M. Filizola, *Differential stability of the crystallographic interfaces of mu- and kappa-opioid receptors*. PloS one, 2014. **9**(2): p. e90694.
73. Kaczor, A.A., M. Jorg, and B. Capuano, *The dopamine D2 receptor dimer and its interaction with homobivalent antagonists: homology modeling, docking and molecular dynamics*. Journal of molecular modeling, 2016. **22**(9): p. 203.
74. Qian, M., et al., *Synthesis toward Bivalent Ligands for the Dopamine D2 and Metabotropic Glutamate 5 Receptors*. Journal of medicinal chemistry, 2018. **61**(18): p. 8212-8225.
75. Tabor, A., et al., *Visualization and ligand-induced modulation of dopamine receptor dimerization at the single molecule level*. Scientific reports, 2016. **6**: p. 33233.
76. Marsango, S., et al., *A Molecular Basis for Selective Antagonist Destabilization of Dopamine D3 Receptor Quaternary Organization*. Scientific reports, 2017. **7**(1): p. 2134.
77. Pediani, J.D., et al., *Dynamic Regulation of Quaternary Organization of the M1 Muscarinic Receptor by Subtype-selective Antagonist Drugs*. The Journal of biological chemistry, 2016. **291**(25): p. 13132-46.
78. Ward, R.J., et al., *Regulation of oligomeric organization of the serotonin 5-hydroxytryptamine 2C (5-HT2C) receptor observed by spatial intensity distribution analysis*. The Journal of biological chemistry, 2015. **290**(20): p. 12844-57.
79. Pediani, J.D., et al., *Spatial Intensity Distribution Analysis: Studies of G Protein-Coupled Receptor Oligomerisation*. Trends in pharmacological sciences, 2018. **39**(2): p. 175-186.
80. Pisterzi, L.F., et al., *Oligomeric size of the m2 muscarinic receptor in live cells as determined by quantitative fluorescence resonance energy transfer*. The Journal of biological chemistry, 2010. **285**(22): p. 16723-38.
81. Shivnaraine, R.V., et al., *Single-Molecule Analysis of the Supramolecular Organization of the M2 Muscarinic Receptor and the Galphai1 Protein*. Journal of the American chemical society, 2016. **138**(36): p. 11583-98.
82. Walsh, S.M., et al., *Single Proteoliposome High-Content Analysis Reveals Differences in the Homo-Oligomerization of GPCRs*. Biophysical journal, 2018. **115**(2): p. 300-312.
83. Canals, M., et al., *Adenosine A2A-dopamine D2 receptor-receptor heteromerization: qualitative and quantitative assessment by fluorescence and bioluminescence energy transfer*. The Journal of biological chemistry, 2003. **278**(47): p. 46741-9.

84. Martinez-Pinilla, E., et al., *Dopamine D2 and angiotensin II type 1 receptors form functional heteromers in rat striatum*. Biochemical pharmacology, 2015. **96**(2): p. 131-42.
85. Mazurkiewicz, J.E., et al., *Single-molecule analyses of fully functional fluorescent protein-tagged follitropin receptor reveal homodimerization and specific heterodimerization with lutropin receptor*. Biology of reproduction, 2015. **92**(4): p. 100.
86. Armando, S., et al., *The chemokine CXCR4 and CC2 receptors form homo- and heterooligomers that can engage their signaling G-protein effectors and betaarrestin*. The FASEB journal, 2014. **28**(10): p. 4509-23.
87. Bonaventura, J., et al., *Allosteric interactions between agonists and antagonists within the adenosine A2A receptor-dopamine D2 receptor heterotetramer*. Proceedings of the national academy of sciences of the United States of America, 2015. **112**(27): p. E3609-18.
88. Casado-Anguera, V., et al., *Evidence for the heterotetrameric structure of the adenosine A2A-dopamine D2 receptor complex*. Biochemical society transactions, 2016. **44**(2): p. 595-600.
89. Sahlholm, K., et al., *Antipsychotic-Like Efficacy of Dopamine D2 Receptor-Biased Ligands is Dependent on Adenosine A2A Receptor Expression*. Molecular neurobiology, 2018. **55**(6): p. 4952-4958.
90. Fernandez-Duenas, V., et al., *Untangling dopamine-adenosine receptor-receptor assembly in experimental parkinsonism in rats*. Disease models & mechanisms, 2015. **8**(1): p. 57-63.
91. Pou, C., et al., *Functional homomers and heteromers of dopamine D2L and D3 receptors co-exist at the cell surface*. The Journal of biological chemistry, 2012. **287**(12): p. 8864-78.
92. Hebert, T.E., et al., *A peptide derived from a beta2-adrenergic receptor transmembrane domain inhibits both receptor dimerization and activation*. The Journal of biological chemistry, 1996. **271**(27): p. 16384-92.
93. Ansonoff, M.A., P.S. Portoghese, and J.E. Pintar, *Consequences of opioid receptor mutation on actions of univalent and bivalent kappa and delta ligands*. Psychopharmacology, 2010. **210**(2): p. 161-8.
94. Cataldo, G., et al., *Bivalent ligand MCC22 potently attenuates nociception in a murine model of sickle cell disease*. Pain, 2018. **159**(7): p. 1382-1391.
95. Chen, J., et al., *Multiplexed Targeting of Barrett's Neoplasia with a Heterobivalent Ligand: Imaging Study on Mouse Xenograft in Vivo and Human Specimens ex Vivo*. Journal of medicinal chemistry, 2018. **61**(12): p. 5323-5331.
96. Karamitri, A., et al., *O-linked melatonin dimers as bivalent ligands targeting dimeric melatonin receptors*. Bioorganic chemistry, 2019. **85**: p. 349-356.
97. Lensing, C.J., et al., *A Direct in Vivo Comparison of the Melanocortin Monovalent Agonist Ac-His-DPhe-Arg-Trp-NH₂ versus the Bivalent Agonist Ac-His-DPhe-Arg-Trp-PEDG20-His-DPhe-Arg-Trp-NH₂: A Bivalent Advantage*. ACS chemical neuroscience, 2017. **8**(6): p. 1262-1278.
98. Lensing, C.J., et al., *An in Vitro and in Vivo Investigation of Bivalent Ligands That Display Preferential Binding and Functional Activity for Different Melanocortin Receptor Homodimers*. Journal of medicinal chemistry, 2016. **59**(7): p. 3112-28.
99. Mathews, J.L., et al., *In vivo characterization of (-)(-)MCL-144 and (+)(-)MCL-193: isomeric, bivalent ligands with mu/kappa agonist properties*. Neurochemical research, 2008. **33**(10): p. 2142-50.
100. Qian, M.C., et al., *Design, Synthesis, and Biological Evaluation of Bivalent Ligands Targeting Dopamine D-2-Like Receptors and the Opioid Receptor*. Medicinal chemistry communications, 2018. **13**(9): p. 944-956.
101. Tanaka, T., et al., *Bivalent ligands of CXCR4 with rigid linkers for elucidation of the dimerization state in cells*. Journal of the American chemical society, 2010. **132**(45): p. 15899-901.
102. Berg, K.A., et al., *Allosteric interactions between delta and kappa opioid receptors in peripheral sensory neurons*. Molecular pharmacology, 2012. **81**(2): p. 264-72.
103. Erbs, E., et al., *A mu-delta opioid receptor brain atlas reveals neuronal co-occurrence in subcortical networks*. Brain structure & function, 2015. **220**(2): p. 677-702.

104. Maurice, P., et al., *Molecular organization and dynamics of the melatonin MT(1) receptor/RGS20/G(i) protein complex reveal asymmetry of receptor dimers for RGS and G(i) coupling*. The EMBO journal, 2010. **29**(21): p. 3646-59.
105. Borroto-Escuela, D.O., et al., *Evidence for the existence of FGFR1-5-HT1A heteroreceptor complexes in the midbrain raphe 5-HT system*. Biochemical and biophysical research communications, 2015. **456**(1): p. 489-93.
106. Romero-Fernandez, W., et al., *Evidence for the existence of dopamine D2-oxytocin receptor heteromers in the ventral and dorsal striatum with facilitatory receptor-receptor interactions*. Molecular psychiatry, 2013. **18**(8): p. 849-50.
107. Trifilieff, P., et al., *Detection of antigen interactions ex vivo by proximity ligation assay: endogenous dopamine D2-adenosine A2A receptor complexes in the striatum*. BioTechniques, 2011. **51**(2): p. 111-8.
108. Kaczor, A.A., M. Jorg, and B. Capuano, *The dopamine D-2 receptor dimer and its interaction with homobivalent antagonists: homology modeling, docking and molecular dynamics*. Journal of molecular modeling, 2016. **22**(9).
109. Iversen, S.D. and L.L. Iversen, *Dopamine: 50 years in perspective*. Trends in neurosciences, 2007. **30**(5): p. 188-93.
110. Benarroch, E.E., *Enteric nervous system: functional organization and neurologic implications*. Neurology, 2007. **69**(20): p. 1953-7.
111. Li, Z.S., et al., *Enteric dopaminergic neurons: definition, developmental lineage, and effects of extrinsic denervation*. The Journal of neuroscience : the official journal of the Society for Neuroscience, 2004. **24**(6): p. 1330-9.
112. Andersen, P.H., et al., *Dopamine receptor subtypes: beyond the D1/D2 classification*. Trends in pharmacological sciences, 1990. **11**(6): p. 231-6.
113. Seeman, P. and H.H. Van Tol, *Dopamine receptor pharmacology*. Trends in pharmacological sciences, 1994. **15**(7): p. 264-70.
114. Sibley, D.R. and F.J. Monsma, Jr., *Molecular biology of dopamine receptors*. Trends in pharmacological sciences, 1992. **13**(2): p. 61-9.
115. Beaulieu, J.M. and R.R. Gainetdinov, *The physiology, signaling, and pharmacology of dopamine receptors*. Pharmacological reviews, 2011. **63**(1): p. 182-217.
116. Missale, C., et al., *Dopamine receptors: from structure to function*. Physiological reviews, 1998. **78**(1): p. 189-225.
117. De Mei, C., et al., *Getting specialized: presynaptic and postsynaptic dopamine D2 receptors*. Current opinion in pharmacology, 2009. **9**(1): p. 53-8.
118. Usiello, A., et al., *Distinct functions of the two isoforms of dopamine D2 receptors*. Nature, 2000. **408**(6809): p. 199-203.
119. Gingrich, J.A. and M.G. Caron, *Recent advances in the molecular biology of dopamine receptors*. Annual review of neuroscience, 1993. **16**: p. 299-321.
120. Chien, E.Y., et al., *Structure of the human dopamine D3 receptor in complex with a D2/D3 selective antagonist*. Science (New York, N.Y.), 2010. **330**(6007): p. 1091-5.
121. Wang, S., et al., *D4 dopamine receptor high-resolution structures enable the discovery of selective agonists*. Science (New York, N.Y.), 2017. **358**(6361): p. 381-386.
122. Wang, S., et al., *Structure of the D2 dopamine receptor bound to the atypical antipsychotic drug risperidone*. Nature, 2018. **555**(7695): p. 269-273.
123. Beaulieu, J.M., S. Espinoza, and R.R. Gainetdinov, *Dopamine receptors - IUPHAR Review 13*. British journal of pharmacology, 2015. **172**(1): p. 1-23.
124. Lee, S.P., et al., *Dopamine D1 and D2 receptor Co-activation generates a novel phospholipase C-mediated calcium signal*. The Journal of biological chemistry, 2004. **279**(34): p. 35671-8.
125. O'Dowd, B.F., et al., *Dopamine receptor oligomerization visualized in living cells*. The Journal of biological chemistry, 2005. **280**(44): p. 37225-35.

126. Rashid, A.J., et al., *D1-D2 dopamine receptor heterooligomers with unique pharmacology are coupled to rapid activation of Gq/11 in the striatum*. Proceedings of the national academy of sciences of the United States of America, 2007. **104**(2): p. 654-9.
127. Scarselli, M., et al., *D2/D3 dopamine receptor heterodimers exhibit unique functional properties*. The Journal of biological chemistry, 2001. **276**(32): p. 30308-14.
128. Borroto-Escuela, D.O., et al., *Dopamine D2 and D4 receptor heteromerization and its allosteric receptor-receptor interactions*. Biochemical and biophysical research communications, 2011. **404**(4): p. 928-34.
129. Gonzalez, S., et al., *Dopamine D4 receptor, but not the ADHD-associated D4.7 variant, forms functional heteromers with the dopamine D2S receptor in the brain*. Molecular psychiatry, 2012. **17**(6): p. 650-62.
130. O'Dowd, B.F., et al., *D5 dopamine receptor carboxyl tail involved in D5-D2 heteromer formation*. Biochemical and biophysical research communications, 2013. **431**(3): p. 586-9.
131. So, C.H., et al., *Calcium signaling by dopamine D5 receptor and D5-D2 receptor heterooligomers occurs by a mechanism distinct from that for dopamine D1-D2 receptor heterooligomers*. Molecular pharmacology, 2009. **75**(4): p. 843-54.
132. Soriano, A., et al., *Adenosine A2A receptor-antagonist/dopamine D2 receptor-agonist bivalent ligands as pharmacological tools to detect A2A-D2 receptor heteromers*. Journal of medicinal chemistry, 2009. **52**(18): p. 5590-602.
133. Popoli, P., et al., *The selective mGlu(5) receptor agonist CHPG inhibits quinpirole-induced turning in 6-hydroxydopamine-lesioned rats and modulates the binding characteristics of dopamine D(2) receptors in the rat striatum: interactions with adenosine A(2a) receptors*. Neuropsychopharmacology, 2001. **25**(4): p. 505-13.
134. Navarro, G., et al., *Detection of heteromers formed by cannabinoid CB1, dopamine D2, and adenosine A2A G-protein-coupled receptors by combining bimolecular fluorescence complementation and bioluminescence energy transfer*. TheScientificWorldJournal, 2008. **8**: p. 1088-97.
135. Niewiarowska-Sendo, A., A. Kozik, and I. Guevara-Lora, *Influence of bradykinin B2 receptor and dopamine D2 receptor on the oxidative stress, inflammatory response, and apoptotic process in human endothelial cells*. PloS one, 2018. **13**(11): p. e0206443.
136. Niewiarowska-Sendo, A., et al., *Bradykinin B2 and dopamine D2 receptors form a functional dimer*. Biochimica et biophysica acta. Molecular cell research, 2017. **1864**(10): p. 1855-1866.
137. Jarrahian, A., V.J. Watts, and E.L. Barker, *D2 dopamine receptors modulate Galpha-subunit coupling of the CB1 cannabinoid receptor*. The Journal of pharmacology and experimental therapeutics, 2004. **308**(3): p. 880-6.
138. Borroto-Escuela, D.O., et al., *G protein-coupled receptor heterodimerization in the brain*. Methods in enzymology, 2013. **521**: p. 281-94.
139. Dasgupta, S., et al., *Regulation of dopamine D2 receptor affinity by cholecystokinin octapeptide in fibroblast cells cotransfected with human CCKB and D2L receptor cDNAs*. Brain research. Molecular brain research, 1996. **36**(2): p. 292-9.
140. Kern, A., et al., *Apo-ghrelin receptor forms heteromers with DRD2 in hypothalamic neurons and is essential for anorexigenic effects of DRD2 agonism*. Neuron, 2012. **73**(2): p. 317-32.
141. Ferrada, C., et al., *Interactions between histamine H3 and dopamine D2 receptors and the implications for striatal function*. Neuropharmacology, 2008. **55**(2): p. 190-7.
142. Borroto-Escuela, D.O., et al., *Dopamine D2 receptor signaling dynamics of dopamine D2-neurotensin 1 receptor heteromers*. Biochemical and biophysical research communications, 2013. **435**(1): p. 140-6.
143. Koschitzky, S., N. Tschammer, and P. Gmeiner, *Cross-receptor interactions between dopamine D2L and neurotensin NTS1 receptors modulate binding affinities of dopaminergics*. ACS chemical neuroscience, 2011. **2**(6): p. 308-16.
144. de la Mora, M.P., et al., *Signaling in dopamine D2 receptor-oxytocin receptor heterocomplexes and its relevance for the anxiolytic effects of dopamine and oxytocin*

- interactions in the amygdala of the rat.* Biochimica et biophysica acta, 2016. **1862**(11): p. 2075-2085.
145. Dunham, J.H., et al., *GPR37 surface expression enhancement via N-terminal truncation or protein-protein interactions.* Biochemistry, 2009. **48**(43): p. 10286-97.
146. Hertz, E., et al., *GPR37 and GPR37L1 differently interact with dopamine 2 receptors in live cells.* Neuropharmacology, 2018.
147. Albizu, L., et al., *Functional crosstalk and heteromerization of serotonin 5-HT_{2A} and dopamine D₂ receptors.* Neuropharmacology, 2011. **61**(4): p. 770-7.
148. Borroto-Escuela, D.O., et al., *Hallucinogenic 5-HT_{2A} agonists LSD and DOI enhance dopamine D_{2R} protomer recognition and signaling of D₂-5-HT_{2A} heteroreceptor complexes.* Biochemical and biophysical research communications, 2014. **443**(1): p. 278-84.
149. Lukasiewicz, S., et al., *Dopamine D₂ and serotonin 5-HT_{1A} receptor interaction in the context of the effects of antipsychotics - in vitro studies.* Journal of neurochemistry, 2016. **137**(4): p. 549-60.
150. Lukasiewicz, S., et al., *Hetero-dimerization of serotonin 5-HT_{2A} and dopamine D₂ receptors.* Biochimica et biophysica acta, 2010. **1803**(12): p. 1347-58.
151. Baragli, A., et al., *Heterooligomerization of human dopamine receptor 2 and somatostatin receptor 2 Co-immunoprecipitation and fluorescence resonance energy transfer analysis.* Cellular signalling, 2007. **19**(11): p. 2304-16.
152. Rocheville, M., et al., *Receptors for dopamine and somatostatin: formation of hetero-oligomers with enhanced functional activity.* Science (New York, N.Y.), 2000. **288**(5463): p. 154-7.
153. Szafran, K., et al., *Antidepressant drugs promote the heterodimerization of the dopamine D₂ and somatostatin Sst5 receptors--fluorescence in vitro studies.* Pharmacological reports, 2012. **64**(5): p. 1253-8.
154. Szafran-Pilch, K., et al., *Antidepressants promote formation of heterocomplexes of dopamine D₂ and somatostatin subtype 5 receptors in the mouse striatum.* Brain research bulletin, 2017. **135**: p. 92-97.
155. Espinoza, S., et al., *Functional interaction between trace amine-associated receptor 1 and dopamine D₂ receptor.* Molecular pharmacology, 2011. **80**(3): p. 416-25.
156. Carli, M., et al., *Dopamine D₂ Receptors Dimers: How can we Pharmacologically Target Them?* Current neuropharmacology, 2018. **16**(2): p. 222-230.
157. Portoghese, P.S., *Bivalent ligands and the message-address concept in the design of selective opioid receptor antagonists.* Trends in pharmacological sciences, 1989. **10**(6): p. 230-5.
158. Shonberg, J., P.J. Scammells, and B. Capuano, *Design strategies for bivalent ligands targeting GPCRs.* ChemMedChem, 2011. **6**(6): p. 963-74.
159. Cordomi, A., et al., *Structures for G-Protein-Coupled Receptor Tetramers in Complex with G Proteins.* Trends in biochemical sciences, 2015. **40**(10): p. 548-551.
160. Perez-Benito, L., et al., *The size matters? A computational tool to design bivalent ligands.* Bioinformatics (Oxford, England), 2018. **34**(22): p. 3857-3863.
161. Huber, D., et al., *Bivalent molecular probes for dopamine D₂-like receptors.* Bioorganic & medicinal chemistry, 2012. **20**(1): p. 455-66.
162. McRobb, F.M., et al., *Homobivalent ligands of the atypical antipsychotic clozapine: design, synthesis, and pharmacological evaluation.* Journal of medicinal chemistry, 2012. **55**(4): p. 1622-34.
163. Gogoi, S., et al., *Novel bivalent ligands for D₂/D₃ dopamine receptors: Significant co-operative gain in D₂ affinity and potency.* ACS medicinal chemistry letters, 2012. **3**(12): p. 991-996.
164. Shonberg, J., et al., *Synthesis, functional and binding profile of (R)-apomorphine based homobivalent ligands targeting the dopamine D-2 receptor.* Medicinal chemistry communications, 2013. **4**(9): p. 1290-1296.

165. Salama, I., et al., *Synthesis and binding profile of haloperidol-based bivalent ligands targeting dopamine D(2)-like receptors*. Bioorganic & medicinal chemistry letters, 2014. **24**(16): p. 3753-6.
166. Jorg, M., et al., *Investigation of novel ropinirole analogues: synthesis, pharmacological evaluation and computational analysis of dopamine D-2 receptor functionalized congeners and homobivalent ligands*. Medicinal chemistry communications, 2014. **5**(7): p. 891-898.
167. Huber, D., H. Hubner, and P. Gmeiner, *1,1'-Disubstituted ferrocenes as molecular hinges in mono- and bivalent dopamine receptor ligands*. Journal of medicinal chemistry, 2009. **52**(21): p. 6860-70.
168. Kuhhorn, J., H. Hubner, and P. Gmeiner, *Bivalent dopamine D2 receptor ligands: synthesis and binding properties*. Journal of medicinal chemistry, 2011. **54**(13): p. 4896-903.
169. Kuhhorn, J., et al., *Development of a bivalent dopamine D(2) receptor agonist*. Journal of medicinal chemistry, 2011. **54**(22): p. 7911-9.
170. Mohr, K., et al., *Rational design of dualsteric GPCR ligands: quests and promise*. British journal of pharmacology, 2010. **159**(5): p. 997-1008.
171. Carriba, P., et al., *Detection of heteromerization of more than two proteins by sequential BRET-FRET*. Nature methods, 2008. **5**(8): p. 727-33.
172. Pulido, D., F. Albericio, and M. Royo, *Controlling multivalency and multimodality: up to pentamodal dendritic platforms based on diethylenetriaminepentaacetic acid cores*. Organic letters, 2014. **16**(5): p. 1318-21.
173. Morphy, R. and Z. Rankovic, *Designed multiple ligands. An emerging drug discovery paradigm*. Journal of medicinal chemistry, 2005. **48**(21): p. 6523-43.
174. Lane, J.R., et al., *A new mechanism of allostery in a G protein-coupled receptor dimer*. Nature chemical biology, 2014. **10**(9): p. 745-52.
175. Earley, C.J., et al., *Connectome and molecular pharmacological differences in the dopaminergic system in restless legs syndrome (RLS): plastic changes and neuroadaptations that may contribute to augmentation*. Sleep medicine, 2017. **31**: p. 71-77.
176. Ferrari-Toninelli, G., et al., *Dopamine receptor agonists for protection and repair in Parkinson's disease*. Current topics in medicinal chemistry, 2008. **8**(12): p. 1089-99.
177. Kehne, J.H., T.H. Andree, and J.N. Heinrich, *D2 receptor partial agonists: treatment of CNS disorders of dopamine function*. Current topics in medicinal chemistry, 2008. **8**(12): p. 1068-88.
178. Simpson, E.H. and C. Kellendonk, *Insights About Striatal Circuit Function and Schizophrenia From a Mouse Model of Dopamine D2 Receptor Upregulation*. Biological psychiatry, 2017. **81**(1): p. 21-30.
179. Bonuccelli, U., P. Del Dotto, and O. Rascol, *Role of dopamine receptor agonists in the treatment of early Parkinson's disease*. Parkinsonism & related disorders, 2009. **15 Suppl 4**: p. S44-53.
180. Deutschlander, A., et al., *Occupancy of pramipexole (Sifrol) at cerebral dopamine D2/3 receptors in Parkinson's disease patients*. Neurolmage. Clinical, 2016. **12**: p. 41-6.
181. Ferre, S., et al., *In search of alternatives to dopaminergic ligands for the treatment of restless legs syndrome: iron, glutamate, and adenosine*. Sleep medicine, 2017. **31**: p. 86-92.
182. Wetsel, W., et al., *Targeting Functional Selectivity of the Dopamine D2 Receptor for Treatment of Schizophrenia-like Behaviors*. International journal of neuropsychopharmacology, 2016. **19**: p. 207-207.
183. Chen, X., et al., *Structure-functional selectivity relationship studies of beta-arrestin-biased dopamine D(2) receptor agonists*. Journal of medicinal chemistry, 2012. **55**(16): p. 7141-53.
184. Mannel, B., et al., *Hydroxy-Substituted Heteroaryl piperazines: Novel Scaffolds for beta-Arrestin-Biased D2R Agonists*. Journal of medicinal chemistry, 2017. **60**(11): p. 4693-4713.
185. Rose, S.J., et al., *Engineered D2R Variants Reveal the Balanced and Biased Contributions of G-Protein and beta-Arrestin to Dopamine-Dependent Functions*. Neuropsychopharmacology :

- official publication of the American College of Neuropsychopharmacology, 2018. **43**(5): p. 1164-1173.
186. Urs, N.M., et al., *Distinct cortical and striatal actions of a beta-arrestin-biased dopamine D2 receptor ligand reveal unique antipsychotic-like properties*. Proceedings of the national Academy of sciences of the United States of America, 2016. **113**(50): p. E8178-E8186.
187. Barone, P., et al., *Sumanitrole versus placebo or ropinirole for the adjunctive treatment of patients with advanced Parkinson's disease*. Movement disorders : official journal of the Movement Disorder Society, 2007. **22**(4): p. 483-9.
188. Garcia-Borreguero, D., et al., *Efficacy and tolerability of sumanitrole in restless legs syndrome: a phase II, randomized, double-blind, placebo-controlled, dose-response study*. Sleep medicine, 2007. **8**(2): p. 119-27.
189. McCall, R.B., et al., *Sumanitrole, a highly dopamine D2-selective receptor agonist: in vitro and in vivo pharmacological characterization and efficacy in animal models of Parkinson's disease*. The Journal of pharmacology and experimental therapeutics, 2005. **314**(3): p. 1248-56.
190. Bonifazi, A., et al., *Novel Bivalent Ligands Based on the Sumanitrole Pharmacophore Reveal Dopamine D2 Receptor (D2R) Biased Agonism*. Journal of medicinal chemistry, 2017. **60**(7): p. 2890-2907.
191. Zou, M.F., et al., *Novel Analogues of (R)-5-(Methylamino)-5,6-dihydro-4H-imidazo[4,5,1-ij]quinolin-2(1H)-one (Sumanitrole) Provide Clues to Dopamine D2/D3 Receptor Agonist Selectivity*. Journal of medicinal chemistry, 2016. **59**(7): p. 2973-88.
192. Bonifazi, A., et al., *Novel and Potent Dopamine D2 Receptor Go-Protein Biased Agonists*. American chemical society: pharmacology & translational science, 2019. **2**(1): p. 52-65.

Chapter 3:

Luminescence- and fluorescence-based complementation assays to screen for GPCR oligomerization: current state of the art

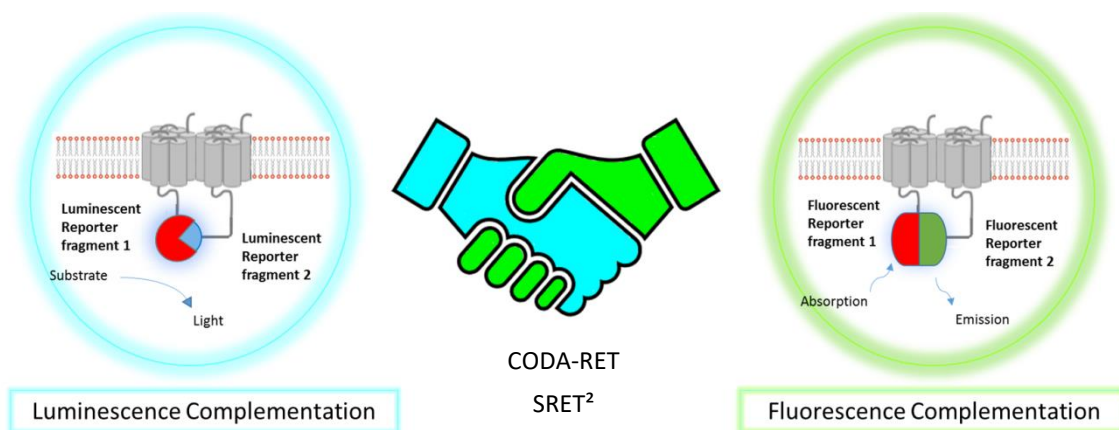
Based on

Elise Wouters[‡], Lakshmi Vasudevan[‡], René A.J. Crans, Deepak K Saini and Christophe Stove. Luminescence- and fluorescence-based complementation assays to screen for GPCR oligomerization: current state of the art. *International Journal of Molecular Sciences*. 2019; 20(12), 2958. [‡]These authors contributed equally.

ABSTRACT

G protein-coupled receptors (GPCRs) have the propensity to form homo- and heterodimers. Dysfunction of these dimers has been associated with multiple diseases, e.g. pre-eclampsia, schizophrenia, depression, among others. Over the past 2 decades, considerable efforts have been made towards the development of screening assays for studying these GPCR dimer complexes in living cells. As a first step, a robust *in vitro* assay in an overexpression system is essential to identify and characterize specific GPCR-GPCR interactions, followed by methodologies to demonstrate association at endogenous levels and eventually *in vivo*. This review focuses on protein complementation assays (PCAs) which have been utilized to study GPCR oligomerization. These approaches are typically fluorescence- and luminescence-based, making identification and localization of protein-protein interactions feasible. The GPCRs of interest are fused to complementary fluorescent or luminescent fragments that, upon GPCR di- or oligomerization, may reconstitute to a functional reporter, of which the activity can be measured. Various protein complementation assays have the disadvantage that the interaction between the reconstituted split fragments is irreversible, which can lead to false positive read-outs. Reversible systems offer several advantages, as they do not only allow to follow the kinetics of GPCR-GPCR interactions, but also allow evaluation of receptor complex modulation by ligands (either agonists or antagonists). PCAs may be used for high-throughput screenings as well, which is highly relevant, given the growing interest and effort to identify small molecule drugs that could potentially target disease-relevant dimers. In addition to providing an overview on how PCAs have allowed to gain better insights into GPCR-GPCR interactions, this chapter also aims at providing practical guidance on how to perform PCA-based assays.

GRAPHICAL ABSTRACT



3.1 Introduction

Membrane receptors are the key players in mediating communication between the cell and the extracellular space. The G protein-coupled receptor (GPCR) protein family represents one of the largest group of cell membrane signaling proteins in the human genome [1]. Currently, approximately 800 members of this superfamily are classified according to the International Union of Pharmacology, Committee on Receptor Nomenclature and Classification (NC-IUPHAR). Herein, GPCRs are grouped into 3 classes, namely Class A (rhodopsin-like), Class B (secretin receptor family) and Class C (metabotropic glutamate-like) [2]. The remaining GPCRs - fungal mating pheromone receptors, cyclic AMP receptors and, frizzled/smoothed - are also included in alternative classification systems [3].

While the traditional view on GPCRs was a “one ligand-one monomeric GPCR unit-one signaling protein” model, an emerging body of evidence shows that GPCRs can form homo- or hetero-oligomeric complexes. This phenomenon adds an additional layer to the complexity of GPCR signaling. Although the concept of GPCR dimerization has been controversial over the past two decades, several sophisticated studies have led scientists to the validation of the GPCR dimerization theory. An indisputable and widely accepted example is the obligate dimer of Class C GABA receptors [4]. These receptors are obligatory dimers, as GABAB1 is necessary for ligand binding and GABAB2 ensures efficient cell trafficking and downstream signaling. Both protomers are not functional when expressed alone. In addition to obligate GPCR dimers observed in Class C receptors, an increasing amount of evidence suggests there is also -transient- dimer formation between Class A GPCRs [5-7].

In general, the phenomenon of oligomerization can exert a significant impact on receptor-ligand binding, downstream signaling, crosstalk, internalization and trafficking. For instance, the interaction of dopamine D2 receptor (D₂R) with dopamine D3 receptor (D₃R) results in a higher potency of certain anti-parkinsonian agents, like pramipexole, compared to their monomers [5]. Furthermore, selective stimulation of D₁R or D₂R or both by the neurotransmitter dopamine triggered co-internalization of the D₁R-D₂R heterodimer [6].

In order to target and study GPCR-GPCR interactions, multiple *in vitro* (and *in vivo*) biochemical, -physical and functional studies have been reported in literature, which applied approaches such as co-immunoprecipitation (co-IP), proximity ligation assays (PLA), and fluorescence- or bioluminescence- based techniques, as already mentioned in **Chapter 2** [8]. Below, we will focus primarily on recent advances in Bioluminescence and Fluorescence-based complementation techniques that have been applied to study GPCR-GPCR interactions.

3.2 Protein complementation assays

Protein complementation assays (PCAs), also referred to as split systems, have been implemented over the past 2 decades to study protein-protein interactions (PPIs). In these assays, a reporter protein with enzymatic or fluorescent properties is engineered or 'split' into non-active or non-fluorescent fragments. These moieties are fused to potential interacting proteins. Upon interaction, the fragments will be brought into close proximity and re-assemble spontaneously into a functional biosensor. Although these assays do not formally prove direct protein-protein interactions, they do suggest co-localization of the GPCRs of interest since PCAs rely on the fusion partners 'interacting'. Complementation-based assays comprise Bimolecular Fluorescence and Luminescence complementation (BiFC/BiLC) as well as β -Lactamase and β -Galactosidase complementation assays. Since 1997, several 'split' fluorescent and luminescent proteins have been developed, of which the most commonly used ones are shown in the timeline in **Figure 3.1**.

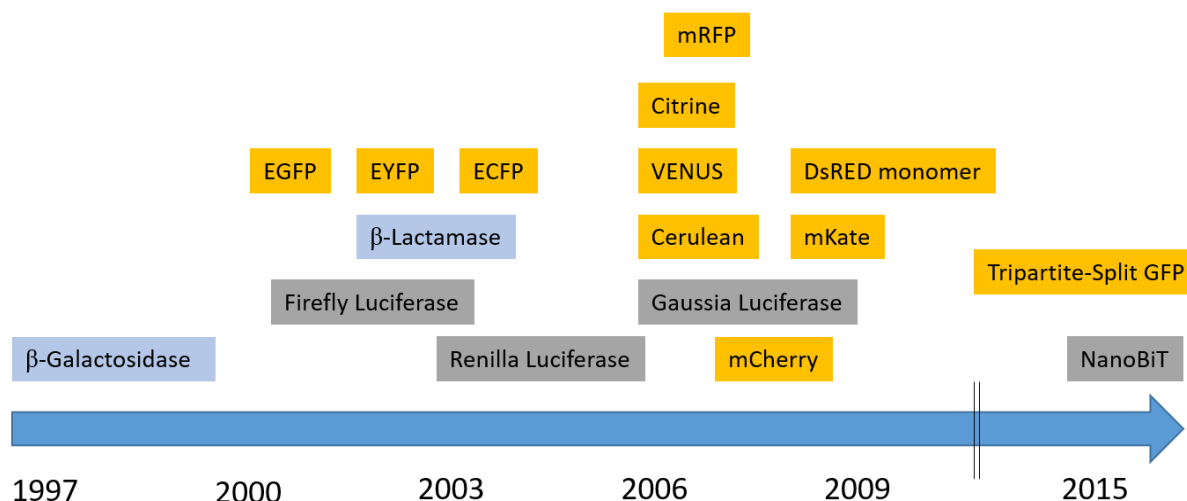


Figure 3.1 History of the development of split protein biosensors. Commonly used fluorescent split proteins (yellow), luminescent split reporters (grey) and enzymes with colorigenic substrates (blue) are shown.

These assays have the potential to be implemented as screening assays to identify GPCR-GPCR interactions, which later on should be confirmed by a variety of complementary approaches, for example Spatial Intensity Distribution Analysis (SpIDA), advanced microscopy techniques, molecular dynamics, among others [9-14]. A benefit of a robust complementation assay is not only its operational simplicity but even more the possibility to test if dimers occur constitutively or whether ligands can alter the oligomeric state of GPCRs. Moreover, these cell-based assays lend themselves for early-stage drug discovery since molecules that potentially exert an impact on the level of dimerization, whether desired or undesired, can be rapidly identified. In addition, off-target effects can be revealed, such as altered receptor expression, localization or cellular signaling. An overview of the available PCAs as of today and their characteristics are presented in **Table 3.1**.

Table 3.1 Overview of proteins, already implemented in fluorescence- and luminescence-based complementation assays. N/A = not applicable, nd = not determined.

Reporter protein	Source species	Readout	Excitation wavelength (nm)	Emission wavelength (nm)	Substrate	Cofactor	Stability (h)	Maturation time (t1/2) (min)	MW (kDa)
VENUS	<i>Aequorea victoria</i>	Fluorescence	515	528	-	N/A	-	40 (in vitro)	27
GFP	<i>Aequorea victoria</i>	Fluorescence	488	510	-	N/A	-	53 (in vitro)	27
mCherry	<i>Discosoma</i>	Fluorescence	587	610	-	N/A	-	17+30 (S. cerevisiae)	29
Cerulean	<i>Aequorea victoria</i>	Fluorescence	433	475	-	N/A	-	nd	27
Tripartite-Split GFP	<i>Aequorea victoria</i>	Fluorescence	488	530	-	N/A	-	nd	23
EYFP	<i>Aequorea victoria</i>	Fluorescence	514	527	-	N/A	-	23 (in vitro)	26.4
ECFP	<i>Aequorea macrodactyla</i>	Fluorescence	405	485	-	N/A	-	49 (S. cerevisiae)	26.8
Citrine	<i>Aequorea victoria</i>	Fluorescence	516	529	-	N/A	-	nd	27
mRFP	<i>Discosoma striata</i>	Fluorescence	584	607	-	N/A	-	<60	25.9
mKate	<i>Discosoma striata</i>	Fluorescence	588	635	-	N/A	-	20	26
DsRed monomer	<i>Discosoma striata</i>	Fluorescence	558	583	-	N/A	-	600	28
Renilla luciferase	<i>Renilla reniformis</i>	Luminescence	-	480	Co-elenterazine	N/A	4.5h (cell)	-	36
Firefly Luciferase	<i>Photinus pyralis</i>	Luminescence	-	550-570	D-luciferin	ATP, O ₂	4.0h (cell)	-	62
Gaussia Luciferase	<i>Gaussia princeps</i>	Luminescence	-	485	Co-elenterazine	N/A	60h (cell media)	-	20
NanoBiT	<i>Oplophorus gracilirostris</i>	Luminescence	-	460	Furimazine	N/A	6.0h (cell)	-	19
β-lactamase	<i>Bacillus licheniformis</i>	Luminescence	-	492	Nitrocefin	N/A	nd	-	29
β-Galactosidase	<i>Escherichia coli</i>	Fluorescence	Reliant on the substrate	Reliant on the substrate	FDG, MUG a.o.	Mg ²⁺	1.1h (yeast cells)	-	464
Click Beetle luciferase	<i>Pyrophorus plagiophthalmus</i>	Luminescence	-	-	D-luciferin	Mg ²⁺ , ATP			64

Many questions remain unanswered in the field of GPCR di- and oligomerization. Therefore, it is a highly warranted first step to fully characterize the *in vitro* assays featuring robust sensitivity in detecting PPIs of interest. This review aims at offering insight into the progress that has been made in the field of protein complementation assays to study GPCR dimerization. This progress concerns for example optimization of complementation assays in stability and light output by consensus sequence driven strategy. Several mutations applied in fluorescent and luminescent complementation assays in the field of GPCR dimerization will be discussed throughout the following sections of this review, for additional information concerning mutational optimization of split reporter genes in general we refer to the excellent review by Wehr and Rossner [15].

3.2.1 Fluorescence-based complementation assays

One of the well-studied PCAs is BiFC, which is based on the structural and functional complementation of two non-fluorescent protein fragments brought into close proximity by their interacting fusion partners (**Figure 3.2**). Upon complementation of the fluorescent protein, the fluorescence can be read via a plate-reader, imaged using a fluorescence microscope or even analyzed by flow cytometry without the need for any treatment of the cells.

In 1999, Regan and colleagues reported BiFC for the first time, in *Escherichia coli* (*E. coli*), by using a strategy based on the non-covalent association of the split fragments of green fluorescent protein (GFP), fused to two antiparallel leucine zippers [16]. Subsequently, Hu *et al.* [17], reported on the development of a BiFC assay based on the split fragments of yellow fluorescent protein (YFP), tagged to two interacting transcription factors in living mammalian cells. Shyu *et al.* [18] developed Venus, one of the brightest fluorescent proteins, for studying PPIs at physiological conditions using BiFC. Since then, numerous types of fluorescence complementation-based assays have been developed to visualize signaling events involving two or even more interacting proteins, ranging from bacteria to mammalian cells.

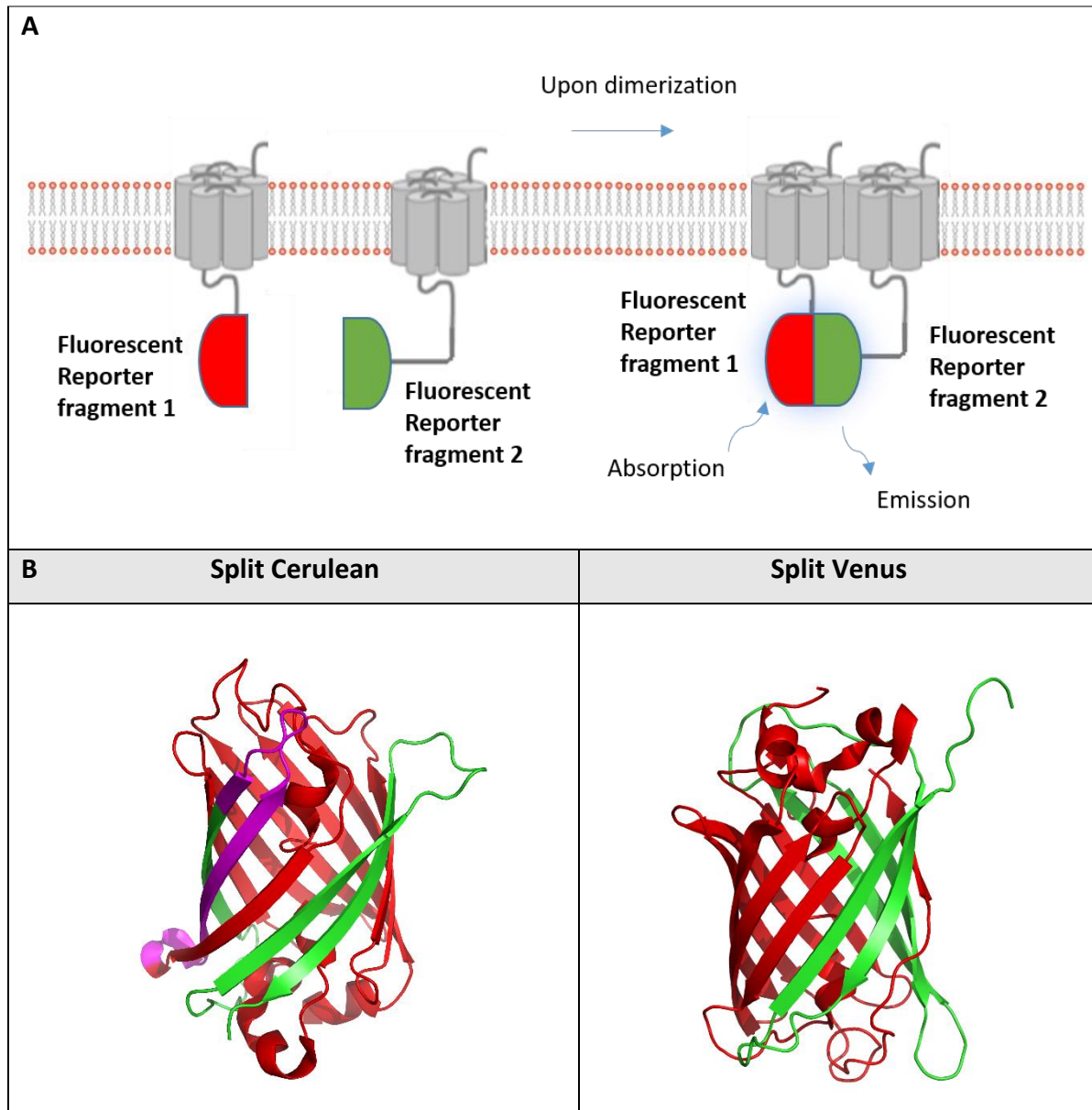


Figure 3.2 Fluorescence-based complementation assay. A. The principle of the fluorescent complementation assay is shown schematically. B. Split versions of the fluorescent reporters Cerulean and Venus are shown in green and red. Purple refers to overlapping sections. (PDB; Accession no. 3AKO for Venus) (PDB: Accession no. 5OXB for Cerulean).

3.2.1.1 Fluorescent proteins

3.2.1.1.1 Green fluorescent protein (GFP)

Regan and colleagues used GFP, the first fluorescent protein, for characterizing BiFC by tagging the split fragments of GFP, i.e. NGFP and CGFP, split at residue 157-158, to strongly interacting antiparallel leucine zippers. The split fragments did not self-assemble in bacteria, whereas upon fusion to antiparallel leucine zippers, the fragments could properly fold to

form a functional GFP protein and hence gain fluorescence. A recent study [19] performed by Son and colleagues made use of enhanced GFP (EGFP), an improved version of GFP that is brighter and more photostable. The EGFP molecule was split to yield N-EGFP (1-158) and C-EGFP (159-238), respectively. These split parts were fused to α -factor receptor (Ste2p), to study homodimerization in *S. cerevisiae*. Both full length and C-terminally truncated forms of the receptors led to fluorescence, indicating dimerization.

A recent advance in BiFC based on GFP is Tripartite GFP, introduced by Cabantous *et al.* in 2013 [20] in an attempt to cope with the problem of poor folding and self-assembly seen with split GFP. Tripartite GFP is based on the tripartite association of two twenty amino-acid residue fragments of GFP, coined as GFP 10 and GFP 11, that can be fused to the proteins under investigation, and the complementary GFP 1-9 detector. Upon interaction between the protein partners, GFP 10 and GFP 11 associate with GFP 1-9 to form the functional GFP molecule. This system was initially characterized in *E. coli* and in mammalian cells, where the rapamycin induced association of FRB (FKBP-rapamycin binding domain of mTOR) and FKBP12 (FK506- and rapamycin-binding protein) was studied. This system has extensively been exploited for the validation of multiple reporter systems. Although use of this Tripartite GFP system has not been reported for studying GPCR dimerization, it could be an advantageous platform to be used over the conventional split GFP.

3.2.1.1.2 Yellow fluorescent protein (YFP)

In 2001, Nagai *et al.* [21] first demonstrated the use of the YFP in BiFC, wherein they used a variant of YFP to study the effect of Ca^{2+} on PPI in living cells. Shortly after, Griesbeck and colleagues [17, 22] tried several permutations and combinations of split regions in EYFP (S65G, S72A, T203Y) to improve the fluorescence signal along with minimal self-assembly of the split fragments. Several variants of YFP have been developed such as Citrine (a variant having a Q69M mutation) and Venus (a variant carrying a F46L mutation), that folds even at a physiological temperature of 37°C [23]. This led to the usage of these fluorescent protein fragments to study GPCR-GPCR interactions.

Vidi *et al.* (2008) [24, 25] used split fragments of Venus fused to the adenosine A_{2A} receptor (A_{2A}) to address the question about A_{2A} oligomerization in the CAD neuronal cell line. Co-expression of A_{2A}-VN and A_{2A}-VC in these cells, as well as in HEK293 cells, resulted in fluorescence, indicating A_{2A} dimerization, in contrast to negative controls wherein cells transfected with A_{2A}-VN/D₁R-VC/M₄R-VC did not show any fluorescence, pointing at the specificity of the interaction.

Similarly, Kilpatrick *et al.* (2014) [26] assessed dimerization of a receptor for NPY, Neuropeptide Y Y1/Y5. This neuropeptide is a widely expressed modulator of the central nervous system, mainly known for its role in the regulation of appetite upon its release from hypothalamic arcuate neurons. The receptors, tagged with split YFP, showed heterodimerization and the irreversible nature of these fragment tags also helped to elucidate the cellular localization of these dimers. Evaluation of the effect of ligands on the internalization of dimers, as opposed to individual protomers, demonstrated that Y1/Y5 receptor dimers displayed altered ligand pharmacology, indicative of allosteric interaction.

Przybyla and Watts in 2010 [27] used Venus-based BiFC to demonstrate heterodimerization between the cannabinoid receptor 1 (CB₁) and the dopamine D_{2Long} receptor (D_{2L}R) in CAD cells, wherein CB₁ and D_{2L}R receptor were fused at their C-terminus to VN and the C-terminal fragment of Cerulean (CC), respectively (see 3.2.1.2.1 MBiFC section).

Ang *et al.* in 2018 [28] assessed homo- and heterodimerization of free fatty acid receptors, GPCRs that are expressed on mammalian cells to sense the short chain fatty acids derived from the microbiota. To study dimerization, HEK293T cells were transfected with VN- or VC-tagged (Free fatty acid receptor 2/3) FFAR2/3 receptor. Homodimerization of FFAR3 and FFAR2, as well as heterodimerization between FFAR2-VN and FFAR3-VC were observed, as compared to negative control FFAR2/3 tagged to VN or VC plus P2RY1-VN or P2RY1-VC (for heterodimerization) and P2RY1-VN plus P2RY1-VC (for homodimerization).

Xue *et al.* in 2018 [29] used a BiFC assay based on split Venus to detect heterodimerization between Growth hormone secretagogue receptor 1 α (GHSR1 α) and Orexin 1 receptor (OX1R). Recently, Navarro *et al.* (2018) [30] used interfering peptides corresponding to

regions in TM1-7 domain for A_{2A} and TM5-7 domain for A₁, each fused to TAT peptides, to disrupt the interaction between the A₁-A_{2A} heteromer. They therefore expressed receptors tagged with split fragments of YFP (nYFP and cYFP) in HEK293T cells. In the absence of the TM peptides, fluorescence complementation was detected for A_{2A}-nYFP and A_{2A}-cYFP in the presence of untagged A₁, suggesting homodimerization of A_{2A}. The interaction sites were mapped to TM4 and 5 of A_{2A} with the help of interfering peptides. In the same way, fluorescence signal corresponding to the heterodimer (A₁-nYFP and A_{2A}-cYFP) was also detected. Upon addition of TM peptides corresponding to regions 5/6, a reduction in fluorescence was observed, suggesting the involvement of these regions in formation of the heterodimer. In the same year (2018), BiFC using split fragments of YFP was utilized by Hinz *et al.* [31] for studying homodimerization between A_{2A} and heterodimerization with A_{2B} receptor. For this purpose, CHO cells were transfected with a constant amount of A_{2A}-NYFP and increasing amounts of HA-A_{2A}-CYFP and a strong fluorescence signal was observed, indicative of the A_{2A}-A_{2A} homodimer. For the purpose of studying A_{2B}-A_{2A} heterodimerization, the GPCRs were tagged with NYFP and CYFP, respectively. CHO cells transfected with constant amounts of A_{2B}-NYFP and increasing amounts of HA-A_{2A}-CYFP showed significantly higher fluorescence when compared to the negative control comprising of GABAB2-NYFP and increasing amounts of HA-A_{2A}-CYFP.

An interesting study was performed by Song *et al.* in 2019 [32], where a homo-molecular fluorescence complementation (homo-FC) probe was designed by splitting a single fluorescent protein (superfolder GFP, sfGFP) into two fragments and linking the C-terminal fragment (strands 8-11) with a short linker N-terminally to the N-terminal fragment (strands 1-7). This “flopped fusion” construct, which does not show intramolecular self-complementation, was used to tag the β_2 adrenergic receptor (β_2 -AR), to study its homodimerization. A fluorescent signal was generated by complementation of strands 1-7 of one “flopped” sfGFP molecule, fused to one β_2 -AR, with strands 8-11 of another “flopped” sGFP molecule, fused to a second β_2 -AR. The advantage of this approach lies in the fact that only one receptor constructs needs to be generated, to allow the assessment of homodimerization.

3.2.1.1.3 Cyan fluorescent protein (CFP)

Apart from using the aforementioned split Venus, Vidi *et al.* [24, 33] also used split fragments of Cerulean to show that A_{2A} homodimerizes in CAD cells (see 3.2.1.2.1 MBiFC section). The same fluorescent protein fragments were also used in 2010 by Przybyla and Watts [27] to illustrate the homodimerization of D_{2L}R.

3.2.1.1.4 Red, far-red and near-infrared fluorescent proteins

Red fluorescent proteins encompass a couple of fluorescent proteins that emit in the red region of the visible spectrum. They have evolved through time to overcome issues such as slow maturation or the tendency to oligomerize (as exhibited by Discosoma Red (DsRed)) [34]. Red variants such as monomer Red fluorescent protein 1 (mRFP1) are not appropriate for BiFC due to their low extinction coefficient, quantum yield and low photostability, despite faster maturation than DsRed and better tissue penetration. Although several variants of RFP have been used for FRET, BiFC assays with the split parts have not been reported for demonstrating GPCR-GPCR interactions.

For imaging deep tissues in animals, fluorescent proteins with emission in the far-red region of the spectrum are chosen. RFP, mcherry and DsRed have limited application in BiFC due to the requirement of low temperatures for their maturation [35, 36]. This led to the development of mKate, a far-red, monomeric form of Katushka fluorescent protein, that matures faster and is photostable [37]. BiFC based on split fragments of mKate fused to transcription factors was successfully applied in COS-7 cells [38], but has not been applied yet for studying GPCR oligomerization.

Table 3.2 An overview of GPCR-GPCR interactions, shown by fluorescence complementation assays.

GPCR dimer	Oligomeric type	PCA	Split biosensor	Fragments	Negative Control	Cell-type	Year	Ref	Evidence in vivo or native tissue	Ref
mGluR ₅ -D ₂ R	Heterodimer	BiFC	YFP	1-155, 155-231	GABA _{B2}	HEK	2009	[39]	Yes	[39]
D ₂ R-D ₂ R	Homodimer	BiFC	YFP	1-155, 156-238	D ₁ R	HEK	2015	[40]	Yes	[41, 42]
A _{2A} -D _{2L} R	Heterodimer	MBiFC	Venus/Cerulean	1-172, 155-238	D ₁	CAD	2008	[24]	Yes	[39, 43-47]
D _{2L} R-CB ₁	Heterodimer	MBiFC	Venus/Cerulean	1-172, 155-238	M ₄	CAD	2010	[27]	Yes	[43]
D _{2L} R-D _{2L} R	Oligomer	MBiFC	Venus/Cerulean	1-172, 155-238	-	CAD	2010	[27]	-	-
D ₂₅ R-D ₂₅ R	Homodimer	BiFC	Venus	1-155, 156-240	CD8	HEK283T	2008	[48]	Yes	[41, 42]
AT ₁ -AT ₂	Homo- and heterodimer	BiFC	Venus	1-158,159-239	ATIP	HEK293FT	2011	[49]	Yes	[50-52]
CXCR4-CXCR4	Homodimer	BiFC	vYFP	1-465, 466-720	D ₂ R	HEK293	2014	[53]	-	-
A _{2A} - A _{2A}	Homodimer	MBiFC	Venus/Cerulean	1-172, 155-238	-	CAD	2008	[24]	-	-
A _{2A} - A _{2A}	Homodimer	BiFC	YFP	1-155, 155-238	Non-fused A ₁ (competition)	HEK293T	2018	[30]	-	-
A _{2A} - A ₁	Heterodimer	BiFC	YFP	1-155, 155-238	-	HEK293T	2018	[30]	Yes	[54]
GHSR1a-OX1R	Heterodimer	BiFC	Venus	1-172, 156-239	-	HEK293T	2018	[29]	-	-
β ₂ AR- β ₂ AR	Oligomer	BiFC	-15sfGFP		-	HeLa	2019	[32]	-	-
A _{2A} -A _{2A}	Homodimer	BiFC	YFP	1-155,156-239	GABA _{B2}	CHO	2018	[31]	-	-
A _{2B} -A _{2A}	Heterodimer	BiFC	YFP	1-155,156-239	GABA _{B2}	CHO	2018	[31]	-	-
FFAR3-FFAR3	Homodimer	BiFC	Venus	1-155 (I152L), 155-239	P2RY1	HEK293T	2018	[28]	-	-
FFAR2-FFAR3	Heterodimer	BiFC	Venus	1-155 (I152L), 155-238	P2RY1	HEK293T	2018	[28]	-	-
mGluR ₂ - mGluR ₂	Homodimer	BiFC	mCitrine	1-172, 155-238	-	HEK293T	2016	[55]	-	-
α _{1b} - α _{1b}	Homodimer	BiFC	eYFP	1-172, 155-238	-	HEK293T	2017	[56]	-	-

3.2.1.2 BiFC assays

3.2.1.2.1 Multicolour BiFC (MBiFC)

Multicolour BiFC (MBiFC) has gained a lot of attention in recent years as it essentially gives the freedom to explore multiple protein-protein interactions inside the same living cell [57]. It has been studied with split parts of Venus and Cerulean, wherein the C terminal part of Cerulean is tagged to protein A (CC), the N-terminal part of Venus is tagged to protein B (VN) and finally the N terminal fragment of Cerulean is fused to protein C (CN). The C-terminal fragment of Cerulean (CC), comprising residues 155-238 (C155), can functionally complement with the N-terminal fragment of VN and CN, comprising residues 1-172 (N173), to produce a Venus (VN+CC) signal or Cerulean (CN+CC) signal. Since these parts are non-fluorescent *per se*, simple employment of different excitation and emission wavelengths allows to study simultaneously the interaction between A-B and A-C within the same cell [24, 58, 59].

MBiFC has aided in the understanding of GPCR oligomerization amongst all its other applications. Vidi *et al.* (2008) [24] used MBiFC to visualize the hetero- and homodimerization capacity of A_{2A} in the CAD neuronal cell line. To this end, D_{2L}R-VN was co-transfected with A_{2A}-CN and A_{2A}-CC in CAD cells. The detection of Venus (D_{2L}R-VN/A_{2A}-CC) and Cerulean (A_{2A}-CN/A_{2A}-CC) fluorescence signals revealed the presence of the A_{2A}-D_{2L}R heteromer and A_{2A} homomer, respectively. In addition, fluorescence microscopy also revealed that the dimers were localized at the plasma membrane as well as in intracellular compartments.

Przybyla and Watts in 2010 [27] showed oligomerization of CB₁ and D_{2L}R. To achieve this, they used CAD cells that expressed CB₁-VN and D_{2L}R fused to the split fragments of Cerulean (D_{2L}R-CN, D_{2L}R-CC) and these cells were imaged using fluorescence microscopy. The heterodimers in the cell formed by CB₁-VN-D_{2L}R-CC produced a Venus signal that was mainly localized in the intracellular compartment, whereas the homodimers of D_{2L}R produced a

Cerulean signal that was localized both in the intracellular compartment and on the plasma membrane.

3.2.1.2.2 BiFC-RET

The fluorescent proteins used in BiFC could also be coupled to FRET or BRET to study GPCR oligomerization, e.g. functionally complemented YFP could act as a FRET/BRET acceptor. BiFC-BRET [60] employs the energy transfer between GPCR-A fused to a luciferase and the complemented fragments of YFP that are fused to GPCR-B and GPCR-C that are as close as 10 nm apart, indicating a trivalent complex of GPCRs.

Navarro *et al.* in 2008 [61] used BiFC-BRET to demonstrate the interaction between D₂R, A_{2A} and CB₁ receptors in HEK cells. The split fragments of YFP fused to CB₁ and A_{2A} acted as the acceptor fluorophore in BRET, *Renilla* luciferase (RLuc) fused to D₂R (D₂R-RLuc) acting as the donor.

BiFC-FRET [62] is similar, offering the additional benefit that the complex can be visualized within the cell. BiFC-FRET was used to understand the existence of higher order oligomers in the case of A_{2A} by using fusion constructs with Cerulean and split parts of Venus. Prior to this, to test if the system could record FRET, A_{2A} dimerization was tested by fusing A_{2A} to Cerulean and Venus. Based on this, CAD neuronal cells were co-transfected with A_{2A}-Cerulean and A_{2A} fused to split parts of Venus. FRET signals were detected, suggesting the existence of A_{2A} oligomers, as opposed to a negative control wherein cells transfected with M₄ as the acceptor only showed very low FRET [63].

In 2017 Bagher *et al.* [64] combined BRET with BiFC which forms the basis of “Sequential resonance energy transfer 2” (SRET²). Herein, the donor for BRET was the RLuc fused to D_{2L}R (D_{2L}R-RLuc), which upon addition of the substrate coelenterazine 400a, excited the acceptor GFP² fused to D_{2L}R (D_{2L}R-GFP²), thereby confirming the homodimerization of D_{2L}R. Sequentially, the GFP² acted as FRET donor for the CB₁-VN/CB₁-VC homodimer, thus providing evidence for heterotetramerization. With increasing concentrations of CB₁-VN/CB₁-VC, there was a hyperbolic increase in net SRET², as opposed to negative control

cells that were transfected with D_{2L}R-RLuc and mGluR6-GFP² and increasing concentrations of CB₁-VN/CB₁-VC, confirming that the homodimers of D_{2L}R and CB₁ associate to form oligomers.

3.2.1.3 Ligand-dependent modulation of dimerization

The level of GPCR dimer formation could possibly be altered by ligands interacting with the receptor(s). The potential of split-protein sensors to monitor the dynamic changes in dimerization, provoked by chemical inducers or inhibitors, was demonstrated using the rapamycin-dependent FKBP/FRB Chemically Induced Dimerization (CID) system[65]. The first demonstration for the use of MBiFC to monitor drug-modulated GPCR oligomerization was published by Vidi *et al.* in 2008 [24] for the A_{2A}-D₂R interaction. Stimulation of D₂R with the D₂R agonist quinpirole led to internalization of D₂R homodimers as well as of A_{2A}-D₂R oligomers, which was blocked by the D₂R antagonist, sulpiride [24]. Furthermore, treatment with quinpirole decreased the formation of A_{2A}-D₂R heterodimers, as compared to A_{2A} homodimers. Also treatment with 5-N-methylcarboxamidoadenosine (MECA), an agonist for the adenosine receptor, increased the proportion of A_{2A}/D_{2L}R heterodimers, as compared to homodimers of A_{2A}, while treatment with its antagonist (CGS15943) had no effect on BiFC. Interestingly, these drug-induced alterations on the formation of oligomers could not be supported by changes in the receptor density.

As discussed above, Przybyla and Watts [27] demonstrated heterodimerization of CB₁-D_{2L}R using MBiFC. Also the influence of ligands on the balance between hetero- and homodimers was analyzed. Quinpirole and CP55,940 shifted the balance towards the formation of CB₁-D_{2L}R heterodimers, as opposed to D_{2L}R-D_{2L}R homodimers. The D₂R antagonist sulpiride favored D_{2L}R homodimerization. Consequently, it was shown that sustained treatment with quinpirole influenced the expression of D_{2L}R, which in turn might affect the dimerization status inside the cell as: D_{2L}R-CB₁ > D_{2L}R-D_{2L}R > A_{2A}-D_{2L}R. In a similar way, studies also indicated that a CB₁ antagonist (1-[7-(2-chlorophenyl)-8-(4-chlorophenyl)-2-methylpyrazolo[1,5-a]-[1,3,5]triazin-4-yl]-3-ethylaminoazetidine-3-carboxylic acid amide

benzenesulfonate) could have a potential therapeutic role in Parkinsonism by enhancing the activity of L-DOPA [66].

In 2018, Navarro *et al.* [30] evaluated if activation of A₁ or A_{2A} alone or by a combination of agonists could modulate the TM interface of the heteromer formed by A_{2A}-nYFP and A₁-cYFP. Selective agonists for A₁, N⁶-cyclopentyladenosine (CPA), and A_{2A}, 4-[2-[[6-Amino-9-(N-ethyl-β-D-ribofuranuronamidosyl)-9H-purin-2-yl] amino] ethyl] benzenepropanoic acid (CGS-21680), were used alone or in combination. None of the agonists, either used in combination or alone, could modify the TM interface of the A₁-A_{2A} heterodimer.

Various ligands were tested for their capacity to affect β₂AR oligomerization by Song *et al.* in 2019 [32]. A panel of compounds consisting of five agonists, two antagonists and two inverse agonists were screened using the above-mentioned homo-FC assay. They observed that agonists induced oligomerization while inverse agonists reduced the signals and a combination of both also resulted in reduced intensity of signal, thus confirming the same.

3.2.2 Luminescence-based complementation assays

Luciferases, which have seen an expansive growth in use as reporter proteins in biological research, are attractive due to the high signal to background ratio associated with their usage, as no excitation light is required to generate a signal [67]. Similar to fluorescent proteins, these enzymes can also be used in applications where the luminescent protein itself is split into two fragments, which are conjugated to proteins of interest (**Figure 3.3**). Several luminescent proteins have served this purpose, with Firefly luciferase (FLuc) [68, 69] and *RLuc* [70, 71] being the two most commonly used bioluminescent proteins (**Table 3.3**). However, many other novel luciferases have also been developed with favorable characteristics in terms of stability, substrate requirement, brightness and emission spectrum, e.g. *Gaussia princeps* luciferase (GLuc) [72] and NanoLuciferase [73-75]. All mentioned split-protein reporters were initially validated using the aforementioned FKBP/FRB CID system [68, 72, 76-78].

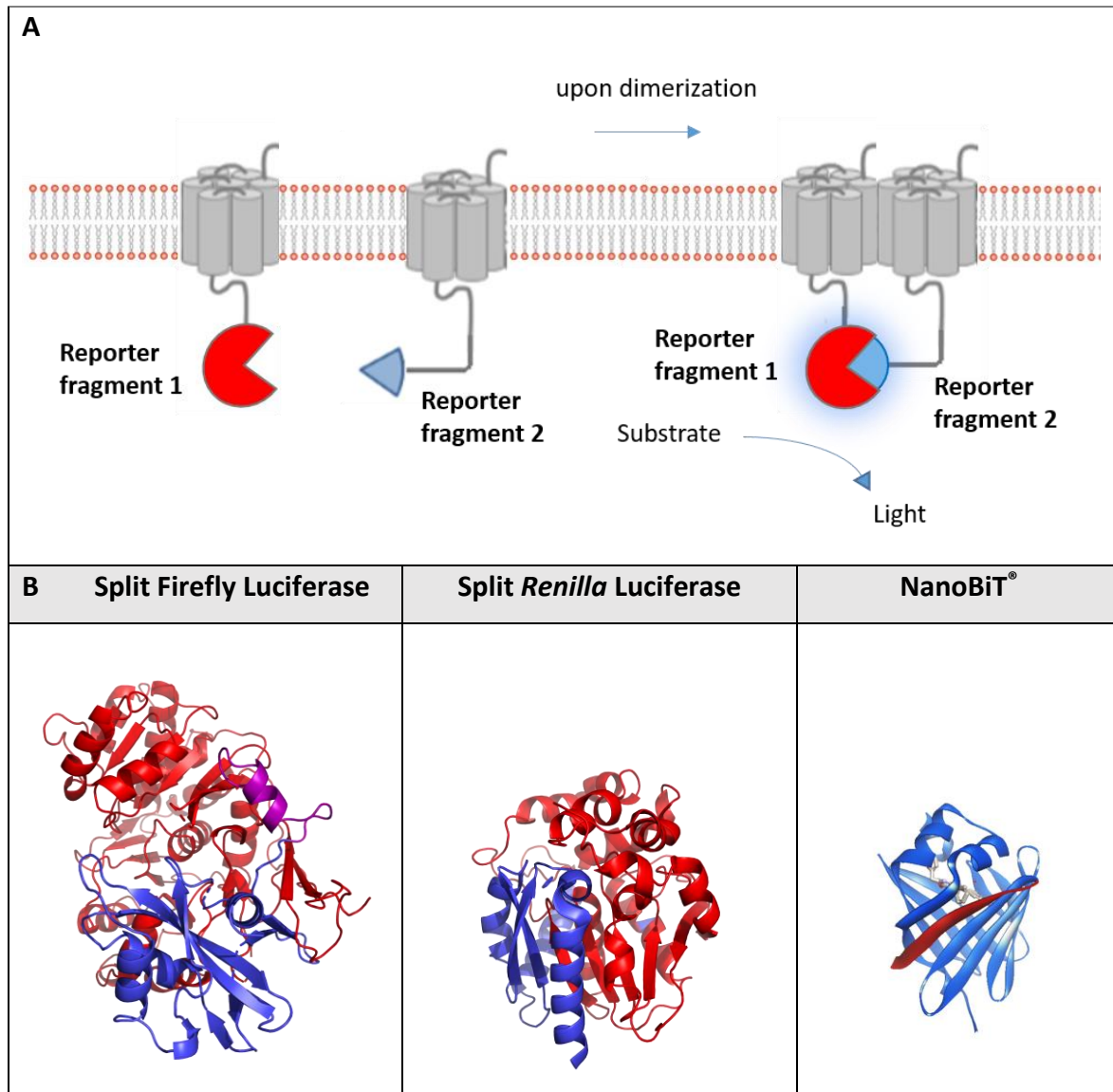


Figure 3.3 Luminescence-based protein complementation assay. A. The principle of the luminescent complementation assay is shown schematically. B. Split versions of the luminescent reporters Firefly, *Renilla* and Nanoluciferase are shown in blue and red. Purple refers to overlapping sections. Split luminescent biosensors are depicted in proportion to their size (Fluc: 62 kDa, Rluc: 36 kDa and NanoBiT[®]: 19 kDa) (PDB Accession no. 1LCI for firefly luciferase, PDB Accession no. 2PSD for *Renilla* luciferase) (NanoBiT[®]: source Promega)

3.2.2.1 Luminescent proteins

3.2.2.1.1 *Renilla*/Firefly Luciferase (RLuc/FLuc)

FLuc is the least optimal reporter for employment as a bioluminescent tag, due to its size (\pm 60 kDa) and its dependence on ATP, molecular oxygen and magnesium for activity. Luciferases that use coelenterazine as a substrate, such as the luciferase from the sea

pansy *Renilla reniformis* *RLuc* [79, 80], have as advantage over *FLuc* that they are not ATP dependent and only require the presence of molecular oxygen for the enzyme-catalyzed conversion of a substrate to a luminescent reaction product. As the bioluminescent activity of formerly used non-truncated luciferases is a limiting factor to permit their application in high throughput screenings, specific mutations of certain luciferases, like in *RLuc*, were selected using a consensus sequence-driven strategy and screened for their ability to confer stability in activity as well as for their light output [81].

For GPCR dimerization purposes, the split-luciferase reporter approaches have not been applied to the same extent as their fluorescence counterparts. Nevertheless, these reporter systems also allow the rapid detection of macromolecular GPCR-GPCR interactions. For instance, the split *FLuc* methodology was used in cell culture models as well as in tumor xenograft models of breast cancer (see section 3.6 *In vivo* applications) to measure changes in chemokine receptor CXCR4 (and CXCR7) homodimerization in response to pharmacological agents [82]. Likewise, the CXCR4 homodimer has also been demonstrated with a split *RLuc* assay [53]. For this *Renilla* luciferase complementation assay, *RlucII* was implemented, which is derived from *RLuc*, wherein two mutations (C124A and M185V) were introduced to make it brighter.

For studying dopamine D₂R oligomers, an alternative *RLuc* construct was implemented, namely *Rluc8* [48]. Owing to eight favorable mutations, this *RLuc8* has a 4-fold improved light output, compared with the parental enzyme [81]. More recently, the same complementation assay was also used by Casado-Anguera *et al.* (2016) [83] to demonstrate the existence of a therapeutically relevant GPCR dimer, namely the A_{2a}-D₂R dimer. This dimer and its inter-protomer allosteric mechanisms have been proposed as a new model that could contribute to our knowledge concerning drug dosage for the treatment of Parkinson's disease.

Table 3.3 An overview of GPCR-GPCR interactions, shown by luminescence complementation assays.

GPCR dimer	Oligomeric type	PCA type	Split biosensor	Fragments	Negative Control	Cell-type	Year	Ref	<i>Evidence in vivo or native tissue</i>	Ref
CXCR4-CXCR4/CC2	Homodimer	BiLC	FLuc	NLuc-416 and CLuc-398	β_2 -AR	HEK293T	2009	[82]	Yes	[84-86]
CXCR7-CXCR7 CXCR4-CXCR7	Homodimer Heterodimer									
A _{2a} -D ₂ R	heterodimer	BiLC	RLuc8	1-229, 230-311	-	HEK293T	2018	[87]	Yes	[39, 43, 44, 46, 47, 88]
A _{2a} -A _{2a}	homodimer	BiLC	RLuc8	1-229, 230-311	A ₁	HEK293	2016	[40, 83]	-	-
D _{2L} R-D _{2L} R	homodimer	NanoBiT®	NanoLuc	1-11, 12-167	CB ₂	HEK293T	2018/2019	[89, 90]	Yes	[41, 42]

3.2.2.1.2 NanoLuciferase

One of the most recent and undoubtedly the most optimized luminescent PCA so far is the ‘NanoLuciferase Binary Technology’ or NanoBiT[®] system, developed by Promega. The assay is based on complementation of the split fragments of NanoLuciferase or NanoLuc. This engineered luciferase reporter is a small (19 kDa), ATP-independent luminescent protein, originating from a luminous deep-sea shrimp, *Oplophorus gracilirostris* [91]. In combination with the development of a novel cell-permeable imidazopyrazinone substrate, furimazine, this bioluminescence system generates a glow-type luminescent signal that is over 150-fold greater compared to that of the former *Renilla* and Firefly luciferases. NanoLuc exhibits high physical stability, in a wide range of environmental conditions such as temperature, pH, urea and ionic strength [92]. As opposed to luminescent protein fragments described earlier, the NanoBiT[®] subunits do not consist of two fragments similar in size but correspond to a small 1.3 kDa subunit (Small BiT; SmBiT) and an 18 kDa subunit (Large BiT; LgBiT). Both subunits have been thoroughly characterized and have a low affinity ($K_D = 190 \mu\text{M}$) for one another, thus providing the ability to follow kinetics of PPIs.

Although the NanoBiT[®] PCA has only recently been developed [76], its broad applicability has proven successful in numerous research fields. NanoBiT[®] has for instance been applied to develop bio-assays based on the recruitment of β -arrestins [93-99] and G proteins [100] for the detection or activity profiling of certain compounds or to elucidate the molecular interaction between the transducer and a GPCR. For GPCR dimerization purposes, NanoBiT[®] has been implemented to detect ligand-dependent modulation of D_{2L}R-D_{2L}R homodimers [89, 90] (**Table 3.3**). The methodology has also been used to perform live-cell monitoring of the dynamics of the interaction between the Melanocortin 4 receptor (MC4R), and the Melanocortin 2 receptor accessory protein 2 (MRAP2), as well as of MC4R homodimerization [101].

The NanoBiT[®] system has been further optimized into a tri-part protein fragment complementation assay by two independent groups [102, 103]. For this purpose, the LgBiT was dissected into a smaller C-terminal part of 11 amino acids (LcBiT) and an N-terminal derivative (LnBiT), serving as a 'detector' protein of 16.5 kDa, similar to the Tripartite GFP mentioned in 2.1.1. Initially, this assay was designed to facilitate the purification of fusion proteins to procure significant quantities and to avoid the lapse of detection of the PPI of interest due to steric hindrance of LgBiT, due to its higher molecular weight. In addition, another novel split-luciferase reporter based on NanoBiT[®] was developed that implements GFP- and mCherry-recognizing nanobodies fused to LgBiT and SmBiT [104]. Using this experimental set-up, GFP- or mCherry-tagged dimers or higher order oligomers can be detected. As fluorescently tagged proteins are already often in use, this luminescent PCA can be directly used and consequently bypasses the tedious protein recloning to explore the different possible configurations for setting up a PCA (also see section 3.4.1). Furthermore, due to the strong affinity of the GFP- and mCherry-recognizing nanobodies, a low limit of detection of PPIs or protein aggregations, from micromolar up to low nanomolar, can be achieved.

3.2.2.2 BiLC-RET

The application of BiLC has already shown its efficiency in combination with a BRET assay, allowing to detect ternary protein complexes. Sahlholm *et al.* (2018) [87] demonstrated, by combining BiLC of D₂R-A_{2a} heterodimers with a YFP-tagged β -arrestin, that a BRET signal could be obtained. Furthermore, it was postulated that D₂R agonists quinpirole or UNC9994 require the formation of D₂R-A_{2a}R heterodimers, to promote β -arrestin2 recruitment.

3.2.3 Combinatorial assays: BiFC and BiLC

For the detection of higher order oligomerization of GPCRs, a combinatorial assay with both BiFC and BiLC can be implemented (**Table 3.4**). Rebois *et al.* (2008) [60] introduced the concept of detection of a tetravalent complex using a combination of BiFC and BiLC, wherein four β_2 ARs were fused to split parts of Venus or GLuc and the homodimerized β_2 AR-GLuc acted as the donor for the homodimerized β_2 AR-Venus acceptor, the presence of a BRET signal indicating the presence of the tetramer. In the same year (2008), Guo and colleagues [48] showed the existence of a D₂R homo-oligomer, using the same technique.

A complemented donor-acceptor resonance energy transfer (CODA-RET) assay showed that the A_{2A}-D₂R dimer not only forms dimers but can also assemble to form a heterotetramer, composed of two receptor homodimers [40, 83]. For this experimental set-up a complemented YFP was implemented and combined with Rluc8.

Table 3.4 Combinatorial assays with BiFC and BiLC for GPCR oligomerization purposes.

GPCR dimer	Oligomeric type	PCA type	Split biosensor	Fragments	Negative Control	Cell-type	Year	Ref
CXCR4- CXCR4/CC2	Hetero-oligomer with CC2, homotetramer	BiLC and BiFC	<i>RLucII</i> , vYFP	<i>RLucII</i> : 1-330, 331- 936 vYFP: 1-465, 466-720	D ₂ R	HEK293	2014	[53]
A _{2a} -D ₂ R	heterotetramer	BiLC and BiFC	<i>RLuc8</i> , YFP	<i>RLuc8</i> : 1-229, 230- 311 YFP: 1-155, 156-238	A ₁ R, D ₁ R	HEK293	2015/2016	[40, 83]
D ₂₅ R-D ₂₅ R	Homo-oligomer	BiLC and BiFC	<i>RLuc8</i> , mVenus	<i>RLuc8</i> : 1-229, 230- 311 mVenus: 1-155, 156- 240	CD8	HEK283T	2008	[48]
β ₂ AR-β ₂ AR	homotetramer	BiLC and BiFC	<i>GLuc</i> , Venus	<i>GLuc</i> : 1-63, 64-185	<i>GLucN</i> , VN, VC	HEK293	2008	[60]

3.3 Comparison of split protein approaches

Protein complementation techniques have shown their applicability in many fields to unravel PPIs. However, every technique has its advantages and limitations, as summarized in **Table 3.5** for BiFC and BiLC.

Table 3.5 Advantages and disadvantages of BiFC and BiLC techniques.

BiFC	
Advantages	Disadvantages
Straightforward technique	Need for tagged proteins (GPCRs)
High-throughput experiments	Autofluorescence
Imaging microscopy: localization of the interaction	Photobleaching
Study intact cells	Measuring dynamics: limited (maturation time)
	Not applicable for studying inhibition of interactions
BiLC	
Advantages	Disadvantages
Straightforward technique	Need for tagged proteins (GPCRs)
High-throughput experiments	Requires a substrate
Kinetic measurements	Detection of localization: more challenging (cfr. sensitive CCD cameras)
Study intact cells	
<i>In vivo</i> application	

3.3.1 Advantages of PCA

A key advantage of BiFC and BiLC lies in the fact that complementation assays offer a robust and straightforward approach to evaluate PPIs in living cells. Consequently, their applicability in high-throughput experiments is a valuable quality. The development of MBiFC, BiFC-RET or CODA-RET has made the detection of multiple protein-protein interactions feasible, such as GPCR oligomers, without the need for cell lysis or fixation. Due to the simplicity of performing these assays, they can be used as a screening platform for drugs [24]. When used with a plate reader, BiFC and BiLC also offer quantitative and rapid results on relatively large cell populations.

The most valuable aspect of BiLC is that kinetic measurements can be performed due to its sensitivity and the limited propensity of self-association events, at least for certain BiLC reporters (e.g. NanoBiT®). For the purpose of studying GPCR dimerization, the NanoBiT® assay has been compared to related bioluminescence- and fluorescence PCAs, including split Venus and *RLuc* [90]. As a benchmark, the generally accepted D₂R-D₂R dimer was compared in the different PCAs. The NanoBiT® assay presented the best signal-to-noise ratio and was considered the most optimal candidate assay for targeting GPCR dimers. In addition, this method can also be implemented to analyze the kinetics of ligand-dependent modulation of dimerization, broadening its application potential [89]. Even high-throughput screenings can be performed, which is highly relevant, given the growing interest and effort to identify small molecule drugs that can target disease-relevant dimers (or even selectively alter GPCR dimer function). Moreover, BiLC has also proven its applicability in an *in vivo* set-up [69, 71].

On the other hand, BiFC has the capacity to visualize and localize the interaction, also offering insight into potential protein aggregation artefacts inside the cell. BiFC doesn't require any exogenous stains or substrate. Thus, depending on the intrinsic fluorescence, it allows the direct measurement of the interaction between proteins.

3.3.2 Limitations of PCA

BiFC and BiLC also come with their own set of drawbacks. First of all, both techniques require the fusion of the target proteins with split fragments of a fluorescent or luminescent protein, which could affect the original proteins' interaction dynamics. Moreover, the amount of proteins expressed by the cell may potentially cause false positive readouts. Therefore, a good set of negative controls is obligatory (see section 3.4.3). In addition, one should bear in mind that these techniques, though indicating the close proximity of the proteins being studied, are not an actual assessment of the physical contact between these proteins.

BiFC needs longer maturation time, has an irreversible nature of complementation, shows a high degree of self-assembly of the split fragments of the fluorescent protein and requires molecular oxygen for the maturation of the fluorophore, thereby making it unsuitable for obligate anaerobes. Since the maturation is a time-dependent process, the data procured from BiFC is not in real time. The irreversibility of the technique also makes it more difficult to study the dynamics of interactions inside the cell and the influence of drugs on the interaction. Despite these limitations, BiFC is still the only protein complementation technique that gives information about the location of PPIs in living cells. For BiLC, limitations are the need of a substrate and the rather limited possibility to detect the localization of the interaction.

3.4 Guidelines to perform accurate PCA-based assays

A potential but inherent drawback of PCA-based assays is the requirement to fuse fragments derived from fluorescent or luminescent proteins to the GPCR, which inherently may alter the GPCR's function or cellular localization. Therefore, a list of recommendations for proper implementation of PCA-based assays can be put forward: 1) Examine all possible combinations of fusion proteins, 2) Verify the functionality and localization of the fused proteins, 3) Include proper controls, i.e. non-interacting partners, to control for self-assembly, 4) Include a normalization reporter, to allow compensation for differences in transfection efficiencies, 5) Preferentially transfect an amount of DNA near to endogenous expression levels of GPCRs, to avoid false positives due to random collisions or potentially generate stable cell lines and 6) Follow the kinetics of the GPCR interaction (**Figure 3.4**).

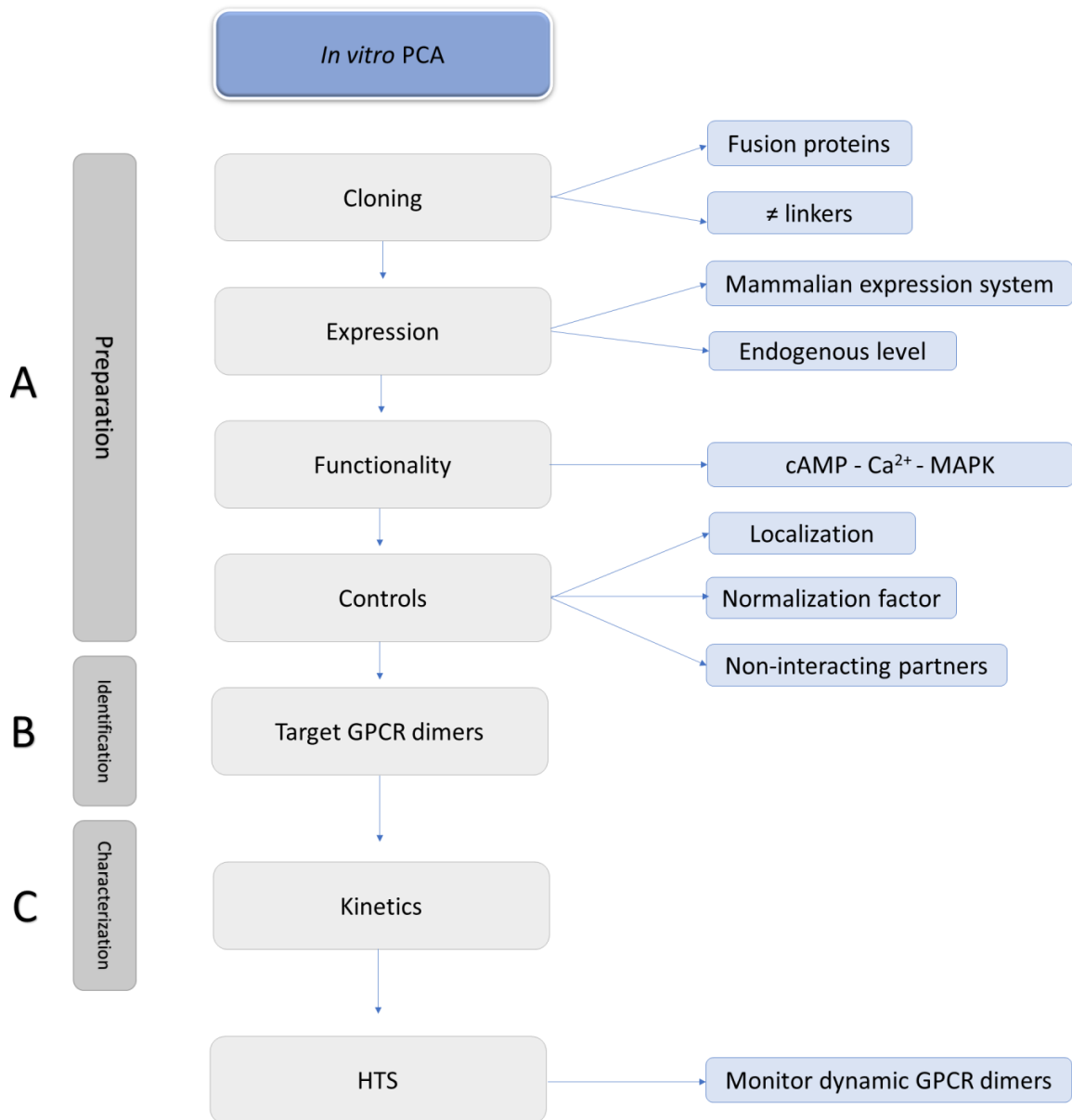


Figure 3.4 A guideline for the set-up of an optimized PCA.

3.4.1 Possible fusions

The development of PCAs requires multiple rounds of cloning, as one needs to design the most optimal 'split' system for each GPCR of interest. Several configurations should be explored, being (i) different reporter systems, (ii) (N- or) C-terminally tagged proteins and (iii) diverse linkers (i.e. length and composition). While this is a time-consuming step, having a certain workload, it is of paramount importance for the development of a robust, sensitive and successful complementation assay.

Selection of the reporter system

A broad variety of fluorescent and luminescent split reporter fragments is available to unravel PPIs. For studying GPCR dimerization, different split reporter systems might be advised, depending on the characteristics of the GPCR dimer of interest (if known). For obligate GPCR dimers, the rules could be less stringent for the choice of the reporter system to be used, whereas for transient GPCR dimers, a dynamic reporter assay with kinetic measurements close to real-time is required. When BiFC is preferred, the truncated YFP fragments YN155 and YC155 are recommended, due to a high signal to noise ratio [105]. Venus, a brighter version of GFP, split at 155 or 173, is also commonly used for studying protein interactions. The benefit of using Venus fragments over YFP is that the complementation can be read at 37°C, thus avoiding the incubation at 30°C which is necessary when dealing with split-YFP. When BiLC is preferred, the NanoBiT® system offers advantages in flexibility and in the low affinity of the SmBiT-LgBiT fragments for each other, so dynamic interactions can be monitored in living cells in real-time [76].

(N- or) C-terminally tagged GPCRs

The site at which the tag is fused to a GPCR plays an important role in the functionality of the GPCR under study and the purpose of the study (**Figure 3.5**). All the published research on PCAs with GPCR dimers involves fusion proteins where the split biosensors are tagged to the C-terminal end of GPCRs, so transport and expression at the membrane surface are not hampered. Especially for monitoring interactions of Class C GPCRs, like the metabotropic glutamate receptors, C-terminal tagging of biosensors is recommended, as modification of the long N-terminus of the receptor could lead to deviating outcomes.

On the other hand, split fragments tagged to the N-termini of GPCRs, though not yet implemented for research on GPCR dimerization, might be an interesting tool as well, as these fusion proteins may enable the simultaneous monitoring of GPCR-GPCR interactions and the signaling properties of the dimer. For example, when a split biosensor is fused to the N-terminus of the GPCRs to monitor the GPCR-GPCR interaction, another split biosensor

fused to the C-terminus of the GPCR can be applied to monitor G protein or β -arrestin recruitment.

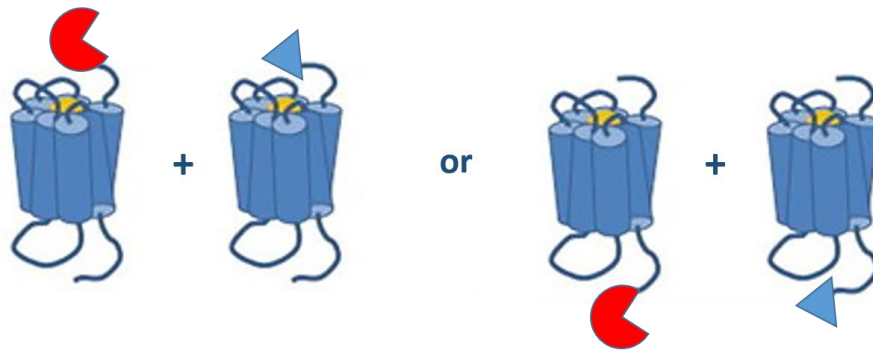


Figure 3.5 N- or C-terminally split biosensor GPCRs.

Linkers

GPCRs of interest and the fragments of the split luminescent or fluorescent partners are usually separated by a linker sequence to assure the flexibility required for the proper folding and ‘settling’ of the biosensor. Multiple linkers with alternating sequences and conformations have been designed, the design of these linkers often being empirical but based on linker sequences derived from natural multi-domain proteins [106].

The most frequently applied linkers in PCAs are composed of non-polar glycine and polar serine amino acids (‘GS’ linker), developed by Argos [107]. The flexibility of these linkers originates from the incorporation of these small residues. Moreover, the use of serine (or threonine) residues in these linkers contributes to the stability in aqueous conditions by the formation of hydrogen bonds with water molecules [108]. A model linker design involves the (GGGS)_n template, where n represents the copy number. By adjusting this copy number, one might obtain the most optimal ‘GS’ linker length to achieve appropriate separation of the GPCR and the split biosensor. For PCA purposes, often utilized GS linkers comprise roughly eight to fifteen amino acids, such as DGGSGGS [109], GGGSGGS [53, 110] or GSSGGGSGGGGSSG [94]. Other -more rigid- linkers have also been implemented in PCA, for example ATGLDLELKASNSAVDGTAGPVAT [87]. The proline residues in linkers might increase stiffness to keep fusion moieties at a distance, whereas lysine residues are often added to improve solubility [108]. Furthermore, proper codon usage (i.e. avoiding rare ones) is advised to not compromise expression levels. Also, depending on the

expression system, sequences which could represent potential protease recognition sites should be avoided.

Overall, the selection of the linker length is crucial to allow proper folding and accomplish optimal biological activity of the fusion proteins. For fusion proteins, the linker length is an essential feature of the PCA set-up since linkers that are too short often result in impaired biological activity due to the inability to accommodate the complementation of the two split proteins, whereas linkers that are too long can create false positives. Therefore, the linker length will vary on a case-by-case basis. With this design in mind, the NanoBiT[®] system offers different restriction sites in the provided biosensor templates, resulting in various GS linkers, ranging from 15 to 21 amino acids [90]. Some examples of linkers that have been applied in PCA assays to detect GPCR dimers are given in **Table 3.6**.

Table 3.6 Linker sequences applied in PCA assays for studying GPCR dimerization.

GPCR dimer	PCA type	Linker	Ref
AT₁-AT₂	BiFC, Venus	GGGSGGGG	[49]
CXCR4-CXCR4	BiLC, Rluc	(GGGS) ₂	[53]
D_{2L}R-D_{2L}R	BiFC, Venus	LG	[48]
D_{2L}R-D_{2L}R A_{2a}-D₂R	BiLC, Rluc	ATGLDLELKASNSAVDGTAGPVAT	[87, 90]
D_{2L}R-D_{2L}R	BiLC, NanoBiT [®]	GNS-GSSGGGGSGGGGSSG	[90]
MOP- NPFF2	BiFC, Venus	DGGSGGGS	[109]

3.4.2 Functionality and localization of the fusion proteins

Occasionally, the fusion of biosensors to a protein of interest (POI) may interfere with the expression level, activity or function of the latter [111, 112]. This may e.g. highly depend on the sequence and length of the linker between the POI and the biosensor (as discussed in section 3.4.1). To verify whether the functional integrity of the fusion POI is not affected, several techniques should ideally be implemented, such as ligand binding as well as functional assays (e.g. calcium signaling, cAMP, β -arrestin recruitment, MAPK activation,

etc.). An immunofluorescence assay can also be used to confirm correct localization of the recombinant proteins at the plasma membrane.

3.4.3 Non-interacting partners

Studying GPCR-GPCR interactions by complementation assays is relatively straightforward. However, the importance of including appropriate controls (i.e. GPCRs that do not bind to the GPCR of interest) should not be underestimated. It is also essential that the split reporter proteins do not spontaneously associate in the absence of binding partners (that normally drive the complementation). If so, a high number of false positives would be generated [90, 113, 114]. Ideally, when the site of interaction is known, a mutation at the specific interaction site of the receptor, is performed to evaluate whether this indeed disrupts the interaction. In those cases where the interaction site is unknown, a screening could be performed to elucidate the perfect non-interacting GPCR partner. Negative controls implemented in already published research articles are shown in **Table 3.2** for the BiFC and in **Table 3.3** for BiLC.

3.4.4 Normalization factor

To allow better comparison between different experimental set-ups, it is advisable to include a normalization factor, i.e. a reporter gene such as a fluorescent marker, as previously described [90, 115]. In a transient expression system, co-transfection of this fluorescent marker, which should not cause cross-excitation, is recommended. A list of PCAs with corresponding fluorescent markers is given in **Table 3.7**. For BiLC in principle, all fluorescent reporters can be used, although it is recommended to avoid cross-excitation by choosing an excitation wavelength more than 20 nm before or after the emission wavelength of the luminescent protein. A potential strategy to cope with alterations in expression levels of the fusion proteins, is the implementation of ratiometric expression systems, consisting of two GPCRs of interest and a fluorescent marker for optical expression control. The so-called ratiometric BiFC (rBiFC) makes it feasible to control the expression through FACS or flow cytometry analysis [115].

Table 3.7 The application of normalization factors. *given as examples

Fluorescence	PCA (excitation/emission)	Fluorescent marker (excitation/emission)
	Venus (515/528)	CFP (433/475)
	mCherry (587/610)	CFP (433/475) / GFP (488/510) / YFP (514/527)
	GFP (488/510)	CFP (433/475)
	Cerulean (452/478)	mTagBFP (402/457)
Luminescence	PCA	Fluorescence marker
	Rluc	CFP (433/475) / mCherry (587/610) *
	Fluc	CFP (433/475) / mCherry (587/610) *
	Nluc	CFP (433/475) / mCherry (587/610) *

3.4.5 Endogenous expression levels

In an arbitrary system, PCAs often involve overexpression of split biosensors since these reporter genes are typically introduced in the cells by transfection. To circumvent excessively high levels of membrane expression, which may ultimately result in random collisions rather than a real interaction, low levels of biosensors should ideally be expressed, preferably close to endogenous expression levels. White *et al.* (2017) [116] have demonstrated that PPIs can be endogenously monitored by BRET when a Nanoluciferase reporter is genetically fused to a natively expressed GPCR of interest by CRISPR/Cas9-mediated homology-directed repair. This methodology also offers the potential to study GPCR-GPCR interactions at endogenous levels.

3.4.6 Kinetics

To follow the dynamics of GPCR interactions in living cells in real-time or to monitor the influence of ligand-dependent modulation on the level of dimerization, one can use a real-time PCA-based method for a certain amount of time. For example, to evaluate the effect of the α -melanocyte-stimulating hormone (α -MSH) on the interaction between MC4R and MRAP2, Habara *et al.* (2018) [101] measured this interaction with a NanoBiT[®]-based PCA for

up to 120 seconds before and after the addition of α -MSH. By doing so, the authors could demonstrate that the stimulation of MC4R with α -MSH slightly decreased the NanoBiT[®] signal, which led to the postulation that the activated structural change of MC4R negatively impacts the interaction with MRAP2. Overall, depending on the half-life of the substrate and the PPI of interest, different timeframes of real-time measurement can be implemented.

3.5 High-throughput screening with cell-based PCAs

High-throughput screening (HTS) assays are powerful ways to assess the influence of ligands that affect the protein complexes, thereby providing a method to measure spatial and temporal changes in the protein association in response to drugs (**Figure 3.6**). This section will focus on the potential use of HTS assays based on BiLC and BiFC for GPCRs.

3.5.1 GPCR oligomerization screening

Given that the protein interaction partners are known, PCAs based on BiLC and BiFC could aid in studying the strength of the interaction compared to a negative control. To find new (unknown) interactions, a screening assay would be handy, in which case the bait protein is fused to a split luminescent/fluorescent fragment and screened against a cDNA library fused to the other half of the reporter fragment. This way, one can identify which GPCRs interact with each other. In conjunction to this is the functional validation of the detected interactions. False readouts can be sidelined upon employment of fusion proteins with mutations at the site of interaction, which consequently inhibit the interaction and decrease the level of complementation of the luminescent or fluorescent fragments. Clearly, this is only feasible if the interaction sites are known, which may be unraveled by alanine screening. For such screening assays, a robust plate reader format would be the best choice.

A non-GPCR example of such a workflow was published by Zych *et al.* in 2013 [117]. These authors established a high-throughput imaging based-screening that was based on the principles of BiFC, with as the aim the study of the dynamics of Vpr (a nonstructural protein encoded by HIV-1) dimerization.

Screening based on BiFC coupled to flow cytometry is a fast way to capture weak interactions and hence, this has been used to screen for mutations that modulate the affinity and specificity of PPIs. For example, in 2013 Morell *et al.* [118] coupled flow cytometry to BiFC to study the weak interaction between the SH3 domain of C-Abl kinase and its natural or mutated binding partners. This combination helps to select for good interacting partners, even if they were deficient in the whole cell population. Hence, this combination has proven to be fast, specific and sensitive and can capture even weak, transient interactions, thus opening up a new dimension in the field of proteomics.

3.5.2 GPCR drug discovery

Since GPCR-GPCR interactions have been implied in several disease patterns, e.g. neurodegenerative disorders, a strong interest in compounds which could interfere with or alter these GPCR-GPCR interactions has arisen. Monitoring these GPCR-GPCR interactions has the potential of unveiling differences in interaction specifics, such as dynamics, as well as identifying potential therapeutic agents.

For an *in vitro* HTS assay, PCAs can be used to screen for compounds that inhibit (BiLC) or enhance (BiLC and BiFC) the PPIs. Upon addition of the modulating compound, the recorded signal changes, depending on its potential to influence the GPCR-GPCR interaction. Counter screens should be implemented to negate the possibility of an artefact, such as compounds which possibly interfere with reporter complementation, show autofluorescence, scatter light, quench luminescence or have toxic side-effects [119-121]. A key advantage of PCA-based approaches is that these include formats using living cells, so GPCR receptors are in their native environment. Overall, this type of HTS strategy would be of great help to further enhance the interest in GPCR drug-discovery research.

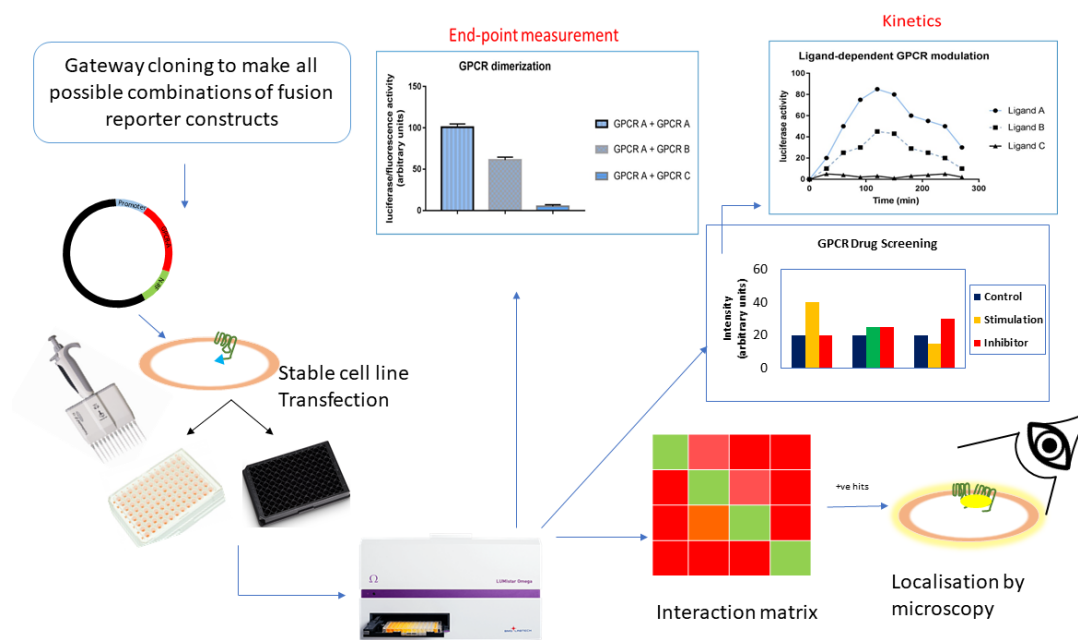


Figure 3.6 High-throughput screening

3.6 *In vivo* application

Besides the potential as HTS assays, in recent years, BiFC and BiLC complementation techniques have also been applied *in vivo*, aiming at a better understanding of the dynamics of homo- or heterodimers in living animals. Several studies established an imaging reporter strategy, which can monitor the specific pharmacological regulation of oligomer complexes.

For GPCR dimerization purposes, Luker *et al.* (2009) [82] applied the FLuc-based PCA (NFLuc-416 and CFLuc-398) to investigate the homo- and heterodimerization of CXCR4 and CXCR7 in a tumor xenograft model of breast cancer. Type 231 cells stably expressing CXCR4-NFLuc and CXCR4-CFLuc or CXCR7-NFLuc and CXCR7-CFLuc were injected bilaterally into 6- to 8-week-old female nude mice. To test whether treatment with chemokine ligands produced time- and dose-dependent changes in reporter signal due to alterations in level of dimerization, fibroblasts stably expressing the chemokine CXCL12 were co-implanted. This chemokine reduced the level of both CXCR4 homodimerization and CXCR4-CXCR7 heterodimerization. Blocking the binding of CXCL12 to CXCR4 resulted in a time-dependent increase in the level of CXCR4 homodimer formation, but no increase in the CXCR4-CXCR7 heterodimerization was detected. In another set-up, mice were injected with 231 cells stably expressing CXCR4 or CXCR7 homodimers and with fibroblasts only transduced with

GFP. After 1 hour of treatment with the CXCR7 modulator CCX754 (100 mg/kg subcutaneous), an increase in CXCR7 homodimer formation, but not CXCR4 homodimer formation, was detected. Overall, it was observed that the chemokine CXCL12 decreased the level of CXCR4 homodimerization and CXCR4-CXCR7 heterodimerization and the CXCR7 modulator CCX754 increased the level of CXCR7 homodimerization. The application of such newly designed drugs that specifically modify the levels of certain dimers could be beneficial in the treatment of not only breast cancer, but also in rheumatoid arthritis, HIV disease, lung and prostate cancers, where these GPCRs play an important role as well.

Rather than trying to bridge the gap between cell culture studies and *in vivo* physiology by the injection of cells stably expressing GPCRs fused to the split biosensors, use of the CRISPR/Cas9 methodology (previously described in section 3.4.5 Endogenous expression levels) to fuse native receptors to split protein fragments would allow the detection of dimerization at endogenous protein levels. This has already successfully been implemented for the β -arrestin2 recruitment to CXCR4 [116], thus could likewise be tested for GPCR dimerization. Most importantly, it has been shown that the bioluminescent reporter is sensitive at all the depths and locations within a live mouse [122], thus making this one of the best platforms to study PPIs as it better mimics a “real-life scenario”.

In the field of fluorescence, Han *et al.* in 2014 [123] applied BiFC based on split fragments of mNeptune, a far-red monomeric Neptune variant (600 nm/650 nm), for *in vivo* applications. The main obstacle of imaging in live animals, being the tissue opacity to excitation light below 600 nm, was overcome by this fluorescent protein. This system was tested by imaging the interaction between bFos and bJun in live mice and could also serve to unravel GPCR-GPCR interactions.

Finally, luminescence- or fluorescence-based systems can be applied to study GPCR oligomerization *in vivo* as these assays allow real-time detection of the interaction and subsequently would help in the screening of pharmacological compounds acting on these oligomers. These noninvasive animal imaging assays, for the quantification of GPCR-GPCR

interactions, might aid in the transformation of treatments targeting specific oligomers (e.g. small molecules or bivalent ligands) from cell-based assays to clinical trials.

3.7 Conclusion

GPCRs are highly dynamic proteins that are subject to multiple spatiotemporal interactions inside the cell to trigger appropriate cellular responses. These interactions involve transducers, kinases as well as other GPCRs, among others [124-126]. While great progress has been made during the past decade in targeting and understanding GPCR-GPCR interactions, some key questions remain unanswered. Although increasing evidence supports the existence of GPCR-GPCR interactions *in vitro* and *in vivo* [127], sophisticated characteristics of these interactions, such as their variation in dynamics, complexity (i.e. dimerization or higher-order oligomerization), binding affinities and the lack of a consensus sequence in the interfaces make GPCR-GPCR interactions a challenging research field. Multiple studies based on PCA techniques have shed new light on the composition, localization and even ligand-induced modulation of these GPCR complexes. Moreover, the potential of these PCA-based methodologies has been further explored by their combination in a variety of ways to investigate not only binary but also ternary or even quaternary partnerships. This chapter described the journey taken by these BiLC- and BiFC-based PCAs and the GPCR-GPCR interactions that have been identified by applying these techniques. PCAs are straightforward and flexible and provide on one hand a convenient approach to visualize the oligomerization processes in living cells or on the other hand an ideal tool to monitor the interaction dynamics. Nevertheless, certain milestones could still be achieved, such as the development of reversible split-fluorescent proteins or the discovery of split-luminescent proteins and their respective substrates that allow enhanced imaging of the GPCR-GPCR interactions. Finally, we anticipate a growing interest in the application of PCA-based high-throughput drug screenings, which makes it possible to identify compounds that selectively modulate the composition of GPCR oligomers in living cells.

References

1. Venter, J.C., et al., *The sequence of the human genome*. Science, 2001. **291**(5507): p. 1304-51.
2. Foord, S.M., et al., *International Union of Pharmacology. XLVI. G protein-coupled receptor list*. Pharmacological reviews, 2005. **57**(2): p. 279-288.
3. Bjarnadottir, T.K., et al., *Comprehensive repertoire and phylogenetic analysis of the G protein-coupled receptors in human and mouse*. Genomics, 2006. **88**(3): p. 263-273.
4. Rondard, P., et al., *Functioning of the dimeric GABA(B) receptor extracellular domain revealed by glycan wedge scanning*. The EMBO journal, 2008. **27**(9): p. 1321-32.
5. Maggio, R. and M.J. Millan, *Dopamine D2-D3 receptor heteromers: pharmacological properties and therapeutic significance*. Current opinion in pharmacology, 2010. **10**(1): p. 100-7.
6. So, C.H., et al., *D1 and D2 dopamine receptors form heterooligomers and cointernalize after selective activation of either receptor*. Molecular pharmacology, 2005. **68**(3): p. 568-78.
7. Petrin, D. and T.E. Hebert, *The functional size of GPCRs - monomers, dimers or tetramers?* Subcellular biochemistry, 2012. **63**: p. 67-81.
8. Van Craenenbroeck, K., *GPCR oligomerization: contribution to receptor biogenesis*. Sub-cellular biochemistry, 2012. **63**: p. 43-65.
9. Ward, R.J., et al., *Regulation of oligomeric organization of the serotonin 5-hydroxytryptamine 2C (5-HT2C) receptor observed by spatial intensity distribution analysis*. Journal of biological chemistry, 2015. **290**(20): p. 12844-57.
10. Ward, R.J., et al., *Spatial intensity distribution analysis quantifies the extent and regulation of homodimerization of the secretin receptor*. Biochemical journal, 2017. **474**(11): p. 1879-1895.
11. Pediani, J.D., et al., *Dynamic Regulation of Quaternary Organization of the M1 Muscarinic Receptor by Subtype-selective Antagonist Drugs*. Journal of biological chemistry, 2016. **291**(25): p. 13132-46.
12. Pediani, J.D., et al., *Spatial Intensity Distribution Analysis: Studies of G Protein-Coupled Receptor Oligomerisation*. Trends in pharmacological sciences, 2018. **39**(2): p. 175-186.
13. Marsango, S., et al., *A Molecular Basis for Selective Antagonist Destabilization of Dopamine D3 Receptor Quaternary Organization*. Science reports, 2017. **7**(1): p. 2134.
14. Kasai, R.S., et al., *The Class-A GPCR Dopamine D2 Receptor Forms Transient Dimers Stabilized by Agonists: Detection by Single-Molecule Tracking*. Cell biochemistry and biophysics, 2018. **76**(1-2): p. 29-37.
15. Wehr, M.C. and M.J. Rossner, *Split protein biosensor assays in molecular pharmacological studies*. Drug discovery today, 2016. **21**(3): p. 415-429.
16. Ghosh, I., A.D. Hamilton, and L. Regan, *Antiparallel leucine zipper-directed protein reassembly: Application to the green fluorescent protein*. Journal of the American chemical society, 2000. **122**(23): p. 5658-5659.
17. Hu, C.D., Y. Chinenov, and T.K. Kerppola, *Visualization of interactions among bZip and Rel family proteins in living cells using bimolecular fluorescence complementation*. Molecular cell, 2002. **9**(4): p. 789-798.

18. Shyu, Y.J., et al., *Identification of new fluorescent protein fragments for bimolecular fluorescence complementation analysis under physiological conditions*. Biotechniques, 2006. **40**(1): p. 61-66.
19. Cevheroglu, O., et al., *The yeast Ste2p G protein-coupled receptor dimerizes on the cell plasma membrane*. Biochimica et biophysica acta-biomembranes, 2017. **1859**(5): p. 698-711.
20. Cabantous, S., et al., *A new protein-protein interaction sensor based on tripartite split-GFP association*. Scientific reports, 2013. **3**: p. 2854.
21. Nagai, T., et al., *Circularly permuted green fluorescent proteins engineered to sense Ca²⁺*. Proceedings of the national academy of sciences of the United States of America, 2001. **98**(6): p. 3197-202.
22. Griesbeck, O., et al., *Reducing the environmental sensitivity of yellow fluorescent protein. Mechanism and applications*. The Journal of biological chemistry, 2001. **276**(31): p. 29188-94.
23. Nagai, T., et al., *A variant of yellow fluorescent protein with fast and efficient maturation for cell-biological applications*. Nature biotechnology, 2002. **20**(1): p. 87-90.
24. Vidi, P.A., et al., *Ligand-dependent oligomerization of dopamine D(2) and adenosine A(2A) receptors in living neuronal cells*. Molecular pharmacology, 2008. **74**(3): p. 544-51.
25. Vidi, P.-A., et al., *Adenosine A2A receptors assemble into higher-order oligomers at the plasma membrane*. FEBS Letters, 2008. **582**(29): p. 3985-3990.
26. Kilpatrick, L.E., L.J. Humphrys, and N.D. Holliday, *A G protein-coupled receptor dimer imaging assay reveals selectively modified pharmacology of neuropeptide Y Y1/Y5 receptor heterodimers*. Molecular pharmacology, 2015. **87**(4): p. 718-32.
27. Przybyla, J.A. and V.J. Watts, *Ligand-induced regulation and localization of cannabinoid CB1 and dopamine D2L receptor heterodimers*. Journal of pharmacology and experimental therapeutics, 2010. **332**(3): p. 710-9.
28. Ang, Z., et al., *FFAR2-FFAR3 receptor heteromerization modulates short-chain fatty acid sensing*. FASEB journal, 2018. **32**(1): p. 289-303.
29. Xue, Q., et al., *Ghrelin Through GHSR1a and OX1R Heterodimers Reveals a Gα_s-cAMP-cAMP Response Element Binding Protein Signaling Pathway in Vitro*. Frontiers in molecular neuroscience, 2018. **11**: p. 245.
30. Navarro, G., et al., *Cross-communication between Gi and Gs in a G-protein-coupled receptor heterotetramer guided by a receptor C-terminal domain*. BMC biology, 2018. **16**(1): p. 24.
31. Hinz, S., et al., *Adenosine A2A receptor ligand recognition and signaling is blocked by A2B receptors*. Oncotarget, 2018. **9**(17): p. 13593-13611.
32. Song, D. and Y. Jung, *Homo-molecular Fluorescence Complementation for Direct Visualization of Receptor Oligomerization in Living Cells*. Angewandte Chemie, 2019. **58**(7): p. 2045-2049.
33. Vidi, P.A., B.R. Chemel, and V.J. Watts, *Direct visualization of adenosine A(2A) and dopamine D-2L receptor oligomers in a neuronal cell model*. FASEB journal, 2008. **22**.
34. Baird, G.S., D.A. Zacharias, and R.Y. Tsien, *Biochemistry, mutagenesis, and oligomerization of DsRed, a red fluorescent protein from coral*. Proceedings of the national academy of sciences of the United States of America, 2000. **97**(22): p. 11984-9.

35. Fan, J.Y., et al., *Split mCherry as a new red bimolecular fluorescence complementation system for visualizing protein-protein interactions in living cells*. Biochemical and biophysical research communications, 2008. **367**(1): p. 47-53.
36. Jach, G., et al., *An improved mRFP1 adds red to bimolecular fluorescence complementation*. Nature methods, 2006. **3**(8): p. 597-600.
37. Shcherbo, D., et al., *Bright far-red fluorescent protein for whole-body imaging*. Nature methods, 2007. **4**(9): p. 741-6.
38. Chu, J., et al., *A novel far-red bimolecular fluorescence complementation system that allows for efficient visualization of protein interactions under physiological conditions*. Biosensors & bioelectronics, 2009. **25**(1): p. 234-9.
39. Cabello, N., et al., *Metabotropic glutamate type 5, dopamine D2 and adenosine A2a receptors form higher-order oligomers in living cells*. Journal of neurochemistry, 2009. **109**(5): p. 1497-507.
40. Bonaventura, J., et al., *Allosteric interactions between agonists and antagonists within the adenosine A2A receptor-dopamine D2 receptor heterotetramer*. Proceedings of the national academy of sciences of the United States of America, 2015. **112**(27): p. E3609-18.
41. Wang, M., et al., *Schizophrenia, amphetamine-induced sensitized state and acute amphetamine exposure all show a common alteration: increased dopamine D2 receptor dimerization*. Molecular brain, 2010. **3**.
42. Zawarynski, P., et al., *Dopamine D2 receptor dimers in human and rat brain*. FEBS letters, 1998. **441**(3): p. 383-386.
43. Bonaventura, J., et al., *Allosteric interactions between agonists and antagonists within the adenosine A2A receptor-dopamine D2 receptor heterotetramer*. Proceedings of the national academy of sciences of the United States of America, 2015. **112**(27): p. E3609-18.
44. Fink, J.S., et al., *Molecular-Cloning of the Rat Adenosine-A2 Receptor - Selective Coexpression with D2-Dopamine Receptors in Rat Striatum*. Molecular brain research, 1992. **14**(3): p. 186-195.
45. Fuxe, K., et al., *Adenosine A(2A) and dopamine D-2 heteromeric receptor complexes and their function*. Journal of molecular neuroscience, 2005. **26**(2-3): p. 209-219.
46. Hillion, J., et al., *Coaggregation, cointernalization, and codesensitization of adenosine A(2A) receptors and dopamine D-2 receptors*. Journal of biological chemistry, 2002. **277**(20): p. 18091-18097.
47. Soriano, A., et al., *Adenosine A(2A) Receptor-Antagonist/Dopamine D-2 Receptor-Agonist Bivalent Ligands as Pharmacological Tools to Detect A(2A)-D-2 Receptor Heteromers*. Journal of medicinal chemistry, 2009. **52**(18): p. 5590-5602.
48. Guo, W., et al., *Dopamine D2 receptors form higher order oligomers at physiological expression levels*. The EMBO journal, 2008. **27**(17): p. 2293-304.
49. Porrello, E.R., et al., *Heteromerization of angiotensin receptors changes trafficking and arrestin recruitment profiles*. Cellular signalling, 2011. **23**(11): p. 1767-76.
50. Riggleman, A., J. Harvey, and C. Baylis, *Endothelin mediates some of the renal actions of acutely administered angiotensin II*. Hypertension, 2001. **38**(1): p. 105-109.
51. Zeng, C.Y., et al., *Altered AT(1) receptor regulation of ETB receptors in renal proximal tubule cells of spontaneously hypertensive rats*. Hypertension, 2005. **46**(4): p. 926-931.

52. Zeng, C.Y., et al., *Aberrant ETB receptor regulation of AT(1) receptors in immortalized renal proximal tubule cells of spontaneously hypertensive rats*. *Kidney international*, 2005. **68**(2): p. 623-631.
53. Armando, S., et al., *The chemokine CXCL4 and CXCR2 receptors form homo- and heterooligomers that can engage their signaling G-protein effectors and betaarrestin*. *The FASEB journal*, 2014. **28**(10): p. 4509-23.
54. Ciruela, F., et al., *Presynaptic control of striatal glutamatergic neurotransmission by adenosine A(1)-A(2A) receptor heteromers*. *Journal of neuroscience*, 2006. **26**(7): p. 2080-2087.
55. Moreno, J.L., et al., *Allosteric signaling through an mGlu2 and 5-HT2A heteromeric receptor complex and its potential contribution to schizophrenia*. *Science signaling*, 2016. **9**(410).
56. Lopez-Gimenez, J.F., et al., *The alpha(1b)-adrenoceptor exists as a higher-order oligomer: Effective oligomerization is required for receptor maturation, surface delivery, and function*. *Molecular pharmacology*, 2007. **71**(4): p. 1015-1029.
57. Hu, C.D. and T.K. Kerppola, *Simultaneous visualization of multiple protein interactions in living cells using multicolor fluorescence complementation analysis*. *Nature biotechnology*, 2003. **21**(5): p. 539-45.
58. Vidi, P.A., et al., *Visualization of G protein-coupled receptor (GPCR) interactions in living cells using bimolecular fluorescence complementation (BiFC)*. *Current protocols in neuroscience*, 2010. **Chapter 5**: p. Unit 5 29.
59. Vidi, P.A. and V.J. Watts, *Fluorescent and bioluminescent protein-fragment complementation assays in the study of G protein-coupled receptor oligomerization and signaling*. *Molecular pharmacology*, 2009. **75**(4): p. 733-9.
60. Rebois, R.V., et al., *Combining protein complementation assays with resonance energy transfer to detect multipartner protein complexes in living cells*. *Methods*, 2008. **45**(3): p. 214-8.
61. Navarro, G., et al., *Detection of heteromers formed by cannabinoid CB1, dopamine D2, and adenosine A2A G-protein-coupled receptors by combining bimolecular fluorescence complementation and bioluminescence energy transfer*. *TheScientificWorldJournal*, 2008. **8**: p. 1088-97.
62. Shyu, Y.J., C.D. Suarez, and C.D. Hu, *Visualization of AP-1 NF-kappaB ternary complexes in living cells by using a BiFC-based FRET*. *Proceedings of the national academy of sciences of the United States of America*, 2008. **105**(1): p. 151-6.
63. Vidi, P.A., et al., *Adenosine A(2A) receptors assemble into higher-order oligomers at the plasma membrane*. *FEBS letters*, 2008. **582**(29): p. 3985-90.
64. Bagher, A.M., et al., *Bidirectional allosteric interactions between cannabinoid receptor 1 (CB1) and dopamine receptor 2 long (D2L) heterotetramers*. *European journal of pharmacology*, 2017. **813**: p. 66-83.
65. Spencer, D.M., et al., *Controlling Signal-Transduction with Synthetic Ligands*. *Science*, 1993. **262**(5136): p. 1019-1024.
66. Cao, X., et al., *Blockade of cannabinoid type 1 receptors augments the antiparkinsonian action of levodopa without affecting dyskinesias in 1-methyl-4-phenyl-1,2,3,6-tetrahydropyridine-treated rhesus monkeys*. *The Journal of pharmacology and experimental therapeutics*, 2007. **323**(1): p. 318-26.

67. Fan, F. and K.V. Wood, *Bioluminescent assays for high-throughput screening*. Assay Drug development technology, 2007. **5**(1): p. 127-36.
68. Luker, K.E., et al., *Kinetics of regulated protein-protein interactions revealed with firefly luciferase complementation imaging in cells and living animals*. Proceedings of the national academy of sciences of the United States of America, 2004. **101**(33): p. 12288-93.
69. Paulmurugan, R., Y. Umezawa, and S.S. Gambhir, *Noninvasive imaging of protein-protein interactions in living subjects by using reporter protein complementation and reconstitution strategies*. Proceedings of the national academy of sciences of the United States of America, 2002. **99**(24): p. 15608-13.
70. Paulmurugan, R. and S.S. Gambhir, *Monitoring protein-protein interactions using split synthetic renilla luciferase protein-fragment-assisted complementation*. Analytical chemistry, 2003. **75**(7): p. 1584-9.
71. Paulmurugan, R., et al., *Molecular imaging of drug-modulated protein-protein interactions in living subjects*. Cancer research, 2004. **64**(6): p. 2113-9.
72. Remy, I. and S.W. Michnick, *A highly sensitive protein-protein interaction assay based on Gaussia luciferase*. Nat Methods, 2006. **3**(12): p. 977-9.
73. Bodle, C.R., et al., *Development of a bimolecular luminescence complementation assay for RGS: G protein interactions in cells*. Analytical biochemistry, 2017. **522**: p. 10-17.
74. Oh-Hashi, K., Y. Hirata, and K. Kiuchi, *SOD1 dimerization monitoring using a novel split NanoLuc, NanoBit*. Cell biochemistry and function, 2016. **34**(7): p. 497-504.
75. Verhoef, L.G., et al., *Multiplex detection of protein-protein interactions using a next generation luciferase reporter*. Biochimica et biophysica acta, 2016. **1863**(2): p. 284-92.
76. Dixon, A.S., et al., *NanoLuc Complementation Reporter Optimized for Accurate Measurement of Protein Interactions in Cells*. ACS chemical biology, 2016. **11**(2): p. 400-8.
77. Galarneau, A., et al., *beta-Lactamase protein fragment complementation assays as in vivo and in vitro sensors of protein-protein interactions*. Nature biotechnology, 2002. **20**(6): p. 619-622.
78. Paulmurugan, R. and S.S. Gambhir, *Novel fusion protein approach for efficient high-throughput screening of small molecule-mediating protein-protein interactions in cells and living animals*. Cancer research, 2005. **65**(16): p. 7413-7420.
79. Matthews, J.C., K. Hori, and M.J. Cormier, *Substrate and substrate analogue binding properties of Renilla luciferase*. Biochemistry, 1977. **16**(24): p. 5217-20.
80. Matthews, J.C., K. Hori, and M.J. Cormier, *Purification and properties of Renilla reniformis luciferase*. Biochemistry, 1977. **16**(1): p. 85-91.
81. Loening, A.M., et al., *Consensus guided mutagenesis of Renilla luciferase yields enhanced stability and light output*. Protein engineering, design and selection, 2006. **19**(9): p. 391-400.
82. Luker, K.E., M. Gupta, and G.D. Luker, *Imaging chemokine receptor dimerization with firefly luciferase complementation*. The FASEB journal, 2009. **23**(3): p. 823-34.
83. Casado-Anguera, V., et al., *Evidence for the heterotetrameric structure of the adenosine A2A-dopamine D2 receptor complex*. Biochemical society transactions, 2016. **44**(2): p. 595-600.
84. Rodriguez-Frade, J.M., et al., *Blocking HIV-1 infection via CCR5 and CXCR4 receptors by acting in trans on the CCR2 chemokine receptor*. EMBO journal, 2004. **23**(1): p. 66-76.

85. Sohy, D., M. Parmentier, and J.Y. Springael, *Allosteric transinhibition by specific antagonists in CCR2/CXCR4 heterodimers*. Journal of biological chemistry, 2007. **282**(41): p. 30062-30069.
86. Sohy, D., et al., *Hetero-oligomerization of CCR2, CCR5, and CXCR4 and the Protean Effects of "Selective" Antagonists*. Journal of biological chemistry, 2009. **284**(45): p. 31270-31279.
87. Sahlholm, K., et al., *Antipsychotic-Like Efficacy of Dopamine D2 Receptor-Biased Ligands is Dependent on Adenosine A2A Receptor Expression*. Molecular neurobiology, 2018. **55**(6): p. 4952-4958.
88. Fuxe, K., et al., *Receptor–receptor interactions within receptor mosaics. Impact on neuropsychopharmacology*. Brain research reviews, 2008. **58**(2): p. 415-452.
89. Wouters, E., et al., *Distinct Dopamine D(2) Receptor Antagonists Differentially Impact D(2) Receptor Oligomerization*. International journal of molecular sciences, 2019. **20**(7).
90. Wouters, E., et al., *Assessing GPCR Dimerization in Living Cells: Comparison of the NanoBiT Assay with Related Bioluminescence- and Fluorescence-Based Approaches*, in *Receptor-Receptor Interactions in the Central Nervous System*, K. Fuxe and D.O. Borroto-Escuela, Editors. 2018, Springer New York: New York, NY. p. 239-250.
91. Hall, M.P., et al., *Engineered luciferase reporter from a deep sea shrimp utilizing a novel imidazopyrazinone substrate*. ACS chemical biology, 2012. **7**(11): p. 1848-57.
92. England, C.G., E.B. Ehlerding, and W. Cai, *NanoLuc: A Small Luciferase Is Brightening Up the Field of Bioluminescence*. Bioconjugate chemistry, 2016. **27**(5): p. 1175-1187.
93. Cannaert, A., et al., *Activity-Based Detection of Consumption of Synthetic Cannabinoids in Authentic Urine Samples Using a Stable Cannabinoid Reporter System*. Analytical chemistry, 2017. **89**(17): p. 9527-9536.
94. Cannaert, A., et al., *Detection and Activity Profiling of Synthetic Cannabinoids and Their Metabolites with a Newly Developed Bioassay*. Analytical chemistry, 2016. **88**(23): p. 11476-11485.
95. Dupuis, N., et al., *Activation of the Orphan G Protein-Coupled Receptor GPR27 by Surrogate Ligands Promotes beta-Arrestin 2 Recruitment*. Molecular pharmacology, 2017. **91**(6): p. 595-608.
96. Noble, C., et al., *Application of an activity-based receptor bioassay to investigate the in vitro activity of selected indole- and indazole-3-carboxamide-based synthetic cannabinoids at CB1 and CB2 receptors*. Drug testing and analysis, 2019. **11**(3): p. 501-511.
97. Storme, J., et al., *Molecular dissection of the human A3 adenosine receptor coupling with beta-arrestin2*. Biochemical pharmacology, 2018. **148**: p. 298-307.
98. Wouters, E., et al., *Functional evaluation of carboxy metabolites of synthetic cannabinoid receptor agonists featuring scaffolds based on L-valine or L-tert-leucine*. Drug testing and analysis, 2019.
99. Cannaert, A., et al., *Activity-Based Concept to Screen Biological Matrices for Opiates and (Synthetic) Opioids*. Clinical chemistry, 2018. **64**(8): p. 1221-1229.
100. Laschet, C., N. Dupuis, and J. Hanson, *A dynamic and screening-compatible nanoluciferase-based complementation assay enables profiling of individual GPCR-G protein interactions*. The Journal of biological chemistry, 2018.

101. Habara, M., et al., *Molecular characterization of feline melanocortin 4 receptor and melanocortin 2 receptor accessory protein 2*. General and comparative endocrinology, 2018. **261**: p. 31-39.
102. Dixon, A.S., et al., *A Tri-part Protein Complementation System Using Antibody-Small Peptide Fusions Enables Homogeneous Immunoassays*. Scientific reports, 2017. **7**.
103. Ohmuro-Matsuyama, Y. and H. Ueda, *Homogeneous Noncompetitive Luminescent Immunodetection of Small Molecules by Ternary Protein Fragment Complementation*. Analytical chemistry, 2018. **90**(5): p. 3001-3004.
104. Moustaqil, M., et al., *A Split-Luciferase Reporter Recognizing GFP and mCherry Tags to Facilitate Studies of Protein-Protein Interactions*. International journal of molecular sciences, 2017. **18**(12).
105. Kerppola, T.K., *Design and implementation of bimolecular fluorescence complementation (BiFC) assays for the visualization of protein interactions in living cells*. Nature protocols, 2006. **1**(3): p. 1278-86.
106. Gokhale, R.S. and C. Khosla, *Role of linkers in communication between protein modules*. Current opinion in chemical biology, 2000. **4**(1): p. 22-27.
107. Argos, P., *An investigation of oligopeptides linking domains in protein tertiary structures and possible candidates for general gene fusion*. Journal of molecular biology, 1990. **211**(4): p. 943-58.
108. Chen, X., J.L. Zaro, and W.C. Shen, *Fusion protein linkers: property, design and functionality*. Advanced drug delivery reviews, 2013. **65**(10): p. 1357-69.
109. Carayon, K., et al., *Heterologous regulation of Mu-opioid (MOP) receptor mobility in the membrane of SH-SY5Y cells*. The Journal of biological chemistry, 2014. **289**(41): p. 28697-706.
110. Stefan, E., et al., *Quantification of dynamic protein complexes using Renilla luciferase fragment complementation applied to protein kinase A activities in vivo*. Proceedings of the national academy of sciences of the United States of America, 2007. **104**(43): p. 16916-21.
111. Lalonde, S., et al., *Fusion to GFP blocks intercellular trafficking of the sucrose transporter SUT1 leading to accumulation in companion cells*. BMC plant biology, 2003. **3**: p. 8.
112. Meyer, E. and P. Fromherz, *Ca²⁺ activation of hSlo K⁺ channel is suppressed by N-terminal GFP tag*. The European journal of neuroscience, 1999. **11**(3): p. 1105-8.
113. Cabantous, S., T.C. Terwilliger, and G.S. Waldo, *Protein tagging and detection with engineered self-assembling fragments of green fluorescent protein*. Nature biotechnology, 2005. **23**(1): p. 102-7.
114. Morell, M., S. Ventura, and F.X. Aviles, *Protein complementation assays: approaches for the in vivo analysis of protein interactions*. FEBS letters, 2009. **583**(11): p. 1684-91.
115. Grefen, C. and M.R. Blatt, *A 2in1 cloning system enables ratiometric bimolecular fluorescence complementation (rBiFC)*. BioTechniques, 2012. **53**(5): p. 311-14.
116. White, C.W., et al., *Using nanoBRET and CRISPR/Cas9 to monitor proximity to a genome-edited protein in real-time*. Scientific reports, 2017. **7**(1): p. 3187.
117. Zych, C., A. Domling, and V. Ayyavoo, *Development of a robust cell-based high-throughput screening assay to identify targets of HIV-1 viral protein R dimerization*. Drug design, development and therapy, 2013. **7**: p. 403-12.

118. Morell, M., et al., *Detection of transient protein-protein interactions by bimolecular fluorescence complementation: The Abl-SH3 case*. Proteomics, 2007. **7**(7): p. 1023-1036.
119. Auld, D.S. and J. Inglese, *Interferences with luciferase reporter enzymes*, in *Assay guidance manual*, G.S. Sittampalam, et al., Editors. 2004: Bethesda (MD).
120. Simeonov, A. and M.I. Davis, *Interference with fluorescence and absorbance*, in *assay guidance manual*, G.S. Sittampalam, et al., Editors. 2004: Bethesda (MD).
121. Wade, M., et al., *Inhibition of protein-protein interactions: cell-based assays*, in *Assay guidance manual*, G.S. Sittampalam, et al., Editors. 2017: Bethesda (MD).
122. Wu, J.C., et al., *Noninvasive optical imaging of firefly luciferase reporter gene expression in skeletal muscles of living mice*. Molecular therapy, 2001. **4**(4): p. 297-306.
123. Han, Y., et al., *In vivo imaging of protein-protein and RNA-protein interactions using novel far-red fluorescence complementation systems*. Nucleic acids research, 2014. **42**(13).
124. Faron-Gorecka, A., et al., *Understanding GPCR dimerization*. Methods in cell biology, 2019. **149**: p. 155-178.
125. Maurice, P., et al., *GPCR-interacting proteins, major players of GPCR function*. Advances in pharmacology, 2011. **62**: p. 349-80.
126. Milligan, G., R.J. Ward, and S. Marsango, *GPCR homo-oligomerization*. Current opinion in cell biology, 2018. **57**: p. 40-47.
127. Gomes, I., et al., *G Protein-Coupled Receptor Heteromers*. Annual review of pharmacology and toxicology, 2016. **56**: p. 403-25.

Chapter 4:

Assessing D₂R dimerization in living cells: comparison of the NanoBiT® assay with related bioluminescence- and fluorescence-based approaches.

Based on

Elise Wouters, Lakshmi Vasudevan, Fransisco Ciruela, Deepak Saini, Christophe Stove, Kathleen Van Craenenbroeck. (2018) Assessing GPCR Dimerization in Living Cells: Comparison of the NanoBiT Assay with Related Bioluminescence- and Fluorescence-Based Approaches. In: FUXE K., Borroto-Escuela D. (eds) Receptor-Receptor Interactions in the Central Nervous System. Neuromethods, vol 140. Humana Press, New York, NY

ABSTRACT

G protein-coupled receptors (GPCRs) modulate cellular signaling pathways, including differentiation, proliferation, hormonal regulation and neuronal activity. Therefore, it is not surprising that one third of the drugs available in the pharmaceutical market target GPCRs. Recently, an emerging body of evidence has proven the formation of GPCR dimers and even higher order oligomers. For neurodegenerative diseases, such as Parkinson's or Alzheimer's disease, it is crucial to characterize these receptor-receptor interactions in the brain to elucidate their role in neuronal disease-relevant processes. As a first step, a robust *in cellulo* assay is essential to identify and characterize specific GPCR-GPCR interactions. In the past 20 years, considerable efforts have been directed towards the development of GPCR dimerization screening assays to evaluate these receptor-receptor interactions in living cells. Interestingly, most of the approaches employ noninvasive fluorescence- and luminescence-based assays. Here, we present an efficient strategy to study GPCR dimerization dynamics, namely a protein complementation assay (PCA) based on the reconstitution of a luminescent protein, the NanoLuciferase (NL). Thus, GPCRs of interest are fused to complementary NL fragments which upon GPCR dimerization may reconstitute to a functional reporter, of which activity can be measured. The experimental procedure takes 2-4 days to complete, depending on the cell type and complexity of the experimental setup. In contrast to alternative protein complementation assays (also described in this Chapter), this method can also be implemented to analyze the kinetics of ligand-dependent modulation of dimerization, broadening its application potential. Additionally, high throughput screenings can also be performed, which is highly relevant given the growing interest and effort to identify small molecule drugs that can target disease-relevant dimers (or even selectively alter GPCR dimer function).

4.1 Introduction

G protein-coupled receptor (GPCR) dimers and/or oligomers have been studied intensively with protein complementation assays (PCAs), of which bimolecular fluorescence and luminescence complementation (BiFC and BiLC, respectively) assays have been applied most. As discussed in **Chapter 3**, several fluorescent proteins have been successfully optimized and applied in BiFC assays, such as GFP, YFP, Venus and mCherry [1]. On the other hand, BiLC uses a split version of a luminescent protein, like *Renilla* or Firefly luciferase (RLuc or FLuc, respectively) or Nanoluciferase (NL). The latter forms the core of one of the more recently optimized luminescence complementation assays, namely the ‘NanoLuciferase Binary Technology’ or NanoBiT[®], commercialized by Promega (**Figure 4.1**) [2-4].

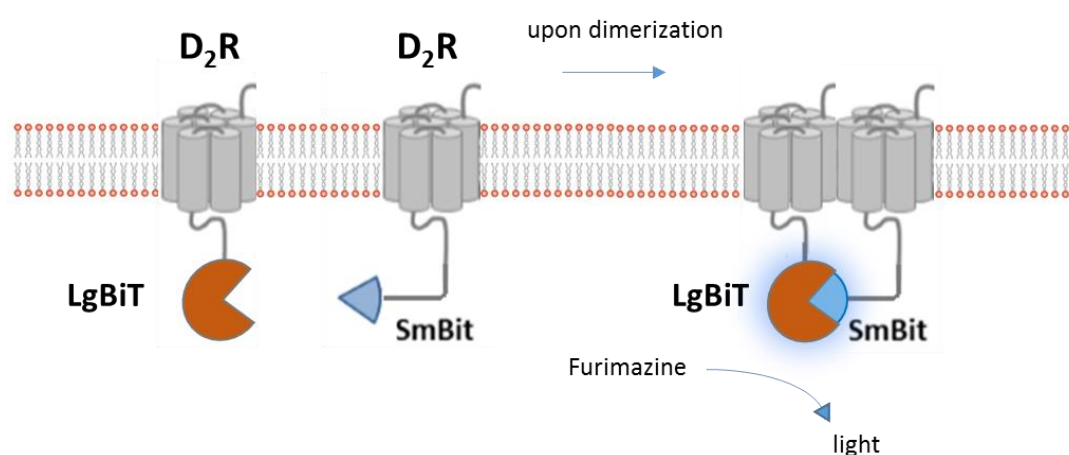


Figure 4.1 Schematic representation of the NanoBiT[®] system. Candidate GPCRs (i.e. D₂R) are fused to SmBiT or LgBiT. Upon GPCR dimerization, the NanoBiT[®] fragments come into close proximity, resulting in NL reconstitution, which can convert the furimazine substrate, leading to the emission of light.

In **Chapter 3**, it has been highlighted that whatever PCA (i.e. BiFC and BiLC) is used to demonstrate the interaction of interest, adequate controls are essential to avoid false positives. In this Chapter, which is somewhat distinct from the other Chapters in this thesis, we provide a practical (‘hands-on’) guideline for the implementation of distinct PCAs based on split biosensors of Venus, *Renilla* luciferase, and NanoLuciferase (see **Table 4.1**) to study homo-dimerization of a prototypical GPCR, the dopamine D₂ receptor (D₂R). In addition, this Chapter aims at providing a direct comparison of the most commonly used/newest PCAs to unravel the PCA with the best signal-to-noise ratio. These findings served as a basis for further research on D₂R homodimerization (see **Chapter 5**).

Table 4.1 Overview of the fluorescent and luminescent proteins, that were compared within this study.

Reporter protein	Readout	Signal-to-noise ratio	Sensor size (kDa)
<i>Renilla</i> luciferase	Luminescence	Low	36
Venus	Fluorescence	Low	27
NanoBiT®	Luminescence	High	19

4.2 Materials

4.2.1 Plasmids

1. GPCR-VN and GPCR-VC plasmids. The fluorescent protein Venus is split in two fragments, namely the N-terminal part (VN155 (aa 1-154)) and the C-terminal part (VC155 (aa 155-238)) (see **Note 1**). The candidate GPCR can be cloned into the backbones, N-terminally of VN or VC, with a short linker between the receptor and the split fragment of Venus, normally a leucine and glutamate residue. The expression of the genes is driven by a CMV promoter. The addition of a VN control plasmid is optional but strongly recommended (see **Note 2**).
2. GPCR-RLuc1 and GPCR-RLuc2 plasmids. For the expression of a candidate GPCR fused to a split fragment of *Renilla* luciferase, the *RLuc1* (aa 1-229) and *RLuc2* (aa 230-311) constructs can be used as backbone plasmids. The linker between the receptor and *RLuc1/RLuc2* consists of 24 amino-acids (ATGLDLELKASNSAVDGTAGPVAT). The expression is driven by a CMV promoter. The addition of *RLuc1* control plasmid is optional but strongly recommended (see **Note 2**).
3. GPCR-LgBiT and GPCR-SmBiT plasmids. The NanoBiT® constructs (Promega) express the small (SmBiT) or large (LgBiT) fragment of the NL, wherein the candidate GPCR can be cloned N-terminally of (preferably both) NL fragments (see **Note 3**). Furthermore, a flexible GS linker of 15-21 amino acids (see **Note 4**) between the receptor and the fragment of the NL is present. These constructs contain a HSV-TK promoter, which is not a very strong promoter and thereby limits overexpression.

4. Plasmids constitutively expressing yellow fluorescent protein (i.e. YFP or Venus) or cyan fluorescent protein (CFP).

4.2.2 Cells

1. Human embryonic kidney 293T (HEK-293T) cells or any other cell line that can give a high transfection efficiency and easily drives the expression of chimeric GPCRs. Although not always possible, it is good to use a cell line which does not show endogenous expression of GPCRs which can interfere with the dimerization assay.

4.3 Reagents

1. Dulbecco's Modified Eagle's Medium (DMEM) supplemented with GlutaMAX supplemented with 10% heat inactivated fetal bovine serum (FBS), 100 mg/ml streptomycin and 100 IU/l penicillin. Serum free medium as well as 2% FBS DMEM medium will also be required. The medium depends on the cell line used.
2. Hank's Balanced Salt Solution (HBSS).
3. Phosphate Buffered Saline (PBS).
4. Transient mammalian cell transfection reagent Polyethylenimine (PEI).
5. Coelenterazine *h* when using *RLuc* or The Nano-Glo Live Cell reagent, a non-lytic detection reagent containing the cell permeable furimazine substrate (Promega) when using the Nanoluciferase.
6. Ligands (i.e. agonist, antagonist) for the candidate receptor.

4.4 Equipment

1. 75 cm² flasks for maintenance and growth of the cell line.
2. Cell culture facility including a laminar hood and incubator set to 5% CO₂ and 37°C.
3. 6-well cell culture plates.
4. 96-well plates (black with a flat bottom for fluorescence-based assays, white with a flat bottom for luminescence-based assays).

5. Fluorescence microscope to check transfection efficiency.
6. Luciferase and/or fluorescence microplate reader, e.g. ClarioSTAR (BMG), Glomax 96 (Promega) or TriStar (Berthold Technologies).

4.5 Methods

1. Design the appropriate (sequence-verified) expression plasmids for the fluorescence-based (GPCR-VN and GPCR-VC) or luminescence-based (GPCR-RLuc1 and GPCR-RLuc2 or GPCR-SmBiT and GPCR-LgBiT) assays. Proper controls need to be included (see **Note 2**).
2. Prepare and purify the required amount of DNA for the assays and dilute the concentration to 100 ng/μl for the transfection.
3. Seed 2.5×10^5 HEK293T cells in 2 ml DMEM with 10% FBS in each well of a 6-well plate. Place the plate in the incubator.
4. Refresh with 1.8 ml of DMEM + 2% FBS the next day.
5. Prepare a DNA mixture containing a combination of candidate GPCR plasmids, which need to be evaluated for dimerization. Prepare at least 2 replicates for each condition (i.e. for 2x a 6-well), so a proper number of transfected cells for the assay will be obtained. To test for dimerization, first use a 1:1 ratio of both GPCR plasmids, i.e. 200 ng each (see **Note 5**). Furthermore, co-transfect a plasmid coding YFP or CFP (or any other suitable fluorescent protein) (100 ng/well) for normalization of the data (see **Note 6**). Add a mock vector, e.g. pcDNA3 (Invitrogen), to have a final DNA concentration of 2 μg for each DNA mixture.
6. Dilute the PEI transfection reagent (stock: 1μg/μl) 20X in serum free DMEM.
7. Pipet the PEI/serum free DMEM mixture onto the DNA mixture (1:1 volume ratio), vortex and incubate for 10 min.
8. Transfer 200 μl of the DNA transfection mix onto the cells.
9. After 4-5h, refresh the medium with 2 ml DMEM supplemented with 10% FBS.
10. Twenty-four hours after transfection (see **Note 7**), it is advisable to check the transfection efficiency (e.g. YFP/CFP expression) with the fluorescence microscope.

11. Additional step if applicable: To test the occurrence of ligand-dependent dimerization, stimulate/block one of the receptors with the appropriate ligand (e.g. 1-10 μ M) in 2 ml of DMEM + 2% FBS. Incubation times can be varied between 4-16h prior to the read-out of the assay.
12. Forty-eight hours after transfection (see **Note 8**), aspirate the medium and wash the cells twice with 1 ml of pre-heated PBS.
13. Scrape the cells with 500 μ l of pre-heated HBSS and transfer them into a microcentrifuge tube.
14. Centrifuge for 5 min at 3000 rpm.
15. Aspirate the buffer and add 400 μ l of fresh pre-heated HBSS (see **Note 9**). Transfer 100 μ l of the cell suspension in a 96-well plate. It is advisable to run at least three replicates per condition to obtain sufficient recordings for statistical analysis.
16. For the fluorescence-based PCA, samples need to be transferred in a 96-well black plate. First, measure the Venus signal and afterwards the CFP signal with the microplate reader (see **Note 10**).
17. For the luminescence-based PCA, the samples need to be transferred into a 96-well white plate. First, measure the YFP signal with the microplate reader. Afterwards, add 25 μ l of coelenterazine *h* (40X dilution into HBSS, see **Note 11**) in the case of the *RLuc*-based PCA. Add 25 μ l of the Nano-Glo Live Cell reagent, containing the cell permeable furimazine substrate (see **Note 12**), in case of the NanoBiT PCA. Avoid light exposure of the substrate at all times! Measure the luminescence with an endpoint measurement with the microplate reader. For an overview of the excitation and emission wavelengths of the fluorescent and luminescent complementation proteins, see **Note 13**.
18. Calculate the mean, standard deviation and standard error of the mean using an Excel spreadsheet or GraphPad Prism (GraphPad Software, San Diego California, USA). Plot a bar graph to visualize the data. Examples of D₂R homodimerization with the fluorescence-based PCA using Venus fragments (**Figure 4.2**)(see **Note 14**), the luminescence-based PCA using *RLuc* fragments (**Figure 4.3**)(see **Note 14**) as well as the NanoBiT[®] PCA (**Figure 4.3**)(see **Note 15**) are shown.

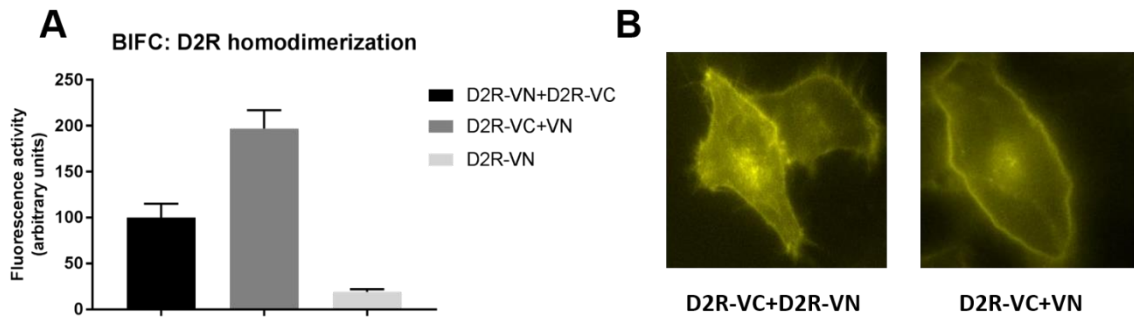


Figure 4.2 Bimolecular fluorescence complementation (BiFC) with D₂R fused to Venus fragments (VN155 and VC155). (A) D₂R constructs were transiently transfected (200 ng each) in HEK293T cells. Fluorescence activity shows the reconstituted Venus signal, normalized for the CFP signal. Endpoint measurement of the fluorescent signal was conducted with the ClarioSTAR. Each value represents the mean \pm SD from 3 independent experiments. (B) D₂R constructs were transiently transfected (50 ng each) in HeLa cells. Microscopy results confirm the high amount of self-assembly of the split Venus fragments.

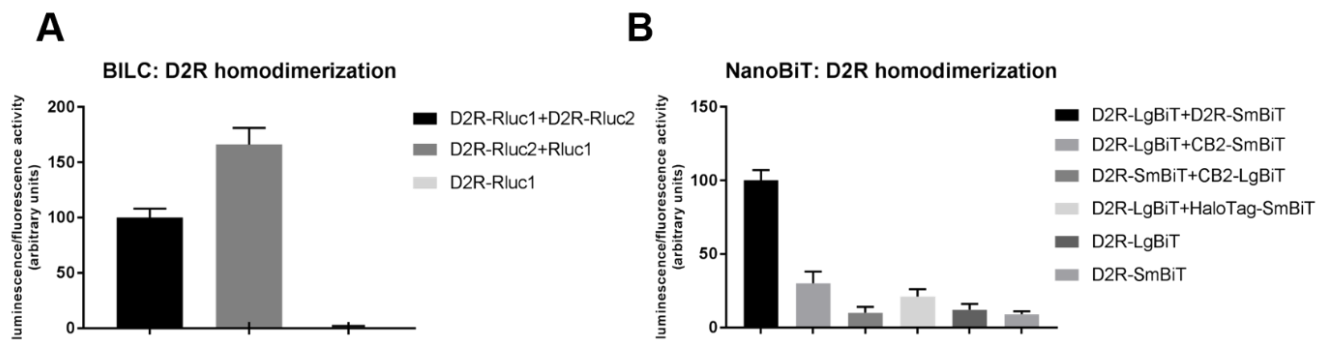


Figure 4.3 Bimolecular luminescence complementation (BiLC) with D₂R fused to *Renilla* luciferase fragments (RLuc1 and RLuc2) (A) or NL fragments (LgBiT and SmBiT) (B). (A & B) D₂R constructs were transiently transfected (200 ng) in HEK293T cells. Venus measurements were included for normalization of the data. The ClarioSTAR was used for endpoint measurements of the luminescent signal. Each value represents the mean \pm SD from 3 independent experiments.

4.6 Notes

1. Plasmids of the fluorescent protein Venus split at other positions are also commercially available, i.e. VN173 (aa 1-173) and VC155 (aa 155-238) (Addgene, Javitch group) [5] but also here a low signal-to-noise ratio was obtained.
2. The fragments of a fluorescent or luminescent protein can show a high affinity for each other, which can be the driving force for reconstitution of the protein, resulting in emission of a signal. Therefore, it is highly recommended to include proper controls in your assay, i.e. a non-interacting partner (another receptor or a mutated version of the receptor at the site of interaction) or the fluorescent or luminescent fragment not fused to a protein of interest (POI). To avoid misleading results, always check the commercially available plasmids will actually encode a protein (e.g. presence of a start codon, correct reading frame, etc.).
3. When assessing heterodimerization instead of homodimerization with the NanoBiT[®] assay, it is highly recommended to test the different constructs (i.e. GPCR fused to LgBiT or SmBiT), since a specific combination always may be favored, i.e. GPCR1-SmBiT and GPCR2-LgBiT or the other way around, depending on the GPCR dimer of interest.
4. Depending on the restriction site which is chosen within the multiple cloning site of the NanoBiT plasmid, a different linker length will be obtained (see **Table 4.2**). In this set-up with the D₂R, the *EcoRI* restriction site was chosen, so an 18-amino acid linker is present between the D₂R and LgBiT as well as between D₂R and SmBiT. More details on the linker length in the different NanoBiT plasmids (protein of interest fused to N- as well as C-terminally) can be found in the manufacturer's manual (Promega).

Table 4.2 Overview of available linker length - and the restriction site needed - in the NanoBiT[®] plasmids when the POI is fused N-terminally of LgBiT or SmBiT.

Fusion protein	Restriction enzyme
POI-GAQGNS-GSSGGGSGGGGSSG-LgBiT	<i>SacI</i>
POI-GNS-GSSGGGSGGGGSSG-LgBiT	<i>EcoRI</i>
POI-GSSGGGSGGGGSSG-LgBiT	<i>XhoI</i>

5. Different GPCR:GPCR ratios need to be validated if one or both of the GPCRs show different expression levels. An indication of the expression levels can be obtained by running a western blot and quantifying the bands with an open-source program, ImageJ. Ideally, the same antibody should be used to visualize both receptors, e.g. by using N-terminally tagged proteins.
6. It is advisable to co-transfect the same amount of DNA of a plasmid expressing YFP or any other fluorescent protein (e.g. 100 ng) in all conditions. This allows normalization of the data and better comparison. Important: when running a fluorescence-based assay with the Venus fragments, CFP (or mCherry) should be used as a control for normalization. Since there is a small overlap between the emission peak of CFP and the excitation peak of Venus, it is advisable to first measure the Venus fluorescence and afterwards the CFP fluorescence signal, to avoid cross-excitation.
7. At this time point, it is also possible to reseed the transfected cells immediately in black or white plates. In this case number 12-15 can be left out of the protocol [24].
8. To obtain more robust experimental results, it is recommended to generate stable cell lines once the ideal combination of GPCR plasmids of interest is known. This way, the experimental set-up can be reduced to 2 instead of 4 days.
9. This volume is adjustable, depending on the number of replicates and the assay setup.
10. Excitation and emission wavelengths of YFP and CFP are shown in **Table 4.3**. A bandwidth of 20 nm is recommended.

Table 4.3 Overview of the excitation and emission maxima of the fluorescent proteins for normalization of the data.

Fluorescent protein	Excitation wavelength (nm)	Emission wavelength (nm)
CFP	434	477
YFP/Venus	497	540

11. A stock solution of coelenterazine *h* of 1 mM can be stored at -20°C. Dilute 40X in HBSS to obtain a final concentration of 25 µM in each well.

12. Dilute the Nano-Glo Live Cell reagent 20X using Nano-Glo LCS Dilution buffer, just prior to measurements.
13. Excitation and emission wavelengths of the complemented proteins are shown in **Table 4.4**.

Table 4.4 An overview of the excitation and emission maxima of the reviewed complementation proteins.

Protein fragments	Excitation wavelength (nm)	Emission wavelength (nm)
Venus (VN155,VC155)	515	528
<i>Renilla</i> Luciferase (RLuc1, RLuc2)	-	480
NanoBiT® (SmBiT, LgBiT)	-	460

14. For the fluorescence-based complementation assay with the Venus fragments (see **Figure 4.2A**) and the luminescence-based complementation assay with the *Renilla* luciferase fragments (see **Figure 4.3A**), a low signal-to-noise ratio was observed due to a high affinity of the VN and VC or the RLuc1 and RLuc2 fragments for one another, whereby an interaction of the fusion partners (in this case: D₂R) is not required. This self-assembly phenomenon of the fluorescence-based complementation assay was confirmed by live cell imaging (see **Figure 4.2B**) [6].
15. With the NanoBiT® assay, a high signal-to-noise is observed due to a low amount of self-assembly of the protein fragments (see **Figure 4.3B**). The cannabinoid receptor 2 (CB₂) is an appropriate non-interacting partner for D₂R in this assay. In addition, ligand-induced modulation of D₂R dimerization can be studied, as described in **Chapter 5** [7].

4.7 Conclusion

To study protein-protein interactions, assays based on the complementation of split biosensors have been intensively applied. This Chapter provides a guideline for the implementation of these PCAs. In addition, distinct PCAs based on fluorescence (split Venus) and luminescence (split *Renilla* Luciferase and NanoBiT®) have been simultaneously compared with one another. From these outcomes it could be concluded that the NanoBiT® assay provides the best signal-to-noise ratio, as the split *Renilla* Luciferase and Venus fragments seem to have a higher affinity for one another, resulting in a higher level of self-assembly.

References

1. Hu, C.D. and T.K. Kerppola, *Simultaneous visualization of multiple protein interactions in living cells using multicolor fluorescence complementation analysis*. Nature biotechnology, 2003. **21**(5): p. 539-45.
2. Cannaert, A., et al., *Detection and Activity Profiling of Synthetic Cannabinoids and Their Metabolites with a Newly Developed Bioassay*. Analytical chemistry, 2016. **88**(23): p. 11476-11485.
3. Dixon, A.S., et al., *NanoLuc Complementation Reporter Optimized for Accurate Measurement of Protein Interactions in Cells*. ACS chemical biology, 2016. **11**(2): p. 400-8.
4. Hall, M.P., et al., *Engineered luciferase reporter from a deep sea shrimp utilizing a novel imidazopyrazinone substrate*. ACS chemical biology, 2012. **7**(11): p. 1848-57.
5. Guo, W., et al., *Dopamine D2 receptors form higher order oligomers at physiological expression levels*. The EMBO journal, 2008. **27**(17): p. 2293-304.
6. Saini, D.K. and N. Gautam, *Live cell imaging for studying g protein-coupled receptor activation in single cells*. Methods in molecular biology (Clifton, N.J.), 2010. **617**: p. 191-207.
7. Wouters, E., et al., *Distinct Dopamine D(2) Receptor Antagonists Differentially Impact D(2) Receptor Oligomerization*. International journal of molecular sciences, 2019. **20**(7).

Chapter 5:

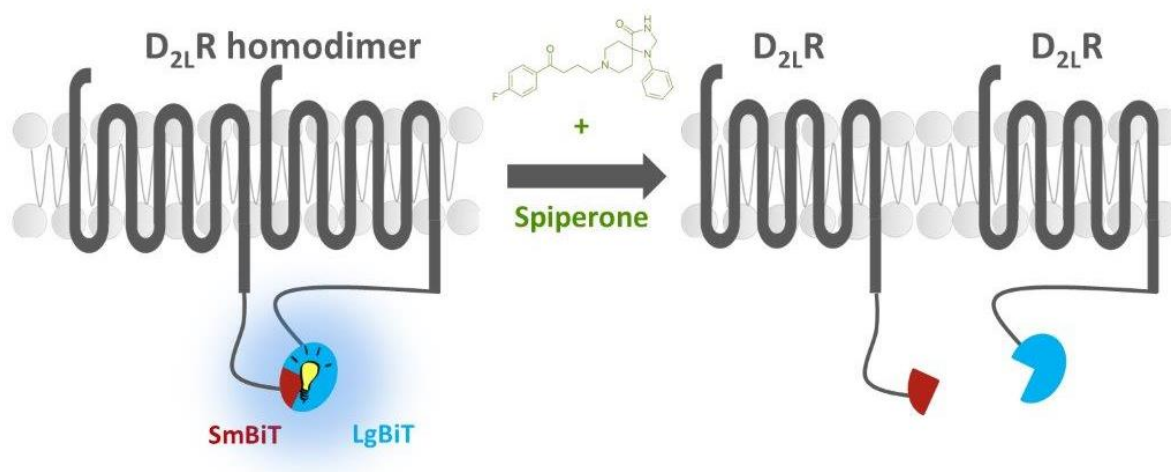
Distinct dopamine D₂ receptor antagonists differentially impact D₂ receptor oligomerization

Based on

Elise Wouters, Adrián Ricarte Marín, James Andrew Rupert Dalton, Jesús Giraldo and Christophe Stove. Distinct Dopamine D₂ Receptor Antagonists Differentially Impact D₂ Receptor Oligomerization. *International Journal of Molecular Sciences*. 2019; 20(7):1686.

ABSTRACT

Dopamine D₂ receptors (D₂R) are known to form transient homodimer complexes, of which the increased formation has already been associated with development of schizophrenia. Pharmacological targeting and modulation of the equilibrium of these receptor homodimers might lead to a better understanding of the critical role played by these complexes in physiological and pathological conditions. Whereas agonist addition has shown to prolong the D₂R dimer lifetime and increase the level of dimer formation, the possible influence of D₂R antagonists on dimerization has remained rather unexplored. Here, using a live-cell reporter assay based on the functional complementation of a split Nanoluciferase, a panel of six D₂R antagonists were screened for their ability to modulate the level of D₂L R dimer formation. Incubation with the D₂R antagonist spiperone decreased the level of D₂L R dimer formation significantly by 40–60% in real-time and after long-term (≥ 16 h) incubations. The fact that dimer formation of the well-studied A_{2a}–D₂L R dimer was not altered following incubation with spiperone supports the specificity of this observation. Other D₂R antagonists, such as clozapine, risperidone, and droperidol did not significantly evoke this dissociation event. Furthermore, molecular modeling reveals that spiperone presents specific Tyr199^{5,48} and Phe390^{6,52} conformations, compared to clozapine, which may determine D₂R homodimerization.

GRAPHICAL ABSTRACT

5.1 Introduction

Dopamine receptors belong to the class A sub-family of G protein-coupled receptors (GPCRs). Five dopamine receptors have been identified in mammals and are classified in the D₁-like family, with the D₁ and D₅ subtypes, and the D₂-like family, with the D₂, D₃, and D₄ subtypes [1]. They are key players in the coordination of motor control, cognitive function, memory, and reward [2, 3]. A growing body of evidence indicates that the signaling function of many GPCRs is diversified and fine-tuned by interaction with other GPCRs [4]. Dimerization of GPCRs has been demonstrated both *in vitro* and *in vivo*, whereby association may take place with the same GPCR (homo-oligomerization) or with different GPCRs (hetero-oligomerization) [5]. Dimerization phenomena have been documented for all five dopamine receptor subtypes [6-9]. Towards this end, extensive work has been directed towards the dopamine D₂ sub-type receptor (D₂R). This receptor plays an important role in the physiological actions of the neurotransmitter dopamine, and it is a target for drugs used to treat schizophrenia and Parkinson's disease, depression, attention deficit hyperactivity, stress, nausea, and vomiting [10-16].

The D₂R exists in two isoforms, D_{2,short} (D_{2S}R) and D_{2,long} (D_{2L}R), generated by alternative splicing [17, 18]. The difference is a 29-amino acid fragment insertion in the third intracellular loop (ICL3) of the D_{2L}R. Although a large number of dimer complexes of D₂R with other GPCRs have been extensively documented ((A_{2a}-D₂R; [19, 20])(β₂AR-D₂R; [21])(CB₁-D₂R; [22, 23])), this receptor can form homodimer complexes as well. It was first reported in 1996 by Ng *et al.* [24] that D_{2L}R forms homodimers, as observed by co-immunoprecipitation (co-IP). Further evidence for homodimerization of both isoforms has been provided by studies using a wide variety of biochemical techniques such as co-IP, ligand binding [25], fluorescence resonance energy transfer (FRET) [26], bioluminescence resonance energy transfer (BRET) [27], single-molecule tracking [28], and protein-protein docking [29, 30]. Furthermore, it has been suggested that the extent of dimerization is subtype-selective (D_{2L}R > D_{2S}R), suggesting a possible role for the 29-amino-acid fragment in ICL3 [31].

In order to better understand the crosstalk between dopamine receptors, the interface(s) should be considered from a molecular point of view. Different transmembrane (TM) regions of the D₂R have been reported to be involved in the D₂R homodimer interface.

Incubation of D₂R homodimers with peptides derived from the putative TM6 regions of the D₂R resulted in dissociation of the dimer to the monomers [24, 32]. On the other hand, successive deletion of TM domains of the D₂R and cysteine cross-linking studies revealed that the most critical areas involved in the intermolecular hydrophobic interactions for dimerization resided in TM4 [33, 34]. In addition, the TM4–TM5–TM4–TM5 and TM5–TM6–TM5–TM6 interfaces have been widely described to be involved in D₂R hetero-oligomerization with other class A GPCRs [35–40]. In 2014, Guitart *et al.* [41] reported that dopamine D₁ receptor (D₁R) TM5- or TM6-derived single peptides were able to reduce D₁R homodimerization. Likewise, a potential TM5–TM6–TM5–TM6 interface could be envisaged in the D₂R homodimer. Collectively, these reported features support the hypothesis of multiple oligomerization interfaces [42], wherein GPCRs undergo multiple cycles of monomer and dimer formation with different interfaces. These interfaces can differ between homo- and heterodimerization processes of GPCRs. This concept of oligomerization of the D₂R has also been confirmed by combined FRET and BRET assays, wherein at least four dopamine D₂R monomers are closely located at the plasma membrane, suggesting higher-order oligomer formation [43, 44].

Although it was first postulated that D₂Rs form constitutive dimers or higher-order oligomers [34], increasing evidence supports the dynamic interconversion between monomers and dimers, suggesting transient dimer formation [28, 42]. Recently, a lifetime of 0.5 s was determined for SNAP-tagged D_{2L}R dimers using single-molecule sensitive total internal reflection fluorescence (TIRF) microscopy [31]. Whereas Tabor *et al.* detected transient D₂R homodimer formation at 24 °C, Kasai *et al.* (2018) [28] performed single-molecule imaging at the physiological temperature of 37 °C, resulting in transient D₂R dimer formation with a lifetime of 68 ms. Similar findings for temperature-dependent lifetimes of homodimer formation were also observed for other class A GPCRs [45–47].

The emerging evidence on transient dynamics of class A GPCR dimers, characterized by fast association and dissociation events, adds to the understanding of the complexity of receptor dimerization. Considering the dynamics and transient nature of D₂R dimers, one might anticipate a functional relevance for alterations in the level of D₂R dimerization. Indeed, an increase in D₂R homodimer formation has been correlated with the pathophysiology of schizophrenia [48]. Therefore, targeting these D₂R dimers might offer

new information about the pathophysiology of diseases related to this GPCR dimer, potentially opening new therapeutic avenues.

Within the concept of altering the level of dimerization or even oligomerization provoked by ligands, different screening methods have been implemented. For example, FRET has been used to monitor dose-dependent increases in the level of D_{2S}R oligomerization by the agonist (-)-norpropylapomorphine [26]. Tabor *et al.* (2016) [31] used TIRF microscopy to investigate the effect of D₂R agonists dopamine and quinpirole on the spatial and temporal organization of D₂R dimer formation. These authors found that agonist stimulation at high concentrations (15 μ M) seemed to prolong the lifetime of the D₂R homodimer by a factor of \sim 1.5, whereas the neutral antagonist UH-232 (0.1 μ M) did not alter the lifetime of the dimer.

To our knowledge, research on monovalent antagonist-mediated modulation of D₂R dimerization is rather limited. The neutral UH-232 and 1,4-DAP have been tested, but no effect was observed [31]. In the present study, the modulating capacity of several clinically used D₂R antagonists/inverse agonists on the level of D₂R homodimerization or higher-order oligomerization was evaluated using complementation-based NanoLuciferase® Binary Technology (NanoBiT®). In addition, an atomistic computational study of D₂R conformational changes induced by specific D₂R antagonists/inverse agonists and its relevance on D₂R homodimerization has been performed using microsecond-length unbiased molecular dynamics (MDs) simulations.

5.2 Materials and methods

5.2.1 Chemicals and reagents

Dulbecco's modified Eagle's medium (DMEM) supplemented with GlutaMAX, Opti-MEM® I reduced serum medium and Gibco™ Penicillin-Streptomycin (10,000 U/mL), Hank's balanced salt solution (HBSS), Phusion high-fidelity (HF) PCR master mix with HF buffer, and T4 DNA ligase were purchased from Thermo Fisher Scientific (Pittsburg, PA, USA). Fetal bovine serum (FBS) was purchased from Biochrom, now part of Merck (Merck KGaA, Darmstadt Germany). Phosphate buffered saline (PBS) was procured from Lonza (Lonza, Walkersville, MD, USA). Transient mammalian cell transfection reagent polyethylenimine (PEI), poly-D-lysine, carbenicillin, Tween 20, and DMSO suitable for cell culture were

purchased from Sigma-Aldrich (Steinheim, Germany). D₂R antagonists spiperone, clozapine, and haloperidol were purchased from Tocris Bioscience (Bio-technie, Abingdon, UK). The Nano-Glo[®] Live Cell reagent and the GoTaq[®] DNA polymerase were from Promega (Madison, WI, USA). Primers were synthesized by Eurofins Genomics (Ebersberg, Germany). Restriction enzymes *Hind*III and *Eco*RI were from New England Biolabs (NEB, Massachusetts, US). E.Z.N.A.[®] MicroElute Gel extraction kit, E.Z.N.A.[®] MicroElute Cycle-Pure kit and E.Z.N.A. plasmid DNA Mini/Midi kit were from VWR International (Radnor, PA, USA). GelRed was purchased from Biotium (Fremont, CA, USA). Luria Bertani broth and agar were procured from Lab M (Heywood, Bury, UK).

5.2.2 Cloning of the dopamine D₂R into the NanoBiT[®] plasmids

The human D₂L_R (NM_000795.3) was cloned into the NanoBiT[®] vectors (NB MCS1 and NB MCS2), which were kindly provided by Promega (Madison, WI, USA). The NanoBiT[®] constructs express a small subunit of the NanoLuciferase of 1 kDa (Small BiT, SmBiT) and a large subunit of 18 kDa (Large BiT, LgBiT). The D₂L_R was cloned into the NanoBiT[®] vectors prior to a 15 amino acid encoding sequence, linking it to the SmBiT or LgBiT fragment, by performing a PCR reaction with primers containing the specific restriction enzyme sites (**Table 5.1**). The PCR reaction was performed with an MJ Research PTC-200 Thermal Cycler (GMI, Minnesota, USA), in a three-step manner: initial denaturation (98 °C, 30 s), denaturation (98 °C, 10 s), annealing (T_m, 35 s), extension (72 °C, 42 s), and final extension (72 °C, 5 min), for 30 cycles. PCR products were run on a 1% agarose gel and purified with a MicroElute Gel extraction kit to remove parental DNA. After digestion with the specific restriction enzymes for 3 h at 37 °C, the PCR product and the NanoBiT[®] vectors were purified with a MicroElute Cycle-Pure kit and a MicroElute Gel extraction kit, respectively. Following ligation using T4 DNA ligase for 1 h at room temperature, the ligated product was transformed into a competent MC1061 *Escherichia coli* strain. After plating on carbenicillin-containing agar, resistant colonies were screened for the presence of the insert by Colony PCR with *Taq* polymerase and subsequent restriction digest. Coding sequences were verified by Sanger sequencing (Eurofins Genomics, Ebersberg, Germany).

As a control, the cDNA coding the human A_{2a} receptor (A_{2a}), a kind gift from F. Ciruela (Unitat de Farmacologia, Barcelona, Spain), was fused to SmBiT and LgBiT in a similar way as for the

D_{2L}R (**Table 5.1**). In addition, cannabinoid receptor 2 (CB₂) fusion constructs, CB₂–LgBiT and CB₂–SmBiT, were developed by performing a PCR reaction on the human CB₂ coding sequence (as described previously by our research group) [49].

Table 5.1 Primers for the development of the GPCR-NanoBiT® fusion constructs.

Fusion protein		Primers (5'>3') ^a	T _m (°C) ^b	RE ^c
D_{2L}R-LgBiT	F	GT TAAAGCTT <u>ATGAAGACGATCATC</u>	64	<i>HindIII</i>
	R	GCAG AATTC GC GCAGTGGAGGATC		<i>EcoRI</i>
D_{2L}R-SmBiT	F	GT TAAAGCTT <u>ATGAAGACGATCATC</u>	64	<i>HindIII</i>
	R	GCAG AATTC GC GCAGTGGAGGATC		<i>EcoRI</i>
A_{2a}-LgBiT	F	CG TAAAGCTT <u>ATGAAGACGATCATCGCCCTG</u>	69	<i>HindIII</i>
	R	TGCAG AATTC GCAGAAACCC CAGCACC		<i>EcoRI</i>

a: Forward (F) and Reverse (R) (5'>3') with restriction enzyme sites (**bold**), start codon (underlined) or extra nucleotides (marked in grey) to ensure a correct reading frame.

b: Annealing temperature.

c: Restriction enzyme.

5.2.3 Cell culture

5.2.3.1 Expression in HEK293T cells

Human Embryonic Kidney 293T (HEK293T) (American Type Culture Collection (ATCC), Manassas, Virginia, USA) cells were maintained in DMEM supplemented with 10% fetal bovine serum (FBS), 100 µg/mL streptomycin, and 100 IU/L penicillin in a controlled environment (37 °C, 98% humidity, 5% CO₂). Prior to transfection, cells were cultured in 6-well plates at a density of 3 × 10⁵ cells/well in 2 mL DMEM + 10% FBS. To ensure low expression levels of GPCRs, only 200 ng of each GPCR fused to a luminescent protein fragment was transiently transfected using PEI transfection reagent in DMEM supplemented with 2% FBS. After 5 h of incubation with the transfection mixture, the medium was refreshed with DMEM + 10% FBS.

5.2.3.2 Cell preparation for dimerization assay with HEK293T cells in suspension

Forty-eight hours after transfection, cells were washed twice with PBS, scraped, and centrifuged for 5 min at 1000× *g*. A bicinchoninic acid assay (BCA) was conducted on an aliquot of the transfected cells in HBSS buffer, and all protein concentrations were

measured. The cell suspensions were diluted to bring them all to a density corresponding to a measured protein concentration of 600 ng/ μ L. For the dimerization assay, the Nano-Glo Live Cell reagent, a non-lytic detection reagent containing furimazine substrate, was 20 \times diluted using Nano-Glo Live Cell System (LCS) dilution buffer, and 25 μ L was added to each 96-well containing 100 μ L cell suspension. End-point fluorescence or luminescence was measured with the ClarioSTAR (BMG LABTECH) in a black and white 96-well plate, respectively.

5.2.3.3 Cell preparation for dimerization assay with adherent HEK293T cells

Twelve hours after transfection, cells were reseeded in poly-D-lysine-pretreated white 96-well plates at 0.5×10^5 cells/well. The next day, cells were washed twice with Opti-MEM[®] and 100 μ L of the reduced serum medium was added to each well. First, 25 μ L of the Nano-Glo Live Cell reagent was added, followed by an incubation of 15 min, monitored by the Tristar (as described previously [49]). Afterwards, 10 μ L of solvent control (blank sample, DMSO $\leq 0.1\%$) or ligand was added to obtain a final concentration of 10 μ M. The read-out was performed immediately upon treatment and monitored for 1 h at room temperature by the TriStar² LB 942 multimode microplate reader controlled by ICE software (Berthold Technologies GmbH & Co., Bad Wildbad, Germany).

5.2.3.4 Fluorescence normalization and signal-to-noise ratio

To circumvent fluctuations in signal resulting from varying transfection efficiencies, a constant amount of a plasmid encoding the fluorescent protein Venus (10% of total DNA transfected) was co-transfected in all conditions. Luminescence data were normalized for the measured fluorescent signal.

As a negative control, the protein fragment SmBiT of the luminescence-based assays, not fused to a receptor but to the HaloTag, was implemented. The luminescent/fluorescent signal obtained for this condition (co-transfected with, e.g., D₂L_R-LgBiT) was considered as background and, consequently, a signal-to-noise ratio could be derived.

5.2.4 NanoBiT®-based validation of the functionality of D_{2L}R luminescent fusion proteins by mini-Gα_i protein-mediated signaling

The plasmid encoding the mini-Gα_i protein was kindly provided by the lab of Dr. A. Chevigné (LIH Luxembourg Institute of Health, Luxembourg). The construct was PCR-amplified using synthesized primers (Forward: 5' ACTCAAGAATTCAATGATCGAGAAGCAGCTGCAG 3' and Reverse: 5' ACTCAAGAATTCTCAGAACAGGCCGCGAGTCTCTC 3') and subcloned into the NanoBiT® constructs expressing LgBiT and SmBiT using *EcoRI* restriction sites flanked at both sites. Sequences were verified by Sanger sequencing.

HEK293T cells were seeded in 6-well plates at a cell density of 5×10^5 cells/well. The next day, cells were transiently transfected with 1.5 µg of each construct (D_{2L}R–LgBiT and SmBiT–mini-Gα_i or D_{2L}R–SmBiT and LgBiT–mini-Gα_i) using FuGENE® HD transfection reagent (Promega) according to the manufacturer's instructions. For reseeding the cells in white 96-well plates, as well as monitoring of the luminescent signal, the same procedure was followed as described in 'Cell preparation for dimerization assay with adherent HEK293T cells'. On the fourth day, cells were treated with quinpirole (0.01 nM–10 µM) to evoke mini-Gα_i protein recruitment to the D_{2L}R.

5.2.5 Detection of the expression levels of D_{2L}R dimers by western blot

Western blot analysis was executed as previously described [50], with some minor adaptations. The day before transfection, HEK293T cells were seeded in 10-cm dishes at a density of 3×10^6 cells/well. PEI-mediated transient transfection was performed with plasmids encoding D_{2L}R–SmBiT and D_{2L}R–LgBiT, each present at 2 µg per dish. The next day, cells were treated with 10 µM haloperidol, spiperone, clozapine, or solvent control for 16 h at 37 °C. On the fourth day, cells were washed two times with PBS, harvested, and lysed using Polytron homogenizer for two 10 s periods in ice-cold PBS buffer. Membrane pellets were obtained by centrifugation at maximum speed for 25 min at 4 °C and dissolving in RIPA buffer (150 mM NaCl; 50 mM Tris HCl, pH 7.5; 1% NP-40; 0.5% deoxycholic acid; supplemented with fresh protease inhibitors: 5 µg/mL aprotinin, 0.4 mg/mL pefabloc and 10 mM β-glycerol-phosphate disodium salt pentahydrate, and 10 µg/mL leupeptin). The membrane pellets were rotated for 1 h at 4 °C, followed by a centrifugation for 20 min at maximum speed. Next, the BCA method was performed on the supernatant to quantify the

protein levels, with bovine serum albumin dilutions as the standard. Cell lysates (50 µg) were heated in Laemmli buffer supplemented with 10% β-mercaptoethanol and 5% bromophenol blue for 10 min at 37 °C. Proteins were separated via a 10% SDS-PAGE for 1 h at 100V and transferred to a nitrocellulose membrane. Membranes were blocked with blocking buffer (LI-COR Biosciences, Lincoln, NE, USA) for 1 h at RT and incubated with rabbit anti-D₂R antibody (RRID: AB_2571596) (Frontier Institute, Hokkaido, Japan) overnight at 4 °C, followed by three washing steps with PBS + 0.05% Tween 20. Afterwards, blots were incubated for 1 h in the dark with goat anti-rabbit IRDye680 LT (1/10,000) (cat. no. 926–68021, LI-COR Biosciences, Lincoln, NE, USA) at RT. Equal loading of all conditions was assessed by normalization by the levels of the constitutively expressed neuronal marker tubulin with the monoclonal anti-α-tubulin antibody (cat. no. T5168, Sigma Aldrich, Steinheim, Germany). After incubation with the primary antibody for 1 h, followed by three washing steps with PBS + 0.05% Tween 20, blots were incubated for 1 h in the dark with the Alexa Fluor® goat anti-mouse secondary antibody (cat. no. A-11001, Invitrogen, Carlsbad, CA, USA). Blots were visualized with the Odyssey® Infrared Imaging system (IGDR, Rennes, France) and quantified by ImageJ software (NIH, Bethesda, MD, USA).

5.2.6 Data analysis

Concentration-response histograms were calculated after correction for the fluorescent signal measured in the same well to compensate for transfection variability. Each experiment was performed three times in triplicate (unless stated otherwise). Statistics were performed using the non-parametric (Kruskal–Wallis) one-way ANOVA, followed by post hoc (Dunn’s multiple comparison test) analysis to detect statistical differences amongst groups ($p < 0.05$) by the GraphPad Prism software (San Diego, CA, USA).

Curve-fitting of concentration–response curves of the mini-Gα_i coupling to the D₂L₁R via a nonlinear regression model (variable slope, four parameters) was employed to determine pEC₅₀ values (a measure of potency). The mean area under the curve (AUC) ± standard error of mean (SEM) was calculated, with a total of 12 replicates for each data point.

The following sections on computational modeling, molecular dynamic simulations and analysis has been performed by Adrián Ricarte Marín.

5.2.7 Computational modeling

A previously published D₂R model [40], based on human D₂R crystal structure (PDB id: 6CM4) [51], was generated using CHIMERA v1.11.2 [52] software (San Francisco, CA, USA) by adding missing residues and converting the crystal mutated residues back to wild-type. In addition, co-crystallized risperidone and endolysin fusion protein were removed from the D₂R structure. This D₂R model was used as initial conformation for construction of three different molecular systems: (i) spiperone-bound D₂R monomer, (ii) clozapine-bound D₂R monomer, and (iii) D₂R homodimer without bound antagonist. Coordinates for clozapine and spiperone were downloaded from PubChem [53]. AUTODOCK v4.2 [54] software (La Jolla, CA, USA) was used to dock clozapine and spiperone into the monomeric D₂R model. The selected docked conformation of each ligand in the receptor represented the top hit identified by best predicted affinity in the largest docking cluster. For construction of the D₂R homodimer model, where two protomers of D₂R interacted via a symmetrical TM5–TM6–TM5–TM6 interface, two D₂R monomers without bound antagonist were initially superimposed onto respective protomers of the μ -opioid receptor homodimer crystal structure (PDB id: 4DKL) [55]. The D₂R homodimer model was then submitted to the ROSIE Web server [56] for protein–protein docking using default parameters. The best docked homodimer structure was identified by two factors: best interface score (“I_sc”) and best membrane-compatible orientation. The D₂R monomer, with bound spiperone or clozapine, and D₂R homodimer without bound antagonist complexes were energy minimized without restraints with CHIMERA [52] in the AMBER-14SB force-field [57] to optimize protein–ligand or protein–protein interactions, respectively.

5.2.8 Molecular dynamic (MD) simulations

D₂R monomer, with bound spiperone or clozapine, and D₂R homodimer without bound antagonist complexes were embedded separately into a 1-Palmitoyl-2-oleoylphosphatidylcholine (POPC) membrane and solvated with TIP3P water molecules using the CHARMM-GUI web-based interface [58]. Complexes were oriented in the membrane according to the OPM database [59] entry of D₂R crystal structure (PDB id: 6CM4) [51] or μ -opioid receptor homodimer crystal structure (PDB id: 4DKL) [55] for monomer and homodimer models, respectively. Charge-neutralizing ions (0.15 M KCl) were introduced into each system. Parameters were automatically generated by CHARMM-GUI

[58]. Membrane, water, and protein parameters were generated according to the CHARMM36 force-field [60], whereas spiperone and clozapine parameters were generated according to CGenFF v1.0.0 [61]. Molecular dynamics (MDs) simulations of D₂R monomer, with bound spiperone or clozapine, and D₂R homodimer were performed using the CHARMM36 force-field [60] with ACEMD [62] on specialized GPU-computer hardware (Stanmore, Middlesex, England). Each system was equilibrated for 28 ns at 300 K and 1 atm, with positional harmonic restraints on protein heavy atoms progressively released over the first 8 ns of equilibration and then continued without constraints. After equilibration, monomer and homodimer models were subjected to unbiased continuous production runs under the same conditions for 3 μ s.

5.2.9 MD simulation analysis

Analysis of MD simulations of D₂R monomer, with bound spiperone or clozapine, and D₂R homodimer without bound antagonist were performed using VMD software v1.9.2 [63] (Chicago, IL, USA). In detail, root mean square deviation (RMSD) measurements of the backbone of the transmembrane domain (TMD) of D₂R was performed to observe receptor conformational change with respect to the initial D₂R monomeric crystal structure (PDB id: 6CM4)[51] or initial D₂R homodimer model. Likewise, RMSD measurements of either clozapine or spiperone in their respective MD simulations were used to monitor ligand stability in the orthosteric pocket of the D₂R monomer. Residues in close contact (protein-ligand distance <3.5 Å) with co-crystallized ligand risperidone were compared, in terms of RMSD with MD conformations of D₂R monomer with bound stable clozapine or spiperone, to observe differences between induced-fit of both ligands. Similarly, residues frequently close-contacted by either clozapine or spiperone in respective MD simulations, within simulation time-periods where ligands remain stable, were identified with a TCL script executed in VMD [63], thus defining ligand-specific D₂R orthosteric pockets. After visual comparisons of the D₂R monomer, with bound spiperone or clozapine, and D₂R homodimer conformations, we performed an analysis of Tyr199^{5.48} and Phe390^{6.52} χ 1 dihedral angle conformations using an in-house custom TCL script executed in VMD [63]. An arbitrary threshold of 240° was selected to classify Tyr199^{5.48} and Phe390^{6.52} χ 1 dihedral angle cis or trans-conformation (> or < 240°, respectively). The proportion of each conformation was measured. Distance analyses of the interface of D₂R homodimer were performed using the TCL script executed in VMD [63]. An energetic analysis of the D₂R homodimer TM5–TM6–

TM5–TM6 interface was performed with FoldX v.4 (Barcelona, Catalonia, Spain) [64]. Alanine scanning of D₂R homodimer Tyr199^{5.48} and Phe390^{6.52}, generating Y199A and F390A mutations, followed by energetical analysis with FoldX v.4 [64], was carried out to measure the contribution of these residues in the homodimer interface.

5.3 Results

5.3.1 Pharmacological properties of the D_{2L}R fusion proteins

For the development of a complementation-based GPCR dimer targeting strategy, the D_{2L}R was C-terminally fused to the small 1 kDa subunit (Small BiT, SmBiT) and to the large 18 kDa subunit (Large BiT, LgBiT) of NanoLuciferase. Upon interaction with D_{2L}R monomers, the NanoLuciferase subunits were brought into close proximity and re-assembled spontaneously into a functional protein. To ensure that these modified D_{2L}R fusion constructs retained functionality, we performed a G protein coupling assay. We therefore cloned the mini-Gα_i protein, corresponding to the engineered GTPase domain of the Gα_i subunit fusion proteins, into the NanoBiT® vectors with either LgBiT or SmBiT at their N-terminus. These mini-Gα_i fusion proteins were transiently co-expressed with the corresponding (complementary) D_{2L}R fusion constructs in HEK293T cells that were stimulated with the dopamine D₂R agonist quinpirole (0.01 nM–10 μM). N-terminally tagged mini-Gα_i proteins showed a concentration-dependent recruitment to the D_{2L}R–SmBiT and D_{2L}R–LgBiT fusion constructs (**Figure 5.1**). This demonstrated (i) that both receptor fusion constructs were expressed at the cell surface, (ii) that both receptor fusion constructs were responsive to ligand-induced activation, and (iii) that both receptor fusion constructs could still undergo a conformational change upon receptor modulation. Interestingly, the different construct combinations resulted in a dissimilar output in terms of sensitivity and signal-to-noise ratio, as published previously for the G protein coupling assay with D₂R [65]. Accordingly, pEC₅₀ values for D_{2L}R–LgBiT and SmBiT–mini-Gα_i in comparison with D_{2L}R–SmBiT and LgBiT–mini-Gα_i deviated substantially (pEC₅₀: 6.62 ± 0.02 and 7.65 ± 0.05, respectively). Although both D_{2L}R fusion proteins can recruit mini-Gα_i in a concentration-dependent manner and, thus, are functional, these observations further underscored the importance of testing several construct combinations when implementing systems like this for deducing EC₅₀ values.

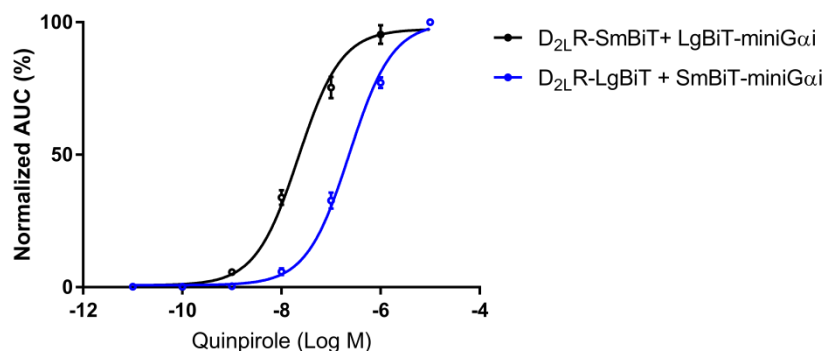


Figure 5.1 Real-time monitoring of mini-G α_i protein recruitment to the D₂L R by the NanoLuciferase Binary Technology (NanoBiT®) assay. Transient overexpression of fusion constructs of the LgBiT and SmBiT of NanoLuciferase C-terminal to D₂L R and N-terminal to the mini-G α_i -protein was achieved in HEK293T cells. Luminescence was monitored for 2 h. Concentration-response curves were generated by the addition of quinpirole (0.01 nM–10 μ M), and the corresponding AUCs (four independent experiments, in triplicate) normalized and plotted to the logarithmic concentration of quinpirole ($n = 12$, \pm SEM).

5.3.2 Targeting the dopamine D₂L R homodimer using the NanoBiT® assay

To target D₂L R homodimers in their native cell environment, the D₂L R-LgBiT and D₂L R-SmBiT fusion constructs were transiently transfected in HEK293T cells. This cell line was selected because of its high transient transfection efficiency as well as its rapid growth characteristics. More importantly, within a comparative study of four different cell lines frequently used for GPCR research, the HEK293 cell line showed the lowest expression (both amount and type) of GPCRs and could thereby serve as an appropriate cell model into which gene constructs of interest can be introduced [66]. Within this experimental setup, a clear luminescent signal was obtained when the D₂L R-LgBiT and D₂L R-SmBiT were co-expressed, indicating interaction of both receptors (**Figure 5.2**). As negative controls, expression of the D₂L R-LgBiT or D₂L R-SmBiT separately only generated a signal that could be considered as background (i.e., seven- to ten-fold lower compared to the signal observed for the D₂L R homodimer), as expected. As an additional negative control, we co-expressed the HaloTag-SmBiT construct, a fusion protein that is diffusively expressed throughout the cell. Again, a response not significantly ($p > 0.05$) different from background was detected (i.e., a five-fold lower signal was observed as compared to the signal provoked by the D₂L R homodimer). Furthermore, from a screening of multiple GPCRs, the cannabinoid receptor 2 (CB₂) was selected as a non-interacting partner for D₂L R since no significant ($p > 0.05$) increase in luminescent signal was observed for the CB₂-D₂L R combination in direct comparison to the negative control D₂L R-LgBiT with HaloTag-SmBiT. To our knowledge, no dimer formation of

CB₂ with D₂R has been reported, in contrast to the CB₁ for which dimerization with the D₂R has been described [67]. Functionality of the CB₂ constructs was demonstrated elsewhere [49]. In addition, the signal obtained for CB₂–D₂L R was significantly (four-fold) lower compared to that obtained for the D₂L R–D₂L R combination. The aforementioned results supported the utility of a NanoLuciferase complementation assay to differentiate between interacting (D₂L R–D₂L R) and non-interacting GPCRs (CB₂–D₂L R), when compared to background.

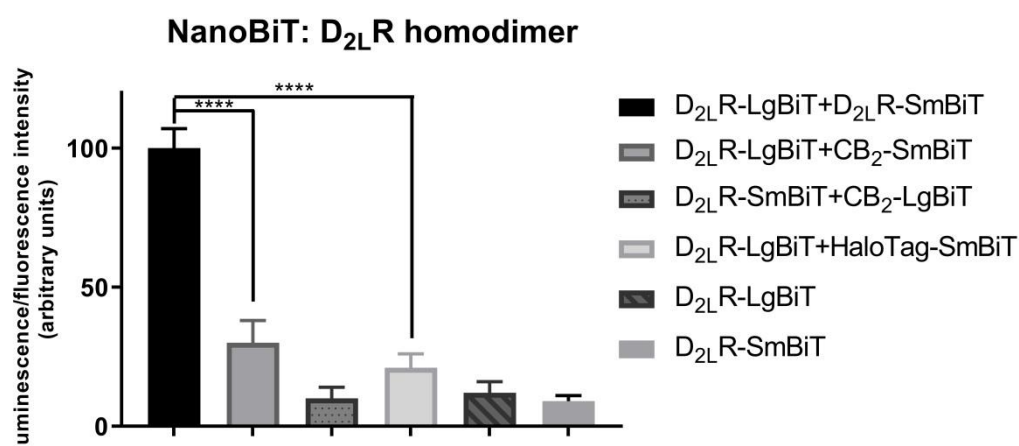


Figure 5.2 Detection of the D₂L R homodimer using the complementation-based NanoLuciferase Binary Technology (NanoBiT®). The SmBiT and LgBiT split parts of the NanoLuciferase are fused to the C-terminus of the GPCRs. Overexpression of these constructs was conducted by transient transfection in HEK293T cells. The luminescent signal was normalized to the fluorescent signal of the co-transfected Venus protein in all conditions. A non-interacting GPCR partner for D₂L R (from a panel of multiple GPCRs) is CB₂, which showed a 4-fold lower signal compared to the D₂L R–D₂L R interaction (n = 3, ± SEM).

5.3.3 Antagonist-dependent modulation of the level of D₂L R homodimer formation

5.3.3.1 Short-term effects

The short-term effect of the D₂R antagonists haloperidol, spiperone and clozapine on the level of dimerization was first evaluated on adherent HEK293T cells transiently transfected with D₂L R–LgBiT and D₂L R–SmBiT. Observed luminescent signals were corrected for solvent control, and the normalized relative luminescence units (RLU) were plotted against time (**Figure 5.3**). A steeper drop in luminescent signal was observed when incubated for 1 h with spiperone (10 μM) compared to haloperidol or clozapine (**Figure 5.3**). Although one should

recognize the possible decay of the NanoGlo substrate, which was considered similar in all conditions, nevertheless, a clear difference in decrease in luminescent signal was observed when incubated with different antagonists (spiperone > haloperidol > clozapine).

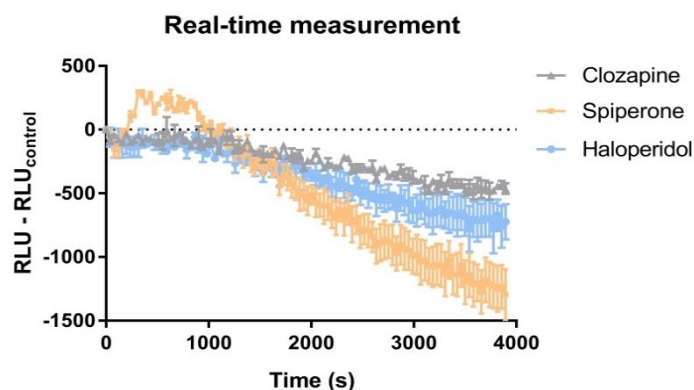


Figure 5.3 Real-time measurement of adherent transfected HEK293T cells incubated with 10 μ M of D₂R antagonists for 1 h. Normalized relative luminescence unit (RLU) is plotted against time (s) (n = 2, \pm SEM).

5.3.3.2 Long-term effects

For longer incubation time points, the capability of modulating the level of dimerization of the D₂R antagonists haloperidol, spiperone and clozapine was validated on cells in suspension. To circumvent fluctuations in the observed effect due to transfection variability, the obtained luminescent signal was normalized to the fluorescent signal obtained from the same amount of co-transfected Venus protein in all conditions. The normalized luminescent signal was measured after 10 min (**Figure 5.4 A**), 30 min (**Figure 5.4 B**), 4 h and 16 h of incubation with the D₂R antagonists (**Figure 5.4 C & D**). The effect of spiperone on the D₂L_R homodimer could be observed after 30 min and was sustained for up to 16 h of incubation. Spiperone reduced the level of D₂L_R dimerization by 40%–60%, depending on the time interval of incubation. This decrease in D₂L_R dimerization levels was only provoked upon incubation with a spiperone concentration ≥ 10 μ M.

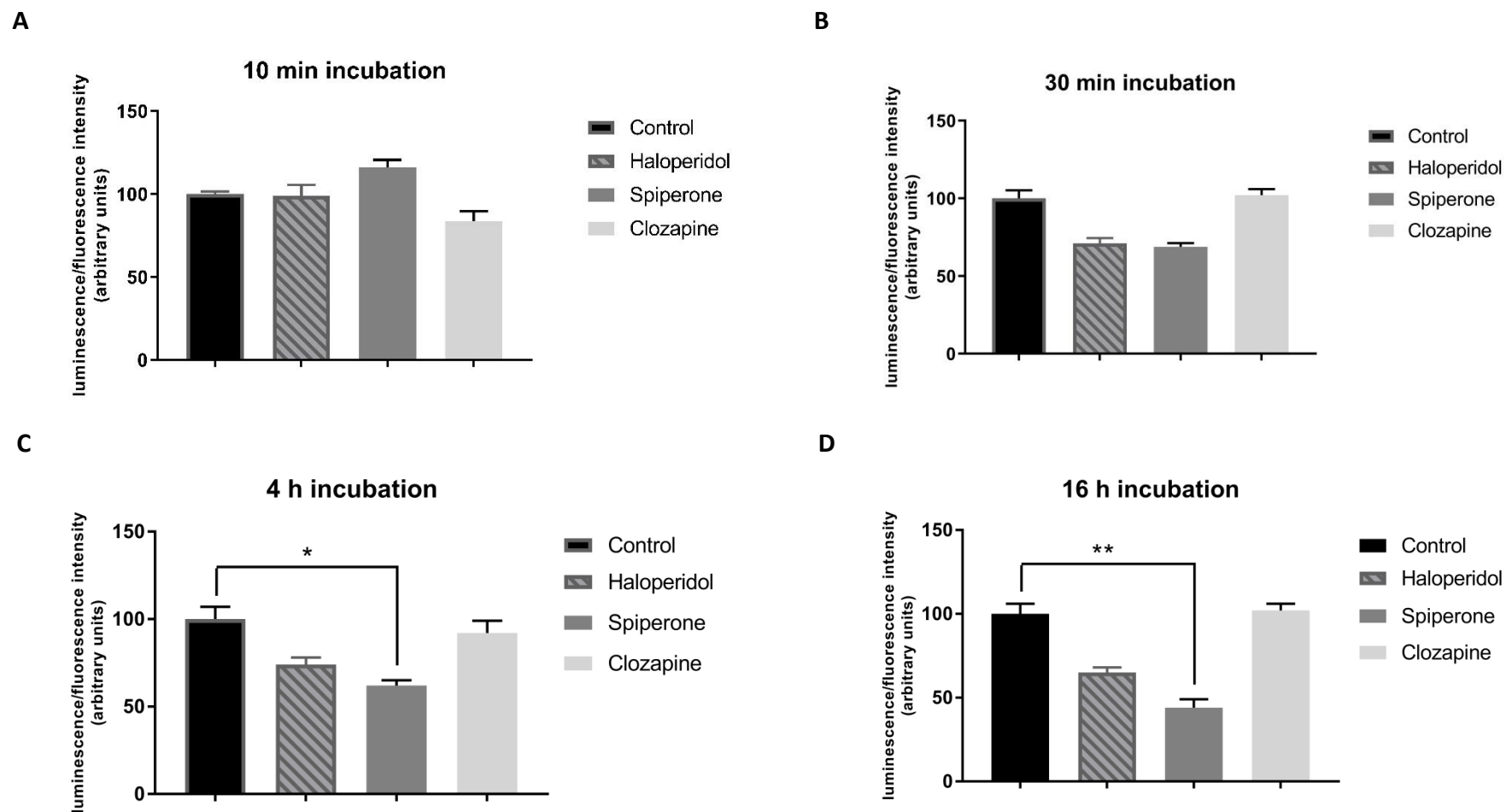


Figure 5.4 Signals obtained following incubation of D₂L-LgBiT and D₂L-SmBiT transfected HEK293T cells with the D₂R antagonists haloperidol, spiperone and clozapine (10 μ M) for 10 min (**A**), 30 min (**B**), 4 h (**C**) or 16 h (**D**). The luminescent signal was normalized to the fluorescent signal of the co-transfected Venus protein in all conditions. Control = solvent-treatment (DMSO \leq 0.1%). (**A & B**) No significant effect was observed after 10 or 30 min of incubation ($n=3$, \pm SEM). (**C & D**) Spiperone reduced the level of D₂L dimerization by $\geq 40\%$ after 4 and 16 h of incubation ($n = 5$, \pm SEM) (non-parametric Kruskal–Wallis one-way Anova, followed by post-hoc analysis (Dunn’s multiple comparison test), * $p < 0.05$, ** $p < 0.01$).

5.3.3.3 Screening of a broader panel of D₂R ligands

To investigate a possible class-dependent effect of D₂R antagonists on the D_{2L}R dimer, a broader panel of D₂R ligands, including droperidol, spiperone, clozapine, olanzapine, risperidone, quinpirole, and haloperidol, was screened for their capacity to modulate the level of D_{2L}R homodimer formation following long-term incubation (16 h). Of these, droperidol, clozapine, risperidone, and the D₂R agonist quinpirole did not significantly ($p > 0.05$) modify the luminescent signal provoked by the dimer (**Figure 5.5**). Haloperidol only slightly decreased the level of dimer formation ($\pm 30\%$). On the other hand, the D₂R antagonist olanzapine clearly enhanced the luminescent signal by 45%. Finally again, the most significant effect was seen upon incubation with spiperone, with a clear reduction of 40–60%.

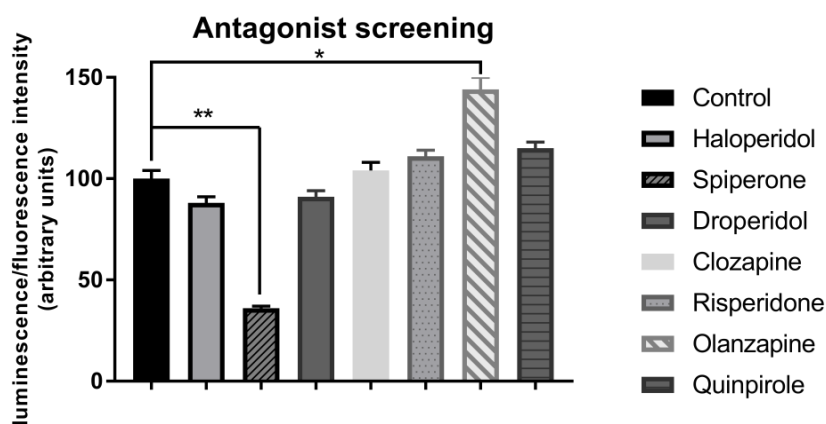


Figure 5.5 A panel of different D₂R ligands was screened via the NanoBiT® assay. Only spiperone reduced the level of dimerization of D_{2L}R significantly. Control = solvent-treatment (DMSO $\leq 0.1\%$). ($n = 3$, \pm SEM) (non-parametric Kruskal–Wallis one-way Anova, followed by post-hoc analysis (Dunn’s multiple comparison test), * $p < 0.05$, ** $p < 0.01$).

5.3.4 Validation of the spiperone-modulating capacity on the D_{2L}R homodimer

Several experimental setups were implemented to validate the modulating capacity of spiperone on the D_{2L}R dimer by investigating: (i) possible artifacts, (ii) expression levels of the D_{2L}R, and (iii) the specificity of the effect of spiperone on the D_{2L}R dimer.

First, to exclude that the observed effect was a result of possible artifacts such as toxicity, the possible influence of spiperone on the activity of native NanoLuciferase, transiently expressed in HEK293T cells, was investigated. Cells expressing the native luminescent

enzyme were incubated for different time points with 10 μ M of the antagonists. No impact on luciferase activity was observed (**Figure 5.6**).

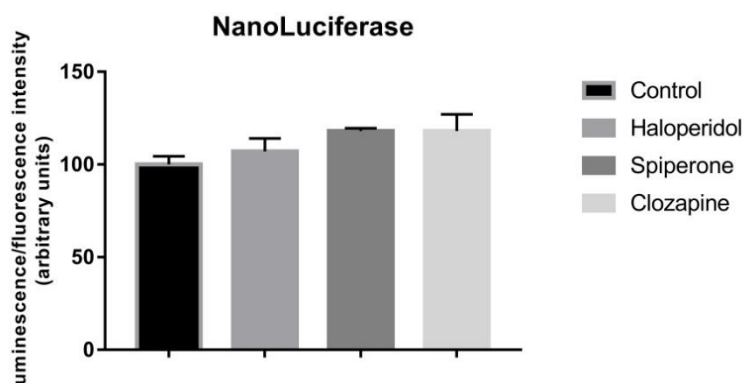


Figure 5.6 Signals obtained following incubation of NanoLuciferase transfected HEK293T cells with D₂R antagonists haloperidol, spiperone and clozapine (10 μ M) for 16 h. Control = solvent-treatment (DMSO \leq 0.1%). No significant effect was observed (n=2, \pm SEM).

Second, to rule out a possible role for spiperone on the expression level of the D_{2L}R, the receptor was fused to yellow fluorescent protein (YFP). HEK293T cells transiently transfected with the fusion construct were incubated with 10 μ M of the D₂R antagonists haloperidol, clozapine and spiperone (**Figure 5.7 A**). Incubation with these D₂R antagonists did not cause any significant alteration in the level of fluorescent signal after 16 h of incubation. Similarly, a western blot experiment under reducing conditions was conducted to analyze the expression of the fusion proteins D_{2L}R–SmBiT and D_{2L}R–LgBiT in both cells that had been and had not been incubated with the antagonists (**Figure 5.7 B**). The aim of this experiment was merely to evaluate whether there was an impact on D_{2L}R expression. After normalization to tubulin as a housekeeping protein, a 14% decrease of D_{2L}R fusion protein expression was observed in cells treated with spiperone, compared to the solvent-treated control. Under these (reducing) conditions, no clear bands of D_{2L}R dimers or higher oligomers could be observed, which might be explained by the fact that lower densities of receptors in the plasma membrane could conceivably reduce the proportion of receptors forming dimers, as reported before [68].

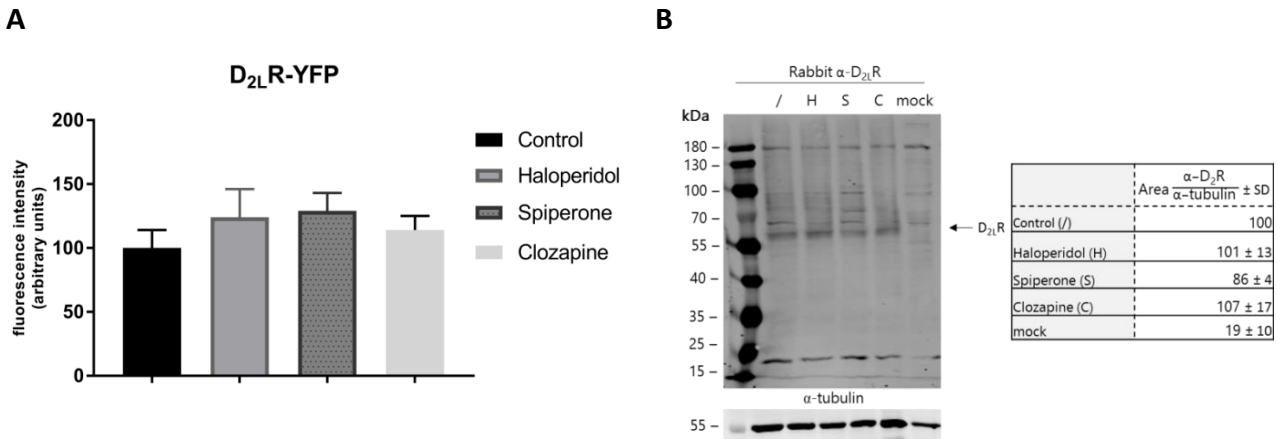


Figure 5.7 Analysis of the specificity of the effect provoked by spiperone on the D_{2L}R homodimer. **(A)** To ensure the effect evoked by spiperone is not simply due to an impact on the expression levels of the D_{2L}R, cells expressing D_{2L}R fused to yellow fluorescent protein (YFP) were incubated with the antagonists for 16 h. No impact was observed. **(B)** In addition, western blot analysis after 16 h of incubation with D₂R antagonists also did not reveal major impact on D_{2L}R (i.e. D_{2L}R-SmBiT and D_{2L}R-LgBiT) expression levels (Control = solvent-treated, H = Haloperidol, S = Spiperone, C= Clozapine, mock = non-transfected HEK293T cells). Results were normalized to tubulin values through analysis with ImageJ. Values of solvent-treated D_{2L}R transfected cells were arbitrarily set as 100% ($n = 3$, \pm SD).

Finally, the specificity of the effect of spiperone on the D_{2L}R homodimer was evaluated by examining its effect on another well-studied GPCR dimer, namely the adenosine A_{2a} receptor–D₂R dimer [19, 20, 69]. We therefore co-expressed A_{2a}–LgBiT and D_{2L}R–SmBiT in HEK293T cells that were treated with 10 μ M spiperone for 16 h (**Figure 5.8**). No significant effect ($p > 0.05$) was observed on the level of A_{2a}–D_{2L}R dimer formation, lending further support to the specificity of the effect of spiperone on the D_{2L}R homodimer.

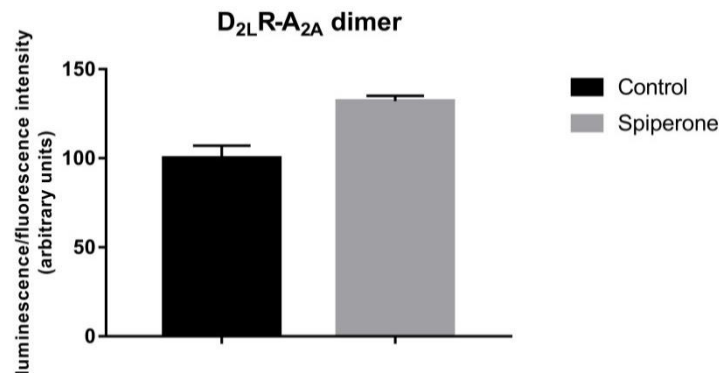


Figure 5.8 Cells expressing another well-known dimer A_{2a}–D₂R, were incubated with 10 μ M spiperone for 16 h. Spiperone did not affect the level of A_{2a}–D₂R dimer formation ($n = 3$, \pm SEM).

5.3.5 Spiperone and clozapine achieve stable binding poses in D₂R during molecular dynamics simulations

In order to comprehend how spiperone might reduce D₂R homodimerization relative to clozapine at the molecular level, we first docked each ligand into the crystal structure of D₂R (PDB id: 6CM4) [51] and then performed unbiased molecular dynamics (MDs) simulations to allow for ligand-induced conformational changes to occur in the monomeric receptor. During respective time periods of 3 μ s, both spiperone and clozapine achieved stable binding poses (**Figure 5.9 A**) despite some initial conformational changes in both ligands, as might be expected (**Figure 5.10 A**). Specifically, clozapine and spiperone achieved stable bound conformations from 0.4 and 1.8 μ s onwards, respectively, where root mean square deviation (RMSD) from their final conformations remained <3.0 Å (average of 1.5 Å \pm 0.5 S.D. for clozapine and 1.9 Å \pm 1.0 S.D. for spiperone). The relative higher conformational fluctuation observed with spiperone can be attributed to its greater flexibility, mainly due to its central alkyl chain. Despite clozapine and spiperone reaching stable binding poses at different times, in both cases the D₂R monomer presented little conformational change of its backbone, with final values of 2.5 Å and 2.2 Å, respectively (**Figure 5.10 B**). In the original crystal structure, residues in close contact with co-crystallized risperidone [55] (<3.5 Å) were located on extracellular loop 1 (ECL1), TM3, TM5, and TM6 (**Table 5.2** and **Figure 5.11**). In terms of the protein–ligand interactions in common between risperidone, spiperone, and clozapine, the most prominent was an electrostatic interaction between the protonated ligand amine group and Asp114^{3.32} (superscript numbers refer to the Ballesteros and Weinstein generic numbering scheme [70], which includes relative TM helix location) on TM3, which was maintained over respective MD simulations. Other common interactions, which occurred once each ligand found its stable binding pose, included contacts with residues on TM3, TM5, and extracellular loop 2 (ECL2): Val115^{3.33}, Ile184^{ECL2}, and Ser193^{5.42} (**Figure 5.9 A** and **Table 5.2**). However, clozapine established several distinct contacts with residues on TM5 and TM6. On the other hand, spiperone was frequently in contact with residues on TM2 and TM3 (**Table 5.2**). These different residues in contact with clozapine and spiperone demonstrated that their binding poses were quite different (**Figure 5.9 A** and **Table 5.2**).

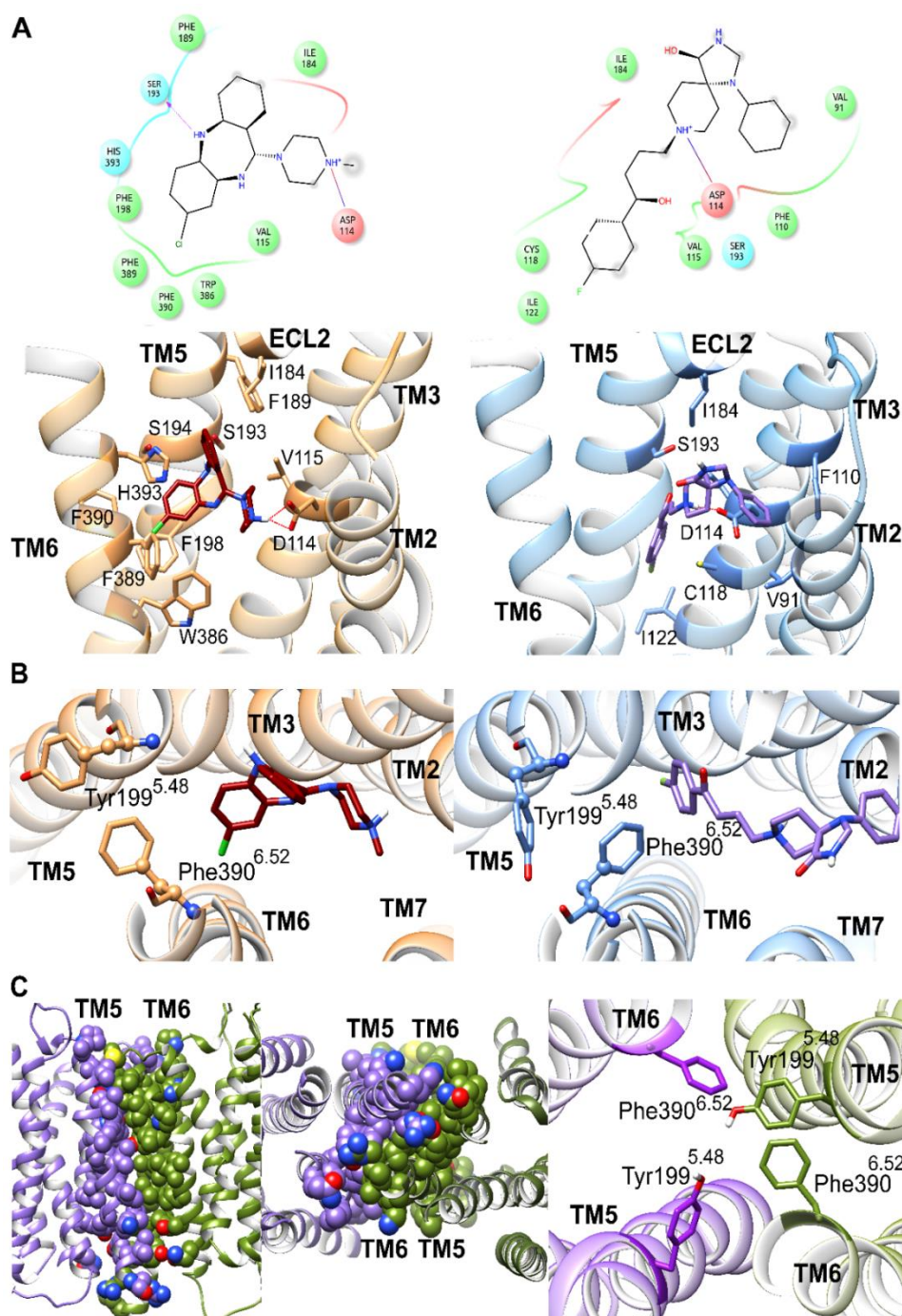


Figure 5.9 D₂R monomer and homodimer complexes. Transmembrane helices are labeled as TM. (A) 2D and 3D (top and bottom, respectively) stable binding poses of residues (abbreviated following three letter or single letter code, respectively) in close contact during molecular dynamics (MD) simulation (<3.5 Å) with clozapine and spiperone (dark red and purple, respectively) bound to respective D₂R monomer (left and right, colored in orange and blue, respectively). (B) Trans and cis conformations of Tyr199^{5.48} and Phe390^{6.52} χ_1 dihedral angles selected by bound clozapine or spiperone (dark red and purple respectively) bound to D₂R monomer (left and right, colored in orange and blue, respectively). (C) From left to right, lateral and intracellular views of TM5–TM6–TM5–TM6 D₂R homodimer model interface, which generates aromatic interactions between Tyr199^{5.48} and Phe390^{6.52} of both D₂R protomers during MD simulation (colored in purple or green, respectively).

Table 5.2 Protein–ligand interactions (<3.5 Å) of co-crystallized risperidone, and stably bound clozapine and spiperone during MD simulations. (i) Common residues in contact between all ligands; (ii) common residues in contact between risperidone and clozapine; (iii) common residues in contact between risperidone and spiperone; (iv) common residues in contact between clozapine and spiperone.

Ligand	Unique interactions	Common interactions	
Risperidone	Trp100 ^{ECL1}	Asp114 ^{3.32}	(I)
	Ser197 ^{5.48}	Cys118 ^{3.36}	(III)
	Phe382 ^{6.44}	Ile122 ^{3.40}	(III)
	Tyr416 ^{7.43}	Trp386 ^{6.48}	(II)
		Phe389 ^{6.51}	(II)
Clozapine	Phe189 ^{5.38}	Asp114 ^{3.32}	(I)
	Ser193 ^{5.42}	Val115 ^{3.33}	(IV)
	Phe198 ^{5.47}	Ile184 ^{ECL2}	(IV)
	Phe390 ^{6.52}	Ser193 ^{5.42}	(IV)
	His393 ^{6.55}	Trp386 ^{6.48}	(II)
		Phe389 ^{6.51}	(II)
Spiperone	Val91 ^{2.61}	Asp114 ^{3.32}	(I)
	Phe110 ^{3.28}	Val115 ^{3.33}	(IV)
		Cys118 ^{3.36}	(III)
		Ile122 ^{3.40}	(III)
		Ile184 ^{ECL2}	(IV)
		Ser193 ^{5.42}	(IV)

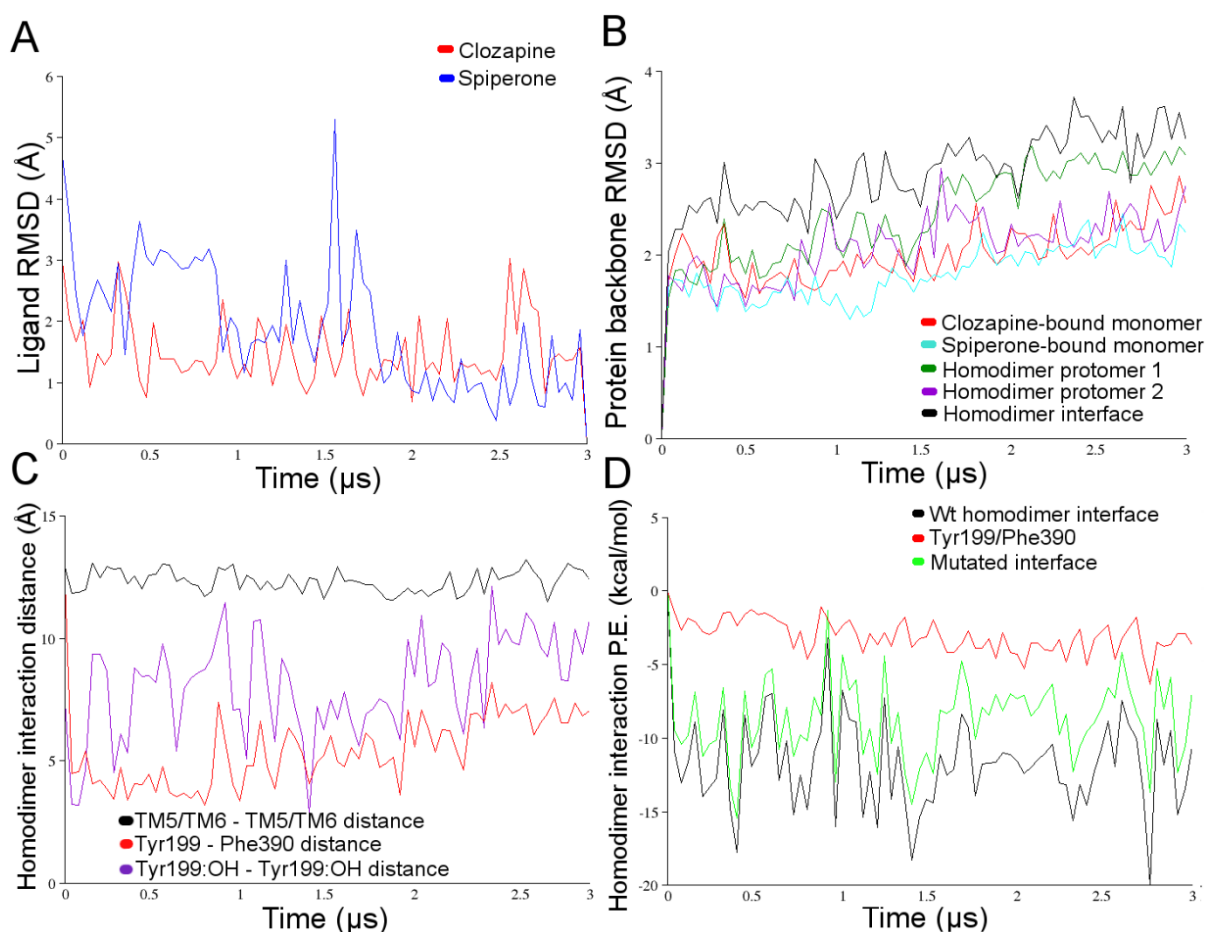


Figure 5.10 (A) Conformational stability of bound clozapine or spiperone (red and blue, respectively) in terms of RMSD compared against last conformation achieved during MD simulations. (B) Conformational change of the backbone of transmembrane domain of D₂R monomer with bound clozapine or spiperone, and protomer 1 or 2 and TM5-TM6-TM5-TM6 interface of D₂R homodimer (red, blue, purple, green and black, respectively) compared against initial conformation. (C) Distance between center of mass (COM) of interacting transmembrane helices (TM5 and TM6, in black), closer distance between residues Tyr199^{5.48} and Phe390^{6.52} (in red), and distance between sidechain oxygen atoms of Tyr199^{5.48} of both protomers (in purple). (D) Energetic analysis of *wt* TM5-TM6-TM5-TM6 D₂R homodimer interface, specific energetic contribution of interactions between Tyr199^{5.48} and Phe390^{6.52}, and mutated D₂R homodimer interface (Tyr199^{5.48} and Phe390^{6.52} replaced with alanine), colored in black, red and green, respectively.

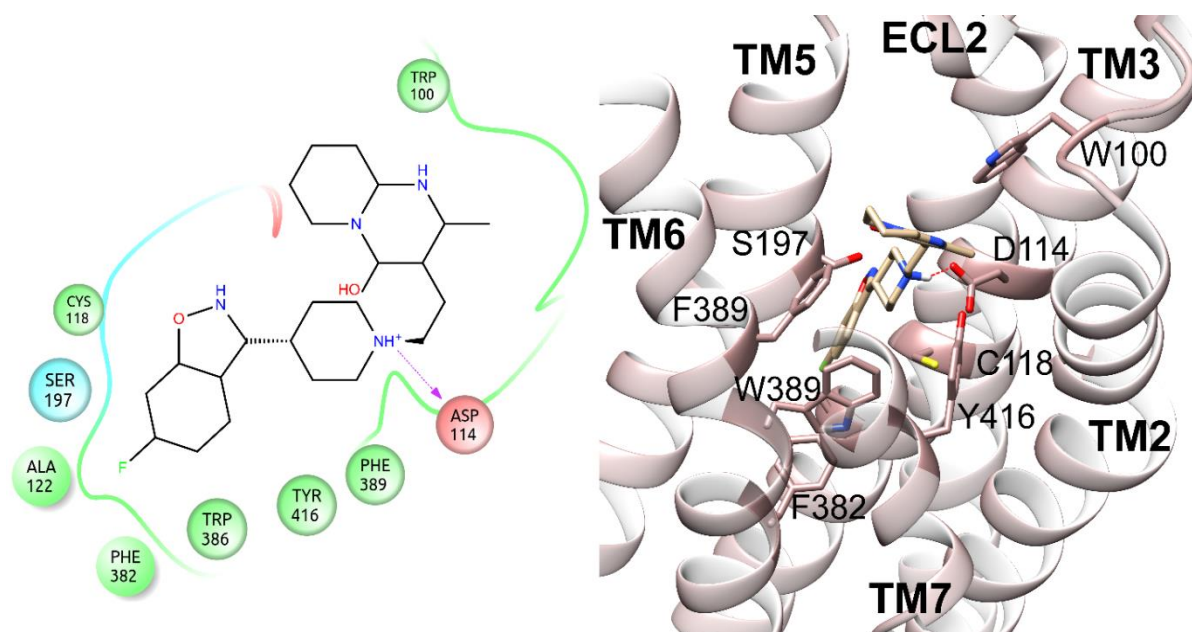


Figure 5.11 Crystallized orthosteric binding pose of risperidone. 2D and 3D binding pose defined by residues close-contacted (<3.5 Å) by risperidone (tan) in D₂R crystal structure (brown, PDBid: 6CM4).

5.3.6 Spiperone and clozapine select for different sidechain conformations in D₂R TM5 and TM6

To ascertain the most important conformational changes selected by the stable binding poses of clozapine and spiperone in D₂R, we carried out residue-level analyses of the monomeric MD simulations. No significant conformational differences between systems were observed in any residues located on TM helices, except for TM5 and TM6. Specifically, neighboring residues Tyr199^{5.48} and Phe390^{6.52} showed different χ_1 dihedral angle conformations with different bound antagonists. In general, for these two aromatic residues, two different pseudo-stable conformations can be observed in our MD simulations, a cis and a trans χ_1 dihedral angle of 300° and 180°, respectively (**Figure 5.9 B**). The D₂R crystal structure presented cis conformations for both Tyr199^{5.48} and Phe390^{6.52}, which underwent conformational changes to trans more frequently when clozapine was bound than with spiperone (**Figure 5.12**). Specifically, considering only time periods where clozapine and spiperone presented stable binding poses (from 0.4 and 1.8 μ s onwards, respectively) clozapine preferentially selected for Tyr199^{5.48} and Phe390^{6.52} χ_1 trans conformations 99% of the time. This “double” χ_1 trans conformation led to an outward orientation (towards the membrane) for Tyr199^{5.48} and Phe390^{6.52}, which potentially may encourage protein–protein interactions through the formation of aromatic contacts, which

are known to be important (**Figure 5.9 B**) [71]. Conversely, spiperone induced rapid fluctuations between χ_1 cis and trans conformations of Tyr199^{5.48}, with the cis selected 25% of the time, whereas the cis conformation of Phe390^{6.52} was exclusively maintained. The χ_1 cis conformation of Tyr199^{5.48} and Phe390^{6.52} oriented them in a more inward position, away from the membrane, which may conceivably discourage protein–protein interactions (**Figure 5.9 B**).

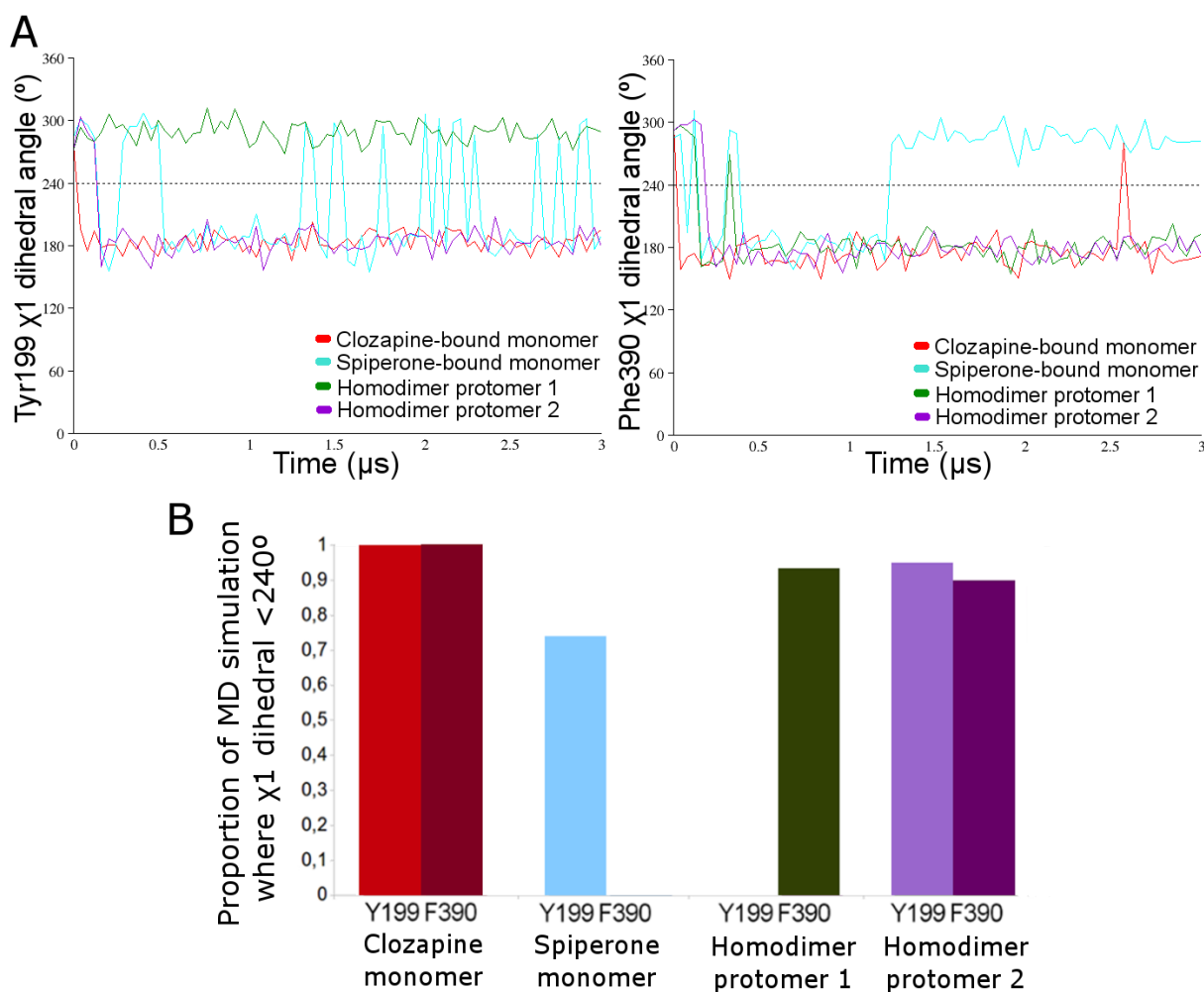


Figure 5.12 (A) Time-dependent plots of Tyr199^{5.48} and Phe390^{6.52} χ_1 dihedral angle induction (left and right graph, respectively) of D₂R monomer with bound clozapine or spiperone, and protomer 1 or 2 of D₂R homodimer (red, blue, green and purple, respectively) during respective MD simulations. Black dotted line indicates *cis/trans* conformation threshold. **(B)** Proportion of selected χ_1 dihedral angle conformation <240° in D₂R monomer with bound stable clozapine or spiperone, and protomer 1 and 2 of D₂R homodimer (red, blue, green and purple, respectively).

5.3.7 Aromatic interactions stabilize D₂R homodimer model interface during MD simulation

In order to probe how a D₂R homodimer might be affected by sidechain conformational changes in TM5 and TM6, a D₂R homodimer without bound antagonist was modeled from the original crystal structure with a TM5–TM6–TM5–TM6 interface (in line with experimental evidence by Pulido, 2018 [32]) by protein–protein docking. This resulted in a D₂R homodimer with a highly favorable interface docking score of –9.7 (on a scale of 0 to –10, where lower than –5.0 was considered satisfactory ([56]); see Methods). This model was subjected to an MD simulation of 3 μ s to investigate homodimer physical stability and receptor conformational changes in individual protomers (**Figure 5.9 C**). During this MD simulation, the TM5–TM6–TM5–TM6 interface remained intact, according to a consistently close interaction distance (**Figure 5.10 C**) between TM5/TM6 helices of each protomer. In the process, participating helices experienced a moderate backbone conformational change of 3.2 Å in order to enhance mutual binding, obtaining an average interaction energy of –11.7 kcal/mol (± 3.2 S.D.) between protomers (**Figure 5.10 B & D**). Furthermore, from an analysis of individual protomers in the homodimer, it can be observed that one protomer underwent slightly more backbone conformational changes than the others during the second half of MD (average RMSDs of 2.9 Å and 2.3 Å, respectively (**Figure 5.10 B**)). To ascertain the relevance of interactions involved in the TM5–TM6–TM5–TM6 homodimer interface, we performed a conformational and energetic analysis of specific residues on TM5 and TM6. Interestingly, the D₂R protomer whose backbone remained relatively unchanged rapidly selected for the cis to trans conformational change of Tyr199^{5.48} and Phe390^{6.52} χ 1 dihedral angles (**Figure 5.9 C**), which occurred at 94% and 90% of the total MD simulation time, respectively (**Figure 5.12**). In addition, a rapid cis to trans conformational change of Phe390^{6.52} χ 1 dihedral angle was observed in the other protomer (occurring at 93% of total time). However, in this second protomer, Tyr199^{5.48} presented no significant conformational change and remained in the cis conformation (**Figure 5.12**). As shown in **Figure 5.9 C**, the outward conformations achieved by Tyr199^{5.48} and Phe390^{6.52} in the homodimer enabled an aromatic interaction network to form, as well as transient H-bond formation between Tyr199^{5.48} sidechains of both protomers (H-bond occupancy of 4%). As a result, the average minimum distance between Tyr199^{5.48}/Phe390^{6.52} residues of each protomer was 5.5 Å (± 1.5 S.D.) (**Figure 5.10 C**). From an energetic point of view, alanine scanning of Tyr199^{5.48} and

Phe390^{6,52} confirmed the relevance of these residues in the D₂R homodimer interface. Removal of these aromatic interactions (by alanine mutation) resulted in a less favorable average interface energy of -8.6 kcal/mol (± 2.8 S.D.), which suggested this aromatic interaction network contributed an average of -3.1 kcal/mol to the homodimer interface.

5.3.8 D_{2L}R oligomerization

HEK293T cells were co-transfected with 400 ng D_{2L}R–SmBiT, D_{2L}R–LgBiT, and increasing DNA concentrations of native D_{2L}R (0–600 ng) (**Figure 5.13**). Co-expression of native D_{2L}R did not circumvent or attenuate the complemented luminescent signal, but in fact it stimulated the D_{2L}R oligomerization (**Figure 5.13 A**) in an expression-dependent manner. To rule out that crowding of GPCRs on the membrane or nonspecific aggregation would result in trivial complementation of the NanoBiT proteins, the muscarinic M₁ receptor (M₁) was co-transfected instead of the native D_{2L}R (**Figure 5.13 B**). Co-expression of the M₁ receptor did not modify the luminescent signal in a significant manner. Furthermore, also in the presence of more D_{2L}Rs, spiperone still had an impact: upon treatment, the increase in oligomerization by increasing amounts of native D_{2L}R was less pronounced (**Figure 5.13 C**). Specifically, when comparing the experimental setup of HEK293T cells transiently expressing D_{2L}R–LgBiT and D_{2L}R–SmBiT with the same setup but with high levels of co-transfected native D_{2L}R (4:4:6) (**Figure 5.13 A**), a significant twenty-fold increase in luminescent signal was observed for the latter. On the other hand, when treated with spiperone, only a five-fold difference between the same two experimental setups could be observed (**Figure 5.13 C**).

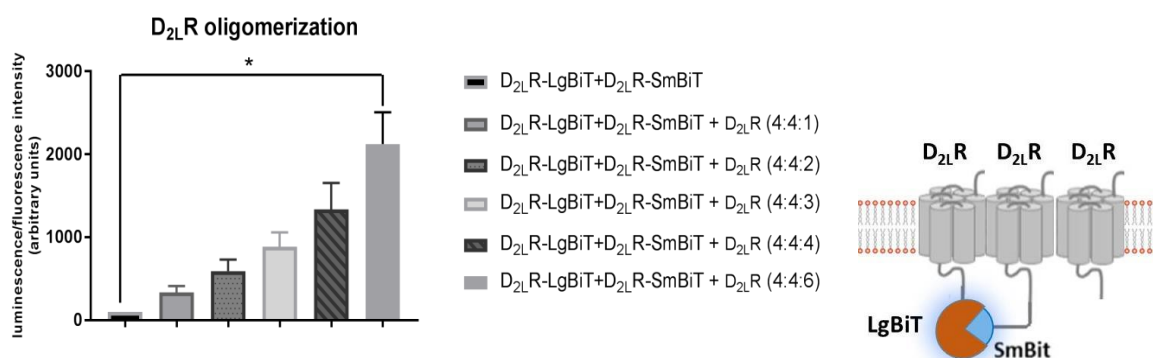
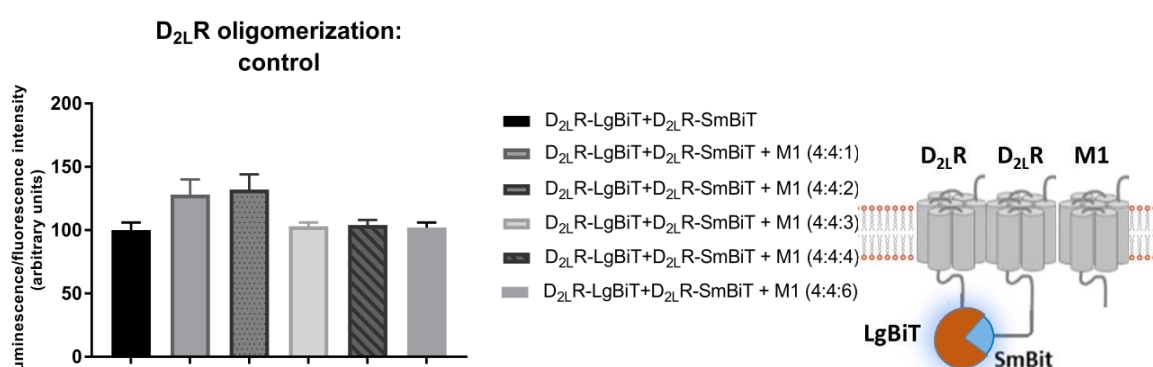
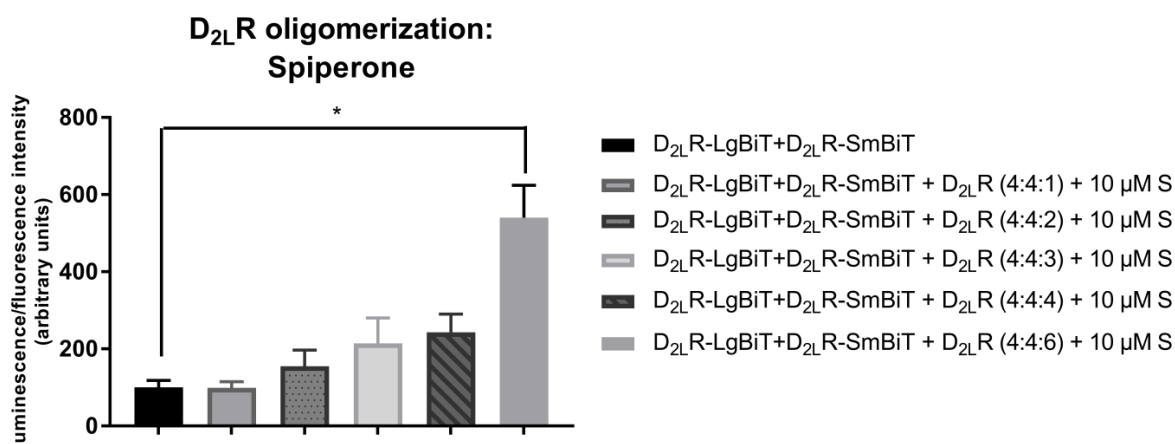
A**B****C**

Figure 5.13 HEK293T cells transiently expressing higher levels of D₂L R (fusion) proteins. **(A)** An increasing amount of native D₂L R was co-transfected with D₂L R-LgBiT and D₂L R-SmBiT vectors. Higher expression levels of D₂L R stimulate D₂L R oligomerization. **(B)** An increasing amount of native muscarinic M₁ receptor does not attenuate nor evoke higher luminescent signals evoked by D₂L R dimerization. **(C)** Incubation of cells with 10 μM spiperone (S) results in a less pronounced increase of D₂L R di- and oligomerization upon expression of increased levels of native D₂L R. Experiments were performed three times in triplicate. ($n = 3$, \pm SEM) (non-parametric Kruskal–Wallis one-way Anova, followed by post-hoc analysis (Dunn’s multiple comparison test), * $p < 0.05$).

5.4 Discussion

Over the past two decades, a growing body of evidence suggests that GPCRs are able to form dimers and/or even higher-order oligomers [72]. Because these GPCRs are involved in many physiological processes, these dimeric or oligomeric GPCR complexes are not only of paramount importance for possible alterations in signaling cascades, compared to their monomers, but also for their association with debilitating diseases.

Interestingly, a significant increase of D₂R dimerization has already been observed in post-mortem striatal tissue of schizophrenia patients [48]. Concerning the dimer formation of D₂Rs, as well as other class A subfamily GPCRs [45, 46], clear evidence for the transient characteristics of the dimer formation has been provided by single-molecule tracking studies [31], with a lifetime of 68 ms being assigned to the D₂R dimer [28, 42]. Although a lot of knowledge has been gathered concerning dimer formation of the D₂R, key questions still remain unanswered. For example, different D₂R dimeric interfaces have been proposed [29, 33], as well as a hypothesis of multiple oligomerization interfaces [42]. Nevertheless, a recent interest has arisen in the establishment of a D₂R TM5–TM6–TM5–TM6 dimeric interface [32, 40, 41]. In our present study we have addressed the computational reliability of this dimeric interface and its implication in the D₂R homodimer by means of computational techniques including microsecond-length MD simulations. In addition, targeting GPCR dimers with ligands or selective chemical tools may elaborate the signaling behavior of dimers as well as their tendency or preference towards GPCR–GPCR interactions. Nonetheless, this topic of ligand-induced modulation of GPCR dimers has been much debated [73–75], with both arguing for and against. In the current study, we further elaborate on this topic and demonstrate the ability of spiperone to alter the dynamic equilibrium between D₂L₂R monomers and dimers, with a clear preference towards monomers.

The Nanoluc[®] Binary Technology (NanoBiT[®]), developed by Promega in 2016 [76], proved to be an interesting tool to study D₂R dimers. In contrast to other complementation-based assays, NanoBiT[®] offers the great advantage of being reversible, which gives opportunity to look into detail on the kinetics of GPCR interactions. Importantly, since this system requires the fusion of LgBiT or SmBiT to the GPCR of interest, the functionality of D₂L₂R fusion proteins

was demonstrated by mini-Gα_i protein recruitment to both receptors upon stimulation with the D₂R agonist quinpirole.

Using this experimental HEK293T-based design, we screened six different D₂R antagonists and one agonist for their ability to modulate the level of D_{2L}R dimer formation. This panel of ligands comprises droperidol, spiperone, clozapine, olanzapine, risperidone, quinpirole, and haloperidol. Although several of the aforementioned ligands have previously been classified as antagonists, one should keep in mind that their inverse agonist capacity has now been recognized [77-80]. Of those, the D₂R antagonist/inverse agonist spiperone could significantly decrease the level of D_{2L}R dimers by 40%–60% in real-time and after long-term (up to 16 h) incubation. Another D₂R antagonist, haloperidol, also modulates the level of D_{2L}R dimerization, but in a less significant manner (±30%). In contrast, the D₂R antagonist olanzapine significantly increases the level of D_{2L}R dimer formation by ± 45%. Furthermore, a class-dependent effect between the butyrophenones (haloperidol, spiperone, and droperidol) and atypical antipsychotics (clozapine, risperidone, and olanzapine) could not be distinguished. For the D₂R agonist quinpirole, only a minor increase in luminescent signal provoked by D_{2L}R dimer formation could be observed. Although it was demonstrated that agonist addition (i.e., dopamine and quinpirole) stabilized the formation of D₂R dimers by a factor of 1.5 in a total measure time of 400 ms by single-molecule tracking [28], we might conclude from this study that this modulating effect does not significantly hold true for long-term effects. Nevertheless, one should keep in mind that findings might differ due to diverse experimental assay setups as well.

In this study, the effect of spiperone on the level of homodimerization of the D_{2L}R was only observed to be significant at high concentrations (i.e. ≥ 10 μM). Nevertheless, the reported affinity of spiperone for D₂R is 0.16 nM [81], which means that the effect of spiperone is only provoked at 1.7×10^5 times its K_i value. Consequently, this concentration is pharmacologically irrelevant *in vivo* as it would be associated with severe toxicity [82]. However, the straightforward translation of *in vitro* concentrations to the *in vivo* situation is difficult. Nevertheless, this effect of spiperone has proven to be reproducible and could not be linked to cytotoxicity, as from control experiments executed in this study (see further). Hypothetically, negative allosteric interactions in the D_{2L}R dimer might occur at high concentrations of spiperone or spiperone might bind to allosteric sites at high

concentrations and thereby inhibit dimerization. Further investigation with lower concentrations and more sensitive techniques is a prerequisite.

In order to further examine the modulating capacity of spiperone on the D_{2L}R dimer, we performed screenings towards incubation time (real-time vs. long-term effects), expression levels of D_{2L}R, and the specificity of the effect on the D_{2L}R dimer. From this, we can conclude that a decrease in the level of D_{2L}R dimerization could readily be observed after approximately 30 min and was still detected after long-term incubation up to 16 h. These data are in agreement with findings for the dopamine D₃R homodimer, for which similar effects were observed after 16 h treatment with spiperone [83]. As a control, we examined whether spiperone altered expression levels of the D_{2L}R, which could cause a decrease in luminescent signal. This possibility was ruled out by both western blot analysis and the fluorescence analysis of a D₂R–YFP fusion protein, expressed in cells that were or were not treated with spiperone for 16 h.

Additionally, to ensure the specificity of the effect of spiperone on the D₂R homodimer, the same experimental set-up with another GPCR dimer was investigated. For this, we selected the well-studied adenosine A_{2a} receptor (A_{2a}) and D₂R dimer since many research groups have reported on: (i) the formation of the dimer by several techniques such as BRET and FRET [20, 84] and protein complementation assays [85], (ii) specific dimer characteristics regarding signaling pathways of the A_{2a}–D₂R dimer [86, 87], (iii) the dimer interface [88], and (iv) allosteric mechanisms [69], among others. Importantly, the fact that several studies have linked this dimer to Parkinson's disease [89–92] lends support to the relevance of research within this field. Nevertheless, to the best of our knowledge, the modulating capacity of the D₂R antagonist spiperone on the level of A_{2a}–D₂R dimer formation has not been investigated yet. Overall, the effect of spiperone on the A_{2a}–D_{2L}R dimer was evaluated by treatment with 10 μ M spiperone for 16 h. However, this did not have a significant effect on the level of A_{2a}–D_{2L}R dimer formation. Thus, since the spiperone-modulating capacity does not hold true for all D₂R dimer complexes, this effect might be specific for the D_{2L}R homodimer or oligomer.

Computational techniques such as MD simulations have shown promise for studying GPCRs, such as D₂R, and their mechanisms of signaling transmission at the atomic level [30]. From a computational point of view, in our study we observed noticeable differences between

the orthosteric binding poses of spiperone and clozapine in a D₂R monomer, which select for different sidechain conformations of Tyr199^{5.48} and Phe390^{6.52} on TM5 and TM6, respectively. Interestingly, the inward conformations adopted by Tyr199^{5.48} and Phe390^{6.52} when spiperone is bound differ from the outward conformations induced by clozapine, which are also favored in the modeled D₂R homodimer. In this study we have observed aromatic interactions between Tyr199^{5.48} and Phe390^{6.52}, as well as occasional H-bonding between Tyr199^{5.48}, of both protomers in a model D₂R homodimer, which could be indicative of the relevance of these two residues in the establishment of a TM5–TM6–TM5–TM6 interface and their role in the homodimerization process. In addition, our D₂R homodimer model with a TM5–TM6–TM5–TM6 interface, in accordance with a previously published D₂R–mGluR₅ heterodimer model presented by Qian *et al.* (2018) [40], is physically stable over microsecond-length MD simulations. In addition to this homodimeric interface, it has been widely described that D₂R heteromerizes through a TM4–TM5–TM4–TM5 interface with other class A GPCRs, such as A_{2a} and AT1 receptors [35–39]. Therefore, our results raise questions about the oligomerization interfaces D₂R may form. In our present study we observe that conformational changes specifically occurring in TM5 and TM6, resulting from bound spiperone and involving inward Tyr199^{5.48} and Phe390^{6.52} sidechain conformations, may alter the TM5–TM6–TM5–TM6 D₂R homodimer interface. This fact may explain the results observed in our experimental approach where spiperone specifically reduces levels of the D₂R homodimer, while having no significant effect on A_{2a}–D₂R heterodimer formation. Altogether, these results indicate that the interfaces involved in homodimerization of D₂R may differ from the interfaces involved in heterodimerization processes with class A GPCRs, which could also differ between different GPCR classes, in agreement with the hypothesis of multiple oligomerization interfaces presented by Kasai *et al.* (2014) [42].

Finally, D_{2L}R oligomerization was investigated in a similar experimental design, using the NanoBiT[®] assay. Although it was first postulated that co-transfection of the native D_{2L}R would attenuate the luminescent signal provoked by D_{2L}R dimer formation by competing for interaction with the D_{2L}R–SmBiT and D_{2L}R–LgBiT fusion proteins, the opposite was observed. Oligomerization of the D_{2L}R appeared to be concentration-dependent, with higher expression levels of native D₂R provoking complementation of the fusion proteins because of the close proximity to their corresponding receptors, suggesting stimulation of

the organization as higher-order oligomers. The fact that the same outcome was not observed when co-expressing increasing amounts of the muscarinic M₁ receptor confirms that this effect was not due to nonspecific aggregation or crowding of GPCRs. The finding of an increased D₂R homo-oligomerization with higher levels of expression is in agreement with literature [26, 31, 43, 44, 93] and has been reported for other dopamine receptors as well [83, 94]. In addition, the effect of spiperone was evaluated on higher expression levels of D_{2L}R as well. Also here we demonstrated that spiperone reduces the level of D_{2L}R–D_{2L}R interactions. Rather than a twenty-fold increase of luminescent signal resulting from higher D_{2L}R expression levels, pre-treatment with spiperone only resulted in a five-fold increase. To conclude, higher expression levels stimulate D_{2L}R–D_{2L}R interaction, suggesting oligomerization. Also at these higher expression levels, spiperone still exerts a negative impact on D_{2L}R–D_{2L}R interactions. Consistent with this concept, one might speculate that spiperone could exert different pharmacological properties in different areas of the brain, in co-relation with the expression level of D_{2L}R.

Interestingly, Ng *et al.* (1996) [24] postulated that spiperone favors binding to the monomer over the dimer, whereas risperidone binds to monomers as well as dimers. In light of our findings, one might hypothesize that spiperone does not necessarily favor binding to the monomers, but simply reduces the number of dimers, as observed in this study.

On the contrary, Armstrong *et al.* (2001) [25] reported quite opposite data obtained from ligand binding experiments. These authors proposed a model wherein D₂Rs can form dimeric units with two orthosteric binding sites for two equivalents, which allows allosteric cooperativity. From experimental data, it was suggested that the first and second equivalent of [³H]spiperone only exerted limited cooperativity between the dimer units, in the absence or presence of sodium ions. On the other hand, [³H]raclopride seems to prefer binding to monomeric units because of an observed negative cooperative effect on the binding of the second equivalent upon binding of the first equivalent, which results in a reduced affinity of the second site of the dimer for [³H]raclopride. Within the mindset of this proposed model by Armstrong *et al.* [25], [³H]spiperone binds to the D₂R dimer, and although no negative effect on affinity of both binding sites due to cooperativity was observed by the authors, from our data we can suggest that conformational changes within the dimer upon spiperone binding might lead to dissociation of the dimer to its monomers.

Interestingly, a similar destabilizing effect of spiperone on D₃R oligomeric complexes was reported by Marsango *et al.* (2017) [83]. Using a spatial intensity distribution analysis (SpIDA) method, the antipsychotics spiperone and haloperidol reduced the level of D₃R dimerization in a ligand-dependent manner. Moreover, this effect could be reversed upon ligand washout. Since the D₃ and D₂ receptors are highly homologous and show a sequence identity of 78% [95], it might not be surprising that certain ligands modulate these receptors in a similar way.

Although the development of the reversible complementation-based NanoBiT[®] assay allows the screening and discovery of ligands that could modulate the level of dimerization, this technique does not provide information about the dynamics of the D₂R dimers or oligomers at the single molecule level. To allow visualization and tracking in real-time of the influence of spiperone on a D₂R dimer in the membrane of living cells, techniques such as single-molecule sensitive total internal reflection fluorescence microscopy (TIRF-M) are recommended. Thus, based on the present understanding, further research to study the effect of the D₂R antagonist spiperone on the D₂R homodimer in detail is required.

References

1. Beaulieu, J.M. and R.R. Gainetdinov, *The physiology, signaling, and pharmacology of dopamine receptors*. Pharmacological reviews, 2011. **63**(1): p. 182-217.
2. Rangel-Barajas, C., I. Coronel, and B. Floran, *Dopamine Receptors and Neurodegeneration*. Aging and disease, 2015. **6**(5): p. 349-68.
3. Missale, C., et al., *Dopamine receptors: from structure to function*. Physiological reviews, 1998. **78**(1): p. 189-225.
4. Farran, B., *An update on the physiological and therapeutic relevance of GPCR oligomers*. Pharmacological research, 2017. **117**: p. 303-327.
5. Ferre, S., et al., *G protein-coupled receptor oligomerization revisited: functional and pharmacological perspectives*. Pharmacological reviews, 2014. **66**(2): p. 413-34.
6. Fiorentini, C., et al., *Dimerization of dopamine D1 and D3 receptors in the regulation of striatal function*. Current opinion in pharmacology, 2010. **10**(1): p. 87-92.
7. Blasiak, E., et al., *Genetic variants of dopamine D2 receptor impact heterodimerization with dopamine D1 receptor*. Pharmacological reports : PR, 2017. **69**(2): p. 235-241.
8. O'Dowd, B.F., et al., *D5 dopamine receptor carboxyl tail involved in D5-D2 heteromer formation*. Biochemical and biophysical research communications, 2013. **431**(3): p. 586-9.
9. Van Craenenbroeck, K., et al., *Role of dimerization in dopamine D(4) receptor biogenesis*. Current protein & peptide science, 2014. **15**(7): p. 659-65.
10. Nakagawa, M., et al., *Dopamine D2 receptor Taq IA polymorphism is associated with postoperative nausea and vomiting*. Journal of anesthesia, 2008. **22**(4): p. 397-403.
11. Pan, Y.Q., et al., *Association between ANKK1 (rs1800497) polymorphism of DRD2 gene and attention deficit hyperactivity disorder: a meta-analysis*. Neuroscience letters, 2015. **590**: p. 101-5.
12. Rocchetti, J., et al., *Presynaptic D2 dopamine receptors control long-term depression expression and memory processes in the temporal hippocampus*. Biological psychiatry, 2015. **77**(6): p. 513-25.
13. Tozzi, A., et al., *Dopamine D2 receptor-mediated neuroprotection in a G2019S Lrrk2 genetic model of Parkinson's disease*. Cell death & disease, 2018. **9**(2): p. 204.
14. Urs, N.M., S.M. Peterson, and M.G. Caron, *New Concepts in Dopamine D2 Receptor Biased Signaling and Implications for Schizophrenia Therapy*. Biological psychiatry, 2017. **81**(1): p. 78-85.
15. Weber, M.A., et al., *Enhanced dopamine D2 autoreceptor function in the adult prefrontal cortex contributes to dopamine hypoactivity following adolescent social stress*. The European journal of neuroscience, 2018. **48**(2): p. 1833-1850.
16. Weinstein, J.J., et al., *PET imaging of dopamine-D2 receptor internalization in schizophrenia*. Molecular psychiatry, 2018. **23**(6): p. 1506-1511.
17. Araki, K., et al., *Structure and expression of human and rat D2 dopamine receptor genes*. Neurochemistry international, 1992. **21**(1): p. 91-8.
18. Dal Toso, R., et al., *The dopamine D2 receptor: two molecular forms generated by alternative splicing*. The EMBO journal, 1989. **8**(13): p. 4025-34.

19. Borroto-Escuela, D.O., et al., *Mapping the Interface of a GPCR Dimer: A Structural Model of the A2A Adenosine and D2 Dopamine Receptor Heteromer*. *Frontiers in pharmacology*, 2018. **9**: p. 829.
20. Canals, M., et al., *Adenosine A2A-dopamine D2 receptor-receptor heteromerization: qualitative and quantitative assessment by fluorescence and bioluminescence energy transfer*. *The Journal of biological chemistry*, 2003. **278**(47): p. 46741-9.
21. Niewiarowska-Sendo, A., et al., *Bradykinin B2 and dopamine D2 receptors form a functional dimer*. *Biochimica et biophysica acta*, 2017. **1864**(10): p. 1855-1866.
22. Kearn, C.S., et al., *Concurrent stimulation of cannabinoid CB1 and dopamine D2 receptors enhances heterodimer formation: a mechanism for receptor cross-talk?* *Molecular pharmacology*, 2005. **67**(5): p. 1697-704.
23. Pinna, A., et al., *L-DOPA disrupts adenosine A(2A)-cannabinoid CB(1)-dopamine D(2) receptor heteromer cross-talk in the striatum of hemiparkinsonian rats: biochemical and behavioral studies*. *Experimental neurology*, 2014. **253**: p. 180-91.
24. Ng, G.Y., et al., *Dopamine D2 receptor dimers and receptor-blocking peptides*. *Biochemical and biophysical research communications*, 1996. **227**(1): p. 200-4.
25. Armstrong, D. and P.G. Strange, *Dopamine D2 receptor dimer formation: evidence from ligand binding*. *The Journal of biological chemistry*, 2001. **276**(25): p. 22621-9.
26. Wurch, T., A. Matsumoto, and P.J. Pauwels, *Agonist-independent and -dependent oligomerization of dopamine D(2) receptors by fusion to fluorescent proteins*. *FEBS letters*, 2001. **507**(1): p. 109-13.
27. Sagar, G.D., et al., *Ubiquitination-induced conformational change within the deiodinase dimer is a switch regulating enzyme activity*. *Molecular and cellular biology*, 2007. **27**(13): p. 4774-83.
28. Kasai, R.S., et al., *The Class-A GPCR Dopamine D2 Receptor Forms Transient Dimers Stabilized by Agonists: Detection by Single-Molecule Tracking*. *Cell biochemistry and biophysics*, 2018. **76**(1-2): p. 29-37.
29. Kaczor, A.A., M. Jorg, and B. Capuano, *The dopamine D2 receptor dimer and its interaction with homobivalent antagonists: homology modeling, docking and molecular dynamics*. *Journal of molecular modeling*, 2016. **22**(9): p. 203.
30. Kaczor, A.A., et al., *Computational methods for studying G protein-coupled receptors (GPCRs)*. *Methods in cell biology*, 2016. **132**: p. 359-99.
31. Tabor, A., et al., *Visualization and ligand-induced modulation of dopamine receptor dimerization at the single molecule level*. *Scientific reports*, 2016. **6**: p. 33233.
32. Pulido, D., et al., *Design of a True Bivalent Ligand with Picomolar Binding Affinity for a G Protein-Coupled Receptor Homodimer*. *Journal of medicinal chemistry*, 2018. **61**(20): p. 9335-9346.
33. Lee, S.P., et al., *D2 dopamine receptor homodimerization is mediated by multiple sites of interaction, including an intermolecular interaction involving transmembrane domain 4*. *Biochemistry*, 2003. **42**(37): p. 11023-31.
34. Guo, W., L. Shi, and J.A. Javitch, *The fourth transmembrane segment forms the interface of the dopamine D2 receptor homodimer*. *The Journal of biological chemistry*, 2003. **278**(7): p. 4385-8.

35. Bonaventura, J., et al., *Allosteric interactions between agonists and antagonists within the adenosine A_{2A} receptor-dopamine D₂ receptor heterotetramer*. Proceedings of the National Academy of Sciences of the United States of America, 2015. **112**(27): p. E3609-18.
36. Ferre, S., et al., *Essential Control of the Function of the Striatopallidal Neuron by Pre-coupled Complexes of Adenosine A_{2A}-Dopamine D₂ Receptor Heterotetramers and Adenylyl Cyclase*. Frontiers in pharmacology, 2018. **9**: p. 243.
37. Martinez-Pinilla, E., et al., *Dopamine D₂ and angiotensin II type 1 receptors form functional heteromers in rat striatum*. Biochemical pharmacology, 2015. **96**(2): p. 131-42.
38. Navarro, G., et al., *Evidence for functional pre-coupled complexes of receptor heteromers and adenylyl cyclase*. Nature communications, 2018. **9**(1): p. 1242.
39. Oliveira, P.A., et al., *Angiotensin II type 1/adenosine A_{2A} receptor oligomers: a novel target for tardive dyskinesia*. Scientific reports, 2017. **7**(1): p. 1857.
40. Qian, M., et al., *Synthesis toward Bivalent Ligands for the Dopamine D₂ and Metabotropic Glutamate 5 Receptors*. Journal of medicinal chemistry, 2018. **61**(18): p. 8212-8225.
41. Guitart, X., et al., *Functional selectivity of allosteric interactions within G protein-coupled receptor oligomers: the dopamine D₁-D₃ receptor heterotetramer*. Molecular pharmacology, 2014. **86**(4): p. 417-29.
42. Kasai, R.S. and A. Kusumi, *Single-molecule imaging revealed dynamic GPCR dimerization*. Current opinion in cell biology, 2014. **27**: p. 78-86.
43. Guo, W., et al., *Dopamine D₂ receptors form higher order oligomers at physiological expression levels*. The EMBO journal, 2008. **27**(17): p. 2293-304.
44. Strange, P.G., *Oligomers of D₂ dopamine receptors: evidence from ligand binding*. Journal of molecular neuroscience : MN, 2005. **26**(2-3): p. 155-60.
45. Hern, J.A., et al., *Formation and dissociation of M₁ muscarinic receptor dimers seen by total internal reflection fluorescence imaging of single molecules*. Proceedings of the National Academy of Sciences of the United States of America, 2010. **107**(6): p. 2693-8.
46. Kasai, R.S., et al., *Full characterization of GPCR monomer-dimer dynamic equilibrium by single molecule imaging*. The Journal of cell biology, 2011. **192**(3): p. 463-80.
47. Calebiro, D., et al., *Single-molecule analysis of fluorescently labeled G-protein-coupled receptors reveals complexes with distinct dynamics and organization*. Proceedings of the National Academy of Sciences of the United States of America, 2013. **110**(2): p. 743-8.
48. Wang, M., et al., *Schizophrenia, amphetamine-induced sensitized state and acute amphetamine exposure all show a common alteration: increased dopamine D₂ receptor dimerization*. Molecular brain, 2010. **3**: p. 25.
49. Cannaert, A., et al., *Detection and Activity Profiling of Synthetic Cannabinoids and Their Metabolites with a Newly Developed Bioassay*. Anal. Chem., 2016. **88**(23): p. 11476-11485.
50. Skietarska, K., et al., *Detection of G protein-coupled receptor (GPCR) dimerization by coimmunoprecipitation*. Methods in cell biology, 2013. **117**: p. 323-40.
51. Wang, S., et al., *Structure of the D₂ dopamine receptor bound to the atypical antipsychotic drug risperidone*. Nature, 2018. **555**(7695): p. 269-273.
52. Pettersen, E.F., et al., *UCSF Chimera--a visualization system for exploratory research and analysis*. Journal of computational chemistry, 2004. **25**(13): p. 1605-12.
53. Kim, S., et al., *PubChem Substance and Compound databases*. Nucleic acids research, 2016. **44**(D1): p. D1202-13.

54. Morris, G.M., et al., *AutoDock4 and AutoDockTools4: Automated docking with selective receptor flexibility*. Journal of computational chemistry, 2009. **30**(16): p. 2785-91.
55. Manglik, A., et al., *Crystal structure of the micro-opioid receptor bound to a morphinan antagonist*. Nature, 2012. **485**(7398): p. 321-6.
56. Lyskov, S., et al., *Serverification of molecular modeling applications: the Rosetta Online Server that Includes Everyone (ROSIE)*. PloS one, 2013. **8**(5): p. e63906.
57. Case, D.A., et al., *The Amber biomolecular simulation programs*. Journal of computational chemistry, 2005. **26**(16): p. 1668-88.
58. Jo, S., et al., *CHARMM-GUI: a web-based graphical user interface for CHARMM*. Journal of computational chemistry, 2008. **29**(11): p. 1859-65.
59. Lomize, M.A., et al., *OPM: orientations of proteins in membranes database*. Bioinformatics (Oxford, England), 2006. **22**(5): p. 623-5.
60. Huang, J. and A.D. MacKerell, Jr., *CHARMM36 all-atom additive protein force field: validation based on comparison to NMR data*. Journal of computational chemistry, 2013. **34**(25): p. 2135-45.
61. Vanommeslaeghe, K., et al., *CHARMM general force field: A force field for drug-like molecules compatible with the CHARMM all-atom additive biological force fields*. Journal of computational chemistry, 2010. **31**(4): p. 671-90.
62. Harvey, M.J., G. Giupponi, and G.D. Fabritiis, *ACEMD: Accelerating Biomolecular Dynamics in the Microsecond Time Scale*. Journal of chemical theory and computation, 2009. **5**(6): p. 1632-9.
63. Humphrey, W., A. Dalke, and K. Schulten, *VMD: visual molecular dynamics*. Journal of molecular graphics, 1996. **14**(1): p. 33-8, 27-8.
64. Schymkowitz, J., et al., *The FoldX web server: an online force field*. Nucleic acids research, 2005. **33**(Web Server issue): p. W382-8.
65. Laschet, C., N. Dupuis, and J. Hanson, *A dynamic and screening-compatible nanoluciferase-based complementation assay enables profiling of individual GPCR-G protein interactions*. The Journal of biological chemistry, 2018.
66. Atwood, B.K., et al., *Expression of G protein-coupled receptors and related proteins in HEK293, AtT20, BV2, and N18 cell lines as revealed by microarray analysis*. BMC genomics, 2011. **12**: p. 14.
67. Przybyla, J.A. and V.J. Watts, *Ligand-induced regulation and localization of cannabinoid CB1 and dopamine D2L receptor heterodimers*. The Journal of pharmacology and experimental therapeutics, 2010. **332**(3): p. 710-9.
68. He, J., et al., *Glycosylation of beta(1)-adrenergic receptors regulates receptor surface expression and dimerization*. Biochemical and biophysical research communications, 2002. **297**(3): p. 565-72.
69. Ferre, S., et al., *Allosteric mechanisms within the adenosine A2A-dopamine D2 receptor heterotetramer*. Neuropharmacology, 2016. **104**: p. 154-60.
70. Ballesteros, J.A. and H. Weinstein, *Integrated methods for the construction of three-dimensional models and computational probing of structure-function relations in G protein-coupled receptors*. Methods in neurosciences, 1995. **25**(ed. Stuart, C.S.): p. 366-428.

71. Madhusudan Makwana, K. and R. Mahalakshmi, *Implications of aromatic-aromatic interactions: From protein structures to peptide models*. Protein science : a publication of the Protein Society, 2015. **24**(12): p. 1920-33.
72. Rossi, M., et al., *Historical Perspectives: From Monomers to Dimers and Beyond, an Exciting Journey in the World of G Protein-Coupled Receptors*, in *G-Protein-Coupled Receptor Dimers*, K. Herrick-Davis, G. Milligan, and G. Di Giovanni, Editors. 2017, Springer International Publishing: Cham. p. 3-14.
73. Ilien, B., et al., *Pirenzepine promotes the dimerization of muscarinic M1 receptors through a three-step binding process*. The Journal of biological chemistry, 2009. **284**(29): p. 19533-43.
74. Milligan, G., *G protein-coupled receptor dimerization: function and ligand pharmacology*. Molecular pharmacology, 2004. **66**(1): p. 1-7.
75. Saenz del Burgo, L. and G. Milligan, *Heterodimerisation of G protein-coupled receptors: implications for drug design and ligand screening*. Expert opinion on drug discovery, 2010. **5**(5): p. 461-74.
76. Dixon, A.S., et al., *NanoLuc Complementation Reporter Optimized for Accurate Measurement of Protein Interactions in Cells*. ACS chemical biology, 2016. **11**(2): p. 400-8.
77. Akam, E. and P.G. Strange, *Inverse agonist properties of atypical antipsychotic drugs*. Biochemical pharmacology, 2004. **67**(11): p. 2039-45.
78. Donthamsetti, P.C., et al., *Optical Control of Dopamine Receptors Using a Photoswitchable Tethered Inverse Agonist*. Journal of the American Chemical Society, 2017. **139**(51): p. 18522-18535.
79. Newton, C.L., M.D. Wood, and P.G. Strange, *Examining the Effects of Sodium Ions on the Binding of Antagonists to Dopamine D2 and D3 Receptors*. PloS one, 2016. **11**(7): p. e0158808.
80. Roberts, D.J. and P.G. Strange, *Mechanisms of inverse agonist action at D2 dopamine receptors*. British journal of pharmacology, 2005. **145**(1): p. 34-42.
81. JE, L. and C. Nlемеgeers, *Neuroleptics*, in *Alterations of metabolites in the nervous system*, A. Lajtha, Editor. 1985, Springer Science: New York. p. 595.
82. D'Souza, R.S. and W.M. Hooten, *Extrapyramidal Symptoms (EPS)*, in *StatPearls*. 2019: Treasure Island (FL).
83. Marsango, S., et al., *A Molecular Basis for Selective Antagonist Destabilization of Dopamine D3 Receptor Quaternary Organization*. Scientific reports, 2017. **7**(1): p. 2134.
84. Navarro, G., et al., *Detection of heteromers formed by cannabinoid CB1, dopamine D2, and adenosine A2A G-protein-coupled receptors by combining bimolecular fluorescence complementation and bioluminescence energy transfer*. TheScientificWorldJournal, 2008. **8**: p. 1088-97.
85. Gandia, J., et al., *Detection of higher-order G protein-coupled receptor oligomers by a combined BRET-BiFC technique*. FEBS letters, 2008. **582**(20): p. 2979-84.
86. Borroto-Escuela, D.O., et al., *On the existence of a possible A2A-D2-beta-Arrestin2 complex: A2A agonist modulation of D2 agonist-induced beta-arrestin2 recruitment*. Journal of molecular biology, 2011. **406**(5): p. 687-99.
87. Sahlholm, K., et al., *Antipsychotic-Like Efficacy of Dopamine D2 Receptor-Biased Ligands is Dependent on Adenosine A2A Receptor Expression*. Molecular neurobiology, 2018. **55**(6): p. 4952-4958.

88. Borroto-Escuela, D.O., et al., *A serine point mutation in the adenosine A2AR C-terminal tail reduces receptor heteromerization and allosteric modulation of the dopamine D2R*. Biochemical and biophysical research communications, 2010. **394**(1): p. 222-7.
89. Antonelli, T., et al., *Experimental studies and theoretical aspects on A2A/D2 receptor interactions in a model of Parkinson's disease. Relevance for L-dopa induced dyskinesias*. Journal of the neurological sciences, 2006. **248**(1-2): p. 16-22.
90. Fuxe, K., et al., *Receptor heteromerization in adenosine A2A receptor signaling: relevance for striatal function and Parkinson's disease*. Neurology, 2003. **61**(11 Suppl 6): p. S19-23.
91. Fuxe, K., et al., *Adenosine A(2A) receptors, dopamine D(2) receptors and their interactions in Parkinson's disease*. Movement disorders : official journal of the movement disorder society, 2007. **22**(14): p. 1990-2017.
92. Soriano, A., et al., *Adenosine A2A receptor-antagonist/dopamine D2 receptor-agonist bivalent ligands as pharmacological tools to detect A2A-D2 receptor heteromers*. Journal of medicinal chemistry, 2009. **52**(18): p. 5590-602.
93. Lee, S.P., et al., *Inhibition of cell surface expression by mutant receptors demonstrates that D2 dopamine receptors exist as oligomers in the cell*. Molecular pharmacology, 2000. **58**(1): p. 120-8.
94. Kong, M.M., et al., *Agonist-induced cell surface trafficking of an intracellularly sequestered D1 dopamine receptor homo-oligomer*. Molecular pharmacology, 2006. **70**(1): p. 78-89.
95. Platania, C.B., et al., *Homology modeling of dopamine D2 and D3 receptors: molecular dynamics refinement and docking evaluation*. PloS one, 2012. **7**(9): p. e44316.

Chapter 6:

Synthesis towards bivalent ligands for the dopamine D₂ and metabotropic glutamate 5 receptors.

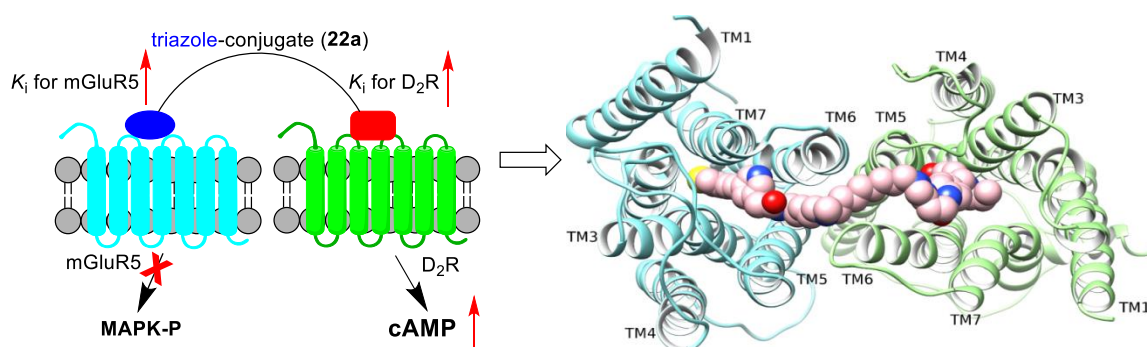
Based on

Mingcheng Qian,[‡] Elise Wouters,[‡] James A. R. Dalton, Martijn D. P. Risseuw, René A. J. Crans, Christophe Stove, Jesús Giraldo, Kathleen Van Craenenbroeck, and Serge Van Calenbergh. Synthesis towards bivalent ligands for the dopamine D₂ and metabotropic glutamate 5 receptors. *Journal of Medicinal Chemistry*, 2018, 61, 18, 8212-8225. [‡]These authors contributed equally. // The same chapter has been incorporated in the thesis of Dr. Mingcheng Qian. Elise Wouters has generated the stable cell lines expressing D₂5R and D₂5R-mGluR₅, performed the cAMP assay and aided with ligand-binding experiments.

ABSTRACT

In this Chapter we designed and synthesized heterobivalent ligands targeting heteromers consisting of the metabotropic glutamate 5 receptor (mGluR₅) and the dopamine D_{2,short} receptor (D₂₅R). Bivalent ligand comprising the D₂R agonist 5-OH-DPAT and the negative allosteric modulator of mGluR₅ MTEP (**22a**) with a linker consisting of 20 atoms showed 4-fold increase in affinity for cells co-expressing D₂₅R and mGluR₅ compared to cells solely expressing D₂₅R. Likewise, the affinity of **22a** for mGluR₅ increased 2-fold in the co-expressing cells. Additionally, **22a** exhibited a 5-fold higher mGluR₅ affinity than its monovalent MTEP azido precursor (**21a**) in cells co-expressing D₂₅R and mGluR₅. These results indicate that **22a** is able to bridge binding sites on both receptors constituting the heterodimer. Likewise, cAMP assays revealed that **22a** had a 4-fold higher potency in stable D₂₅R and mGluR₅ co-expressing cell lines compared to its monovalent precursor DPAT alkyne (**1**). Furthermore, molecular modeling revealed that **22a** is able to simultaneously bind both receptors by bridging the TM5-TM6 interface and establishing six protein-ligand H-bonds.

GRAPHICAL ABSTRACT



6.1 Introduction

The metabotropic glutamate receptors (mGluRs) constitute a family of G protein-coupled receptors (GPCRs) characterized by the presence of large, ectocytic, N-terminal orthosteric binding domains, which are activated by L-glutamate [1-3]. Based on sequence homology, receptor pharmacology and signaling pathways the eight mGluR subtypes are divided into three groups (Group I, II, and III). Group I mGluRs (mGluR₁ and mGluR₅) are mainly localized postsynaptically and are extensively present in numerous brain areas, including the hippocampus, thalamic nuclei and spinal cord. Stimulation of Gα_q protein coupled mGluR₁ and mGluR₅ results in phosphoinositide (PI) hydrolysis and intracellular formation of the second messengers inositol triphosphate (IP₃), which prompts the release of intracellular Ca²⁺, and diacylglycerol (DAG), which stimulates protein kinase C activity (PKC) [2, 4, 5]. In contrast, Group II (mGluR₂ and mGluR₃) and group III (mGluR₄, mGluR₆, mGluR₇, and mGluR₈) are primarily located presynaptically and, upon stimulation, suppress adenylyl cyclase (AC), thereby reducing intracellular cAMP levels upon stimulation [6-8].

Excessive activation of mGluR₅ is related to the development of neurodegenerative diseases like Alzheimer's [9, 10], Parkinson's disease [11, 12], or numerous CNS disorders including neuropathic pain [13], anxiety and depression [14], drug addiction [15] and fragile X syndrome [16, 17].

On the other hand, the dopamine receptor subtypes are divided into two distinct subfamilies: D₁-like (D₁R and D₅R) and D₂-like (D₂R, D₃R, and D₄R) dopamine receptors. Whereas the D₁-like family couples to Gα_{s/olf} or Gα_q and subsequently stimulates AC and increases the levels of cAMP, the D₂-like family recruits Gα_{i/o} and reduces intracellular cAMP levels. The D₂R has been associated with multiple diseases as well, including Parkinson's disease [18] and schizophrenia [19], among others.

Interestingly, mounting evidence shows that D₂R may form heteromers with mGluR₅ at the plasma membrane. Cabello *et al.* [20] first suggested the occurrence of these mGluR₅ and D₂R heterodimers in living cells using a fluorescence complementation assay. Additionally, bioluminescence resonance energy transfer and sequential resonance energy transfer assays also allowed detecting receptor oligomers having at least two protomers, in which the mGluR₅ and D₂R also assembled with the adenosine A_{2A} receptor (A_{2A}). Co-immunoprecipitation in

native tissue confirmed the oligomerization of mGluR₅, D₂R and A_{2A} in rat striatum homogenates. Overall, the above results indicate the existence of mGluR₅-D₂R-A_{2A} heteromers in living cells and support their presence in the GABAergic striatopallidal neurons, where they may represent important targets for the potential treatment of locomotion, neuropsychiatric disorders and drug addiction [20, 21].

A recent study by Beggiato *et al.* [22] revealed a functional role for A_{2A}, D₂R and mGluR₅ in modulating the activity of rat basal ganglia using dual-probe microdialysis in free-moving rats. The results suggested that A_{2A} and mGluR₅ interact synergistically in regulating the D₂R-mediated control of striatopallidal GABA neurons. D₂R appears to suppress synaptic delivery of mGluR₅ by limiting Src family kinase (SFK)-mediated tyrosine phosphorylation of mGluR₅ in rat striatum [23]. In the basal ganglia, mGluR₅ negative allosteric modulators (NAM) regulate the L-3,4-dihydroxyphenylalanine (L-DOPA) induced changes of D₂R, the connected signaling proteins including ERK1/2 and Akt/GSK3 β and neuropeptides preproenkephalin and preprodynorphin, along with the expression of A_{2A} [24]. As is well known, cocaine can improve extracellular glutamate and dopamine (DA) levels in the nucleus accumbens (NAc), which are boosted with repeated administration [25].

Nowadays, heterobivalent ligands have emerged as pharmacological probes to validate the existence of GPCR dimers without the need for receptor modification [26-28]. Heterobivalent ligands having a linker of optimal length are envisioned to show a greater potency than that stemming from the sum of their two constituting pharmacophores [27, 29, 30]. Compounds able to modulate GPCR dimers may eventually also evolve to useful pharmacological agents that target selected heteromeric subtypes, thereby potentially increasing selectivity [28].

In this Chapter we describe the design and synthesis of a series of mGluR₅ negative allosteric modulator-D₂R agonist/antagonist bivalent ligands as pharmacological tools to further study mGluR₅-D₂R heteromers. Towards this end, ligands for the protomeric D₂R and the mGluR₅ were conjugated through a spacer of variable length. These bivalent ligands were evaluated in radioligand binding and functional assays both in cells in which the mGluR₅ and D₂R were expressed separately and in cells co-expressing both target receptors.

6.2 Materials and methods

6.2.1 Chemistry

The synthesis of all the bivalent ligands and precursors has been performed by Dr. Mingcheng Qian. Interested readers are referred to the publication by Qian *et al.* (2018). For the readers' convenience, we have retained the same numbering of the synthesized ligands in this thesis as in the publication.

6.2.2 Generation of the stable mGluR₅-D₂R co-expressing cell line

Production of the stable mGluR₅-D₂R co-expressing cell line was conducted by a retroviral transduction of D₂R (human) into both human embryonic kidney (HEK) 293T cells and the *mGluR_{5a}-HEK293-TREx* stable cell line (a kind gift of Janssen Pharmaceutical Companies of Johnson & Johnson), stably transfected with the mGluR_{5a}/pcDNA4-TO construct (RefSeq NM_000842; RefSeqP NP_000833).

The retroviral construct of D₂R was generated by PCR-amplifying the D₂R sequence (RefSeq NM_016574.3) flanked by the *Sna*BI/*Not*I restriction enzyme sites and cloned into the digested retroviral vector pLZRS-IRES-EGFP. The integrity of the insert was confirmed by DNA sequencing. The pLZRS-D₂R-IRES-EGFP plasmid leads to co-expression of the D₂R and eGFP, the latter can be used as a marker for cell sorting and to check the stability of the cell lines by flow cytometry.

For the production of retroviruses the Phoenix-Amphotropic packaging cell line was used (a kind gift from prof. Bruno Verhasselt, Department of Clinical Chemistry, Microbiology, and Immunology, Ghent University, Belgium). The cells were transfected with LZRS-D₂R-IRES-EGFP, by calcium phosphate precipitation (Invitrogen, San Diego, CA, USA). After puromycin selection for 2 weeks, the retroviral supernatant was harvested, spun down (10 min at 350 × g) and aliquots of the supernatant were stored at -80 °C until use. For the retroviral transduction of HEK293T and HEK293 mGluR₅ cells, 10⁴ cells/well were seeded in a transparent 96-well plate. After 24 h, the medium was refreshed with the retroviral supernatant, which had been preincubated for 10 min with Dotap (Roche Diagnostics). To increase transduction efficiency, the plates were spun down (90 min, 950 × g, 32 °C).

Transduction efficiency was measured by flow cytometry 48 h after transduction, via assessment of expression of EGFP. Cell sorting was done on a BD FACSAria III, equipped with 405, 488, 561, and 640 nm lasers (BD Biosciences, Erembodegem, Belgium).

6.2.3 Cell culture and transfection

HEK293T cells, HEK293 mGluR₅ and HEK293 mGluR₅-D₂R stably expressing cells were cultured in Dulbecco's modified Eagle's medium (DMEM; Invitrogen), supplemented with 10% fetal bovine serum, penicillin (100 U/ml), and streptomycin (100 µg/ml) in a controlled environment (37 °C, 98% humidity, 5% CO₂). For ligand binding experiments, HEK293T cells were transiently transfected using the Polyethylenimine (PEI) method as described before [31]. A total amount of 10 µg of DNA was used for transfection of cells in one 10-cm dish.

6.2.4 Membrane preparation and protein determination

Membrane suspensions from HEK293T D₂R, HEK293 mGluR₅ and HEK293 mGluR₅-D₂R stable cell lines were prepared according to previously described protocols [32]. In brief, cells were disrupted by a Polytron homogenizer for two 10-second periods in proper volumes of ice-cold Tris-HCl buffer (50 mM, pH 7.4). Membrane pellets were obtained by centrifugation at 16500g for 25 min at 4 °C. The resulting membrane pellets were stored at -80 °C and were washed once more as described above and resuspended in the relevant binding buffer for direct use. BCA method was used to quantify the membrane protein using bovine serum albumin dilutions as the standard.

6.2.5 [³H]Raclopride binding

A saturation binding assay for [³H]raclopride was carried out as described previously [32, 33]. In brief, a suspension of cell membranes (20 µg) were incubated with varying concentrations (0–20 nM) of [³H]raclopride in 50 mM Tris-HCl, pH 7.4 buffer (containing 100 mM NaCl, 5 mM KCl, 4 mM MgCl₂, 1.5 mM CaCl₂ and 1 mM EDTA) at 37 °C for 1 h. For competition binding assays, 2.0 nM [³H]raclopride (specific activity = 73.8 Ci/mmol, PerkinElmer, USA) was used and incubated with 20 µg of cell membranes in the absence or presence of varying concentrations (0.1 nM–10 µM) of unlabeled ligands at 37 °C for 1 h. Non-specific binding was measured by the addition of 1 µM haloperidol. Rapid filtration through GF/C glass-fiber filters

(Whatman Schleicher and Schuell, Keene, NH) embedded in 0.1% PEI and mounted on a Brandel cell harvester was utilized to terminate the incubation. Filters were washed three times with cold 50 mM Tris-HCl, pH 7.4 buffer and transferred to vials containing 3 mL of scintillation cocktail to soak the filter overnight. The radioactivity counts were measured with a Tri-Carb 2800TR liquid scintillation analyzer (PerkinElmer).

6.2.6 [³H]MPEP binding

A saturation binding assay for [³H]MPEP was adapted from a previous protocol [34]. Membranes (20 µg) were incubated with different concentrations (0–10 nM) of [³H]MPEP in 50 mM Tris-HCl and 2 mM MgCl₂, pH 7.4 buffer at 25 °C for 1 h. For competition binding assays, 3.0 nM [³H]MPEP (specific activity = 60 Ci/mmol, American Radiolabeled Chemicals, Inc.) was incubated together with 20 µg of membranes in the absence or presence of varying concentrations (0.1 nM–100 µM) of unlabeled ligands at 25 °C for 1 h. Nonspecific binding was determined in the presence of 10 µM MPEP. Filtration and measuring were as described above.

6.2.7 Data analysis

All results shown represent means ± SEM for at least three independent experiments, each performed in duplicate or triplicate. Statistical analysis and curve fits of concentration-response curves were performed by GraphPad Prism 7. *K_i* values were calculated by using the Cheng-Prusoff equation [35].

6.2.8 GloSensor cAMP protocol

HEK293 mGluR₅-D₂₅R co-expressing cells and HEK293T D₂₅R cells were seeded in 6-well plates at 500 000 cells/well. The day after, cells were transfected with the pGloSensor-22F cAMP plasmid, using the FuGene transfection reagent (as described previously) [36]. Cells were washed with CO₂-independent medium and afterwards incubated with equilibration medium containing 2% v/v GloSensor cAMP reagent stock solution in 10% FBS CO₂-independent medium. After an incubation of 30 min at 37 °C, the luminescence signal was measured until a steady-state basal signal was obtained. Serial concentrations of monovalent agonist DPAT-alkyne (**1**) or bivalent ligand (**22a**) (0.1 nM–10 µM) were added. After 15 min, 10 µM Forskolin (FSK) was added. The agonist profile of the compounds was evaluated by assessing their

ability to counteract the Forskolin-induced increase of cAMP accumulation. Finally, concentration-response curves were generated enabling the calculation of IC₅₀-values.

6.2.9 Computational modeling

Computational modeling of the mGluR₅-D₂R heterodimer and the docking of the bivalent ligand onto this heteromer has been performed by Dr. James Dalton (Universitat Autònoma de Barcelona, Spain).

6.2.9.1 Receptor structure preparation

Crystallographic missing residues and/or atoms in the human D₂R crystal structure [37] (PDB id: 6CM4) were added using CHIMERA v1.11.2 software [38] by selecting the most probable rotamer at relevant positions with fewest possible steric clashes. Mutated residues: I122A, L375A, L379A were converted back to wild-type using the same procedure. The four-residue missing segment of intracellular loop 2 (ICL2) was *ab initio* modeled with MODELLER v9.18 [39]. Co-crystallized risperidone and endolysin fusion protein were removed from the D₂R structure. Energy minimization was then performed on added residues/loops and any clashing atoms in the AMBER14SB force-field [40].

From a previously published molecular dynamics (MD) simulation of mGluR₅ with bound NAM [41], a conformation of mGluR₅ was extracted which has a larger extracellular gap between TM5 and TM6 than the original crystal structure [42] (PDB id: 4009). The simulated NAM was removed from this structure.

6.2.9.2 Protein-protein docking

For construction of an mGluR₅-D₂R heterodimer model, where D₂R and mGluR₅ interact via a symmetrical TM5-TM6 interface, both receptors were systematically superimposed onto relevant monomers of the mu-opioid receptor homodimer crystal structure [43] (PDB id: 4DKL). The mGluR₅-D₂R heterodimer model was then submitted to the ROSIE webserver [44] for protein-protein docking using default parameters. The best docked heterodimer structure was identified by two factors: best interface score (“I_sc”) and best membrane-compatible orientation.

6.2.9.3 Bivalent ligand docking

Coordinates for 3-[(2-methyl-4-thiazolyl)ethynyl]pyridine (MTEP) and 5-hydroxy-2-(dipropylamino)tetralin (5-OH-DPAT) were downloaded from PubChem [45]. Autodock v4.2 [46] was used to dock MTEP into mGluR₅ and 5-OH-DPAT into D₂R in the heterodimer model. Gridpoints were extended to cover total allosteric and orthosteric pocket volumes, respectively. The selected docked conformation of each ligand in its receptor represents the top hit identified by best predicted affinity in the largest docking cluster. The linker between MTEP and 5-OH-DPAT components, corresponding to compound **22a**, was modeled with CHIMERA by manually extending the chain from both sides and connecting at the heterodimer interface between TM5 and TM6 of both receptors. The **22a** linker was modeled to follow the shortest path possible between receptors whilst avoiding steric clashes. The heterodimer-ligand complex was energy minimized without restraints with CHIMERA in the AMBER-14SB force-field [40] to relax the **22a** linker and optimize protein-ligand interactions.

6.3 Results and Discussion

6.3.1 Design of heterobivalent ligands

Dr. Mingcheng Qian constructed bivalent ligands encompassing spacers of varying length that were functionalized with a primary amine on one end and an azide on the other to allow orthogonal coupling to the appropriately derivatized dopamine and mGluR₅ ligands, respectively (**Figure 6.1**).

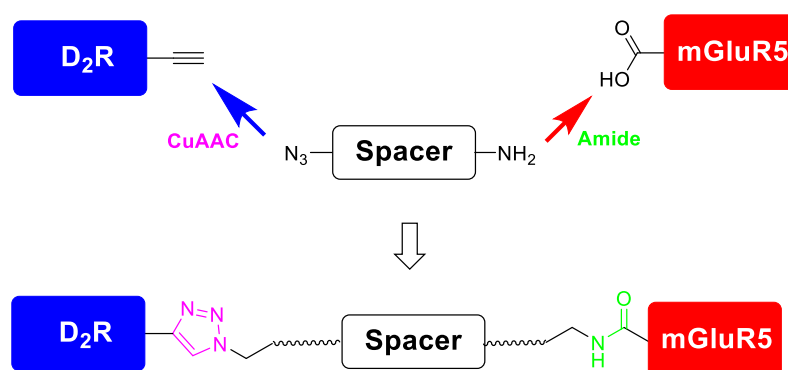


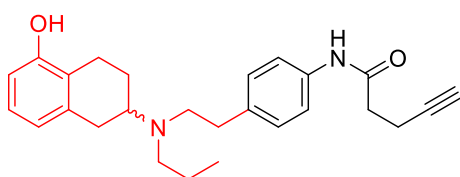
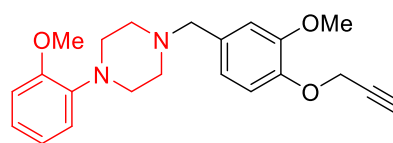
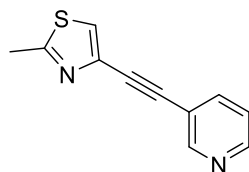
Figure 6.1 Construction of the heterobivalent ligands.

As D₂R ligands we selected the 5-OH-DPAT [32] and the 1,4-disubstituted aromatic piperazine (1,4-DAPs) [47] that were equipped with an alkyne ligation handle to afford **1** and **2**, which may be swiftly connected to the azide group of the spacer via a copper-catalyzed azide–alkyne cycloaddition (CuAAC) reaction (**Figure 6.2**).

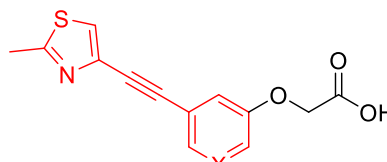
5-OH-DPAT is a prototypical D₂R/D₃R agonist suitable for constructing bivalent ligands [48]. Site-directed mutagenesis has demonstrated that the interaction between the 2-aminotetralin moiety and an agonist binding domain linking TM3 and TM5 leads to either D₂R or D₃R activation. The 5-OH group and the basic N are critical for binding affinity.

The D₂R antagonistic activity of 1,4-DAPs originates from the aromatic head group and the amine moiety that forms a strong hydrogen bond with Asp^{3.32} [47]. A lipophilic appendage enhances affinity. Because proper lengthening of the lipophilic appendage is anticipated to lead to the “entrance region” of the receptor and from there reaching out to the binding pocket of the neighboring protomer, the para-position of the benzylic appendage is considered an appropriate attachment point for a linker unit [47].

As mGluR₅ ligand we opted for the selective and potent allosteric mGluR₅ antagonist MTEP [5]. Although MTEP analogues substituted at the 5-position of the 3-pyridyl moiety showed moderately lower affinity compared to the parent MTEP, they have been demonstrated to be more potent allosteric mGluR₅ antagonists than those modified at the 2- or 6-positions [25]. Hence, we introduced a carboxylic acid at the 5-position of the 3-pyridyl moiety to afford two carboxylic acid analogues of MTEP **3a-b** which are amenable for coupling to the amine group of the bifunctional spacers.

D₂-likeR ligandsDPAT-alkyne (**1**)DAP-alkyne (**2**)mGluR₅ ligands

MTEP



3a: X = N
3b: X = CH

Linkers

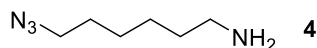
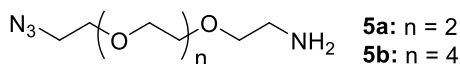
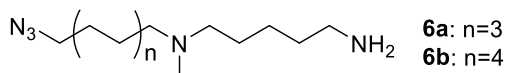
**4****5a:** n = 2**5b:** n = 4**6a:** n=3**6b:** n=4

Figure 6.2 Overview of appropriately modified monovalent ligands and linkers used in this Chapter. Parent ligands are indicated in red.

To construct the desired bivalent ligands, we considered three types of linkers with an azido group on one and an amino group on the other end, as to allow swift conjugation to alkyne modified dopamine ligands **1** and **2**, and the carboxylic acid containing MTEP analogues **3a-b**, respectively (**Figure 6.2**).

The first linker **4** is composed of a simple bifunctional hexamethylene chain. The polyethylene glycol (PEG) linkers **5a-b** were previously used to construct bivalent D₂R-μOR ligands [32]. These two types of spacers have been frequently employed to compose bivalent ligands and they allow for a gradual increase in spacer length [30, 47-49]. In a third type of linkers **6a-b**, we decided to introduce a protonatable nitrogen atom near the center of the bifunctional

polymethylene chain to moderate incremental increase in lipophilicity upon extension, which may result in aggregation in aqueous media.

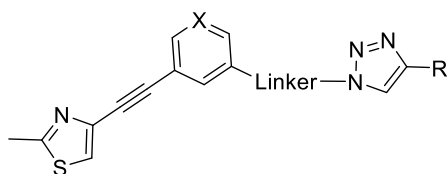
6.3.2 Synthesis

The synthesis of all the bivalent ligands and precursors has been performed by Dr. MingCheng Qian. Interested readers are referred to the publication by Qian *et al.* (2018).

6.3.3 Pharmacological evaluation

6.3.3.1 Affinity of the bivalent ligands for the D_{2S}R

We performed a competition assay to evaluate the binding affinity of the bivalent ligands for the D_{2S}R (**Table 6.1**). First, the binding affinity of nine bivalent ligands along with the alkynylated precursors of DPAT (**1**) and DAP (**2**) was measured by displacement of [³H]raclopride from the D_{2S}R stably expressed in HEK293T cells. Raclopride is a selective D₂R antagonist that, due to its more pronounced hydrophilic character, shows substantially less non-specific binding than spiperone [32]. All bivalent ligands retained good to moderate affinity for the D_{2S}R (**Table 6.1**). The DPAT-based ligand **22a**, featuring a type 3 linker consisting of 20 atoms showed the best affinity (50 ± 6.4 nM) for D_{2S}R. Interestingly, amongst the DAP-based ligands, compounds **23a** and **23c**, featuring the same spacer as **22a**, displayed the lowest K_i value (132 nM and 147 nM, respectively). A substantial reduction (5- to 17-fold) in D_{2S}R binding affinities, upon comparison to the precursor **1** was observed for the DPAT-based (**18**, **22a**, **22b**) bivalent ligands with hexamethylene linkers. This also held true for the DAP-based bivalent ligands (**20a** and **20b**), where a 5-fold reduction in affinities was observed in comparison to precursor **2**.

Table 6.1 Binding affinities (K_i) for D₂₅R and D₂₅R-mGluR₅.

Compd	X	R	Linker	K_i (nM) for D ₂₅ R	K_i (nM) for D ₂₅ R-mGluR ₅
1	-	-	-	17 ± 2.6	19 ± 1.8
2	-	-	-	77 ± 6.8	69 ± 22
18	N	DPAT	-OCH ₂ CONH (CH ₂) ₆ -	295 ± 99	142 ± 10
22a	N	DPAT	-OCH ₂ CONH(CH ₂) ₅ NCH ₃ (CH ₂) ₈ -	50 ± 6.4	13 ± 3.6
22b	N	DPAT	-OCH ₂ CONH (CH ₂) ₅ NCH ₃ (CH ₂) ₁₀ -	79 ± 16	171 ± 12
23a	N	DAP	-OCH ₂ CONH (CH ₂) ₅ NCH ₃ (CH ₂) ₈ -	132 ± 44	45 ± 5.3
23b	N	DAP	-OCH ₂ CONH (CH ₂) ₅ NCH ₃ (CH ₂) ₁₀ -	303 ± 43	115 ± 32
23c	CH	DAP	-OCH ₂ CONH (CH ₂) ₅ NCH ₃ (CH ₂) ₈ -	147 ± 24	94 ± 21
23d	CH	DAP	-OCH ₂ CONH (CH ₂) ₅ NCH ₃ (CH ₂) ₁₀ -	398 ± 100	252 ± 54
20a	CH	DAP	-OCH ₂ CONH-PEG ₄ -	438 ± 89	251 ± 42
20b	CH	DAP	-OCH ₂ CONH-PEG ₆ -	352 ± 94	186 ± 75

Binding affinities (K_i) obtained by competitive displacement of [³H]raclopride from HEK293T D₂₅R and HEK293 D₂₅R-mGluR₅ cell membranes. All values are expressed as the mean ± SEM of three independent assays.

Next, we determined the affinity of nine bivalent ligands and their corresponding alkyne precursors **1** and **2** for D₂₅R in the presence of mGluR₅. Interestingly, the affinity of **22a** to cells expressing both D₂₅R and mGluR₅ (13 ± 3.6 nM) increased 4-fold compared to cells expressing only D₂₅R (50 ± 6.4 nM). Likewise, the affinity for D₂₅R of the DAP-containing bivalent ligand **23a** was 3-fold higher in cells co-expressing the mGluR₅ (45 ± 5.3 nM versus 132 ± 44 nM). Furthermore, **22a** showed moderately higher affinity than **1** (19 ± 1.8 nM) and 10-fold higher affinity compared to the two other DPAT-based bivalent ligands **18** and **22b** in D₂₅R and

mGluR₅ co-expressing cells. All these data indicate that bivalent ligands **22a** and **23a** possibly bridge the binding sites of the D₂₅R and mGluR₅ heterodimers. Furthermore, DPAT-based compound **18** containing a short hexamethylene linker showed a lower affinity for D₂₅R-mGluR₅ relative to **22a**, probably because its linker is too short to bridge the binding sites of the heterodimer. The preference for a tertiary amine linker as deduced from the superior affinities of **22a** and **23a** in the co-expressing cells may be partly due to the H-bond that is formed between the tertiary amine group of the linker and D400 located on extracellular loop 3 (ECL3) of D₂R (see 6.3.4 Computational modeling), which may compensate for the entropic penalty of the flexible linker. Based on the results discussed above, a type 3 linker of appropriate length is preferred in this study.

6.3.3.2 Affinity of the bivalent ligands for the mGluR₅

Competitive ligand binding assays in plasma membranes from HEK293 cells stably expressing mGluR₅ in the absence or presence of D₂₅R, allowed to assess the binding affinity for said receptor using [³H]MPEP, a nonselective mGluR₅ antagonist. First, saturation binding assays for HEK293 cells expressing mGluR₅ and mGluR₅-D₂₅R with [³H]MPEP were performed (**Figure 6.3** and **Table 6.2**).

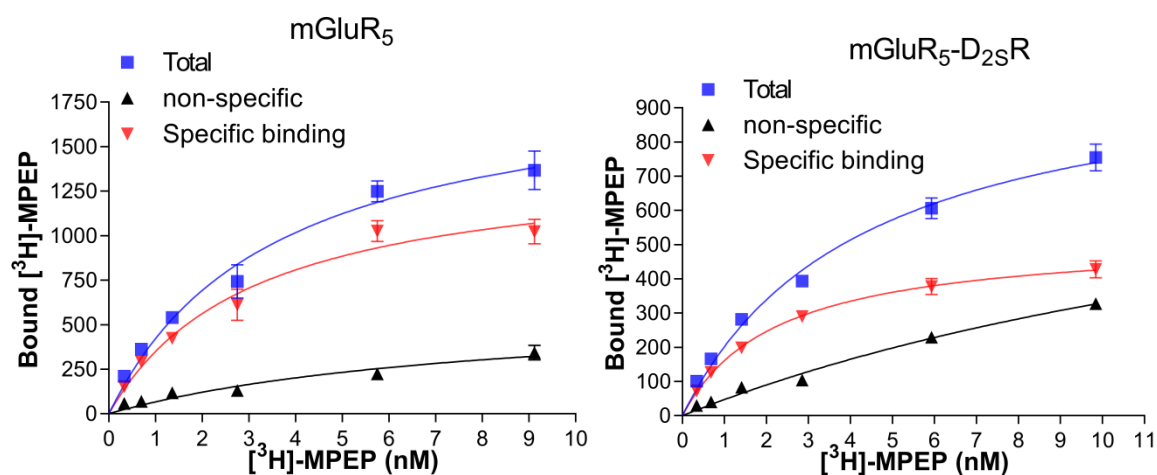


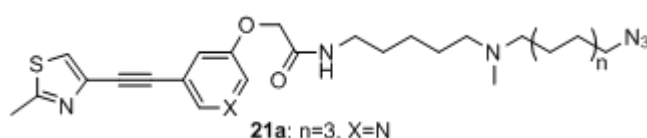
Figure 6.3 Saturation assay for mGluR₅ and mGluR₅-D₂₅R with [³H]MPEP. All points are expressed as the mean \pm SEM of two independent assays performed in duplicate.

Table 6.2 B_{max} and K_d values from saturation assay

Entry	B _{max} (fmol/mg)	K _d (nM)
mGluR ₅	1488 ± 153	2.2 ± 0.7
mGluR ₅ -D ₂₅ R	522 ± 19	2.0 ± 0.2

All values are expressed as the mean ± SEM of two independent assays performed in duplicate.

The binding affinities of the azido precursor **21a** for mGluR₅ and D₂₅R-mGluR₅ were 5.8 ± 0.9 μM and 5.7 ± 0.8 μM, respectively (**Table 6.3**). In addition, the affinity of **3a** for mGluR₅ was 6.5 ± 0.6 μM, which is comparable to that of **21a**. This led us to use **21a** as control in ligand binding and further functional assays for mGluR₅. Bivalent ligand **22a** showed a 2-fold gain in binding affinity in cells expressing both D₂₅R and mGluR₅ compared to cells solely expressing mGluR₅. Interestingly, **22a** exhibited a 5-fold higher affinity (1.1 ± 0.2 μM) for D₂₅R-mGluR₅ compared to its azido precursor **21a** lacking a D₂R ligand (5.7 ± 0.8 μM). Likewise, **23a** displayed 4-fold higher affinity (1.3 ± 0.2 μM) for D₂₅R-mGluR₅ relative to **21a**. All these results indicate that bivalent ligands **22a** and **23a** bridge the orthosteric and allosteric binding sites of the D₂₅R and mGluR₅ heteromer, respectively.

Table 6.3 Binding affinities (K_i) for mGluR₅ and mGluR₅-D₂₅R.

Entry	X	R	Linker	K _i (μM) for mGluR ₅	K _i (μM) for D ₂₅ R-mGluR ₅
21a	N	-	-OCH ₂ CONH(CH ₂) ₅ NCH ₃ (CH ₂) ₈ -	5.8 ± 0.9	5.7 ± 0.8
22a	N	DPAT	-OCH ₂ CONH(CH ₂) ₅ NCH ₃ (CH ₂) ₈ -	2.3 ± 0.5	1.1 ± 0.2
23a	N	DAP	-OCH ₂ CONH(CH ₂) ₅ NCH ₃ (CH ₂) ₈ -	1.0 ± 0.3	1.3 ± 0.2

Binding affinities (K_i) obtained by competitive displacement of [³H]MPEP from HEK293T cell membranes expressing mGluR₅ and D₂R-mGluR₅. All values are expressed as the mean ± SEM of three independent assays performed in duplicate.

6.3.3.3 cAMP assay to study potency of the selected D₂R ligands

To further understand the potency of nine bifunctional ligands and their corresponding monovalent precursors **1** and **2** consisting of the pharmacophore of a D₂R agonist and a D₂R antagonist, respectively, we performed a bioluminescence based cAMP accumulation assay (**Figure 6.4** and **Table 6.4**) [36]. Coupled to inhibitory G $\alpha_{i/o}$ proteins, activation of the D₂R decreases cAMP production.

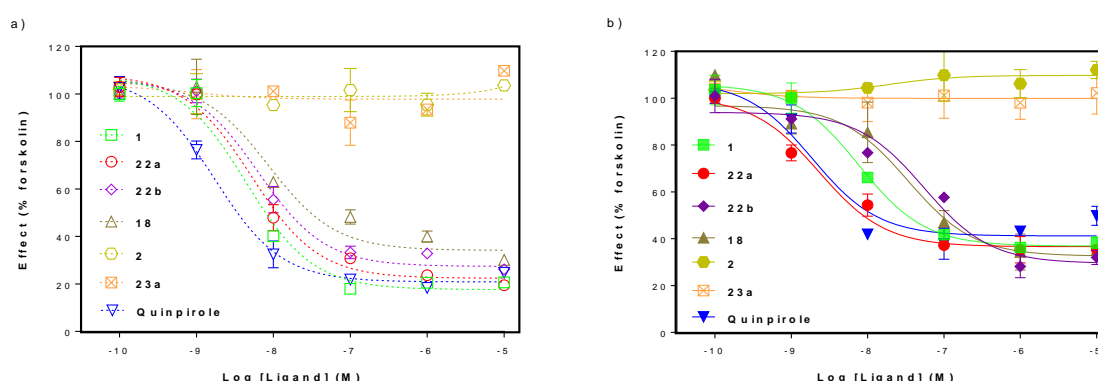


Figure 6.4 Concentration-response curves of cAMP accumulation for representative ligands. Functional activity of selected bivalent ligands and their precursors **1** and **2**, determined in HEK293T cells stably expressing D₂₅R (left, a) or HEK293 cells expressing both D₂₅R and mGluR₅ (right, b) and transiently co-expressing the pGloSensor-22F cAMP plasmid. Cells were stimulated with the selected ligands of varying concentrations (0.1 nM–10 μ M) in the presence of 10 μ M forskolin. cAMP production was normalized to the percentage of forskolin stimulated cAMP concentration (100%). Data represent mean \pm SEM of three independent experiments, each performed in duplicate.

Similar to the reference D₂R agonist quinpirole, bivalent ligands **18**, **22a**, **22b** and their alkyne precursor **1** inhibited forskolin-stimulated cAMP formation both in cells mono-expressing D₂₅R or in cells co-expressing D₂₅R and mGluR₅. Interestingly, in the latter cells a substantially lower IC₅₀ value was observed for bivalent ligand **22a** (IC₅₀ = 1.5 \pm 0.5 nM) compared to **1** (IC₅₀ = 6.5 \pm 0.6 nM), indicating that the bivalent binding requires a lower receptor occupation to exert signaling. However, **18** and **22b** exhibited 3- and 5-fold lower potencies (20 nM and 32 nM, respectively) in the co-expressing cell line relative to **1**, revealing weak D₂R agonism. In D₂₅R-mGluR₅-co-expressing cells, quinpirole inhibited cAMP accumulation with similar potencies as in cells mono-expressing D₂₅R, while monovalent precursor **1** showed an unexpected 2-fold lower potency in co-expressing cells compared to mono-expressing cells. In addition, **18** and **22b** displayed 2- and 6-fold lower potencies in the co-expressing cells than

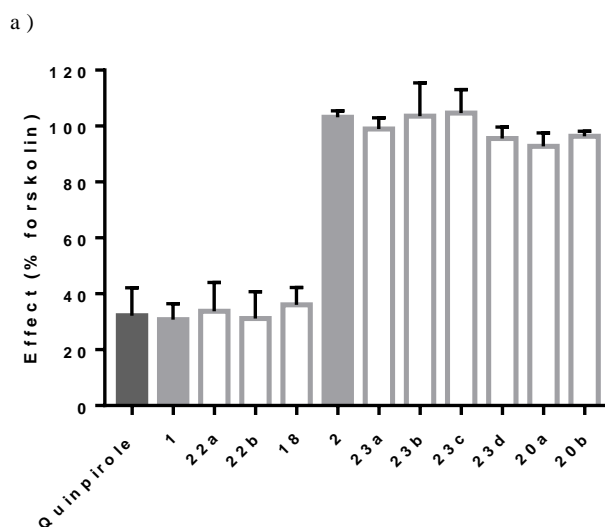
in the mono-expressing cells. On the other hand, bivalent ligand **22a** is the only compound that was able to decrease cAMP production with a 2-fold higher potency in the co-expressing cells than in mono-expressing D₂R cells.

Table 6.4 Potency of inhibition of forskolin mediated cAMP accumulation for bivalent ligands based on D₂R agonist DPAT-alkyne.

Compd	cAMP IC ₅₀ (nM)	cAMP IC ₅₀ (nM)
	D ₂ R	D ₂ R-mGluR ₅
Quinpirole	1.8 ± 0.4	1.9 ± 0.3
1	3.0 ± 0.8	6.5 ± 0.6
18	7.6 ± 0.7	20 ± 9.8
22a	3.3 ± 0.7	1.5 ± 0.5
22b	5.5 ± 0.6	32 ± 15

Data shown represent the mean ± SEM of three independent experiments.

In addition, bivalent ligands based on DAP-alkyne and their alkyne precursor **2** failed to inhibit cAMP accumulation (**Figure 6.4** and **Figure 6.5**), both in the cells solely expressing and in the D₂R-mGluR₅ co-expressing cells, suggesting that DAP-based bivalent ligands show D₂R antagonist behavior, which is in line with results reported by others [47].



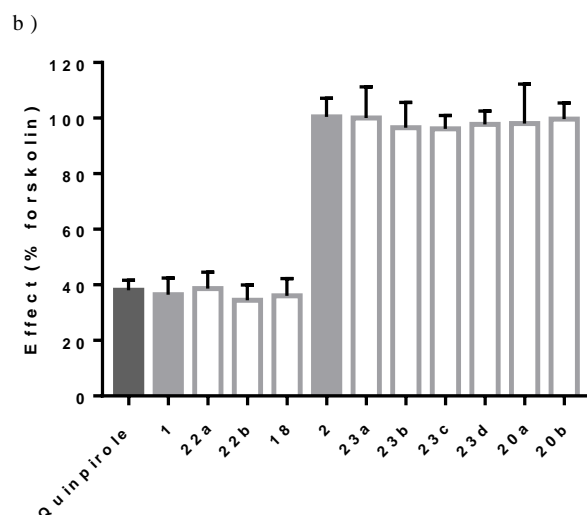


Figure 6.5 Effect of bivalent ligands to inhibit forskolin-induced cAMP accumulation. Functional activity of bivalent ligands and their precursors **1** and **2**, determined in HEK293T cells stably expressing the D₂₅R (a) or HEK293 cells stably expressing both D₂₅R and mGluR₅ (b) and co-expressing the pGloSensor-22F cAMP plasmid via transient transfection. Cells were stimulated with 10 μ M ligands in the presence of 10 μ M forskolin. cAMP production was normalized to the percentage of forskolin-induced cAMP concentration (100%). Data represent mean \pm SEM of three independent experiments each performed in triplicate.

6.3.4 Computational modeling of a bivalent ligand bound to an mGluR₅-D₂R heterodimer

The binding pose of compound **22a** was investigated *in silico* through protein-protein docking of crystal structures: transmembrane domains (TMD) of mGluR₅ and D₂R, followed by docking of the bivalent ligand into the modeled heterodimer (see Experimental Section). As both receptors are co-crystallized with either a NAM [42] or antagonist [37], they can be considered to be in their respective inactive states. As the bivalent ligand **22a** is a fusion of mGluR₅ NAM and a D₂R agonist, this means mGluR₅ is in an ideal conformation but not D₂R, which would theoretically be active in such a heterodimer-ligand complex.

Furthermore, as the original crystal structure of mGluR₅ has no clear entrance or exit for NAMs because of its tightly closed extracellular loops and TMD [42], a modified conformation of the receptor was deemed necessary to correctly bind a bivalent compound. Such a conformation has been observed previously, first with a Monte Carlo sampling technique employed for the purposes of docking photo-sensitive [50] and long linear [51] mGluR₅ NAMs, and secondly during MD simulations of mGluR₅ with bound NAM [41]. In summary, this

alternative mGluR₅ conformation is in an inactive state and similar to the original mGluR₅ crystal structure [42] but undergoes a partial separation of the extracellular ends of TM5 and TM6, which are highly flexible [41]. This potentially allows NAMs to enter or leave and is conducive for the linker of a bivalent ligand to pass outside of the receptor. As such, we utilized this MD-generated mGluR₅ conformation [41] for modeling interactions with D₂R, whose crystal structure has no such limitations regarding the binding of a bivalent ligand.

In terms of modeling an mGluR₅-D₂R heterodimer, referring to experimental information is important as these proteins can potentially interact in a number of ways. Interestingly, TM5 and TM6 have been experimentally observed to dynamically participate in the interface(s) of an mGluR₂ homodimer [52], whereas TM5 has also been involved in cross-talk between mGluR₂ and the Class A GPCR, 5-HT_{2A} receptor [53-55]. Based on homology between mGluR₂ and mGluR₅ TMDs (sequence identity of 51%), physical interaction between mGluR₅ and D₂R may follow a similar pattern. In addition, participation of mGluR₅ TM5 and/or TM6 in a direct interaction with D₂R would provide a means of bridging a bivalent ligand between the receptors. Likewise for D₂R, TM5 and TM6 have been observed to participate in its experimentally characterized homodimeric and heteromeric receptor interactions [56-59]. As such, we modeled an mGluR₅-D₂R heterodimer via its respective TM5-TM6 helices by using the mu-opioid homodimer crystal structure as a template [43], which contains an analogous interface. This initial mGluR₅-D₂R model was refined with protein-protein docking to identify an optimal interaction between the receptors [44] (see Experimental Section). The best docked mGluR₅-D₂R conformation results in close packing of residues at the TM5-TM6 interface (**Figure 6.6 B**). However, as D₂R is in an inactive state, with its TM6 in an inward rather than outward orientation [37], the contact surface between both receptors is possibly not as extensive as it could be. Nevertheless, the reported docking score is respectable, suggesting a favorable interaction (*I_{sc}* of -6.6 on a scale of 0 to -10, where better than -5 is considered satisfactory [44]).

Compound **22a** was bound to the mGluR₅-D₂R heterodimer model by first automatically docking its separate mGluR₅ NAM (MTEP) and D₂R agonist (DPAT-alkyne, **1**) components, second, by manually connecting these with the appropriate linker, and third, energy minimizing the resulting complex (see Experimental Section). It was found that by following this process, **22a** is able to simultaneously bind both receptors, passing between TM5 and

TM6 of each (**Figure 6.6 A**), with the linker residing at the membrane surface or just beneath (**Figure 6.6 B**). In the modeled complex, compound **22a** is able to make six protein-ligand H-bonds: two with mGluR₅ and four with D₂R (**Figure 6.6 C**). In mGluR₅, these H-bonds involve residues S805 and S809 on TM7, both of which interact with the MTEP component of **22a** (**Figure 6.6 C**). These observed protein-ligand H-bonds are consistent with known mGluR₅ NAM binding modes previously identified in mGluR₅ crystal structures [42, 60] and published mGluR₅ MD simulations [41, 50]. In D₂R, the DPAT component of **22a** makes an H-bond with D114 on TM3 in the same manner as co-crystallized risperidone in the original D₂R crystal structure [37]. However, in line with its potential D₂R agonism and unlike risperidone, **22a** makes additional H-bonds with the backbone oxygen of S193 on TM5 and Y408 hydroxyl group on TM7 (**Figure 6.6 C**). The importance of S193 for the binding of D₂R agonists has been noted before [61], along with neighboring residues, S194 and S197. Due to the closeness of these three particular serine residues in the D₂R crystal structure, only moderate conformational changes in TM5 (due to receptor activation, for example) would be required for **22a** to make H-bonds with the sidechain hydroxyl groups of either S193, S194 or S197. Finally, the tertiary amine on the linker of **22a** makes an H-bond with D400 located on extracellular loop 3 (ECL3) of D₂R (**Figure 6.6 C**). This interaction is likely conducive to the conformational stability of this particular linker, which might otherwise (e.g. PEG-linkers) become a destabilizing factor.

Overall, due to the number of observed protein-ligand H-bonds with both receptors, as well as consistency with known mGluR₅ and D₂R ligand binding modes, the modeled heterodimer-ligand complex appears to be compatible with the reported biological activity of compound **22a**.

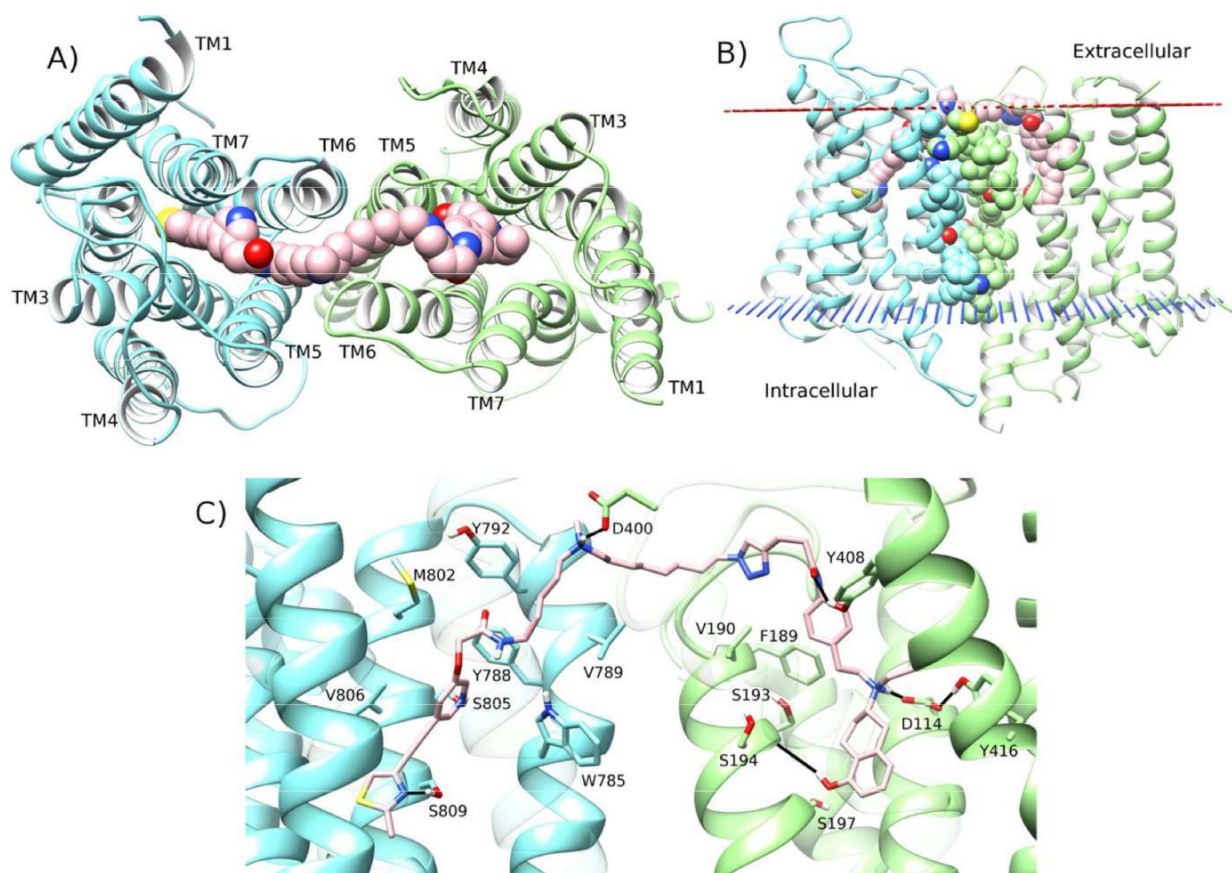


Figure 6.6 The modeled mGluR₅-D₂R-compound **22a complex.** A) Extracellular top-view of the interaction between mGluR₅ (blue ribbon, derived from PDB id: 4009) and D₂R (green ribbon, PDB id: 6CM4) via symmetrical TM5-TM6 interface, including bound compound **22a** (carbons as pink spheres). B) Side-view of mGluR₅-D₂R heterodimer with bound **22a** (carbon, nitrogen, oxygen and sulphur atoms as pink, dark blue, red and yellow spheres, respectively), showing contact interface (carbons as blue and green spheres, respectively) within a model membrane (red dots and blue lines, representing upper and lower leaflets, respectively). C) Modeled binding mode of compound **22a** (pink) within respective allosteric and orthosteric pockets of mGluR₅-D₂R heterodimer (blue and green ribbons, respectively). Protein-ligand H-bonds are displayed as solid black lines (S805 is partially obscured by the ligand). Selected residues on mGluR₅: TM6, TM7 and D₂R: TM3, TM5, TM7 and ECL3 are displayed (mGluR₅: TM3, TM5 and D₂R: TM6 are transparent for visualization purposes).

6.4 Conclusion

To conclude, we have designed and synthesized nine potential bivalent ligands comprising two distinct D₂R agonist/antagonist and an mGluR₅ negative allosteric antagonist. Ligation of D₂R ligands shows that bivalent ligands with PEG (PEG₄ and PEG₆) and hexamethylene linkers exhibit relatively low affinity for D₂₅R, contrary to bivalent ligands with alkylamine spacers. Interestingly, bivalent ligand **22a**, with a 20-atom alkylamine spacer, showed a 4-fold affinity increase for the D₂₅R in cells expressing both the D₂₅R and the mGluR₅, compared to cells only expressing D₂₅R, suggesting that **22a** may bridge the binding sites of the D₂₅R and mGluR₅ receptors. Moreover, **22a** shows a 5-fold higher affinity for the mGluR₅ than its MTEP azido precursor **21a** in D₂₅R-mGluR₅ cells, also pointing towards its capacity to simultaneously occupy both binding sites of the heteromer. From a functional point of view, **22a** inhibits forskolin stimulated cAMP formation with a 4-fold higher potency compared to alkyne **1** in the co-expressing cells, indicating that the bivalent binding requires a lower receptor occupation to exert signaling. In addition, a docking study reveals that **22a** is indeed able to simultaneously bind both receptors by bridging the heterodimeric interface, comprised of TM5 and TM6 of both receptors, and establishing six protein-ligand H-bonds.

Overall, we demonstrated that the length and nature of the spacer between the two receptor pharmacophores strongly affect binding affinity and functional potency both from a D₂₅R and from an mGluR₅ viewpoint. Most importantly, this study allowed us to identify bivalent ligand **22a**, which emerges as a promising molecular probe to further investigate D₂₅R and mGluR₅ heterodimerization.

References

1. Brauner-Osborne, H., et al., *Ligands for glutamate receptors: design and therapeutic prospects*. Journal of medicinal chemistry, 2000. **43**(14): p. 2609-45.
2. Pin, J.P. and F. Acher, *The metabotropic glutamate receptors: structure, activation mechanism and pharmacology*. Current drug targets. CNS and neurological disorders, 2002. **1**(3): p. 297-317.
3. Roppe, J.R., et al., 5-[(2-Methyl-1,3-thiazol-4-yl)ethynyl]-2,3'-bipyridine: a highly potent, orally active metabotropic glutamate subtype 5 (mGlu5) receptor antagonist with anxiolytic activity. Bioorganic & medicinal chemistry letters, 2004. **14**(15): p. 3993-6.
4. Conn, P.J. and J.P. Pin, *Pharmacology and functions of metabotropic glutamate receptors*. Annual review of pharmacology and toxicology, 1997. **37**: p. 205-37.
5. Cosford, N.D., et al., 3-[(2-Methyl-1,3-thiazol-4-yl)ethynyl]-pyridine: a potent and highly selective metabotropic glutamate subtype 5 receptor antagonist with anxiolytic activity. Journal of medicinal chemistry, 2003. **46**(2): p. 204-6.
6. Alagille, D., et al., *Synthesis and receptor assay of aromatic-ethynyl-aromatic derivatives with potent mGluR5 antagonist activity*. Bioorganic & medicinal chemistry, 2005. **13**(1): p. 197-209.
7. Baumann, C.A., et al., *Structure-activity relationships of fluorinated (E)-3-((6-methylpyridin-2-yl)ethynyl)cyclohex-2-enone-O-methyloxime (ABP688) derivatives and the discovery of a high affinity analogue as a potential candidate for imaging metabotropic glutamate receptors subtype 5 (mGluR5) with positron emission tomography (PET)*. Journal of medicinal chemistry, 2010. **53**(10): p. 4009-17.
8. Kulkarni, S.S., et al., *Structure-activity relationships comparing N-(6-methylpyridin-yl)-substituted aryl amides to 2-methyl-6-(substituted-arylethynyl)pyridines or 2-methyl-4-(substituted-arylethynyl)thiazoles as novel metabotropic glutamate receptor subtype 5 antagonists*. Journal of medicinal chemistry, 2009. **52**(11): p. 3563-75.
9. Bruno, V., et al., *Selective blockade of metabotropic glutamate receptor subtype 5 is neuroprotective*. Neuropharmacology, 2000. **39**(12): p. 2223-30.
10. Wang, Q., et al., *Block of long-term potentiation by naturally secreted and synthetic amyloid beta-peptide in hippocampal slices is mediated via activation of the kinases c-Jun N-terminal kinase, cyclin-dependent kinase 5, and p38 mitogen-activated protein kinase as well as metabotropic glutamate receptor type 5*. The Journal of neuroscience : the official journal of the Society for neuroscience, 2004. **24**(13): p. 3370-8.
11. Ossowska, K., et al., *An influence of ligands of metabotropic glutamate receptor subtypes on parkinsonian-like symptoms and the striatopallidal pathway in rats*. Amino acids, 2007. **32**(2): p. 179-88.
12. Rouse, S.T., et al., *Distribution and roles of metabotropic glutamate receptors in the basal ganglia motor circuit: implications for treatment of Parkinson's disease and related disorders*. Pharmacology & therapeutics, 2000. **88**(3): p. 427-35.
13. Varney, M.A. and R.W.t. Gereau, *Metabotropic glutamate receptor involvement in models of acute and persistent pain: prospects for the development of novel analgesics*. Current drug targets. CNS and neurological disorders, 2002. **1**(3): p. 283-96.
14. Pilc, A., et al., *Multiple MPEP administrations evoke anxiolytic- and antidepressant-like effects in rats*. Neuropharmacology, 2002. **43**(2): p. 181-7.
15. Chiamulera, C., et al., *Reinforcing and locomotor stimulant effects of cocaine are absent in mGluR5 null mutant mice*. Nature neuroscience, 2001. **4**(9): p. 873-4.
16. Bear, M.F., *Therapeutic implications of the mGluR theory of fragile X mental retardation*. Genes, brain, and behavior, 2005. **4**(6): p. 393-8.
17. Todd, P.K., K.J. Mack, and J.S. Malter, *The fragile X mental retardation protein is required for type-I metabotropic glutamate receptor-dependent translation of PSD-95*. Proceedings of the national academy of sciences of the United States of America, 2003. **100**(24): p. 14374-8.

18. Obeso, J.A., et al., *Pathophysiology of the basal ganglia in Parkinson's disease*. Trends in neurosciences, 2000. **23**(10 Suppl): p. S8-19.
19. Seeman, P., *Dopamine D2 receptors as treatment targets in schizophrenia*. Clinical schizophrenia and related psychoses, 2010. **4**(1): p. 56-73.
20. Cabello, N., et al., *Metabotropic glutamate type 5, dopamine D2 and adenosine A2a receptors form higher-order oligomers in living cells*. Journal of neurochemistry, 2009. **109**(5): p. 1497-507.
21. Diaz-Cabiale, Z., et al., *Metabotropic glutamate mGlu5 receptor-mediated modulation of the ventral striopallidal GABA pathway in rats. Interactions with adenosine A(2A) and dopamine D(2) receptors*. Neuroscience letters, 2002. **324**(2): p. 154-8.
22. Beggiato, S., et al., *Functional role of striatal A2A, D2, and mGlu5 receptor interactions in regulating striatopallidal GABA neuronal transmission*. Journal of neurochemistry, 2016. **138**(2): p. 254-64.
23. Mao, L.M. and J.Q. Wang, *Dopamine D2 receptors are involved in the regulation of Fyn and metabotropic glutamate receptor 5 phosphorylation in the rat striatum in vivo*. Journal of neuroscience research, 2016. **94**(4): p. 329-38.
24. Morin, N., et al., *mGlu5, Dopamine D2 and Adenosine A2A Receptors in L-DOPA-induced Dyskinesias*. Current neuropharmacology, 2016. **14**(5): p. 481-93.
25. Iso, Y., et al., *Synthesis and structure-activity relationships of 3-[(2-methyl-1,3-thiazol-4-yl)ethynyl]pyridine analogues as potent, noncompetitive metabotropic glutamate receptor subtype 5 antagonists; search for cocaine medications*. Journal of medicinal chemistry, 2006. **49**(3): p. 1080-100.
26. Milligan, G. and M. Bouvier, *Methods to monitor the quaternary structure of G protein-coupled receptors*. The FEBS journal, 2005. **272**(12): p. 2914-25.
27. Soriano, A., et al., *Adenosine A2A receptor-antagonist/dopamine D2 receptor-agonist bivalent ligands as pharmacological tools to detect A2A-D2 receptor heteromers*. Journal of medicinal chemistry, 2009. **52**(18): p. 5590-602.
28. Yekkirala, A.S., et al., *N-naphthoyl-beta-naltrexamine (NNTA), a highly selective and potent activator of mu/kappa-opioid heteromers*. Proceedings of the national academy of sciences of the United States of America, 2011. **108**(12): p. 5098-103.
29. Jacobson, K.A., et al., *A novel pharmacological approach to treating cardiac ischemia. Binary conjugates of A1 and A3 adenosine receptor agonists*. The Journal of biological chemistry, 2000. **275**(39): p. 30272-9.
30. Portoghese, P.S., *From models to molecules: opioid receptor dimers, bivalent ligands, and selective opioid receptor probes*. Journal of medicinal chemistry, 2001. **44**(14): p. 2259-69.
31. Rondou, P., et al., *KLHL12-mediated ubiquitination of the dopamine D4 receptor does not target the receptor for degradation*. Cellular signalling, 2010. **22**(6): p. 900-13.
32. Qian, M., et al., *Design, Synthesis, and Biological Evaluation of Bivalent Ligands Targeting Dopamine D2 -Like Receptors and the mu-Opioid Receptor*. ChemMedChem, 2018. **13**(9): p. 944-956.
33. Kiss, B., F. Horti, and A. Bobok, *In vitro and in vivo comparison of [(3)H](+)-PHNO and [(3)H]raclopride binding to rat striatum and lobes 9 and 10 of the cerebellum: a method to distinguish dopamine D(3) from D(2) receptor sites*. Synapse (New York, N.Y.), 2011. **65**(6): p. 467-78.
34. Domenici, M.R., et al., *Chronic treatment with the mGlu5R antagonist MPEP reduces the functional effects of the mGlu5R agonist CHPG in the striatum of 6-hydroxydopamine-lesioned rats: possible relevance to the effects of mGlu5R blockade in Parkinson's disease*. Journal of neuroscience research, 2005. **80**(5): p. 646-54.
35. Cheng, Y. and W.H. Prusoff, *Relationship between the inhibition constant (K1) and the concentration of inhibitor which causes 50 per cent inhibition (I50) of an enzymatic reaction*. Biochemical pharmacology, 1973. **22**(23): p. 3099-108.

36. Buccioni, M., et al., *Innovative functional cAMP assay for studying G protein-coupled receptors: application to the pharmacological characterization of GPR17*. Purinergic signalling, 2011. **7**(4): p. 463-8.
37. Wang, S., et al., *Structure of the D2 dopamine receptor bound to the atypical antipsychotic drug risperidone*. Nature, 2018. **555**(7695): p. 269-273.
38. Pettersen, E.F., et al., *UCSF Chimera--a visualization system for exploratory research and analysis*. Journal of computational chemistry, 2004. **25**(13): p. 1605-12.
39. Sali, A., *Comparative protein modeling by satisfaction of spatial restraints*. Molecular medicine today, 1995. **1**(6): p. 270-7.
40. Case, D.A., et al., *The Amber biomolecular simulation programs*. Journal of computational chemistry, 2005. **26**(16): p. 1668-88.
41. Dalton, J.A.R., J.P. Pin, and J. Giraldo, *Analysis of positive and negative allosteric modulation in metabotropic glutamate receptors 4 and 5 with a dual ligand*. Scientific reports, 2017. **7**(1): p. 4944.
42. Dore, A.S., et al., *Structure of class C GPCR metabotropic glutamate receptor 5 transmembrane domain*. Nature, 2014. **511**(7511): p. 557-62.
43. Manglik, A., et al., *Crystal structure of the micro-opioid receptor bound to a morphinan antagonist*. Nature, 2012. **485**(7398): p. 321-6.
44. Lyskov, S., et al., *Serverification of molecular modeling applications: the Rosetta Online Server that Includes Everyone (ROSIE)*. PloS one, 2013. **8**(5): p. e63906.
45. Kim, S., et al., *PubChem Substance and Compound databases*. Nucleic acids research, 2016. **44**(D1): p. D1202-13.
46. Morris, G.M., et al., *AutoDock4 and AutoDockTools4: Automated docking with selective receptor flexibility*. Journal of computational chemistry, 2009. **30**(16): p. 2785-91.
47. Kuhhorn, J., H. Hubner, and P. Gmeiner, *Bivalent dopamine D2 receptor ligands: synthesis and binding properties*. Journal of medicinal chemistry, 2011. **54**(13): p. 4896-903.
48. Gogoi, S., et al., *Novel bivalent ligands for D2/D3 dopamine receptors: Significant co-operative gain in D2 affinity and potency*. ACS medicinal chemistry letters, 2012. **3**(12): p. 991-996.
49. Zhang, Y., et al., *Synthesis and biological evaluation of bivalent ligands for the cannabinoid 1 receptor*. Journal of medicinal chemistry, 2010. **53**(19): p. 7048-60.
50. Dalton, J.A., et al., *Shining Light on an mGlu5 Photoswitchable NAM: A Theoretical Perspective*. Current neuropharmacology, 2016. **14**(5): p. 441-54.
51. Gomez-Santacana, X., et al., *Positional isomers of bispyridine benzene derivatives induce efficacy changes on mGlu5 negative allosteric modulation*. European journal of medicinal chemistry, 2017. **127**: p. 567-576.
52. Xue, L., et al., *Major ligand-induced rearrangement of the heptahelical domain interface in a GPCR dimer*. Nature chemical biology, 2015. **11**(2): p. 134-40.
53. Fribourg, M., et al., *Decoding the signaling of a GPCR heteromeric complex reveals a unifying mechanism of action of antipsychotic drugs*. Cell, 2011. **147**(5): p. 1011-23.
54. Gonzalez-Maeso, J., et al., *Identification of a serotonin/glutamate receptor complex implicated in psychosis*. Nature, 2008. **452**(7183): p. 93-7.
55. Moreno, J.L., et al., *Allosteric signaling through an mGlu2 and 5-HT2A heteromeric receptor complex and its potential contribution to schizophrenia*. Science signaling, 2016. **9**(410): p. ra5.
56. Bonaventura, J., et al., *Allosteric interactions between agonists and antagonists within the adenosine A2A receptor-dopamine D2 receptor heterotetramer*. Proceedings of the national academy of sciences of the United States of America, 2015. **112**(27): p. E3609-18.
57. Ferre, S., et al., *Essential Control of the Function of the Striatopallidal Neuron by Pre-coupled Complexes of Adenosine A2A-Dopamine D2 Receptor Heterotetramers and Adenylyl Cyclase*. Frontiers in pharmacology, 2018. **9**: p. 243.

58. Guo, W., et al., *Crosstalk in G protein-coupled receptors: changes at the transmembrane homodimer interface determine activation*. Proceedings of the national academy of sciences of the United States of America, 2005. **102**(48): p. 17495-500.
59. Navarro, G., et al., *Evidence for functional pre-coupled complexes of receptor heteromers and adenylyl cyclase*. Nature communications, 2018. **9**(1): p. 1242.
60. Christopher, J.A., et al., *Fragment and Structure-Based Drug Discovery for a Class C GPCR: Discovery of the mGlu5 Negative Allosteric Modulator HTL14242 (3-Chloro-5-[6-(5-fluoropyridin-2-yl)pyrimidin-4-yl]benzonitrile)*. Journal of medicinal chemistry, 2015. **58**(16): p. 6653-64.
61. Malo, M., et al., *Investigation of D(2) receptor-agonist interactions using a combination of pharmacophore and receptor homology modeling*. ChemMedChem, 2012. **7**(3): p. 471-82, 338.

Part II

Chapter 7:

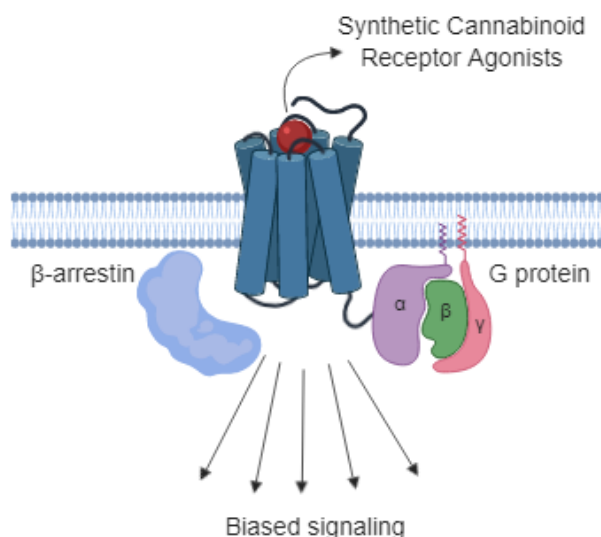
Insights into biased signaling at cannabinoid receptors:
synthetic cannabinoid receptor agonists

Based on

Elise Wouters, Jolien Walraed, Samuel Banister and Christophe Stove. Insights into biased signaling at cannabinoid receptors: synthetic cannabinoid receptor agonists. *Biochemical Pharmacology*. 2019; 169C; 113623.

ABSTRACT

Cannabinoid receptors type 1 (CB₁) and type 2 (CB₂) are promising targets for a number of diseases, including obesity, neuropathic pain, and multiple sclerosis, among others. Upon ligand-mediated activation of these receptors, multiple receptor conformations could be stabilized, resulting in a complex pattern of possible intracellular effects. Although numerous compounds have been developed and widely used to target cannabinoid receptors, their mode of action and signaling properties are often only poorly characterized. From a drug development point of view, unraveling the underlying complex signaling mechanism could offer the possibility to generate medicines with the desired therapeutic profile. Recently, an increased interest has emerged for the development of agonists that are signaling pathway-selective and thereby do not evoke on-target adverse effects. This phenomenon, in which specific pathways are preferred upon receptor activation by certain ligands, is also known as 'biased signaling'. For a particular group of cannabinoid receptor ligands (i.e. CB₁/CB₂ agonists), namely the synthetic cannabinoid receptor agonists (SCRAs), the research on biased signaling is still in its infancy and interesting outcomes are only recently being revealed. Therefore, this review aims at providing insights into the recent knowledge about biased agonism mediated by SCRAs *so far*. In addition, as these outcomes are obtained using a distinct panel of functional assays, the accompanying difficulties and challenges when comparing functional outcomes are critically discussed. Finally, some guidance on the conceptualization of ideal *in vitro* assays for the detection of SCRA-mediated biased agonism, which is also relevant for compounds belonging to other chemical classes, is provided.

GRAPHICAL ABSTRACT

Chapter outline

7.1 Introduction

7.1.1 Synthetic cannabinoid receptor agonists

7.2 Biased signaling

7.2.1 What is known for SCRAbs?

7.2.2 Strategies for identifying biased signaling

7.2.2.1 Challenges in comparing different experimental set-ups

7.2.2.2 Ideal *in vitro* activity-based techniques for assessing biased signaling

7.2.3 Reference compounds selection for SCRA bias detection

7.2.4 Cell system selection

7.3 Concluding remarks

7.1 Introduction

New psychoactive substances (NPS) are defined by the United Nations Office on Drugs and Crime Early Warning Advisory (UNODC EWA) as “substances of abuse, either in a pure form or a preparation, that are not controlled by the 1961 Single Convention on Narcotic Drugs or the 1971 Convention on Psychotropic Substances, but which may pose a public health threat” [1]. NPS, also referred to as ‘legal highs’, encompass a multitude of substances marketed as alternatives to traditional recreational drugs [2]. By modifying the chemical structure of traditional illicit drugs or psychoactive pharmaceuticals, clandestine medicinal chemists are purposely designing these psychoactive substances in order to evade current structure-based detection methods and/or bypass legislation. Consequently, specific NPS are often only transiently prevalent in drug markets, with typical life cycles of months to years for a given substance. NPS are constantly replaced with newer examples to stay one step ahead of law enforcement agencies, analytical laboratories and regulators [3].

By the end of 2018, more than 730 NPS had been identified in Europe by the European Monitoring Centre for Drugs and Drug Addiction (EMCDDA)[2]. Although NPS represent

approximately 5.0% of all drug abuse in Europe [4, 5], NPS use

is increasingly associated with serious harms, including death, in Europe and abroad [6]. Up to December 2018, over 110 countries worldwide have reported on nearly 900 NPS to the UNODC EWA on NPS [1].

NPS can be broadly categorized into six groups based on pharmacological similarity to the ‘traditional drugs’ (illicit or psychoactive) they intend to mimic, with structural heterogeneity both between and within groups. The proportional classification of these groups on the NPS

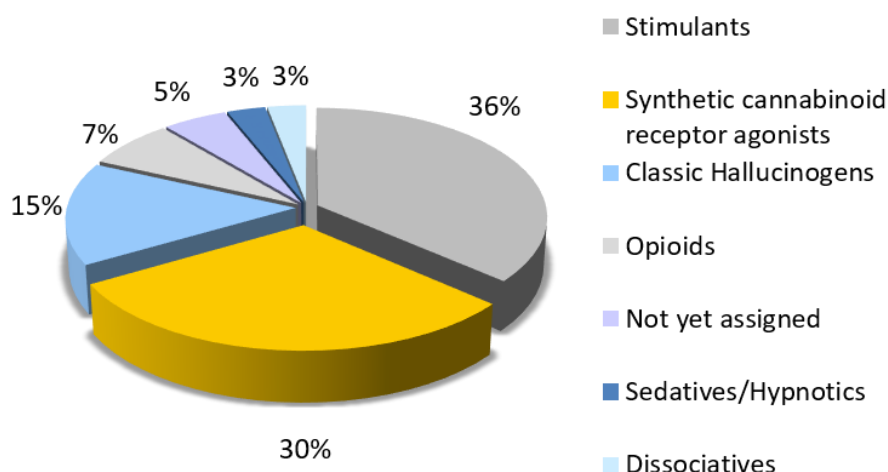


Figure 7.1 New psychoactive substances, proportionally divided in psychoactive groups, up to December 2018. Figure adapted from: UNODC EWA on NPS, 2019 [4].

market worldwide is depicted in **Figure 7.1** [1]. The majority are stimulants (36%), followed by synthetic cannabinoid receptor agonists (30%) and classic hallucinogens (15%), with these three classes accounting for more than 80% of the total number of NPS currently monitored by the UNODC.

7.1.1 Synthetic cannabinoid receptor agonists

Synthetic cannabinoid receptor agonists (SCRAs) are referred to as ‘cannabimimetics’ based on pharmacological similarities to the plant-derived Δ^9 -tetrahydrocannabinol (Δ^9 -THC), the major psychoactive component of cannabis [7]. Similar to Δ^9 -THC, SCRAs exert their cannabimimetic effects primarily through interaction with cannabinoid receptors type 1 (CB₁) [8-11] and type 2 (CB₂) [12] present in the human body. Although both receptors are Class A G protein-coupled receptors (GPCRs), CB₁ and CB₂ show only 44% overall sequence identity and differ in their tissue distribution and ligand sensitivity [13]. CB₁ is primarily expressed in the central nervous system, where its activation is associated with euphoria and relaxation effects. To a lesser extent, CB₁ expression has also been observed in the peripheral nervous system [14], where it has been associated with peripheral metabolism [15]. CB₂ is predominantly located in the periphery and mediates immune functions. Additionally, recent evidence has demonstrated that CB₂ is also expressed in neuronal terminals and mediates neuropsychiatric effects [16].

Both cannabinoid receptors were primarily known to be the main molecular targets of endocannabinoids, which are endogenous lipid-based neurotransmitters. Endocannabinoids, of which the two most thoroughly studied endogenous modulators encompass anandamide (AEA) and 2-arachidonoylglycerol (2-AG) (**Figure 7.2**), are all derived from long-chain polyunsaturated fatty acids [17]. More in particular, these endocannabinoids are produced following the hydrolysis of glycerol(phospho)lipid precursors, which successively originate from the remodeling of other membrane phospholipids [18]. It is quite well established that lipid-derived messengers can be produced through multiple biogenetic routes, however, for AEA the most common synthesis pathway involves phospholipase D whereas for 2-AG the enzymes phospholipase C and diacylglycerol lipase play a vital role [19]. Biosynthesis of endocannabinoids and its release from neurons is known to be regulated by the enhancement of intracellular calcium (Ca²⁺) concentrations, following Ca²⁺ influx by cell depolarization or

calcium mobilization [18, 20, 21]. Accordingly, the enzymes involved in the last step of AEA and 2-AG biosynthesis are all Ca^{2+} -sensitive. On the other hand, inactivation of these endocannabinoids is regulated by re-uptake or enzymatic degradation mechanisms involving fatty acid amide hydrolase (FAAH) and monoacylglycerol lipase (MAGL) for AEA and 2-AG, respectively [22].

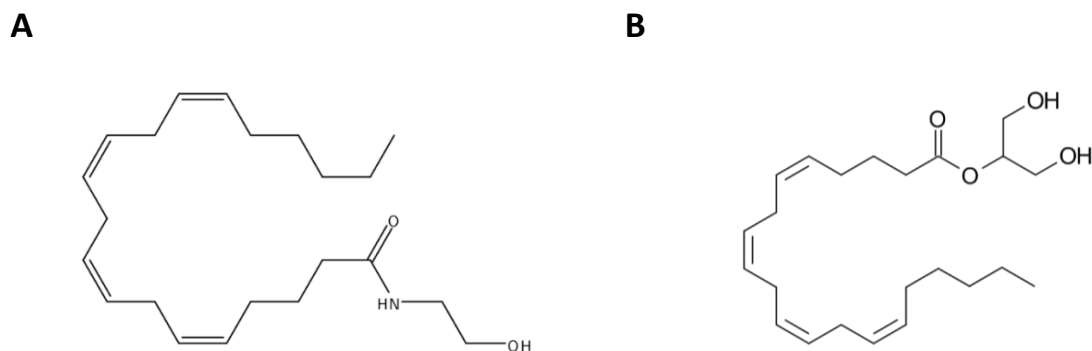


Figure 7.2 Chemical structure of the endocannabinoids AEA (A) and 2-AG (B).

Stimulation of CB₁ or CB₂ by endogenous or exogenous cannabinoid receptor ligands or SCRA promotes coupling to the G protein G $\alpha_{i/o}$ (although coupling of CB₁ with G α_s and G α_q has also been reported [23, 24]) as well as β -arrestin recruitment (see **Figure 7.3**) [25-27]. Upon activation of cannabinoid receptors, both type of transducers, G proteins and β -arrestins, provoke the activity of multiple downstream effectors. The recruitment of the pertussis toxin (PTX)-sensitive G $\alpha_{i/o}$ -type G protein leads to the inhibition of adenylyl cyclase (AC) and, consequently, results in a rapid decrease in 3',5'-cyclic adenosine monophosphate (cAMP) levels [28] or coupling to the mitogen-activated protein kinase (MAPK) pathway (**Figure 7.3**). Furthermore, the G $\beta\gamma$ subunits, upon dissociation from G $\alpha_{i/o}$, are known to activate G protein-gated inwardly rectifying potassium channels (GIRKs) and phosphatidylinositol-3-kinase (PI3K) and inhibit voltage-gated calcium channels (VGCC) [25].

On the other hand, β -arrestin2 recruitment to CB₁ results in desensitization and internalization of the receptor, while the recruitment of β -arrestin1 has been suggested to provoke the activation of the extracellular signal-regulated kinase (ERK) pathway (**Figure 7.3**) [29, 30]. Several studies have also investigated β -arrestin recruitment by CB₂, although still less is known about this signaling pathway [25]. The recruitment of β -arrestin2 to CB₂ has been demonstrated using the PathHunter[®] and NanoBiT[®] complementation assays [26, 31-34], as

well as by translocation studies using fluorescently tagged β -arrestin2 to the cell membrane [35, 36] and, like CB₁, this mechanism is physiologically linked to internalization and desensitization [37, 38]. Moreover, a recent study by Nogueras-Otíz et al. (2017) [36] suggested recruitment of β -arrestin1 to the 2-AG activated and internalized CB₂ as well, which led to ERK1/2 phosphorylation. In contrast to β -arrestin2, which was observed to be robustly recruited to the plasma membrane upon CB₂ activation, β -arrestin1 seems to associate and co-localize with CB₂ only at endosomal compartments such as the Rab4/5 compartments [36].

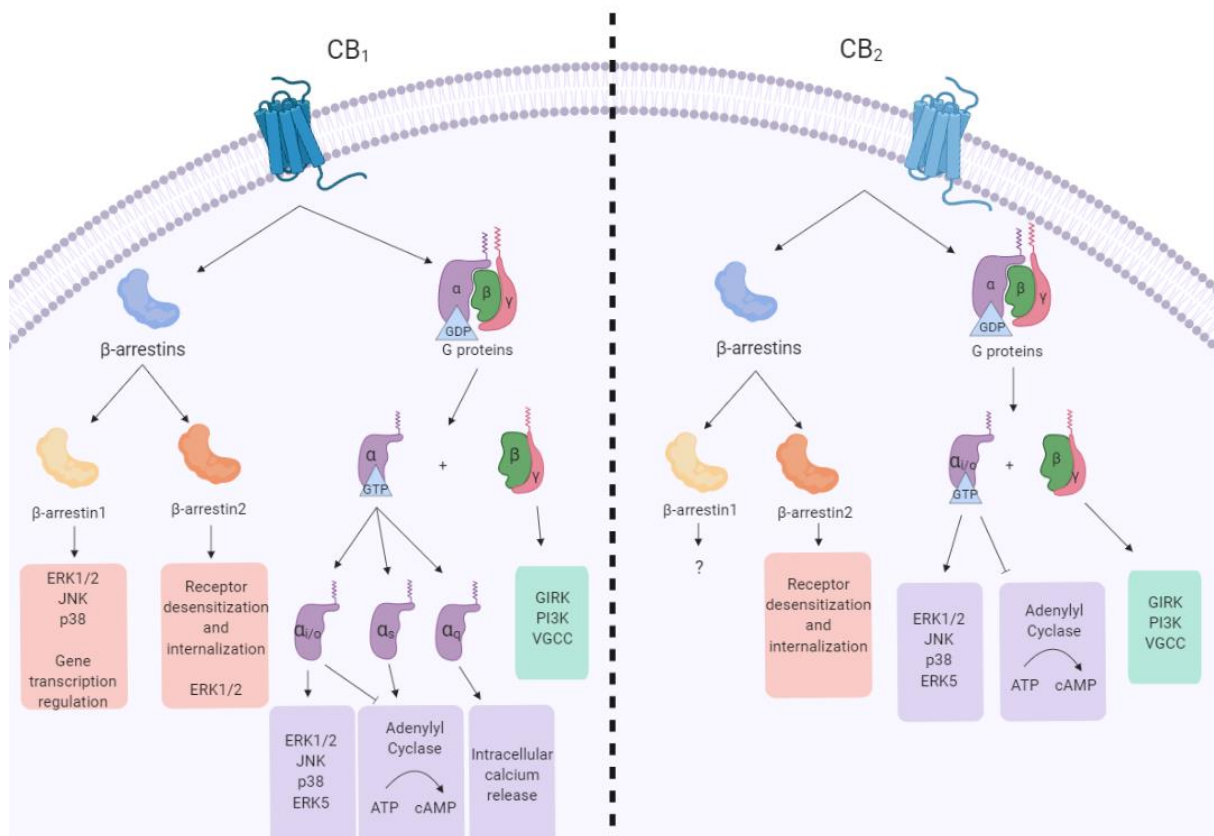


Figure 7.3 Signaling pathways mediated by CB₁ and CB₂ activation with focus on the Gα proteins and β-arrestins. Signaling through CB receptors can be mediated via G proteins and β-arrestins, each with their own downstream effectors. A knowledge gap is observed for CB₂ signaling through β-arrestin1, caused by a lack of in-depth studies concerning this signaling pathway. Abbreviations: ERK1/2 and ERK5: extracellular signal-regulated kinase (members of the mitogen activated protein kinase (MAPK) family), JNK: c-Jun N-terminal kinase, p38: p38 mitogen-activated protein kinase, GIRK: G protein-gated inwardly rectifying potassium channels, PI3K: phosphatidylinositol-3-kinase and VGCC: voltage-gated calcium channels.

In general, the recruitment of β-arrestins to activated GPCRs has been thought to occur in the absence of bound G proteins to prevent further G protein-mediated downstream signaling. This concept was recently challenged by studies by Thomsen *et al.* (2016) [39], who observed

the simultaneous binding of G proteins and β -arrestin to certain receptors, resulting in so-called super-complexes. Moreover, one should also keep in mind that for certain receptors, it has recently been proposed that β -arrestin signaling is only mediated downstream of G protein-mediated signaling, whereby β -arrestin would thus function as a regulator and thus not as an independent signaling scaffold [40]. Overall, activation of these downstream effectors (i.e. G proteins and β -arrestins) of the cannabinoid signaling pathways impacts biological processes, including immune-system activity, neuromodulation, appetite control, body weight regulation and pain modulation [20, 41-44].

Cannabinoid receptors are involved in the regulation of a broad panel of central and peripheral physiological processes, prompting exploration of these sites as drug targets for a variety of disorders. Whereas CB₁-selective ligands are of interest for the treatment of obesity, anorexia, cardiometabolic disorder and neuropathic pain [41, 45-47], CB₂-selective ligands represent a potential therapeutic treatment for pain and neuro-inflammatory diseases such as multiple sclerosis [48-51].

Many SCRA were primarily developed by scientists as research tools to investigate the function of the endocannabinoid system and subsequently as potential therapeutics for the treatment of distinct aforementioned diseases. Although many hundreds of SCRA were developed by academic laboratories and the pharmaceutical industry, most cannabinoid drug development programs never proceeded beyond preliminary preclinical investigation, and few cannabinoid receptor ligands are approved for human use. Several cannabinoid receptor ligands have currently entered phase II clinical trials registered by the US National Institutes of Health, such as the CB₂ agonist ajulemic acid (also known as JBT-101) for the treatment of systemic lupus erythematosus (from ClinicalTrials.gov: NCT03093402). Amongst the few CB₁ and CB₂ agonists that have already been approved are Marinol® (INN: dronabinol, synthetic THC), as an anti-emetic and appetite stimulant and Cesamet® (INN: nabilone, synthetic THC analogues) as anti-emetic. Furthermore, several formulations of Δ^9 -THC have been approved, such as nabiximols (Sativex®), being a standardized cannabis extract containing Δ^9 -THC and cannabidiol in a precisely formulated ratio. Sativex is an oromucosal spray which is an add-on therapy for the management of spasticity associated with multiple sclerosis [52, 53].

The CB₁ activation elicited by SCRAs, and presumed psychoactivity associated with this pharmacological profile [10, 12], led to the emergence of SCRAs on the illicit drug market in the mid-2000s. The earliest SCRA products were marketed under the brand ‘Spice’ (consisting of JWH-018 and CP47,497 C8 homologue, among other SCRAs) [54], although hundreds of SCRAs and product brands have been identified since [55]. Entirely new SCRA structures with no precedent in the scientific literature have also emerged, resulting in an apparent trend for more toxic compounds over time [56, 57]. Abuse of these SCRAs poses serious health risks, and adverse effects like agitation, hypertension, organ specific toxicity, heart attack, stroke, and even death, have been reported [58-64].

SCRAs can be classified into three broad, chemotypic groups: phytocannabinoid-like terpenophenolic derivatives, lipidic endocannabinoid analogues and heteroaromatic small molecules (see **Figure 7.4**). While several phytocannabinoid-like SCRAs have been detected in the NPS market (see Class I, **Figure 7.4**), the majority of SCRAs are heteroaromatic small molecules (see Classes II-VI, **Figure 7.4**). The Markush structure for this latter group of SCRAs is comprised of 4 subunits, including a core, a head, a linker and a tail. The core consists of a (hetero)aromatic structure, typically represented by indoles or azaindoles, although compounds with a pyrrole, naphthalene or thiazole core have also been identified. A linker, mostly a ketone, ester or amide group, connects the core to the head structure of the SCRA. This head group is characterized by a great diversity of chemical structures including substituted aromatic, heteroaromatic, alicyclic, polycyclic, and amino acid-derived moieties. Finally, diverse groups like alkyl, alicyclic, heterocyclic, aromatic and heteroaromatic chains can serve as the tail [65].

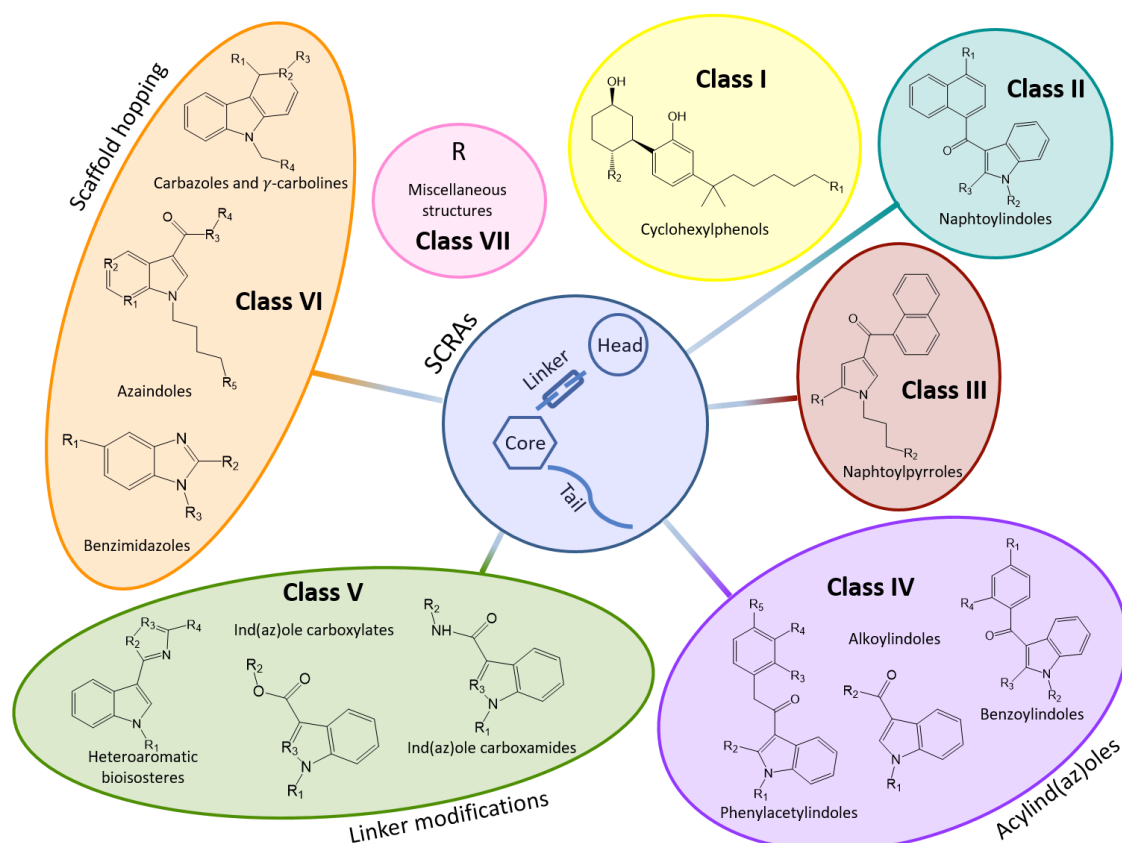


Figure 7.4 Classification of SCRA, based on their chemical structure (Based on Banister (2018) & Abbate (2018))[66-68].

Although several studies have reported on the structure-activity relationships and pharmacological evaluation of distinct SCRA classes [33, 57, 67-72], it has proven challenging to separate the desired medicinal properties from (often undesired) psychoactivity and adverse on-target effects [73]. The generation of CB_{1/2}-targeted ligands that selectively activate signaling pathways that mediate desired effects while minimizing adverse effects may lead to highly effective therapeutics for multiple indications [74]. To realize cannabinoid receptor ligands with new modes of action, a better understanding of the phenomenon known as ‘biased signaling’ is required for this class of ligands.

7.2 Biased signaling

Upon activation of a GPCR by an agonist, a cascade of cellular signals is elicited through specific transducers such as G proteins or β -arrestins. Historically, it was thought that GPCRs act as ligand-controlled ‘on/off’ switches, in which all agonists stabilize a single active conformation of the GPCR [75]. Nowadays, it is well-recognized that GPCRs act as allosteric microprocessors that sample a variety of active conformations upon response to different ligands [76]. Consequently, these ligand-induced stabilizations of active GPCR conformational states could preferentially transduce certain downstream signaling pathways over others, a phenomenon known as ‘biased signaling’, ‘ligand bias’ or ‘functional selectivity’. This ‘multi-state’ model is revolutionizing drug discovery as the selective activation of certain signaling pathways could result in improved targeted drugs with reduced side effects [76-79].

To be able to distinguish true ligand bias from ‘observational’ bias, also referred to as ‘apparent’ bias, care must be taken when selecting the effector systems (see section 2.2 ‘Strategies for identifying biased agonism’ and section 2.4 ‘Cell system selection’) and in implementing appropriate data analysis. Observational bias can occur upon differential expression of recruited transducers proximal to the receptor or following inappropriate interpretation of the data [76, 80].

For the quantification of true ligand bias *in vitro*, distinct quantitative methods based on mathematical models have been developed. Increasingly applied theoretical methods are (i) the operational model of Black and Leff [81], to estimate the transduction coefficients ($\Delta\Delta\log(\tau/K_A)$) or (ii) a model based on ratios of changes in *intrinsic* relative activity (RA_i) ($\Delta\Delta\log(RA_i)$). Whereas the latest mentioned model is calculated from the efficacy (E_{max}) and potency (EC_{50}) values of a ligand compared to a reference compound (**BOX 7.1**) and can only be applied if the Hill coefficient is unity, the model based on the $\Delta\Delta\log(\tau/K_A)$ ratio, in which τ is a measure for the efficacy and system amplification, allows quantification of relative bias taking into account the receptor density (**BOX 7.1**) and can be applied with a Hill coefficient of non-unity. Interested readers are referred to the excellent reviews written by Kenakin *et al.* (2013) [77], Onaran *et al.* (2017) [82] and Smith *et al.* (2018) [70] for a comprehensive overview of the analytical methods and their respective pitfalls. Moreover, these

quantification models have been validated and compared with one another in experimental set-ups [76,77].

BOX 7.1: Quantitative methods for the quantification of true ligand bias, defined by ‘the bias factor β’, <i>in vitro</i>.	
Transduction coefficients	Intrinsic relative activity (RA_i)
<p>The bias factor β is calculated by the ratios of the τ/K_a :</p> $\beta = \Delta \log(\tau/K_a)_{\text{ligand}} - \text{reference ligand}$ $= \Delta \log(\tau/K_a)_{\text{ligand}}$ $- \Delta \log(\tau/K_a)_{\text{reference ligand}}$ <p>In this formula K_a represents the conditional affinity for a specific pathway and τ the transduction coefficient which can be estimated by applying the operational model of Black and Leff:</p> $\frac{E}{E_m} = \frac{\tau^n [A]^n}{\tau^n [A]^n + (K_a + [A])^n}$ <p>With: E = effect E_m = maximal effect n = Hill factor $[A]$ = agonist concentration</p>	<p>The bias factor β is calculated by the ratios of the RA_i :</p> $\beta = \log \left(\frac{RA_{i,reference}^{pathwayA}}{RA_{i,reference}^{pathwayB}} \right)$ <p>The RA_i for each pathway of interest is calculated from the ratios of the E_{max} and EC_{50}'s of a ligand compared to a reference compound of both pathways:</p> $RA_{i,reference}^{pathwayA/B} = \frac{E_{max,i} \times EC_{50,ref}}{EC_{50,i} \times E_{max,ref}}$ <p>With: $E_{max,i}$ = efficacy of the ligand $EC_{50,i}$ = potency of the ligand $E_{max,ref}$ = efficacy of the reference $EC_{50,ref}$ = potency of the reference</p>

For suitable application to high-throughput screening (HTS) assays, a comparative study by Winpenny *et al.* (2016) [83] has shown that the more straightforward quantification method based on the $\Delta \log(RA_i)$ ratios can be applied, rather than the operational model by Black & Leff. Since both quantification methods generated similar outcomes, the $\Delta \log(RA_i)$ analysis is preferred as no additional re-fitting of concentration-response curves to a more complex model is needed.

Overall, biased signaling has grown into an increasingly active area of research with a plethora of endogenous and exogenous biased ligands identified for multiple GPCRs [84-87], including the cannabinoid receptors.

7.2.1 What is known for SCRAAs?

The pharmacological profiles of synthetic cannabinoid receptor agonists vary greatly between and within classes in terms of potency, efficacy, and signaling bias. SCRAAs identified as NPS on the drugs market typically act as potent, highly efficacious dual agonists of CB₁ and CB₂, however, there are noted exceptions [88-91]. In contrast, the Δ^9 -THC found in cannabis is a potent but only moderately efficacious agonist at CB₁; a “partial agonist”. As successive generations of SCRAAs with increasing CB₁ potency have emerged, reports of acute and fatal intoxications have increased in both frequency and scale [64, 92]. The structural and pharmacological features contributing to cannabinoid toxicity are not well understood, but CB₁ likely mediates at least some adverse effects, such as seizures, following SCRA use [93-95]. Deconvoluting the structural features that confer therapeutic cannabinoid effects from those associated with toxicity is a prerequisite for the rational design of new therapeutic cannabinoid receptor ligands that are devoid of the undesired effects mediated by CB₁. Most of the research on cannabinoid biased agonism has mainly focused on CB₁, although CB₂-mediated biased signaling has also been reported (**Table 7.1**).

CB₁ predominantly couples to G $\alpha_{i/o}$, but under certain circumstances CB₁ can also signal through G α_s and G α_q [23, 24]. For endogenous or plant-derived cannabinoid receptor ligands, as well as for allosteric SCRAAs, several studies have investigated the prevalence of preferred signaling through certain pathways upon CB₁ activation [23, 96, 97], but for orthosteric SCRAAs studies are rather limited. For example, it has been reported that the classical cannabinoid receptor agonist WIN55,212 (Class IV, **Figure 7.4**) preferentially permits coupling of CB₁ to G α_q over the recruitment of other G proteins (**Table 7.1**), while CB₁ stimulation with the structurally dissimilar molecule CP55,940 (Class I) shows a preference for coupling to G α_s [98-101]. WIN55,212 also preferentially recruits β -arrestin1 over β -arrestin2, while CP55,940 seems to favor coupling to G α_s over β -arrestin1 recruitment (**Table 7.1**) [99, 100, 102, 103].

Table 7.1 SCRAs showing biased agonism towards certain signaling pathways, reported in literature.

SCRA	Functional selectivity	Functional assays	Cell system	Ref.
hCB ₁				
CP55,940	G α_s > β -arrestin1 > G α_i > G α_q > G $\beta\gamma$	pERK1/2, pCREB, BRET	STHdh ^{Q7/Q7}	[99, 100]
	G proteins = β -arrestins	cAMP, [³⁵ S]GTP γ S, PathHunter [®]	CHO	[104]
		NanoBiT [®]	HEK293T	[105]
	G $\alpha_{i/o}$ > pERK	cAMP, in-cell western	HEK293	[97]
JWH-018	G proteins = β -arrestins	cAMP, [³⁵ S]GTP γ S, PathHunter [®]	CHO	[104]
HU-210	G α_o > G α_i = G α_s > G α_q	[³⁵ S]GTP γ S	Sf9 cells	[98, 106]
	G $\alpha_{i/o}$ > pERK	cAMP, in-cell western	HEK293	[97]
WIN55,212	G α_q > G α_i = G α_s > G α_o	[³⁵ S]GTP γ S	Sf9 cells	[98, 106]
	β -arrestin1 > β -arrestin2	Total surface fluorescence	HEK293T	[102, 107]
5F-APINACA	β -arrestin2 > G α_i	NanoBiT [®]	HEK293T	[105]
EG-018	G α_i > β -arrestin2	NanoBiT [®]	HEK293T	[105]
hCB ₂				
CP55,940	G $\alpha_{i/o}$ = β -arrestin2	cAMP, PathHunter [®]	HEK293T	[35, 108]
JWH-133	G $\alpha_{i/o}$ > β -arrestin2	cAMP, PathHunter [®]	HEK293T	[23]
WIN55,212	G $\alpha_{i/o}$ > β -arrestin2	cAMP, PathHunter [®]	HEK293T	[35, 108, 109]
AM-1710	β -arrestin2 > G proteins	Antibody-based internalization assay	HEK293T	[35]
AM-1241	β -arrestin & pERK > GIRK	PathHunter [®] , Alphascreen and FLIPR	CHO, AtT20	[31]
HU-308 and HU-910	G protein = β -arrestin2	[³⁵ S]GTP γ S, cAMP, PathHunter [®] , pERK and FLIPR [®]	AtT20, HEK293 and CHO	[31]
UOSD017 (triazine)	β -arrestin > pERK & cAMP	Antibody-based internalization assay, pERK1/2, cAMP	HEK293	[110]

Abbreviations in Table 7.1: SCRA: synthetic cannabinoid receptor agonist, Ref.: references, hCB₁: human CB₁, hCB₂: human CB₂, pERK1/2: phosphorylation of ERK1/2 (members of the mitogen activated protein kinase (MAPK) family), pCREB: phosphorylation of cyclic AMP response element binding (a cellular transcription factor), BRET: bioluminescence resonance energy transfer, cAMP: 3',5'-cyclic adenosine monophosphate.

Although biased signaling has been observed upon stimulation of CB₁ by CP55,940, other studies such as those from Ford *et al.* [104] have reported that CP55,940 is an overall unbiased ligand for CB₁, also coined a ‘balanced agonist’, meaning that it signals equally through G protein-dependent pathways and through β -arrestin recruitment (see 7.2.2.1 ‘Challenges in comparing different experimental set-ups for the transducers’). Therefore, the development of new accurate techniques for the measurement of bias, as well as new structural insights, might elucidate seemingly contradictory aspects in different reports about biased signaling [96, 111].

Similarly to CB₁, CB₂ can be activated by SCRA that differentially signal through various intracellular pathways. Whereas it has been reported that CP55,940 behaves as an unbiased ligand [35, 108], JWH-133 (Class II) and WIN55,212 can both signal through the G $\alpha_{i/o}$ signaling pathway, but reportedly failed to recruit β -arrestins (**Table 7.1**) [35, 108, 109, 112]. In contrast, AM-1710 (Class II) and AM-1241 (Class II) were reported to preferentially signal through β -arrestin2 over G protein-dependent signaling [24, 35, 113]. Finally, whereas HU-308 and HU-910 were observed to act as balanced agonists [31], the triazine (UOSD017) preferred signaling through β -arrestin [110].

For multiple SCRA the potencies (EC₅₀) and efficacies (E_{max}) of distinct signaling pathways have been investigated. For a selected group of SCRA, the pharmacological evaluation of both G protein- and β -arrestin-mediated signaling pathways has been reported, of which an overview is given in **Table 7.2** for CB₁ and **Table 7.3** for CB₂. **Tables 7.2** and **7.3** summarize reported values for measures of SCRA potency and efficacy across signaling pathways, however, direct quantitative comparisons should be drawn cautiously due to differences in experimental design, cellular systems, and protein expression levels. Differences in EC₅₀ values of a certain ligand in distinct studies are overall often only limited (**Table 7.2 and 7.3**). In certain instances however, there is a substantial variation. For example, an 88-fold difference was observed in the EC₅₀ values for CP55,940, following CB₁ stimulation, using either a [³⁵S]GTP γ S assay (EC₅₀ of 0.359 nM) (**Table 7.2**) [114] or a cAMP assay (EC₅₀ of 31.62 nM) (**Table 7.2**) [115]. Moreover, differences in reported EC₅₀ values were also observed when applying the same assay ([³⁵S]GTP γ S) within the same cell line (HEK293T), as exemplified by a 30-fold difference in EC₅₀ values for the CP55,940-activated CB₂ (EC₅₀: 0.294 nM [114] vs. EC₅₀: 9.07 nM [116] (**Table 7.3**). Also for the reported efficacies a certain range in E_{max} values can be observed, which may be

related to differences in normalization strategies applied in distinct studies (as indicated in **Tables 7.2 and 7.3**). An example is the efficacy of CP55,940, which ranges from 47% in a cAMP assay (**Table 7.2**) [115] up to 163.3% in a [³⁵S]GTPyS assay (**Table 7.2**) [116]. In the latter mentioned, the efficacy is presented as a percentage activation over basal stimulation [116], whereas in the first case the efficacy was normalized to the E_{\max} of a reference compound WIN55,212 [115]. Besides differences in efficacy values due to different normalization strategies, the possible effect of ‘receptor reserve’ (discussed further in more detail in section 7.2.1.1 Challenges in comparing different experimental set-ups) on the maximum response reached by the ligand should also be taken into account. Although multiple lines of evidence support the thesis that SCRA-mediated biased agonism does occur, many details remain to be elucidated. There are several requirements to unravel the potential ligand-biased properties of SCRA: (i) consistent assays should be used for the detection of bias, (ii) suitable reference compounds should be selected and (iii) evaluation should be conducted in the same cellular system.

Table 7.2 Overview of the potencies (EC_{50}) and efficacies (E_{max}) for a panel of SCRA, for which both the G protein and β -arrestin mediated signaling pathways have been investigated at CB₁.

Common name	Cell/Tissue type	K _i for CB ₁ (nM)	EC ₅₀ (nM)			E _{max}	Ref. compound	Assay	Ref.
			G protein	β-arrestin1	β-arrestin2				
Class I: Cyclohexylphenols									
CP55,940	HEK293T cells	0.59	23.3			124% ^a		[³⁵ S]GTPyS	[117]
		1.15 ± 0.13	16.9 ± 3.8			163.3% ^a		[³⁵ S]GTPyS	[116]
			31.62			47 ± 7.5% ^b	WIN55,212	cAMP	[115]
			15.85			47 ± 6.1% ^b	WIN55,212	cAMP	[115]
			0.359			94.5 ± 3.23% ^e		[³⁵ S]GTPyS	[114]
	Whole brain homogenate		13.5 ± 3.6					[³⁵ S]GTPyS	[118]
	AtT20-FlpIn neuroblastoma cells	18	42			100% ^c	CP55,940	FLIPR®	[69, 119]
	CHO cells	0.67	0.30			100% ^c	CP55,940	cAMP	[120]
			0.735					[³⁵ S]GTPyS	[121]
					5.62			PathHunter®	[122]
CHO-β2-hCB1 cells				19.0 (IC50)	114 ± 14% ^c (I _{max})	CP55,940	cAMP	[104]	
CHO-hCB1-Rx cells		1.80			91 ± 11%	CP55,940	[³⁵ S]GTPyS	[104]	
STHdh ^{Q7/Q7} cells				350		86 ± 4% ^d		BRET	[100]
Class II: Naphtoylindoles									
AM-2201	HEK293T cells				23.5	98.8% ^c	JWH-018	NanoBiT®	[70]
	AtT20-FlpIn neuroblastoma cells	1.0	38			111 ± 6% ^c	WIN55,212	FLIPR®	[123, 124]
EAM-2201	HEK293T cells	0.41	46.8 ± 5.0			270.3% ^a		[³⁵ S]GTPyS	[116]
					4.8			NanoBiT®	[33]
			79.43			71 ± 3.0% ^b	WIN55,212	cAMP	[115]
JWH-018	HEK293T cells				41.0	100% ^c	JWH-018	NanoBiT®	[70]
					38.2			NanoBiT®	[33]
					36.8	102.0% ^c	JWH-018	NanoBiT®	[125]
					23.9			NanoBiT®	[32]
			1584.89			55 ± 3.5% ^b	WIN55,212	cAMP	[115]
				45.1	102.6% ^c	JWH-018	NanoBiT®	[126]	
	AtT20-FlpIn neuroblastoma cells		18			116 ± 9% ^c	CP55,940	FLIPR®	[124]
		9.00	102			107 ± 6% ^c	WIN55,212	FLIPR®	[123, 124]
	CHO cells		1.132					cAMP	[127]
	CHO-β2-hCB1 cells				1.73 (IC50)	90 ± 5% ^c (I _{max})	CP55,940	cAMP	[104]
Whole brain homogenate		20.2			163 ± 3% ^a		[³⁵ S]GTPyS	[128]	
JWH-122	HEK293T cells				71.7			NanoBiT®	[33]
	CHO cells	3.35	2.8			101.9% ^c	CP55,940	cAMP	[120]
JWH-210	HEK293T cells	1.43 ± 0.39	116.1 ± 8.2			287.4% ^a		[³⁵ S]GTPyS	[116]
					25.3			NanoBiT®	[33]
	CHO cells	1.01	111			287.4% ^c	CP55,940	cAMP	[120]
MAM-2201	HEK293T cells	1.86 ± 0.29	36.1 ± 4.7			310.2% ^a		[³⁵ S]GTPyS	[116]
					60.5			NanoBiT®	[33]
			79.43			65 ± 3.9% ^b	WIN55,212	cAMP	[115]
Class IV: Acylindoles/Acylindazoles									
Aromatic									
WIN 55, 212	AtT20-FlpIn neuroblastoma cells		27			100% ^c	WIN55,212	FLIPR®	[129]
			284			100% ^c	WIN55,212	FLIPR®	[124]
	HEK293T cells	1.89	47.2			113% ^c	CP55,940	cAMP	[71, 130]
			31.6			65 ± 5.2% ^b	WIN55,212	cAMP	[115]
			5.01			64 ± 6.2% ^b	WIN55,212	cAMP	[131]

Common name	Cell/Tissue type	K _i for CB ₁ (nM)	EC ₅₀ (nM)			E _{max}	Ref. compound	Assay	Ref.
			G protein	β-arrestin1	β-arrestin2				
	STHdh ^{Q7/Q7} cells			570		59 ± 13% ^d		BRET	[100]
	CHO cells				158.49			PathHunter®	[122]
Alicyclic									
UR-144	AtT20-FlpIn neuroblastoma cells	150	421			94 ± 4% ^c	WIN55,212	FLIPR®	[123, 124]
	HEK293T cells				426			NanoBiT®	[32]
XLR-11 (5F-UR-144)	AtT20-FlpIn neuroblastoma cells	29.4	98			110 ± 4% ^c	WIN55,212	FLIPR®	[123, 124]
	HEK293T cells				179			NanoBiT®	[32]
			3981.07			65 ± 5.4% ^b	WIN55,212	cAMP	[115]
Class V: Linker modifications									
Indole/indazole esters/carboxylates									
5F-PB-22	whole brain homogenate	0.13 ± 0.01	3.7 ± 0.6			203 ± 3% ^a		[³⁵ S]GTPyS	[128]
	AtT20-FlpIn neuroblastoma cells		2.8			108 ± 5% ^c	WIN55,212	FLIPR®	[124]
	HEK293T cells				0.84			NanoBiT®	[33]
PB-22			39.81			67 ± 7.8% ^b	WIN55,212	cAMP	[115]
	HEK293T cells				0.86			NanoBiT®	[33]
			251.19			69 ± 5.9% ^b	WIN55,212	cAMP	[115]
	AtT20-FlpIn neuroblastoma cells		5.1			114 ± 3% ^c	WIN55,212	FLIPR®	[124]
Indole/indazole carboxamides									
Amino acid derivatives									
AB-CHMINACA	AtT20-FlpIn neuroblastoma cells	0.519	2.55					FLIPR®	[67]
			7.8					FLIPR®	[132]
	CHO cells		0.278					cAMP	[127]
	HEK293T cells				3.45	390.5% ^c	JWH-018	NanoBiT®	[125]
					6.1			NanoBiT®	[32]
		0.78	7.4			205% ^a		[³⁵ S]GTPyS	[117]
ADB-CHMINACA (MAB-CHMINACA)	AtT20-FlpIn neuroblastoma cells	0.289	0.620					FLIPR®	[67]
	HEK293T cells				0.34	262.6% ^c	JWH-018	NanoBiT®	[125]
					1.49			NanoBiT®	[32]
AB-PINACA	HEK293T cells				18.5	287.9% ^c	JWH-018	NanoBiT®	[70]
			79.34			69 ± 3.3% ^b	WIN55,212	cAMP	[115]
		2.87	71			192% ^a		[³⁵ S]GTPyS	[117]
	AtT20-FlpIn neuroblastoma cells		1.2			103 ± 4% ^c	CP55,940	FLIPR®	[119]
	HEK293T cell membrane	8.89	7.63			122 ± 7% ^e	CP55,940	[³⁵ S]GTPyS	[114]
5F-AB-PINACA	HEK293T cells				65.5	267.8% ^c	JWH-018	NanoBiT®	[70]
					55.4	216.8% ^c	JWH-018	NanoBiT®	[125]
		8.72	2.45			102 ± 6.55% ^e	CP55,940	[³⁵ S]GTPyS	[114]
	AtT20-FlpIn neuroblastoma cells		0.48			94 ± 6% ^c	CP55,940	FLIPR®	[119]
5F-ADB-PINACA	AtT20-FlpIn neuroblastoma cells		0.24			91 ± 7%	CP55,940	FLIPR®	[119]
	HEK293T cells				2.76	308.4% ^c	JWH-018	NanoBiT®	[125]
ADB-FUBICA	AtT20-FlpIn neuroblastoma cells		2.6			113 ± 8% ^c	CP55,940	FLIPR®	[119]
	HEK293T cells				12.3	313.6% ^c	JWH-018	NanoBiT®	[125]

Common name	Cell/Tissue type	K _i for CB ₁ (nM)	EC ₅₀ (nM)			E _{max}	Ref. compound	Assay	Ref.
			G protein	β-arrestin1	β-arrestin2				
AB-FUBINACA	HEK293T cells				15.6	323.7% ^c	JWH-018	NanoBiT®	[70]
					12.9	283% ^c	JWH-018	NanoBiT®	[126]
	AtT20-FlpIn neuroblastoma cells		1.8			108 ± 7% ^c	CP55,940	FLIPR®	[119]
	CHO cells		1.36 ± 0.09 (IC ₅₀)					cAMP	[133]
ADB-FUBINACA	HEK293T cells				0.69	338.8% ^c	JWH-018	NanoBiT®	[70]
					0.81				[125]
	AtT20-FlpIn neuroblastoma cells		1.2			152 ± 11% ^c	CP55,940	FLIPR®	[119]
5F-AMB-PINACA (5F-AMB)	HEK293T cells	8.29	1.3		15.1	258.6% ^c	JWH-018	NanoBiT®	[125]
						95.6 ± 8.02% ^e	CP55,940	[³⁵ S]GTPyS	[114]
	AtT20-FlpIn neuroblastoma cells		2.4					FLIPR®	[134]
			1.9			109 ± 3% ^c	CP55,940	FLIPR®	[65]
5F-MDMB-PINACA (5F-ADB)	AtT20-FlpIn neuroblastoma cells		0.45					FLIPR®	[67]
			0.59			108 ± 5% ^c	CP55,940	FLIPR®	[65]
	HEK293T cells	0.692	0.294			111 ± 9.14% ^e	CP55,940	[³⁵ S]GTPyS	[114]
					0.84	319.3% ^c	JWH-018	NanoBiT®	[125]
					1.78	331% ^c	JWH-018	NanoBiT®	[126]
MDMB-CHMICA	AtT20-FlpIn neuroblastoma cells		10			112 ± 3% ^c	CP55,940	FLIPR®	[65]
	CHO cells		0.142					cAMP	[127]
	HEK293T cells				1.77	285.1% ^c	JWH-018	NanoBiT®	[125]
AMB-CHMINACA	AtT20-FlpIn neuroblastoma cells		5.1			109 ± 4% ^c	CP55,940	FLIPR®	[65]
	HEK293T cells				3.91	360.1% ^c	JWH-018	NanoBiT®	[125]
MDMB-CHMINACA	AtT20-FlpIn neuroblastoma cells		10			111 ± 2% ^c	CP55,940	FLIPR®	[65]
	HEK293T cells				0.78	226.7% ^c	JWH-018	NanoBiT®	[125]
MDMB-FUBICA	AtT20-FlpIn neuroblastoma cells		2.7			109 ± 3% ^c	CP55,940	FLIPR®	[65]
	HEK293T cells				5.79	270.6% ^c	JWH-018	NanoBiT®	[125]
MDMB-FUBINACA	AtT20-FlpIn neuroblastoma cells		3.9			108 ± 3% ^c	CP55,940	FLIPR®	[65]
	CHO cells		0.6569			216.2% ^f		cAMP	[135]
	HEK293T cells				0.36	240.9% ^c	JWH-018	NanoBiT®	[125]
		1.14	0.2668			74.77% ^a		[³⁵ S]GTPyS	[135]

^a The E_{max} (%) was calculated as percentage activation over basal stimulation

^b The E_{max} (%) was normalized to the reference compound WIN55,212, of which the E_{max} was calculated from the inhibition of forskolin-stimulated cAMP production and resulted in ±65%

^c The E_{max} (%) was normalized to the reference compound, of which the E_{max} was set as 100%

^d The E_{max} (%) was calculated from the BRET efficiency curve

^e The E_{max} (%) was normalized to the reference compound CP55,940, of which the E_{max} was calculated as percentage activation over basal

^f The E_{max} (%) was expressed as percentage inhibition of forskolin-stimulated cAMP production

Table 7.3 Overview of the potencies (EC_{50}) and efficacies (E_{max}) for a panel of SCRA, for which both the G protein and β -arrestin mediated signaling pathways have been investigated at CB₂.

Common name	Cell/Tissue type	K _i for CB ₂ (nM)	EC ₅₀ (nM)			E _{max}	Ref. compound	Assay	Ref.
			G protein	β-arrestin1	β-arrestin2				
Class I: Cyclohexylphenols									
CP55,940	AtT20-Flpln neuroblastoma cells		68			100% ^c	CP55,940	FLIPR®	[65]
			13			100% ^c	CP55,940	FLIPR®	[119]
			22					FLIPR®	[69]
	HEK293T cells	0.55	9.07			55.1% ^a		[³⁵ S]GTPyS	[116]
		0.30	2.1			63% ^a		[³⁵ S]GTPyS	[117]
			0.294			92.4 ± 3.27% ^e		[³⁵ S]GTPyS	[114]
	CHO cells		0.735					[³⁵ S]GTPyS	[121]
			0.69 ± 0.23			100 ± 7.4% ^c	CP55,940	[³⁵ S]GTPyS	[136]
					2.88			PathHunter®	[122]
Class II: Naphtoylindoles									
AM-2201	AtT20-Flpln neuroblastoma cells	2.6	58			102 ± 7% ^c	WIN55,212	FLIPR®	[123, 124]
	HEK293T cells				6.59	125.0% ^c	JWH-018	NanoBiT®	[70]
EAM-2201	HEK293T cells				3.7			NanoBiT®	[33]
			91.9			40.2% ^a		[³⁵ S]GTPyS	[116]
	AtT20-Flpln neuroblastoma cells	0.371							[123]
JWH-018 (AM678)	AtT20-Flpln neuroblastoma cells		22			87 ± 7% ^c		FLIPR®	[119]
			133			95 ± 5% ^c	WIN55,212	FLIPR®	[124]
	HEK293T cells				12.8			NanoBiT®	[33]
					6.8			NanoBiT®	[32]
JWH-133	CHO cells		4.0 ± 1.0			111.5 ± 13.6% ^c	CP55,940	[³⁵ S]GTPyS	[136]
					10.72			PathHunter®	[122]
JWH-210	HEK293T cells				17.5			NanoBiT®	[33]
MAM-2201	HEK293T cells		51.0			43.6% ^a		[³⁵ S]GTPyS	[116]
					2.7			NanoBiT®	[33]
			1.93			23.2% ^a		[³⁵ S]GTPyS	[116]
Class IV: Acylindoles/Acylindazoles									
Aromatic									
WIN 55, 212	AtT20-Flpln neuroblastoma cells		117			100% ^c	WIN55,212	FLIPR®	[129]
	Whole brain homogenate	0.28 ± 0.16							[137]
	HEK293T cells		0.650			98% ^c	CP55,940	cAMP	[130]
	CHO cells				11.22			PathHunter®	[122]
Alicyclic									
UR-144	AtT20-Flpln neuroblastoma cells	1.8	72			104 ± 3% ^c	WIN55,212	FLIPR®	[123, 124]
	HEK293T cells				7.4			NanoBiT®	[32]
XLR-11 (5F-UR-144)	AtT20-Flpln neuroblastoma cells	0.608	83			117 ± 10% ^c	WIN55,212	FLIPR®	[67, 124]
	HEK293T cells				2.8			NanoBiT®	[32]

Common name	Cell/Tissue type	K _i for CB ₂ (nM)	EC ₅₀ (nM)			E _{max}	Ref. compound	Assay	Ref.
			G protein	β-arrestin1	β-arrestin2				
Class V: Linker modifications									
Indole/indazole esters/carboxylates									
5F-PB-22	AtT20-FlpIn neuroblastoma cells	0.633	11			101 ± 3% ^c	WIN55,212	FLIPR®	[67, 124]
	HEK293T cells				0.70			NanoBiT®	[33]
PB-22	HEK293T cells				0.82			NanoBiT®	[33]
	AtT20-FlpIn neuroblastoma cells		37			101 ± 5% ^c	WIN55,212	FLIPR®	[124]
Indole/indazole carboxamides									
Amino acid derivatives									
AB-CHMINACA	HEK293T cells	0.45	232.4			35% ^a		[³⁵ S]GTPyS	[117]
					3.7			NanoBiT®	[32]
			251.19			51 ± 1.8% ^b	WIN55,212	cAMP	[131]
AB-PINACA	AtT20-FlpIn neuroblastoma cells		2.5					FLIPR®	[67]
			8.60 ± 0.13			104 ± 7% ^c	CP55,940	FLIPR®	[119]
	HEK293T cells				2.77	143.7% ^c	JWH-018	NanoBiT®	[70]
		0.88	14.9			41% ^a		[³⁵ S]GTPyS	[117]
			2.4			83.7 ± 5.34% ^e	CP55,940	[³⁵ S]GTPyS	[114]
5F-AB-PINACA	AtT20-FlpIn neuroblastoma cells		2.6					FLIPR®	[67]
			8.59 ± 0.25			110 ± 13% ^c	CP55,940	FLIPR®	[119]
	HEK293T cells				7.06	173.0% ^c	JWH-018	NanoBiT®	[70]
			5.22			84.5 ± 9% ^e	CP55,940	[³⁵ S]GTPyS	[114]
AB-FUBINACA	AtT20-FlpIn neuroblastoma cells		3.2					FLIPR®	[67]
			8.50 ± 0.20			95 ± 12% ^c	CP55,940	FLIPR®	[119]
	HEK293T cells				1.78	106.5% ^c	JWH-018	NanoBiT®	[70]
					1.60	121% ^c	JWH-018	NanoBiT®	[126]
	CHO cells		42.4 ± 3.8 (IC ₅₀)					cAMP	[133]
ADB-FUBINACA	AtT20-FlpIn neuroblastoma cells		3.5					FLIPR®	[67]
			8.46 ± 0.13			104 ± 7% ^c	CP55,940	FLIPR®	[119]
	HEK293T cells				0.59	134.5% ^c	JWH-018	NanoBiT®	[70]
5F-AMB-PICA	AtT20-FlpIn neuroblastoma cells		4.6					FLIPR®	[67]
	HEK293T cells				15.3	167.1% ^c	JWH-018	NanoBiT®	[70]
5F-MDMB-PICA	AtT20-FlpIn neuroblastoma cells		7.4					FLIPR®	[67]
			4.6			94 ± 3% ^c	CP55,940	FLIPR®	[65]
	HEK293T cells				0.87	244.0% ^c	JWH-018	NanoBiT®	[70]

^a The E_{max} (%) was calculated as percentage activation over basal stimulation

^b The E_{max} (%) was normalized to the reference compound WIN55,212, of which the E_{max} was calculated from the inhibition of forskolin-stimulated cAMP production and resulted in ±65%

^c The E_{max} (%) was normalized to the reference compound, of which the E_{max} was set as 100%

^d The E_{max} (%) was calculated from the BRET efficiency curve

^e The E_{max} (%) was normalized to the reference compound CP55,940, of which the E_{max} was calculated as percentage activation over basal

^f The E_{max} (%) was expressed as percentage inhibition of forskolin-stimulated cAMP production

7.2.2 Strategies for identifying biased signaling

For the identification of biased agonism properties of ligands, sensitive techniques measuring downstream signaling are required. A panel of distinct functional assays has been employed to quantify the extent of canonical or non-canonical signaling at CB₁ and CB₂ (**Table 7.4**). For canonical or G protein-mediated signaling pathways, the functional assays Fluorescence Imaging Plate Reader (FLIPR®), [³⁵S]guanosine 5'-O-[gamma-thio]triphosphate (GTPγS), or assays measuring cAMP levels can be applied. For the non-canonical pathways, functional assays such as PathHunter® or Tango™ can be employed. Both assays measure the recruitment of β-arrestins to the activated GPCR, but whereas PathHunter® is a complementation-based assay with β-galactosidase split fragments fused to the GPCR of interest and β-arrestin, the principle of the Tango™ assay encompasses the fusion of a protease to β-arrestin and a transcription factor to the GPCRs, ultimately leading to the transcription of the β-lactamase reporter gene (**Table 7.4**). In addition, certain techniques allow the quantification of both canonical and non-canonical signaling pathways by measuring the recruitment of the transducers. These techniques include complementation-based assays based on NanoBiT® (employing a split NanoLuciferase)[105] or resonance energy transfer (RET)-based assays like fluorescence RET (FRET) or bioluminescence RET (BRET) or mitogen-activated protein kinase (MAPK/ERK) assay (**Table 7.4**).

7.2.2.1 Challenges in comparing different experimental set-ups

Upon implementation of the aforementioned distinct experimental set-ups, different outcomes for biased agonism, sometimes with apparently contradictory results, may be obtained. In the case of CP55,940 (**Table 7.1**) a BRET assay revealed that the recruitment of Gα_s-protein was preferred over β-arrestin1 recruitment as well as over the remaining G proteins [99, 100]. In contrast, Ford *et al.* [104] reported that CP55,940 acted as a balanced agonist, as demonstrated by cAMP, [³⁵S]GTPγS and PathHunter® assays. This apparent discrepancy may be a reflection of differences in the measurement systems or the cell systems that were used (*STHdh*^{Q7/Q7} striatal cell line [99, 100] vs. Chinese hamster ovary (CHO) cells [104]). Moreover, deviating outcomes for potency and efficacy values have been observed upon the implementation of distinct techniques (**Table 7.2 & 7.3**). When screening for biased agonism, it is therefore crucial to apply approaches that can separate true ligand bias, which

should be present across different assays, from observational bias upon screening for biased agonists [82].

For the evaluation of the outcome of functional assays, 'receptor reserve' is an important aspect. This term refers to the phenomenon wherein only submaximal receptor occupancy is required for the system to reach its maximal response [138]. In general, assays measuring events proximal to the receptor, like G protein and β -arrestin recruitment or GTP exchange (e.g. NanoBiT[®], BRET, FRET, PathHunter[®] and [³⁵S]GTPyS assays), typically have lower levels of 'receptor reserve'. Therefore, these techniques allow differentiation between agonists of differing efficacies [139]. On the other hand, second-messenger assays (e.g. cAMP, FLIPR[®] and MAPK) are typically more prone to providing potentially skewed results due to a higher degree of 'receptor reserve'. Accordingly, the maximal response is reached faster upon lower degree of receptor occupation, due to signal amplification (**Table 7.4**). Hence, a partial and full agonist may both yield the same maximal effect and may not be distinguished in these experimental set-ups. Furthermore, although the Tango[™] assay measures recruitment of β -arrestin, its dependence on the transcription of β -lactamase renders the read-out heavily affected by signal amplification [140]. This level of receptor reserve has already been investigated for the CB₁-based FLIPR[®] assay via receptor depletion, accomplished by pre-treatment with the irreversible CB₁ antagonist AM6544 [141]. This allowed the quantitative determination of efficacy by fitting the concentration-response curves to the operational model of Black and Leff before and after receptor depletion. It was observed that pretreatment with AM6544 caused an overall 94% reduction in receptors available in the FLIPR[®] assay for CB₁ agonist stimulation [141].

Table 7.4 Selected assays for assessing biased signaling (G protein-based assays: Orange, β -arrestin-based assays: Blue, Applicable for both transducers: Green).

ASSAY	MEASURING		READ-OUT		AMPLIFICATION OF SIGNAL VIA 2 ND MESSENGER	MEASUREMENT*
	WHAT	HOW	WHAT	HOW		
FLIPR®	Membrane potential	Via voltage-sensitive fluorescent dyes	Fluorescence	CCD camera	YES	End-point
[³⁵ S]GTP γ S	Level of G protein activation	Via [³⁵ S]GTP γ S labeled G α -subunits	Radioactivity	Scintillation counter	YES	Real-time for 30 – 60 min or End-point
cAMP	Change in intracellular cAMP level	Via immune-competitive assay	Antibody labeling	Plate reader (FRET or ELISA)	YES	End-point
		Via mutant luciferase with a cAMP binding domain (Glosensor™)	Bioluminescence	Plate reader		Real-time for 15 min
PathHunter®	β -arrestin recruitment	Via the fusion of ProLink™ and enzyme acceptor (EA) (β -galactosidase) [°]	Chemiluminescence	Plate reader	NO	End-point: after 90 min
Tango™	β -arrestin recruitment	Via fusion of a transcription factor and a protease (Transcription of β -lactamase)	Fluorescence	Plate reader	NO	End-point after 16 h incubation (transcription)
NanoBiT®	G protein or β -arrestin recruitment	Via the complementation of SmBiT and LgBiT (split NanoLuciferase) [°]	Bioluminescence	Plate reader	NO	Real-time for 2 h
BRET	G protein or β -arrestin recruitment	Via the proximity of a luminescent donor and a fluorescent acceptor [°]	Bioluminescence	Plate reader	NO	End-point: after 1 min
FRET	G protein or β -arrestin recruitment	Via the proximity of 2 fluorophores [°]	Fluorescence	Plate reader	NO	End-point
MAPK	G protein or β -arrestin recruitment	In-cell western	Antibody labeling	LI-COR® Odyssey® Infrared Imaging System	YES	End-point

*End-point measurement: a single measurement is performed after a fixed incubation period

[°]Complementation- or RET-based assays: both techniques rely on the fusion of a (split) protein to the GPCR and an additional (split) protein to the transducer.

Besides receptor reserve, one should also bear in mind that second messenger assays do not necessarily demonstrate that a specific G protein or β -arrestin mediated the observed response. For example, changes in cAMP levels might also be evoked by the regulation of phosphodiesterases or via signaling by the beta-gamma subunits of G proteins ($G_{\beta\gamma}$) [142]. The latter mentioned is known to activate or inhibit adenylyl cyclase, leading to an intracellular increase or decrease of cAMP [142]. For cannabinoid signaling, both CB₁ and CB₂ primarily signal through the pertussis toxin (PTX)-sensitive $G\alpha_i$ protein, for which incubation with PTX has been successfully used as a control of $G\alpha_i$ -mediated cAMP signaling [108]. An intrinsic drawback of the complementation- and RET-based assays is that these require labeling of the receptor and transducer via fusion with other (split)proteins, which may have a physical impact on recruitment of the transducer. In contrast, the key advantage of second-messenger signaling pathways includes the possibility of measuring signaling bias mediated by the native, unmodified receptor at lower expression levels.

Another phenomenon involves the dynamic aspects of biased signaling, designated as ‘temporal bias’ [143]. Most experimental set-ups do not allow the capturing of temporal information of the GPCR/transducer complex. Therefore, assays like the NanoBiT[®] assay might serve as a good *in vitro* technique for the quantification of biased agonism, as these also allows kinetic measurements. This makes it possible to evaluate ligand bias at different time points, e.g. at the time point when the maximal response is reached, or a given timeframe thereafter [105].

Overall, the difficulties in comparing different experimental set-ups for identifying biased agonism encompass several aspects (see **BOX 7.2**). Firstly, intrinsic properties of the system might generate deviating outcomes due to: (i) the possible saturability of the read-out, (ii) different expression levels of the utilized constructs, or (iii) the requirement of modification of the GPCR and transducer (versus the native GPCR and transducer). A second aspect relates to the cell context, which might influence observed outcomes due to: (i) different expression levels of the native transducers and/or GPCRs or (ii) the expression of off-target proteins or isoforms of the GPCR (see section ‘cell system selection’ for a more detailed discussion).

BOX 7.2: Difficulties in comparing distinct experimental set-ups for identifying of biased agonism.

The system	Cell context
<ul style="list-style-type: none"> • System characteristics (e.g. endpoint vs. real-time detection, direct or inferred measurement (i.e. via transcription factor), among others). • Saturability of the read-out (i.e. receptor reserve) • Distinct expression levels of utilized constructs • Native vs. modified receptor/transducer • Capturing of temporal bias 	<ul style="list-style-type: none"> • Cell species • Different expression levels of the native receptor and the transducer • Expression (levels) of isoforms of the GPCR • Expression (levels) of off-target proteins e.g. orphan receptors GPR18, GPR55, GPR119

7.2.2.2 Ideal *in vitro* activity-based techniques for assessing biased signaling:

Ideal *in vitro* assays for the assessment of biased signaling should have the following characteristics:

❖ **Common detection technique for recruitment of different transducers.**

Preferentially, the same experimental set-up is used to investigate the distinct transducer signaling pathways, to avoid ‘observational’ bias of one assay compared to another [144].

❖ **Real-time measurement.** Real-time measurement, in which the effect of biased agonism is analyzed over multiple time points, gives a better view on the biological relevance of the time scale in which the biased agonism persists [145].❖ **Equivalent amplification.** When opting for certain assays to analyze specific signaling pathways, a similar level of amplification for both pathways should be generated [144, 146]. More specifically, functional assays based on receptor-proximal events (e.g. G protein and β -arrestin recruitment to the receptor) are

preferentially compared with each other, rather than with second-messenger assays (e.g. cAMP and FLIPR®) – and *vice versa*.

- ❖ **Simplicity.** A straightforward experimental set-up to allow fast detection should be implemented. In particular, direct measurement of the signaling event is favored over the implementation of additional steps as for example the activation of a transcription factor. Also the use of living cell cultures (ideally stable cell lines), allowing live assay measurements, may prove beneficial in terms of simplicity.
- ❖ **Sensitivity.** Although the concept of ‘sensitivity’ is always a prerequisite in HTS, in this case this concept might be less straightforward since it is still unclear what the magnitude of bias should be to provoke a relevant change in psychological response.
- ❖ **Reproducibility.** *In vitro* screening assays to identify bias should be robust, i.e. deliver reproducible results, notwithstanding variations inherent to execution of the assay (e.g. small deviations in cell number, age of the substrate, among others). Independently performed experiments should provide consistent outcomes.
- ❖ **Detection in appropriate cell systems.** The host cell line should be consistent across the different assays for measuring biased agonism. Furthermore, one should keep in mind that although the Black and Leff operational model corrects for receptor expression levels, the effect of the endogenous expression of off-target receptors and other modulating proteins (e.g. G protein-coupled receptor kinase) cannot always be ruled out [146]. Finally, as cellular and *in vivo* bias responses may deviate from one another, it is highly recommended to choose a cell line as similar to the targeted *in vivo* area as possible, such as Neuro 2a or the STHdh^{Q7/Q7} cell lines, as discussed in more detail in section ‘7.2.4 Cell system selection’.
- ❖ **Throughput.** Several assays capable of detecting both G protein and β -arrestin signaling pathways are amenable to HTS when applied with appropriate quantifying methods [83]. As first-line screening tool for the development of pathway-selective compounds, one should also consider the associated cost.

7.2.3 Reference compound selection for SCRA bias detection

Whereas selective agonists could specifically target certain preferred signaling pathways, other ligands ‘equally’ target distinct signaling pathways and may serve as reference

compounds. These compounds, also known as ‘balanced agonists’, are a key requirement for all aforementioned methods for biased ligand quantification. Furthermore, these reference compounds allow the comparison of the relative activity of ligands across distinct methods. CP55,940, JWH-018 and WIN55,212-2 have been reported to act as balanced agonists and have been implemented as reference compounds in multiple studies (**Table 7.1**) [31, 99, 104, 105, 108, 110].

7.2.4 Cell system selection

The implementation of different cell lines might result in different patterns of biased agonism of the same ligands, also referred to as ‘system bias’. Each cell line has a distinct pattern of protein expression, as demonstrated by Atwood *et al.* (2011) [147], who reported on significant differences in endogenous expression levels of GPCRs, G proteins, β -arrestins and adenylyl cyclase, among other proteins. These distinct patterns could alter the stoichiometry of receptors and their respective signaling molecules (either native or transiently or stably introduced) in a cell type-dependent manner. A comprehensive study by Priestley [148] confirmed this by analyzing agonist bias profiles of three SCRA (CP55,940, HU-210 and WIN 55,212-2) by the same receptor-coupled signaling pathways in three distinct cell lines (CB₁-transfected CHO and HEK 293 cells, and murine neuroblastoma Neuro 2a cell line). As expected, these cell lines yielded slightly different ligand bias profiles (represented by the calculated intrinsic relative activity values).

In line with this, G protein-coupled receptor kinase isoforms (GRK 1-6) may differentiate distinct, ligand-induced or -stabilized CB₁ conformations, and, consequently, may provoke distinct β -arrestin1-mediated downstream effects via differential phosphorylation profiles [25, 103, 149]. Consequently, the host cells should be consistent across assays measuring agonist bias.

SCRAs may also act on other pharmacological targets besides CB₁ and CB₂, and these potential off-target activities may contribute to the many adverse effects reported following SCRA use [150-152]. For instance, the orphan receptors GPR18, GPR55 and GPR119 have been demonstrated to interact with certain natural and synthetic cannabinoids [153-156]. Moreover, certain SCRAs also behaved as weakly potent GPR55 and GPR18 antagonists [57, 154]. Importantly, in contrast to the reported CB₁-mediated

suppression of intestinal tumor growth, GPR55 has been reported to play an opposing role to CB₁, acting as a tumor-promotor [153].

Consequently, when screening novel SCRA for functional selectivity, one should ensure the effects are mediated exclusively by cannabinoid receptors. Transiently transfected cell systems are suited for delineating biased responses since high receptor expression levels result in large signals, which may aid in discerning the often subtle differences in preferences of SCRA towards signaling pathways. Nevertheless, to ascertain the physiological relevance of these observed patterns, the functional selectivity of SCRA should also ideally be determined *in vivo*. As a first step, neuronal cell lines endogenously expressing the cannabinoid receptors are well-suited, such as the CB₁-expressing mouse neuroblastoma N18 and N18TG2 cell lines [157, 158], the CB₁/CB₂-expressing murine neuroblastoma Neuro 2a cell line [159, 160] or the CB₁-expressing mouse STHdh^{Q7/Q7} cell culture model of striatal medium spiny projection neurons [100, 161]. Besides neuronal cell lines, also CB₁-expressing astrocytes (C6 glioma cells) or CB₁/CB₂-expressing microglia (BV2 cells) have already been applied successfully in studies analyzing endogenous cannabinoid receptor signaling [158]. Investigation of signaling via endogenous CB receptors is most easily achieved using second-messenger assays (e.g. cAMP, FLIPR®, MAPK, [³⁵S]GTPγS). However, complementation- and RET-based techniques can also be used to observe biased agonism at the level of endogenous expression of GPCR and transducer in the aforementioned cell lines. Both BRET and NanoBiT®, in combination with CRISPR/Cas9 technology for genome-editing of the GPCR and transducer, have proven successful [162-165]. Importantly, different outcomes may be observed depending on the dynamics of the interaction of the transducer with the GPCR. A recent report by White *et al.* (2017) [165] elegantly demonstrated this. When studying the transient interaction of β-arrestin with the chemokine receptor CXCR4, these authors observed only minimal differences in read-out when comparing the recruitment of exogenously transfected vs. endogenously genome-edited β-arrestin. In contrast, for the vasopressin V2 receptor, which is known to form more stable complexes with β-arrestin, the experimental set-up did show a substantial difference in signal between endogenously genome-edited and exogenously transfected β-arrestin.

7.3 Concluding remarks

Cannabinoid receptors are considered as key drug targets for a number of diseases. As of today, most of the typical orthosteric cannabinoid receptor ligands (especially CB₁ agonists) still provoke psychotropic side effects that limit their broad therapeutic utility.

Although the research on biased signaling of SCRA is still in its infancy, the outcome of these studies could contribute to the development of compounds that are receptor- and signaling pathway-selective, thereby mitigating *on-target* adverse effects. In addition, structural studies may elucidate potential mechanisms via which SCRA functional selectivity is mediated. The recent cryo-EM structure of CB₁ in complex with the SCRA MDMB-FUBINACA and the intracellular binding partner Gα_i provides structural and dynamic insights regarding the binding and propagation of SCRA activity at the molecular level [10]. This may reveal information on the dynamic properties of a SCRA-CB₁-transducer complex, which is a prerequisite for understanding biased signaling.

This review aimed at providing an overview of what is known about biased signaling mediated by SCRA. Although the underlying mechanisms of SCRA that provoke the desired medicinal properties or the psychoactive effects remain to be elucidated, a strong interest has arisen in unravelling this complex signaling mechanism, as evidenced by the growing amount of published research on this matter. To identify the presence of biased signaling properties of ligands, distinct functional assays have been employed to characterize the signaling of GPCRs such as CB₁ and CB₂. The deployment of these assays has proven useful to determine the potencies and efficacies of many SCRA. These data also allow for the assessment of biased signaling whereby the use of balanced reference compounds such as CP55,940 and WIN55,212-2 has proven successful. However, one should keep in mind that in certain cases deviating outcomes might be observed due to several causes, including distinct experimental designs and different cell systems.

Once considerable reports have added to the understanding of potential biased properties of SCRA in heterologously expressed cannabinoid receptor systems, a next step would involve the generation of data from systems endogenously expressing cannabinoid receptors. In this context, endogenously CB₁/CB₂ expressing neuronal cell lines, such as Neuro 2a and STHdh^{Q7/Q7} cell cultures, have been shown to provide relevant

information. In a next step, *in vivo* experiments involving preclinical animal models may be used. The pharmacological *in vitro* and *in vivo* effects of SCRA might be influenced by several factors, e.g. tissue-specific characteristics [76], natural cannabinoid variants [166-168] or even oligomerization [169, 170]. GPCR-GPCR interactions involving CB₁ have been reported, with homodimer formation of CB₁ splice variants [171] or heterodimer formation with other receptors, including the dopamine D₂ receptor [172]. The potential involvement of dimerized CB receptors in biased signaling is still unexplored, but represents an exciting avenue of future pursuit.

Interestingly, antitumor effects of the SCRA WIN55,212-2 have been reported in a murine cancer model [173]. The psychoactive effects observed *in vivo* were milder when a nanomicellar formulation of WIN55,212-2 (SMA-WIN) was administered compared to a solution of the drug. In combination with other chemotherapeutic agents, SMA-WIN might be a potential therapeutic treatment for triple-negative breast cancer [173]. As with other aspects of cannabinoid therapeutic activity, the anticancer effects of cannabinoid receptor agonists are mediated through distinct signaling pathways, predominantly Gα_i/Gα_q-proteins [174], p38 mitogen-activated protein kinase (MAPK) [175], as well as through non-CB₁/CB₂ targets such as GPR55 [153, 176, 177]. Overall, one might hypothesize that the design of novel SCRA with a reduced preference for β-arrestin2 coupling might be advantageous due to decreased internalization and tolerance [80].

A major challenge for the interpretation of data obtained from *in vitro* biased agonism screening assays is the fact that the extent to which a biased ligand must favor one pathway over another to produce a therapeutic benefit is unknown [178]. As in most cases differences in coupling of the distinct transducers are only subtle, we might assume that true biased agonism is a rare phenomenon.

Progress in this field will depend on the determination of the most efficient and most reliable *in vitro* techniques to characterize biased agonism, on insights into the required degree of bias factor, and on translation of the observed *in vitro* effects to the clinically-relevant *in vivo* state.

References

1. United Nations Office on Drugs and Crime (UNODC). What are NPS? 2019; Available from: <https://www.unodc.org/LSS/Page/NPS>.
2. European Monitoring Centre for Drugs and Drug Addiction (EMCDDA). *European Drug report 2019: Trends and developments*. 2019.
3. Karila, L., et al., *The Synthetic Cannabinoids Phenomenon*. Curr. Pharm. Des., 2016. **22**(42): p. 6420-6425.
4. Hondebrink, L., A. Zwartsen, and R.H.S. Westerink, *Effect fingerprinting of new psychoactive substances (NPS): What can we learn from in vitro data?* Pharmacol. Ther., 2018. **182**: p. 193-224.
5. United Nations Office on Drugs and Crime (UNODC). World Drug Report, United Nations publication, Sales No. E.17.XI.7. via: <https://www.unodc.org/wdr2017/index.html> (2017), Accessed 8th May 2019. 2017.
6. Kraemer, M., et al., *Death cases involving certain new psychoactive substances: A review of the literature*. Forensic Sci. Int., 2019. **298**: p. 186-267.
7. Banister, S.D., et al., *Dark Classics in Chemical Neuroscience: Delta(9)-Tetrahydrocannabinol*. ACS Chem. Neurosci., 2019. **10**(5): p. 2160-2175.
8. Hua, T., et al., *Crystal structures of agonist-bound human cannabinoid receptor CB1*. Nature, 2017. **547**(7664): p. 468-471.
9. Hua, T., et al., *Crystal Structure of the Human Cannabinoid Receptor CB1*. Cell, 2016. **167**(3): p. 750-762 e14.
10. Krishna Kumar, K., et al., *Structure of a signaling cannabinoid receptor 1-G protein complex*. Cell, 2019. **176**(3): p. 448-458 e12.
11. Shao, Z., et al., *High-resolution crystal structure of the human CB1 cannabinoid receptor*. Nature, 2016. **540**(7634): p. 602-606.
12. Li, X., et al., *Crystal Structure of the Human Cannabinoid Receptor CB2*. Cell, 2019. **176**(3): p. 459-467 e13.
13. Howlett, A.C., et al., *International Union of Pharmacology. XXVII. Classification of cannabinoid receptors*. Pharmacol. Rev., 2002. **54**(2): p. 161-202.
14. Mackie, K., *Distribution of cannabinoid receptors in the central and peripheral nervous system*. Handbook of experimental pharmacology, 2005(168): p. 299-325.
15. Nogueiras, R., et al., *Peripheral, but not central, CB1 antagonism provides food intake-independent metabolic benefits in diet-induced obese rats*. Diabetes, 2008. **57**(11): p. 2977-91.
16. Stempel, A.V., et al., *Cannabinoid Type 2 Receptors Mediate a Cell Type-Specific Plasticity in the Hippocampus*. Neuron, 2016. **90**(4): p. 795-809.
17. Mechoulam, R., E. Friede, and V. Di Marzo, *Endocannabinoids*. European journal of pharmacology, 1998. **359**(1): p. 1-18.
18. Di Marzo, V., *Endocannabinoids: synthesis and degradation*. Reviews of physiology, biochemistry and pharmacology, 2008. **160**: p. 1-24.
19. Jung, K. and D. Piomelli, *Cannabinoids and Endocannabinoids*, in *Neuroscience in the 21st Century*, D. Pfaff and N.D. Volkow, Editors. 2016, Springer: New York.
20. Di Marzo, V., *'Endocannabinoids' and other fatty acid derivatives with cannabimimetic properties: biochemistry and possible physiopathological relevance*. Biochim. Biophys. Acta 1998. **1392**(2-3): p. 153-75.
21. Di Marzo, V., et al., *Endocannabinoids: endogenous cannabinoid receptor ligands with neuromodulatory action*. Trends in neurosciences, 1998. **21**(12): p. 521-8.
22. Iannotti, F.A., V. Di Marzo, and S. Petrosino, *Endocannabinoids and endocannabinoid-related mediators: Targets, metabolism and role in neurological disorders*. Progress in lipid research, 2016. **62**: p. 107-28.
23. Laprairie, R.B., A.M. Bagher, and E.M. Denovan-Wright, *Cannabinoid receptor ligand bias: implications in the central nervous system*. Curr. Opin. Pharmacol., 2017. **32**: p. 32-43.

24. Mallipeddi, S., et al., *Functional selectivity at G-protein coupled receptors: Advancing cannabinoid receptors as drug targets*. *Biochem. Pharmacol.*, 2017. **128**: p. 1-11.
25. Ibsen, M.S., M. Connor, and M. Glass, *Cannabinoid CB1 and CB2 Receptor Signaling and Bias*. *Cannabis Cannabinoid Res.*, 2017. **2**(1): p. 48-60.
26. McGuinness, D., et al., *Characterizing cannabinoid CB2 receptor ligands using DiscoverX PathHunter beta-arrestin assay*. *J. Biomol. Screen.*, 2009. **14**(1): p. 49-58.
27. van der Lee, M.M., et al., *Pharmacological characterization of receptor redistribution and beta-arrestin recruitment assays for the cannabinoid receptor 1*. *J. Biomol. Screen.*, 2009. **14**(7): p. 811-23.
28. Howlett, A.C., et al., *Cannabinoid physiology and pharmacology: 30 years of progress*. *Neuropharmacology*, 2004. **47 Suppl 1**: p. 345-58.
29. Bakshi, K., R.W. Mercier, and S. Pavlopoulos, *Interaction of a fragment of the cannabinoid CB1 receptor C-terminus with arrestin-2*. *FEBS Lett.*, 2007. **581**(25): p. 5009-5016.
30. Singh, S.N., et al., *Binding between a Distal C-Terminus Fragment of Cannabinoid Receptor 1 and Arrestin-2*. *Biochemistry-Us*, 2011. **50**(12): p. 2223-2234.
31. Soethoudt, M., et al., *Cannabinoid CB2 receptor ligand profiling reveals biased signalling and off-target activity*. *Nat. Commun.*, 2017. **8**: p. 13958.
32. Cannaert, A., et al., *Activity-Based Detection of Consumption of Synthetic Cannabinoids in Authentic Urine Samples Using a Stable Cannabinoid Reporter System*. *Anal. Chem.*, 2017. **89**(17): p. 9527-9536.
33. Cannaert, A., et al., *Detection and Activity Profiling of Synthetic Cannabinoids and Their Metabolites with a Newly Developed Bioassay*. *Anal. Chem.*, 2016. **88**(23): p. 11476-11485.
34. Cannaert, A., et al., *Activity-based detection of cannabinoids in serum and plasma samples*. *Clin. Chem.*, 2018. **64**(6): p. 918-926.
35. Atwood, B.K., et al., *Functional selectivity in CB(2) cannabinoid receptor signaling and regulation: implications for the therapeutic potential of CB(2) ligands*. *Mol. Pharmacol.*, 2012. **81**(2): p. 250-63.
36. Nogueras-Ortiz, C., et al., *Retromer stops beta-arrestin 1-mediated signaling from internalized cannabinoid 2 receptors*. *Molecular biology of the cell*, 2017. **28**(24): p. 3554-3561.
37. Chen, X., et al., *Involvement of beta-arrestin-2 and clathrin in agonist-mediated internalization of the human cannabinoid CB2 receptor*. *Curr. Mol. Pharmacol.*, 2014. **7**(1): p. 67-80.
38. Morales, P., P. Goya, and N. Jagerovic, *Emerging strategies targeting CB2 cannabinoid receptor: Biased agonism and allosterism*. *Biochem Pharmacol*, 2018. **157**: p. 8-17.
39. Thomsen, A.R.B., et al., *GPCR-G Protein-beta-Arrestin Super-Complex Mediates Sustained G Protein Signaling*. *Cell*, 2016. **166**(4): p. 907-919.
40. Grundmann, M., et al., *Lack of beta-arrestin signaling in the absence of active G proteins*. *Nature communications*, 2018. **9**(1): p. 341.
41. Engeli, S., *Central and peripheral cannabinoid receptors as therapeutic targets in the control of food intake and body weight*. *Handb. Exp. Pharmacol.*, 2012(209): p. 357-81.
42. Hohmann, A.G. and R.L. Suplita, 2nd, *Endocannabinoid mechanisms of pain modulation*. *AAPS J.*, 2006. **8**(4): p. E693-708.
43. Kaminski, N.E., *Evidence for a cannabinoid receptor in immunomodulation by cannabinoid compounds*. *Adv. Exp. Med. Biol.*, 1993. **335**: p. 115-20.
44. Kirkham, T.C., *Cannabinoids and appetite: food craving and food pleasure*. *Int. Rev. Psychiatry*, 2009. **21**(2): p. 163-71.
45. Kogan, N.M. and R. Mechoulam, *Cannabinoids in health and disease*. *Dialogues Clin. Neurosci.*, 2007. **9**(4): p. 413-30.
46. Pacher, P., S. Batkai, and G. Kunos, *The endocannabinoid system as an emerging target of pharmacotherapy*. *Pharmacol. Rev.*, 2006. **58**(3): p. 389-462.
47. Banister, S.D., et al., *Selective modulation of the cannabinoid type 1 (CB1) receptor as an emerging platform for the treatment of neuropathic pain*. *Medchemcomm*, 2019. **10**: p. 647-659.

48. Murineddu, G., et al., *Different classes of CB2 ligands potentially useful in the treatment of pain*. Recent Pat. CNS Drug Discov., 2013. **8**(1): p. 42-69.
49. Evlice, A., et al., *Rare onset symptoms in multiple sclerosis*. Acta Clin. Belg., 2016. **71**(3): p. 154-7.
50. Han, S., et al., *Therapeutic utility of cannabinoid receptor type 2 (CB₂) selective agonists*. J. Med. Chem., 2013. **56**(21): p. 8224-56.
51. Navarro, G., et al., *Targeting Cannabinoid CB₂ Receptors in the Central Nervous System. Medicinal Chemistry Approaches with Focus on Neurodegenerative Disorders*. Front. Neurosci., 2016. **10**: p. 406.
52. Flachenecker, P., T. Henze, and U.K. Zettl, *Nabiximols (THC/CBD oromucosal spray, Sativex(R)) in clinical practice--results of a multicenter, non-interventional study (MOVE 2) in patients with multiple sclerosis spasticity*. Eur Neurol, 2014. **71**(5-6): p. 271-9.
53. Sastre-Garriga, J., et al., *THC and CBD oromucosal spray (Sativex(R)) in the management of spasticity associated with multiple sclerosis*. Expert Rev Neurother, 2011. **11**(5): p. 627-37.
54. Auwarter, V., et al., *'Spice' and other herbal blends: harmless incense or cannabinoid designer drugs?* J. Mass. Spectrom., 2009. **44**(5): p. 832-7.
55. European Monitoring Centre for Drugs and Drug Addiction (EMCDDA). European Drug Report 2018: Trends and Developments, Publications Office of the European Union, Luxembourg. 2018.
56. Graddy, R., M.E. Buresh, and D.A. Rastegar, *New and Emerging Illicit Psychoactive Substances*. Med. Clin. North Am. , 2018. **102**(4): p. 697-714.
57. Hess, C., et al., *Pharmacological evaluation of synthetic cannabinoids identified as constituents of spice*. Forensic Toxicol., 2016. **34**: p. 329-343.
58. Abouchedid, R., et al., *Analytical confirmation of synthetic cannabinoids in a cohort of 179 presentations with acute recreational drug toxicity to an Emergency Department in London, UK in the first half of 2015*. Clin. Toxicol. (Phila), 2017. **55**(5): p. 338-345.
59. Basavarajappa, B.S. and S. Subbanna, *Potential Mechanisms Underlying the Deleterious Effects of Synthetic Cannabinoids Found in Spice/K2 Products*. Brain Sci., 2019. **9**(1).
60. Behonick, G., et al., *Four postmortem case reports with quantitative detection of the synthetic cannabinoid, 5F-PB-22*. J. Anal. Toxicol., 2014. **38**(8): p. 559-62.
61. Gurney, S.M., et al., *Pharmacology, Toxicology, and Adverse Effects of Synthetic Cannabinoid Drugs*. Forensic Sci. Rev., 2014. **26**(1): p. 53-78.
62. Hermanns-Clausen, M., et al., *Acute side effects after consumption of the new synthetic cannabinoids AB-CHMINACA and MDMB-CHMICA*. Clin. Toxicol. (Phila), 2018. **56**(6): p. 404-411.
63. Thornton, S.L., et al., *Synthetic cannabinoid use associated with acute kidney injury*. Clin. Toxicol. (Phila), 2013. **51**(3): p. 189-90.
64. Trecki, J., R.R. Gerona, and M.D. Schwartz, *Synthetic Cannabinoid-Related Illnesses and Deaths*. N. Engl. J. Med., 2015. **373**(2): p. 103-7.
65. Banister, S.D., et al., *Pharmacology of Valinate and tert-Leucinate Synthetic Cannabinoids 5F-AMBICA, 5F-AMB, 5F-ADB, AMB-FUBINACA, MDMB-FUBINACA, MDMB-CHMICA, and Their Analogues*. ACS Chem. Neurosci., 2016. **7**(9): p. 1241-54.
66. Abbate, V., et al., *The ongoing challenge of novel psychoactive drugs of abuse. Part I. Synthetic cannabinoids (IUPAC Technical Report)*. Pure Appl. Chem., 2018. **90**(8): p. 1255-1282.
67. Banister, S.D. and M. Connor, *The Chemistry and Pharmacology of Synthetic Cannabinoid Receptor Agonist New Psychoactive Substances: Evolution*. Handb. Exp. Pharmacol., 2018.
68. Banister, S.D. and M. Connor, *The Chemistry and Pharmacology of Synthetic Cannabinoid Receptor Agonists as New Psychoactive Substances: Origins*. Handb. Exp. Pharmacol., 2018. **252**: p. 165-190.
69. Longworth, M., et al., *Synthesis and pharmacological profiling of the metabolites of synthetic cannabinoid drugs APICA, STS-135, ADB-PINACA, and 5F-ADB-PINACA*. ACS Chem. Neurosci., 2017. **8**(8): p. 1673-1680.

70. Noble, C., et al., *Application of an activity-based receptor bioassay to investigate the in vitro activity of selected indole- and indazole-3-carboxamide-based synthetic cannabinoids at CB1 and CB2 receptors*. Drug Test. Anal., 2018.
71. Wiley, J.L., J.A. Marusich, and J.W. Huffman, *Moving around the molecule: relationship between chemical structure and in vivo activity of synthetic cannabinoids*. Life Sci., 2014. **97**(1): p. 55-63.
72. Wiley, J.L., J.A. Marusich, and B.F. Thomas, *Combination Chemistry: Structure-Activity Relationships of Novel Psychoactive Cannabinoids*. Curr. Top. Behav. Neurosci., 2017. **32**: p. 231-248.
73. Logan, B.K., et al., *Reports of Adverse Events Associated with Use of Novel Psychoactive Substances, 2013-2016: A Review*. J. Anal. Toxicol., 2017. **41**(7): p. 573-610.
74. Bosier, B., et al., *Functionally selective cannabinoid receptor signalling: therapeutic implications and opportunities*. Biochem. Pharmacol., 2010. **80**(1): p. 1-12.
75. Wisler, J.W., et al., *Recent developments in biased agonism*. Curr. Opin. Cell Biol., 2014. **27**: p. 18-24.
76. Smith, J.S., R.J. Lefkowitz, and S. Rajagopal, *Biased signalling: from simple switches to allosteric microprocessors*. Nat. Rev. Drug. Discov., 2018. **17**(4): p. 243-260.
77. Kenakin, T. and A. Christopoulos, *Signalling bias in new drug discovery: detection, quantification and therapeutic impact*. Nat. Rev. Drug. Discov., 2013. **12**(3): p. 205-16.
78. Rankovic, Z., T.F. Brust, and L.M. Bohn, *Biased agonism: An emerging paradigm in GPCR drug discovery*. Bioorg. Med. Chem. Lett., 2016. **26**(2): p. 241-250.
79. Violin, J.D., et al., *Biased ligands at G-protein-coupled receptors: promise and progress*. Trends Pharmacol. Sci., 2014. **35**(7): p. 308-16.
80. Priestley, R., M. Glass, and D. Kendall, *Functional Selectivity at Cannabinoid Receptors*. Adv. Pharmacol., 2017. **80**: p. 207-221.
81. Black, J.W. and P. Leff, *Operational models of pharmacological agonism*. Proc. R. Soc. Lond. B. Biol. Sci., 1983. **220**(1219): p. 141-62.
82. Onaran, H.O., et al., *Systematic errors in detecting biased agonism: Analysis of current methods and development of a new model-free approach*. Sci. Rep., 2017. **7**.
83. Winpenny, D., M. Clark, and D. Cawkill, *Biased ligand quantification in drug discovery: from theory to high throughput screening to identify new biased mu opioid receptor agonists*. Br. J. Pharmacol., 2016. **173**(8): p. 1393-403.
84. Bonifazi, A., et al., *Novel and Potent Dopamine D2 Receptor Go-Protein Biased Agonists*. ACS Pharmacol. Transl. Sci., 2019. **2**(1): p. 52-65.
85. Chun, L.S., et al., *Structure-Activity Investigation of a G Protein-Biased Agonist Reveals Molecular Determinants for Biased Signaling of the D2 Dopamine Receptor*. Front. Synaptic. Neurosci., 2018. **10**: p. 2.
86. Ehrlich, A.T., et al., *Biased Signaling of the Mu Opioid Receptor Revealed in Native Neurons*. iScience, 2019. **14**: p. 47-57.
87. Tan, L., et al., *Biased Ligands of G Protein-Coupled Receptors (GPCRs): Structure-Functional Selectivity Relationships (SFSRs) and Therapeutic Potential*. J. Med. Chem., 2018. **61**(22): p. 9841-9878.
88. Banister, S.D., et al., *The chemistry and pharmacology of putative synthetic cannabinoid receptor agonist (SCRA) new psychoactive substances (NPS) 5F-PY-PICA, 5F-PY-PINACA, and their analogs*. Drug Test Anal, 2019. **11**(7): p. 976-989.
89. Banister, S.D., et al., *The chemistry and pharmacology of synthetic cannabinoid SDB-006 and its regioisomeric fluorinated and methoxylated analogs*. Drug Test Anal, 2018.
90. Banister, S.D., et al., *The synthesis and pharmacological evaluation of adamantane-derived indoles: cannabimimetic drugs of abuse*. ACS Chem Neurosci, 2013. **4**(7): p. 1081-92.
91. Longworth, M., et al., *The 2-alkyl-2H-indazole regioisomers of synthetic cannabinoids AB-CHMINACA, AB-FUBINACA, AB-PINACA, and 5F-AB-PINACA are possible manufacturing impurities with cannabimimetic activities*. Forensic Toxicol, 2016. **34**: p. 286-303.

92. De Luca, D., et al., *Reply to Giesinger and McNamara: The Impact of Therapeutic Hypothermia on Pulmonary Hemodynamics of Meconium Aspiration Syndrome*. Am. J. Respir. Crit. Care. Med., 2018. **198**(2): p. 287-288.
93. Funada, M. and M. Takebayashi-Ohsawa, *Synthetic cannabinoid AM2201 induces seizures: Involvement of cannabinoid CB1 receptors and glutamatergic transmission*. Toxicol. Appl. Pharmacol., 2018. **338**: p. 1-8.
94. Kevin, R.C., et al., *CUMYL-4CN-BINACA Is an Efficacious and Potent Pro-Convulsant Synthetic Cannabinoid Receptor Agonist*. Front. Pharmacol., 2019. **10**: p. 595.
95. Wallace, M.J., et al., *Assessment of the role of CB1 receptors in cannabinoid anticonvulsant effects*. Eur. J. Pharmacol., 2001. **428**(1): p. 51-7.
96. Al-Zoubi, R., P. Morales, and P.H. Reggio, *Structural Insights into CB1 Receptor Biased Signaling*. Int. J. Mol. Sci., 2019. **20**(8).
97. Khajehali, E., et al., *Biased Agonism and Biased Allosteric Modulation at the CB1 Cannabinoid Receptor*. Mol. Pharmacol., 2015. **88**(2): p. 368-79.
98. Glass, M. and J.K. Northup, *Agonist selective regulation of G proteins by cannabinoid CB(1) and CB(2) receptors*. Mol. Pharmacol., 1999. **56**(6): p. 1362-9.
99. Laprairie, R.B., et al., *Biased Type 1 Cannabinoid Receptor Signaling Influences Neuronal Viability in a Cell Culture Model of Huntington Disease*. Mol. Pharmacol., 2016. **89**(3): p. 364-75.
100. Laprairie, R.B., et al., *Type 1 cannabinoid receptor ligands display functional selectivity in a cell culture model of striatal medium spiny projection neurons*. J. Biol. Chem., 2014. **289**(36): p. 24845-62.
101. Lauckner, J.E., B. Hille, and K. Mackie, *The cannabinoid agonist WIN55,212-2 increases intracellular calcium via CB1 receptor coupling to Gq/11 G proteins*. Proc. Natl. Acad. Sci. U.S.A., 2005. **102**(52): p. 19144-9.
102. Daigle, T.L., C.S. Kearn, and K. Mackie, *Rapid CB1 cannabinoid receptor desensitization defines the time course of ERK1/2 MAP kinase signaling*. Neuropharmacology, 2008. **54**(1): p. 36-44.
103. Delgado-Peraza, F., et al., *Mechanisms of Biased beta-Arrestin-Mediated Signaling Downstream from the Cannabinoid 1 Receptor (vol 89, pg 618, 2016)*. Mol. Pharmacol., 2016. **90**(1): p. 62-62.
104. Ford, B.M., et al., *Characterization of structurally novel G protein biased CB1 agonists: Implications for drug development*. Pharmacol. Res., 2017. **125**(Pt B): p. 161-177.
105. Wouters, E., et al., *Assessment of biased agonism amongst distinct synthetic cannabinoid receptor agonist scaffolds*. Submitted, 2019.
106. Lauckner, J.E., B. Hille, and K. Mackie, *The cannabinoid agonist WIN55,212-2 increases intracellular calcium via CB1 receptor coupling to Gq/11 G proteins*. P Natl Acad Sci USA, 2005. **102**(52): p. 19144-9.
107. Delgado-Peraza, F., et al., *Mechanisms of Biased beta-Arrestin-Mediated Signaling Downstream from the Cannabinoid 1 Receptor*. Mol. Pharmacol., 2016. **89**(6): p. 618-29.
108. Dhopeswarkar, A. and K. Mackie, *Functional Selectivity of CB2 Cannabinoid Receptor Ligands at a Canonical and Noncanonical Pathway*. J. Pharmacol. Exp. Ther., 2016. **358**(2): p. 342-51.
109. Chicca, A., et al., *4'-O-methylhonokiol increases levels of 2-arachidonoyl glycerol in mouse brain via selective inhibition of its COX-2-mediated oxygenation*. J. Neuroinflammation, 2015. **12**: p. 89.
110. Oyagawa, C.R.M., et al., *Cannabinoid Receptor 2 Signalling Bias Elicited by 2,4,6-Trisubstituted 1,3,5-Triazines*. Front. Pharmacol., 2018. **9**: p. 1202.
111. Diaz, O., J.A.R. Dalton, and J. Giraldo, *Revealing the Mechanism of Agonist-Mediated Cannabinoid Receptor 1 (CB1) Activation and Phospholipid-Mediated Allosteric Modulation*. J. Med. Chem., 2019.
112. Laprairie, R.B., A.M. Bagher, and E.M. Denovan-Wright, *Cannabinoid receptor ligand bias: implications in the central nervous system*. Current opinion in pharmacology, 2017. **32**: p. 32-43.
113. Vecchio, E.A., et al., *New paradigms in adenosine receptor pharmacology: allostery, oligomerization and biased agonism*. Brit J Pharmacol, 2018. **175**(21): p. 4036-4046.

114. Gamage, T.F., et al., *Synthetic Cannabinoid Hydroxypentyl Metabolites Retain Efficacy at Human Cannabinoid Receptors*. J. Pharmacol. Exp. Ther., 2019. **368**(3): p. 414-422.
115. Costain, W.J., et al., *Pharmacological characterization of emerging synthetic cannabinoids in HEK293T cells and hippocampal neurons*. Eur. J. Pharmacol., 2016. **786**: p. 234-245.
116. Marusich, J.A., et al., *Finding order in chemical chaos - Continuing characterization of synthetic cannabinoid receptor agonists*. Neuropharmacology, 2018. **134**(Pt A): p. 73-81.
117. Wiley, J.L., et al., *AB-CHMINACA, AB-PINACA, and FUBIMINA: Affinity and Potency of Novel Synthetic Cannabinoids in Producing Delta9-Tetrahydrocannabinol-Like Effects in Mice*. J Pharmacol Exp Ther, 2015. **354**(3): p. 328-39.
118. Grim, T.W., et al., *Pharmacological characterization of repeated administration of the first generation abused synthetic cannabinoid CP47,497*. J Basic Clin Physiol Pharmacol, 2016. **27**(3): p. 217-28.
119. Banister, S.D., et al., *Pharmacology of Indole and Indazole Synthetic Cannabinoid Designer Drugs AB-FUBINACA, ADB-FUBINACA, AB-PINACA, ADB-PINACA, 5F-AB-PINACA, 5F-ADB-PINACA, ADBICA, and 5F-ADBICA*. ACS Chem. Neurosci., 2015. **6**(9): p. 1546-59.
120. Gatch, M.B. and M.J. Forster, *Delta(9)-Tetrahydrocannabinol-like effects of novel synthetic cannabinoids in mice and rats*. Psychopharmacology, 2016. **233**(10): p. 1901-10.
121. Asada, A., et al., *Cannabimimetic activities of cumyl carboxamide-type synthetic cannabinoids*. Forensic Toxicol., 2018. **36**(1): p. 170-177.
122. Soethoudt, M., et al., *Protocol to Study beta-Arrestin Recruitment by CB1 and CB2 Cannabinoid Receptors*. Methods Mol Biol, 2016. **1412**: p. 103-11.
123. Banister, S.D. and M. Connor, *The Chemistry and Pharmacology of Synthetic Cannabinoid Receptor Agonists as New Psychoactive Substances: Origins*. Handb. Exp. Pharmacol., 2018.
124. Banister, S.D., et al., *Effects of bioisosteric fluorine in synthetic cannabinoid designer drugs JWH-018, AM-2201, UR-144, XLR-11, PB-22, 5F-PB-22, APICA, and STS-135*. ACS Chem. Neurosci., 2015. **6**(8): p. 1445-58.
125. Wouters, E., et al., *Functional evaluation of carboxy metabolites of synthetic cannabinoid receptor agonists featuring scaffolds based on L-valine or L-tert-leucine*. Drug Test. Anal., 2019.
126. Antonides, L.H., et al., *Enantiospecific Synthesis, Chiral Separation, and Biological Activity of Four Indazole-3-Carboxamide-Type Synthetic Cannabinoid Receptor Agonists and Their Detection in Seized Drug Samples*. Front. Chem., 2019. **7**(321).
127. Franz, F., et al., *Phase I metabolism of the highly potent synthetic cannabinoid MDMB-CHMICA and detection in human urine samples*. Drug Test. Anal., 2017. **9**(5): p. 744-753.
128. De Luca, M.A., et al., *Native CB1 receptor affinity, intrinsic activity and accumbens shell dopamine stimulant properties of third generation SPICE/K2 cannabinoids: BB-22, 5F-PB-22, 5F-AKB-48 and STS-135*. Neuropharmacology, 2016. **105**: p. 630-638.
129. Banister, S.D., et al., *The synthesis and pharmacological evaluation of adamantane-derived indoles: cannabimimetic drugs of abuse*. ACS Chem. Neurosci., 2013. **4**(7): p. 1081-92.
130. Yao, B.B., et al., *In vitro and in vivo characterization of A-796260: a selective cannabinoid CB2 receptor agonist exhibiting analgesic activity in rodent pain models*. Br J Pharmacol., 2008. **153**(2): p. 390-401.
131. Costain, W.J., et al., *Analysis of the pharmacological properties of JWH-122 isomers and THJ-2201, RCS-4 and AB-CHMINACA in HEK293T cells and hippocampal neurons*. Eur. J. Pharmacol., 2018. **823**: p. 96-104.
132. Adams, A.J., et al., *"Zombie" Outbreak Caused by the Synthetic Cannabinoid AMB-FUBINACA in New York*. N Engl J Med, 2017. **376**(3): p. 235-242.
133. Canazza, I., et al., *Pharmaco-toxicological effects of the novel third-generation fluorinate synthetic cannabinoids, 5F-ADBINACA, AB-FUBINACA, and STS-135 in mice. In vitro and in vivo studies*. Hum. Psychopharmacol., 2017. **32**(3).
134. Banister, S.D., et al., *Synthesis and pharmacology of new psychoactive substance 5F-CUMYL-P7AICA, a scaffold- hopping analog of synthetic cannabinoid receptor agonists 5F-CUMYL-PICA and 5F-CUMYL-PINACA*. Drug Test. Anal., 2018.

135. Gamage, T.F., et al., *Molecular and Behavioral Pharmacological Characterization of Abused Synthetic Cannabinoids MMB- and MDMB-FUBINACA, MN-18, NNEI, CUMYL-PICA, and 5-Fluoro-CUMYL-PICA*. J. Pharmacol. Exp. Ther., 2018. **365**(2): p. 437-446.
136. Huffman, J.W., et al., *Structure-activity relationships for 1-alkyl-3-(1-naphthoyl)indoles at the cannabinoid CB(1) and CB(2) receptors: steric and electronic effects of naphthoyl substituents. New highly selective CB(2) receptor agonists*. Bioorg. Med. Chem. , 2005. **13**(1): p. 89-112.
137. Huffman, J.W., et al., *1-Alkyl-2-aryl-4-(1-naphthoyl)pyrroles: new high affinity ligands for the cannabinoid CB1 and CB2 receptors*. Bioorg. Med. Chem. Lett., 2006. **16**(20): p. 5432-5.
138. Neubig, R.R., et al., *International Union of Pharmacology Committee on Receptor Nomenclature and Drug Classification. XXXVIII. Update on terms and symbols in quantitative pharmacology*. Pharmacol. Rev., 2003. **55**(4): p. 597-606.
139. DeLapp, N.W., et al., *GTPgammaS Binding Assays*, in *Assay Guidance Manual*, G.S. Sittampalam, et al., Editors. 2012: Bethesda (MD).
140. Littmann, T., A. Buschauer, and G. Bernhardt, *Split luciferase-based assay for simultaneous analyses of the ligand concentration- and time-dependent recruitment of beta-arrestin2*. Anal. Biochem., 2019. **573**: p. 8-16.
141. Sachdev, S., et al., *In vitro determination of the CB1 efficacy of illicit synthetic cannabinoids*. bioRxiv, 2018: p. 385583.
142. Tang, W.J. and A.G. Gilman, *Type-specific regulation of adenylyl cyclase by G protein beta gamma subunits*. Science (New York, N.Y.), 1991. **254**(5037): p. 1500-3.
143. Grundmann, M. and E. Kostenis, *Temporal Bias: Time-Encoded Dynamic GPCR Signaling*. Trends Pharmacol. Sci., 2017. **38**(12): p. 1110-1124.
144. Stott, L.A., D.A. Hall, and N.D. Holliday, *Unravelling intrinsic efficacy and ligand bias at G protein coupled receptors: A practical guide to assessing functional data*. Biochem. Pharmacol., 2016. **101**: p. 1-12.
145. Klein Herenbrink, C., et al., *The role of kinetic context in apparent biased agonism at GPCRs*. Nat. Commun., 2016. **7**: p. 1-14.
146. Gundry, J., et al., *A Practical Guide to Approaching Biased Agonism at G Protein Coupled Receptors*. Front. Neurosci., 2017. **11**: p. 17.
147. Atwood, B.K., et al., *Expression of G protein-coupled receptors and related proteins in HEK293, AtT20, BV2, and N18 cell lines as revealed by microarray analysis*. BMC genomics, 2011. **12**: p. 14.
148. Priestley, R., *A study of functional selectivity at the cannabinoid type 1 receptor*. PhD thesis, . 2015, University of Nottingham.
149. Ibsen, M.S., et al., *Cannabinoid CB1 and CB2 Receptor-Mediated Arrestin Translocation: Species, Subtype, and Agonist-Dependence*. Front. Pharmacol., 2019. **10**: p. 350.
150. Taylor, L., et al., *Primary Macrophage Chemotaxis Induced by Cannabinoid Receptor 2 Agonists Occurs Independently of the CB2 Receptor*. Sci. Rep., 2015. **5**: p. 10682.
151. Elmore, J.S. and M.H. Baumann, *Repeated Exposure to the "Spice" Cannabinoid JWH-018 Induces Tolerance and Enhances Responsiveness to 5-HT1A Receptor Stimulation in Male Rats*. Front. Psychiatry, 2018. **9**: p. 55.
152. Pertwee, R.G., *Receptors and channels targeted by synthetic cannabinoid receptor agonists and antagonists*. Curr. Med. Chem., 2010. **17**(14): p. 1360-81.
153. Hasenoehl, C., et al., *G protein-coupled receptor GPR55 promotes colorectal cancer and has opposing effects to cannabinoid receptor 1*. Int. J. Cancer, 2018. **142**(1): p. 121-132.
154. Schoeder, C.T., et al., *Pharmacological evaluation of new constituents of "Spice": synthetic cannabinoids based on indole, indazole, benzimidazole and carbazole scaffolds*. Forensic Toxicol., 2018. **36**(2): p. 385-403.
155. Syed, S.K., et al., *Regulation of GPR119 receptor activity with endocannabinoid-like lipids*. Am. J. Physiol. Endocrinol. Metab., 2012. **303**(12): p. E1469-78.
156. Yang, H., J. Zhou, and C. Lehmann, *GPR55 - a putative "type 3" cannabinoid receptor in inflammation*. J. Basic Clin. Physiol. Pharmacol., 2016. **27**(3): p. 297-302.

157. Abood, M.E., et al., *Isolation and expression of a mouse CB1 cannabinoid receptor gene. Comparison of binding properties with those of native CB1 receptors in mouse brain and N18TG2 neuroblastoma cells*. *Biochemical pharmacology*, 1997. **53**(2): p. 207-14.
158. Leishman, E., et al., *Cannabidiol's Upregulation of N-acyl Ethanolamines in the Central Nervous System Requires N-acyl Phosphatidyl Ethanolamine-Specific Phospholipase D*. *Cannabis and cannabinoid research*, 2018. **3**(1): p. 228-241.
159. Graham, E.S., et al., *Induction of Krox-24 by endogenous cannabinoid type 1 receptors in Neuro2A cells is mediated by the MEK-ERK MAPK pathway and is suppressed by the phosphatidylinositol 3-kinase pathway*. *J. Biol. Chem.*, 2006. **281**(39): p. 29085-95.
160. T.N., H. and R. Iyengar, *Heterotrimeric G proteins and their effector pathways*, in *The G protein-coupled receptors handbook*, L. Devi, Editor. 2005, Humana Press.
161. Laprairie, R.B., M.E. Kelly, and E.M. Denovan-Wright, *Cannabinoids increase type 1 cannabinoid receptor expression in a cell culture model of striatal neurons: implications for Huntington's disease*. *Neuropharmacology*, 2013. **72**: p. 47-57.
162. Oh-Hashi, K., et al., *Application of a novel HiBiT peptide tag for monitoring ATF4 protein expression in Neuro2a cells*. *Biochem. Biophys. Rep.*, 2017. **12**: p. 40-45.
163. Schwinn, M.K., et al., *CRISPR-Mediated Tagging of Endogenous Proteins with a Luminescent Peptide*. *ACS Chem. Biol.*, 2018. **13**(2): p. 467-474.
164. White, C.W., et al., *NanoBRET ligand binding at a GPCR under endogenous promotion facilitated by CRISPR/Cas9 genome editing*. *Cell. Signal.*, 2019. **54**: p. 27-34.
165. White, C.W., et al., *Using nanoBRET and CRISPR/Cas9 to monitor proximity to a genome-edited protein in real-time*. *Sci. Rep.*, 2017. **7**(1): p. 3187.
166. Ruehle, S., et al., *Discovery and characterization of two novel CB1 receptor splice variants with modified N-termini in mouse*. *J. Neurochem.*, 2017. **142**(4): p. 521-533.
167. Smith, D.R., et al., *Rare genetic variants in the endocannabinoid system genes CNR1 and DAGLA are associated with neurological phenotypes in humans*. *PloS one*, 2017. **12**(11): p. e0187926.
168. Zou, S. and U. Kumar, *Cannabinoid Receptors and the Endocannabinoid System: Signaling and Function in the Central Nervous System*. *Int. J. Mol. Sci.*, 2018. **19**(3).
169. Hudson, B.D., T.E. Hebert, and M.E. Kelly, *Ligand- and heterodimer-directed signaling of the CB(1) cannabinoid receptor*. *Mol. Pharmacol.*, 2010. **77**(1): p. 1-9.
170. Wouters, E., et al., *Luminescence- and Fluorescence-Based Complementation Assays to Screen for GPCR Oligomerization: Current State of the Art*. *Int J Mol Sci*, 2019. **20**(12).
171. Bagher, A.M., et al., *Co-expression of the human cannabinoid receptor coding region splice variants (hCB(1)) affects the function of hCB(1) receptor complexes*. *Eur. J. Pharmacol.*, 2013. **721**(1-3): p. 341-54.
172. Przybyla, J.A. and V.J. Watts, *Ligand-induced regulation and localization of cannabinoid CB1 and dopamine D2L receptor heterodimers*. *J. Pharmacol. Exp. Ther.*, 2010. **332**(3): p. 710-9.
173. Greish, K., et al., *Synthetic cannabinoids nano-micelles for the management of triple negative breast cancer*. *J. Control. Release*, 2018. **291**: p. 184-195.
174. Scotter, E., S. Graham, and M. Glass, *Cannabinoid Receptor Signal Transduction Pathways*, in *The Cannabinoid Receptors*, P.H. Reggio, Editor. 2009, Humana Press: Totowa, NJ. p. 153-171.
175. Giuliano, M., et al., *Apoptosis induced in HepG2 cells by the synthetic cannabinoid WIN: involvement of the transcription factor PPARgamma*. *Biochimie*, 2009. **91**(4): p. 457-65.
176. Morales, P. and N. Jagerovic, *Advances Towards The Discovery of GPR55 Ligands*. *Curr. Med. Chem.*, 2016. **23**(20): p. 2087-100.
177. Moreno, E., et al., *The Endocannabinoid System as a Target in Cancer Diseases: Are We There Yet?* *Front. Pharmacol.*, 2019. **10**: p. 339.
178. Luttrell, L.M., S. Maudsley, and L.M. Bohn, *Fulfilling the Promise of "Biased" G Protein-Coupled Receptor Agonism*. *Mol. Pharmacol.*, 2015. **88**(3): p. 579-88.

Chapter 8:

Assessment of biased agonism amongst distinct
synthetic cannabinoid receptor agonist scaffolds

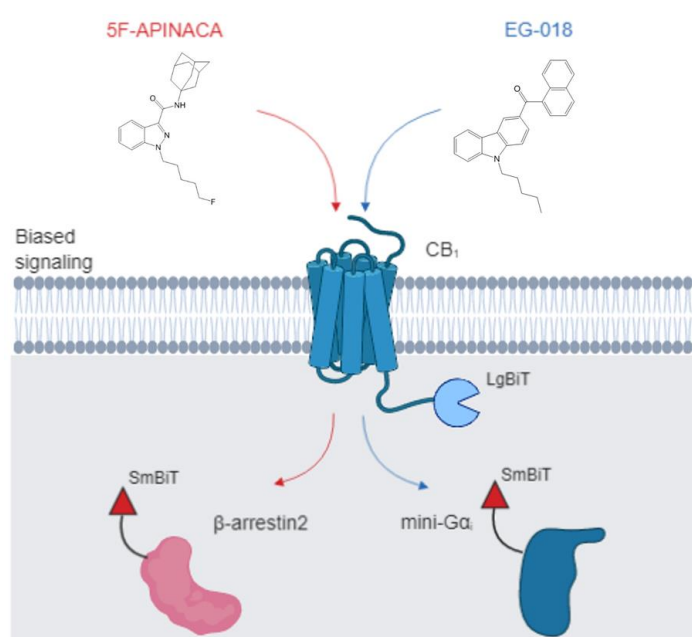
Based on

Elise Wouters, Jolien Walraed, Michael Joseph Robertson, Max Meyrath, Martyna Szpakowska, Andy Chevigné, Georgios Skinotis and Christophe Stove. Assessment of biased agonism amongst distinct synthetic cannabinoid receptor agonist scaffolds. Submitted.

ABSTRACT

The cannabinoid receptor 1 (CB₁) is a key drug target for a number of diseases, including metabolic syndromes and neuropathic pain. Most of the typical cannabinoid ligands provoke psychotropic side effects that impair their therapeutic utility. As of today, it is not yet clearly known which structural features of cannabinoid ligands determine a preference towards specific signaling pathways. Distinct bio-assays are typically used to elucidate signalling preferences. However, these are often based on different cell lines and use different principles and/or read-outs, which makes straightforward assessment of “ligand bias” difficult. Within this context, this study is the first to investigate ligand bias among synthetic cannabinoid receptor agonists (SCRAs) in as closely analogous conditions as possible, by applying a new functional complementation-based assay panel to assess the recruitment of Gα_i protein or β-arrestin2 to CB₁. In a panel of 21 SCRAs, chosen to cover a broad diversity in chemical structures, distinct, although often subtle, preferences towards specific signaling pathways were observed. Most of the selected SCRAs (e.g. 5F-APINACA, CUMYL-PEGACLONE, among others) displayed a preferred signaling through the β-arrestin2 pathway, whereas MMB-CHMICA could serve as a potential ‘balanced’ agonist. Interestingly, EG-018 was the only SCRA showing a significant (10-fold) preference towards G protein over β-arrestin2 recruitment. While it is currently unclear what this exactly means in terms of abuse potential and/or toxicity, the approach proposed here may allow to build a knowledge base that, in the end, may allow better insight into the structure-‘functional’ activity-relationship of these compounds. This may aid the development of new therapeutics with less unwanted psychoactive effects.

GRAPHICAL ABSTRACT



8.1 Introduction

Since the discovery and identification of the cannabinoid receptor type 1 (CB₁) in the late 80s [1], many efforts have been made to gain insights into the mechanisms and physiological signaling systems mediated by this seven trans-membrane G-protein coupled receptor (GPCR). CB₁ receptor is one of the most abundantly expressed receptors in the central nervous system and regulate neurotransmission [2, 3]. The CB₁ receptor has been associated with distinct diseases, including metabolic syndromes (e.g. obesity and anorexia) [4-6], neurodegenerative diseases (e.g. in early stages of Huntington's disease, Parkinson's disease or schizophrenia) [7-9], as well as depression and suicidal behavior [10] and cancers [11]. Consequently, both CB₁ agonists and antagonists have been explored as therapeutic agents in various fields of medicine [6, 12, 13]. Nevertheless, when exploiting its therapeutic utility, one should bear in mind that several studies have reported on the occurrence of psychiatric disorders, such as anxiety, mood and psychotic disorders [14, 15] as well as cognitive deficits after long-term cannabinoid exposure [16].

Cannabinoid agonists that modulate CB₁ activity can be classified into three main groups: the endogenous cannabinoids (e.g. anandamide), the natural cannabinoids (e.g. Δ^9 -tetrahydrocannabinol (Δ^9 -THC)) and the synthetic cannabinoid receptor agonists (SCRAs) (e.g. CP55,940). Upon ligand binding and receptor activation, CB₁ is known to recruit different transducers, primarily the pertussis toxin-sensitive $G\alpha_{i/o}$ type G protein. Heterotrimeric G proteins encompass the alpha ($G\alpha$) and the obligate dimer beta and gamma subunit ($G\beta\gamma$). The alpha domain of the heterotrimeric G protein encompasses a conserved GTPase domain and a unique helical domain. Activation of the $G\alpha_{i/o}$ type G protein leads to the inhibition of adenylyl cyclase, which, consequently, results in a rapid decrease in cAMP levels [16]. Interestingly, under certain circumstances, CB₁ also couples to $G\alpha_s$ or $G\alpha_q$, via which stimulation of cAMP or calcium production, respectively, is provoked [17-19].

Besides the well-characterized G protein-mediated signaling pathways of CB₁, also the non-canonical signaling pathways involving β -arrestins and their downstream regulatory effects have received attention. Both β -arrestin1 (arrestin2) and β -arrestin2 (arrestin3) have been shown to be implicated in CB₁ signaling. Upon binding of β -arrestin2 to CB₁, desensitization and internalization of the receptor is induced [20]. While some studies have reported only

little to no β -arrestin1 recruitment to CB₁ following receptor activation [20], other studies indicated that β -arrestin1 provoked the activation of the extracellular signal-regulated kinase pathway, thus also regulating long-term cellular events [21, 22]. This was corroborated by structural studies that observed binding of β -arrestin1 to the distal part of CB₁'s C-terminus [23, 24].

Interestingly, upon GPCR activation, including CB₁, certain ligands have been shown to preferentially activate specific downstream signaling pathways over others, also referred to as 'biased signaling' or 'biased agonism' [25-28]. As selective activation of certain signaling pathways could potentially result in improved drugs with less side effects, this research domain has gained a lot of interest lately.

For different GPCRs, like for example for the dopamine D₂ receptor or the melanocortin 4 receptor, it has been demonstrated that ligands preferentially mediating β -arrestin dependent events could be exploited for the development of novel pharmaceutical agents [29-33]. For other GPCRs, like the μ opioid receptor, G protein biased agonists have been shown to reduce adverse opioid effects [34-36]. For CB₁ it is not completely clear whether the adverse effects are G protein or β -arrestin mediated, although certain studies have suggested that β -arrestin2 negatively influences the acute (e.g. antinociception) and increases chronic (e.g. development of tolerance) responses upon CB₁ activation [37-39]. Consequently, cannabinoid ligands that exert biased signaling towards G protein-mediated signaling might exhibit reduced side effects.

Whereas for endogenous and natural cannabinoids only a few studies have investigated the prevalence of biased signaling upon CB₁ activation [18, 40, 41], for orthosteric SCRA this has not been the case [42]. In fact, very little is known about the structural features of SCRA that could mediate preference towards the distinct CB₁-mediated signaling pathways in specific cell types or tissues.

Therefore, the objective of this study was to systematically investigate the ability of a structurally diverse panel of SCRA to preferentially drive G protein or β -arrestin recruitment upon activation of CB₁. Selected SCRA encompassed distinct structural classes, including: Cyclohexylphenols ((C8)-CP 47,497), Naphthoylindoles (AM-2201, JWH-018), Benzoylindoles (WIN48,098, RCS-4), Phenylacetylindoles (JWH-250, RCS-8), Alkoylindoles (XLR-11, UR-144),

Ind(az)ole esters/carboxylates (5F-PB-22, BB-22), Ind(az)ole carboxamides (5F-APINACA), Amino acid derivatives (MDMB-CHMICA, MMB-CHMICA, (S)-5F-MDMB-PINACA, 4F-MDMB-BINACA), Cumylamine derivatives (5F-CUMYL-PINACA) and Carbazoles and γ -Carbolines (CUMYL-PEGACLONE, EG-018, EG-2201 and MDMB-CHMCZCA). For the screening of these SCRA, *in vitro* CB₁ activation bio-assays were used to assess recruitment of an engineered GTPase domain of the G α_i subunit, referred to as the mini-G α_i protein, or an engineered β -arrestin2, in which the predominant binding site for clathrin was eliminated [43]. The recruitment of both transducers to the same CB₁ construct was investigated in the same cellular context, using the same assay principle (luminescence following functional complementation of a split luciferase (NanoBiT® Technology)). This approach allows a better insight into the structural features of certain SCRA that provoke biased signaling, which ultimately may aid the development of new therapeutic compounds with less unwanted psychoactive effects.

8.2 Materials and methods

8.2.1 Chemicals and reagents

A panel of 21 SCRA was investigated: JWH-018 ((naphthalen-1-yl)(1-pentyl-1*H*-indol-3-yl)methanone), (C8)-CP47,497 (2-[(1*S*,3*R*)-3-hydroxycyclohexyl]-5-(2-methylnonan-2-yl)phenol), AM-2201 ([1-(5-fluoropentyl)-1*H*-indol-3-yl](naphthalen-1-yl)methanone), WIN48,098 ((4-methoxyphenyl{2-methyl-1-[2-(morpholin-4-yl)ethyl]-1*H*-indol-3-yl}methanone), RCS-4 ((4-methoxyphenyl)(1-pentyl-1*H*-indol-3-yl)methanone), JWH-250 (2-(2-methoxyphenyl-1-(1-pentyl-1*H*-indol-3-yl)ethan-1-one), RCS-8 (1-[1-(2-cyclohexylethyl)-1*H*-indol-3-yl]-2-(2-methoxyphenyl)ethan-1-one), XLR-11 ([1-(5-fluoropentyl)-1*H*-indol-3-yl](2,2,3,3-tetramethylcyclopropyl)methanone), UR-144 ((1-pentyl-1*H*-indol-3-yl)(2,2,3,3-tetramethylcyclopropyl)methanone), 5F-PB-22 (quinolin-8-yl 1-(5-fluoropentyl)-1*H*-indole-3-carboxylate), BB-22 (quinolin-8-yl 1-(cyclohexylmethyl)-1*H*-indole-3-carboxylate), 5F-APINACA (*N*-(adamantan-1-yl)-1-(5-fluoropentyl)-1*H*-indazole-3-carboxamide), MDMB-CHMICA (methyl (2*S*)-2-[[1-(cyclohexylmethyl)-1*H*-indole-3-carbonyl]amino]-3,3-dimethylbutanoate), MMB-CHMICA (methyl (2*S*)-2-[[1-(cyclohexylmethyl)-1*H*-indole-3-carbonyl]amino]-3-methylbutanoate), 5F-MDMB-PINACA (methyl (2*S*)-2-[[1-(5-fluoropentyl)-1*H*-indazole-3-carbonyl]amino]-3,3-dimethylbutanoate), 5F-CUMYL-PINACA (1-(5-

fluoropentyl-*N*-(2-phenylpropan-2-yl)-1*H*-indazole-3-carboxamide), CUMYL-PEGACLONE (5-pentyl-2-(2-phenylpropan-2-yl)-2,5-dihydro-1*H*-pyrido[4,3-*b*]indol-1-one), EG-018 ((naphthalen-1-yl)(9-pentyl-9*H*-carbazol-3-yl)methanone), EG-2201 ([9-(5-fluoropentyl)-9*H*-carbazol-3-yl](naphthalen-1-yl)methanone), MDMB-CHMCZCA (methyl (2*S*)-2-{[9-(cyclohexylmethyl)-9*H*-carbazole-3-carbonyl]amino}-3,3-dimethylbutanoate, 4F-MDMB-BINACA (methyl (2*S*)-2-{[1-(4-fluorobutyl)-1*H*-indazole-3-carbonyl]amino}-3,3-dimethylbutanoate).

All SCRA were purchased from Chiron (Trondheim, Norway), except the reference compound (rc) CP55,940 (2-[(1*R*,2*R*,5*R*)-5-hydroxy-2-(3-hydroxypropyl)cyclohexyl]-5-(2-methyloctan-2-yl)phenol), which was purchased from Sigma-Aldrich (Steinheim, Germany) and EG-2201, MDMB-CHMCZCA and 4F-MDMB-BINACA, which were kindly provided by the Institute for Forensic Medicine from the University Hospital in Freiburg. Chloroquine and puromycin were procured from Sigma Aldrich (Steinheim, Germany). Thermosensitive Alkaline Phosphatase was purchased from Promega (Madison, WI, USA), anti-dNGFR antibody was procured from Chromaprobe (Maryland Heights, MO, USA). Iscove's Modified Dulbecco's Medium (IMDM) and a Calcium Phosphate Transfection kit were purchased from Thermo Fisher Scientific (Pittsburgh, PA, USA). Methanol and DMSO were purchased from Fisher Scientific (Leicestershire, UK). All other chemicals and reagents used were procured from the same suppliers as described previously [44].

8.2.2 Development of mini-G α_i protein NanoBiT[®] construct plasmids

For the implementation of the NanoBiT[®] system (Promega), fusion constructs consisting of the human CB₁ receptor and the mini-G α_i protein were developed in a similar manner as previously described for the CB₁ and β -arrestin2 experimental set-up [43, 45]. Fusion of the human CB₁ receptor (**NM_016083**) to the SmBiT and LgBiT fragments of NanoLuciferase was previously described by Cannaert *et al.*, 2016 [45]. For this study, four different mini-G α_i -containing fusion constructs were developed: mini-G α_i -SmBiT, mini-G α_i -LgBiT, SmBiT-mini-G α_i and LgBiT-mini-G α_i . To assure flexibility, a linker sequence was added between the mini-G α_i and the split NanoLuciferase (LgBiT/SmBiT-GSSGGGGSGGGGSSG-GAQGNS-mini-G α_i or mini-G α_i -GNS-GSSGGGGSGGGGSSG-SmBiT/LgBiT).

The sequence encoding the mini-G α_i protein, the engineered GTPase domain of the G α_i subunit [46, 47] was synthesized by Thermo Fisher Scientific. This coding sequence was PCR-amplified using *EcoRI* restriction sites-containing primers (**Table 7.1A**). The PCR reaction was performed with the Phusion High-Fidelity PCR Master Mix according to the manufacturer's instructions, using a MastercyclerTM Nexus Thermal Cycler (Eppendorf, Hamburg, Germany) at the following three-step conditions: initial denaturation (98 °C – 30 s), denaturation (98 °C – 10 s), annealing (T_m – 35 s), extension (72 °C – 40 s), final extension (72 °C – 5 min), for 35 cycles. PCR products were run on a 1% agarose gel and purified with a MicroElute Gel extraction kit. Following digestion with the restriction enzyme *EcoRI* for 2h at 37 °C, the PCR insert and the vectors of destination were purified with a MicroElute Cycle-Pure kit and a MicroElute Gel extraction kit, respectively. To avoid re-association of the vectors, the 5' prime ends were dephosphorylated by Thermosensitive Alkaline Phosphatase for 15 min at 37 °C, followed by deactivation of the enzyme at 74 °C for 15 min. Finally, the inserts were ligated into the digested vectors using T4 DNA ligase for 30 min at room temperature (RT) and the ligated products were transformed into a competent MC1061 *E. coli* strain. After plating on carbenicillin containing agar, resistant colonies were screened for the presence of the insert by Colony PCR with *Taq* polymerase and subsequent restriction digest. Coding sequences were verified by Sanger sequencing.

8.2.3 Development of the CB₁-NanoBiT®- mini-G α_i reporter bio-assay

For the development of a CB₁ NanoBiT® reporter bio-assay, based on the recruitment of mini-G α_i , the most optimal combination of distinct C-terminal CB₁ (CB₁-LgBiT or CB₁-SmBiT) and N- and C-terminal mini-G α_i (mini-G α_i -SmBiT, mini-G α_i -LgBiT, SmBiT-mini-G α_i and LgBiT-mini-G α_i) fusion constructs was selected, using a transient HEK293T experimental set-up. Briefly, on day one HEK293T cells were seeded in a 6-well plate at a density of 5×10^5 cells/well in 2 mL DMEM. The next day, cells were transiently transfected with the different combinations of the CB₁ and mini-G α_i fusion constructs (in a 1:1 ratio, 1.5 μ g each), using FuGENE HD reagent, according to the manufacturer's instructions. On the third day, cells were treated with EDTA/trypsin and reseeded in a poly-D-lysine pre-coated white 96-well plate at a cell density of 5×10^4 cells/96-well. Forty-eight hours after transfection, cells were washed twice with Opti-MEM I Reduced Serum Medium and 100 μ l Opti-MEM I was added to the wells. Next, 25 μ l of furimazine substrate (20-fold diluted in aqueous Nano-Glo LCS dilution buffer) was added to each well

and luminescence was monitored in a TriStar² LB 942 multimode microplate reader controlled by ICE software (Berthold Technologies GmbH & Co., Bad Wildbad, Germany). After an equilibration period of 15 minutes, 10 μ L of a solvent control (blank, \leq 0.1% DMSO) or 13.5 x concentrated solution of the CB₁ agonist JWH-018 in Opti-MEM I/methanol (50:50) was added, yielding a final concentration of 100 nM JWH-018. Luminescence was monitored for 120 minutes.

8.2.4 Generation of a stable HEK293T cell line expressing CB₁ and mini-G α_i protein

To generate a HEK293T cell line stably expressing CB₁-LgBiT and SmBiT-mini-G α_i , retroviral vectors encoding these sequences were developed for the production of retroviruses in a Phoenix-AMPHO (Φ NX-A) packaging cell line. Generation of the pLZRS-CB₁-LgBiT-IRES-EGFP expression vector, which leads to co-expression of the fusion protein CB₁-LgBiT and enhanced green fluorescent protein (EGFP), was already described by Caninaert *et al.*, 2017 [48]. For this study, the fusion protein SmBiT-mini-G α_i was transferred into the pLZRS-IRES-dNGFR viral vector using similar standard cloning procedures, by which the fusion construct was flanked by restriction sites *NotI* and *SnaBI* (**Table 7.1B**). The integrity of the insert was verified via Sanger sequencing.

Retrovirus generation was executed similarly -with only minor adaptations- as previously published by our group [49]. Briefly, the day before transfection the Φ NX-A packaging cell line was seeded at a density of 1.5×10^6 cells/6cm dish in IMDM supplemented with 10% heat-inactivated fetal bovine serum (FBS), 2 mM glutamine, 100 IU/mL penicillin, 100 μ g/mL streptomycin and 0.25 μ g/mL amphotericin B under humidified atmosphere at 37°C, 5% CO₂. The next day, cells were transiently transfected using the Calcium Phosphate Transfection method according to the manufacturer's instructions, using a total of 20 μ g retroviral expression vector DNA (1:1 ratio of pLZRS-CB₁-LgBiT-IRES-EGFP:pLZRS-SmBiT-mini-G α_i -IRES-dNGFR). After an incubation of 30 min of the transfection mixture and 5 min prior to the dropwise addition of the mixture to the cells, chloroquine was added to the cells at a final concentration of 25 μ M, to inhibit DNA degradation by lysosomes. After overnight incubation, the medium was refreshed. Forty-eight hours after transfection, puromycin selection (2 μ g/mL) was carried out for 3 rounds of 48 h, alternating each time with a 48-h incubation in puromycin-free IMDM. After two weeks of these selection rounds, the viral supernatant was

harvested and centrifuged (10 min, 350×g, 4°C), after which the supernatant was aliquoted and stored at -80°C.

For retroviral transduction, HEK293T cells were seeded in a 24-well plate at 5×10^4 cells/well in complete DMEM. The next day, the medium was aspirated and replaced by retroviral supernatant (containing a mixture of CB₁- and mini-Gα_i-sequence containing retroviruses), pre-incubated with 10 µL DOTAP Liposomal Transfection Reagent. Subsequently, the plate was centrifuged for 90 min at 950×g (32°C) to increase transduction efficiency. After overnight incubation, the medium was refreshed. Expression efficiency was evaluated 48 hours after transduction with the CytoFLEX flow-cytometer (Beckman Coulter Life Sciences, Brea, USA) by measuring the level of EGFP or dNGFR (by 30 min pre-incubation with an Allophycocyanin-linked anti-dNGFR antibody), which are co-expressed with the CB₁- and mini-Gα_i-fusion proteins, respectively.

Cell sorting of stably transduced HEK293T cells

Cell sorting was performed using a BD FACS Aria III Fusion equipped with 405, 640, 488 and 561 nm lasers (BD Biosciences, Erembodegem, Belgium). Stably transduced HEK293T cells were selected for their desired co-expression levels of EGFP and dNGFR. Stability of the obtained cell lines was monitored every 3-5 passages by flow cytometry, as described in the previous section.

Table 7.1 PCR conditions for the development of mini-Gα_i-NanoBiT® constructs and the SmBiT-mini-Gα_i coding retroviral vector.

A. Generation of mini-G _{α_i} protein NanoBiT® construct				
Fusion construct		Primers (5'>3') ^a	Tm (°C) ^b	RE ^c
mini-G _{α_i} -LgBiT & mini-G _{α_i} -SmBiT	F	ACTCAAGA AATTC ACCATGATCGAGAAGCAGCTGCAG	71°C	<i>EcoRI</i>
	R	ACTCAAGA AATTC CCGAACAGGCCGCGAGTCTC		
LgBiT-mini-G _{α_i} & SmBiT-mini-G _{α_i}	F	ACTCAAGA AATTC <u>AA</u> TGATCGAGAAGCAGCTGCAG	70°C	<i>EcoRI</i>
	R	ACTCAAGA AATTC <u>TCT</u> CAGAACAGGCCGCGAGTCTCTC		
B. Generation of SmBiT-mini-G _{α_i} in a retroviral expression vector construct				
Fusion construct		Primers (5'>3') ^a	Tm (°C) ^b	RE ^c
pLZRS-SmBiT-mini-G _{α_i} -IRES-dNGFR	F	ATTCAAG CGGCCG <u>CA</u> CCATGGTGACCGGC	72°C	<i>NotI</i>
	R	ACTCAAT ACGTAT <u>CAG</u> AACAGGCCGCGAGTC		<i>SnaBI</i>

a: Forward (F) and Reverse (R) primers (5'>3') with restriction enzyme sites (**bold**), start codon (underlined), Kozak sequence (*italic*), stop codon (double underlined) or extra nucleotides (marked in grey) to ensure a correct reading frame.

b: Annealing temperature.

c: Restriction enzyme.

8.2.5 Screening of SCRA in bio-assays of mini-G α_i and β -arrestin2 signaling

All SCRA were screened applying the developed stable HEK293T cell systems, expressing CB₁ and a transducer (mini-G α_i or β -arrestin2), using a two-day protocol. On the first day, cells were washed twice with Opti-MEM I before adding 100 μ L Opti-MEM I and 25 μ L diluted furimazine substrate to each well of a 96-plate and equilibrating for 15 minutes, to allow stabilization of the luminescent signal. Thereafter, luminescence measurement was shortly interrupted for the addition of the compounds. Serial dilutions of each compound were freshly prepared each time and the same preparations were used for the CB₁-NanoBiT[®]- β arr2 and CB₁-NanoBiT[®]-mini-G α_i reporter bio-assays, to avoid inter-assay fluctuations. Ten μ L of 13.5 x concentrated solutions were applied, resulting in final concentrations from 0.1 pM up to 10 μ M (dependent on the potency of the SCRA). Luminescence was monitored for 120 minutes. A solvent control (blank, \leq 0.1% DMSO), as well as a reference compound (CP55,940), were included in duplicate on each plate.

8.2.6 Data analysis

Relative Luminescence units (RLU) over time of all SCRA that provoked β -arrestin2 or mini-G α_i coupling to CB₁ were corrected for inter-well variability and solvent control. The mean area under the curve (AUC) \pm standard error of mean (SEM) was derived from three or four independent experiments ($n = 3-4$). Each of these experiments encompassed the analysis of duplicates (hence, each data point is the result of 6-8 determinations). All AUCs were normalized to the maximum response of the reference compound CP55,940 (arbitrarily set as 100%). Sigmoidal curve-fitting of concentration–response curves via nonlinear regression (three parameters, Hill slope $n_H = 1$) with GraphPad Prism software (San Diego, CA, USA) was employed to determine EC₅₀ values (a measure of potency).

8.2.7 Quantifying biased signaling

For the quantification of the signaling bias, the bias factor β was calculated using the relative activity-based model, as described previously [50]. First, the *intrinsic relative activity* (RA_i) was calculated for each SCRA, for both the mini-G protein and β -arrestin2 recruitment, using the formula in (1).

$$RA_{i,CP55,940}^{pathX} = \frac{E_{max,i} \times EC_{50,CP55,940}}{EC_{50,i} \times E_{max,CP55,940}} \quad (1)$$

Herein, the $E_{max,i}$ and $EC_{50,i}$ represent the maximal response (E_{max}) and the potency (EC_{50}) of each SCRA of the panel of 21 SCRA that were screened, whereas the $E_{max,CP55,940}$ and $EC_{50,CP55,940}$ represent the efficacy and potency values of the reference compound.

Subsequently, the *bias factor* was calculated for each SCRA using the formula in (2), which entails the logarithm of the ratio of the RA_i value for β -arrestin2 recruitment to the RA_i value for G protein signaling.

$$\beta = \log \left(\frac{RA_{i,CP55,940}^{\beta\text{-arrestin2}}}{RA_{i,CP55,940}^{mini-G\alpha_i}} \right) \quad (2)$$

Statistical analysis on the calculated bias factors was performed using the non-parametric (Kruskal–Wallis) one-way ANOVA, followed by post hoc (Dunn’s multiple comparison test) analysis to detect statistical differences amongst calculated bias factors of SCRA, compared to the non-biased reference compound CP55,940 ($p < 0.05$), by the GraphPad Prism software (San Diego, CA, USA).

Furthermore, bias plots were generated to graphically express the differential activation of both pathways. The normalized AUCs (expressed as % vs. CP55,940) of the SCRA observed in the β -arrestin2 bio-assay were plotted to those in the mini-G α_i bio-assay. For each bio-assay, this normalization was relative to the reference compound CP55,940, for which - per definition - we assigned equal values for both bio-assays at each of the tested concentrations, with 100% corresponding to the maximum observed for CP55,940 in both bio-assays. Finally, curves were fitted using the centered second order polynomial (quadratic) fitting using the GraphPad Prism software.

For the investigation of temporal bias, the E_{\max} values of all SCRA were derived from the relative luminescence units (RLU) plots and not from the normalized AUC concentration-response curves. The maximal responses, upon incubation with all SCRA at their highest concentration (i.e. 10 μ M, 1 μ M or 100 nM, dependent on the potency of the SCRA) were corrected for their respective blank and were normalized to the CP55,940 reference. This was done for the maximal response (E_{\max} , max values) provoked by the SCRA and for 30 minutes after the maximal response (E_{\max} , max values + 30'). Next, the bias factors were recalculated based on the different E_{\max} , max values and E_{\max} , max values + 30'.

8.2.8 Molecular Docking

Recently, the cryo-EM structure of the CB₁-G α_i complex with the highly potent MDMB-FUBINACA has been unraveled [51]. In this study, the molecular docking of (subtle) β -arrestin2-biased 5F-APINACA (**12**), CUMYL-PEGACLONE (**19**) and (subtle) mini-G α_i protein-biased EG-018 (**18**) and EG-2201 (**20**) on the CB₁ structure, activated by MDMB-FUBINACA was performed, as previously described by Krishna Kumar, *et al.* (2019) [51]. The cryo-EM structure of CB₁/G α_i (PDB: 6n4b) was prepared with Schrodinger's Maestro. Missing atoms were built and hydrogen bonding was optimized with the protein preparation tool. All ligands were docked with GLIDE extra precision docking [52].

8.3 Results and discussion

8.3.1 Development of the stable CB₁ NanoBiT[®] reporter bio-assay for real-time monitoring of mini-Gα_i recruitment in HEK293T cells

To obtain a system that measures G protein recruitment and that allows a straightforward comparative analysis with the CB₁-β-arrestin2 NanoBiT[®] bio-assay [48], a stable CB₁-mini-Gα_i reporter cell line was developed by retroviral transduction. This way, a panel of SCRA could be screened for their preferential recruitment of β-arrestin2 or mini-Gα_i, using a very similar experimental set-up. Prior to generating a stable cell reporter system, the four possible combinations of the CB₁ and mini-Gα_i fusion proteins were tested in a transient set-up (**Figure 8.1**).

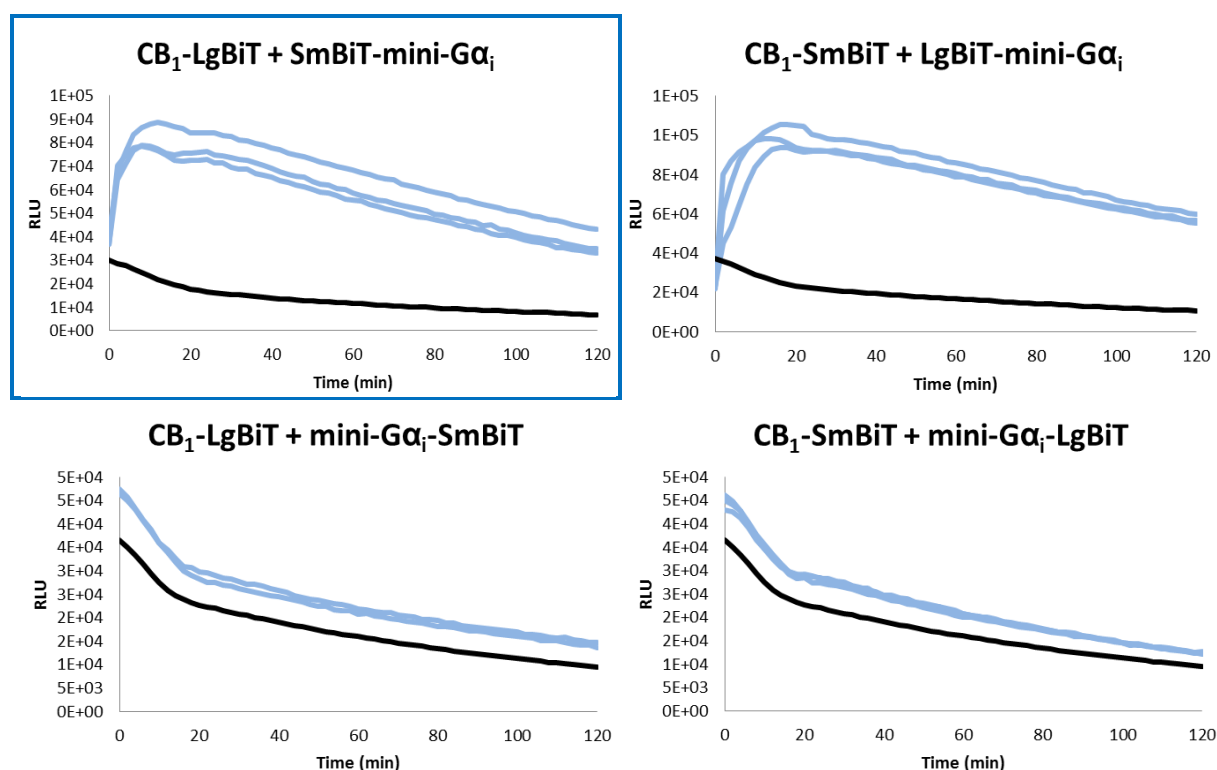


Figure 8.1 Selection of the most optimal combination of the NanoBiT[®] fusion proteins of CB₁ and the mini-Gα_i protein. All combinations were incubated with 100 nM of reference compound JWH-018 (blue lines) or solvent control (black lines). Luminescence was monitored for 120 minutes. Measurements of triplicate wells and the average solvent control are depicted of one representative experiment (n=3).

As expected, the combinations with C-terminally tagged mini-Gα_i fusion proteins yielded no luminescent signal, as the C-terminal α5-helical domain of the mini-Gα_i plays a crucial role in the interaction with CB₁ [51, 53, 54]. In contrast, both the LgBiT- and SmBiT- N-terminal fusions with the mini-Gα_i protein were efficiently recruited to respectively the SmBiT- and LgBiT-CB₁ C-terminal fusion proteins following stimulation with 100 nM JWH-018. In this manner, the C-

terminus of the mini-G α_i is free to interact with the cavity created at the transmembrane (TM) 3/5/6 region of the activated CB₁, resulting in complementation of the split biosensor, of which the luminescent signal can be measured.

As both SmBiT-mini-G α_i and LgBiT-mini-G α_i provoked similar patterns in fold increase of luminescent signal upon CB₁ stimulation compared to background, we opted for the same experimental set-up as in the CB₁- β -arrestin2 NanoBiT® bio-assay, i.e. CB₁-LgBiT combined with SmBiT-mini-G α_i . Hence, differences in recruitment of the transducers due to different tagging of the receptor or transducer could be ruled out. Thus, a HEK293T cell line stably expressing both fusion proteins was generated following retroviral transduction and cell sorting. In both the CB₁-LgBiT:SmBiT-mini-G α_i and the CB₁-LgBiT:SmBiT- β -arrestin2 cell lines, the expression levels of CB₁ and the transducers were monitored every 3-5 passages by flow cytometry (**Figure 8.2**). This was easily achieved by monitoring the expression of the co-expressed markers EGFP and dNGFR. In the Y-axis of **Figure 8.2**, the level of EGFP (FL1-A: FITC-A) is displayed. This fluorescent protein is a marker for the expression level of the CB₁ receptor construct. The X-axis (FL5-A: APC-A) shows the level of the fluorophore APC (allophycocyanin), which is a marker for the expression level of the β -arrestin2 or the mini-G α_i construct. Both are co-expressed with dNGFR, which can be visualized with an APC-linked antibody against dNGFR. Untransduced cells are double negative (bottom left quadrant). After retroviral transduction and cell sorting, ≥ 95.8 % of the CB₁- β -arrestin2 HEK293T cells and 96.8 % of the CB₁-mini-G α_i HEK293T cells are double positive (upper right quadrant), meaning they express the receptor construct, as well as the transducer construct. After 10 passages, during which the experiments for biased agonism screening were performed expression levels of > 80 % (of total population) for both stable HEK293T cell lines remained. Importantly, both cell lines had similar expression levels of both EGFP and dNGFR.

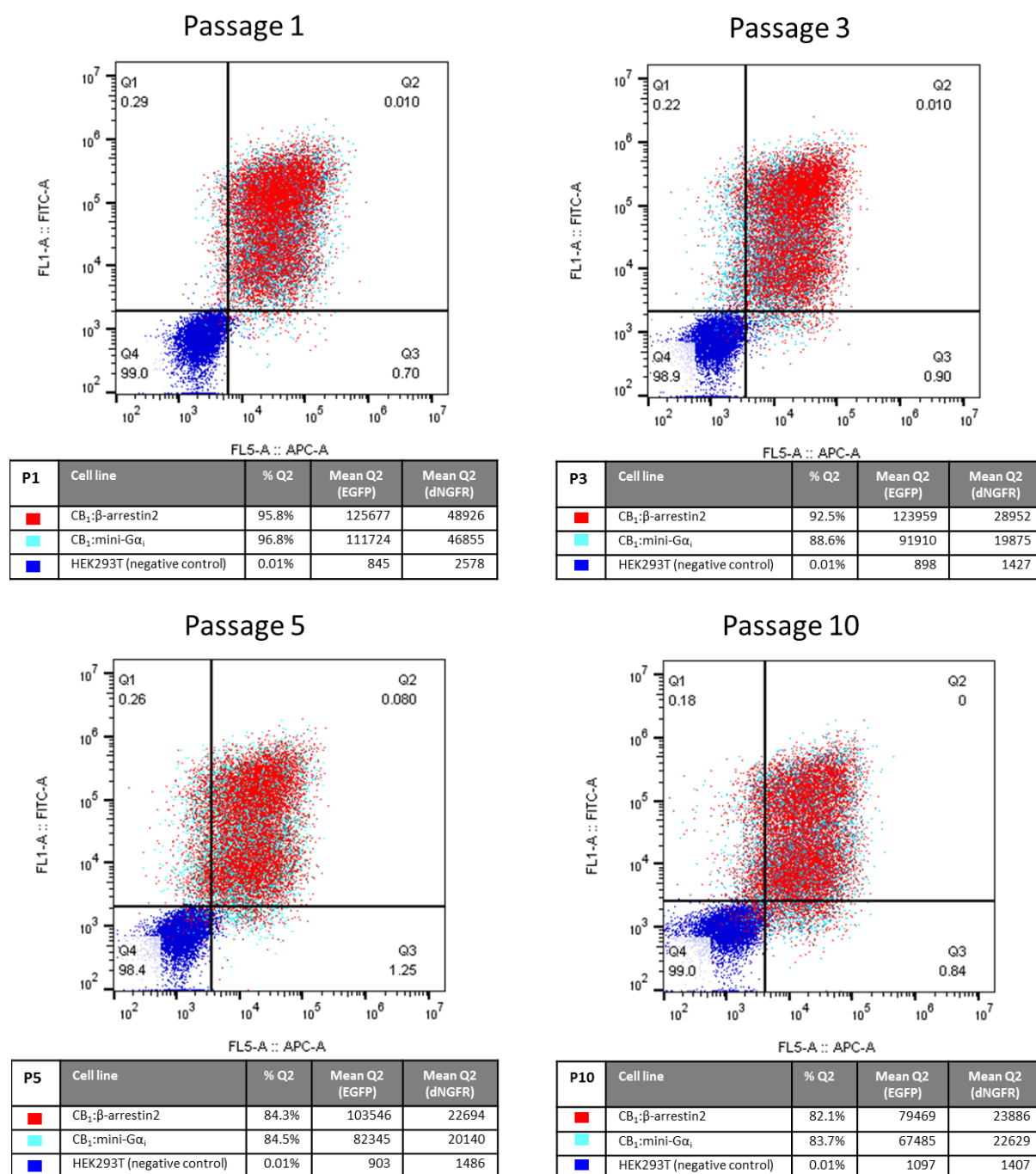


Figure 8.2 Percentage of double positive stable HEK293T cell lines (Q2) from passage 1 to passage 10. The CB₁-β-arrestin2 HEK293T, the CB₁-mini-Gα_i HEK293T and the double negative HEK293T cell lines are superimposed and depicted in light blue, red and dark blue, respectively. The percentage double positive expressing cells and the mean of the FITC-A (EGFP) and APC-A (dNGFR) are given. The percentage indicated for each quadrant represents double-negative cells.

8.3.2 Selection of a non-biased reference compound in the NanoBiT® bio-assays

Once the stable HEK293T cell line expressing the CB₁-LgBiT and SmBiT-mini-Gα_i had been established, a reference compound had to be selected that could serve as a ‘balanced ligand’, equally recruiting β-arrestin2 and mini-Gα_i. Both JWH-018 and CP55,940 have been reported

to act as balanced compounds [37] and were evaluated here. Both the new SmBiT-mini- $G\alpha_i$ system, as well as the readily available SmBiT- β -arrestin2 system, each in a HEK293T cell background co-expressing similar levels of CB₁-LgBiT, were used to generate concentration-response curves for JWH-018 (10 pM – 10 μ M) and CP55,940 (1 pM – 1 μ M) (**Figure 8.3**). Similar EC₅₀ and E_{max} values were obtained for CP55,940 in both the CB₁- β -arrestin2 (EC₅₀: 0.53 nM, E_{max}: 7.59*10⁸) and the CB₁-mini- $G\alpha_i$ NanoBiT[®] cell system (EC₅₀: 0.15 nM, E_{max}: 1.03*10⁸), as was the case for JWH-018 (CB₁- β -arrestin2 assay: EC₅₀: 5.57 nM, E_{max}: 8.77*10⁸ and CB₁-mini- $G\alpha_i$ assay: EC₅₀: 3.23 nM, E_{max}: 1.51*10⁸). From this data, it can be concluded that both SCRA can function as relatively non-biased agonists. As CP55,940 has already successfully served as a reference compound previously [37], we selected this SCRA as the main non-biased reference compound within this study. Nonetheless, we also evaluated the pathway bias for all the 21 SCRA relative to JWH-018 (see section 8.3.3, pathway bias).

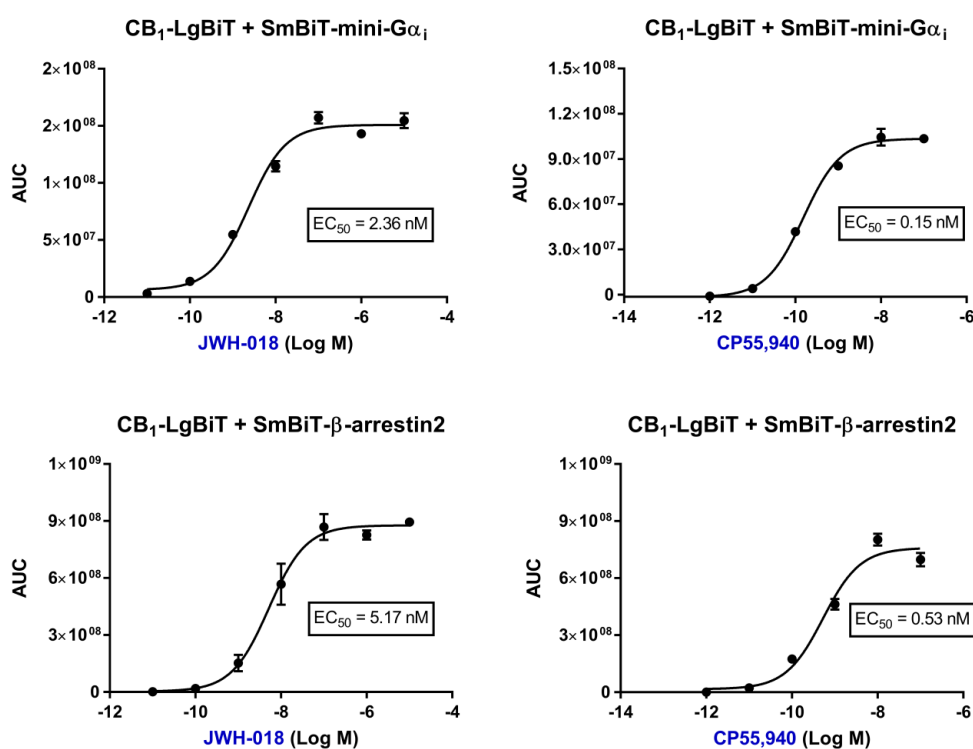


Figure 8.3 Selection of a non-biased reference compound JWH-018 (left) or CP55,940 (right) on the stable CB₁-mini- $G\alpha_i$ - and the CB₁- β -arrestin2-NanoBiT[®] bio-assays.

8.3.3 Screening of a panel of SCRA for biased signaling in β -arrestin2 and mini- $G\alpha_i$ recruitment assays

An initial panel of 19 SCRA, encompassing a remarkable degree of chemical diversity and belonging to distinct classes, was evaluated for the ability to recruit β -arrestin2 *versus* mini- $G\alpha_i$. As outlined further in the section ‘Pathway bias’, 2 additional compounds, EG-2201 (**20**) and MDMB-CHMCZCA (**21**) were only included at a later stage, bringing the total panel of evaluated SCRA on 21. An overview of the chemical structures of the selected SCRA is given in **Figure 8.4**. For all SCRA, different concentrations (ranging from 0.1 pM up to 10 μ M, depending on the potency of the SCRA) were tested in both bio-assays. This yielded the concentration-response curves depicted in **Figure 8.5**.

Potency values (EC_{50})

In **Table 8.2**, the potency (EC_{50}) and efficacy (E_{max} , relative to CP55,940) for all selected SCRA are shown for both pathways. A broad diversity in efficacy and potency of the investigated SCRA can be observed (**Table 8.2**), with 5F-PB-22 (**10**), (S)-5F-MDMB-PINACA (**14**) and CUMYL-PEGACLONE (**19**) being the most potent SCRA in both bio-assays, whereas EG-018 (**18**), EG-2201 (**20**) and MDMB-CHMCZCA (**21**) are amongst the least potent SCRA. The cause of these observed differences in potency could be elucidated by means of molecular docking of these SCRA in the orthosteric CB_1 binding pocket, based on the recently published cryo-EM structure of the CB_1 - $G\alpha_i$ complex [51] (**Figure 8.6**). This revealed that 5F-APINACA (**12**) and CUMYL-PEGACLONE (**19**) can be positioned in a very similar manner as the highly potent MDMB-FUBINACA, although the larger ring system of CUMYL-PEGACLONE (**19**) occupies more of the pocket. More importantly, these SCRA possess an oxygen at a key position, allowing these compounds to establish an interaction with a serine in TM7 of CB_1 , more specifically S383^{7.39} (superscript indicates Ballesteros-Weinstein numbering for GPCRs) [55]. It has previously been reported that mutation of S383^{7.39} results in reduced agonist binding [51, 56] and structure-activity-relationship studies revealed that ligands without the hydrogen bonding group had a lower potency [51, 57]. As EG-018 (**18**) and EG-2201 (**20**) do not possess this oxygen group in the key position (which is also the case for compound **21**) to establish a hydrogen bonding network with water molecules and S383^{7.39} (**Figure 8.6**, circled in red), this likely explains why these SCRA seem to interact only poorly with CB_1 , as also reflected by the low receptor activation potential, observed in both bio-assays.

The general trend in the observed potencies for the investigated SCRA scaffolds leans towards lower EC_{50} values in the mini- $G\alpha_i$ bio-assay compared to the β -arrestin2 recruitment assay (**Figure 8.7 B**). This might be explained by the fact that for the mini- $G\alpha_i$ system the assay ceiling is already reached at lower concentrations, whereas for the β -arrestin2 assay the signals continue to rise, only reaching the plateau at higher concentrations. Only for 5F-APINACA (**12**) a slightly lower EC_{50} value was obtained with the β -arrestin2 recruitment assay as compared to the mini- $G\alpha_i$ assay, the differences between both EC_{50} values not being significant, though. On the other hand, the most pronounced shift in potency was observed for EG-018 (**18**) (EC_{50} β -arrestin2: 2012 nM vs. EC_{50} mini- $G\alpha_i$ assay: 76.5 nM)(**Table 8.2** and **Figure 8.7 B**).

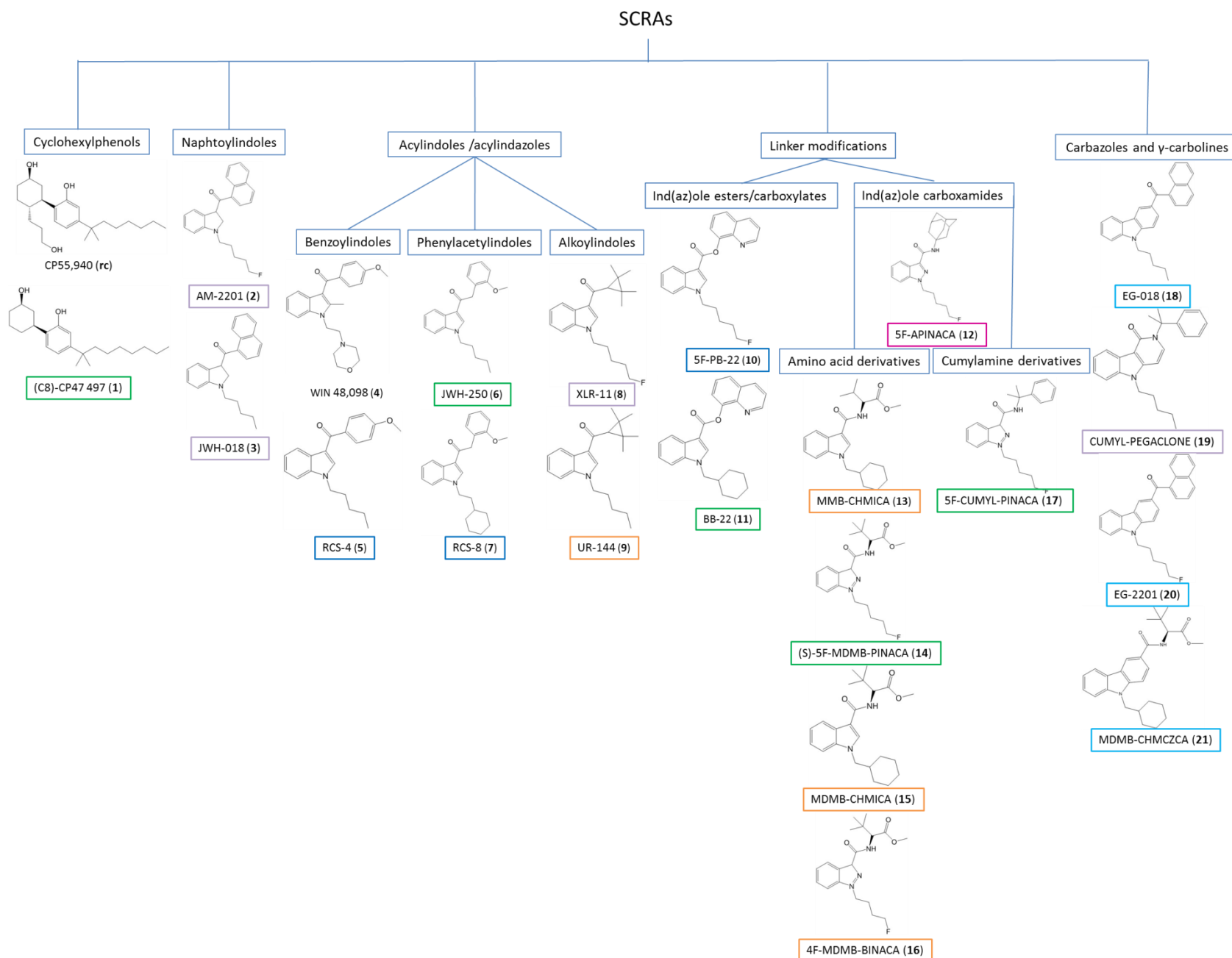


Figure 8.4 Chemical structures of the selected twenty-one SCRAs. The distinct colors reflect the distinct profiles observed in the bias plots (cfr. Figure 8.11).

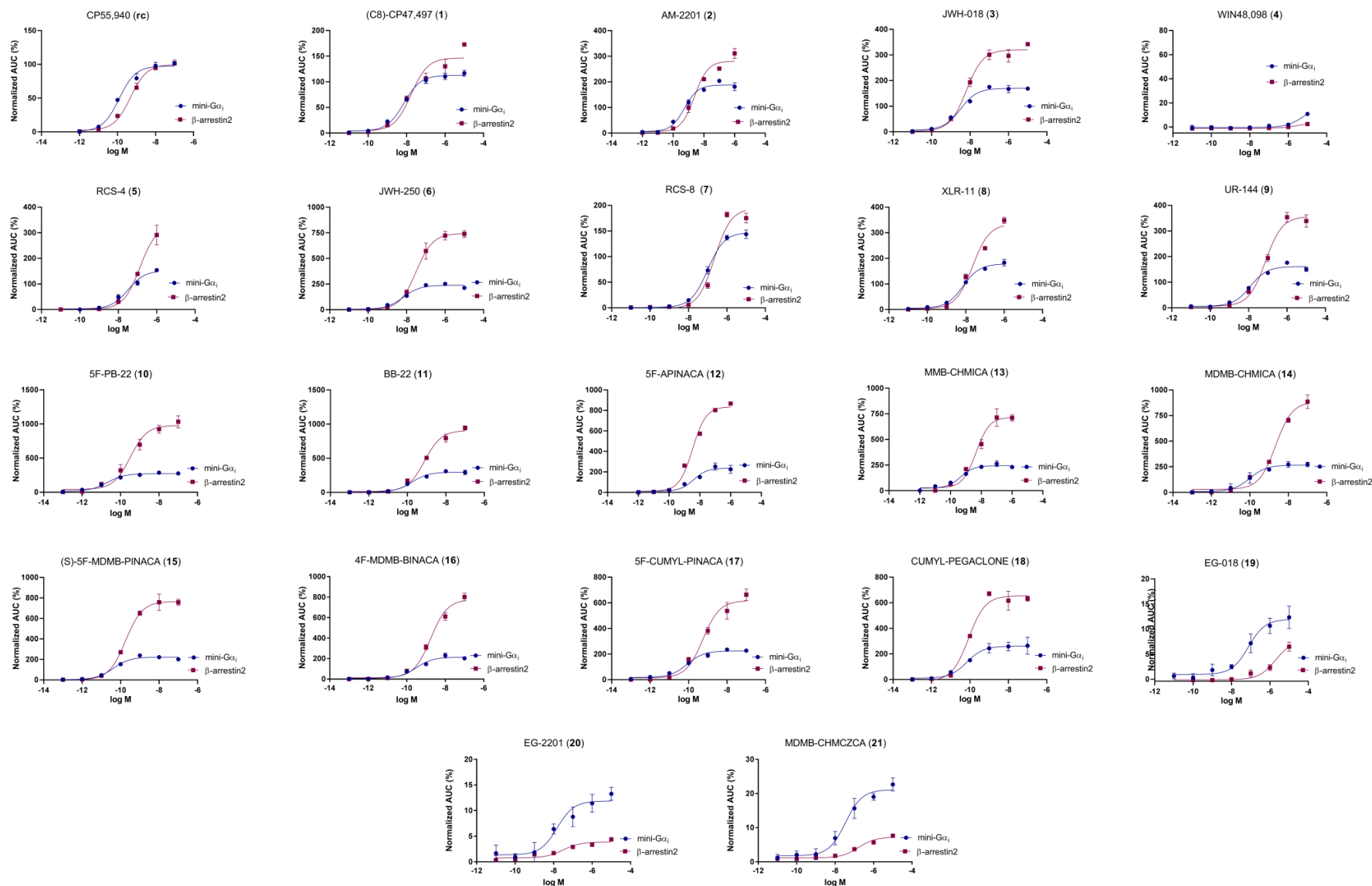


Figure 8.5 Overview of the sigmoidal concentration-response curves of twenty-one SCRAs and the reference compound CP55,940. Curves derived from the table HEK293T CB₁-miniGα_i NanoBiT[®] assay are depicted in purple, SCRAs tested in the HEK293T CB₁-β-arrestin2 NanoBiT[®] assay are depicted in blue (n=3, ± SEM).

Table 8.2 Overview of the potency (EC_{50}), efficacy (E_{max} , relative to CP55,940), each with the corresponding 95% confidential intervals (CI), the calculated intrinsic relative activity (RA_i) of the β -arrestin2 and mini- $G\alpha_i$ pathways and the bias factor β for the selected SCRAs.

Compound	Mini- $G\alpha_i$		β -arrestin2		$RA_i^{\text{mini-}G\alpha_i}$	$RA_i^{\beta\text{-arrestin2}}$	β
	EC_{50} (nM)	E_{max} (%)	EC_{50} (nM)	E_{max} (%)			
(C8)-CP47,497 (1)	6.56 (4.26-9.80)	109.9 (103.1-116.8)	9.34 (4.93-17.7)	125.2 (112.7-138.4)	0.020	0.041	0.322
AM-2201 (2)	0.60 (0.36-0.96)	192.2 (179.1-205.8)	1.64 (1.20-2.27)	251.7 (238.0-265.9)	0.430	0.546	0.103
JWH-018 (3)	3.23 (1.73-5.97)	170.7 (157.9-184.1)	5.57 (3.41-8.82)	306.5 (284.0-329.5)	0.067	0.238	0.551
WIN48,098 (4)	ND	ND	ND	ND	ND	ND	ND
RCS-4 (5)	32.4 (16.3-47.1)	151.8 (135.2-171.3)	136 (77.9-243)	329.9 (285.7-382.9)	0.006	0.012	0.302
JWH-250 (6)	6.77 (4.19-10.6)	238.4 (224.1-252.8)	31.4 (20.4-48.4)	744.7 (696.8-793.9)	0.044	0.114	0.415
RCS-8 (7)	99.4 (74.9-132)	147.3 (140.0-154.8)	225 (152-335)	194.5 (178.4-211.3)	0.002	0.004	0.352
XLR-11 (8)	5.04 (2.43-10.0)	159.3 (144.8-174.2)	16.0 (9.64-27.6)	303.5 (282.2-325.6)	0.030	0.072	0.372
UR-144 (9)	12.2 (8.08-18.6)	160.9 (152.1-169.9)	75.6 (50.4-111)	356.9 (333.8-380.6)	0.016	0.023	0.141
5F-PB-22 (10)	0.04 (0.03-0.09)	281.8 (264.3-299.6)	0.13 (0.08-0.23)	913.2 (848.8-979.5)	7.126	33.55	0.673
BB-22 (11)	0.17 (0.10-0.31)	296.7 (274.3-320.0)	0.79 (0.53-1.15)	907.2 (851.7-964.0)	2.163	5.541	0.409
5F-APINACA (12)	3.98 (1.61-8.79)	237.0 (212.1-263.0)	3.39 (1.39-8.11)	836.1 (740.6-938.7)	0.074	1.187	1.204
MMB-CHMICA (13)	0.45 (0.20-0.94)	244.0 (224.8-263.6)	4.54 (2.14-8.83)	717.2 (650.1-786.8)	0.673	0.760	0.053
(S)-5F-MDMB-PINACA (14)	0.04 (0.03-0.07)	222.5 (209.4-235.8)	0.18 (0.13-0.27)	765.9 (724.1-808.5)	6.765	20.25	0.476
MDMB-CHMICA (15)	0.10 (0.03-0.32)	266.4 (230.0-304.5)	2.21 (1.41-3.52)	885.7 (818.5-958.0)	3.321	1.929	-0.236
4F-MDMB-BINACA (16)	0.31 (0.15-0.70)	214.3 (192.7-235.9)	1.74 (1.22-2.49)	777.4 (726.7-828.0)	0.863	2.150	0.397
5F- CUMYL-PINACA (17)	0.09 (0.05-0.14)	224.6 (211.1-238.4)	0.56 (0.26-1.09)	616.8 (556.4-679.5)	3.314	5.311	0.205
EG-018 (18)	76.5 (24.9-234)	11.9 (9.8-14.1)	2012 (769-5279)	7.8 (5.9-12.0)	$1.94 \cdot 10^{-4}$	$1.87 \cdot 10^{-5}$	-1.018
CUMYL-PEGACLONE (19)	0.07 (0.02-0.22)	260.9 (223.2-299.9)	0.09 (0.05-0.13)	655.1 (611.9-698.8)	4.700	37.18	0.898
EG-2201 (20)	15.3 (4.01-58.3)	11.9 (9.8-13.9)	31.5 (6.76-146)	3.9 (3.2-4.6)	$9.70 \cdot 10^{-4}$	$5.92 \cdot 10^{-4}$	-0.214
MDMB-CHMCZCA (21)	34.4 (14.1-84.1)	21.1 (18.5-23.7)	164 (77.4-349)	7.3 (6.4-8.1)	$7.65 \cdot 10^{-4}$	$2.12 \cdot 10^{-4}$	-0.557
CP55,940 (rc)	0.12 (0.08-0.20)	97.5 (91.7-103.5)	0.48 (0.31-0.72)	99.8 (94.0-105.8)	1.0	1.0	0

ND: not determined since saturation was not reached

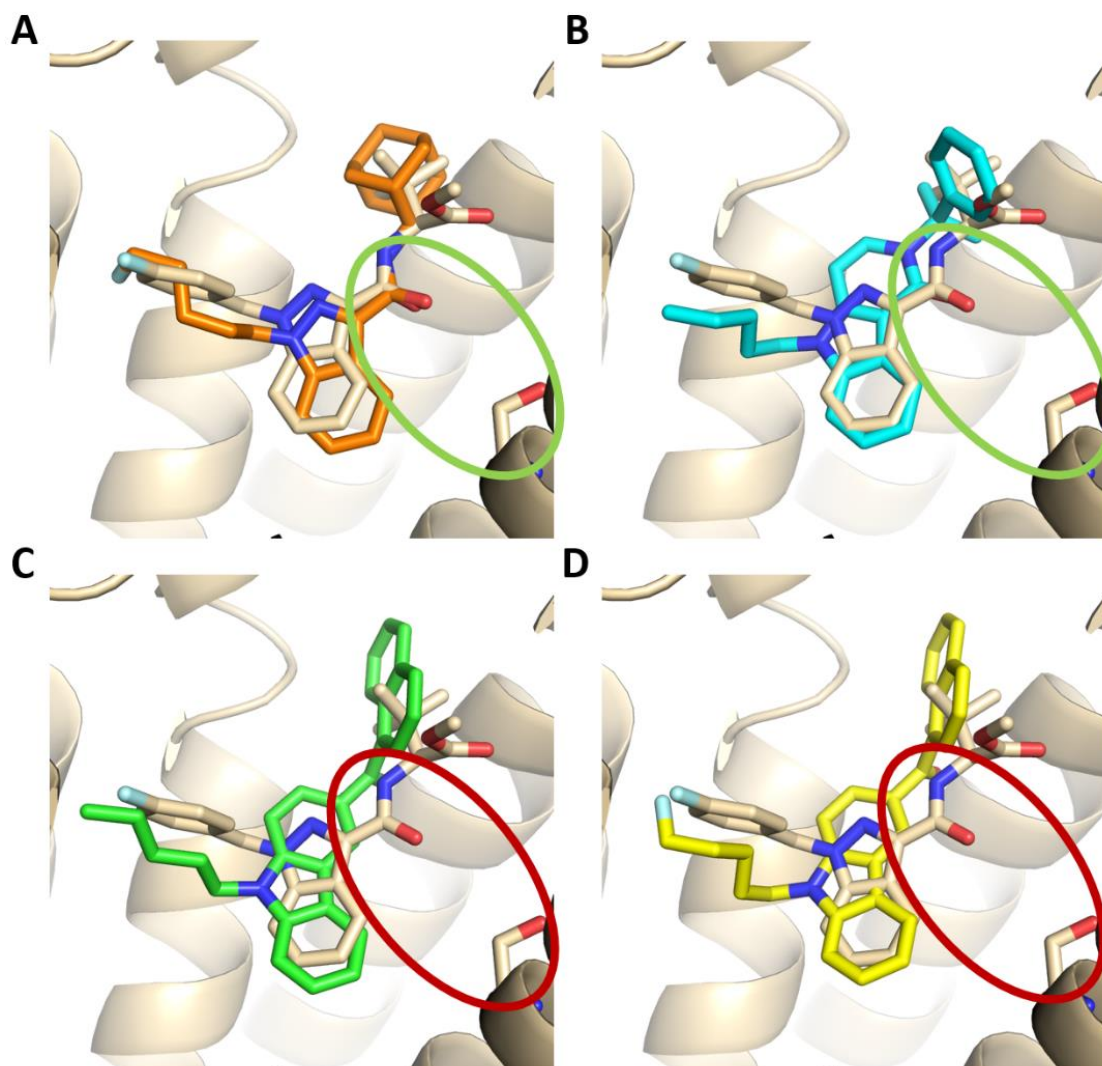


Figure 8.6 Molecular docking of (subtle) β -arrestin2-biased 5F-APINACA (**12**) and CUMYL-PEGACLONE (**19**) and (subtle) mini- $G\alpha_i$ protein-biased EG-018 (**18**) and EG-2201 (**20**) in the orthosteric CB₁ binding site. (A&B) Comparison of the similar binding modes of 5F-APINACA (**12**) (orange) and CUMYL-PEGACLONE (**19**) (blue) with MDMB-FUBINACA (light yellow), in which both can mediate a hydrogen bonding network with S383^{7,39} and water molecules in the pocket (circled in green). (C&D) Comparison of the binding modes of EG-018 (**18**) (green) and EG-2201 (**20**) (yellow) and with MDMB-FUBINACA (light yellow), in which only the latter can make hydrogen bonds with S383^{7,39} (circled in red), since compound **18** and **20** lacks the oxygen in the key position.

Efficacy values (E_{\max})

CP55,940, also described by others as a non-biased full agonist [37], was selected as a reference compound (**rc**) here and its efficacy was arbitrarily set as 100%. Remarkably, with 2 exceptions (WIN48,098 (**4**) and EG-018 (**18**)) all of the initial 19 SCRA reached higher E_{\max} values, in both the β -arrestin2 and the mini- $G\alpha_i$ NanoBiT[®] bio-assay (Figure 8.7). In other

studies published by our research group, similar high efficacies have been obtained using the CB₁- β -arrestin2 NanoBiT[®] assay [44, 45, 48, 58]. For WIN48,098 (**4**), no E_{max} values could be determined as this SCRA shows only little activity at the highest tested concentration of 10 μ M (**Figure 8.4**), which is in agreement with previous studies [59]. Nevertheless, a slight preference towards G protein signaling could still be observed. Although also EG-018 (**18**) was a relatively poor agonist, E_{max} values could be obtained for this compound, at 11.9% (mini-G α_i) and 7.8% (β -arrestin2) of the CP55,940 reference (**Table 8.2**). In both bio-assays, EG-018 (**18**) behaved as a partial CB₁ agonist with a low efficacy, as well as a low potency, which is in agreement with the reported affinity of this compound for CB₁ (K_i: 291 nM) [60], which is relatively low compared to other second generation SCRA. The SCRA that provoked the highest observed maximal responses in both bio-assays were 5F-PB-22 (**10**) and BB-22 (**11**), with E_{max} values ~9-fold and ~3-fold higher than the CP55,940 reference in the β -arrestin2 and mini-G α_i NanoBiT[®] assays, respectively (**Figure 8.7**)(**Table 8.2**).

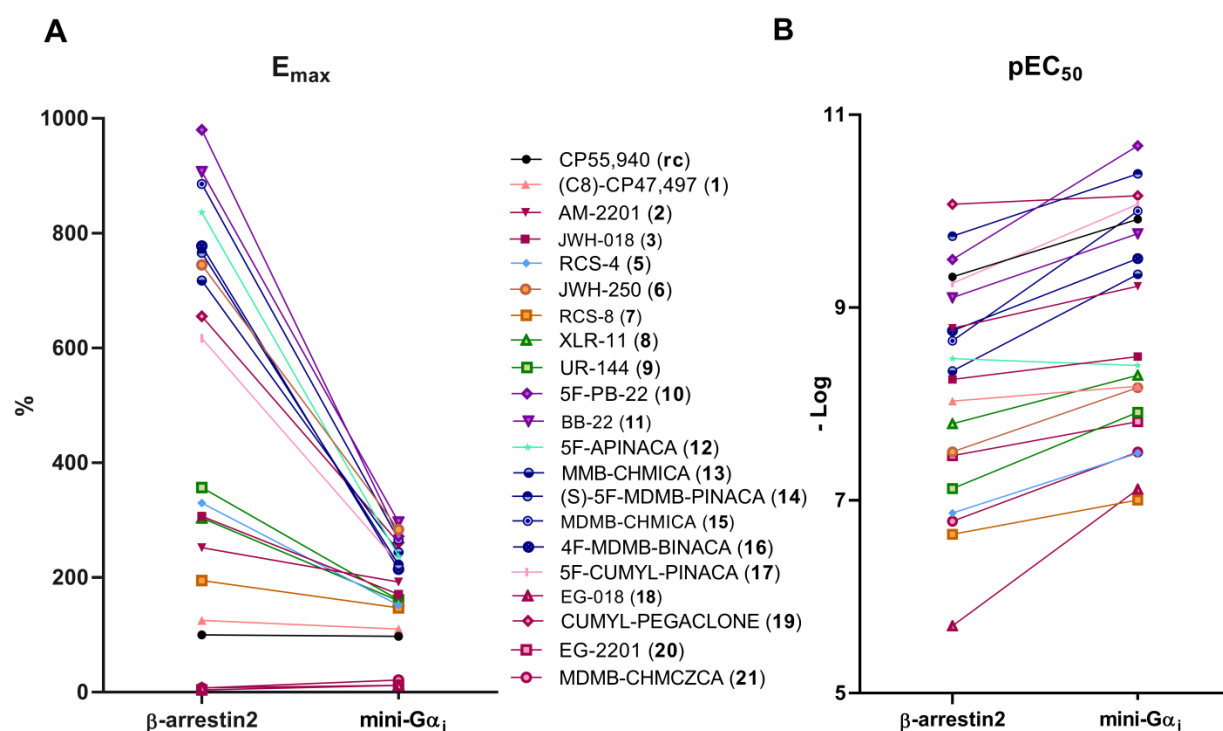


Figure 8.7 Comparison of the E_{max} values (%) relative to the reference compound (rc) CP55,940 (arbitrarily set as 100%) (**A**) and pEC₅₀ values (**B**) of the 21 SCRA screened in the β -arrestin2 NanoBiT[®] bio-assay versus the mini-G α_i NanoBiT[®] bio-assay (n=3).

Overall, the efficacy values of the investigated SCRA show a different pattern in the β -arrestin2 recruitment bio-assay compared to the mini-G α_i bio-assay (**Figure 8.7**). It is clear that

a more dynamic range in efficacies can be observed for the β -arrestin2 recruitment bio-assay. In contrast, the mini- $G\alpha_i$ bio-assay seems to have reached a system ceiling at $\pm 300\%$ (relative to CP55,940). Therefore, it might be postulated that the β -arrestin2 NanoBiT[®] bio-assay allows a better determination of the true intrinsic efficacy provoked by SCRA in comparison to the mini- $G\alpha_i$ NanoBiT[®] bio-assay. One might hypothesize that the mini- $G\alpha_i$ NanoBiT[®] bio-assay has reached a system ceiling due to issues related to 'receptor reserve'. This phenomenon, in which only submaximal receptor occupancy is required for the system to reach its maximal response, has already been investigated for the CB₁-based FLIPR[®] assay by receptor depletion via pre-treatment with the CB₁ antagonist AM6544 [61]. It has already been suggested by Smith and Rajagopal (2016) [62] that β -arrestin recruitment assays are less likely to be subject to 'receptor reserve', due to less signal amplification as compared to second messenger assays, in which the assay ceiling may be reached more easily. As in our case the mini- $G\alpha_i$ and β -arrestin2 bio-assays are based on analogous experimental set-ups, both being proximal to the receptor, the concept of 'receptor reserve' cannot simply explain the apparent lower ceiling for the $G\alpha_i$ bio-assay. Detector (luminescence) saturation is also not an explanation, as the absolute signals for the β -arrestin2 assay were higher than those for the $G\alpha_i$ assay.

In **Figure 8.7** the E_{\max} values were calculated based on the concentration-response curves, wherein the AUCs were plotted as a function of time. To make sure that the patterns that we observed were not owing to the data analysis approach *per se*, we reanalyzed the data, with E_{\max} values being deducted from the maximal signals provoked by the SCRA (Figure 8.8A). This analysis was also performed for the signals 30 minutes after the maximum had been reached (Figure 8.8B). In both cases, a similar pattern, with a more dynamic range in efficacies for the β -arrestin2 recruitment bio-assay, could be observed. We can thus conclude that this phenomenon is independent from the data analysis method. Overall, there are various hypotheses that may explain the interesting observation that there is a broader range of efficacies in the β -arrestin2 as compared to the mini- $G\alpha_i$ recruitment bio-assay, such as different transducer dynamics and/or coupling efficiencies.

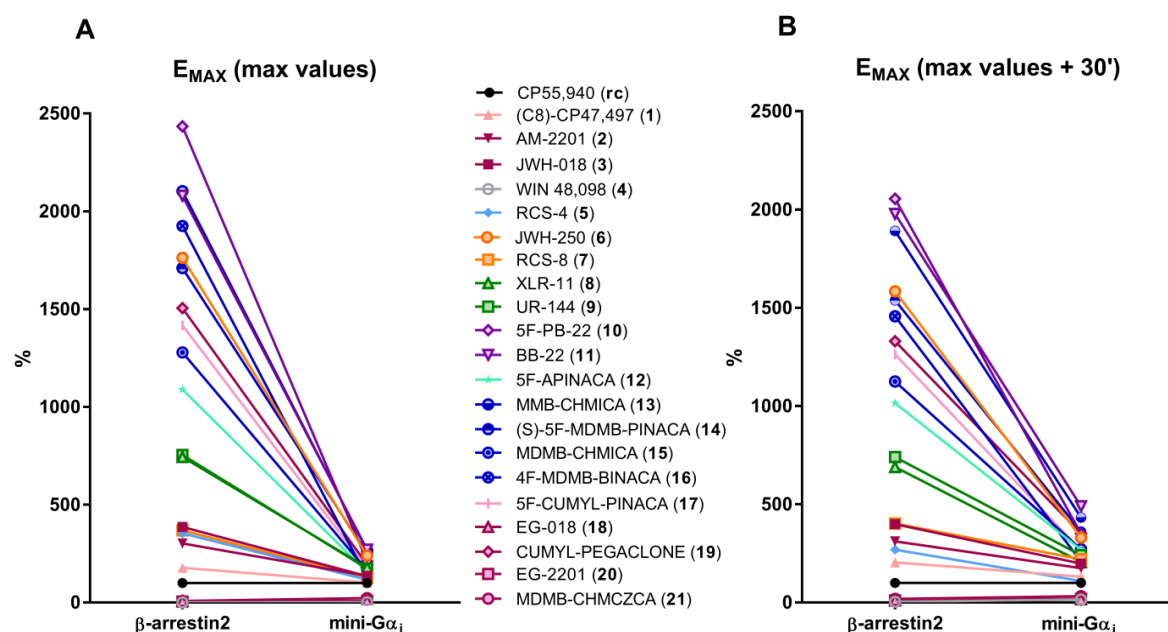


Figure 8.8 The E_{max} values (%) obtained by the normalization of the maximal relative luminescent response (RLU) observed for all the 21 SCRA at 10 μ M, 1 μ M or 100 nM (dependent on the potency of the SCRA) to CP55,940 (rc) (A) and 30 minutes after the maximal response (B) (n=3).

Pathway bias

To estimate the prevalence of biased signaling among the selected SCRA the bias factor β was calculated, which is based on the logarithmic ratio of the intrinsic relative activities of the SCRA, as assessed by the β -arrestin2 and mini- $G\alpha_i$ bio-assays (see section 8.2.7)(Table 8.2). In both bio-assays the same CB₁ construct, C-terminally fused to LgBiT, was applied, resulting in the set-up of highly analogous systems.

With CP55,940 as a reference, the majority of the panel of selected SCRA seemed to act in such a way that CB₁ preferentially recruited β -arrestin2 over mini- $G\alpha_i$. These β -arrestin2 biased SCRA include 5F-APINACA (12) > CUMYL-PEGACLONE (19) > JWH-018 (3) > (C8)-CP47,497 (1), among others (Figure 8.9)(Table 8.2). Of those, 5F-APINACA (12) is the only SCRA that significantly shows a 16-fold preferred β -arrestin2 biased recruitment ($p < 0.05$), as compared to the reference compound. Interestingly, the chemical structure of 5F-APINACA (12) is identical to that of 5F-CUMYL-PINACA (17), except for the head group, the adamantane group in (12) replacing a cumyl group in (17). As 5F-APINACA (12) is the only SCRA of the panel that has an adamantane substituent as head group, the influence of this group on β -arrestin2-mediated signaling should be further investigated. On the other hand, certain SCRA show a similar pattern as that of CP55,940 (rc), of which MMB-CHMICA (13) can be considered as a

‘non-biased’ SCRA (bias factor $\beta = 0.053$) within this study (**Figure 8.9**)(**Table 8.2**). Finally, only two out of the original panel of 19 SCRA, MDMB-CHMICA (**15**) and EG-018 (**18**), seem to be mini- $G\alpha_i$ biased SCRA, with only EG-018 (**18**) showing a significant ($p < 0.05$; 10-fold) preference towards mini- $G\alpha_i$, as compared to the reference compound. Structurally, EG-018 (**18**) can be considered an analogue of JWH-018 (**3**) (**Figure 8.4**), only deviating in the core group, which is an indole in JWH-018 (**3**) and a carbazole in EG-018 (**18**). We reasoned that this structural difference may not only result in a pronounced difference in potency (**Table 8.2**), but that it may also underlie the dissimilarity in their preference towards evoking a certain bias.

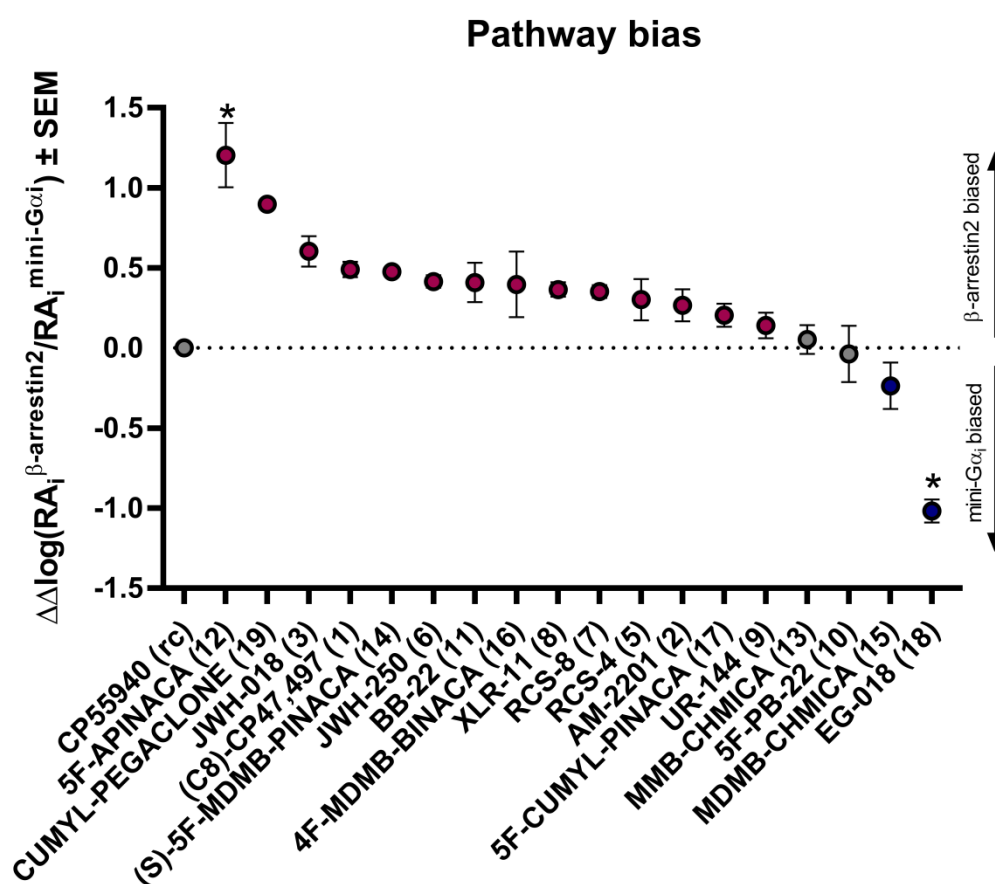


Figure 8.9 Pathway Bias with CP55,940 as the reference compound. The logarithmic ratio of the intrinsic relative activities of the β -arrestin2 over the mini- $G\alpha_i$ pathways for the selected SCRA are plotted. The (subtle) β -arrestin2 biased SCRA, the non-biased SCRA and the (subtle) mini- $G\alpha_i$ biased SCRA are depicted in red, grey and blue, respectively. Statistical analysis was performed with a Kruskal-Wallis test followed by the post hoc Dunn's multiple comparison test ($n = 3$, \pm SEM), * $p < 0.05$.

Consequently, two additional structural analogues of EG-018 (**18**) with a carbazole as core group, namely EG-2201 (**20**) and MDMB-CHMCZCA (**21**), were investigated. Both SCRA also displayed a tendency towards preferred G protein-mediated signaling (**Figure 8.10**), thus

confirming the aforementioned hypothesis that the carbazole group might have a role in preferentially evoking this signaling outcome.

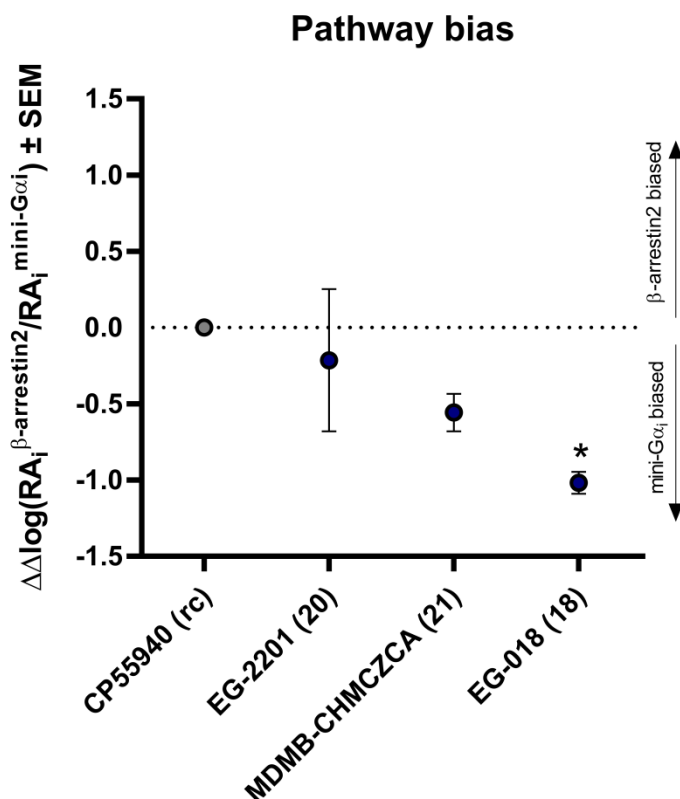


Figure 8.10 Pathway Bias with CP55,940 as the reference compound. The logarithmic ratio of the intrinsic relative activities of the β -arrestin2 over the mini-G α_i pathways for the selected SCRA scaffolds are plotted. The non-biased SCRA and the (subtle) mini-G α_i biased SCRA scaffolds are depicted in grey and blue, respectively. Statistical analysis was performed with a Kruskal-Wallis test followed by the post hoc Dunn's multiple comparison test ($n = 3$, \pm SEM), * $p < 0.05$.

Another visual representation of the pathway bias was generated by plotting the signal intensities (represented by AUCs) resulting from β -arrestin2 and mini-G α_i recruitment, relative to equimolar concentrations of CP55,940 (**Figure 8.11**). Distinct patterns can be observed in the resulting bias plots, allowing the SCRA scaffolds to be grouped into 6 classes (each represented in **Figure 8.11** and **Figure 8.12** in a different color). Also here, 5F-APINACA (**12**) and EG-018 (**18**) (as well as EG-2201 (**20**) and MDMB-CHMCZCA (**21**)) stand out as unique SCRA scaffolds, clearly displaying distinct shapes in the bias plot as compared to the remaining SCRA scaffolds (represented in **Figure 8.11** in dark pink and light blue, respectively). (C8)-CP47,497 (**1**), JWH-250 (**6**), BB-22 (**11**) and 5F-CUMYL-PINACA (**17**) display a similar pattern as (S)-5F-MDMB-PINACA (**14**) (depicted in green in **Figure 8.11**), all showing a subtle preference towards β -arrestin2 signaling. For JWH-018 (**3**), XLR-11 (**8**) and CUMYL-PEGACLONE (**19**), a similar pattern as for

AM-2201 (**2**) (depicted in purple in **Figure 8.11**) is observed. In addition, UR-144 (**9**), MDMB-CHMICA (**15**) and 4F-MDMB-BINACA (**16**) show a similar shape in the bias plot as MMB-CHMICA (orange) (**13**), showing at lower concentrations the same pattern as the non-biased compound, while at higher concentrations the curve subtly starts leaning towards preferred β -arrestin2 signaling. Finally, both RCS-4 (**5**), RCS-8 (**7**) and 5F-PB-22 (**10**) seem to display at lower concentrations a subtle preference towards mini- $G\alpha_i$, while favoring β -arrestin2 signaling at higher concentrations. Importantly, all these observations are relative to the reference compound CP55,940. Apart from the similar profiles for the carbazole-core-containing EG-018 (**18**), EG-2201 (**20**) and MDMB-CHMCZCA (**21**), no obvious structural features could be found that may underlie these distinct patterns. An overview of the bias plots of all SCRA, individually plotted together with the reference compound CP55,940, is given in **Figure 8.12**.

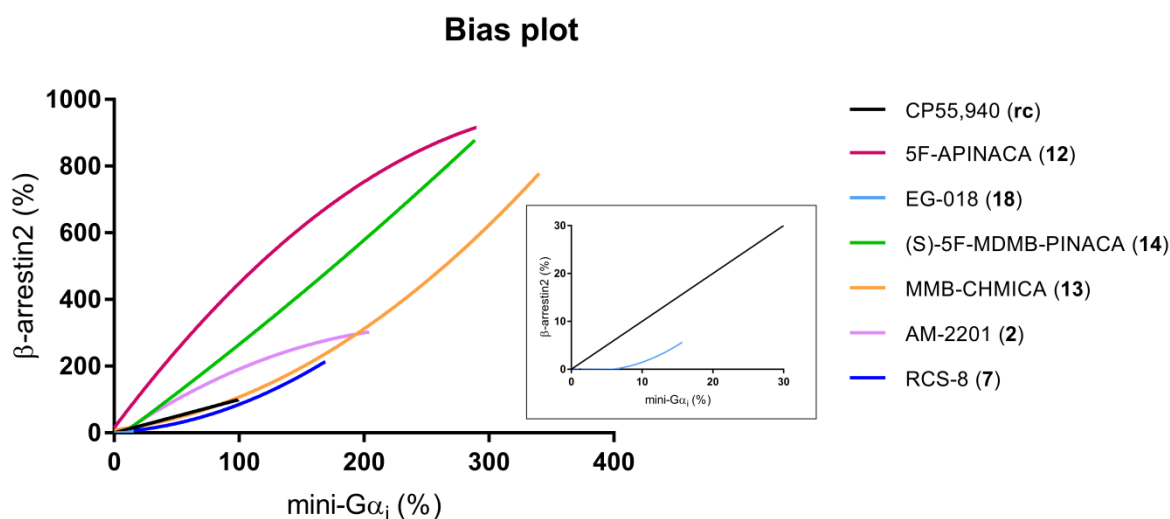


Figure 8.11 Bias plot. A visual representation of the pathway bias of a selected group of SCRA. The normalized AUCs (to CP55,940, depicted in black) of the SCRA in the β -arrestin2 bio-assay were plotted against the normalized AUCs in the mini- $G\alpha_i$ bio-assay. The SCRA 5F-APINACA (**12**), EG-018 (**18**), (S)-5F-MDMB-PINACA (**14**), MMB-CHMICA (**13**), AM-2201 (**2**) and RCS-8 (**7**) represent all the distinct patterns that were observed for the 21 investigated SCRA (depicted in dark pink, light blue, green, orange, purple and dark blue, respectively). A zoom-in of mini- $G\alpha_i$ -biased EG-018 (**18**) (depicted in light blue) is provided. Curves were fitted using the centered second order polynomial (quadratic) fitting.

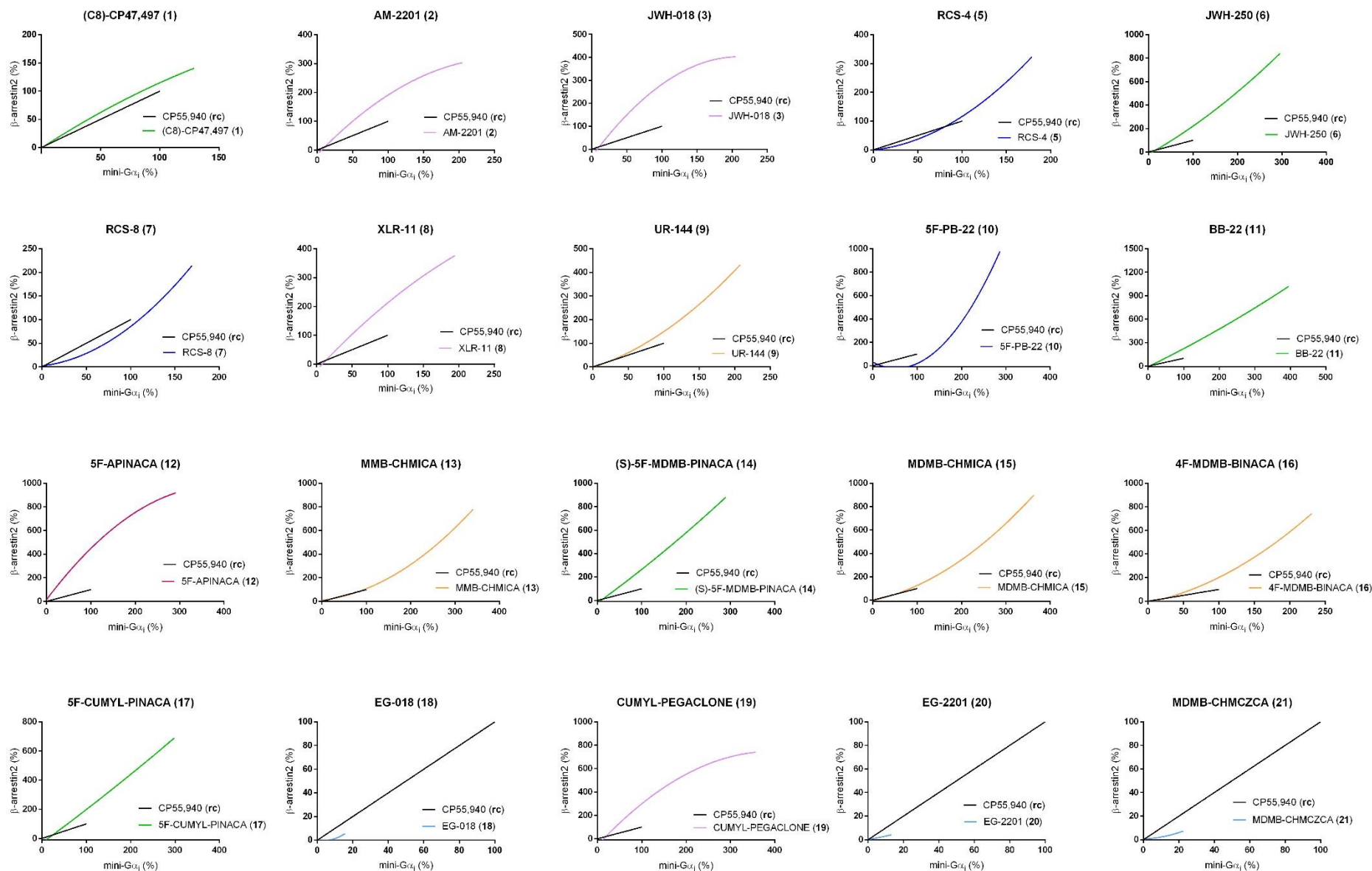


Figure 8.12 A Individual Bias plots of the screened SCRA's with CP55,940 as the non-biased reference compound. All SCRA's are grouped into 6 classes (visualized in green, purple, dark blue, dark pink, orange and light blue), dependent on the similarity of the observed pattern in the bias plot.

Pathway bias (rc = JWH-018)

As mentioned earlier, for both CP55,940 and JWH-018 (**3**) similar EC_{50} and E_{max} values were observed in both bio-assays (see section 8.3.2) and therefore both compounds could serve as balanced reference compounds within these experimental set-ups. To verify the impact of choosing another compound as a reference, we also evaluated the pathway bias (**Figure 8.13**) and generated bias plots (**Figure 8.15**) with JWH-018 as the reference compound. By doing so, the pathway bias showed an overall shift towards mini- $G\alpha_i$ -biasedness, as expected. Nonetheless, the overall order, ranging from subtle β -arrestin2-biased (i.e. 5F-APINACA (**12**)) towards significant mini- $G\alpha_i$ -biased (i.e. EG-018 (**18**) and MDMB-CHMCZCA (**21**)), remains similar. For (C8)-CP47,497 (**1**) and AM-2201 (**2**) a milder shift, although not substantial, could be observed. This might be explained by the fact that the observed bias factors for these compounds are generally low and the applied correction factors may have had a more pronounced effect in these cases. Somewhat surprisingly, EG-2201 (**20**) made a substantial shift to the left, no longer clustering with EG-018 (**18**) and MDMB-CHMCZCA (**21**). A review of the raw data revealed that this shift was primarily driven by a different impact on the E_{max} of EG-2201 (**20**) in the distinct bio-assays when using JWH-018 rather than CP55,940 as a reference compound.

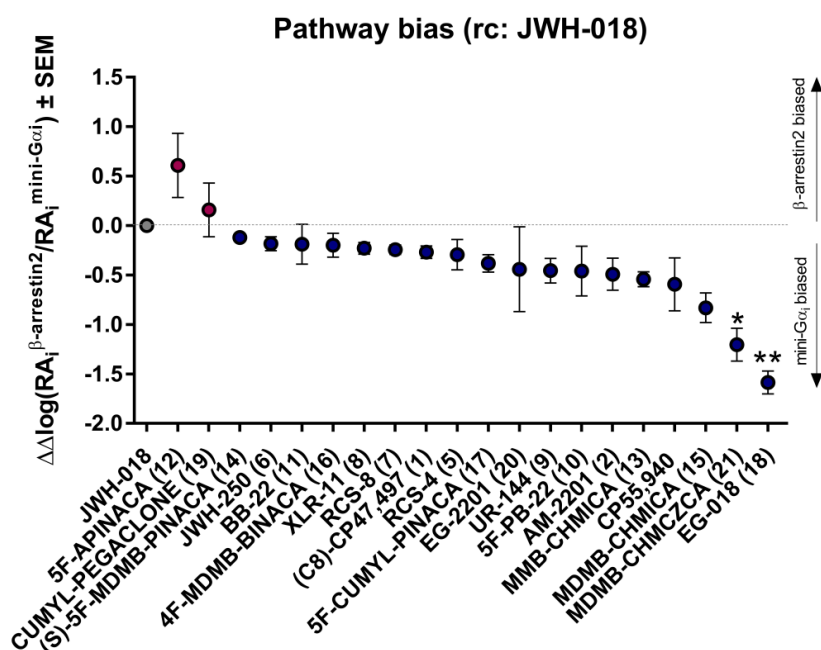


Figure 8.13 Pathway bias with JWH-018 (**3**) as a reference compound. The logarithmic ratio of the intrinsic relative activities of the β -arrestin2 (β -arr2) over the mini- $G\alpha_i$ pathways for the selected SCRA are plotted. The (subtle) β -arrestin2 biased SCRA, the non-biased with the reference compound and the (subtle) mini- $G\alpha_i$ biased SCRA are depicted in red, grey and blue respectively. Statistical analysis was performed with a Kruskal-Wallis test followed by the post hoc Dunn's multiple comparison test ($n = 3$, \pm SEM), * $p < 0.05$, ** $p < 0.01$.

With JWH-018 as the reference compound, overall lower efficacy values are observed, with a maximum of 3-fold higher as compared to JWH-018 (arbitrarily set as 100%)(**Figure 8.14**). Nevertheless, similarly as with CP55,940 as the reference compound, also here a wider dynamic range in E_{\max} values for the β -arrestin2 bio-assay as compared to the mini- $G\alpha_i$ bio-assay was observed.

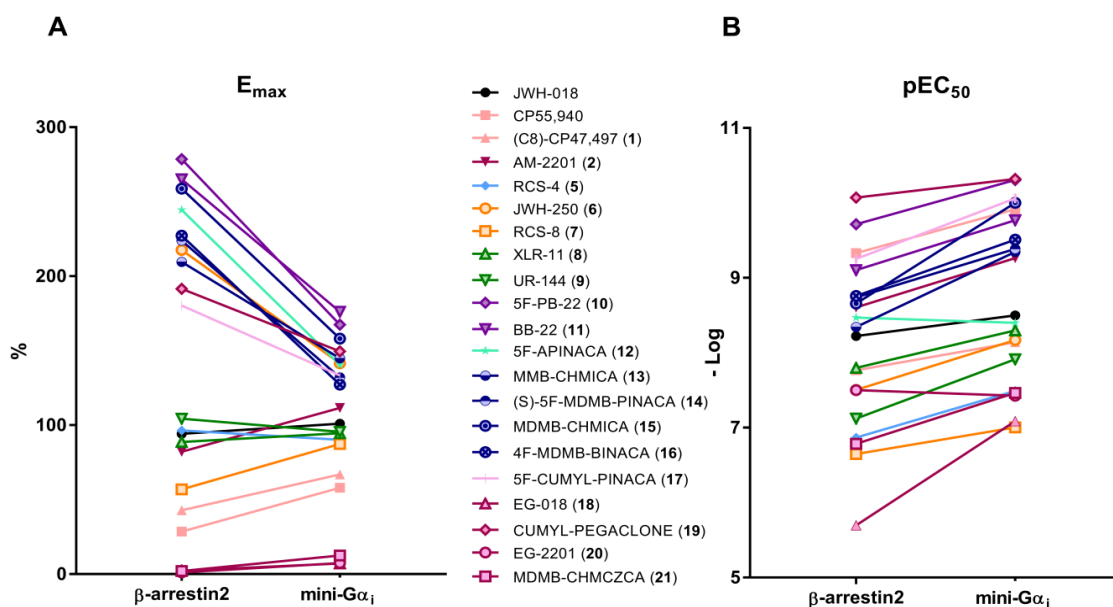


Figure 8.14 Comparison of the E_{\max} values (%) relative to the reference compound (rc) JWH-018 (arbitrarily set as 100%) (A) and pEC_{50} values (B) of the 21 SCRA's screened in the β -arrestin2 NanoBiT[®] bio-assay versus the mini- $G\alpha_i$ NanoBiT[®] bio-assay (n=3).

Finally, in the bias plot with JWH-018 as the reference compound, only 5F-APINACA (**12**) shows a subtle β -arrestin2-bias, whereas all the other SCRA's prefer mini- $G\alpha_i$ signaling (**Figure 8.15**).

Individual bias plots are depicted in **Figure 8.16**.

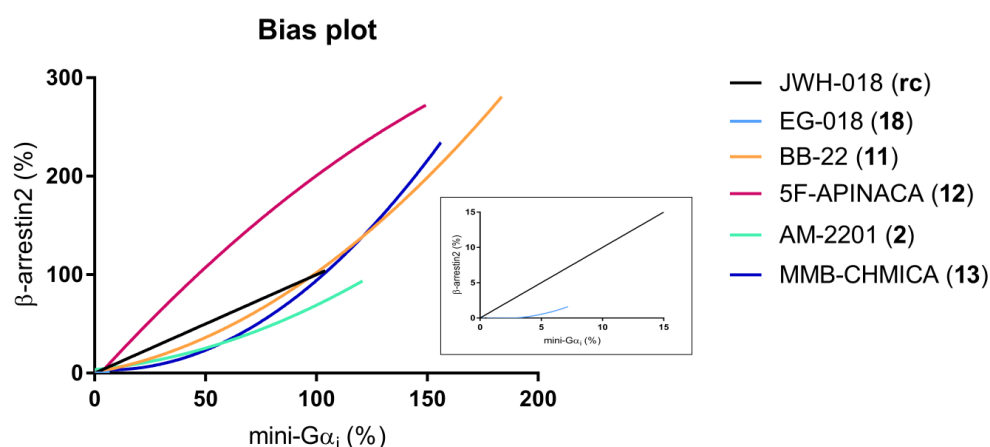


Figure 8.15 Bias plot. A visual representation of the pathway bias of a selected group of SCRA's. The normalized AUCs (to JWH-018, depicted in black) of the SCRA's in the β -arrestin2 bio-assay were plotted against the normalized AUCs in the mini- $G\alpha_i$ bio-assay. The SCRA's EG-018 (**18**), BB-22 (**11**), 5F-APINACA (**12**), AM-2201 (**2**) and MMB-CHMICA (**13**) represent all the distinct patterns that were observed for the 21 SCRA's (depicted in light blue, orange, dark pink, green and dark blue, respectively). An inset of mini- $G\alpha_i$ -biased EG-018 (**18**) (depicted in light blue) is provided. Curves were fitted using the centered second order polynomial (quadratic) fitting.

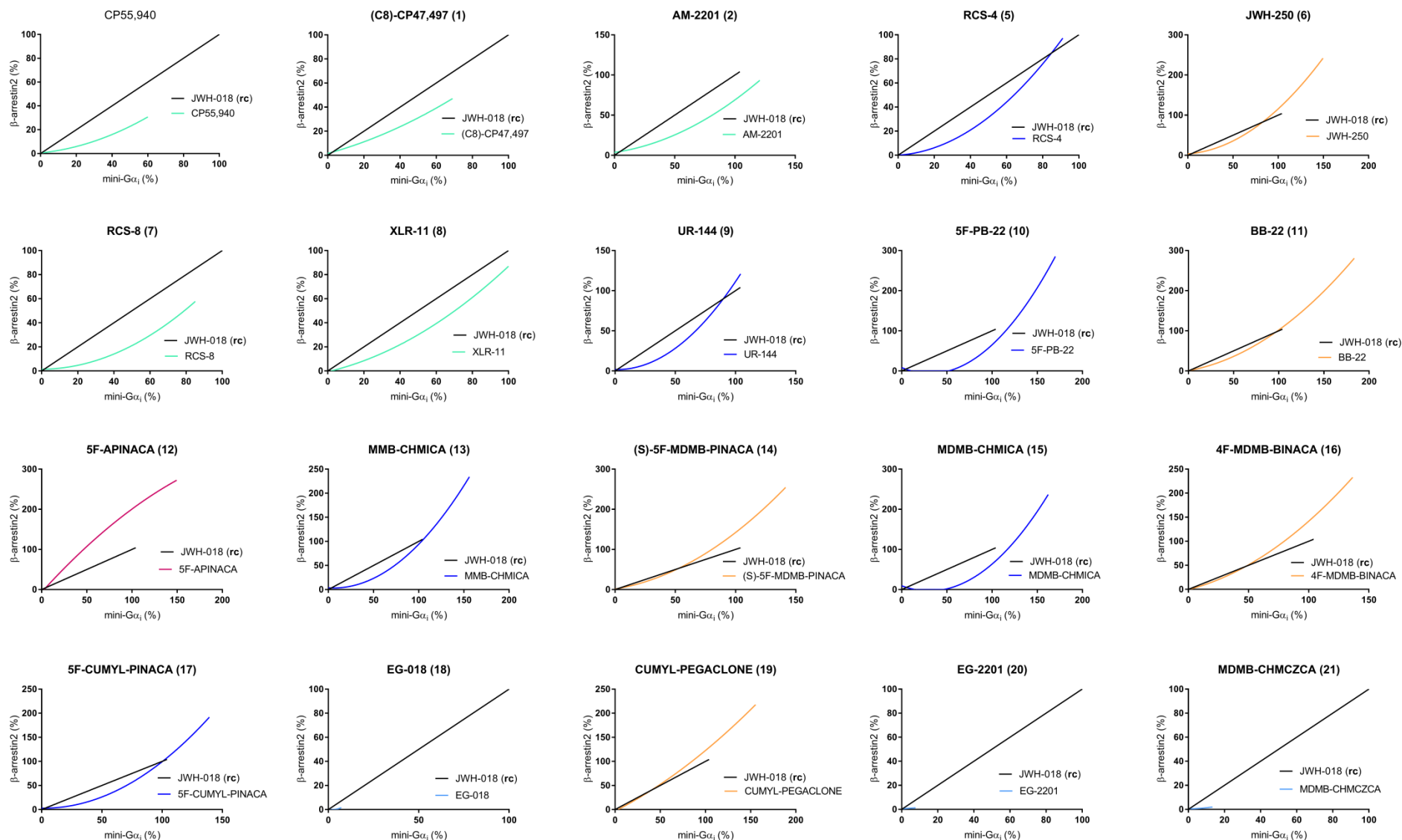


Figure 8.16 A Individual Bias plots of the screened SCRA with JWH-018 as the non-biased reference compound. All SCRA are grouped into 5 classes – which slightly differ from the patterns with CP55,940 as the reference compound – (visualized in green, dark blue, dark pink, orange and light blue), dependent on the similarity of the observed pattern in the bias plot.

compound reached its maximum response. Statistical analysis was performed with a Kruskal-Wallis test followed by the post hoc Dunn's multiple comparison test ($n = 3$, \pm SEM), $^{**}p < 0.01$.

Since overall only minor changes were observed when comparing pathway bias at the maximum luminescence level and 30 minutes thereafter, we consider it more plausible that these changes are due to the experimental approach, rather than to true temporal bias. Nevertheless we consider it useful to also evaluate in future research the potential presence of a temporal bias for SCRA.

7.4 Conclusions

Using two distinct but highly analogous bio-assays, SCRA-induced recruitment of β -arrestin2 versus recruitment of a mini- $G\alpha_i$ protein to CB_1 was assessed. The CB_1 receptor has emerged as a promising target for the treatment of several diseases, including obesity and neuropathic pain [5, 64]. Although tremendous efforts have been undertaken to develop therapeutic compounds, these compounds have shown to cause psychoactive side effects, hampering their therapeutic utility. Upon ligand binding, distinct conformational changes are induced in CB_1 , which will subsequently lead to distinct intracellular – whether desired or undesired – signaling pathways. Within this context, this is the first study that reports on the screening for ligand bias in an extended panel of SCRA scaffolds, chosen to cover a broad diversity of chemical structures. For the first time, this was achieved by using two distinct bio-assays in a consistent cellular context (HEK293T cells stably expressing the same CB_1 construct in both assays), by applying the same assay principle (luminescence following functional complementation of a split-luciferase) and by investigating CB_1 activation at the same level of signal transduction proximal to the receptor, i.e. to avoid potentially skewed results due to differences in signal amplification. Application of this approach might contribute to the understanding of how specific chemical structures preferentially or exclusively activate specific signaling pathways.

Several general conclusions can readily be drawn from the concentration-response curves observed in both bio-assays. First, the newer-generations of SCRA, being CUMYL-PEGACLONE (**19**), (S)-5F-MDMB-PINACA (**14**), 5F-CUMYL-PINACA (**17**), 5F-PB-22 (**10**) and BB-22 (**11**) (first reported during 2013-2016), are more potent than earlier-stage SCRA, such as RCS-4 (**5**), RCS-

8 (**7**) and JWH-250 (**6**) (first reported in 2009-2012). This is in agreement with the previously described structural evolution of SCRA scaffolds [65-68].

Second, the reported beneficial effect of fluorination of the aliphatic tail for the overall activity of the compound [69] was observed for JWH-018 (**3**) (EC_{50} mini- $G\alpha_i$: 3.23 nM and EC_{50} β -arrestin2: 5.57 nM) and its 5F-variant AM-2201 (**2**) (EC_{50} mini- $G\alpha_i$: 0.60 nM and EC_{50} β -arrestin2: 1.64 nM), but also for UR-144 (**9**) (EC_{50} mini- $G\alpha_i$: 12.2 nM and EC_{50} β -arrestin2: 75.6 nM) and its 5F-variant XLR-11 (**8**) (EC_{50} mini- $G\alpha_i$: 5.04 nM and EC_{50} β -arrestin2: 16.0 nM).

Third, SCRA scaffolds with a lower potency, including EG-018 (**18**) and EG-2201 (**20**) (mini- $G\alpha_i$ EC_{50} : 15.3 – 76.5 nM, β -arrestin2 EC_{50} : 31.5 – 2012 nM), do not contain the hydrogen-bonding group that mediates an interaction with S383^{7,39}, which is beneficial for CB₁ activation [51]. In contrast, the most potent SCRA scaffolds of the screened panel, 5F-APINACA (**12**) and CUMYL-PEGACLONE (**19**) (mini- $G\alpha_i$ EC_{50} : 0.07 – 3.98 nM, β -arrestin2 EC_{50} : 0.09 – 3.39 nM), do possess an oxygen group in the key position to establish a hydrogen bonding network with water molecules and S383^{7,39}, as confirmed by molecular docking in this study.

Our screening of a selection of twenty-one SCRA scaffolds with a diverse palette of chemical structures, using both recruitment-based bio-assays, revealed an overall subtle preference for the β -arrestin2 recruitment, with 5F-APINACA being the only SCRA that showed a significant β -arrestin2 biased agonism (16-fold preference as compared to the reference compound CP55,940). In addition, certain SCRA scaffolds, such as MMB-CHMICA, showed a more balanced profile, whereas the carbazole-core-containing EG-018 showed a pronounced 10-fold preference towards mini- $G\alpha_i$ over β -arrestin2 recruitment. Interestingly, a potential role for this carbazole core in imposing a bias towards mini- $G\alpha_i$ was confirmed by two other carbazole-core-containing compounds, EG-2201 and MDMB-CHMICA. It should be noted that suboptimal fitting of concentration-response curves of these 3 partial agonists may affect the bias factors, primarily by an impact on the calculated EC_{50} values. Ideally, the bias of these compounds should be confirmed by the operational model by Black and Leff, in which inclusion of the dissociation constant could result in an even better estimation of the bias factor [50]. The potential issue of suboptimal fitting of the concentration-response curve does not hold true for the highly potent β -arrestin2-biased 5F-APINACA, and thus in the used experimental set-up we can consider 5F-APINACA as a SCRA showing true biased agonism.

Importantly, in our case study, upon using a threshold of 10-fold bias relative to CP55,940, the overall prevalence of bias among the selected SCRA is 10% (2 out of 21 tested compounds), whereas if the threshold is modified to a threefold bias, the prevalence shifts towards 67%. This highlights the importance of unraveling what a significant level of bias factor is to provoke a relevant biological *in vivo* effect. Interestingly, but not surprisingly, the percentage of observed bias slightly alters when selecting another reference compound. For example, using JWH-018 as the non-biased reference compound, and in this case a bias prevalence of 10% and 52% was observed (using a threshold of 10-fold and 3-fold, respectively). With this study new insights have been gathered into the preferred recruitment of β -arrestin2 or $G\alpha_i$ -protein to CB₁ using highly analogous *in vitro* screening assays. Yet, still, one should keep in mind that even in a given cell system one assay may be favoured over the other because of issues such as receptor reserve or context-dependent efficacy (e.g. presence and expression level of GRKs), different transducer dynamics among others [42]. Thus, as the 'ideal' *in vitro* assay, which is not subject to underlying misleading factors, does not yet exist, the outcomes concerning the prevalence of biased signaling amongst SCRA need to be considered as an indication and should be further investigated, ideally in an *in vivo* setting.

Moreover, biased signaling is a complex phenomenon that not only involves spatiotemporal dependent signaling [63] but also involves dynamic underlying mechanisms, such as prolonged signaling in endosomes or ligand-specific endocytic dwell times [70, 71]. The latter mentioned encompasses ligand-mediated prolonged β -arrestin signaling by preventing endocytosis. Overall, to further reveal the underlying mechanism(s) of ligand-induced activation and the subsequent activated signaling pathway(s) of CB₁, biological assays screening for a broader set of cannabinoid ligands or a broader set of signaling pathways (i.e. simultaneous investigation of the recruitment of distinct transducers: β -arrestin1, β -arrestin2, $G\alpha_i$, $G\alpha_s$ and $G\alpha_o$) might help. Also concerted in-depth studies involving computational modeling, site-directed mutagenesis, unraveling ligand-GPCR-transducer structures and spectroscopic techniques are a prerequisite. In the end, this should allow a better understanding of biased agonism at CB₁.

References

1. Devane, W.A., et al., *Determination and characterization of a cannabinoid receptor in rat brain*. Molecular pharmacology, 1988. **34**(5): p. 605-13.
2. Pertwee, R.G., *Pharmacology of cannabinoid CB1 and CB2 receptors*. Pharmacology & therapeutics, 1997. **74**(2): p. 129-80.
3. Pertwee, R.G., *Receptors and channels targeted by synthetic cannabinoid receptor agonists and antagonists*. Current medicinal chemistry, 2010. **17**(14): p. 1360-81.
4. Engeli, S., *Central and peripheral cannabinoid receptors as therapeutic targets in the control of food intake and body weight*. Handb. Exp. Pharmacol., 2012(209): p. 357-81.
5. Kogan, N.M. and R. Mechoulam, *Cannabinoids in health and disease*. Dialogues Clin. Neurosci., 2007. **9**(4): p. 413-30.
6. Sink, K.S., et al., *The novel cannabinoid CB1 receptor neutral antagonist AM4113 suppresses food intake and food-reinforced behavior but does not induce signs of nausea in rats*. Neuropsychopharmacology : official publication of the American College of Neuropsychopharmacology, 2008. **33**(4): p. 946-55.
7. Giuffrida, A. and L.R. McMahon, *In vivo pharmacology of endocannabinoids and their metabolic inhibitors: therapeutic implications in Parkinson's disease and abuse liability*. Prostaglandins & other lipid mediators, 2010. **91**(3-4): p. 90-103.
8. More, S.V. and D.K. Choi, *Promising cannabinoid-based therapies for Parkinson's disease: motor symptoms to neuroprotection*. Molecular neurodegeneration, 2015. **10**: p. 17.
9. Ujike, H., et al., *CNR1, central cannabinoid receptor gene, associated with susceptibility to hebephrenic schizophrenia*. Molecular psychiatry, 2002. **7**(5): p. 515-8.
10. Hungund, B.L., et al., *Upregulation of CB1 receptors and agonist-stimulated [35S]GTPgammaS binding in the prefrontal cortex of depressed suicide victims*. Molecular psychiatry, 2004. **9**(2): p. 184-90.
11. Moreno, E., et al., *The Endocannabinoid System as a Target in Cancer Diseases: Are We There Yet?* Front. Pharmacol., 2019. **10**: p. 339.
12. Ignatowska-Jankowska, B.M., et al., *A Cannabinoid CB1 Receptor-Positive Allosteric Modulator Reduces Neuropathic Pain in the Mouse with No Psychoactive Effects*. Neuropsychopharmacology : official publication of the American College of Neuropsychopharmacology, 2015. **40**(13): p. 2948-59.
13. Shekhar, A. and G.A. Thakur, *Cannabinoid Receptor 1 Positive Allosteric Modulators for Posttraumatic Stress Disorder*. Neuropsychopharmacology : official publication of the American College of Neuropsychopharmacology, 2018. **43**(1): p. 226-227.
14. De Aquino, J.P., et al., *The Psychiatric Consequences of Cannabinoids*. Clinical therapeutics, 2018. **40**(9): p. 1448-1456.
15. Moreira, F.A., M. Grieb, and B. Lutz, *Central side-effects of therapies based on CB1 cannabinoid receptor agonists and antagonists: focus on anxiety and depression*. Best practice & research. Clinical endocrinology & metabolism, 2009. **23**(1): p. 133-44.
16. Howlett, A.C., et al., *Cannabinoid physiology and pharmacology: 30 years of progress*. Neuropharmacology, 2004. **47 Suppl 1**: p. 345-58.
17. Finlay, D.B., et al., *Galphas signalling of the CB1 receptor and the influence of receptor number*. British journal of pharmacology, 2017. **174**(15): p. 2545-2562.
18. Laprairie, R.B., A.M. Bagher, and E.M. Denovan-Wright, *Cannabinoid receptor ligand bias: implications in the central nervous system*. Curr. Opin. Pharmacol., 2017. **32**: p. 32-43.
19. Mallipeddi, S., et al., *Functional selectivity at G-protein coupled receptors: Advancing cannabinoid receptors as drug targets*. Biochem. Pharmacol., 2017. **128**: p. 1-11.
20. Gyombolai, P., et al., *Differential beta-arrestin2 requirements for constitutive and agonist-induced internalization of the CB1 cannabinoid receptor*. Molecular and cellular endocrinology, 2013. **372**(1-2): p. 116-27.

21. Delgado-Peraza, F., et al., *Mechanisms of Biased beta-Arrestin-Mediated Signaling Downstream from the Cannabinoid 1 Receptor* (vol 89, pg 618, 2016). Mol. Pharmacol., 2016. **90**(1): p. 62-62.
22. Laprairie, R.B., et al., *Biased Type 1 Cannabinoid Receptor Signaling Influences Neuronal Viability in a Cell Culture Model of Huntington Disease*. Mol. Pharmacol., 2016. **89**(3): p. 364-75.
23. Bakshi, K., R.W. Mercier, and S. Pavlopoulos, *Interaction of a fragment of the cannabinoid CB1 receptor C-terminus with arrestin-2*. FEBS Lett., 2007. **581**(25): p. 5009-5016.
24. Singh, S.N., et al., *Binding between a Distal C-Terminus Fragment of Cannabinoid Receptor 1 and Arrestin-2*. Biochemistry, 2011. **50**(12): p. 2223-2234.
25. Bangasser, D.A., et al., *Corticotropin-releasing factor overexpression gives rise to sex differences in Alzheimer's disease-related signaling*. Molecular psychiatry, 2017. **22**(8): p. 1126-1133.
26. Kenakin, T. and A. Christopoulos, *Signalling bias in new drug discovery: detection, quantification and therapeutic impact*. Nature reviews. Drug discovery, 2013. **12**(3): p. 205-16.
27. Smith, J.S., R.J. Lefkowitz, and S. Rajagopal, *Biased signalling: from simple switches to allosteric microprocessors*. Nat. Rev. Drug. Discov., 2018. **17**(4): p. 243-260.
28. Yang, Y., et al., *D1 dopamine receptors intrinsic activity and functional selectivity affect working memory in prefrontal cortex*. Molecular psychiatry, 2018.
29. Donthamsetti, P., et al., *Arrestin recruitment to dopamine D2 receptor mediates locomotion but not incentive motivation*. Mol. Psychiatry, 2018.
30. Lotta, L.A., et al., *Human Gain-of-Function MC4R Variants Show Signaling Bias and Protect against Obesity*. Cell, 2019. **177**(3): p. 597-607 e9.
31. Bonifazi, A., et al., *Novel and Potent Dopamine D2 Receptor Go-Protein Biased Agonists*. ACS Pharmacol Transl Sci, 2019. **2**(1): p. 52-65.
32. Park, S.M., et al., *Effects of beta-Arrestin-Biased Dopamine D2 Receptor Ligands on Schizophrenia-Like Behavior in Hypoglutamatergic Mice*. Neuropsychopharmacology : official publication of the American College of Neuropsychopharmacology, 2016. **41**(3): p. 704-15.
33. Rose, S.J., et al., *Engineered D2R Variants Reveal the Balanced and Biased Contributions of G-Protein and beta-Arrestin to Dopamine-Dependent Functions*. Neuropsychopharmacology : official publication of the American College of Neuropsychopharmacology, 2018. **43**(5): p. 1164-1173.
34. DeWire, S.M., et al., *A G protein-biased ligand at the mu-opioid receptor is potently analgesic with reduced gastrointestinal and respiratory dysfunction compared with morphine*. J. Pharmacol. Exp. Ther., 2013. **344**(3): p. 708-17.
35. Schmid, C.L., et al., *Bias Factor and Therapeutic Window Correlate to Predict Safer Opioid Analgesics*. Cell, 2017. **171**(5): p. 1165-1175 e13.
36. Valentino, R.J. and N.D. Volkow, *Untangling the complexity of opioid receptor function*. Neuropsychopharmacology : official publication of the American College of Neuropsychopharmacology, 2018. **43**(13): p. 2514-2520.
37. Ford, B.M., et al., *Characterization of structurally novel G protein biased CB1 agonists: Implications for drug development*. Pharmacol. Res., 2017. **125**(Pt B): p. 161-177.
38. Nguyen, P.T., et al., *beta-arrestin2 regulates cannabinoid CB1 receptor signaling and adaptation in a central nervous system region-dependent manner*. Biological psychiatry, 2012. **71**(8): p. 714-24.
39. Raehal, K.M. and L.M. Bohn, *beta-arrestins: regulatory role and therapeutic potential in opioid and cannabinoid receptor-mediated analgesia*. Handbook of experimental pharmacology, 2014. **219**: p. 427-43.
40. Al-Zoubi, R., P. Morales, and P.H. Reggio, *Structural Insights into CB1 Receptor Biased Signaling*. Int. J. Mol. Sci., 2019. **20**(8).
41. Khajehali, E., et al., *Biased Agonism and Biased Allosteric Modulation at the CB1 Cannabinoid Receptor*. Molecular pharmacology, 2015. **88**(2): p. 368-79.

42. Wouters, E., et al., *Insights into biased signaling at cannabinoid receptors: synthetic cannabinoid receptor agonists*. Submitted, 2019.
43. Cannaert, A., et al., *Activity-based detection of cannabinoids in serum and plasma samples*. Clin. Chem., 2018. **64**(6): p. 918-926.
44. Wouters, E., et al., *Functional evaluation of carboxy metabolites of synthetic cannabinoid receptor agonists featuring scaffolds based on L-valine or L-tert-leucine*. Drug Test. Anal., 2019.
45. Cannaert, A., et al., *Detection and Activity Profiling of Synthetic Cannabinoids and Their Metabolites with a Newly Developed Bioassay*. Anal. Chem., 2016. **88**(23): p. 11476-11485.
46. Nehme, R., et al., *Mini-G proteins: Novel tools for studying GPCRs in their active conformation*. PLoS one, 2017. **12**(4): p. e0175642.
47. Wan, Q.W., et al., *Mini G protein probes for active G protein-coupled receptors (GPCRs) in live cells*. Journal of biological chemistry, 2018. **293**(19): p. 7466-7473.
48. Cannaert, A., et al., *Activity-based detection of consumption of synthetic cannabinoids in authentic urine samples using a stable cannabinoid reporter system*. Anal. Chem., 2017. **89**(17): p. 9527-9536.
49. Storme, J., et al., *Probing structure-activity relationship in beta-arrestin2 recruitment of diversely substituted adenosine derivatives*. Biochemical pharmacology, 2018. **158**: p. 103-113.
50. Rajagopal, S., et al., *Quantifying ligand bias at seven-transmembrane receptors*. Molecular pharmacology, 2011. **80**(3): p. 367-77.
51. Krishna Kumar, K., et al., *Structure of a signaling cannabinoid receptor 1-G protein complex*. Cell, 2019. **176**(3): p. 448-458 e12.
52. Friesner, R.A., et al., *Extra precision glide: docking and scoring incorporating a model of hydrophobic enclosure for protein-ligand complexes*. Journal of medicinal chemistry, 2006. **49**(21): p. 6177-96.
53. Carpenter, B. and C.G. Tate, *Expression, Purification and Crystallisation of the Adenosine A2A Receptor Bound to an Engineered Mini G Protein*. Bio-Protocol, 2017. **7**(8).
54. Weis, W.I. and B.K. Kobilka, *The Molecular Basis of G Protein-Coupled Receptor Activation*. Annual review of biochemistry, 2018. **87**: p. 897-919.
55. Ballesteros, J.A. and H. Weinstein, *Integrated methods for the construction of three-dimensional models and computational probing of structure-function relations in G protein-coupled receptors*. Methods in neurosciences, 1995. **25**(ed. Stuart, C.S.): p. 366-428.
56. Hua, T., et al., *Crystal structures of agonist-bound human cannabinoid receptor CB1*. Nature, 2017. **547**(7664): p. 468-471.
57. Bow, E.W. and J.M. Rimoldi, *The Structure-Function Relationships of Classical Cannabinoids: CB1/CB2 Modulation*. Perspectives in medicinal chemistry, 2016. **8**: p. 17-39.
58. Noble, C., et al., *Application of an activity-based receptor bioassay to investigate the in vitro activity of selected indole- and indazole-3-carboxamide-based synthetic cannabinoids at CB1 and CB2 receptors*. Drug testing and analysis, 2018.
59. Haubrich, D.R., et al., *Pharmacology of pravadoline: a new analgesic agent*. The Journal of pharmacology and experimental therapeutics, 1990. **255**(2): p. 511-22.
60. Banister, S.D. and M. Connor, *The Chemistry and Pharmacology of Synthetic Cannabinoid Receptor Agonist New Psychoactive Substances: Evolution*. Handb. Exp. Pharmacol., 2018.
61. Sachdev, S., et al., *In vitro determination of the CB1 efficacy of illicit synthetic cannabinoids*. bioRxiv, 2018: p. 385583.
62. Smith, J.S. and S. Rajagopal, *The beta-Arrestins: Multifunctional Regulators of G Protein-coupled Receptors*. The Journal of biological chemistry, 2016. **291**(17): p. 8969-77.
63. Grundmann, M. and E. Kostenis, *Temporal Bias: Time-Encoded Dynamic GPCR Signaling*. Trends in pharmacological sciences, 2017. **38**(12): p. 1110-1124.
64. Pacher, P., S. Batkai, and G. Kunos, *The endocannabinoid system as an emerging target of pharmacotherapy*. Pharmacol. Rev., 2006. **58**(3): p. 389-462.
65. Graddy, R., M.E. Buresh, and D.A. Rastegar, *New and Emerging Illicit Psychoactive Substances*. The Medical clinics of North America, 2018. **102**(4): p. 697-714.

66. Hess, C., et al., *Pharmacological evaluation of synthetic cannabinoids identified as constituents of spice*. Forensic toxicology, 2016. **34**: p. 329-343.
67. Zanda, M.T. and L. Fattore, *Old and new synthetic cannabinoids: lessons from animal models*. Drug metabolism reviews, 2018. **50**(1): p. 54-64.
68. European Monitoring Centre for Drugs and Drug Addiction (EMCDDA). European Drug Report 2018: Trends and Developments, Publications Office of the European Union, Luxembourg. 2018.
69. Gurney, S.M., et al., *Pharmacology, toxicology, and adverse effects of synthetic cannabinoid drugs*. Forensic science review, 2014. **26**(1): p. 53-78.
70. Flores-Otero, J., et al., *Ligand-specific endocytic dwell times control functional selectivity of the cannabinoid receptor 1*. Nature communications, 2014. **5**: p. 4589.
71. Irannejad, R., et al., *Conformational biosensors reveal GPCR signalling from endosomes*. Nature, 2013. **495**(7442): p. 534-8.

Chapter 9:

Functional evaluation of carboxy metabolites of synthetic cannabinoid receptor agonists featuring scaffolds based on L-valine or L-*tert*-leucine.

Based on

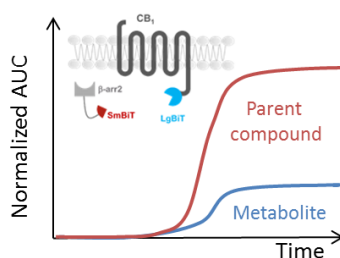
Elise Wouters, Lukas Mogler, Annelies Canaert, Volker Auwärter and Christophe Stove. (2019) Functional evaluation of carboxy metabolites of synthetic cannabinoid receptor agonists featuring scaffolds based on L-valine or L-*tert*-leucine. *Drug Testing and Analysis*. 2019.

ABSTRACT

Indole and indazole-based synthetic cannabinoid receptor agonists (SCRAs), featuring valine or *tert*-leucine substituents, are commonly abused new psychoactive substances (NPS). A major metabolic pathway for these SCRAs is hydrolysis of the terminal amide or methylester functionalities. Although these hydrolysis products were already detected as main ingredients in some ‘legal highs’, these metabolites are often poorly characterized. Here, we report a systematic investigation of the activity of seven common hydrolysis metabolites of fifteen SCRAs featuring scaffolds based on L-valine or L-*tert*-leucine in direct comparison to their parent compounds. An activity-based cannabinoid receptor 1 (CB₁) bio-assay was used for activity profiling of SCRAs and their metabolites in a stable HEK293T cell system. The recruitment of β -arrestin2 to the activated CB₁ (each fused to one part of a split Nanoluciferase) was provoked by adding the (putative) SCRAs. Luminescence of the functionally complemented luciferase was monitored by a 96-well plate-reader. The major hydrolysis metabolites of 5F-AB-PINACA, ADB-CHMICA, ADB-CHMINACA, ADB-FUBICA, and their methyl- and ethylester derivatives showed no detectable CB₁ activation at concentrations up to 1 μ M. On the other hand, metabolites of 5F-ADB-PINACA, AB-CHMINACA and ADB-FUBINACA did retain activity, although significantly reduced as compared to the parent compounds (EC₅₀ values > 100 nM). Activity-based characterization of SCRAs and their metabolites at CB₁ may not only allow a better insight into the complex interplay between SCRAs and their metabolites in intoxications, but may also allow to apply the concept of ‘activity equivalents’ present in biological fluids or, alternatively, in confiscated materials.

GRAPHICAL ABSTRACT

The implementation of an activity-based cannabinoid receptor 1 bio-assay for the activity profiling of 15 SCRAs and their common hydrolysis metabolites revealed that metabolites did retain activity, although significantly reduced as compared to the parent compounds. As the efficacy of certain metabolites is still higher than that of JWH-018, these metabolites could potentially contribute to the overall pharmacological or toxicological response *in vivo*.



Functional evaluation of carboxy metabolites of synthetic cannabinoid receptor agonists featuring scaffolds based on L-valine or L-*tert*-leucine

Elise Wouters, Lukas Mogler, Annelies Caninaert, Volker Auwärter and Christophe Stove*

9.1 Introduction

During the last decade, new psychoactive substances (NPS) have emerged on the illicit drug market, with synthetic cannabinoid receptor agonists (SCRA) being the most prominent class in Europe [1]. SCRA are man-made substances that exert their effects through binding to two G-protein coupled receptors (GPCRs), namely cannabinoid receptors 1 (CB₁) and 2 (CB₂) [2, 3]. CB₁ receptors are primarily located in the central nervous system (the brain and spinal cord) and mediate the psychotropic effect of cannabis (alternatives), whereas CB₂ receptors are mostly expressed in the peripheral nervous system, the spleen and the immune system and are involved in immunosuppression and pain perception mediation [4, 5].

Synthetic cannabimimetics, which mimic the actions of endogenous and natural compounds acting on the cannabinoid receptors, are often far more potent than the main psychoactive substance found in cannabis, delta-9-tetrahydrocannabinol (Δ^9 -THC). The intake of these highly potent drugs of abuse has caused considerable morbidity and mortality in the United States, Europe and Japan, as well as in many other countries [6-8]. Observed adverse effects include agitation, hypertension, acute kidney injury and tachycardia and may even result in fatalities [9-16].

As xenobiotics, SCRA undergo extensive metabolism and clearance, mainly by the liver, to remove these substances from the human body. The goal of drug metabolism is to detoxify potentially harmful compounds and excrete them from the body. In certain cases, bioactivation of these compounds, which might lead or contribute to toxicological effects, has been reported. For example, major hydroxylated metabolites of JWH-018 and AM-2201 retained full agonist activity at nanomolar concentrations [17, 18].

Although hydroxylation of the pentyl side chain of SCRA is a common metabolism pathway, the major pathway for SCRA featuring scaffolds based on L-valine and L-*tert*-leucine involves amide hydrolysis of the L-valinamide or L-*tert*-leucinamide functional groups [19-21] or methyl- or ethylester hydrolysis of L-valinate or L-*tert*-leucinate groups [22, 23]. Hydrolysis of the terminal functionality is more pronounced for compounds containing an L-valinate or L-*tert*-leucinate group compared to their amide analogs, due to the more metabolically labile characteristic of the methylester functionality [24]. The enzyme responsible for the biotransformation of the primary amide moiety, resulting in major carboxylic acid metabolites,

was identified in human liver microsomes (HLMs) as carboxylesterase 1 (CES1) [23, 24]. In addition to a transformation catalyzed by enzymes, a pyrolytic formation of the carboxylic acids has to be considered when the drugs are smoked [25, 26].

Further adding to the complexity of the SCRA problem is that, in addition to the rapid and constant emergence of new SCRA, relatively little is known about the pharmacology of these SCRA and their metabolites. More particularly, only few studies have focused on the pharmacological characteristics of hydrolysis metabolites [17, 27-34]. Recently, there has been an increased interest, since knowledge about SCRA metabolite activity data might empower forensic laboratories to elaborate on the possible contributory role of these metabolites in human intoxications and in side-effects related to SCRA. A concept of 'total cannabinoid activity', rather than merely the cannabinoid activity related to a main compound can be envisaged. When referring the activity in a biological matrix relative to that of a given concentration of a reference compound, this concept can further be defined as 'activity equivalents' being present in e.g. blood or serum of an intoxicated or deceased person.

In this context, we investigated here the activity of fifteen parent compounds, featuring scaffolds based on L-valine and L-*tert*-leucine, and their respective carboxy metabolites, using a bio-assay that monitors activation of the CB₁ receptor. Compounds of this structural family, carrying carboxamide L-valine and L-*tert*-leucine moieties, are highly prevalent on the European market and show a high potency, resulting in numerous cases of severe intoxications [26, 35].

SCRA and their structural analogues, derived from L-valinamide or L-valinate investigated in this study, include 5F-AB-PINACA, 5F-AMB-PINACA, 5F-AEB-PINACA, AB-CHMINACA and AMB-CHMINACA (**Figure 8.1**). SCRA and their structural analogues, derived from L-*tert*-leucinamide or L-*tert*-leucinate, include 5F-ADB-PINACA, 5F-MDMB-PINACA, ADB-CHMICA, MDMB-CHMICA, ADB-CHMINACA, MDMB-CHMINACA, ADB-FUBICA, MDMB-FUBICA, ADB-FUBINACA and MDMB-FUBINACA (**Figure 8.1**). As the same hydrolysis metabolite featuring a carboxylic acid moiety might derive from more than one parent compound, hydrolysis of these fifteen SCRA results in seven carboxy metabolites, i.e. 5F-AB-PINACA-COOH, AB-CHMINACA-COOH, 5F-ADB-PINACA-COOH, ADB-CHMICA-COOH, ADB-CHMINACA-COOH, ADB-FUBICA-COOH and ADB-FUBINACA-COOH. Pharmacological properties of the above-mentioned

hydrolysis metabolites were compared with those of their parent compounds. The objective of this study was to clarify the possible impact of amide or ester hydrolysis across a range of SCRA featuring scaffolds based on L-valine or L-*tert*-leucine, to allow a better insight into their potential contribution to the *in vivo* toxicity profile.

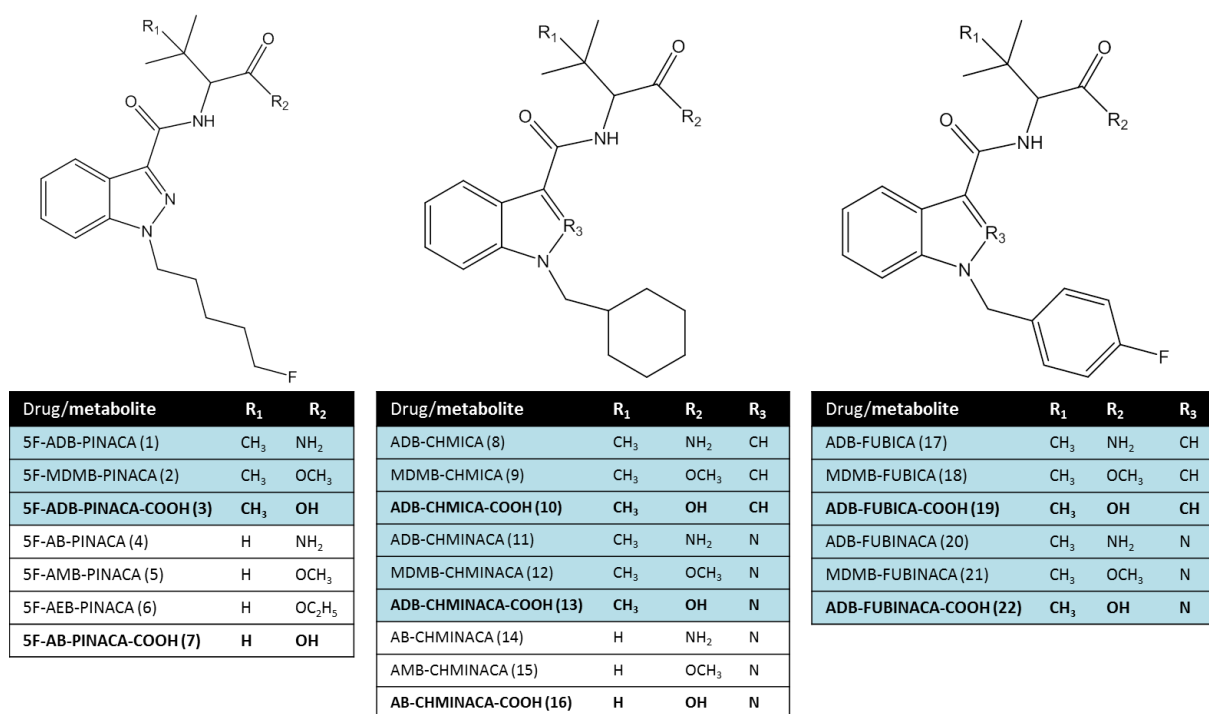


Figure 8.1 Structures of SCRA featuring a scaffold based on L-valine (white) and L-*tert*-leucine (blue) and their respective most common carboxy hydrolysis metabolites.

9.2 Materials and methods

9.2.1 Chemicals and reagents

Reference standards of all parent compounds including 5F-ADB-PINACA (*N*-[(2*S*)-1-amino-3,3-dimethyl-1-oxobutan-2-yl]-1-(5-fluoropentyl)-1*H*-indazole-3-carboxamide), 5F-MDMB-PINACA (methyl (2*S*)-2-[[1-(5-fluoropentyl)-1*H*-indazole-3-carbonyl]amino]-3,3-dimethylbutanoate), 5F-AB-PINACA (*N*-[(2*S*)-1-(amino-3-methyl-1-oxobutan-2-yl)-1-(5-fluoropentyl)-1*H*-indazole-3-carboxamide], 5F-AMB-PINACA (methyl (2*S*)-2-[[1-(5-fluoropentyl)-1*H*-indazole-3-carbonyl]amino]-3-methylbutanoate), 5F-AEB-PINACA (ethyl (2*S*)-2-[[1-(5-fluoropentyl)-1*H*-indazole-3-carbonyl]amino]-3-methylbutanoate), ADB-

CHMINACA (*N*-[(2*S*)-1-amino-3,3-dimethyl-1-oxobutan-2-yl]-1-(cyclohexylmethyl)-1*H*-indazole-3-carboxamide), MDMB-CHMICA (methyl (2*S*)-2-[[1-(cyclohexylmethyl)-1*H*-indole-3-carbonyl]amino]-3,3-dimethylbutanoate), ADB-CHMICA (*N*-[(2*S*)-1-amino-3,3-dimethyl-1-oxobutan-2-yl]-1-(cyclohexylmethyl)-1*H*-indole-3-carboxamide), MDMB-CHMINACA (methyl (2*S*)-2-[[1-(cyclohexylmethyl)-1*H*-indazole-3-carbonyl]amino]-3,3-dimethylbutanoate), AB-CHMINACA (*N*-[(2*S*)-1-amino-3-methyl-1-oxobutan-2-yl]-1-(cyclohexylmethyl)-1*H*-indazole-3-carboxamide), AMB-CHMINACA (methyl (2*S*)-2-[[1-(cyclohexylmethyl)-1*H*-indazole-3-carbonyl]amino]-3-methylbutanoate), ADB-FUBICA (*N*-[(2*S*)-1-amino-3,3-dimethyl-1-oxobutan-2-yl]-1-[(4-fluorophenyl)methyl]-1*H*-indole-3-carboxamide), MDMB-FUBICA (methyl (2*S*)-2-[[1-[(4-fluorophenyl)methyl]-1*H*-indole-3-carbonyl]amino]-3,3-dimethylbutanoate), ADB-FUBINACA (*N*-[(2*S*)-1-amino-3,3-dimethyl-1-oxobutan-2-yl]-1-[(4-fluorophenyl)methyl]-1*H*-indazole-3-carboxamide), MDMB-FUBINACA (methyl (2*S*)-2-[[1-[(4-fluorophenyl)methyl]-1*H*-indazole-3-carbonyl]amino]-3,3-dimethylbutanoate) and their metabolites 5F-AB-PINACA-COOH ((2*S*)-3-methyl-2-[[1-(5-fluoropentyl)-1*H*-indazole-3-carbonyl]amino]butanoic acid), 5F-ADB-PINACA-COOH ((*S*)-2-[[1-(5-fluoropentyl)-1*H*-indazole-3-carbonyl]amino]-3,3-dimethylbutanoic acid), ADB-FUBICA-COOH ((*S*)-2-[[1-(4-fluorobenzyl)-1*H*-indole-3-carbonyl]amino]-3,3-dimethylbutanoic acid), ADB-CHMINACA-COOH ((2*S*)-2-[[1-(cyclohexylmethyl)-1*H*-indazole-3-carbonyl]amino]-3,3-dimethylbutanoic acid), AB-CHMINACA-COOH ((2*S*)-2-[[1-(cyclohexylmethyl)-1*H*-indazole-3-carbonyl]amino]-3-methylbutanoic acid), ADB-CHMICA-COOH ((*S*)-2-[[1-(5-fluoropentyl)-1*H*-indazole-3-carbonyl]amino]-3,3-dimethylbutanoic acid) were purchased from Cayman Chemical (Ann Arbor, MI, USA).

JWH-018 ((Naphthalen-1-yl)(1-pentyl-1*H*-indol-3-yl)methanone) was purchased from LGC (Wesel, Germany). Poly-D-lysine and fetal bovine serum (FBS) were procured from Sigma-Aldrich (Steinheim, Germany). Dulbecco's modified eagle medium (DMEM) + GlutaMAX, Opti-MEM I Reduced Serum, trypsin, penicillin and streptomycin were procured from Thermo Fisher Scientific (Pittsburg, PA, USA). Nano-Glo® Live Cell substrate furimazine and Nano-Glo® dilution buffer were purchased from Promega (Madison, WI, USA). Methanol and DMSO were purchased from Fisher Scientific (Leicestershire, UK).

9.2.2 Cannabinoid reporter bio-assay

A live cell-based assay, based on the NanoLuc Binary Technology (NanoBiT[®], Promega) was used to evaluate activity at CB₁. Upon activation of CB₁, an intracellular protein, β -arrestin2 (β -arr2), which participates in the agonist-mediated desensitization of GPCRs, will be recruited. The generation of a HEK293T cell line stably expressing both the CB₁ receptor (C-terminally fused to the large part of the NanoLuciferase; LgBiT) and β -arr2 (N-terminally fused to the small part of NanoLuciferase; SmBiT) has been described previously [29]. This cell line can be used for structure-activity relationship determination of reference compounds, as well as for the screening of biological matrices for cannabinoid activity [32, 36, 37].

HEK293T cells stably expressing CB₁-LgBiT and SmBiT- β -arr2 were maintained in Dulbecco's Modified Eagle's Medium (DMEM) + GlutaMAX, supplemented with 10% fetal bovine serum (FBS), 100 μ g/mL streptomycin and 100 IU/l penicillin in a humidified environment (37°C, 5% CO₂). For the bio-assay, cells were seeded on a poly-D-lysine coated white 96-well plate at 5 x 10⁴ cells/well. The next day, cells were washed twice with Opti-MEM I Reduced Serum Medium and 100 μ l Opti-MEM I was added to the wells. First, the Nano-Glo Live Cell detection reagent (Promega) was prepared by a 20-fold dilution of the cell-permeable furimazine substrate in aqueous Nano-Glo LCS dilution buffer. Twenty-five μ L of this reagent was added to each well and luminescence was monitored in a TriStar² LB 942 multimode microplate reader controlled by ICE software (Berthold Technologies GmbH & Co., Bad Wildbad, Germany) during an equilibration period of 15 minutes. Once the luminescent signal had stabilized, monitoring was shortly interrupted for the addition of 10 μ L of the 13.5x concentrated agonist solutions in Opti-MEM I/methanol (50:50), ranging from 0.01 nM up to 10 μ M end concentration in the 96-well. This resulted in a final volume percentage of 3.7% methanol in each 96-well, which does not pose a problem to the cells within the timeframe of the assay. Subsequently, luminescence was detected for 120 minutes. A solvent control (blank), as well as a reference compound (JWH-018) was included in duplicate or triplicate on each plate.

9.2.3 Data processing

Relative Luminescence units (RLU) over time of all SCRA were corrected for solvent control and inter-well variability. Concentration-responses (area under the curve; AUC) were calculated and normalized to the maximum response of the reference compound, JWH-018, arbitrarily set as 100%. The mean and standard error of the mean (SEM) were derived from three independent experiments (hence, $n = 3$), the results from each of these experiments stemming from the analysis of duplicates or triplicates (hence, each data point is the result of 7-9 determinations). EC_{50} values were determined using the GraphPad Prism software (San Diego, CA, USA), via non-linear regression analysis (variable slope, four parameters).

9.3 Results and discussion

The SCRA investigated in this study can be divided into 3 main categories: (1) PINACA derivatives (1-pentyl-1*H*-indazole-3-carboxamide derivatives), (2) CHMICA and CHMINACA derivatives (1-(cyclohexylmethyl)-1*H*-indole-3-carboxamide and 1-(cyclohexylmethyl)-1*H*-indazole-3-carboxamide, respectively) and (3) FUBICA and FUBINACA derivatives (1-[(4-fluorophenyl)methyl]-1*H*-indole-3-carboxamide and 1-[(4-fluorophenyl)methyl]-1*H*-indazole-3-carboxamide, respectively). Each category is subdivided into scaffolds based on L-valine or L-*tert*-leucine, and are hereafter referred to as the numbers depicted in **Figure 9.1**. To quantify the potency and efficacy of the 15 SCRA and their common metabolites, the EC_{50} and E_{max} values were determined. As JWH-018 was the first detected SCRA in the end of 2008 [38] and the most commonly used standard SCRA in the field of toxicology, it was chosen as the reference compound. The observed EC_{50} value for JWH-018 in the bio-assay expressing CB₁ was 36.8 nM, with a 95% confidence interval (CI) of 28.6-50.4 nM, which is in agreement with earlier published data from our research group [17, 32].

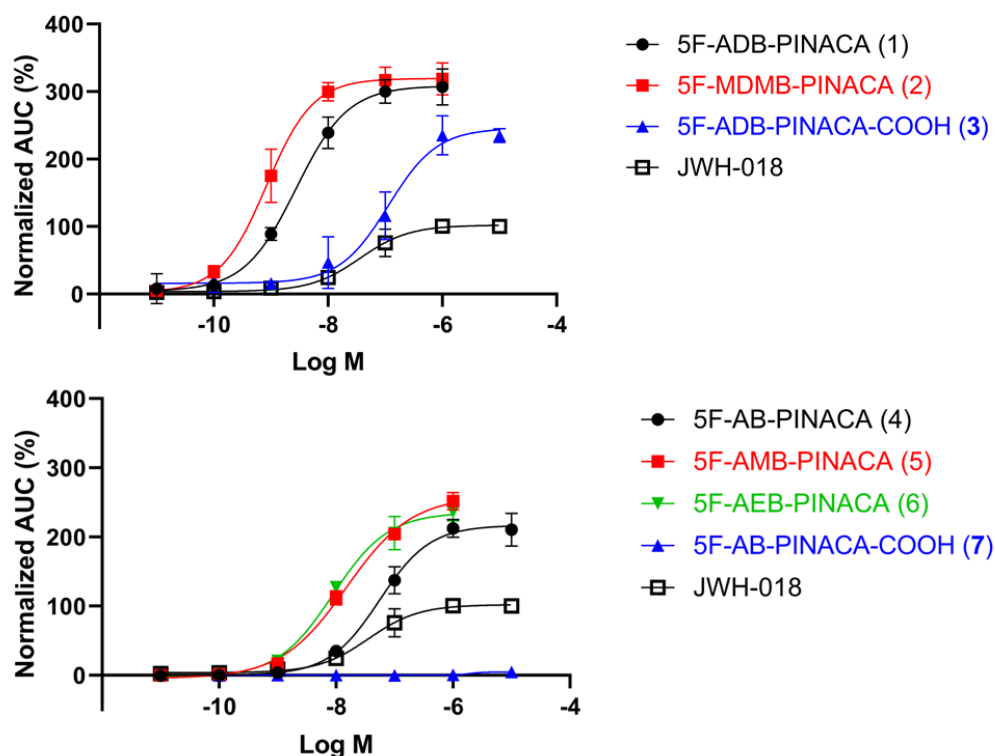
9.3.1 1-Pentyl-1*H*-indazole-3-carboxamide derivatives (PINACA)

Figure 9.2 Sigmoidal concentration-response curves of PINACA-based SCRA derivatives for the CB₁ receptor. Each data point represents the mean value \pm SEM of 3 experiments ($n = 3$).

All derivatives of the 1-Pentyl-1*H*-indazole-3-carboxamide family investigated in this study contain a 5-fluoropentyl group linked to N₁ of the indazole ring (**Figure 9.1**). The *L*-*tert*-leucinamide derivative 5F-ADB-PINACA (**1**) and the *L*-*tert*-leucinate derivatives 5F-MDMB-PINACA (**2**) showed a high potency at CB₁, with EC₅₀ values of 2.76 nM (95% CI: 1.24-5.41 nM) and 0.84 nM (0.52-1.24 nM), respectively (**Figure 9.2**)(**Table 9.1**). A fatal intoxication in Japan due to intake of 5F-MDMB-PINACA (**2**), also referred to as 5F-ADB, resulted in postmortem blood concentrations of 0.19 ng/mL (0.5 nM) of the parent compound [39]. In that case, investigation of the urinary metabolites revealed the presence of the carboxy metabolite **3**, generated after ester hydrolysis by carboxylesterase. However, no blood or urinary concentration was reported for that metabolite.

Despite having a strongly reduced potency when compared to the parent compounds **1** and **2**, hydrolyzed metabolite **3** still shows a higher E_{max} value than that of reference compound JWH-018 (\pm 2.5-fold) (**Figure 9.2**)(**Table 9.1**). Furthermore, the potency of metabolite **3** was 41-fold

reduced when compared to parent compound **1**, resulting in an EC₅₀ value of 113 nM for 5F-ADB-PINACA-COOH (**3**). Longworth *et al.* [31] investigated the activity of the non-fluorinated structural analogue ADB-PINACA and its hydrolyzed metabolite ADB-PINACA-COOH, using a fluorometric assay of membrane potential. These authors reported a 256-fold reduction in potency of the metabolite ADB-PINACA-COOH compared to its parent compound (EC₅₀ value of 1.3 nM for the parent compound vs. 333 nM for its metabolite). The fact that hydrolysis of parent compound **1** is apparently less detrimental for CB₁ activation than hydrolysis of its non-fluorinated structural analogue ADB-PINACA might be explained by the reported beneficial effect of fluorination of the aliphatic tail for the overall activity of the compound [14], attributable to the electronegativity of the halogen. Alternatively, we cannot exclude that assay differences underlie this dissimilarity.

Investigation of the L-valinamide derivative, 5F-AB-PINACA (**4**), as well as the methyl and ethyl L-valinate derivatives, 5F-AMB-PINACA (**5**) and 5F-AEB-PINACA (**6**), respectively, revealed notable structure activity relationships (SARs) in this study. The EC₅₀ values for **4**, **5** and **6** at CB₁ were 55.4 nM (31.2-85.1), 15.1 nM (10.2-23.9) and 8.76 nM (5.5-17.0) (**Figure 9.2**)(**Table 9.1**). Substitution of the amide group by methyl or ethyl ester groups resulted in higher potency towards CB₁. However, this finding is somewhat discordant with the findings by Banister *et al.*, [38] who reported a lower potency at CB₁ for **5** than **4** (1.9 nM vs 0.48 nM) by the implementation of a Fluorometric Imaging Plate Reader (FLIPR®) assay. Whereas this assay measures the Gβγ-mediated activation of inwardly rectifying potassium channels, the NanoBiT®-based bio-assay measures the direct recruitment of β-arr2 to the CB₁ receptor. Therefore, one should keep in mind that findings might differ due to different experimental assay set-ups (canonical vs. non-canonical), which could even reflect - although still mostly unexplored for SCRA - biased signaling. On the other hand, similar efficacies for compounds **4**, **5** and **6** were observed, namely an efficacy about 2.5-fold that of JWH-018 (**Table 9.1**).

The amide hydrolysis product of parent compound **4**, 5F-AB-PINACA-COOH (**7**), was the third most prevalent metabolite generated in human hepatocytes [21]. In the bio-assay, metabolite **7** of parent compounds **4**, **5** and **6** shows almost no activity at CB₁, which is in agreement with earlier observations by Noble *et al.* [32] for the hydrolyzed metabolite of the structural analogue AB-PINACA. As even the most 'inactive' metabolite within this study, i.e. metabolite

7, still shows some minor activity at high concentration (10 μ M), none of the screened metabolites are considered to be an antagonist.

Overall, consistent with earlier published data [38, 40], the L-*tert*-leucine-functionalized SCRA ($R_1 = \text{CH}_3$) (**Figure 9.1**), like **1** and **2** ($\text{EC}_{50} = 0.84\text{--}2.76$ nM), are more potent than their L-valine-functionalized SCRA counterparts **4**, **5** and **6** ($\text{EC}_{50} = 8.76\text{--}55.4$ nM). This also holds true for the carboxy metabolite **3** of the L-*tert*-leucine-functionalized SCRA, which has an EC_{50} value of 113 nM, whereas no activity could be observed for the hydrolyzed metabolite **7** of the L-valine-functionalized SCRA derivatives.

Table 9.1 Potency (EC_{50}), efficacy (E_{max} , relative to JWH-018) of the selected SCRA and metabolites ($n = 3$).

Compound	EC_{50} (nM)	E_{max} (%)	Metabolite/Parent EC_{50}
5F-ADB-PINACA (1)	2.76 (1.24-5.41)	308.4 (277.8-346.4)	40.9
5F-MDMB-PINACA (2)	0.84 (0.52-1.24)	319.3 (291.0-353.6)	
5F-ADB-PINACA-COOH (3)	113 (51.3-242)	245.6 (204.2-349.6)	
5F-AB-PINACA (4)	55.4 (31.2-85.1)	216.8 (196.4-241.5)	
5F-AMB-PINACA (5)	15.1 (10.2-23.9)	258.6 (238.2-287.0)	
5F-AEB-PINACA (6)	8.76 (5.5-17.0)	235.4 (211.3-273.3)	
5F-AB-PINACA-COOH (7)	ND	ND	
ADB-CHMICA (8)	3.31 (0.94-12.4)	327.2 (280.4-459.4)	44.9
MDMB-CHMICA (9)	1.77 (0.79-3.83)	285.1 (258.5-321.5)	
ADB-CHMICA-COOH (10)	ND	57.6 (35.7-92.4)*	
ADB-CHMINACA (11)	0.34 (0.02-0.91)	262.6 (236.7-301.1)	
MDMB-CHMINACA (12)	0.78 (0.22-1.90)	226.7 (202.9-261.2)	
ADB-CHMINACA-COOH (13)	ND	68.2 (63.5-73.0)*	
AB-CHMINACA (14)	3.45 (1.96-6.14)	390.5 (358.4-435.0)	548.8
AMB-CHMINACA (15)	3.91 (1.86-8.44)	360.1 (322.2-421.2)	
AB-CHMINACA-COOH (16)	155 (97.4-277.6)	254.8 (227.3-292.3)	
ADB-FUBICA (17)	12.3 (9.68-16.1)	313.6 (297.0-333.2)	
MDMB-FUBICA (18)	5.79 (2.97-10.25)	270.6 (243.7-303.0)	
ADB-FUBICA-COOH (19)	ND	81.8 (65.4-99.6)*	
ADB-FUBINACA (20)	0.82 (0.46-1.34)	273.6 (254.7-295.6)	
MDMB-FUBINACA (21)	0.36 (0.17-0.69)	240.9 (221.4-263.3)	548.8
ADB-FUBINACA-COOH (22)	450 (176-749)	176.6 (141.0-314.7)	
JWH-018	36.8 (28.6-50.4)	102.0 (97.6-107.5)	

*Maximum effect seen at 10 μ M

ND: not determined since saturation has not been reached

9.3.2 1-(Cyclohexylmethyl)-1*H*-indole-3-carboxamide (CHMICA) and 1-(cyclohexylmethyl)-1*H*-indazole-3-carboxamide (CHMINACA)

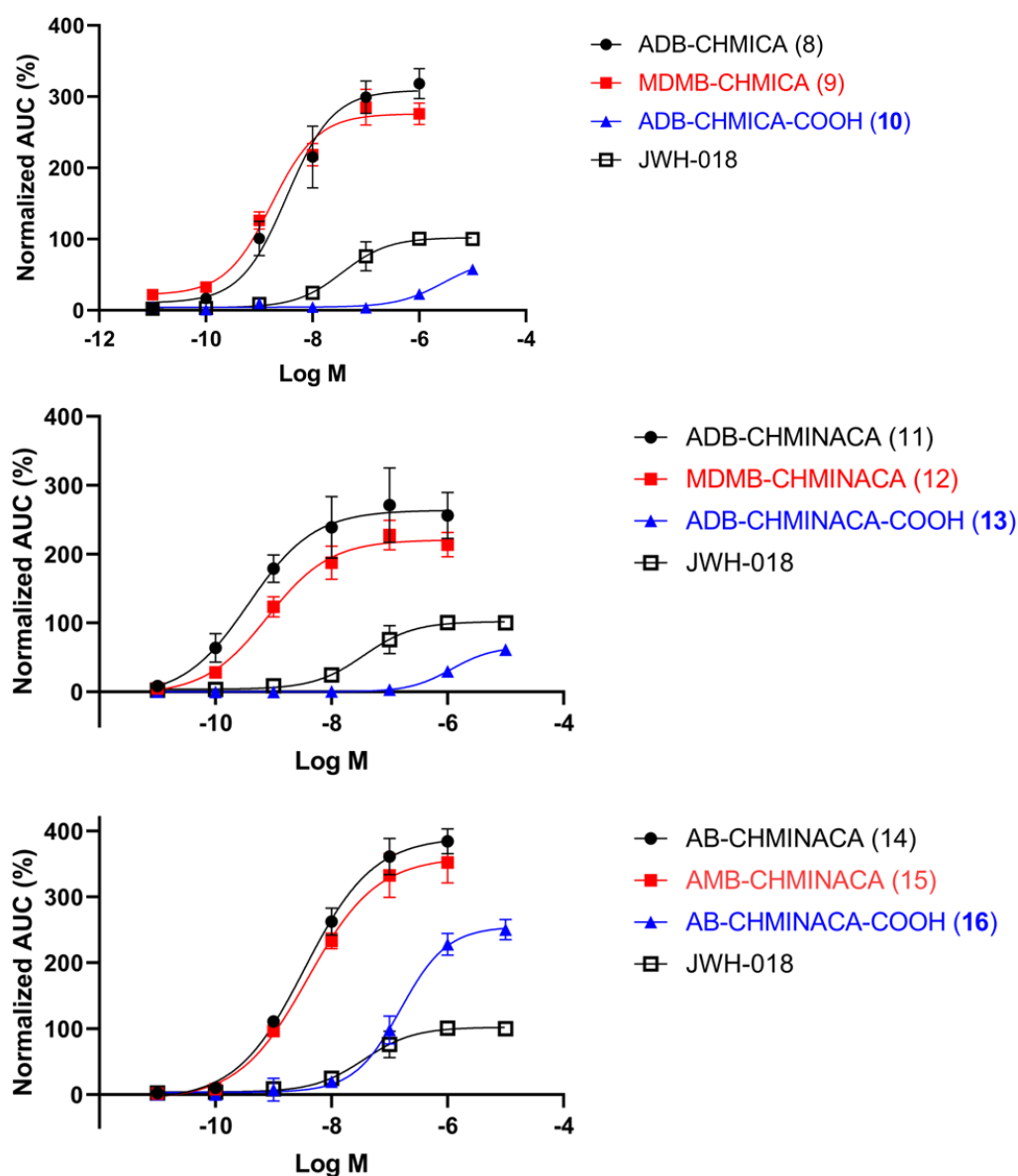


Figure 9.3 Sigmoidal concentration-response curves of CHMICA- and CHMINACA-based SCRA derivatives for the CB₁ receptor. Each data point represents the mean value \pm SEM of 3 experiments ($n = 3$).

Since 2014, numerous non-fatal and fatal intoxications with the *L*-*tert*-leucine derivative MDMB-CHMICA (9) have been reported [9, 12, 41-46]. Subsequently, the UK Government implemented the ‘Psychoactive Substances Act’ in 2016 to counteract MDMB-CHMICA-related intoxications. Nevertheless, only a minor reduction in the availability of MDMB-CHMICA from internet-based suppliers could be observed [47]. Although there is only limited

data published concerning its structural analogue, ADB-CHMICA (**8**), which features a primary amide moiety, both parent compounds **8** and **9** are extremely potent at CB₁, with EC₅₀ values of 3.31 nM for compound **8** and 1.77 nM for compound **9** (**Figure 9.3**)(**Table 9.1**). Their hydrolysis metabolite **10** was found to be one of the most abundant *in vivo* Phase I metabolites in urine samples [26]. Hydrolysis of the primary amide or methylester severely impairs the activity of the metabolite compared to the parent compounds **8** and **9** (**Figure 9.3**). Notwithstanding, an efficacy of 57.6% of the E_{max} value of JWH-018 at high concentrations (10 μM) was retained.

ADB-CHMINACA (**11**) is one of the most potent CB₁ agonists from the panel of SCRA investigated in this study, with an EC₅₀ value of 0.34 nM (**Figure 9.3**)(**Table 9.1**), which is in agreement with earlier published data [29, 32, 34, 48]. ADB-CHMINACA (**11**), also referred to as MAB-CHMINACA, is sold over the Internet as a white powder and is mostly smoked in order to get 'high' [49]. Typical doses reported by users, who mix it with herbs, vary from 0.25 mg up to heavy doses of 2 mg. In a fatal case in 2015, the presence of ADB-CHMINACA (**11**) was shown for the first time in human specimens, with the highest concentration of the parent compound found in the liver (156 ng/g) [15]. Subsequently, various intoxications with the highly potent ADB-CHMINACA have been reported, with blood concentrations of four individuals ranging from 5.2 up to 14.6 ng/mL (or 14 nM up to 39 nM) [48]. The adverse effects observed in these individuals included vomiting, seizures, limb twisting, muscle tremors, aggression, agitation, slurred speech, among others. Amide hydrolysis was detected in ADB-CHMINACA (**11**) as well as in AB-CHMINACA (**14**) metabolism, but only as a minor transformation, since the cyclohexylmethyl tail appeared to be the preferred site of transformation [20, 50, 51]. Although no EC₅₀ value could be determined for hydrolysis metabolite **13** of parent compounds **11** and **12**, it still showed significant activity at CB₁ at high concentrations, with an efficacy of 68.2% relative to JWH-018 (in agreement with findings of Cannaert *et al.*, 2017 [29]). While the human consumption of this metabolite has not been reported before, metabolite **13**, also referred to as DMBA-CHMINACA, has recently been identified in a white powder-type product delivered in an airmail package to Korea [52].

Besides MDMB-CHMICA (**9**), the chemically closely related L-valine derivative AB-CHMINACA (**14**) has also frequently been encountered in forensic case work. It was identified amongst prevalently consumed drugs of abuse in patients presenting to an emergency department in

London in the first half of 2015 [9]. The use of these drugs has been associated with adverse effects including cardiovascular effects, neurotoxicity and neuropsychiatric effects, potentially even more serious severe toxicity effects compared to the earlier generation SCRA [12]. The L-valine derivatives **14** and **15** showed a lower potency compared to their L-*tert*-leucine counterparts **11** and **12** (**Figure 9.3**). An EC₅₀ value of 3.45 nM (1.96-6.14) was determined for compound **14** (**Table 9.1**), which is in agreement with the low EC₅₀ value of 7.4 ± 1.5 nM reported by Wiley *et al.* [53], which was determined by the binding of a slowly hydrolysable GTP analog to the Gα-subunit using [³⁵S]GTPγS turnover assay, instead of the β-arr2 recruitment assay used in this study. Hydrolysis metabolite **16** has been identified as a hydrolysis product of parent compounds **14** and **15** in a number of studies in urine and hair of abusers [54-56]. Metabolite **16** clearly retains activity (EC₅₀ = 155 nM), although with a 45-fold impaired potency when compared to the parent compounds (**Table 9.1**). It has been reported by the European Monitoring Centre for Drugs and Drug Addiction (EMCDDA) that the hydrolysis product of **14** and **15**, also listed under the name MBA-CHMINACA, has been sold as a 'research chemical' under the name 'AB-CHMINACA' [35]. This research chemical was purchased via the Internet from online vendors and analyzed at the Institute of Forensic Medicine, Freiburg, Germany.

9.3.3 1-[4-Fluorophenyl)methyl]-1*H*-indole-3-carboxamide (FUBICA) and 1-[(4-fluorophenyl)methyl]-1*H*-indazole-3-carboxamide derivatives (FUBINACA)

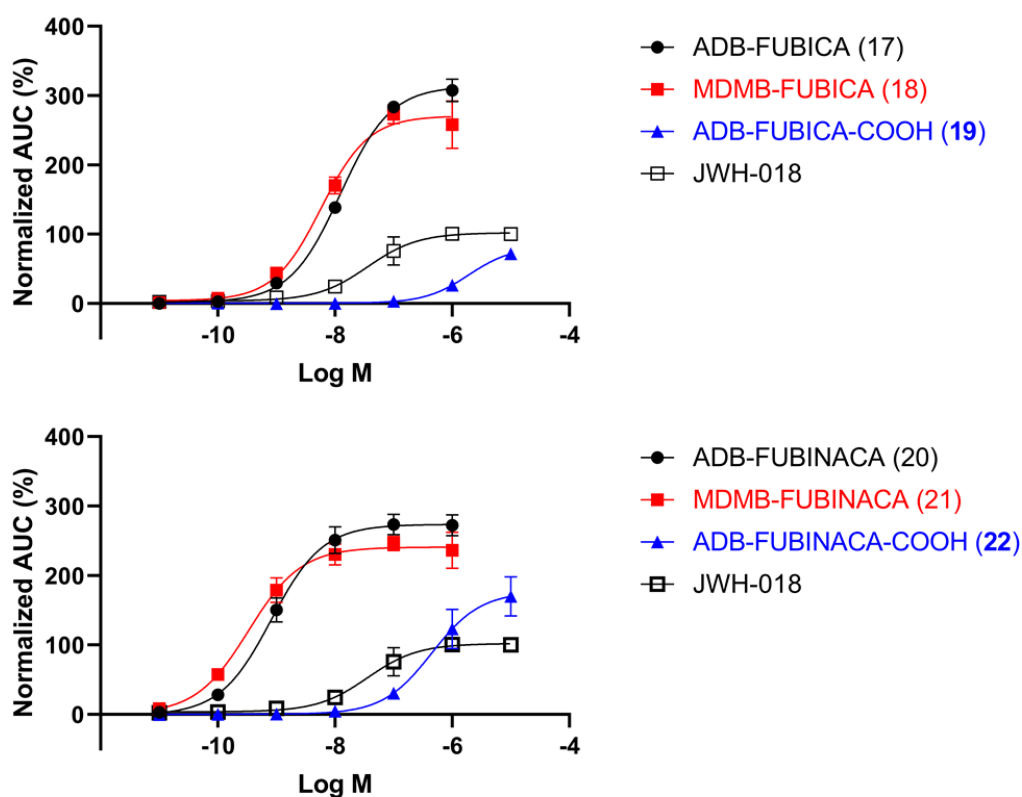


Figure 9.4 Sigmoidal concentration-response curves of FUBICA- and FUBINACA-based SCRA derivatives for the CB₁ receptor. Each data point represents the mean value \pm SEM of 3 experiments ($n = 3$).

Of the FUBICA and FUBINACA derivatives, featuring a fluorinated benzene ring coupled to N₁ of the indole or indazole ring, only L-*tert*-leucine derivatives were investigated in this study (**Figure 9.1**). For ADB-FUBICA (**17**) an EC₅₀ value of 12.3 nM (9.68-16.1) and an E_{max} value 3-fold higher than that of JWH-018 was determined (**Figure 9.4**)(**Table 9.1**). MDMB-FUBICA (**18**), which has been reported to be more selective towards CB₂ compared to the CB₁ receptor, shows an efficacy of 5.79 nM for CB₁, in agreement with GTPγS binding results by Doi *et al.* (2018) [57] (EC₅₀ = 9.72 nM) and FLIPR® assay results by Banister *et al.* (2016) [40] (EC₅₀ = 2.7 nM). HLM incubation studies yielded the Phase I metabolite **19** from the parent compound ADB-FUBICA (**17**) following carboxamide hydrolysis [58]. At high concentrations, metabolite **19** reached an E_{max} value comparable with 81.8% of the efficacy of the reference compound JWH-018.

ADB-FUBINACA (**20**) intake has led to multiple severe intoxications [59-61]. In a fatal case reported in the USA, related to the intake of compound **20**, a concentration of 7.3 ng/mL (19.1 nM) was detected in postmortem blood [61]. In a nonfatal case, an even higher serum concentration of 15.6 ng/mL (41 nM) was determined after intake of ADB-FUBINACA (**20**) by ingesting two drops of e-cigarette fluid [59]. Its structural analogue, MDMB-FUBINACA (**21**) has similarly been linked to more than 600 poisonings, including 15 deaths over 2 weeks in Russia in 2014 [62]. Consequently, compound **21** has been designated as one of the deadliest cannabimimetics sold to date [63]. Interestingly, the structure of this highly potent agonist bound to the CB₁-Gα_i complex has recently been unraveled [63]. Delineating the structural basis of this complex revealed a C-shape binding mode of **21**, which stabilizes the active conformation of CB₁ to a greater extent compared to the partial agonist Δ⁹-THC. Also in this study, both compounds **20** and **21** show extremely high potency as CB₁ agonists, with EC₅₀ values of 0.82 nM and 0.36 nM, respectively (**Figure 9.4**)(**Table 9.1**). Whereas the estimated EC₅₀ value of compound **20** is in agreement with the low EC₅₀ value of 1.2 nM determined by Banister *et al.* [38] using a FLIPR[®] membrane potential assay, the EC₅₀ value of compound **21** estimated here (0.36 nM) deviates to a larger extent from the result obtained by Banister *et al.* (3.9 nM) but is in good agreement with the EC₅₀ value of 0.26 nM, as determined by [³⁵S]GTPγS assay by Gamage *et al.* [30]. As already mentioned earlier, different EC₅₀ value outcomes can be explained by the implementation of different functional signaling assays, different cell lines (CHO vs HEK293T cells) or even biased signaling. Hydrolysis of the terminal moieties (primary amide and methylester for ADB-FUBINACA (**20**) and MDMB-FUBINACA (**21**), respectively) was found to be a common major metabolic pathway for both parent compounds [64, 65]. Metabolite **22** was the most abundant metabolite in 9 postmortem urine samples, associated with MDMB-FUBINACA (**21**) intake [65]. This metabolite **22** still showed significant, albeit impaired, activity at CB₁ at high concentrations, with an EC₅₀ value of 450 nM and an E_{max} of 176.6 %, relative to the efficacy of the reference compound JWH-018.

9.4 Conclusion

The present study provides critical and missing data related to the potential toxicological characteristics of common hydrolysis metabolites of 15 SCRA featuring scaffolds based on L-valine and L-*tert*-leucine. Our results indicate an overall severely impaired activity of these metabolites at CB₁. Nevertheless, a broad variety in metabolite activity could be detected in the chemically closely related SCRA panel in this study, ranging from no activity detected to EC₅₀ values around 150 nM. Comparison of our data to already published activity data on the investigated compounds once more revealed that EC₅₀ values may markedly vary among different assays, possibly due to differences in functional signaling and choice of cell lines. Nevertheless, our data highlight that the hydrolysis metabolites of closely related SCRA can possess markedly distinct pharmacological characteristics. Although we observed a strong reduction in efficacy (E_{max}) of the carboxy metabolites of L-valine and L-*tert*-leucine SCRA for CB₁, when compared to the parent compounds, the efficacy of certain metabolites is still higher than that of JWH-018. This might imply that metabolites from ADB-FUBINACA, 5F-ADB-PINACA and AB-CHMINACA and their methyl- and ethylester functionalities could potentially contribute to the overall pharmacological or toxicological response *in vivo*.

References

1. European Monitoring Centre for Drugs and Drug Addiction (EMCDDA). Perspectives on drugs: Synthetic cannabinoids in Europe. 2017. http://www.emcdda.europa.eu/system/files/publications/2753/POD_Synthetic%20cannabinoids_0.pdf. Accessed 21 December 2018.
2. Matsuda, L.A., et al., *Structure of a cannabinoid receptor and functional expression of the cloned cDNA*. Nature, 1990. 346(6284): p. 561-4.
3. Munro, S., K.L. Thomas, and M. Abu-Shaar, *Molecular characterization of a peripheral receptor for cannabinoids*. Nature, 1993. 365(6441): p. 61-5.
4. Mechoulam, R. and L.A. Parker, *The endocannabinoid system and the brain*. Annual review of psychology, 2013. 64: p. 21-47.
5. Pertwee, R.G., *Pharmacology of cannabinoid CB1 and CB2 receptors*. Pharmacology & therapeutics, 1997. 74(2): p. 129-80.
6. Kikura-Hanajiri, R., N.U. Kawamura, and Y. Goda, *Changes in the prevalence of new psychoactive substances before and after the introduction of the generic scheduling of synthetic cannabinoids in Japan*. Drug testing and analysis, 2014. 6(7-8): p. 832-9.
7. Spiller, H.A., et al., *Clinical experience with and analytical confirmation of "bath salts" and "legal highs" (synthetic cathinones) in the United States*. Clinical toxicology (Philadelphia, Pa.), 2011. 49(6): p. 499-505.
8. Zawilska, J.B. and D. Andrzejczak, *Next generation of novel psychoactive substances on the horizon - A complex problem to face*. Drug and alcohol dependence, 2015. 157: p. 1-17.
9. Abouchedid, R., et al., *Analytical confirmation of synthetic cannabinoids in a cohort of 179 presentations with acute recreational drug toxicity to an Emergency Department in London, UK in the first half of 2015*. Clinical toxicology (Philadelphia, Pa.), 2017. 55(5): p. 338-345.
10. Hermanns-Clausen, M., et al., *Adverse effects after the use of JWH-210 - a case series from the EU Spice II plus project*. Drug testing and analysis, 2016. 8(10): p. 1030-1038.
11. Hermanns-Clausen, M., et al., *Acute toxicity due to the confirmed consumption of synthetic cannabinoids: clinical and laboratory findings*. Addiction (Abingdon, England), 2013. 108(3): p. 534-44.
12. Hermanns-Clausen, M., et al., *Acute side effects after consumption of the new synthetic cannabinoids AB-CHMINACA and MDMB-CHMICA*. Clinical toxicology (Philadelphia, Pa.), 2018. 56(6): p. 404-411.
13. Behonick, G., et al., *Four postmortem case reports with quantitative detection of the synthetic cannabinoid, 5F-PB-22*. Journal of analytical toxicology, 2014. 38(8): p. 559-62.
14. Gurney, S.M., et al., *Pharmacology, toxicology, and adverse effects of synthetic cannabinoid drugs*. Forensic science review, 2014. 26(1): p. 53-78.
15. Hasegawa, K., et al., *Postmortem distribution of AB-CHMINACA, 5-fluoro-AMB, and diphenidine in body fluids and solid tissues in a fatal poisoning case: usefulness of adipose tissue for detection of the drugs in unchanged forms*. Forensic toxicology, 2015. 33(1): p. 45-53.
16. Thornton, S.L., et al., *Synthetic cannabinoid use associated with acute kidney injury*. Clinical toxicology (Philadelphia, Pa.), 2013. 51(3): p. 189-90.
17. Cannaert, A., et al., *Detection and activity profiling of synthetic cannabinoids and their metabolites with a newly developed bioassay*. Analytical chemistry, 2016. 88(23): p. 11476-11485.
18. Chimalakonda, K.C., et al., *Cytochrome P450-mediated oxidative metabolism of abused synthetic cannabinoids found in K2/Spice: identification of novel cannabinoid receptor ligands*. Drug metabolism and disposition: the biological fate of chemicals, 2012. 40(11): p. 2174-84.
19. Castaneto, M.S., et al., *Identification of AB-FUBINACA metabolites in human hepatocytes and urine using high-resolution mass spectrometry*. Forensic toxicology, 2015. 33(2): p. 295-310.

20. Erratico, C., et al., *In vitro and in vivo human metabolism of the synthetic cannabinoid AB-CHMINACA*. Drug testing and analysis, 2015. 7(10): p. 866-76.
21. Wohlfarth, A., et al., *Pentylindole/Pentylindazole synthetic cannabinoids and their 5-Fluoro analogs produce different primary metabolites: metabolite profiling for AB-PINACA and 5F-AB-PINACA*. The AAPS journal, 2015. 17(3): p. 660-77.
22. Andersson, M., et al., *Metabolic profiling of new synthetic cannabinoids AMB and 5F-AMB by human hepatocyte and liver microsome incubations and high-resolution mass spectrometry*. Rapid communications in mass spectrometry : RCM, 2016. 30(8): p. 1067-78.
23. Thomsen, R., et al., *Synthetic cannabimimetic agents metabolized by carboxylesterases*. Drug testing and analysis, 2015. 7(7): p. 565-76.
24. Franz, F., et al., *Structure-metabolism relationships of valine and tert-leucine-derived synthetic cannabinoid receptor agonists: a systematic comparison of the in vitro phase I metabolism using pooled human liver microsomes and high-resolution mass spectrometry*. Forensic toxicology, 2019.
25. Franz, F., et al., *Metabolites of synthetic cannabinoids in hair--proof of consumption or false friends for interpretation?* Analytical and bioanalytical chemistry, 2016. 408(13): p. 3445-52.
26. Franz, F., et al., *Phase I metabolism of the highly potent synthetic cannabinoid MDMB-CHMICA and detection in human urine samples*. Drug testing and analysis, 2017. 9(5): p. 744-753.
27. Brents, L.K., et al., *Monohydroxylated metabolites of the K2 synthetic cannabinoid JWH-073 retain intermediate to high cannabinoid 1 receptor (CB1R) affinity and exhibit neutral antagonist to partial agonist activity*. Biochemical pharmacology, 2012. 83(7): p. 952-61.
28. Brents, L.K., et al., *Phase I hydroxylated metabolites of the K2 synthetic cannabinoid JWH-018 retain in vitro and in vivo cannabinoid 1 receptor affinity and activity*. PloS one, 2011. 6(7): p. e21917.
29. Cannaert, A., et al., *Activity-based detection of consumption of synthetic cannabinoids in authentic urine samples using a stable cannabinoid reporter system*. Analytical chemistry, 2017. 89(17): p. 9527-9536.
30. Gamage, T.F., et al., *Molecular and behavioral pharmacological characterization of abused synthetic cannabinoids MMB- and MDMB-FUBINACA, MN-18, NNEI, CUMYL-PICA, and 5-Fluoro-CUMYL-PICA*. The Journal of pharmacology and experimental therapeutics, 2018. 365(2): p. 437-446.
31. Longworth, M., et al., *Synthesis and pharmacological profiling of the metabolites of synthetic cannabinoid drugs APICA, STS-135, ADB-PINACA, and 5F-ADB-PINACA*. ACS chemical neuroscience, 2017. 8(8): p. 1673-1680.
32. Noble, C., et al., *Application of an activity-based receptor bioassay to investigate the in vitro activity of selected indole- and indazole-3-carboxamide-based synthetic cannabinoids at CB1 and CB2 receptors*. Drug testing and analysis, 2018.
33. Rajasekaran, M., et al., *Human metabolites of synthetic cannabinoids JWH-018 and JWH-073 bind with high affinity and act as potent agonists at cannabinoid type-2 receptors*. Toxicology and applied pharmacology, 2013. 269(2): p. 100-8.
34. Buchler, I.P., M.J. Hayes, and H. S.G., *Indazole derivatives*. 2009.
35. European Monitoring Centre for Drugs and Drug Addiction (EMCDDA). . <https://ednd.emcdda.europa.eu/html.cfm/index6555EN.html>. Accessed 13 December 2018.
36. Cannaert, A., et al., *Activity-based detection of cannabinoids in serum and plasma samples*. Clinical chemistry, 2018. 64(6): p. 918-926.
37. Cannaert, A., et al., *Validation of activity-based screening for synthetic cannabinoid receptor agonists in a large set of serum samples*. Clinical chemistry, 2019. 65(2): p. 347-349.
38. Banister, S.D. and M. Connor, *The chemistry and pharmacology of synthetic cannabinoid receptor agonist new psychoactive substances: evolution*. Handbook of experimental pharmacology, 2018.

39. Kusano, M., et al., *Fatal intoxication by 5F-ADB and diphenidine: Detection, quantification, and investigation of their main metabolic pathways in humans by LC/MS/MS and LC/Q-TOFMS*. Drug testing and analysis, 2018. 10(2): p. 284-293.
40. Banister, S.D., et al., *Pharmacology of valinate and tert-leucinate synthetic cannabinoids 5F-AMBICA, 5F-AMB, 5F-ADB, AMB-FUBINACA, MDMB-FUBINACA, MDMB-CHMICA, and their analogues*. ACS chemical neuroscience, 2016. 7(9): p. 1241-54.
41. Adamowicz, P., *Fatal intoxication with synthetic cannabinoid MDMB-CHMICA*. Forensic science international, 2016. 261: p. e5-10.
42. Angerer, V., et al., *Reply to 'sudden cardiac death following use of the synthetic cannabinoid MDMB-CHMICA'*. Journal of analytical toxicology, 2016. 40(3): p. 240-2.
43. Gaunitz, F., et al., *Post-mortem distribution of the synthetic cannabinoid MDMB-CHMICA and its metabolites in a case of combined drug intoxication*. International journal of legal medicine, 2018. 132(6): p. 1645-1657.
44. Hill, S.L., et al., *Clinical toxicity following analytically confirmed use of the synthetic cannabinoid receptor agonist MDMB-CHMICA. A report from the Identification Of Novel psychoActive substances (IONA) study*. Clinical toxicology (Philadelphia, Pa.), 2016. 54(8): p. 638-43.
45. Seywright, A., et al., *Analysis and clinical findings of cases positive for the novel synthetic cannabinoid receptor agonist MDMB-CHMICA*. Clinical toxicology (Philadelphia, Pa.), 2016. 54(8): p. 632-7.
46. Westin, A.A., et al., *Sudden cardiac death following use of the synthetic cannabinoid MDMB-CHMICA*. Journal of analytical toxicology, 2016. 40(1): p. 86-7.
47. Haden, M., D.M. Wood, and P.I. Dargan, *The impact of the Psychoactive Substances Act 2016 on the online availability of MDMB-CHMICA*. QJM : monthly journal of the association of physicians, 2017. 110(10): p. 619-622.
48. Adamowicz, P. and J. Gieron, *Acute intoxication of four individuals following use of the synthetic cannabinoid MAB-CHMINACA*. Clinical toxicology (Philadelphia, Pa.), 2016. 54(8): p. 650-4.
49. Wurita, A., et al., *Identification and quantitation of 5-fluoro-ADB-PINACA and MAB-CHMINACA in dubious herbal products*. Forensic toxicology, 2015. 33(2): p. 213-220.
50. Carlier, J., et al., *Identification of new synthetic cannabinoid ADB-CHMINACA (MAB-CHMINACA) metabolites in human hepatocytes*. The AAPS journal, 2017. 19(2): p. 568-577.
51. Hasegawa, K., et al., *Identification and quantification of predominant metabolites of synthetic cannabinoid MAB-CHMINACA in an authentic human urine specimen*. Drug testing and analysis, 2018. 10(2): p. 365-371.
52. Lee, J.H., et al., *Identification and characterization of an indazole-3-carboxamide class synthetic cannabinoid: 2-[1-(cyclohexylmethyl)-1H-indazole-3-carboxamido]-3,3-dimethylbutanoic acid (DMBA-CHMINACA)*. Forensic science international, 2018. 291: p. 167-174.
53. Wiley, J.L., et al., *AB-CHMINACA, AB-PINACA, and FUBIMINA: Affinity and potency of novel synthetic cannabinoids in producing delta9-tetrahydrocannabinol-like effects in mice*. The Journal of pharmacology and experimental therapeutics, 2015. 354(3): p. 328-39.
54. Sim, J., et al., *Determination of AB-CHMINACA and its metabolites in human hair and their deposition in hair of abusers*. Journal of pharmaceutical and biomedical analysis, 2017. 140: p. 162-168.
55. Tyndall, J.A., et al., *An outbreak of acute delirium from exposure to the synthetic cannabinoid AB-CHMINACA*. Clinical toxicology (Philadelphia, Pa.), 2015. 53(10): p. 950-6.
56. Wurita, A., et al., *Identification and quantification of metabolites of AB-CHMINACA in a urine specimen of an abuser*. Legal medicine (Tokyo, Japan), 2016. 19: p. 113-8.
57. Doi, T., et al., *Evaluation of carboxamide-type synthetic cannabinoids as CB1/CB2 receptor agonists: difference between the enantiomers*. Forensic toxicology, 2018. 36(1): p. 51-60.

58. Li, J., et al., *UPLC-HR-MS/MS-based determination study on the metabolism of four synthetic cannabinoids, ADB-FUBICA, AB-FUBICA, AB-BICA and ADB-BICA, by human liver microsomes*. Biomedical chromatography : BMC, 2018. 32(3).
59. Lam, R.P.K., et al., *Supraventricular tachycardia and acute confusion following ingestion of e-cigarette fluid containing AB-FUBINACA and ADB-FUBINACA: a case report with quantitative analysis of serum drug concentrations*. Clinical toxicology (Philadelphia, Pa.), 2017. 55(7): p. 662-667.
60. Nacca, N., et al., *Coma, seizures, atrioventricular block, and hypoglycemia in an ADB-FUBINACA body-packer*. The Journal of emergency medicine, 2018. 55(6): p. 788-791.
61. Shanks, K.G., W. Clark, and G. Behonick, *Death associated with the use of the synthetic cannabinoid ADB-FUBINACA*. Journal of analytical toxicology, 2016. 40(3): p. 236-9.
62. Shevyrin, V., et al., *Identification and analytical characteristics of synthetic cannabinoids with an indazole-3-carboxamide structure bearing a N-1-methoxycarbonylalkyl group*. Analytical and bioanalytical chemistry, 2015. 407(21): p. 6301-15.
63. Krishna Kumar, K., et al., *Structure of a signaling cannabinoid receptor 1-G protein complex*. Cell, 2019. 176(3): p. 448-458 e12.
64. Carlier, J., et al., *In vitro metabolite profiling of ADB-FUBINACA, a new synthetic cannabinoid*. Current neuropharmacology, 2017. 15(5): p. 682-691.
65. Kavanagh, P., A. Grigoryev, and N. Krupina, *Detection of metabolites of two synthetic cannabimimetics, MDMB-FUBINACA and ADB-FUBINACA, in authentic human urine specimens by accurate mass LC-MS: a comparison of intersecting metabolic patterns*. Forensic toxicology, 2017. 35(2): p. 284-300.

Chapter 10:

Broader international context, relevance and future perspectives

G protein-coupled receptors (GPCRs) are one of the most intensively studied drug targets, due to their pivotal role in the regulation of (patho-)physiological processes in the human body. As GPCRs have accessible druggable sites at the cell surface, almost one third of the modern drug therapies target these receptors. Most targeted GPCRs comprise Class A (Rhodopsin) GPCRs, with adrenergic, histamine and serotonin receptors being the most prominent targeted families by the US Food and Drug Administration (FDA)-approved drugs (**Figure 10.1**). Those drugs mostly encompass small molecules that function as agonists or antagonists, although other modalities such as peptides and monoclonal antibodies (mAbs) are becoming more popular in Phase I trials (**Figure 10.1**)[1].

Most of the currently marketed drugs were developed with the assumption that GPCRs function as on/off switches, as also reflected in the descriptions of these drugs (e.g. beta-blockers or dopamine agonists). Over the last few years, recent advances made in structural biology and pharmacology have unveiled the functional complexity of GPCRs and have proven that there is much more to the story of GPCR signaling than just on/off switches. Our knowledge about receptor activation and altered signaling has expanded with two phenomena known as ‘GPCR-GPCR interactions’ and ‘biased signaling’, due to which new avenues for GPCR drug discovery have emerged.

GPCR-GPCR interactions

The discovery that GPCRs can not only function as monomers but also as receptor complexes, and thus modulate intracellular communication by direct allosteric interactions, has brought our understanding of GPCR-mediated signaling to another dimension. However, the formation of these macromolecular receptor complexes, also referred to as oligomerization, appears to be a common feature to regulate receptor function among other receptor families as well [2]. For example, this oligomeric organization has also been observed for the ligand-gated ion channel (LGIC) family that mainly consists of pentameric ion channels, such as the GABA_A receptor. Furthermore, the appearance of GPCR oligomerization is not only limited to the central nervous system (CNS), but has also been observed in peripheral tissue, including cells of cardiovascular or endocrine systems and in cancer cells [3].

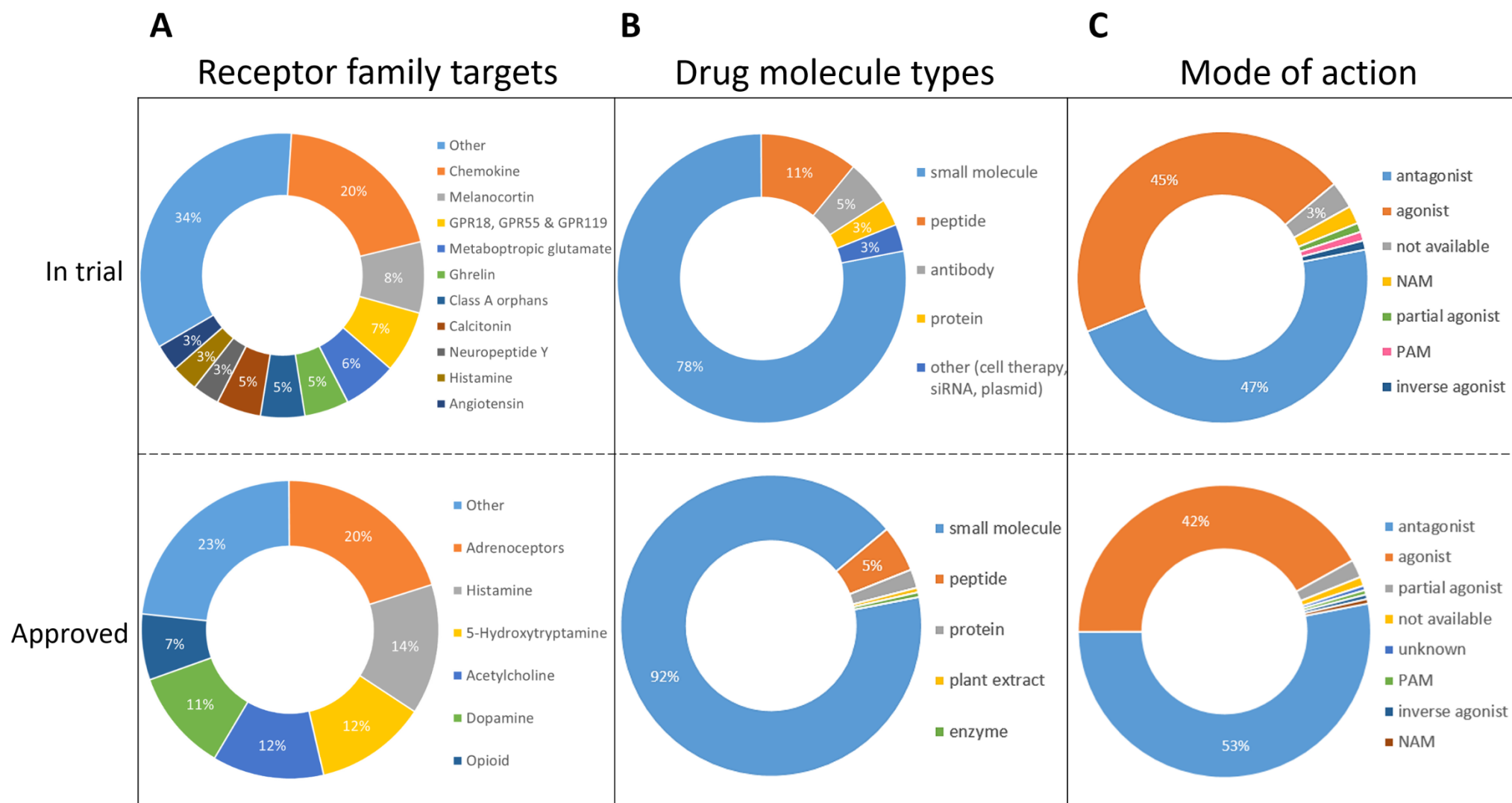


Figure 10.1 Trends in the drug discovery process of GPCR targets in 2017. (A) The receptor family targets for which distinct drug molecule types are in clinical trial or FDA-approved. (B) The different drug molecule types in trial and approved and (C) The mode of action of the different molecule types in trial and approved. Source: GPCRdb. PAM = positive allosteric modulator, NAM = negative allosteric modulator, siRNA = small interfering RNA.

The existence of these GPCR-GPCR complexes actually offers the opportunity to develop new therapeutic approaches for the treatment of distinct diseases. Several pharmacological strategies have already been proposed, including heteromeric-selective mAbs [4], bivalent ligands or allosteric ligands that affect oligomeric assemblies, among others [5].

In **Chapter 5** of this thesis, the aim was to target the dopamine D₂ receptor (D₂R) homodimer, for which an increase in dimer formation has already been associated with schizophrenia [6]. A panel of distinct D₂R antagonists, including spiperone, haloperidol, risperidone and clozapine was screened for their capacity to modulate the level of D₂R dimerization. Interestingly, spiperone was able to decrease the level of dimerization by 40-60% at high concentrations. In Japan, spiperone is licensed for clinical use for the treatment of schizophrenia, under the brand name Spiropitan®. Nevertheless, the administration of high doses of these antipsychotic drugs have been associated with extrapyramidal and autonomic nervous system side effects [7].

Although an effect of spiperone on the D₂R homodimer was observed, the underlying mechanism remains elusive. Consequently, it would be of interest to further investigate the dynamics of the D₂R dimers or oligomers at the single molecule level in real-time by techniques such as single-molecule sensitive total internal reflection fluorescence microscopy (TIRF-M) or the spatial intensity distribution analysis (SpIDA) method to quantify the monomer-dimer(oligomer) ratio present at the plasma membrane.

Besides research in an academic environment, interest in GPCR-GPCR interactions has reached the industry as well. In 2004, a drug discovery company in Melbourne, Dimerix, was built on a platform referred to as the Receptor-Heteromer Investigation Technology (Receptor-HIT), allowing the identification of druggable GPCR dimers (**Figure 10.2**)[8]. This assay employs proximity-based reporter systems, such as a bioluminescence resonance energy transfer (BRET) assay, involving i) a GPCR-A fused to *Renilla* Luciferase (RLuc), also referred to as the donor, ii) an untagged GPCR-B and iii) a yellow fluorescent protein (YFP)-tagged Protein-C, or the acceptor. Protein-C involves a protein that interacts with GPCRs in a ligand-dependent manner, such as β -arrestins or G proteins. Consequently, a BRET signal will only be generated when the ligand-activated GPCR-B recruits Protein-C and simultaneously heterodimerizes with GPCR-A.

Dimerix's lead candidate, DMX-200, has reached a Phase II clinical trial for the treatment of patients suffering from proteinuria (i.e. excessive protein in the urine), which is symptomatic in a range of kidney problems. DMX-200 comprises two drugs, a former blockbuster blood pressure drug irbesartan plus a less-well-known anti-inflammatory drug called propagermanium. The latter mentioned targets the chemokine receptor type 2 (CCR2), that forms heterodimers with angiotensin II receptor type 1 (AT₁R) GPCRs, which is the target of irbesartan. *In vivo* data showed that DMX-200 could decrease the level of proteinuria by 50%, which is considered a clinically meaningful outcome.

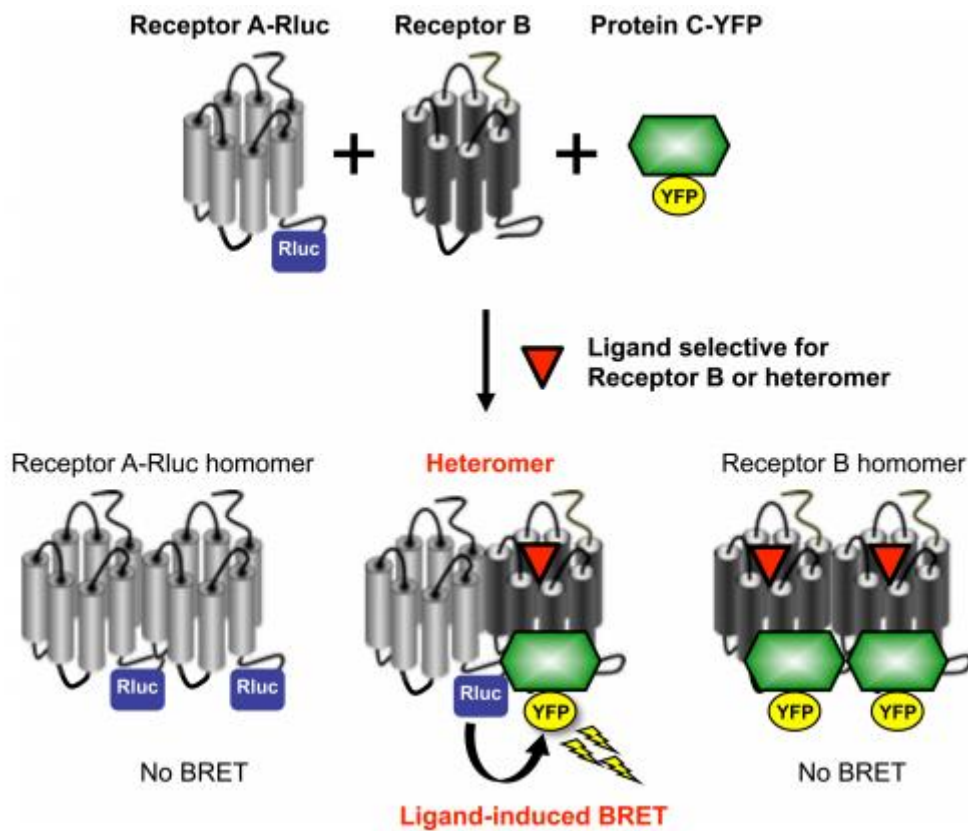


Figure 10.2 The Receptor-Heteromer Investigation Technology (Receptor-HIT) of Dimerix. Upon co-transfection of GPCR-A-RLuc, untagged GPCR-B and Protein-C-YFP, a BRET signal can only be generated when Protein-C-YFP is recruited to the activated GPCR-B, which simultaneously forms a dimer with GPCR-A-RLuc. Source: Johnstone *et al.*, 2012 [8].

Besides targeting a dimer by co-administration of two separate ligands, another approach utilized to target GPCR dimers is the development of bivalent ligands. Those ligands comprise two pharmacophores, linked by a spacer, with the aim to simultaneously bind to both protomers of the dimer with a higher affinity than upon binding to the receptors separately.

In **Chapter 6** bivalent ligands for the D₂R-mGluR₅ heterodimer were synthesized and pharmacologically tested for their ability to bridge both receptors.

Bivalent ligands have proven their utility as pharmacological tools to target GPCRs dimers *in vitro* as well as in animal models. Nevertheless, one should always keep in mind that in cases where negative cooperativity would occur between the two orthosteric sites of the GPCR homo- or heteromer, this will be detrimental for the simultaneous binding of the bivalent ligand to both binding sites [9].

It should be noted that the potential of bivalent ligands to serve as therapeutic compounds for human consumption is currently rather limited. As these compounds typically do not meet all the criteria of the Lipinski's rule of five (see **BOX 10.1**), it is a challenge to formulate these compounds for oral administration. However, intravenous infusion of these ligands could potentially mediate targeting of dimers present in peripheral tissues. To target GPCR dimers in the CNS, crossing of the blood-brain barrier is required, for which a typically low molecular weight and high degree of lipid solubility is required [10], which is not in line with the typical characteristics of bivalent ligands.

BOX 10.1: Lipinski's rule of five

1. No more than 5 hydrogen bond donors (total sum of NH and OH bonds)
2. No more than 10 hydrogen bond acceptors (all N and O atoms)
3. A molecular weight less than 500 daltons
4. An octanol-water participation coefficient (LogP) not greater than 5

Biased signaling

Besides GPCR-GPCR interactions, another phenomenon known as 'biased signaling' or 'functional selectivity' has gained a lot of interest lately. To mediate signaling, GPCRs recruit various intracellular binding partners, e.g. G proteins and β -arrestins. However, every receptor has a natural preference towards a certain signaling pathway (e.g. D₂R and cannabinoid receptor type 1 (CB₁) preferentially couple to G α_i proteins, whereas mGluR₅ prefers signaling through G α_q proteins), also referred to as 'receptor bias'. On the other hand,

biased signaling can also be controlled by the intracellular expression levels of transducers and/or modulating proteins, known as 'system bias'. Finally, the term 'ligand bias' defines the capacity of a ligand to modulate or shift the signaling repertoire of a certain receptor towards a specific signaling pathway while blocking or diminishing other pathways. Mostly, studies have focused on the ligand-mediated distinguishing between the β -arrestin and G protein signaling pathways. However, shifts in the preference of coupling to G protein subtypes (e.g. $G\alpha_i$ over $G\alpha_s$) have also been observed [11]. From a drug development point of view, this offers the possibility to generate ligands with a desired therapeutic profile with less side effects, as the preferred signaling pathway(s) will be activated, while reducing the activation of pathways that mediate the adverse effects.

As of today, several biased ligands acting on distinct GPCRs are in various stages of the drug development process, with some even in clinical trials. For example, G protein biased ligands are being characterized for the μ -opioid receptor (MOR) or CB_1 [12-14], whereas β -arrestin biased ligands show therapeutic potential for diseases involving D_2R or the melanocortin 4 receptor (MC4R) [15, 16].

A well-characterized example comprises the functional selectivity at MOR. MOR agonists, such as morphine and fentanyl, have extensively been used for the treatment of moderate-to-severe acute pain. However, their use is restricted by various undesired side effects, such as respiratory depression, nausea, vomiting and constipation. Interestingly, studies using β -arrestin2 knockout mice reported on the fact that the analgesic effect were retained, yet, the adverse effects were largely attenuated [17, 18]. Consequently, tremendous efforts have been done for the development of G protein-biased MOR ligands as these retain the analgesic properties but hold improved safety profiles [19]. Such an example of a MOR agonist that preferentially signals through the $G\alpha_i$ protein over β -arrestin recruitment, is oliceridine, also known as TRV130 [20, 21]. Recently, the outcomes of a Phase III clinical trial comparing the effects of oliceridine to placebo and morphine treatment in patients with moderate-to-severe postoperative pain were reported [22]. Treatment with oliceridine resulted in a rapid onset of analgesia with reduced gastrointestinal adverse effects as compared to morphine and may thus provide a new short-term treatment option with lower risks of adverse effects.

In the context of the treatment of chronic pain, the over-prescription of opioid medications has led to an ‘addiction opioid crisis’ in the United States. Consequently, health authorities and research laboratories are now focusing on the development of nonopioid treatments. Targeting the endocannabinoid system has already been proposed as an alternative, since there is some evidence of the efficacy of cannabinoids in treatment of chronic pain. More specifically, Δ^9 -tetrahydrocannabinol (Δ^9 -THC) and cannabidiol (CBD), the primary constituents of cannabis, have been applied for medical use. Formulations containing distinct Δ^9 -THC/CBD profiles have been evaluated [23]. But whereas Δ^9 -THC causes the typical ‘high’, CBD is not intoxicating at typical doses. Nevertheless, as convincing evidence on the efficacy of cannabis is still lacking, debates on whether physicians should recommend cannabis as a replacement of opioids is ongoing [24]. Especially for young adolescents for whom the brain has proven to be intrinsically more vulnerable as compared to a mature brain to the adverse effects of the use of cannabis, the impairment in brain connectivity has been associated with exposure to cannabis which is consistent with findings that the cannabinoid system plays a prominent role in synapse formation during brain development [25, 26]. Other adverse effects associated with cannabis usage, such as risk of addiction, paranoia, cognitive impairment, among others have also been reported [26]. Nevertheless, most of these adverse effects of cannabis usage have been observed among heavy or long-term users, which complicates our ability to assess the true effects of exposure to cannabis for medicinal use.

A biopharmaceutical company, Cara Therapeutics Inc., based in Stamford Connecticut, is testing (synthetic) medicinal marijuana, known as CR701, as an alternative for opioids in preclinical trials for the treatment of neuropathic pain. CR701 aims at targeting peripheral CB₂ receptors, thus potentially avoiding the CB₁-mediated psychotropic side effects [27]. Besides for chronic pain treatment, cannabis has also been used or has been suggested for other medical purposes, including management of vomiting and nausea associated with chemotherapy as well as an antiseizure treatment in epilepsy or as an anti-spasmodic in multiple sclerosis (MS) [28-31].

For example, Sativex® is a cannabis-based mouth spray (1:1 ratio of Δ^9 -THC/CBD) used as adjunctive treatment for the symptomatic relief of neuropathic pain (i.e. spasticity) in adult patients with MS [32]. As of today, Sativex® is the only cannabis-based product that is legally available in Belgium, following the 2015 Royal Decree by the health minister. In contrast to

legislation laws in the US (2012) [33] and the UK (2016) [34], which are controlling and banning all substances with psychoactive properties, the Belgian legislation is based on ‘analogue laws’ or ‘generic structure laws’ [35]. The generic legislation not only prohibits all currently known drugs but also illegalizes future analogues of a given structure, as depicted in **Figure 10.3** on the next page for SCRAAs [35]. Interestingly, in Belgium a legal limit of 0.2% Δ^9 -THC content is fixed, thus cannabis plants or products containing less than 0.2% THC are legal and can be sold in cannabis shops [37]. Besides that, cannabis for medical reasons with a higher Δ^9 -THC content is only accessible in Belgium through illegal networks including social supply (e.g. Cannabis social clubs [36]), street circuits, personal cultivation, online sales, or through crossing the border in Dutch pharmacies and coffee shops. Obtaining cannabis from a Dutch pharmacy is possible when prescribed by a Belgian physician. In Belgium, physicians are allowed to prescribe unlicensed medicines, such as cannabis, due to what is called “therapy freedom” [37], yet, the import of cannabis in Belgium is still prohibited. Nevertheless, also in Belgium a new wave in favor of the legislation of cannabis has emerged [38].

Also synthetic cannabinoid receptor agonists (SCRAAs) have been implemented for medicinal use, under the name of dronabinol (marketed as Marinol) and nabilone (marketed as Cesamet). Whereas dronabinol has the identical chemical structure as Δ^9 -THC, nabilone has a related structure and is more potent. The use of both synthetic medicines has been licensed in several countries, including the US, the Netherlands, Germany, Austria, and Croatia [23]. Dronabinol can be prepared through organic chemical synthesis in a relatively high yield and high stereoselectivity [39], however, also the biosynthesis of SCRAAs in *Saccharomyces cerevisiae*, from the simple sugar galactose has been reported [40]. Nevertheless, current clinical use of SCRAAs is limited and underdeveloped, with only a few examples available today (**Table 10.1**).

Similarly as for cannabis, human studies done so far to investigate the therapeutic benefits of SCRAAs have mainly focused on reducing pain, spasticity and cognitive deficits in CNS disorders [41]. Unfortunately, short-term usage of SCRAAs provokes undesired psychotropic effects whereas chronic administration of these agonists results in the development of tolerance and dependence, both limiting the therapeutic utility of these ligands.

BELGIAN GENERIC STRUCTURE LAW FOR SYNTHETIC CANNABINOID RECEPTOR AGONISTS (ROYAL DECREE. 06.09.2017)

For the indoles (A, D), indazoles (B,E) and benzodiazoles (C,F,G,H)

X = -CH₂-, -C(=O)-, -CH₂O-, -C(=O)O- or -C(=O)NH-.

R₁: C_nH_{2n+1}, C_nH_{2n-1}, C_nH_{2n-3} (n = 1-7), phenyl, benzyl, cyclohexylmethyl; with potential extra substitutions with one of the following groups or combination thereof: OH, C(=O)OH, halogen, CN, tetrahydropyranyl, morpholinyl, N-methylpyrrolidinyl, N-methylpiperidinyl or another functional group with maximum 7 C-atoms.

R₂: H, C_nH_{2n+1}, C_nH_{2n-1}, C_nH_{2n-3} (n = 1-7).

R₃: phenyl, benzyl, phenylethyl, naphthalenyl, adamantanyl, quinolinyl, tetracyclopropyl or another functional group with maximum 7 C-atoms; with potential extra substitutions with one of the following groups or combination thereof: halogen, OH, CH₂OH, C(=O)OH, azide, dimethylamino, CN, NO₂ or another functional group with maximum 7 C-atoms.

R₄: H, halogen, methyl, OH, OCH₃, NO₂, CN (on any position the 6-ring of the indole-, indazole- or benzodiazole-group).

R₅: H, phenyl, benzyl, phenylethyl, naphthalenyl, adamantanyl, quinolinyl, tetracyclopropyl or another functional group with maximum 7 C-atoms; with potential extra substitutions with one of the following groups or combination thereof: halogen, OH, CH₂OH, C(=O)OH, azide, dimethylamino, CN, NO₂ or another functional group with maximum 7 C-atoms.

For the pyrroles (I)

X = -CH₂-, -C(=O)-, -CH₂O-, -C(=O)O- or -C(=O)NH-.

R₁: C_nH_{2n+1}, C_nH_{2n-1}, C_nH_{2n-3} (n = 1-7), phenyl, benzyl, cyclohexylmethyl; with potential extra substitutions with one of the following groups or combination thereof: OH, C(=O)OH, halogen, CN, tetrahydropyranyl, morpholinyl, N-methylpyrrolidinyl, N-methylpiperidinyl or another functional group with maximum 7 C-atoms.

R₂: H, halogen, phenyl, halogenphenyl, naphthyl, or another functional group with maximum 7 C-atoms.

R₃: H, halogen, phenyl, halogenphenyl, naphthyl, or another functional group with maximum 7 C-atoms.

R₄: H, halogen, phenyl, halogenphenyl, naphthyl, or another functional group with maximum 7 C-atoms.

R₅: naphthylgroup, or one or more mono- or polycycloalkylgroups (maximum 7 C-atoms), potentially with extra halogen substitutions.

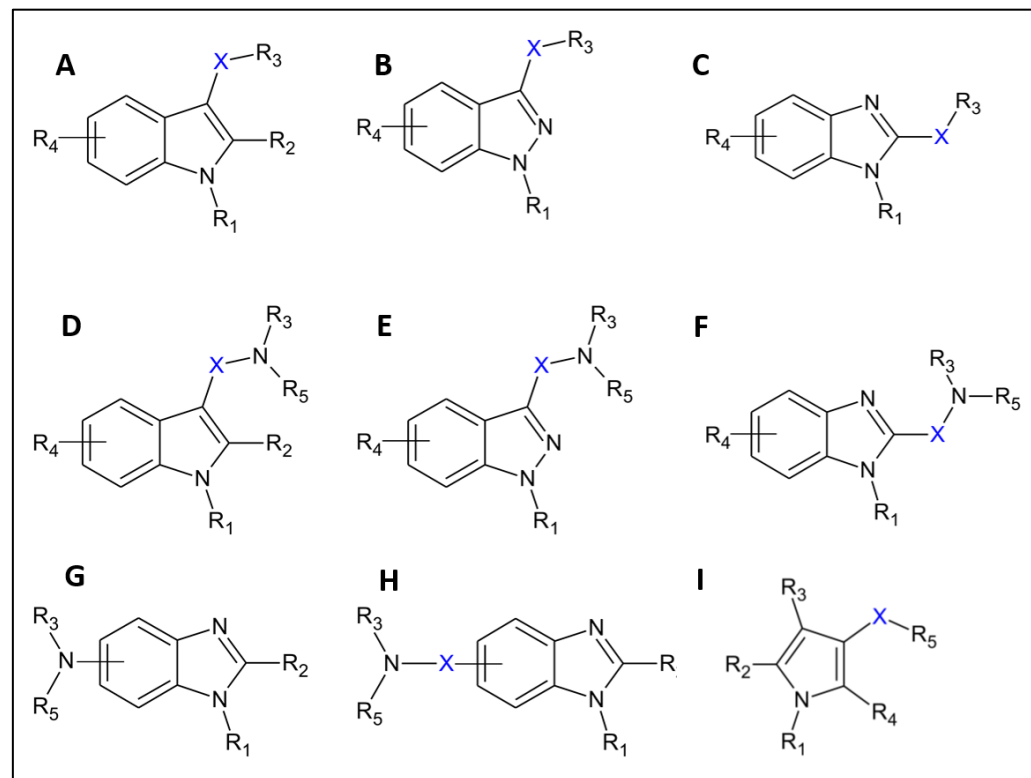


Figure 10.3 The Belgian Generic structure law for SCRA.

Table 10.1 Synthetic cannabinoid receptor agonists (SCRAs) for which therapeutic benefits have been investigated in (pre-)clinical studies, reported in literature. SCRAs investigated in preclinical studies are depicted in white, FDA-approved SCRAs are depicted in green and SCRAs that are withdrawn are depicted in red. Their mode of action, pharmacological effect and comparison with natural cannabinoids are provided. Source: Reddy, 2019 [41].

Synthetic cannabinoid	Mode of action	Pharmacological effect	Comparison with Δ^9 -THC
JWH-175	High affinity for CB ₁	Hypomotility and abuse potential	More potent than Δ^9 -THC
JWH-018 (spice, K2 type herbal blends)	Full agonist for CB ₁ and CB ₂ with some selectivity for CB ₂	Vomiting, agitation, confusion, tachycardia and hallucinations; increase in blood pressure, myocardial ischemia, impairment of neurocognition at lower doses	Higher potency than Δ^9 -THC (four to five times more potent than Δ^9 -THC)
JWH-030	Higher affinity for CB ₁ as compared to CB ₂ ; partial agonist of CB ₁	Analgesic, severe harmful effects on cardiovascular system; mediates cytotoxicity by acting on CB ₂ receptor	Nearly half the potency of Δ^9 -THC
JWH-250	CB ₁ and CB ₂ agonist	Analgesic, severe harmful effects on cardiovascular system	-
JWH-176	High affinity for CB ₁	Analgesic	More potent than Δ^9 -THC
JWH-133	Potent selective CB ₂ agonist; and a lower affinity for CB ₁	Effective in Alzheimer's disease prevention, potent analgesic, anti-inflammatory, effective against pathogenesis of psoriasis; chemotherapeutic effect against gliomas	-
CP 47, 497	CB ₁ agonist	Analgesic, anticonvulsant, hypothermic effects	Equivalent potency to Δ^9 -THC
HU-210	Synthetic agonist analog of Δ^9 -THC, potent CB ₁ and CB ₂ agonists; involves ATP sensitive K ⁺ channels	Effective in prevention of Alzheimer's disease, potent analgesic; neuroprotection; anti-arrhythmic; anti-nociceptive	100–800 times more potent than Δ^9 -THC with extended duration of action
WIN55,212-2	Binds with both CB ₁ and CB ₂ ; full agonist of CB ₁	Effective in Alzheimer's disease and Parkinson's disease prevention, potent analgesic, anti-inflammatory, intra-ocular pressure reduction; reduction of cardiac ischemia-reperfusion injury in rat models; effective against multiple sclerosis in mice model, anti-tumor effects	Higher affinity for cannabinoid receptors than Δ^9 -THC
SR141716 (Rimonabant)	Antagonist or inverse agonist for CB ₁	Anorectic anti-obesity drug, causes sleep disorders, nausea, skin irritation, diarrhea, fatigue, cramps, and spasms	Opposite activity to Δ^9 -THC
Nabilone	CB _{1/2} agonist	Treatment of cannabis dependence; antiemetic, analgesic, Chemotherapy induced nausea, and vomiting	Mimics Δ^9 -THC
Dronabinol	CB _{1/2} agonist	Anti-emetic, anti-anorexic	Synthetic form of Δ^9 -THC; chemically known as Δ^9 tetrahydrocannabinol

Evidence suggests that, similarly as for MOR, G protein-biased ligands may exhibit reduced adverse effects as both acute (e.g. antinociception) and chronic (e.g. tolerance) responses to Δ^9 -THC improved in β -arrestin2 knockout mice [42, 43].

As of today, the discovery of biased CB_{1/2} ligands has been minimal [44, 45]. In addition, the exact mode of action underlying the toxic effects remains unknown. Hence, there is a need for research in this field to unravel the mechanism(s) responsible for the therapeutic or toxic effects by specific SCRA. In **Chapter 8**, a first attempt to unravel these underlying mechanisms involved the investigation of the prevalence of biased signaling mediated by a panel of structurally diverse SCRA. Certain SCRA, with a carbazole group as head group (e.g. EG-018), displayed a preference towards G protein signaling. To what extent these *in vitro* results can be projected to the *in vivo* situation remains elusive. However, studies by Ehrlich *et al.* (2019) [46] involving *in vitro* BRET assays for the characterization of MOR biased agonists, showed similar results as the *in vivo* outcomes. Moreover, also in the case of SCRA, such as PNR-4-20, *in vitro* observations involving the preferential G protein-dependent signaling over β -arrestin2 signaling could be translated to fewer adverse effects (e.g. reduced tolerance) measured *in vivo* [12, 13].

Although several advances have already been reached in the field of biased signaling, future structure-relationship studies are a prerequisite for the development of high affinity, highly selective and bioactive (i.e. considering the drug solubility, drug metabolism and adequately crossing the blood-brain barrier) G protein-biased cannabinoid agonists that could serve as potential therapeutics.

Pharmacokinetic properties of these SCRA, such as drug metabolism, are not only important for the consequences on the half-life and circulating levels of a bioactive parent drug for therapeutic purposes, but also for the potential contribution to the overall toxicological profile associated with SCRA. Given the aforementioned undesired effects (or 'desired', depending on the context) of the parent compounds, including psychotropic effects, tolerance and dependence, one might wonder to what extent rapid metabolization of the parent compound contributes to the rapid detoxification of these compounds. SCRA are typically subjected to rapid Phase I metabolism by a panel of possible enzymes, including cytochrome P450 enzymes and carboxylesterases. These Phase I metabolites will be further deactivated by the

conjugation of for example glutathione by glutathione-S-transferases to produce more polar metabolites that cannot cross membranes and will be subsequently excreted. Yet, in many instances it remains elusive whether Phase I metabolites could still contribute to the overall toxicological profile provoked by the parent compounds.

In **Chapter 9**, this was investigated for the carboxy metabolites of SCRA with scaffolds based on L-valine and L-*tert*-leucine. *In vitro* studies revealed that certain Phase I metabolites still retain activity, although significantly impaired as compared to the parent compounds. Nevertheless, the possible toxicological effect of Phase I SCRA metabolites *in vivo* remains an unexplored research field. Consequently, an important question remaining is whether and to what extent these metabolites can cross the blood-brain barrier. Thus, to fully explore the possible contribution of active metabolites of parent SCRA compounds to the toxicological profile *in vivo*, the most straightforward manner would involve the intravenous injection of distinct metabolites in animal models, characterization of the effects elicited by these drugs and, linked to this, analysis of brain extracts for the presence of these drugs [47].

Overall, the activity-based bio-assays applied in **Chapter 8 & 9**, based on the recruitment of different transducers to CB₁, have shown here to successfully serve as a first-line screening tool in unraveling preferences towards certain signaling pathways as well as for activity profiling of metabolites. Interestingly, besides being useful in the context of drug development, these assays have also been successfully exploited by our research group for drug detection in biological fluids [48-51]. As the currently available ‘targeted screening assays’, including liquid chromatography with tandem mass spectrometry (LC-MS/MS), ELISA and immunoassays, require the knowledge of chemical structures and their spectral profiles of NPS, these ‘untargeted’ activity-based bio-assays may serve as a straightforward first-line detection screening tool. The already developed bio-assays are currently based on the recruitment of β -arrestin2 to the activated CB₁, CB₂ and MOR [48-51]. Nevertheless, although biased signaling is considered to be a ‘rare phenomenon’, the co-expression of both transducers, i.e. mini-G α_i and β -arrestin2 in these bio-assays could potentially further increase the sensitivity of these bio-assays for NPS detection.

The merging of two distinct worlds: GPCR-GPCR interactions and biased signaling

Until recently, biased signaling and GPCR di-/oligomerization were considered and investigated as two distinct phenomena. Nevertheless, GPCR-GPCR allosteric interactions have already been proposed as a possible explanation for biased signaling effects.

For the ligand-dependent modulation of GPCR-GPCR interactions, two possible mechanisms have already been proposed, including dose-dependent modulation and heteromer-biased ligands. Within the perspective of dose-dependent modulation of dimer signaling, it has been hypothesized by Zou *et al.* (2018) [52] that these findings could be explained by yet another phenomenon, involving a single occupied dimer versus a double occupied dimer preferentially signaling through G protein-dependent and -independent signaling pathways, respectively. This might contribute to the understanding of complex dosing regimens of certain drugs to provoke the desired therapeutic effect. On the other hand, an alternative approach in drug development, although highly complex, involves heteromer-biased ligands, which are ligands that specifically target the heterodimer and consequently alter the preferred signaling pathway mediated by the dimer.

For the two main GPCRs of interest within this thesis, namely D₂R and CB₁, biased signaling has been observed for each GPCR as well as the formation of heteromers comprising these GPCRs [53, 54]. Interestingly, heteromer-biased signaling has already been observed for the CB₁-D₂R heterodimer [55, 56]. Co-stimulation of both receptors in striatal neurons led to increased cAMP levels, whereas stimulation of both receptors separately decreases the levels of cAMP. Therefore, it is believed that the (constitutive) active D₂R promotes an increased coupling of the G α_s protein instead of the G α_i protein to the CB₁ receptor [55]. Although it has already been speculated that there might be a link with Huntington's disease, the real underlying mechanism of this dimer as well as to what extent this dimer might be related to a pathophysiological process, remains unknown and requires further investigation.

One thing is sure:

There are interesting days ahead.

References

1. Hauser, A.S., et al., *Trends in GPCR drug discovery: new agents, targets and indications*. Nature reviews. Drug discovery, 2017. **16**(12): p. 829-842.
2. Changeux, J.P. and A. Christopoulos, *Allosteric modulation as a unifying mechanism for receptor function and regulation*. Diabetes, obesity and metabolism, 2017. **19** p. 4-21.
3. Guidolin, D., et al., *Receptor-Receptor Interactions as a Widespread Phenomenon: Novel Targets for Drug Development?* Frontiers in endocrinology 2019. **10**: p. 53.
4. Gomes, I., et al., *Antibodies to probe endogenous G protein-coupled receptor heteromer expression, regulation, and function*. Frontiers in pharmacology, 2014. **5**: p. 268.
5. Carli, M., et al., *Dopamine D2 Receptors Dimers: How can we Pharmacologically Target Them?* Current neuropharmacology, 2018. **16**(2): p. 222-230.
6. Wang, M., et al., *Schizophrenia, amphetamine-induced sensitized state and acute amphetamine exposure all show a common alteration: increased dopamine D2 receptor dimerization*. Molecular brain, 2010. **3**: p. 25.
7. Sukegawa, T., et al., *Study protocol: safety correction of high dose antipsychotic polypharmacy in Japan*. BMC psychiatry, 2014. **14**: p. 103.
8. Johnstone, E.K. and K.D. Pflieger, *Receptor-Heteromer Investigation Technology and its application using BRET*. Frontiers in endocrinology, 2012. **3**: p. 101.
9. Daniels, D.J., et al., *Opioid-induced tolerance and dependence in mice is modulated by the distance between pharmacophores in a bivalent ligand series*. Proceedings of the national academy of sciences of the United States of America, 2005. **102**(52): p. 19208-13.
10. Banks, W.A., *Characteristics of compounds that cross the blood-brain barrier*. BMC neurology, 2009. **9** p. S3.
11. Seyedabadi, M., M.H. Ghahremani, and P.R. Albert, *Biased signaling of G protein coupled receptors (GPCRs): Molecular determinants of GPCR/transducer selectivity and therapeutic potential*. Pharmacology & therapeutics, 2019.
12. Ford, B.M., et al., *Reduced Tolerance and Asymmetrical Crosstolerance to Effects of the Indole Quinuclidinone Analog PNR-4-20, a G Protein-Biased Cannabinoid 1 Receptor Agonist in Mice: Comparisons with Delta(9)-Tetrahydrocannabinol and JWH-018*. Journal of pharmacology and experimental therapeutics, 2019. **369**(2): p. 259-269.
13. Ford, B.M., et al., *Characterization of structurally novel G protein biased CB1 agonists: Implications for drug development*. Pharmacol. Res., 2017. **125**(Pt B): p. 161-177.
14. Schmid, C.L., et al., *Bias Factor and Therapeutic Window Correlate to Predict Safer Opioid Analgesics*. Cell, 2017. **171**(5): p. 1165-1175 e13.
15. Donthamsetti, P., et al., *Arrestin recruitment to dopamine D2 receptor mediates locomotion but not incentive motivation*. Mol. Psychiatry, 2018.
16. Lotta, L.A., et al., *Human Gain-of-Function MC4R Variants Show Signaling Bias and Protect against Obesity*. Cell, 2019. **177**(3): p. 597-607 e9.
17. Bohn, L.M., et al., *Enhanced morphine analgesia in mice lacking beta-arrestin 2*. Science 1999. **286**(5449): p. 2495-8.
18. Raehal, K.M., J.K. Walker, and L.M. Bohn, *Morphine side effects in beta-arrestin 2 knockout mice*. The Journal of pharmacology and experimental therapeutics, 2005. **314**(3): p. 1195-201.
19. Kennedy, N.M., et al., *Optimization of a Series of Mu Opioid Receptor (MOR) Agonists with High G Protein Signaling Bias*. Journal of medicinal chemistry, 2018. **61**(19): p. 8895-8907.
20. Singla, N., et al., *A randomized, Phase IIb study investigating oliceridine (TRV130), a novel micro-receptor G-protein pathway selective (mu-GPS) modulator, for the management of moderate to severe acute pain following abdominoplasty*. Journal of pain research, 2017. **10**: p. 2413-2424.
21. Soergel, D.G., et al., *Biased agonism of the mu-opioid receptor by TRV130 increases analgesia and reduces on-target adverse effects versus morphine: A randomized, double-blind, placebo-controlled, crossover study in healthy volunteers*. Pain, 2014. **155**(9): p. 1829-35.

22. Viscusi, E.R., et al., *APOLLO-1: a randomized placebo and active-controlled phase III study investigating oliceridine (TRV130), a G protein-biased ligand at the micro-opioid receptor, for management of moderate-to-severe acute pain following bunionectomy*. Journal of pain research, 2019. **12**: p. 927-943.
23. Freeman, T.P., et al., *Medicinal use of cannabis based products and cannabinoids*. British medical journal, 2019. **365**: p. l1141.
24. Humphreys, K. and R. Saitz, *Should Physicians Recommend Replacing Opioids With Cannabis?* Journal of the American medical association, 2019.
25. Gaffuri, A.L., D. Ladarre, and Z. Lenkei, *Type-1 cannabinoid receptor signaling in neuronal development*. Pharmacology, 2012. **90**(1-2): p. 19-39.
26. Volkow, N.D., et al., *Adverse health effects of marijuana use*. The New England journal of medicine, 2014. **370**(23): p. 2219-27.
27. Urits, I., et al., *An Update of Current Cannabis-Based Pharmaceuticals in Pain Medicine*. Pain and therapy, 2019. **8**(1): p. 41-51.
28. Albertson, T.E., et al., *The Changing Drug Culture: Medical and Recreational Marijuana*. FP essentials, 2016. **441**: p. 11-7.
29. Bar-Sela, G., et al., *Cannabis-related cognitive impairment: a prospective evaluation of possible influences on patients with cancer during chemotherapy treatment as a pilot study*. Anticancer drugs, 2019. **30**(1): p. 91-97.
30. Schleider, L.B.L., et al., *Prospective analysis of safety and efficacy of medical cannabis in large unselected population of patients with cancer*. European journal of internal medicine, 2018. **49**: p. 37-43.
31. Friedman, D. and O. Devinsky, *Cannabinoids in the Treatment of Epilepsy*. The New England journal of medicine, 2015. **373**(11): p. 1048-58.
32. Markova, J., et al., *Sativex(R) as add-on therapy vs. further optimized first-line ANTispastics (SAVANT) in resistant multiple sclerosis spasticity: a double-blind, placebo-controlled randomised clinical trial*. The International journal of neuroscience, 2019. **129**(2): p. 119-128.
33. USA, Synthetic Drug Abuse Prevention Act of 2012. *Food and Drug Administration Safety and Innovation Act (FDASIA)*. 2012. Section 1151-1153, 126 STAT. 1130-1132.
34. UK, Psychoactive Substances Act 2016. 2016. Chapter 2, 1-57.
35. Belgisch Staatsblad, Koninklijk Besluit houdende regeling van verdovende middelen, psychotrope stoffen (Federale overheidsdienst Volksgezondheid Veiligheid van de voedselketen en leefmilieu). KB. 06.09.2017. Brussels, 2017.
36. Pardal, M. and F. Bawin, *The Supply of Cannabis for Medical Use Through Cannabis Social Clubs in Belgium*. Contemporary Drug Problems, 2018. **45**(2): p. 127-145.
37. Federaal Agentschap voor Geneesmiddelen en Gezondheidsproducten. *FAQ cannabis*. 2017; Available from: https://www.fagg-afmps.be/nl/MENSELIJK_gebruik/bijzondere_producten/speciaal_gereguleerde_stoffen/verdovende_middelen/faq_cannabis.
38. Leus, X. and G. Van Hal, *A new wave of marijuana legalization: country case study from Belgium*. European journal of public health, 2019. **29**(3): p. 388.
39. Souza, F.E.S., et al., *Synthetic route to dronabinol*. 2004, Sandoz Inc: US.
40. Luo, X., et al., *Complete biosynthesis of cannabinoids and their unnatural analogues in yeast*. Nature, 2019. **567**(7746): p. 123-126.
41. Muralidhar Reddy, P., N. Maurya, and B.K. Velmurugan, *Medicinal Use of Synthetic Cannabinoids—a Mini Review*. Current pharmacology reports, 2019. **5**(1): p. 1-13.
42. Nguyen, P.T., et al., *beta-arrestin2 regulates cannabinoid CB1 receptor signaling and adaptation in a central nervous system region-dependent manner*. Biological psychiatry, 2012. **71**(8): p. 714-24.
43. Raehal, K.M. and L.M. Bohn, *beta-arrestins: regulatory role and therapeutic potential in opioid and cannabinoid receptor-mediated analgesia*. Handbook of experimental pharmacology, 2014. **219**: p. 427-43.

44. Al-Zoubi, R., P. Morales, and P.H. Reggio, *Structural Insights into CB1 Receptor Biased Signaling*. Int. J. Mol. Sci., 2019. **20**(8).
45. Oyagawa, C.R.M., et al., *Cannabinoid Receptor 2 Signalling Bias Elicited by 2,4,6-Trisubstituted 1,3,5-Triazines*. Frontiers in pharmacology, 2018. **9**: p. 1202.
46. Ehrlich, A.T., et al., *Biased Signaling of the Mu Opioid Receptor Revealed in Native Neurons*. iScience, 2019. **14**: p. 47-57.
47. Loryan, I., et al., *Mechanistic understanding of brain drug disposition to optimize the selection of potential neurotherapeutics in drug discovery*. Pharmaceutical research, 2014. **31**(8): p. 2203-19.
48. Cannaert, A., et al., *Activity-based detection of consumption of synthetic cannabinoids in authentic urine samples using a stable cannabinoid reporter system*. Anal. Chem., 2017. **89**(17): p. 9527-9536.
49. Cannaert, A., et al., *Detection and Activity Profiling of Synthetic Cannabinoids and Their Metabolites with a Newly Developed Bioassay*. Anal. Chem., 2016. **88**(23): p. 11476-11485.
50. Cannaert, A., et al., *Activity-Based Detection of Cannabinoids in Serum and Plasma Samples*. Clin Chem, 2018.
51. Cannaert, A., et al., *Activity-Based Concept to Screen Biological Matrices for Opiates and (Synthetic) Opioids*. Clinical chemistry, 2018. **64**(8): p. 1221-1229.
52. Zhou, B. and J. Giraldo, *An operational model for GPCR homodimers and its application in the analysis of biased signaling*. Drug discovery today, 2018. **23**(9): p. 1591-1595.
53. Bagher, A.M., et al., *Bidirectional allosteric interactions between cannabinoid receptor 1 (CB1) and dopamine receptor 2 long (D2L) heterotetramers*. European journal of pharmacology, 2017. **813**: p. 66-83.
54. Marcellino, D., et al., *Antagonistic cannabinoid CB1/dopamine D2 receptor interactions in striatal CB1/D2 heteromers. A combined neurochemical and behavioral analysis*. Neuropharmacology, 2008. **54**(5): p. 815-23.
55. Hudson, B.D., T.E. Hebert, and M.E. Kelly, *Ligand- and heterodimer-directed signaling of the CB(1) cannabinoid receptor*. Molecular pharmacology, 2010. **77**(1): p. 1-9.
56. Mustafa, S., M.A. Ayoub, and K.D. Pflieger, *Uncovering GPCR heteromer-biased ligands*. Drug discovery today. Technologies, 2010. **7**(1): p. e1-e94.

Chapter 11:

Conclusion and Summary

G protein-coupled receptors (GPCRs) are involved in the regulation of multiple physiological processes. An altered regulation and/or expression level of these GPCRs has already frequently been linked to distinct diseases. As a direct consequence, one third of the modern medicinal drugs target GPCRs. However, in certain cases adverse events or side effects are observed after long-term use of these drugs, which hampers their therapeutic utility. As scientific research is continuously evolving, new strategies for the development of novel drug therapies are nonstop being explored. Two of those strategies that currently gained a lot of interest in the scientific community involve targeting GPCR dimers/oligomers as well as a phenomenon known as ‘biased signaling’. The fact that both strategies could possibly open up new avenues in drug development processes are briefly discussed in **Chapter 1**.

In this thesis, those two strategies were further investigated for two different members of the Rhodopsin family, namely the dopamine D₂ receptor (D₂R) (**Part I**, for GPCR-GPCR interactions) and the cannabinoid receptor type 1 (CB₁) (**Part II**, for biased signaling).

In **Part I** of this thesis, the focus lies on GPCR-GPCR interactions. Over the past 2 decades, a growing body of evidence suggests that GPCRs are able to form dimers and/or even higher-order oligomers. An introduction on GPCR oligomerization, mainly involving the D₂R, and a detailed description on the reason why and how to target these complexes is provided in **Chapter 2**.

For the identification and characterization of specific GPCR-GPCR interactions of interest, a robust *in vitro* assay in an overexpression system can be implemented. A straightforward biochemical technique that has often been applied involves protein complementation assays (PCAs). These assays rely on the fusion of two split fragments of a fluorescent or luminescent protein to the proteins of interest (POI). Upon interaction of the POI, the two split fragments come into close proximity, and fluorescence or luminescence can be measured. A panel of distinct fluorescent and luminescent PCAs have been developed and described previously. In **Chapter 3** an overview of the available PCAs which have been utilized to study GPCR oligomerization is given and their respective pros and cons are described.

In **Chapter 4**, different PCAs, based on split fragments of Venus, *Renilla* luciferase and Nanoluciferase were compared in similar experimental set-ups, using the D₂R homodimer as a reference. When compared to the other evaluated PCAs, a higher signal-to-noise ratio was

observed for approach applying the NanoLuciferase Binary Technology (NanoBiT®), compromising functional complementation of a large (LgBiT, 18 kDa) and a small fragment (SmBiT, 1 kDa) of NanoLuciferase.

In **Chapter 5**, the modulating capacity of several clinically used D₂R antagonists on the level of D₂R homodimerization or higher-order oligomerization was evaluated using the aforementioned NanoBiT® bio-assay. As an increase in D₂R homodimer formation has been correlated with the pathophysiology of schizophrenia, targeting these D₂R dimers might offer new information about the pathophysiology of diseases related to this GPCR dimer, potentially opening new therapeutic avenues. In this study, incubation with the D₂R antagonist spiperone decreased the level of D₂L₁R dimer formation significantly by 40–60% in real-time and after long-term (≥16 h) incubations. The fact that dimer formation of the well-studied A_{2a}–D₂L₁R dimer was not altered following incubation with spiperone supports the specificity of this observation.

Besides the formation of homo-oligomers, D₂R can mediate heterodimer interactions with numerous other GPCRs, including the metabotropic glutamate receptor 5 (mGluR₅). A pharmacological tool to validate the existence of these GPCRs involves bivalent ligands. These ligands are envisioned to show a greater potency than that stemming from the sum of their two constituting pharmacophores. In **Chapter 6**, bivalent ligands comprising the D₂R agonist 5-OH-DPAT and a negative allosteric modulator of mGluR₅ (MTEP) were evaluated in radioactive ligand binding and cyclic AMP (cAMP) assays. A 2- and 4-fold increase in affinity was observed for HEK293T cells co-expressing D₂S₁R and mGluR₅, when compared to cells solely expressing mGluR₅ or D₂S₁R, respectively. Likewise, cAMP assays revealed that the bivalent ligand had a 4-fold higher potency in stable D₂S₁R and mGluR₅ co-expressing cell lines compared to its monovalent precursor. The outcome of this study indicates that the bivalent ligand is able to bridge binding sites of both receptors constituting the heterodimer.

In **Part II** of this thesis, the focus lies on GPCR-transducer interactions, more specifically on the recruitment of β -arrestin2 or the G α_i protein to CB₁, provoked by the addition of synthetic cannabinoid receptor agonists (SCRAs).

Interestingly, it has been previously observed that certain ligands can preferentially activate specific signaling pathways, while blocking others, a phenomenon known as ‘biased signaling’

or ‘functional selectivity’. **Chapter 7** provides insights into the recent knowledge about biased agonism mediated by SCRA. In addition, a comprehensive overview of the pharmacological evaluation of SCRA reported in literature is given. As these are obtained using a distinct panel of functional assays, the accompanying difficulties and challenges when comparing functional outcomes are critically discussed.

To investigate SCRA-mediated biased signaling, stable HEK293T cell lines were generated, again utilizing NanoBiT® technology. These cell lines co-express CB₁ (C-terminally tagged with LgBiT) and the transducer, either mini-Gα_i or β-arrestin2 (N-terminally tagged to SmBiT) (**Chapter 8**). Consequently, the occurrence of biased signaling upon SCRA activation of CB₁ could be evaluated in analogous experimental set-ups and in the same cellular context. CP55,940 was selected as the non-biased reference compound as this SCRA equally provokes mini-Gα_i or β-arrestin2 recruitment. From a panel of 21 SCRA, one β-arrestin2-biased SCRA (5F-APINACA) and one mini-Gα_i-biased SCRA (EG-018) could be identified.

In **Chapter 9**, we further explore the applicability of the stable CB₁:β-arrestin2 NanoBiT® cell system for the activity profiling of a panel of seven common hydrolysis metabolites of fifteen SCRA featuring scaffolds based on L-valine or L-*tert*-leucine in direct comparison to their parent compounds. From this study, it could be concluded that certain carboxy metabolites, such as 5F-ADB-PINACA-COOH, AB-CHMINACA-COOH and ADB-FUBINACA-COOH, still do retain activity at high concentrations. Specifically, efficacies of 2 to 3-fold higher than that of the reference compound JWH-018 were observed for these carboxy metabolites. Therefore, it might be concluded that these metabolites could still contribute to the toxicological profile of SCRA *in vivo*.

Overall, the outcomes of both parts of this thesis contribute a small piece to the puzzle of the complex world of GPCR oligomerization and biased signaling. In both parts the work done here involves *in vitro* experiments from which a general knowledge base could be built that allows better insights into both investigated phenomena. Further concerted in-depth studies involving computational modeling, functional screening or activity profiling, site-directed mutagenesis and *in vivo* animal model studies will allow us and others to better understand the underlying mechanisms of GPCR oligomerization and biased signaling. Nevertheless, for now we can conclude with the fact that it is safe to say that, whether it is the action of dopamine or ‘dope’, it is all about interaction!

Samenvatting

G proteïne-gekoppelde receptoren (GPCR's) zijn betrokken bij de regulatie van meerdere fysiologische processen. Een gewijzigde regulatie en/of expressieniveau van deze GPCR's is al vaak in verband gebracht met verschillende ziekten. Als een direct gevolg is één derde van de moderne geneesmiddelen gericht op GPCR's. In bepaalde gevallen worden echter nadelige bijwerkingen waargenomen na langdurig gebruik van deze geneesmiddelen, hetgeen hun therapeutisch nut belemmert. Terwijl het wetenschappelijk onderzoek voortdurend evolueert, worden nieuwe strategieën voor de ontwikkeling van nieuwe geneesmiddeltherapieën continu onderzocht. Twee van die strategieën die momenteel veel belangstelling van de wetenschappelijke onderzoekswereld hebben gekregen, zijn gericht op GPCR-dimeren/oligomeren en een fenomeen dat bekend staat als '*biased* signalisatie'. Het feit dat beide strategieën mogelijk nieuwe wegen kunnen openen voor de ontwikkeling van geneesmiddelen, wordt kort besproken in **Hoofdstuk 1**.

In dit proefschrift werden deze twee strategieën verder onderzocht voor twee verschillende leden van de Rhodopsine-familie, namelijk de dopamine D₂-receptor (D₂R) (**Deel I**, voor GPCR-GPCR-interacties) en de cannabinoïde receptor type 1 (CB₁) (**Deel II**, voor *biased* signalisatie).

In **Deel I** van dit proefschrift ligt de focus op GPCR-GPCR interacties. In de afgelopen 2 decennia suggereert een toenemend aantal experimenten dat GPCR's in staat zijn om dimeren en/of zelfs hogere orde oligomeren te vormen. Een inleiding over GPCR-oligomerisatie, voornamelijk met betrekking tot de D₂R, en een gedetailleerde beschrijving van de reden waarom en hoe deze complexen kunnen *getarget* worden, wordt gegeven in **Hoofdstuk 2**.

Voor de identificatie en karakterisering van specifieke GPCR-GPCR-interacties kan een robuuste *in vitro assay* in een overexpressiesysteem worden geïmplementeerd. Een eenvoudige biochemische techniek die reeds vaak is toegepast, omvat proteïne complementatie-*assays* (PCA's). Deze *assays* berusten op de fusie van twee gesplitste fragmenten van een fluorescent of luminescent proteïne aan de proteïnes van interesse (POI). Bij interactie van de POI komen de twee gesplitste fragmenten dicht in elkaars buurt en kan fluorescentie of luminescentie worden gemeten. Een panel van verschillende fluorescente en luminescente PCA's is eerder al ontwikkeld en beschreven. In **Hoofdstuk 3** wordt een overzicht gegeven van de beschikbare PCA's die reeds zijn toegepast om GPCR-oligomerisatie te bestuderen en worden hun respectievelijke voor- en nadelen beschreven.

In **Hoofdstuk 4** werden verschillende PCA's, gebaseerd op gesplitste fragmenten van Venus, *Renilla* luciferase en Nanoluciferase vergeleken in analoge experimentele opstellingen, met behulp van het D₂R-homodimeer als referentie. In vergelijking met de andere geëvalueerde PCA's, werd een hogere signaal-ruisverhouding waargenomen bij de NanoLuciferase binaire technologie (NanoBiT®), die gebaseerd is op de functionele complementatie van een groot (LgBiT, 18 kDa) en een klein fragment (SmBiT, 1 kDa) van NanoLuciferase.

In **Hoofdstuk 5** werd de modulerende capaciteit van verschillende klinisch toegepaste D₂R-antagonisten op het niveau van D₂R-homodimerisatie (of hogere orde oligomerisatie) geëvalueerd met behulp van de hiervoor genoemde NanoBiT® bio-assay. Omdat een toename van de vorming van het D₂R-homodimeer gecorreleerd is met de pathofysiologie van schizofrenie, zou het *targeten* van deze D₂R-dimeren nieuwe informatie kunnen bieden over de pathofysiologie van ziekten gerelateerd aan dit GPCR-dimeer, waardoor mogelijk nieuwe therapeutische wegen worden geopend. In deze studie verminderde incubatie met de D₂R-antagonist spiperone het niveau van D₂L-dimeervorming aanzienlijk met 40-60% in *real-time* en na lange termijn (> 16 uur) incubaties. Het feit dat de dimeervorming van het goed bestudeerde A_{2a}-D₂L-dimeer niet veranderde na incubatie met spiperone, ondersteunt de specificiteit van deze waarneming.

Naast de vorming van homo-oligomeren, kan de D₂R eveneens heterodimeer-interacties aangaan met tal van andere GPCR's, waaronder de metabotrope glutamaatreceptor 5 (mGluR₅). Een farmacologisch hulpmiddel om het bestaan van deze GPCR dimeren te valideren zijn bivalente liganden. Het doel van deze liganden is een grotere affiniteit van de liganden voor de receptoren te verkrijgen dan diegene die afkomstig is van de som van hun twee samenstellende farmacoforen. In **Hoofdstuk 6** werden bivalente liganden, die de D₂R-agonist 5-OH-DPAT en een negatieve allosterische modulator van mGluR₅ (MTEP) omvatten, geëvalueerd in radioactieve ligandbinding en cyclische AMP (cAMP)-assays. Een 2- en 4-voudige toename in affiniteit werd waargenomen voor HEK293T-cellen die gelijktijdig D₂S₂R en mGluR₅ tot expressie brengen, indien vergeleken met cellen die uitsluitend mGluR₅ of D₂S₂R tot expressie brengen. Evenzo onthulde de cAMP-assay dat het bivalent ligand een 4-voudig hogere potentie had in stabiele cellijnen die D₂S₂R en mGluR₅ tot co-expressie brengen in vergelijking met zijn monovalente precursor. De uitkomst van deze studie geeft aan dat het

bivalente ligand in staat is om de bindingsplaatsen van beide receptoren die het heterodimeer vormen te overbruggen.

In **Deel II** van dit proefschrift ligt de nadruk op GPCR-transducer-interacties, meer specifiek op de rekrutering van β -arrestin2 of het $G\alpha_i$ -eiwit naar CB_1 , veroorzaakt door de toevoeging van synthetische cannabinoïde receptor agonisten (SCRA's).

Interessant is dat eerder is waargenomen dat bepaalde liganden bij voorkeur specifieke signalisatiesroutes kunnen activeren, terwijl andere worden geblokkeerd, een verschijnsel dat bekend staat als '*biased* signalisatie' of 'functionele selectiviteit'. **Hoofdstuk 7** biedt inzicht in de recente kennis over *biased* signalisatie gemedieerd door SCRA's. Daarnaast wordt een uitgebreid overzicht gegeven van de farmacologische karakteristieken van SCRA's die in de literatuur zijn gerapporteerd. Omdat deze verkregen werden met behulp van een heel divers panel van functionele testen, worden de bijbehorende moeilijkheden en uitdagingen bij het vergelijken van deze functionele uitkomsten kritisch besproken.

Om SCRA-gemedieerde *biased* signalisatie te onderzoeken, werden stabiele HEK293T-cellijnen gegenereerd, opnieuw met behulp van de NanoBiT®-technologie. Deze cellijnen brengen tegelijkertijd CB_1 tot expressie (C-terminaal gelabeld met LgBiT) en de transducer, ofwel mini- $G\alpha_i$ of β -arrestin2 (N-terminaal gelabeld aan SmBiT) (**Hoofdstuk 8**). Bijgevolg kon het optreden van *biased* signalisatie na SCRA-activering van de CB_1 worden geëvalueerd in analoge experimentele opstellingen en in dezelfde cellulaire context. CP55,940 werd geselecteerd als het niet-*biased* referentie ligand, omdat deze SCRA een gelijkaardige mini- $G\alpha_i$ of β -arrestin2 rekrutering uitlokt. Uit een heel divers panel van 21 SCRA's konden één β -arrestin2-*biased* SCRA (5F-APINACA) en één mini- $G\alpha_i$ -*biased* SCRA (EG-018) worden geïdentificeerd.

In **Hoofdstuk 9** onderzoeken we verder de toepasbaarheid van het stabiele CB_1 : β -arrestin2 NanoBiT®-celsysteem voor de activiteitsprofilering van een panel van zeven gemeenschappelijke hydrolyse metabolieten van vijftien SCRA's met scaffolds op basis van L-valine of L-*tert*-leucine in directe vergelijking met hun moedercomponenten. Uit deze studie kon worden geconcludeerd dat bepaalde carboxymetabolieten, zoals 5F-ADB-PINACA-COOH, AB-CHMINACA-COOH en ADB-FUBINACA-COOH, nog steeds activiteit behouden bij hoge

concentraties. In het bijzonder werd voor deze carboxymetabolieten een *efficacy* van 2 tot 3 maal hoger dan die van de referentie ligand JWH-018 waargenomen. Daarom kan worden geconcludeerd dat deze metabolieten nog steeds kunnen bijdragen aan het toxicologische profiel van SCRA's *in vivo*.

Over het algemeen dragen de uitkomsten van beide delen van dit proefschrift een klein stukje bij tot de puzzel van de complexe wereld van GPCR-oligomerisatie en *biased* signalisatie. In beide delen bestaat het hier uitgevoerde werk uit *in vitro* experimenten, waaruit een algemene kennis kan worden opgebouwd die betere inzichten biedt in beide onderzochte verschijnselen. Verdere gecoördineerde diepgaande onderzoeken met computationele modellering, functionele screening of activiteitsprofilering, mutagenese en *in vivo* diermodelstudies zullen ons en anderen in staat stellen de onderliggende mechanismen van GPCR-oligomerisatie en *biased* signalering beter te begrijpen. Desalniettemin kunnen we voorlopig besluiten met het feit dat het veilig is om te zeggen dat, of het nu de werking betreft van dopamine of 'dope', alles draait om interactie!

Curriculum Vitae

ELISE WOUTERS

Personal Information

Address	Ruiseleedsesteenweg, 8700 Tielt, Belgium
Date of Birth	17/01/1992
Place of Birth	Jette, Belgium
Email address	elise.wouters@ugent.be elisewouters@hotmail.com
Telephone number	+32 475 36 86 05

Education

2015-2019	PhD in Pharmaceutical Sciences, Ghent University
2012-2014	Master of Science, Bio-engineering sciences: Cell- and Gene biotechnology/ Medical Biotechnology, University of Brussels (Magna cum Laude) Thesis: 'Identification of biological receptors of fimbrial adhesins expressed by pathogenic <i>Escherichia coli</i> ' Research group: Structural Biology Brussels
2009-2012	Bachelor of Science (BSc), Bio-engineering, University of Brussels (Cum Laude)
2003-2009	Mathematics-Sciences, Koninklijk Atheneum Grimbergen

Work experience**Scientific experience**

2017-2019	PhD student at the Laboratory of Toxicology, Department of Bioanalysis, Faculty of Pharmaceutical Sciences, Ghent University (Prof. Dr. C. Stove)
2015-2017	PhD student at the Laboratory of G-protein coupled receptor Expression and Signal Transduction (L-GEST), Department of Biochemistry and Microbiology, Faculty of Sciences, Ghent University (Prof. Dr. Kathleen Van Craenenbroeck)
2013	Internship student at ProDigest (Ghent), entitled: Study of the microbial metabolism of polyphenols in an <i>in vitro</i> simulation platform for the human intestinal microbial ecosystem.

Educational experience

2019	Supervision of Master dissertation, Master in Drug development: 'NanoLuciferase-based bio-assays to shed a new light on functional selectivity of synthetic cannabinoid receptor agonists' - Jolien Walraed
------	---

2017-2018	Support of practical courses Bioanalysis (3 rd Bachelor in Pharmaceutical Sciences)
2015-2016	Lab instructor, Biochemistry and Biotechnology Bachelor dissertation: <ul style="list-style-type: none"> - Justine Naessens - Domien Vanneste - Daan Verhaege
2015-2017	Support of practical courses Biochemistry and Biotechnology: 'Advanced Biotechnology: Part 2' (3 rd Bachelor in Biochemistry and Biotechnology)

Scientific Curriculum

1. Wouters E., Vasudevan L., Ciruela F., Saini D., Stove C., Van Craenenbroeck K. (2018) Assessing GPCR dimerization in living cells: comparison of the NanoBiT assay with related bioluminescence- and fluorescence-based approaches. In: Fuxe k., Borroto-Escuela d. (eds) Receptor-receptor interactions in the central nervous system. Neuromethods, vol 140. Humana press, New York
2. Qian M.[‡], Wouters E.[‡], Dalton J., Risseuw M., Crans R., Stove C., Giraldo J., Van Craenenbroeck K., Van Calenbergh S. (2018) Synthesis toward bivalent ligands for the dopamine D₂ and metabotropic glutamate 5 receptors. *Journal of Medicinal Chemistry*. 61(18):8212-8225. [‡]: equally contributed.
IF (2018): 6.054; Q1 (3/61) of 'Chemistry, Medicinal'
3. Crans R., Janssens J., Daelemans S., Wouters E., Raedt R., Van Dam D., *et al.* (2019) The validation of Short Interspersed Nuclear Elements (SINEs) as a RT-qPCR normalization strategy in a rodent model for temporal lobe epilepsy. *PLoS ONE* 14(1): e0210567.
IF (2018): 2.776; Q2 (24/69) of 'Multidisciplinary Sciences'
4. Wouters E., Marin A.R., Dalton J., Giraldo J., Stove C. (2019) Distinct Dopamine D₂ receptor antagonists differentially impact D₂ receptor oligomerization. *International Journal of Molecular Sciences*. 20, 1686.
IF (2018): 4.183; Q2 (78/298) of 'Biochemistry & Molecular Biology'
5. Wouters E., Mogler L., Cannaert A., Auwärter V. and Stove C. (2019) Functional evaluation of carboxy metabolites of synthetic cannabinoid receptor agonists featuring scaffolds based on L-valine or L-tert-leucine. *Drug Testing and Analysis*. 11: 1183- 1191.
IF (2018): 2.799; Q2 (28/84) of 'Chemistry, Analytical'
6. Wouters E.[‡], Vasudevan L.[‡], Crans R., Saini K. and Stove C. (2019) Luminescence- and fluorescence-based complementation assays to screen for GPCR oligomerization: current state of the art. *International Journal of Molecular Sciences*. 20, 12, (2958). [‡]: equally contributed.
IF (2018): 4.183; Q2 (78/298) of 'Biochemistry & Molecular Biology'

7. Wouters E., Walraed J., Banister S.D. and Stove C. (2019) Insights into biased signaling at cannabinoid receptors: synthetic cannabinoid receptor agonists. *Biochemical Pharmacology*. 169C, 113623.
IF (2018): 4.825; Q1 (25/267) of 'Pharmacology & Pharmacy'
8. Wouters E., Walraed J., Robertson M.J., Meyrath M., Szpakowska M., Chevigne A., *et al.* (2019) Assessment of biased agonism amongst distinct synthetic cannabinoid receptor agonist scaffolds. Submitted.

Oral presentation

1. Scientific session of the Toxicological society of Belgium and Luxembourg (BLT), Brussels, Belgium, March 12th 2019. Functional evaluation of carboxy metabolites of synthetic cannabinoid receptor agonists featuring scaffolds based on valine or tert-leucine.' (Wouters E., Mogler L., Cannaert A., Auwärter V. and Stove C.)
2. Research Day & Student Research Symposium, Ghent, Belgium, April 4th 2019. 'Functional evaluation of carboxy metabolites of synthetic cannabinoid receptor agonists featuring scaffolds based on valine or tert-leucine.' (Wouters E., Mogler L., Cannaert A., Auwärter V. and Stove C.)
3. VI International Conference on Novel Psychoactive Substances, Maastricht, The Netherlands, April 8-9th 2019. 'Functional evaluation of carboxy metabolites of synthetic cannabinoid receptor agonists featuring scaffolds based on valine or tert-leucine.' (Wouters E., Mogler L., Cannaert A., Auwärter V. and Stove C.)
4. Discover Glo Tour by Promega, Brussels, Belgium, May 14th 2019. 'Application of the NanoBiT[®] assay for the activity profiling of new psychoactive substances.' (Wouters E., Vasudevan L.)

Posters

1. 3rd GPCR targeted screening conference by GTC, Berlin, 12-13th of May 2016. 'Evaluation of several complementation assays to identify G protein-coupled receptor dimers.' (Wouters E., Vasudevan L., Crans R.A.J., Heyninck K., Ciruela F. and Van Craenenbroeck K.)
2. 'Integrative modeling of bio-molecular interactions' organized by EMBO, Barcelona, Spain, July 4-9th 2016. 'Evaluation of several complementation assays to identify G protein-coupled receptor dimers.' (Wouters E., Vasudevan L., Crans R.A.J., Heyninck K., Ciruela F. and Van Craenenbroeck K.)
3. The 28th conference of European comparative endocrinologists by CECE, Leuven, 21-25th of August 2016. 'Evaluation of several complementation assays to identify G protein-coupled receptor dimers.' (Wouters E., Vasudevan L., Crans R.A.J., Heyninck K., Ciruela F. and Van Craenenbroeck K.)

4. GPCR Structure and Function: Taking GPCR Drug Development and Discovery to the Next Level by Keystone Symposia, Santa Fe, United States of America, 16-20th of February 2018. 'A new approach to study GPCR dimer kinetics: ligand-induced modulation of the Dopamine D₂ and the Muscarinic M₁ receptor dimer.' (Wouters E., Crans R.A.J., Ciruela F., Van Craenenbroeck K. and Stove C.)
5. Discover Glo Tour by Promega, Brussels, Belgium, May 14th 2019. 'Functional evaluation of carboxy metabolites of synthetic cannabinoid receptor agonists featuring scaffolds based on L-valine or L-*tert*-leucine.' (Wouters E., Mogler L., Cannaert A., Auwärter V. and Stove C.)
6. International congress of analytical, forensic and clinical toxicology by SFTA/STC/SoHT/BLT, Lille, France, 22-24th of May 2019. 'Functional evaluation of carboxy metabolites of synthetic cannabinoid receptor agonists featuring scaffolds based on L-valine or L-*tert*-leucine.' (Wouters E., Mogler L., Cannaert A., Auwärter V. and Stove C.)
7. TIAFT 2019, Birmingham, United Kingdom, September 2-6th 2019. 'Assessment of biased agonism amongst distinct synthetic cannabinoid receptor agonist scaffolds.' (Wouters E., Walraed J., Robertson M.J., Meyrath M., Szpakowska M., Chevigne A., Skiniotis G. and Stove C.)

Scientific Events and workshops

1. New vistas in GPCR research: the Dawn of an Exciting Drug Discovery Era? by Medchem, Braine-L'alleud, November 21st 2014.
2. Bioluminescent Cell-based Assay symposium Discover Glo! by Promega, Free University of Brussels, March 9th 2015.
3. The 11th congress of Belgian Society for Neuroscience, Mons, May 22nd 2015
4. 'Integrative modeling of bio-molecular interactions' organized by EMBO, Barcelona, Spain, July 4-9th 2016.
5. Practical course on isolation of synaptosomes in the lab of Prof. F. Ciruela in Barcelona, Spain, June 6th 2016-July 5th 2016. Travel grant obtained from GLISTEN.

Scientific prize

Promega Poster award during the Discover Glo Tour by Promega, Brussels, Belgium, May 14th 2019

Membership of Scientific organization

BLT (Belgium Luxembourg Toxicological Society)

